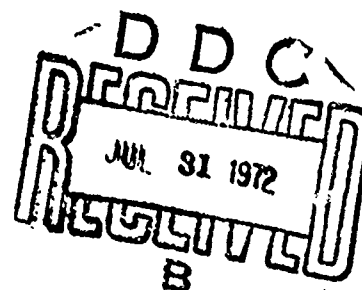


NUSC Technical Report 4331

# The Response of Cable-Moored Axisymmetric Buoys To Ocean Wave Excitation

KIRK T. PATTON  
*Ocean Science Department*

AD 745749



15 June 1972

## NAVAL UNDERWATER SYSTEMS CENTER

Details of illustrations in  
this document may be better  
studied on microfiche

Approved for public release; distribution unlimited.

Reproduced by  
NATIONAL TECHNICAL  
INFORMATION SERVICE  
U S Department of Commerce  
Springfield VA 22151

Hob

# ADMINISTRATIVE INFORMATION

This study was prepared originally as a dissertation in partial fulfillment of the requirements for the degree of Doctor of Philosophy in Mechanical Engineering at the University of Rhode Island. The work was accomplished under NUSC Project No. A-071-00-00, "Buoy Dynamics," Principal Investigator, K. T. Patton (Code TA12), and Navy Subproject and Task No. ZR-001-01-611-1N, Program Manager, Dr. J. H. Huth (DLP/MAT 03L4).

REVIEWED AND APPROVED: 15 June 1972

ACCESSION for	
NTIS	White Section <input checked="" type="checkbox"/>
DCC	Buff Section <input type="checkbox"/>
UNANNOUNCED	<input type="checkbox"/>
JUSTIFICATION .....	
BY .....	
DISTRIBUTION/AVAILABILITY CODES	
Dis.	Avail. and/or SPECIAL
A	

*W. A. Von Winkle*

W. A. Von Winkle  
Director of Science and Technology

Inquiries concerning this report may be addressed to the author,  
New London Laboratory, Naval Underwater Systems Center,  
New London, Connecticut 06320

UNCLASSIFIED

Security Classification

## DOCUMENT CONTROL DATA - R &amp; D

Security classification of title, body of abstract and index, annotation must be entered when the overall report is classified

1. ORIGINATING ACTIVITY (Corporate author) Naval Underwater Systems Center Newport, Rhode Island 02840		2a. REPORT SECURITY CLASSIFICATION <b>UNCLASSIFIED</b>	
		2b. GROUP	
3. REPORT TITLE <b>THE RESPONSE OF CABLE-MOORED AXISYMMETRIC BUOY TO OCEAN WAVE EXCITATION</b>			
4. DESCRIPTIVE NOTES (Type of report and inclusive dates) <b>Research Report</b>			
5. AUTHOR(S) (First name, middle initial, last name) <b>Kirk T. Patton</b>			
6. REPORT DATE <b>15 June 1972</b>	7a. TOTAL NO. OF PAGES <b>402</b>	7b. NO. OF REFS <b>87</b>	
8a. CONTRACT OR GRANT NO.		9a. ORIGINATOR'S REPORT NUMBER(S)	
b. PROJECT NO. <b>A-071-00-00</b>		<b>4331</b>	
c. <b>ZR-011-01-01-611-1N</b>		9b. OTHER REPORT NO(S) (Any other numbers that may be assigned this report)	
d.			
10. DISTRIBUTION STATEMENT <b>Approved for public release; distribution unlimited</b>			
11. SUPPLEMENTARY NOTES		12. SPONSORING MILITARY ACTIVITY <b>Department of the Navy</b>	
13. ABSTRACT Forces and motions imposed upon a moored buoy system by the oceanic environment are investigated using numerical methods on a digital computer. Equations of motion for axisymmetric buoys are developed for six degrees of freedom including cross-coupled hydrostatic and hydrodynamic forces. Equations of motion for the mooring cable are developed to allow simultaneous axial and transverse wave propagation. A unique method of characteristics numerical technique is shown for digital computer simulation of cable dynamics. The equations of motion for the buoy and its mooring cable are coupled and are excited by winds, currents, and a quasi-random wind wave model. Simulated buoy system parameter response characteristics are compared with response characteristics observed from actual oceanographic buoy system moorings. This comparison indicates that steady state buoy system forces and configurations can be predicted within 5 percent and that dynamic motions can be predicted within 50 percent using the digital computer simulation.			

UNCLASSIFIED

Security Classification

14 KEY WORDS	LINK A		LINK B		LINK C	
	ROLE	WT	ROLE	WT	ROLE	WT
Ocean Buoys Axisymmetric Buoys Moored Buoys						

DD FORM 1473 (BACK)  
1 NOV 65

UNCLASSIFIED

Security Classification



## ABSTRACT

Motions and dynamic forces imposed upon a moored buoy system by the oceanic environment are of vital interest to the user of the system. If instrumentation for monitoring the environment is motion sensitive, it is of little value if its response to platform motion is greater than its response to the changing environment. The buoy system designer is also concerned with motions and forces in buoy systems in order to design for the highest probability of system survival under extreme conditions.

In response to these needs, this study investigates digital computer simulation of buoy system dynamics for simple buoy systems, i.e., a surface buoy moored on a single mooring line. The buoy system can be excited by winds, waves, and currents. Winds can act from any compass direction, and currents can vary in strength and direction as a function of depth in the water column. Wind waves are simulated by first computing their properties with the Sverdrup-Munk-Bretschneider method and then by using Borgman's energy partitioning scheme on a two-parameter Bretschneider spectrum to compute component sine wave amplitudes and frequencies. Since the component Stokesian waves are linear, the principle of superposition can be used to sum component magnitudes in order to compute water particle motions.

Equations of motion for the buoy are developed for six degrees of freedom--three translational and three rotational. Hydrostatic and hydrodynamic forces

and moments acting on an oblate spheroid moving on the free surface of an infinite body of water are investigated in detail. The set of integro-differential equations for buoy motions are reduced to a set of nonlinear, ordinary differential equations with nonconstant coefficients by using the Haskind hypothesis to evaluate the hydrodynamic force and moment integrals and to represent them as frequency dependent coefficients. Buoy motions are coupled through hydrostatic, hydrodynamic, and mooring line forces.

Cable dynamics are also investigated. A set of coupled, hyperbolic, partial differential equations for cable motions are developed, and characteristic equations are derived to effect a method of characteristics solution. A unique numerical method of characteristics technique, based upon Hartree's method, is developed for the solution of the cable equations in the time-space domain. Buoy motions, which are dependent upon the cable tensions, serve as the upper boundary conditions. Lower boundary conditions are prescribed at the anchor, where there can be no motion.

For certain buoy systems, where many mass discontinuities exist along the cable, or for shallow water moorings, where slack cable conditions can exist, a lumped-mass method of computing cable dynamics is developed as opposed to the finite-difference method just described. In general, for cable dynamics the lumped-mass numerical method is an order of magnitude faster in computation time than the finite difference method.

The equations of motion developed for the buoy were solved numerically in the time domain using a fourth-order, Runge-Kutta integration method. Cable

equations can be solved either by finite-difference methods or by integrating with the Runge-Kutta algorithm for the lumped-mass model.

In order to validate the numerical models developed, two buoy systems were instrumented and deployed in Block Island Sound. The motion data from these experiments, along with data published in the literature, are compared with simulated buoy motion data. This comparison indicates that steady-state buoy system forces and configurations can be predicted within approximately 5 percent and that buoy system dynamics can be predicted within approximately 50 percent. There are some indications that the surge and sway hydrodynamic forces acting on the buoy are being underestimated by the computer model.

## ACKNOWLEDGMENTS

I am grateful to the Faculty of the Mechanical Engineering and Applied Mechanics Department and of the Ocean Engineering Department at the University of Rhode Island for their continuing inspiration and guidance. In particular, I would like to thank my advisor, Dr. Rodger B. Dowdell and the members of my dissertation committee, Drs. Charles D. Nash and Everett E. McEwen.

This research would not have been possible without the support of my colleagues at the Naval Underwater Systems Center. Many helpful discussions were held with Dr. Robert G. Williams, Messrs. Stanley L. Rupinski, Louis F. DiRienzo, and Gary T. Griffin. The instrumentation and telemetry circuitry were designed and constructed by Mr. George F. Battista. Field support was offered by Messrs. Hector F. Bernier and Carl T. Milner, of the BIFI acoustic range.

The buoys were installed and removed through the efforts of Lt. Robert B. Doughty, Master, and the crew of the U.S. Coast Guard buoy tender, REDWOOD. The many trips required to inspect and service the buoys were made possible by Dr. Andrew J. Nalwalk, of the University of Connecticut, and Oram A. Campbell, Master of the R/V UCONN and his crew.

I am thankful for the support I received from the Naval Underwater Systems Center under the Advanced Professional Development Program and

from my supervisor, Mr. Kenneth L. Moothart. Support for the research was furnished by NUSC Project A-071-00-00, "Buoy Dynamics," Principal Investigator, Kirk T. Patton (Code TA12), and Navy Subproject and Task ZR-011-01-01-611-1N, Program Manager, Dr. J. H. Huth (DLP/MAT 03L4).

## TABLE OF CONTENTS

	Page
ABSTRACT . . . . .	i
ACKNOWLEDGMENTS . . . . .	iv
LIST OF TABLES . . . . .	viii
LIST OF ILLUSTRATIONS . . . . .	ix
LIST OF SYMBOLS AND NOTATIONS . . . . .	xv
Chapter	
I INTRODUCTION . . . . .	1
II PROCEDURE . . . . .	12
2.1 System Dynamics . . . . .	12
2.2 Experimental Validation . . . . .	15
III ANALYTICAL DEVELOPMENT AND DISCUSSION . . . . .	16
3.1 Buoy Dynamics . . . . .	16
3.1.1 Wind Forces . . . . .	22
3.1.2 Mooring Line Forces . . . . .	26
3.1.3 Hydrostatic Forces . . . . .	27
3.1.4 Hydrodynamic Forces . . . . .	37
3.1.5 Ocean Waves . . . . .	57
3.1.6 Numerical Solution of the Equations of Motion . . . . .	72
3.2 Cable Dynamics . . . . .	79
3.2.1 The Cable Equations . . . . .	79
3.2.2 Finite-Difference Methods . . . . .	104
3.2.3 Cable Loading Functions . . . . .	113
3.2.4 Lumped-Mass Model . . . . .	120

## TABLE OF CONTENTS (Cont'd)

Chapter	Page
3.3 Steady-State Buoy System Configurations . . . . .	128
IV EXPERIMENTAL MEASUREMENTS AND COMPARISON WITH MODELS . . . . .	138
4.1 Steady-State Buoy System Configurations . . . . .	138
4.1.1 Torroid and Current Meter Array at Station BRAVO . . . . .	136
4.1.2 WHOI Mooring No. 279 . . . . .	152
4.2 Experimental Measurements of Buoy System Dynamics . . . . .	156
4.2.1 Spherical Buoy at Station D . . . . .	157
4.2.2 Torroidal Buoy at Station BRAVO . . . . .	172
4.3 Simulation and Comparison of Buoy System Dynamics . . . . .	212
4.3.1 Spherical Buoy at Station D . . . . .	212
4.3.2 Torroidal Buoy at Station BRAVO . . . . .	220
4.3.3 WHOI Mooring No. 238 . . . . .	240
V SUMMARY . . . . .	246
5.1 Restatement of the Problem . . . . .	246
5.2 Conclusions . . . . .	248
5.3 Suggestions for Further Study . . . . .	250
REFERENCES . . . . .	252
Appendix	
A ANGULAR STABILITY OF AXISYMMETRIC BUOYS . . . . .	260
B COMPUTER PROGRAMS FOR THE MODELS . . . . .	267
C DERIVATION OF THE CABLE CHARACTERISTICS . . . . .	352
D COMPUTED INPUT DATA FOR THE SIMULATIONS . . . . .	361
E BUOYANT FORCES AND MOMENTS FOR A TORROIDAL BUOY . . . . .	373

## LIST OF TABLES

Table	Page
1. Current Meter Data — Station BRAVO . . . . .	142
2. Comparison of Observed Current Meter Tilt Angles With Data Computed by Integration of Cable Equations . . .	144
3. Comparison of Observed Current Meter Tilt Angles With Data Computed by Assuming No Cable Curvature . . .	150
4. Summary of Observed Environmental and Buoy Response Data for the Torroidal Buoy BRAVO . . . . .	180



## LIST OF ILLUSTRATIONS

Figure		Page
1	A Current Meter Energy Spectrum . . . . .	6
2	An Anemometer Power Spectrum . . . . .	5
3	A Simple Buoy System . . . . .	13
4	Buoy Coordinate Systems . . . . .	17
5	Energy Flow in Buoy System . . . . .	19
6	Immersed Volume of an Oblate Spheroid . . . . .	29
7	An Object on a Free Surface . . . . .	39
8	Hydrodynamic Mass and Wave Damping for Swaying or Surging Oblate Spheroids . . . . .	46
9	Hydrodynamic Mass and Wave Damping for Heaving Oblate Spheroids . . . . .	47
10	Hydrodynamic Mass Moment of Inertia for Pitching or Rolling Oblate Spheroids . . . . .	48
11	Least-Squares Fits to Kim's Parameters . . . . .	51
12	Borgman's Energy Partitioning in a Bretschneider Spectrum . . . . .	67
13	Free Body of a Cable Segment . . . . .	80
14	Cable Coordinates . . . . .	85
15	Grid for Adaptation of Hartree's Method . . . . .	105
16	Cable Loading Functions . . . . .	114
17	Segments for a Five-Element, Lumped-Mass Model . . . . .	121

# LIST OF ILLUSTRATIONS (Cont'd)

Figure		Page
18	Lumped-Mass Model . . . . .	123
19	Buoy System Configuration Computation Procedures . . .	133
20	Free Body of an Object on the Mooring Line . . . . .	135
21	Current Meter Array at Station BRAVO . . . . .	139
22	Torroidal Buoy Used for the Three-Current-Meter Array .	140
23	Current Meter Tilt Angles Computed by Integrating Down the Cable Compared With Observed Data . . . . .	145
24	A Simple Statics Model of the Current Meter Array . . .	147
25	Comparison of Computed Buoy System Configurations . .	149
26	Current Meter Tilt Angles Computed by Simple Statics Model Compared With Observed Data . . . . .	151
27	Woods Hole Oceanographic Institution Mooring No. 279 . .	153
28	Comparisons of WHOI Data With Computed Mean Mooring Line Tensions . . . . .	155
29	Spherical Buoy at Block Island Station D . . . . .	158
30	Spherical Buoy System at Block Island . . . . .	160
31	Statistical Accelerometer Data for Heave Motions . . . .	161
32	Conditional Probabilities for Heave Motions . . . . .	162
33	Spherical Buoy Heave Acceleration Amplitude Distributions . . . . .	163
34	Spherical Buoy Motion Parameter Statistics . . . . .	165
35	Spherical Buoy Motion Amplitude Histograms — Wave Height, Heave, and Surge . . . . .	166
36	Spherical Buoy Amplitude Histograms — Pitch and Roll . .	167

# LIST OF ILLUSTRATIONS (Cont'd)

Figure		Page
37	Spherical Buoy Motion Amplitude Histograms — Cable Pitch and Cable Roll . . . . .	168
38	Heave Response of the Spherical Buoy . . . . .	170
39	Torroidal Buoy at Station BRAVO . . . . .	173
40	The Shore Station at Watch Hill Lighthouse . . . . .	174
41	Telemetry Receiver and Recording Equipment . . . . .	175
42	Torroidal Buoy Motion Experiment Setup . . . . .	176
43	Buoy Motion Telemetry System . . . . .	177
44	Torroidal Buoy Motion Statistics for 6-week Period . . . . .	182
45	Buoy Motions versus Wind Speed — Heave and Sway . . . . .	184
46	Buoy Motions versus Wind Speed — Surge and Roll . . . . .	185
47	Buoy Motions versus Wave Height — Heave and Sway . . . . .	186
48	Buoy Motions versus Wave Height — Surge and Roll . . . . .	187
49	Surge and Sway Motions versus Heave Motion . . . . .	188
50	Roll Motion versus Heave Motion . . . . .	189
51	Empirical Equations for Significant Buoy Motion Amplitudes. . . . .	190
52	Empirical Equations for Mean Buoy Motion Amplitudes . . . . .	191
53	Wind and Current Cumulative Distributions . . . . .	192
54	Significant Wave Height Cumulative Distributions . . . . .	193
55	Significant Buoy Motion Cumulative Distributions . . . . .	194
56	Computed Wind Wave Spectral Levels — 2030 hr, 11 June 1970 . . . . .	195
57	Observed Heave Spectral Levels . . . . .	196

# LIST OF ILLUSTRATIONS (Cont'd)

Figure		Page
58	Observed Surge Spectral Levels . . . . .	197
59	Observed Sway Spectral Levels . . . . .	198
60	Observed Pitch Spectral Levels . . . . .	199
61	Observed Roll Spectral Levels . . . . .	200
62	Cross-Spectral Levels of Surge and Heave . . . . .	202
63	Cross-Spectral Levels of Sway and Heave . . . . .	203
64	Cross-Spectral Levels of Pitch and Heave . . . . .	204
65	Cross-Spectral Levels of Roll and Heave . . . . .	205
66	Gain Function for Heave and Wave Height . . . . .	207
67	Gain Function for Sway and Wave Height . . . . .	208
68	Gain Function for Surge and Wave Height . . . . .	209
69	Gain Function for Pitch and Wave Height . . . . .	210
70	Gain Function for Roll and Wave Height . . . . .	211
71	Computed Steady-State Configurations of the Spherical Buoy System . . . . .	213
72	Observed and Simulated Heave Motions of the Spherical Buoy . . . . .	215
73	Bretschneider Spectrum — 1200 hr; 16 March 1970, Station D . . . . .	217
74	Simulated Spherical Buoy Motion Parameter Statistics . .	218
75	Observed Spherical Buoy Motion Parameter Statistics . .	219

# LIST OF ILLUSTRATIONS (Cont'd)

Figure		Page
76	Torroidal Buoy BRAVO With Ebb Current and Southwest Winds . . . . .	222
77	Computed Mean Wave Heights and Periods at Station BRAVO . . . . .	223
78	Computed Wind Wave Spectra . . . . .	224
79	Simulated and Observed Buoy Motions versus Wind Speed . . . . .	226
80	Simulated and Observed Buoy Motions versus Wave Height . . . . .	227
81	Simulated and Observed Surge and Pitch versus Heave . . . . .	228
82	Wave Height Spectrum — 2030 hr, 11 June 1970 . . . . .	231
83	Simulated Wave Height Spectral Levels . . . . .	232
84	Simulated Heave Spectral Levels . . . . .	234
85	Simulated Sway Spectral Levels . . . . .	235
86	Simulated Surge Spectral Levels . . . . .	236
87	Simulated Pitch Spectral Levels . . . . .	237
88	Simulated Roll Spectral Levels . . . . .	238
89	Initial Strains for WHOI Mooring No. 238 . . . . .	242
90	Initial Angles for WHOI Mooring No. 238 . . . . .	243
91	Computed and Observed Tension Amplitudes at 12 m For WHOI Mooring No. 238 . . . . .	244

## Appendix A

A-1	Axisymmetric Buoy Shapes . . . . .	262
A-2	Spar Buoy Phase Planes . . . . .	263

## LIST OF ILLUSTRATIONS (Cont'd)

Figure		Page
A-3	Torroid or Discus Buoy Phase Planes . . . . .	266
Appendix B		
B-1	Steady-State Buoy System Configuration Flow Chart . . .	268
B-2	Spherical Buoy Dynamics Simulation Flow Chart . . . .	283
B-3	Torroidal Buoy BRAVO Dynamics Simulation Flow Chart .	300
B-4	Torroidal Buoy WHOI Mooring No. 238 Dynamics Simulation Flow Chart . . . . .	329
B-5	Finite-Difference Cable Dynamics Simulation Flow Chart .	330
Appendix E		
E-1	Torroid Section . . . . .	374
E-2	Torroid (8-ft) Displacement versus Draft . . . . .	377
E-3	Torroid (8-ft) Righting Moment versus Tilt Angle . . . .	378
E-4	Torroid (8-ft) Coupled Moment versus Tilt Angle . . . .	379
E-5	Torroid (8-ft) Coupled Buoyancy versus Tilt Angle . . .	380

## LIST OF SYMBOLS AND NOTATIONS

### Buoy Dynamics

$a$	Spheroid minor half-diameter
$a$	Frequency parameter
$A$	Transform matrix from inertial to cable coordinates
$A_H$	Plan area of immersed buoy volume
$A_s$	Profile area of immersed buoy volume
$A_1$	Buoy windage — profile area above free surface
$A_2$	Plan area of buoy
$b$	Spheroid major half-diameter
$B$	Hydrostatic force vector
$C_D$	Buoy hull drag coefficient
$CV$	Current component in $y$ direction
$CW$	Current component in $z$ direction
$C_L$	Buoy hull lift coefficient
$d$	Spheroid buoyant force moment arm
$d$	Viscous drag force component
$D$	Viscous drag force vector
$D$	Wind duration
$\bar{D}$	Dimensionless duration parameter
$e$	2.7182 . . .

### Buoy Dynamics (Cont'd)

$F$	Fetch
$F_D$	Force vector on an immersed body $B$
$\bar{F}$	Dimensionless fetch parameter
$F_1$	Dimensionless wave height parameter for Bretschneider spectra
$F_2$	Dimensionless wave period parameter for Bretschneider spectra
$g$	Gravitation constant
$G$	Gravity vector
$G_D$	Moments on an immersed body $B$
$H$	Hydrodynamic force vector
$H_D$	Buoy draft
$H$	Angular wave damping coefficient
$H_{CB}$	Height of center of buoyancy below free surface
$H_{CG}$	Height of center of gravity
$H_{CP}$	Height of center of pressure
$H_{ML}$	Height of the center of gravity of the buoy above mooring line termination
$H_w$	Height of wind center of pressure from center of gravity
$H_{1/3}$	Significant wave height
$\bar{H}$	Dimensionless significant wave height parameter
$i$	$\sqrt{-1}$
$I$	Structural mass moment of inertia
$I$	Hydrodynamic mass moment of inertia coefficient
$I^A$	Area of the intersection of a body $B$ with the free surface



### Buoy Dynamics (Cont'd)

$I_x^A, I_y^A$	Moments of $I^A$ about vertical planes
$J_0$	Bessel function of first kind of order 0
$K$	Wave number
$L$	Wind lift force
$m$	Structural mass of the buoy
$M$	Structural mass matrix
$M$	Hydrodynamic mass coefficient
$M_h$	Hydrodynamic mass dyadic
$M_\beta$	Pitch buoyant moment
$M_\gamma$	Roll buoyant moment
$n$	Unit normal to immersed surface of body B
$N$	Wave damping coefficient
$N$	Wave damping dyadic
$P_k$	Components of unit normal $n$
$q_k$	Components of moment of $n$ about center of gravity of body B
$Q$	Displacement vector of the buoy center of gravity
$\bar{r}$	Position vector of a point on the immersed surface of body B
$R$	Coordinate system center
$Re$	Reynold's number
$S$	Immersed surface of body B
$S_0$	Struve function of order 0
$t$	Time
$T$	Mooring line tension vector

Buoy Dynamics (Cont'd)

$u_j$	Pressure function
$u, v, w$	Velocity components of the buoy center of gravity
$V$	Wind velocity vector.
$W$	Wind force vector
$W_D$	Wind drag force on buoy
$W_L$	Wind lift force on buoy
$WV$	Wind velocity components
$x, y, z$	Spatial coordinates
$Y_0$	Bessel function of second kind of order 0
$\alpha$	Yaw angle
$\beta$	Pitch angle
$\beta$	Dimensionless frequency
$\gamma$	Roll angle
$\epsilon$	Wave component phase angle
$\eta$	Instantaneous free surface height below mean free surface
$\theta$	Cable tilt angle
$\theta$	Rotation vector
$\theta', \theta'', \theta'''$	Angular displacements of body B
$\lambda$	Wavelength
$\mu$	Absolute viscosity
$\nu$	Kinematic viscosity
$\xi$	Instantaneous wave surface slope
$\pi$	3.1416 . . .

### Buoy Dynamics (Cont'd)

$\rho$	Fluid mass density
$\rho_A$	Air mass density
$\sigma$	Angular frequency of buoy motion
$\tau_{1/3}$	Significant wave period
$\bar{\tau}$	Dimensionless significant period parameter
$\phi$	Cable transverse tilt angle
$\Phi(s, y, z; t)$	Velocity potential
$\omega$	Angular frequency of wind waves
$\Omega$	Buoy rotation matrix

### Subscripts

d	Viscous drag
D	Drag
h	Hydrodynamic
i	Coordinate system
L	Lift
max.	Maximum
min.	Minimum
o	Static position
og	Static position of center of gravity
S	Surface
w	Wave
x, y, z	Coordinate directions
$\alpha, \beta, \gamma$	Buoy rotations
1/3	Statistically significant

### Cable Dynamics

$a$	Cable section radius
$A$	Transform matrix from inertial to cable coordinates
$C_{DN}$	Normal drag coefficient
$C_{DT}$	Tangential drag coefficient
$Ch$	Characteristic velocity
$C_s$	Current velocity vector
$d$	Cable diameter
$D$	Viscous drag
$F_H$	Hydrodynamic inertia force
$g$	Gravitational constant
$G$	Cable loading function
$h$	Node separation in grid
$H$	Cable loading function
$\hat{i}, \hat{j}, \hat{k}$	Direction indices
$I$	Cable loading function
$k$	Time step size in grid
$K$	Linearized tension - strain derivative
$m_h$	Hydrodynamic mass
$\vec{Q}$	Force vector on a cable segment
$\vec{r}$	Vector from origin to point on cable
$Re$	Reynolds number
$S$	Stokes number
$t$	Time
$\vec{T}$	Tension vector

### Cable Dynamics (Cont'd)

$U, V, W$	Velocity components
$w_c$	Cable in-water weight per unit length
$x, y, z$	Spatial coordinates
$X, Y, Z$	Force components on cable
$\epsilon$	Strain
$\theta$	Cable tilt angle
$\lambda$	Characteristic velocities
$\mu$	Cable structural mass per unit length
$\nu$	Kinematic viscosity
$\pi$	3.1416 . . .
$\rho$	Fluid mass density
$\phi$	Cable transverse tilt angle
$\omega$	Angular frequency of oscillation

### Subscripts

A	Point (i, j) in time-space grid
B	Point (i-1, j) in time-space grid
B	Buoy
C	Point (i-1, j-1) in time-space grid
D	Point (i+1, j) in time-space grid
E	Point (i, j-1) in time-space grid
F	Point (i+1, j-1) in time-space grid
H	High
i	Space

Subscripts (Cont'd)

j	Time
L	Low
N	Normal
P <sub>1</sub>	Point between B-A in grid for tensile characteristic
P <sub>2</sub>	Point between A-D in grid for tensile characteristic
Q <sub>1</sub>	Point between B-A in grid for transverse characteristic
Q <sub>2</sub>	Point between A-D in grid for transverse characteristic
R	Point (i, j+1) in time-space grid
S	Current velocity
T	Tangential

## I. INTRODUCTION

Clean, green, windy billows notching out the sky,  
Grey clouds tattered into rags, sea-winds blowing high,  
And the ships under topsails, beating, thrashing by,  
And the mewling of the herring gulls.

Dancing, flashing green seas shaking white locks,  
Boiling in blind eddies over hidden rocks,  
And the wind in the rigging, the creaking of the blocks,  
And the straining of the timber hulls.

John Masefield  
"Cardigan Bay"

This study is concerned with the analysis and simulation of the dynamics of simple oceanic buoy systems. The analysis must include the effect of the significant forces that act on the buoy system and are imposed by the ocean environment — wind, waves, and currents. Because of the highly nonlinear nature of the problem, numerical methods are favored in order to provide a realistic simulation.

Buoys have been employed by mariners for centuries as aids to navigation and to support mooring chains. In this country, navigational buoys were in service in the Delaware River in 1767 and in Boston Harbor by 1808. At present, the United States Coast Guard maintains over 24,000 buoys in the navigable waters of the United States and its possessions. Navigational buoy system design is largely a matter of employing "rules of thumb" evolved over decades of experience with these buoys. The vast majority of navigational

buoys are moored in waters less than 100 ft deep, and the most common cause of failure is collision with a vessel. Thus, these buoy systems are characterized by massive steel buoys moored with heavy chain to large concrete clumps. They are serviced on a regular basis and are recovered and overhauled annually.

In recent years, oceanographers have used buoy systems to support current meters, thermistor chains, and other oceanographic instrumentation. The state of the art in oceanography has advanced to the point where oceanographers are no longer satisfied with data taken at a single point over a rather short time duration. Multiple measurements to be made simultaneously over wide areas of the ocean or long-duration measurements are made most economically with a buoy system equipped with self-recording or telemetering instrumentation. This economy can be realized only if the buoy system is designed to have a life on station greater than the desired measurement time.

The basic design philosophy of deep-sea oceanographic buoy systems is quite different from that of the navigational buoys. Oceanographic vessels are usually small and are not equipped for handling heavy objects over the side at sea; thus, the buoys and mooring line components must be of relatively light weight. The mooring lines are miles long and thus preclude the use of heavy chains (except at the bottom) and tend to be made up of light, high-strength wire ropes or of synthetic fiber ropes. Designers of oceanographic buoy systems are faced with the near-impossible task of designing a lightweight, highly compliant structure to survive for periods of a year or more in one of the harshest environments known to man.



Isaacs<sup>1</sup> describes a mean time between failure (MTBF) of 121 days for the taut-moored Scripps Institution of Oceanography "Catamaran" buoys. The observed system failures were due to parting of the nylon mooring line near the surface. The writers hypothesize that high tensile loads in the nylon line are caused by tensile waves propagating up and down the cable. Richardson<sup>2</sup> of the Woods Hole Oceanographic Institution (WHOI), anchored 106 buoy systems between Cape Cod and Bermuda. The MTBF for these systems was found to be about 90 days. The WHOI buoy system failures were attributed to mooring line failures, fish bite of synthetic mooring lines, and theft. In 1967, WHOI<sup>3</sup> set nine long term buoy moorings of which only one was recovered on station after 60 days. Three of these were found adrift. WHOI was more successful in 1968,<sup>4</sup> when only 3 of 14 long-term buoy moorings failed.

All the oceanographic buoy systems described above were taut-moored systems, the majority of which utilized synthetic rope in their mooring lines. Their short life on station and their low recovery rate indicate a need for an accurate engineering method of computing the dynamic response of the buoy system to the ocean environment.

Slack moored buoy systems have a much greater MTBF and are more reliable. The catenary of the mooring line provides the necessary compliance; thus, dynamic tensions in the mooring line are reduced. Navigational buoy systems are slack moored and are very reliable. Smith<sup>5</sup> cites a long history of successful moorings in the Gulf of Mexico for the NOMAD buoy system. Over a 5-year period, a number of the NOMAD buoys were kept on station for periods of a year or more. Smith also describes fifteen, 25-ton barges that

were slack moored for 8 months in water depths over 12,000 ft with no failures.

Oceanographers are also concerned with the effects of buoy system motions on their instrumentation. For example, instrumentation fastened to the mooring line of a slack-moored system will undergo depth excursions that are dependent on the current structure. Webster<sup>6,7</sup> discusses errors in self-recording current meter data due to buoy system motion. Webster shows a current energy spectrum developed from a current meter that is attached to the mooring line of a buoy system (figure 1). The energy introduced into the current data by the buoy system motions is far greater than the energy of the currents themselves.

Marcus<sup>8</sup> compared anemometer data taken from a NOMAD buoy in the Gulf of Mexico with other meteorological observations in the area over a 6-month period. The mean error of the wind speed data was 0.2 knot with a standard deviation of the error of  $\pm 4.67$  knots. Huff<sup>9</sup> shows a power spectrum of anemometer data taken from another NOMAD buoy system moored off Fermuda. This spectrum (figure 2) indicates that a large amount of energy was introduced into the spectrum by the motion of the buoy. Huff also shows an increase in the average wind speed deviation from the mean with increasing mean wind speed that levels out at high wind speeds. This variation is characteristic of sea surface slopes, which have an upper limit due to gravity. This upper limit implies that the wind speed error is due to the pitch and roll motions of the buoy. Day<sup>10</sup> found that wind data sampled every 10 min from a

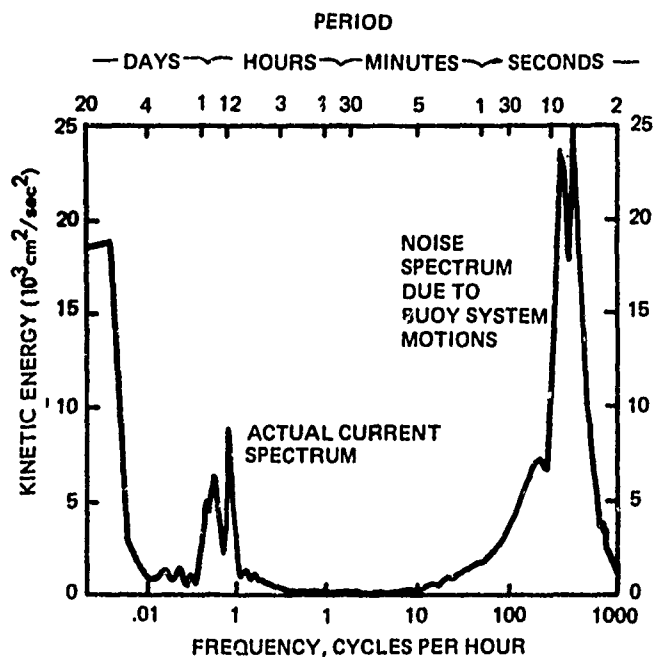


Figure 1. A Current Meter Energy Spectrum  
(From Webster, reference 7.)

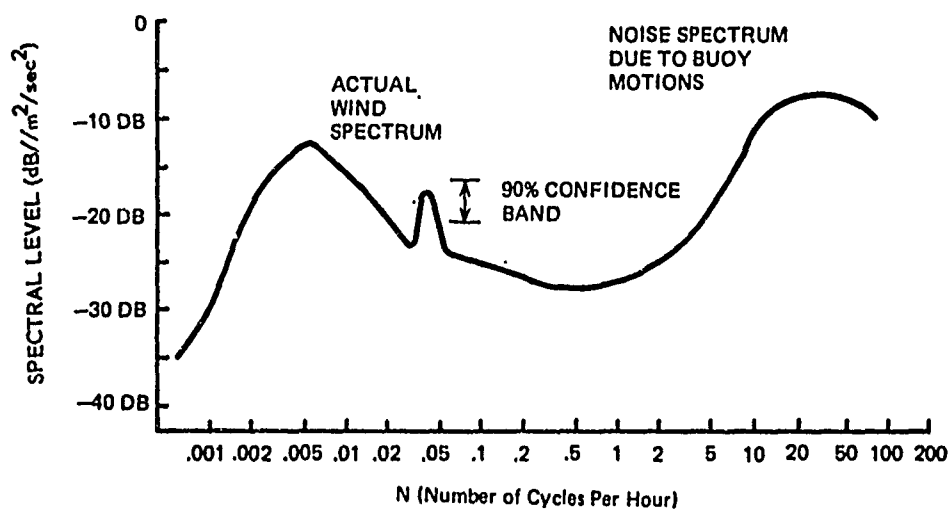


Figure 2. An Anemometer Power Spectrum  
(From Webster, reference 9.)

buoy-mounted anemometer had to be time averaged over a 2-hr period to remove errors due to buoy motions.

The two-dimensional, steady-state configurations of buoy cable systems have been investigated by Wilson.<sup>11, 12</sup> Wilson constrained the upper end of the cable to be at the mean ocean surface and did not consider cable elasticity. Patton,<sup>13</sup> as part of this dissertation research, developed a numerical method to determine the equilibrium configuration of buoy cable systems. The three-dimensional configuration for any current structure (currents may vary in strength and direction as a function of depth), as well as the buoy draft, is computed. The elasticity of the cable is considered and the stretch is also computed. Martin<sup>14</sup> developed a numerical method similar to Patton's, but it is restricted to two dimensions. Martin also experimentally investigated the elastic properties of nylon rope and the drag of buoy models. Smith<sup>5</sup> presented a graphical method for two-dimensional buoy system configurations but neglected tangential drag and elasticity.

The study of the motions of bodies floating on the ocean surface and being excited by waves originated in 1749 with Euler<sup>15</sup> in his classic work, Scientia Navalis. Froude<sup>16</sup> was concerned with the rolling and roll stability of ships. Froude recognized the nonlinearity of the problem and included viscous resistance in the equations of motion. Kriloff<sup>17</sup> investigated ship motions and wrote coupled equations of motion. Both Froude and Kriloff assumed that the ship did not influence the waves, which allowed them to treat the hydrodynamic properties of the ship as a body oscillating on a free surface. By far, the

single greatest problem in ship dynamics is the description of the hydrodynamic forces acting on the ship. Lewis<sup>18</sup> introduced the "strip theory" in 1929, which allowed computation of three-dimensional hydrodynamic characteristics from two-dimensional theory. Haskind<sup>19, 21</sup> assumed that the hydrodynamic equations could be linearized in such a manner that velocity potentials could be superimposed. This method allowed the use of three velocity potentials: (1) incident wave potential, i.e., the velocity potential of the waves alone; (2) diffracted wave potential, i.e., the velocity potential of the body fixed on a free surface exposed to waves; and (3) forced heave potential, i.e., the velocity potential of the body oscillating in still water. Naval architects currently favor the Haskind hypothesis as opposed to the earlier Froude-Kriloff hypothesis, which assumes that body dimensions are small compared with the waves.

John<sup>22, 23</sup> wrote complete sets of coupled equations of motion for floating bodies in harmonic waves and considered the influence of the body on the waves (after Haskind). John also included an external force term that could be used to describe a mooring cable. Heave and surge motions of a sphere were computed for various wave frequencies.

St. Denis and Pierson<sup>24</sup> linearized the decoupled equations of motion for a ship and investigated ship motions in confused seas by summing the ship's responses to sine wave seas of different frequencies. Korvin-Kroukovsky<sup>25-27</sup> used the "strip" method to compute the hydrodynamic characteristics of the ship and included cross-coupled hydrodynamic forces. A complete discussion of the state of the art in the prediction of ship motions is presented in the proceedings of the fifth symposium on naval hydrodynamics.<sup>28</sup> Current

research indicates that cross-coupled hydrodynamic forces are the same order of magnitude as other hydrodynamic forces and can not be neglected.

A large oceanographic buoy was built in 1965 by General Dynamics/Convair Division. As part of the design process,<sup>29</sup> model tests were conducted in a towing tank for various buoy hull shapes, and buoy motions were simulated on an analog computer. The analog computer simulation considered the dynamics of the planar motions of the buoy alone; the mooring line was treated as an elastic spring. The following quote is from reference 29:

The simulation was not fully successful; some results are considered inconclusive. Due to the difficulty in obtaining reasonable agreement with the model data, the analog computer study was terminated short of its goal.

The 40-ft-diameter "MONSTER" buoy described in reference 29 has proven to be a successful ocean data station. At sea motions of this buoy are described by Devereux<sup>30</sup> and Uyeda.<sup>31</sup> Gaul and Brown<sup>32</sup> correlated buoy heave acceleration power spectra from the "MONSTER" buoy and from a small wave sensing buoy.

Paquette<sup>33</sup> developed a two-dimensional, lumped-mass analog computer model for buoy system dynamics. The buoy was assumed to follow an elliptical orbit (major axis vertical and equal to the wave height), and its motions were not integrated as part of the system dynamics. The lumped-mass cable elements were acted upon by tensions on adjacent elements, weight and buoyancy forces, and velocity-squared drag forces. Cable hydrodynamic masses and linear

damping forces were neglected. Paquette concluded that at least ten mass elements are needed for a deep-sea mooring line to adequately describe the system dynamics in the band of ocean wave frequencies that were considered (0 to 0.5 Hz). The coupling of tensile waves into transverse waves due to the steady-state curvature of the cable was also noted.

Bivens and Swann<sup>34</sup> also developed a two-dimensional, lumped-mass simulation of buoy system dynamics but included the buoy dynamics. However, hydrodynamic cross-coupled terms were neglected. Rudnick<sup>35</sup> measured motions of the "FLIP" spar buoy at sea and compared motion power spectra with the power spectra predicted from a linear, decoupled buoy motion model. Blumberg and Osborn<sup>36</sup> developed a digital computer simulation for submerged buoy motions. The mooring line was considered to be a rigid, massless, and dragless link. Hydrodynamic forces acting on the buoy included no cross-coupled terms, and the equations of motion were linearized. Millard<sup>37</sup> describes tension measurements made at sea as part of the Woods Hole Oceanographic Institution buoy reliability program. Tension amplitudes were correlated with recorded currents and wind speeds. Millard's data indicate that the tension amplitudes are attenuated with length down the mooring cable. A very comprehensive study of buoy system dynamics has been conducted by Prof. Nath, of Oregon State University.<sup>38</sup> The two-dimensional motions of a buoy and its mooring cable were considered. Buoy motions were solved by use of recurrence formulas and served as boundary conditions for the cable. Cable dynamics were solved by using a numerical method of characteristics solution.

Hydrodynamic forces acting on the buoy and cable were included, and nonlinear stress-strain properties of the cable were used. Transfer functions between wave spectra and line tension spectra along the cable were developed and compared with MONSTER buoy data.

Hsu and Blenkarn<sup>39</sup> utilized momentum flux equations to compute the hydrodynamic forces acting on a moored ship. Equations of motion were solved numerically, and the mooring lines were considered as elastic springs. Each wave was assumed to impart an impulse; thus, the forcing function was composed of a series of impulses acting on the ship. Burke<sup>40</sup> assumed that a set of linear response functions for the vessel were known and developed sets of statistical relations for vessel motions in a random sea. This technique was applied to predict drilling vessel motions, and the results were compared with drilling vessel motions recorded at sea.

The present investigation has produced a three-dimensional, numerical model for buoy system dynamics. The model includes cross-coupled hydrodynamic forces and can be excited by wind, current, and wave forces. Cable dynamics are investigated with both finite-element (lumped masses) and finite-difference (distributed mass) methods. In this study, finite-element methods were found to be attractive because of their relative economy with regard to numerical computational time. Finite-difference methods, while more rigorous, are more involved numerically and require relatively large amounts of computer time.

The deterministic model is excited by a numerical wave model having the same spectral characteristics as the ocean waves. The computed buoy system



3 response is then sampled to provide motion spectra by using Fast Fourier Transform (FFT) techniques.

To validate the model, two oceanographic buoys were equipped with motion sensing instrumentation and installed in Block Island Sound. Buoy motions were monitored and recorded for various wind, current, and wave conditions. These data are compared with buoy motions computed with the numerical model for the same environmental conditions.

## II. PROCEDURE

In order to predict the response of the buoy system (figure 3) to the ocean environment, a deterministic model of the system dynamics must be constructed and excited by a random model of the oceanic conditions. The two major structural components of the system (the buoy and the mooring line) are treated separately and then are combined to form the deterministic buoy system model.

### 2.1 System Dynamics

Buoy motions can be described by the equations of motion for a body with six degrees of freedom floating on the free surface of a fluid.<sup>28</sup> The major problem encountered in the solution of the set of six, coupled, elliptical, differential equations of motion is the description of the hydrodynamic forces acting on the buoy. In their most rigorous form, the buoy equations of motion would be integro-differential equations since the dynamic pressures must be integrated over the immersed surface of the buoy. Analytical solution of these equations of motion for an arbitrary body in a random sea state has not been accomplished up to this time. If the hydrodynamic forces can be expressed as variable coefficients in the equations of motion, the equations can be written as a set of six, ordinary differential equations that can be solved by using the approximate methods of numerical techniques. The problem now is to define the variable hydrodynamic coefficients. If the fluid is assumed to be incompressible and

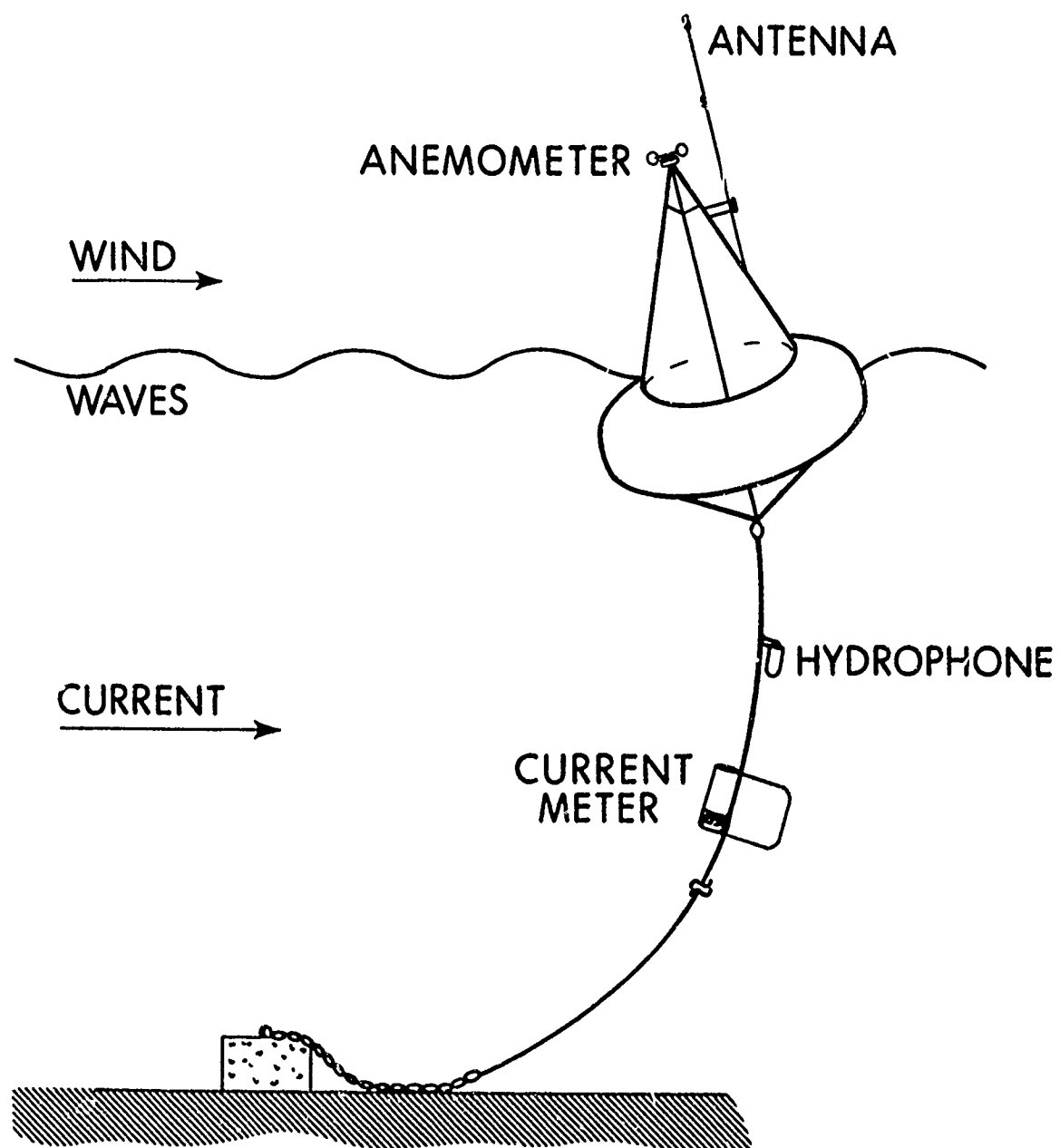


Figure 3. A Simple Buoy System

irrotational, the hydrodynamic properties of certain simple two- and three-dimensional bodies can be computed. Also, if the waves on the free surface of the fluid are deterministic and linear, the velocity potentials for various body motion modes can be superimposed to construct the case of a body floating on a free surface and responding to waves propagating on that free surface.

This study employs the technique described above. Equations of motion are written as a set of six, coupled, ordinary differential equations with variable coefficients; hydrodynamic coefficients are computed by assuming that the fluid is incompressible and irrotational and that velocity potentials can be superimposed; aerodynamic and hydrodynamic viscous forces are assumed to follow a velocity-squared law; and the body is assumed to be axisymmetric about a vertical axis (as are most oceanographic and navigational buoys), which simplifies the computation of the hydrodynamic coefficients.

Dynamics of cables are investigated and simulated. The most direct approach, i.e., solution of the cable equations of motion by a finite-difference method, is developed first. Since the cable equations are a set of nonlinear, hyperbolic, partial differential equations, analytical solutions are intractable, and a numerical method of solution is devised. Although more accurate, the finite-difference method can be very expensive with regard to digital computer time. A lumped-mass simulation of cable dynamics is also investigated and developed. Lumped-mass methods offer significant savings in computational time at the expense of truncation of the higher frequency cable dynamics.

The buoy equations of motion and the two sets of cable equations (finite-difference and lumped-mass) are then coupled and solved numerically on a

UNIVAC 1108 digital computer. A numerical model of ocean waves is used to excite the buoy system dynamics model. Steady-state buoy system configurations are solved as the zeroth-order case of buoy system dynamics.

## 2.2 Experimental Validation

In order to validate the computer model, two oceanographic buoys were equipped with motion sensing instrumentation and were monitored. The recorded buoy motion data have been reduced in statistical form and will be correlated with buoy motions predicted from the computer models. Also, buoy motion data reported in the literature have been used to validate the computer models.

### III. ANALYTICAL DEVELOPMENT AND DISCUSSION

#### 3.1. Buoy Dynamics

Consider an axisymmetric buoy having six degrees of freedom, floating on the free surface of a fluid, constrained by a mooring line, and exposed to wind, waves, and currents (figure 4). The buoy is being acted on by the following:

Inertial forces and moments

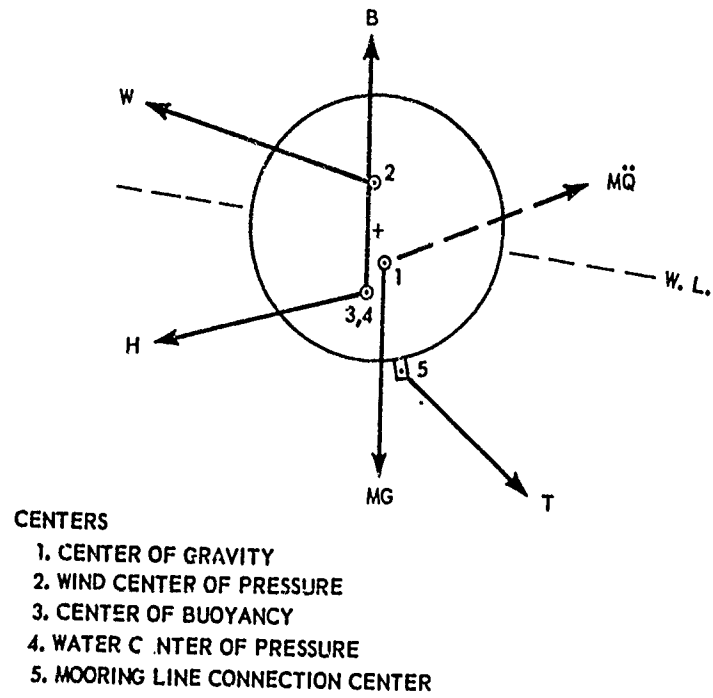
Hydrostatic forces and moments

Hydrodynamic forces and moments

Wind forces

Mooring line tensions.

The inertial forces can be separated into those due to gravity (weight) and those due to the motion of the buoy. Hydrostatic forces can be obtained by integration of the hydrostatic pressure acting on the submerged surface of the buoy. Likewise, hydrodynamic forces can be obtained by integration of the hydrodynamic pressures acting on the submerged surface of the buoy. Hydrodynamic forces are classified as inertial or dissipative. Energy is being dissipated through viscous effects, radiation of pressure waves, and radiation of surface waves generated by the motion of the buoy. Energy is introduced to the system through hydrostatic and hydrodynamic forces due to currents and surface waves.



A FREE BODY OF THE BUOY

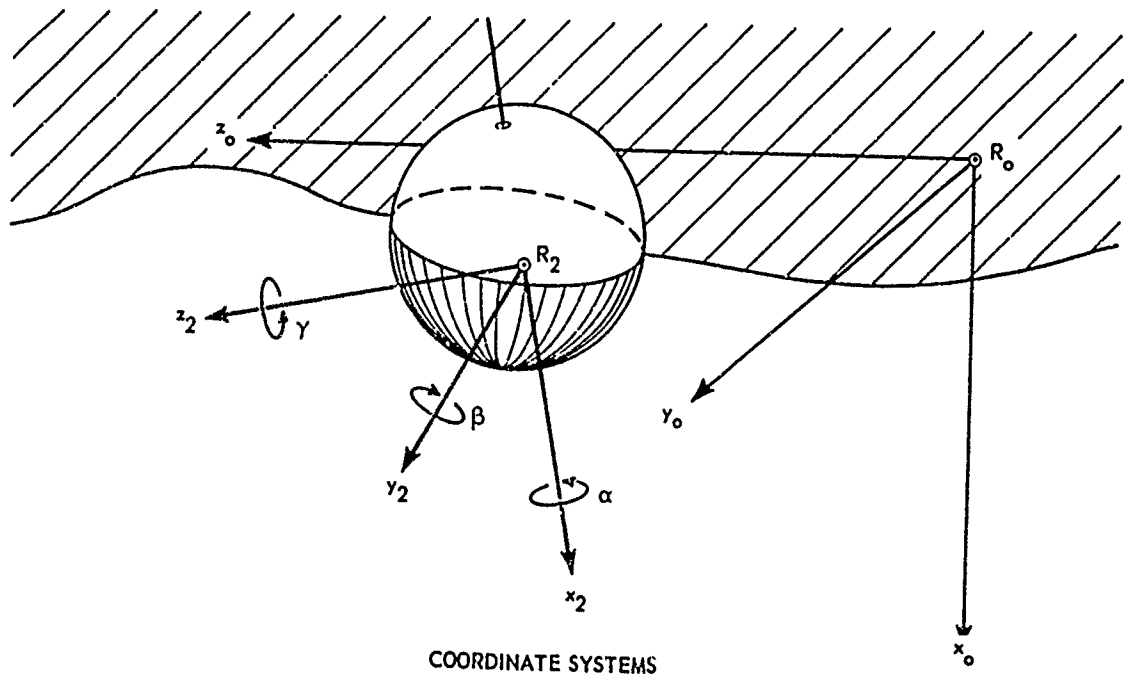


Figure 4. Buoy Coordinate Systems

Wind forces acting on the exposed surface of the buoy also introduce energy into the system. Mooring line tensions indicate a path of energy removal from the system. If the buoy were treated as a "black box" that transforms energy from one form to another, we can draw a schematic as shown in figure 5.

From figure 4, it is seen that four sets of coordinates must be considered. It is desired to solve for the coordinates of the center of gravity of the buoy in inertial coordinates,  $(x_{og}, y_{og}, z_{og})$ , but the hydrostatic and hydrodynamic forces and moments are due to fluid motions relative to the buoy. Any point in space has coordinates  $x_i, y_i, z_i$  relative to  $R_i$  ( $i = 0, 1, 2, 3$ ); therefore,

$$\begin{aligned}x_o &= x_{og} + x_i \\y_o &= y_{og} + y_i \\z_o &= z_{og} + z_i\end{aligned}$$

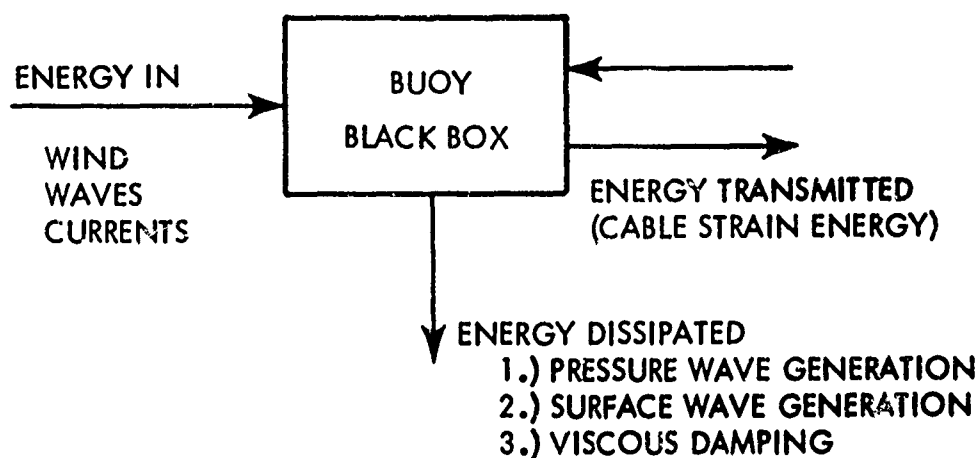
The only difference between  $R_1$  and  $R_2$  is a space rotation about the axes of the buoy. Thus, we have

$$\begin{bmatrix} X_2 \\ Y_2 \\ Z_2 \end{bmatrix} = \Omega \cdot \begin{bmatrix} X_1 \\ Y_1 \\ Z_1 \end{bmatrix}, \quad (1)$$

where  $\Omega$  is a 3-by-3 orthogonal rotation matrix,

$$\Omega = \begin{bmatrix} \cos \gamma \cos \beta & -\cos \gamma \sin \beta \sin \alpha & \cos \gamma \sin \beta \cos \alpha \\ & + \sin \gamma \cos \alpha & + \sin \gamma \sin \alpha \\ -\sin \gamma \cos \beta & \sin \gamma \sin \beta \sin \alpha & -\sin \gamma \sin \beta \cos \alpha \\ & + \cos \gamma \cos \alpha & + \cos \gamma \sin \alpha \\ -\sin \beta & -\cos \beta \sin \alpha & \cos \beta \cos \alpha \end{bmatrix}. \quad (2)$$





#### MATRIX EQUATIONS OF MOTION

$$M\ddot{Q} = MG - B - H + W - T$$

WHERE:

M - MASS MATRIX

$\ddot{Q}$  - ACCELERATION VECTOR

G - GRAVITY VECTOR

B - HYDROSTATIC FORCE & MOMENT VECTOR

H - HYDRODYNAMIC FORCE & MOMENT VECTOR

W - WIND FORCE VECTOR

T - CABLE TENSION VECTOR

Figure 5. Energy Flow in Buoy System

Since  $\Omega$  is orthogonal, we see that  $\Omega^{-1} = \Omega^T$ ; thus,

$$\Omega^{-1} = \begin{bmatrix} \cos \gamma \cos \beta & -\sin \gamma \cos \beta & -\sin \beta \\ -\cos \gamma \sin \beta \sin \alpha + \sin \gamma \cos \alpha & \sin \gamma \sin \beta \sin \alpha + \cos \gamma \cos \alpha & -\cos \beta \sin \alpha \\ \cos \gamma \sin \beta \cos \alpha + \sin \gamma \sin \alpha & -\sin \gamma \sin \beta \cos \alpha + \cos \gamma \sin \alpha & \cos \beta \cos \alpha \end{bmatrix}. \quad (3)$$

The spatial coordinates become

$$X_0 = X_{0g} + X_2 \cos \gamma \cos \beta - Y_2 \sin \gamma \cos \beta - Z_2 \sin \beta, \quad (4A)$$

$$Y_0 = Y_{0g} + X_2 (-\cos \gamma \sin \beta \sin \alpha + \sin \gamma \cos \alpha) + Y_2 (\sin \gamma \sin \beta \cos \alpha + \cos \gamma \sin \alpha) + Z_2 (-\cos \beta \sin \alpha), \quad (4B)$$

and

$$Z_0 = Z_{0g} + X_2 (\cos \gamma \sin \beta \cos \alpha + \sin \gamma \sin \alpha) + Y_2 (-\sin \gamma \sin \beta \cos \alpha + \cos \gamma \sin \alpha) + Z_2 (\cos \beta \cos \alpha). \quad (4C)$$

The center of the coordinate system, which is aligned with the waterplane area, is located directly above the center of gravity of the buoy. Motions of fluid particles due to waves are described relative to this coordinate system. The dynamical equations of motion will be written in buoy coordinates, but displacements will be transformed to the  $R_0$  coordinate system in order to solve for cable tensions.

Using the free body of the buoy (figure 4) and applying Newton's Second Law, we can develop the equations of motion for the buoy. In matrix form, the

equations of motion for the buoy are

$$M \ddot{Q} = M G - B - H - W - T, \quad (5)$$

where

$M$  is the structural mass matrix

$\ddot{Q}$  is the acceleration vector

$G$  is the gravitational acceleration vector

$B$  is the hydrostatic force vector

$H$  is the hydrodynamic force vector

$W$  is the wind force vector

$T$  is the mooring line tension vector.

Each of these forces will be considered in turn.

Using a coordinate system with the origin located at the center of gravity of the buoy and including moments and products of inertial, we can write the structural mass matrix as

$$M = \begin{bmatrix} m & 0 & 0 & 0 & 0 & 0 \\ 0 & m & 0 & 0 & 0 & 0 \\ 0 & 0 & m & 0 & 0 & 0 \\ 0 & 0 & 0 & I_{\alpha\alpha} & I_{\alpha\beta} & I_{\alpha\gamma} \\ 0 & 0 & 0 & I_{\beta\alpha} & I_{\beta\beta} & I_{\beta\gamma} \\ 0 & 0 & 0 & I_{\gamma\alpha} & I_{\gamma\beta} & I_{\gamma\gamma} \end{bmatrix}.$$

(6)

If the coordinate system is aligned with the principal axes of the buoy,  
the structural mass matrix is

$$M = \begin{bmatrix} m & 0 & 0 & 0 & 0 & 0 \\ 0 & m & 0 & 0 & 0 & 0 \\ 0 & 0 & m & 0 & 0 & 0 \\ 0 & 0 & 0 & I_{\alpha\alpha} & 0 & 0 \\ 0 & 0 & 0 & 0 & I_{\beta\beta} & 0 \\ 0 & 0 & 0 & 0 & 0 & I_{\gamma\gamma} \end{bmatrix} . \quad (7)$$

The acceleration vectors are

$$\ddot{Q} = \begin{bmatrix} \ddot{x} \\ \ddot{y} \\ \ddot{z} \\ \ddot{\alpha} \\ \ddot{\beta} \\ \ddot{\gamma} \end{bmatrix} \quad \text{and} \quad G = \begin{bmatrix} G \cos \gamma \cos \beta \\ -G \sin \gamma \cos \beta \\ -G \sin \beta \\ 0 \\ 0 \\ 0 \end{bmatrix} . \quad (8)$$

### 3.1.1 Wind Forces

The wind force vector is now considered. For an axisymmetric buoy about the  $x_2$  axis and assuming a velocity-squared viscous drag, the drag and lift forces acting on the body are given by

$$D = \frac{1}{2} \rho_n C_D A_1 W V^2 \quad (9)$$

and

$$L = \frac{1}{2} \rho C_L A_2 WV^2, \quad (10)$$

where

$D$  is the drag force

$L$  is the lift force

$\rho$  is the air density

$C_D$  is the drag coefficient (subcritical,  $\frac{WV \mu \rho}{\mu_R} < 5 \times 10^5$ )

$C_L$  is the lift coefficient (subcritical,  $\frac{WV \mu \rho}{\mu_R} < 5 \times 10^5$ )

$A_1$  is the vertical projected area

$A_2$  is the horizontal projected area

$WV$  is the wind velocity

$\mu_R$  is the absolute viscosity of the air

$\mu$  is the buoy width.

Because of the axial symmetry, the drag and lift coefficients of the buoy are the same in the  $y_2$  and  $z_2$  directions. Given wind velocity components  $WV_{y0}$  and  $WV_{z0}$  in the  $R_0$  coordinate system and assuming that the wind velocities are an order of magnitude greater than the displacement velocities of the buoy, we can transform to the  $R_2$  coordinate system and can compute the wind forces and moments. For forces acting on a point that lies on the axis of symmetry of the buoy, the transform from inertial coordinates to buoy coordinates is independent of  $\alpha$  rotations.

The wind components in the  $R_2$  coordinate system are

$$\begin{bmatrix} WV_{x2} \\ WV_{y2} \\ WV_{z2} \end{bmatrix} = \Omega \cdot \begin{bmatrix} 0 \\ WV_{y0} \\ WV_{z0} \end{bmatrix}, \quad (11)$$

Neglecting the small wind velocity component acting along the axis of symmetry, the magnitude of the wind velocity in the  $R_2$  coordinate system is

$$WV_{R2} = \sqrt{WV_{y2}^2 + WV_{z2}^2}, \quad (12)$$

and the wind forces become

$$W_{D2} = \frac{1}{2} \rho C_D A_1 WV_{R2} |WV_{R2}| \quad (13)$$

and

$$W_{L2} = \frac{1}{2} \rho C_L A_2 WV_{R2} |WV_{R2}|. \quad (14)$$

(Note that velocities squared is written as the product of the velocity and its absolute value in order to maintain the sign convention.) Resolving the wind drag force into  $y_2$  and  $z_2$  components, we find that

$$W_{y2} = \frac{WV_{y2}}{WV_{R2}} \cdot W_{D2} \quad (15)$$

and

$$W_{z_2} = \frac{WV_{z_2}}{WV_{R_2}} \cdot W_{D_2} \quad (16)$$

The wind moments are computed by using the wind forces and the moment arm:

$$W_{\alpha_2} = 0 \quad (17A)$$

$$W_{\beta_2} = -W_{z_2} \cdot H_w \quad (17B)$$

and

$$W_{\gamma_2} = -W_{y_2} \cdot H_w \quad (17C)$$

where  $H_w$  is the height from C. of G. to the wind force center of pressure.

In the  $R_2$  coordinate system, the wind forces and moments are

$$W_{R_2} = \begin{bmatrix} -W_{x_2} \\ W_{y_2} \\ W_{z_2} \\ 0 \\ W_{\beta_2} \\ W_{\gamma_2} \end{bmatrix} .$$

(18)

### 3.1.2 Mooring Line Forces

Mooring line tensions are acting on the buoy at the mooring line termination point. This point is taken to be below the center of gravity and along the axis of symmetry a distance  $H_{ML}$  from the center of gravity. If the space orientation of the cable is described by angles  $\theta$  and  $\phi$  relative to the  $R_0$  coordinate system (figure 4), we can develop a 3-by-3 orthogonal rotation matrix to transform from inertial to cable coordinates. The inverse of the matrix can be used to compute the tension components acting on the buoy. This rotation matrix,  $(A)$ , is developed in the next section on cable dynamics but is used here.

The tension components at the buoy end of the cable are

$$T_{B_0} = A^{-1} \begin{bmatrix} T \\ 0 \\ 0 \end{bmatrix} = \begin{bmatrix} T_{x_0} \\ T_{y_0} \\ T_{z_0} \end{bmatrix}. \quad (19)$$

In the  $R_2$  coordinate system, they become

$$T_{B_2} = \Omega \cdot T_{B_0} = \begin{bmatrix} T_{x_2} \\ T_{y_2} \\ T_{z_2} \end{bmatrix}. \quad (20)$$

The moments due to the mooring line tension are

$$T_{\alpha_2} = 0 \quad (21A)$$



$$T_{\beta_2} = T_{x_2} \cdot H_{ML} \quad (21B)$$

$$T_{\gamma_2} = T_{y_2} \cdot H_{ML} \quad (21C)$$

The forces and moments due to cable tensions are then

$$T = \begin{bmatrix} T_{x_2} \\ T_{y_2} \\ T_{z_2} \\ 0 \\ T_{\beta_2} \\ T_{\gamma_2} \end{bmatrix} \quad (22)$$

### 3.1.3 Hydrostatic Forces

The hydrostatic forces are considered next. If the displacements of an elemental volume of fluid just below the free surface and in the immediate vicinity of the buoy are given relative to the inertial coordinates ( $\eta$ ), and if the slope of the free surface above this particle is also given ( $\xi$ ), the buoyant forces and moments can be computed. The assumptions that the buoy diameter is small relative to the wavelength and that the presence of the buoy does not influence the shape of the free surface (Froude-Kriloff hypothesis) allow representation of the sea surface as a plane intersecting with the body volume.

Most oceanographic buoys have axial symmetry, and their shape can be approximated by an oblate spheroid. Consider an ellipsoid of revolution (figure 6) with a major diameter of  $2b$  and a minor diameter of  $2a$ . The equation of the surface is

$$\frac{x_b^2}{a^2} + \frac{y_b^2}{b^2} + \frac{z_b^2}{b^2} = 1. \quad (23)$$

Let a plane intersect the oblate spheroid at a height  $H_d$  from the geometric center at an angle  $\beta'$ . The intercepts of the plane are

$$\begin{aligned} x &= -H_d \\ y &= \infty \\ z &= -H_d / \tan \beta'. \end{aligned}$$

The equation of the plane becomes

$$\frac{x_b}{-H_d} + \frac{z_b}{-H_d / \tan \beta'} = 1 \quad (24)$$

or

$$x_b + z_b \tan \beta' + H_d = 0. \quad (24A)$$

The intersection of the body and the plane is therefore given by

$$\frac{x_b^2}{a^2} + \frac{y_b^2}{b^2} + \frac{z_b^2}{b^2} - 1 = x_b + z_b \tan \beta' + H_d \quad (25)$$

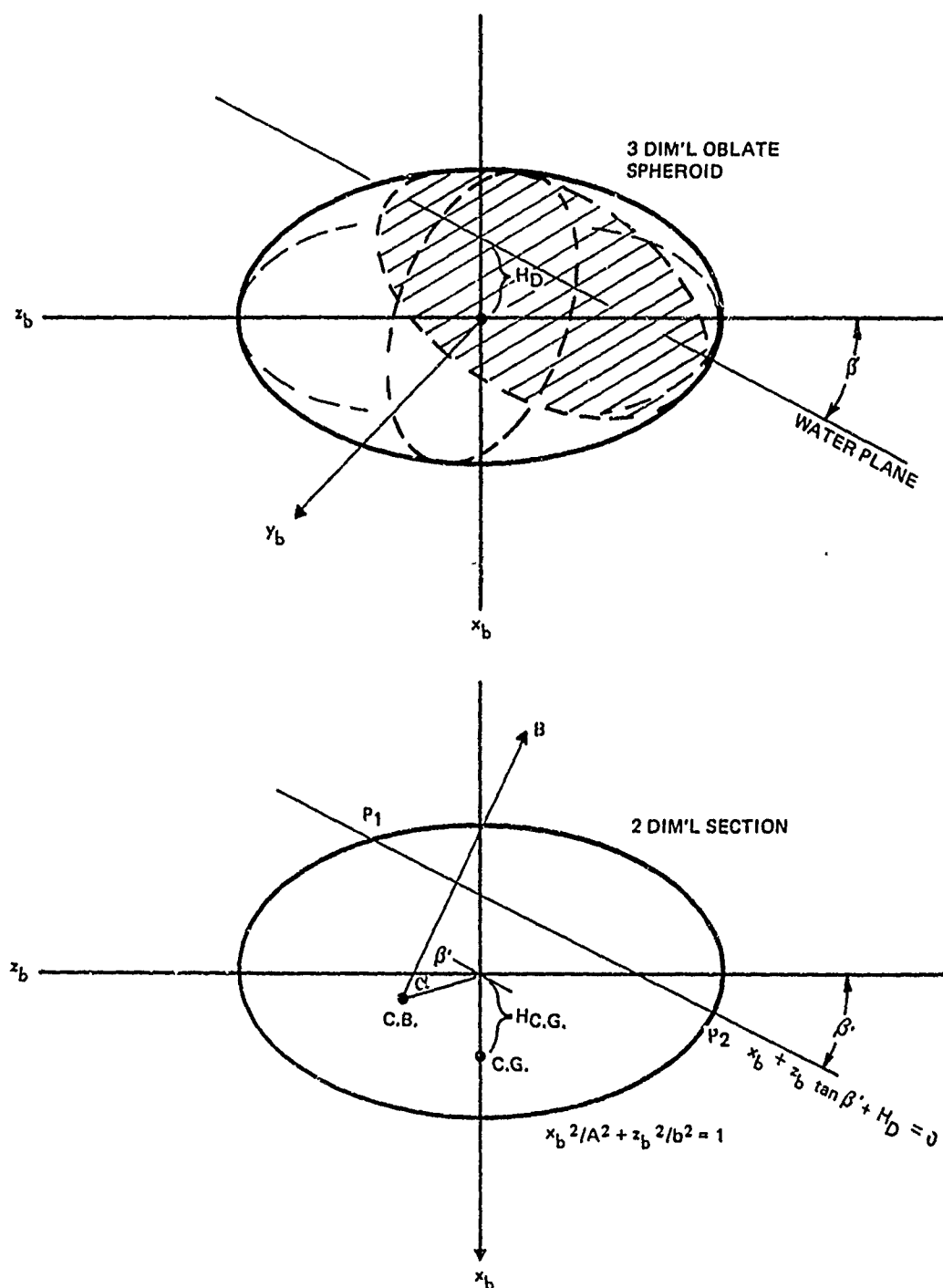


Figure 6. Immersed Volume of an Oblate Spheroid

or

$$\frac{X_b^2}{A^2} + \frac{Y_b^2}{b^2} + \frac{z_b^2}{b^2} - X_b - z_b \tan \beta' - H_b - 1 = 0, \quad (25A)$$

which is an ellipse. In order to compute the volume of the "cut" oblate spheroid, the area of any section parallel to the cutting plane must be defined. In the  $x_b - z_b$  plane, we find that on the ellipse

$$X_b^2 = A^2 - \frac{A^2}{b^2} z_b^2 \quad (26)$$

and on the line

$$X_b^2 = z_b^2 \tan^2 \beta' + 2 H_b z_b \tan \beta' + H_b^2. \quad (27)$$

Equating (26) and (27), we can compute the  $z$  coordinates of intersecting points  $P_1$  and  $P_2$  by

$$\left( \tan^2 \beta' + \frac{A^2}{b^2} \right) z_b^2 + 2 z_b H_b \tan \beta' + (H_b^2 - A^2) = 0. \quad (28)$$

Solving for  $z_b$ , we find

$$z_b = \frac{-H_b \tan \beta' \pm A/b \sqrt{b^2 \tan^2 \beta' + A^2 - H_b^2}}{(\tan^2 \beta' + A^2/b^2)} \quad (29)$$

For  $P_1$ , the coordinates are

$$z_{b1} = \frac{-H_b \tan \beta' + A/b \sqrt{b^2 \tan^2 \beta' + A^2 - H_b^2}}{(\tan^2 \beta' + A^2/b^2)} \quad (30)$$

and

$$X_{b_1} = -Z_{b_1} \tan \beta' - H_D ; \quad (31)$$

for  $P_2$ , the coordinates are

$$Z_{b_2} = \frac{-H_D \tan \beta' - H_D/b \sqrt{b^2 \tan^2 \beta' + H^2 - H_D^2}}{(\tan^2 \beta' + H^2/b^2)} \quad (32)$$

and

$$X_{b_2} = -Z_{b_2} \tan \beta' - H_D ; \quad (33)$$

thus,

$$Z_{b_1} - Z_{b_2} = \frac{2 H_D/b \sqrt{b^2 \tan^2 \beta' + H^2 - H_D^2}}{(\tan^2 \beta' + H^2/b^2)} \quad (34)$$

The  $b'$  axis of the intersecting ellipse is

$$b' = \frac{1}{2} \frac{(Z_{b_1} - Z_{b_2})}{\cos \beta'} .$$

From equation (34), we substitute and find

$$b' = \frac{H_D/b \sqrt{b^2 \tan^2 \beta' + H^2 - H_D^2}}{\cos \beta' (\tan^2 \beta' + H^2/b^2)} \quad (35)$$

The  $z$  coordinate of the center of the elliptical section is

$$Z_c = Z_{b_1} - b' \cos \beta' = \frac{-H_D \tan \beta'}{(\tan^2 \beta' + H^2/b^2)} \quad (36)$$

The x coordinate of the center of the elliptical section is

$$x_c = \frac{H_b \tan^2 \beta'}{(\tan^2 \beta' + H_b^2/b^2)} - H_b \quad (37)$$

The dimension of the  $a'$  axis of the intersecting ellipse is one-half the y dimension at the center. The y dimension at the center is

$$y_b = \pm \sqrt{b^2 - \frac{H_b^2 \tan^2 \beta'}{(\tan^2 \beta' + H_b^2/b^2)} - \frac{b^2}{H_b^2} \left( \frac{H_b \tan^2 \beta'}{(\tan^2 \beta' + H_b^2/b^2)} - H_b \right)^2} \quad (38)$$

and the axis length is

$$H' = \sqrt{b^2 - \frac{H_b^2}{(\tan^2 \beta' + H_b^2/b^2)}} \quad (39)$$

The area of the intersecting ellipse is

$$A = \pi H' b' = \pi \sqrt{b^2 - \frac{H_b^2}{(\tan^2 \beta' + H_b^2/b^2)}} \cdot \frac{H_b \sqrt{b^2 \tan^2 \beta' + H_b^2 - H_b^2}}{\cos \beta' (\tan^2 \beta' + H_b^2/b^2)}$$

or

$$A = \frac{\pi H_b}{\cos \beta'} \left( \frac{1}{(\tan^2 \beta' + H_b^2/b^2)^{1/2}} - \frac{H_b^2}{b^2 (\tan^2 \beta' + H_b^2/b^2)^{3/2}} \right) \quad (40)$$

The volume of the "cut" oblate spheroid is given by

$$V = \int_{-H_{b0}}^{H_b'} A dH' \quad (41)$$

The lower limit of the integral can be found by setting the area of the cutting plane equal to zero ( $A = 0$ ). The deepest draft is

$$H_{L0} = \sqrt{b^2 \tan^2 \beta' + A^2} ; \quad (42)$$

thus, with this lower limit, the volume is

$$V = \int_{-\cos \beta' \sqrt{b^2 \tan^2 \beta' + A^2}}^{H_0 \cos \beta'} \frac{\pi A b}{\cos \beta'} \left( \frac{1}{(\tan^2 \beta' + A^2/b^2)^{1/2}} - \frac{H'^2 / \cos^2 \beta'}{b^2 (\tan^2 \beta' + A^2/b^2)^{3/2}} \right) dH' ,$$

or, when integrating, it becomes

$$V = \pi A b^2 \left[ \frac{2}{3} + \frac{H_0}{(b^2 \tan^2 \beta' + A^2)^{1/2}} - \frac{H_0^3}{3(b^2 \tan^2 \beta' + A^2)^{3/2}} \right] . \quad (43)$$

The location of the centroid is given by

$$H'_{CB} = \frac{\int H' dV}{V} .$$

Expanding, we find

$$H'_{CB} = \frac{1}{V} \int_{-\cos \beta' \sqrt{b^2 \tan^2 \beta' + A^2}}^{H_0 \cos \beta'} \frac{\pi A b}{\cos \beta'} \left( \frac{1}{(\tan^2 \beta' + A^2/b^2)^{1/2}} - \frac{H'^2 / \cos^2 \beta'}{b^2 (\tan^2 \beta' + A^2/b^2)^{3/2}} \right) H' dH' .$$

Thus, carrying out the integration, we see that the centroid location becomes

$$H'_{CB} = \frac{\frac{\cos \beta'}{2} \left[ H_0^2 - \frac{(b^2 \tan^2 \beta' + A^2)}{2} - \frac{H_0^4}{2(b^2 \tan^2 \beta' + A^2)} \right]}{\left[ \frac{2}{3} \sqrt{b^2 \tan^2 \beta' + A^2} + H_0 - \frac{H_0^3}{3(b^2 \tan^2 \beta' + A^2)} \right]} . \quad (44)$$

The H dimension of the centroidal plane is

$$H_{CB} = \frac{\frac{1}{2} \left[ \frac{H_D^4}{2(b^2 \tan^2 \beta' + \kappa^2)} - H_D^2 + \frac{(b^2 \tan^2 \beta' + \kappa^2)}{2} \right]}{\left[ \frac{2}{3} \sqrt{b^2 \tan^2 \beta' + \kappa^2} + H_D - \frac{H_D^3}{3(b^2 \tan^2 \beta' + \kappa^2)} \right]} \quad (45)$$

The x coordinate of the centroid is

$$X_{CB} = \left( \frac{\tan^2 \beta'}{(\tan^2 \beta' + \kappa^2/b^2)} - 1 \right) \cdot H_{CB} \quad (46)$$

The z coordinate of the centroid is

$$Z_{CB} = \left( \frac{-\tan \beta'}{(\tan^2 \beta' + \kappa^2/b^2)} \right) \cdot H_{CB} \quad (47)$$

The moment arm for the buoyant force is

$$d = d_1 + d_2,$$

where the distances  $d_1$  and  $d_2$  are given by

$$d_1 = \sqrt{X_{CB}^2 + Z_{CB}^2} \cdot \cos(\alpha' + \beta'),$$

or

$$d_1 = Z_{CB} \cos \beta' + X_{CB} \sin \beta',$$

and

$$d_2 = H_{CG} \sin \beta'.$$

The angle  $\alpha'$  is defined as

$$\alpha' = \tan^{-1} \frac{X_{CB}}{Z_{CB}}.$$



The moment arm is

$$d = z_{CB} \cos \beta' + (H_{CG} - x_{CB}) \sin \beta'. \quad (48)$$

For the special case of a sphere of radius  $A$ , the immersed volume is

$$V = \pi A^3 \left[ \frac{2}{3} + \frac{H_D}{A} \cos \beta' - \frac{H_D^3}{3A^3} \cos^3 \beta' \right]. \quad (49)$$

The height of the plane intersecting the center of buoyancy is

$$H_{CB} = \frac{3 \left[ \frac{H_D^4}{A^2} \cos^2 \beta' - 2 H_D^2 + A^2 \sec^2 \beta' \right]}{4 \left[ 2 A \sec \beta' + 3 H_D - \frac{H_D^3}{A^2} \cos^2 \beta' \right]}. \quad (50)$$

The coordinates of the center of buoyancy are

$$x_{CB} = -\cos^2 \beta' \cdot H_{CB} \quad (51)$$

and

$$z_{CB} = -\sin \beta' \cos \beta' \cdot H_{CB}. \quad (52)$$

The buoyancy moment arm is then

$$d = z_{CB} \cos \beta' + (H_{CG} - x_{CB}) \sin \beta'. \quad (53)$$

If the buoy is pitched and rolled with angles  $\beta$  and  $\gamma$  and the sea surface slope at the buoy is  $\beta_w$  and  $\gamma_w$ , the slope of the sea surface relative to buoy coordinates is  $\beta_s = \beta - \beta_w$  and  $\gamma_s = \gamma - \gamma_w$ . The angle between the sea surface plane and the buoy vertical axis is

$$\beta' = \cos^{-1}(\cos \gamma_s \cos \beta_s).$$

With the buoy tilt angle defined, along with the location of the buoy center of gravity relative to the sea surface, the buoyant force and moment can be computed for an oblate spheroid. The buoyant force  $B$  acts normal to the plane of the sea surface through the center of buoyancy. In buoy coordinates, the buoyant force vector is

$$B_{R_2} = \begin{bmatrix} -B \cos \gamma_s \cos \beta_s \\ -B \sin \gamma_s \\ -B \cos \gamma_s \sin \beta_s \end{bmatrix}. \quad (54)$$

The  $\beta$  buoyant moment becomes

$$M_\beta = (B \cos \gamma_s \cos \beta_s)(z_{CB} \cos \alpha) - (H_{CG} - x_{CB})(B \cos \gamma_s \sin \beta_s), \quad (55)$$

and the  $\gamma$  buoyant moment becomes

$$M_\gamma = (B \cos \gamma_s \cos \beta_s)(z_{CB} \sin \alpha) - (H_{CG} - x_{CB})(B \sin \gamma_s), \quad (56)$$

The same transformations as used above can be applied to any axisymmetric buoy if the buoyancy can be defined as a function of the draft and tilt angle of

the buoy. The angular stability of axisymmetric buoy hulls, as defined by the locations of the centers of buoyancy and gravity, is discussed in appendix A.

#### 3.1.4 Hydrodynamic Forces

The hydrodynamic forces acting on the buoy that are due to the waves incident on the buoy and the motion of the buoy in the fluid must be included in the equations of motion. Ideally, the computation of these forces should be made for a buoy moving in a viscous fluid exposed to a random sea state. However, the solution to this general problem is not tractable and the forces acting on a buoy moving sinusoidally in an ideal fluid is considered in this study. These forces are considered as being composed of two components -- inertial and dissipative. Energy is dissipated from the buoy, which is moving in an ideal fluid, by the generation of surface waves that radiate cylindrically to infinity. Dissipative forces due to viscosity will be included in the equations of motion as separate force components.

The separation of dissipative forces into those due to surface wave generation and those due to viscous drag is supported by Havelock,<sup>41</sup> who concluded through dimensional analysis of the decay of oscillations of a prism on a free surface that the viscous damping is an order of magnitude less than the damping due to surface wave generation. Ogilvie<sup>28</sup> cites other model experiments which support Havelock's conclusions. Ogilvie also lists generalized equations of motion for ships in a seaway in which the viscous damping is either neglected or included as a separate force term, which is the current practice among naval architects.

The analysis of the motion of floating bodies conducted by John<sup>22, 23</sup> illustrates the computation of the hydrodynamic forces. Consider a mechanical system consisting of a liquid and a partly immersed body  $B$ . The liquid is assumed to be incompressible and to have irrotational motion. The free surface extends to infinity in all directions (figure 7). The body  $B$  is assumed to be rigid and to describe a forced motion under the influence of external forces. The state of the liquid is described by the velocity potential  $\phi(x, y, z; t)$ , which satisfies Laplace's equation. The boundary condition that the normal velocity of the particles along with the pressure is continuous across the surface must be satisfied. In addition, the pressure on the free surface is assumed constant and equal to the atmospheric pressure. Under these conditions, energy is gained or lost by the system only through waves arriving or departing at infinity or through the external forces.

The difficulties arising from the fact that the velocity potential,  $\phi$ , is a solution of the potential equation determined by nonlinear boundary conditions on a variable boundary force linearization of the problem in order to make it tractable. Restricting the analysis to infinitesimal motions, note that the boundary conditions become linear conditions for the potential function  $\phi$  on fixed surfaces corresponding to the rest or equilibrium position. The average free surface lies in a horizontal plane, and the average immersed surface  $S^0$  for the body  $B$  is for a position of equilibrium for  $B$ . On the average free surface,  $y = 0$ , the wave equation is

$$\phi_{tt} + g\phi_y = 0. \quad (57)$$

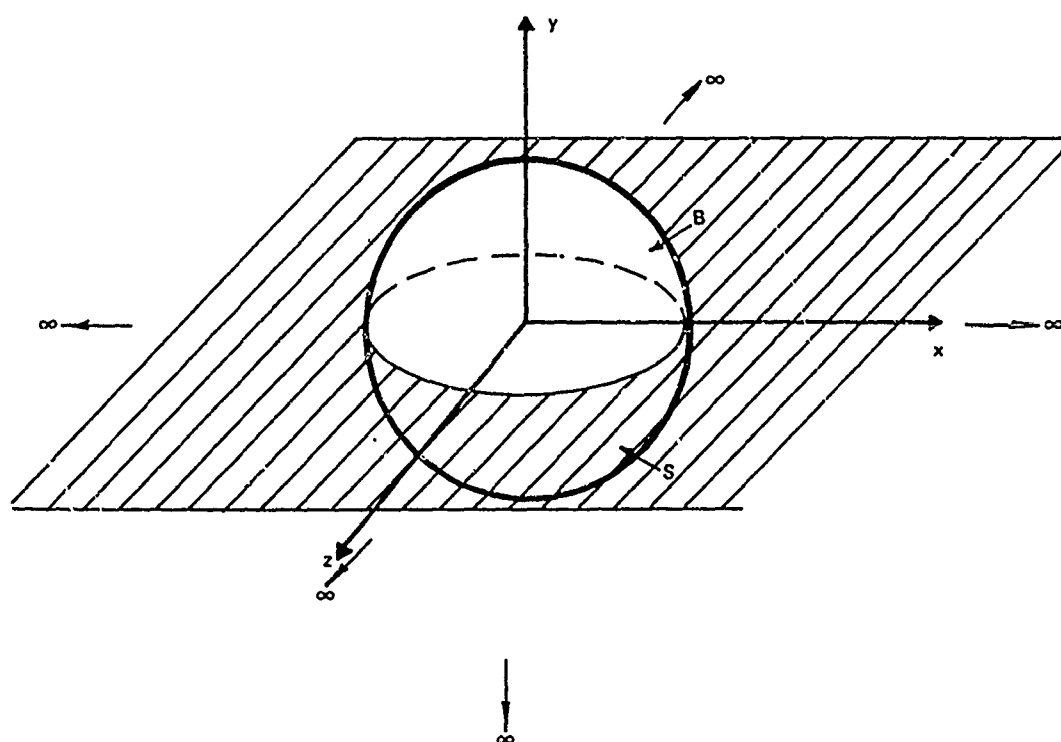


Figure 7. An Object on a Free Surface

On the average immersed surface, we find

$$\frac{\partial \phi}{\partial n} = X_t p_1 + Y_t p_2 + Z_t p_3 + \theta'_t q_1 + \theta''_t q_2 + \theta'''_t q_3, \quad (58)$$

where

$X, Y, Z$  are the coordinates of the center of gravity of  $B$

$\theta', \theta'', \theta'''$  are the angular displacements of  $B$

$n$  is the unit normal of  $S^\circ$

$p_k$  are the components of  $n$

$q_k$  are the components of the moment of  $n$  about the center of gravity.

Six differential equations of motion for  $B$  must also be written. For small perturbations, they are linear, second-order differential equations in  $x, y, z, \theta', \theta'', \theta'''$  with constant coefficients and integrals of  $\phi$  in the inhomogeneous part. They are of the form

$$\frac{M}{\rho} Y_{tt} = - \iint_{S^\circ} \phi_t p_2 dS - g \left[ I^A (Y - Y_0) + I_x^A \theta''' - I_z^A \theta' \right], \quad (59)$$

where

$M$  is the mass of  $B$

$\rho$  is the fluid density

$I^A$  is the area of  $A$ , the intersection of the body and free surface

$I_x^A, I_z^A$  are the moments of  $A$  about vertical planes

$g$  is the acceleration of gravity.

The integral expresses the hydrodynamic forces, whereas the right-hand term represents the hydrostatic forces.

For a buoy undergoing simple harmonic oscillations,  $\phi$  can be defined as

$$\phi(\bar{x}, \bar{y}, \bar{z}; t) = \text{Re} \left[ V(\bar{x}, \bar{y}, \bar{z}) e^{-i\sigma t} \right], \quad (60)$$

where

$\sigma$  is the angular frequency of the oscillation.

For an incompressible fluid,  $V$  is a solution to

$$\nabla^2 V(\bar{x}, \bar{y}, \bar{z}) = 0 \quad \text{in } \bar{y} < 0,$$

where  $V$  is complex valued. For small oscillations of the buoy, the amplitude of induced wave motion will be small compared with the wavelength. Thus, the linearized dynamic condition for  $\phi$  on the free surface is

$$g\bar{\eta}(\bar{x}, \bar{z}; t) + \phi_t(\bar{x}, 0, \bar{z}; t) = 0, \quad (61)$$

where

$\bar{\eta}$  is the free surface elevation.

Equation (61) with the linearized kinematic condition,

$$\phi_{\bar{y}}(\bar{x}, 0, \bar{z}; t) = \bar{\eta}_t(\bar{x}, \bar{z}; t), \quad \text{yields}$$

$$\frac{\partial}{\partial \bar{y}} V(\bar{x}, 0, \bar{z}) - k V(\bar{x}, 0, \bar{z}) = 0 \quad \text{on } \bar{y} = 0, \quad (62)$$

where

$k$  is the wave number,  $k = \sigma^2/g = 2\pi/\bar{\lambda}$ ,

$\bar{\lambda}$  is the free wavelength.

The normal velocity across the immersed surface of the buoy is continuous;

thus, we find

$$\frac{\partial}{\partial n} \phi(\bar{x}, \bar{y}, \bar{z}; t) = (\dot{\bar{Q}} + \dot{\theta} \times \bar{r}) \cdot n, \quad (63)$$

which is equation (58) restated in vector form where

$\bar{Q}$  is the position vector of the body  $C$ , of  $G$ ;  $\bar{Q} = Xp_1 + Yp_2 + Zp_3$ ,

$\theta$  is the rotation vector of body  $B$ ;  $\theta = \theta'q_1 + \theta''q_2 + \theta'''q_3$ ,

$\bar{r}$  is the position vector of some point on the immersed surface of the body.

The kinematic condition is to be satisfied on the immersed surface in the undisturbed position, i.e.,

$$\frac{\partial}{\partial n} V(\bar{x}, \bar{y}, \bar{z}) = \sum_{j=1}^6 \frac{\partial}{\partial n} V_j(\bar{x}, \bar{y}, \bar{z}) = -i\sigma [\bar{Q} \cdot n + \theta \cdot (\bar{r} \times n)] \quad (64)$$

Applying a Sommerfeld radiation condition at infinity, we find that a disturbance in the finite region should only produce an outgoing wave at a large distance:

$$V(\bar{d}, \psi, \bar{r}) - A(\psi) \bar{d}^{-\frac{1}{2}} e^{k\bar{y} + ik\bar{d}} \rightarrow 0 \text{ as } \bar{d} \rightarrow \infty, \quad (65)$$

where

$$\bar{d} = (\bar{x}^2 + \bar{z}^2)^{\frac{1}{2}}$$

$$\psi = \tan^{-1}(\bar{z}/\bar{x}).$$



To put the equations in dimensionless form, let

$$\Omega = \bar{\Omega} k \quad \text{the frequency}$$

$$x = \bar{x}/k$$

$$y = \bar{y}/k$$

$$z = \bar{z}/k$$

space variables

$$Q = \bar{Q}/k$$

the space parameters,

where  $k$  is a typical buoy dimension. Introduce the pressure function  $u_j$

by

$$i\sigma V_j(\bar{x}, \bar{y}, \bar{z}) / g \bar{\Omega} Q_j^0 = k u_j(x, y, z) \quad j=1, 2, 3 \quad (66A)$$

and

$$i\sigma V_j(\bar{x}, \bar{y}, \bar{z}) / g \bar{\Omega} \Theta_j^0 = k u_j(x, y, z) \quad j=4, 5, 6 \quad (66B)$$

The boundary value problem is to find a potential  $u_j(x, y, z)$ ,  $j=1, 2, \dots, 6$  that is continuous in the fluid space in such a manner that

$$\nabla^2 u_j(x, y, z) = 0 \quad \text{in } y < 0,$$

$$\frac{\partial}{\partial y} u_j(x, 0, z) - k u_j(x, 0, z) = 0 \quad \text{outside } S^0,$$

$$\frac{\partial}{\partial n} u_j(x, y, z) = h_j(x, y, z) \quad \text{on } S^0,$$

$$u_j(d, y, z) - A_j(y) d^{-\frac{1}{2}} e^{ny+ind} \rightarrow 0 \quad \text{as } d \rightarrow \infty,$$

where  $h_j$  represents the prescribed function that depends on the mode of oscillation. The  $h_j$  are given as

$$h_1(x, y, z) = n_x$$

$$h_2(x, y, z) = n_y$$

$$h_3(x, y, z) = n_z$$

$$h_4(x, y, z) = y n_z - z n_y$$

$$h_5(x, y, z) = z n_x - x n_z$$

$$h_6(x, y, z) = x n_y - y n_x.$$

The source potentials  $G$  of unit strength in the lower half-space which satisfy the sets of boundary conditions are

$$G(x, y, z; \xi, \eta, \zeta) = R^{-1} + R'^{-1} - \pi h e^{h(y+\eta)} [S_0(h\bar{\omega}) + Y_0(h\bar{\omega}) - i2J_0(h\bar{\omega})] - 2h e^{h(y+\eta)} \int_{y+\eta}^0 e^{-h\mu} (\mu^2 + \bar{\omega}^2)^{-\frac{1}{2}} d\mu, \quad (67)$$

where

$$\bar{\omega} = [(x-\xi)^2 + (y-\eta)^2]^{\frac{1}{2}}, \quad \bar{\omega}' = [(x-\xi)^2 + (y+\eta)^2]^{\frac{1}{2}}, \\ R = [\bar{\omega}^2 + (z-\zeta)^2]^{\frac{1}{2}}, \quad R' = [\bar{\omega}'^2 + (z-\zeta)^2]^{\frac{1}{2}}.$$

$S_0(h\bar{\omega})$  is the Struve function of order 0

$J_0(h\bar{\omega}), Y_0(h\bar{\omega})$  is the Bessel functions of first and second kind of order 0.

The solution to the boundary value problem is now in the form

$$u_j(x, y, z) = \frac{1}{4\pi} \iint_S f_j(\xi, \eta, \zeta) G(x, y, z; \xi, \eta, \zeta) dS, \quad (68)$$

where  $f$  is the strength of the distributed sources over the immersed surface and is a continuous complex function. If the forces and moments are written as components in phase with the acceleration and velocity, we find that

$$F_d = -\rho \bar{h}^3 M \ddot{\bar{Q}}_j - \rho \sigma \bar{h}^3 N \dot{\bar{Q}}_j \quad j=1, 2, 3. \quad (69)$$

For simple harmonic motions, the body vectors become

$$Q_j(t) = \text{Re} [\bar{Q}_j^o(t) e^{-i\sigma t}] \quad j=1,2,3$$

and

$$\Theta_j(t) = \text{Re} [\bar{\Theta}_j^o(t) e^{-i\sigma t}] \quad j=4,5,6 \quad (70)$$

The moments are

$$G_d = -\rho \bar{H}^4 I \ddot{\Theta}_j - \rho \sigma \bar{H}^4 H \dot{\Theta}_j \quad j=4,5,6.$$

Then,  $\bar{M}$  and  $\bar{N}$  are the hydrodynamic mass and the linear damping coefficients, and  $\bar{I}$  and  $\bar{H}$  are the hydrodynamic mass moment of inertia and rotational damping coefficients. The dimensionless coefficients are

$$\bar{M} = \frac{\bar{M}}{\rho \bar{H}^3} = \text{Re} \left[ \iint_S u_j(x,y,z) n \, dS \right] \quad j=1,2,3, \quad (71)$$

$$\bar{N} = \frac{\bar{N}}{\rho \sigma \bar{H}^3} = \text{Im} \left[ \iint_S u_j(x,y,z) n \, dS \right] \quad j=1,2,3, \quad (72)$$

$$\bar{I} = \frac{\bar{I}}{\rho \bar{H}^4} = \text{Re} \left[ \iint_S u_j(x,y,z) \cdot (r \times n) \, dS \right] \quad j=4,5,6, \quad (73)$$

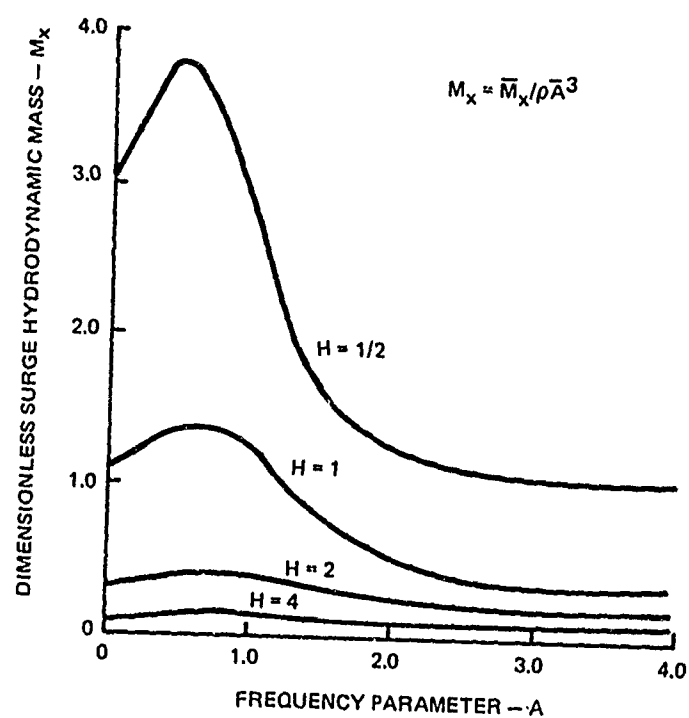
and

$$\bar{H} = \frac{\bar{H}}{\rho \sigma \bar{H}^4} = \text{Im} \left[ \iint_S u_j(x,y,z) \cdot (r \times n) \, dS \right] \quad j=4,5,6. \quad (74)$$

Kim<sup>42</sup> has evaluated these integrals numerically for spheroids of various aspect ratios and has plotted the dimensionless hydrodynamic coefficients versus the frequency parameter. Barakat<sup>43</sup> evaluated the Fredholm integrals with an approximate analytical solution for the case of a sphere on the free surface.

Kim's data are shown in figures 8, 9, and 10. A curve-fitting program

(CURFIT) built into the Government Services Administration remote terminal



SPHEROID  
 $H = \frac{\text{HALF-BEAM}}{\text{DRAFT}}$

$$A = \bar{A} \sigma^2 / g$$

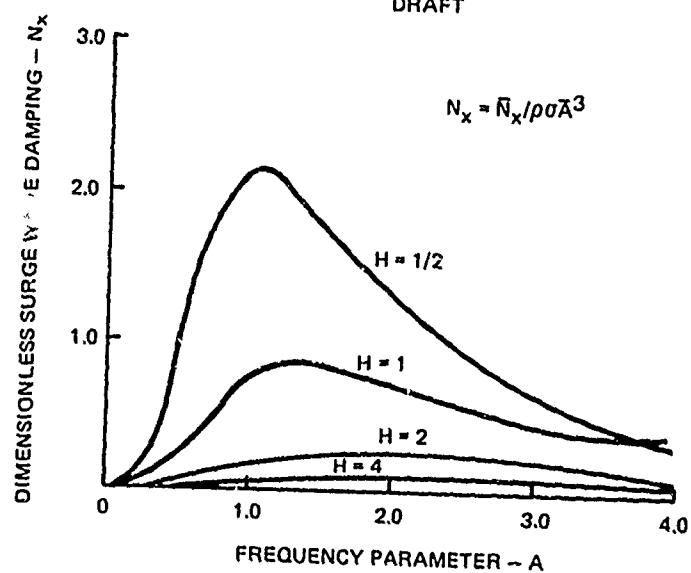


Figure 8. Hydrodynamic Mass and Wave Damping for Swaying or Surging Oblate Spheroids  
 (From Kim, reference 42.)

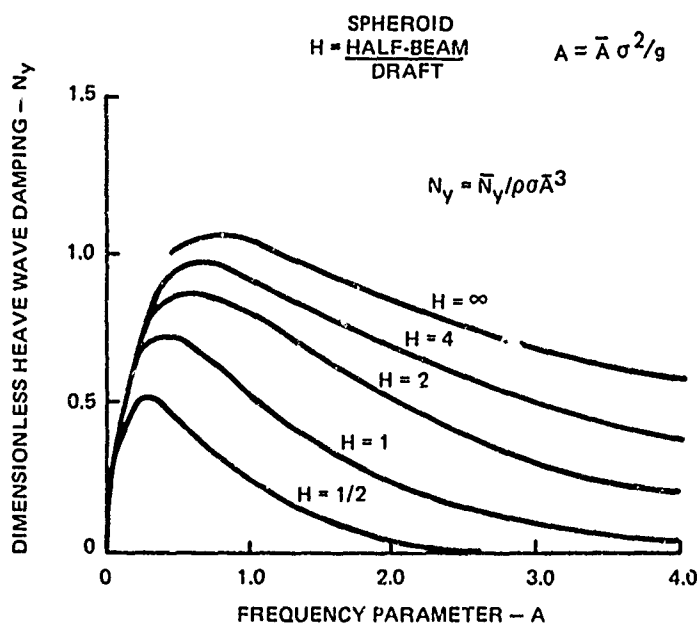
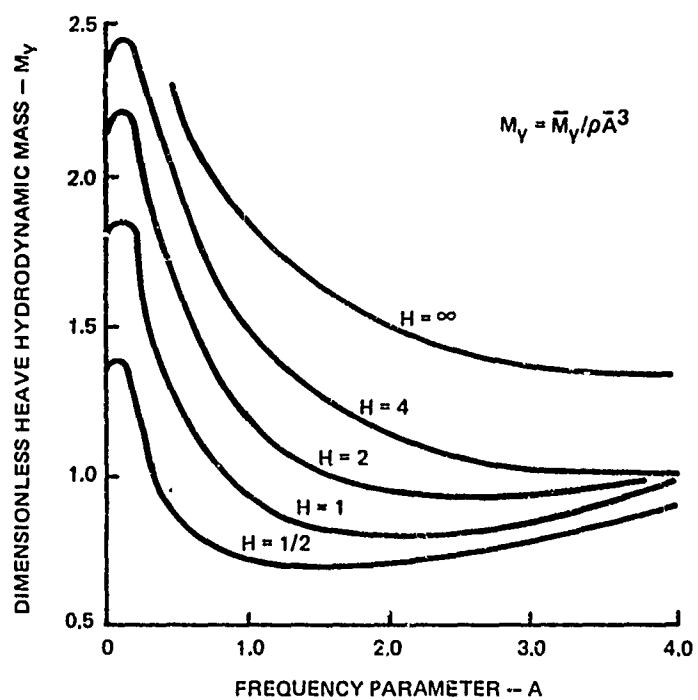


Figure 9. Hydrodynamic Mass and Wave Damping for Heaving Oblate Spheroids  
 (From Kim, reference 42.)

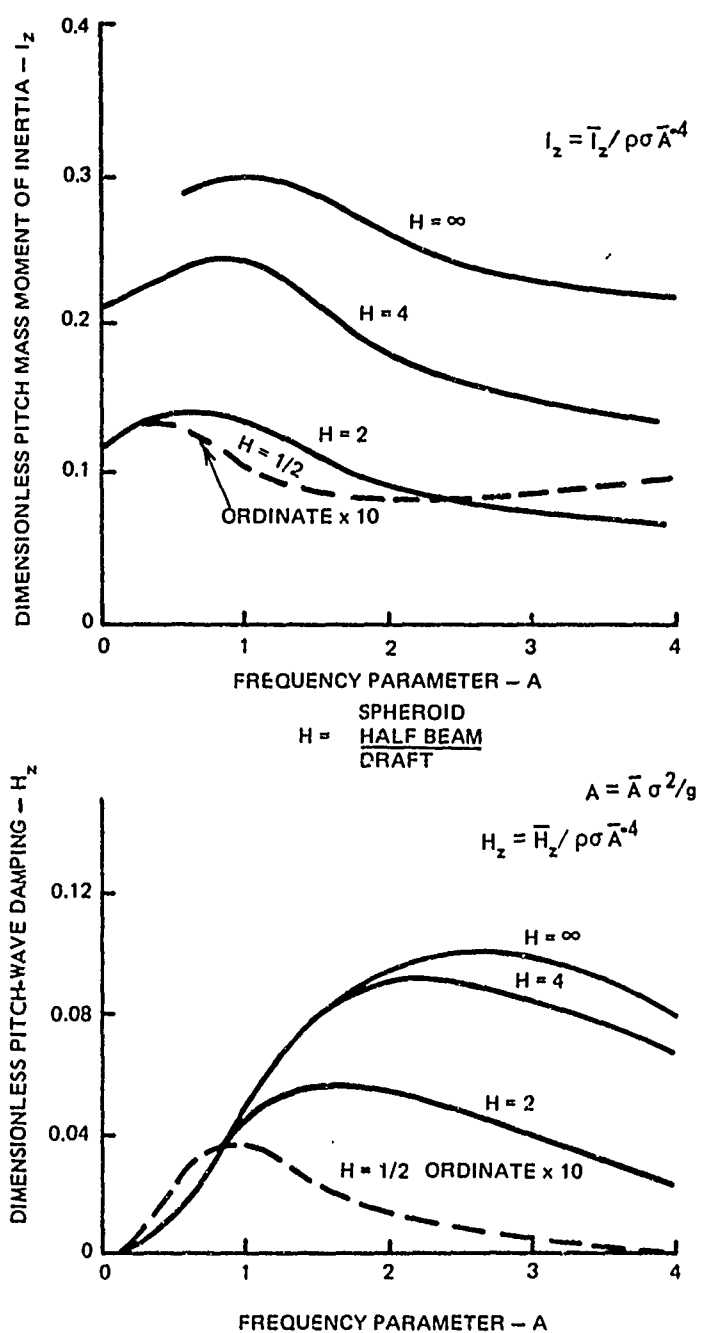


Figure 10. Hydrodynamic Mass Moment of Inertia  
For Pitching or Rolling Oblate Spheroids

(From Kim, reference 42.)

computer system was used to develop approximate equations for Kim's data for a sphere. Program CURFIT fits six curves to the data by a least-squares fit of the candidate curve's linear transform. The six curves are of the following types:

$$Y = A + B \cdot X$$

$$Y = A e^{BX}$$

$$Y = A X^B$$

$$Y = A + B/X$$

$$Y = 1/(A + B \cdot X)$$

$$Y = X/(A + B \cdot X)$$

Coefficients for each curve and an index of determination (best fit) are computed.

Kim's data for the sphere are approximated by the following functions:

#### Sway-Surge

##### HYDRODYNAMIC MASS

$$M_z = M_x = 1.089 + 0.529 H' \quad 0 < H' < 0.74 \quad (75A)$$

$$= 1/(-0.0318 + 0.954 H') \quad 0.74 < H' < 3.4 \quad (75B)$$

##### DAMPING

$$N_z = N_x = 0 \quad 0 < H' < 0.1 \quad (76A)$$

$$= -0.069 + 0.71 H' \quad 0.1 < H' < 1.37 \quad (76B)$$

$$= 1.595 e^{-0.415 H'} \quad 1.37 < H' < 3.4 \quad (76C)$$

#### Heave

##### HYDRODYNAMIC MASS

$$M_y = 1.85 \quad 0 < H' < 0.1 \quad (77A)$$

$$= 1.02 \cdot H'^{-0.256} \quad 0.1 < H' < 3.4 \quad (77B)$$

## DAMPING

$$N_y = 0.126 + 1.7 A' \quad 0 < A' < 0.4 \quad (78A)$$

$$= 1.18 e^{-0.83 A'} \quad 0.4 < A' < 3.4 \quad (78B)$$

Dimensionless hydrodynamic mass and wave damping coefficients for a sphere based upon Kim's study along with the above approximate curves are shown in figure 11. The set of approximate functions will be used in the computer simulation of buoy dynamics for a spherical buoy.

Birkoff<sup>44</sup> has investigated the influence of body symmetry on the hydrodynamic mass dyadic. An oblate spheroid possessing an axis of symmetry has five hydrodynamic mass values along the main diagonal: heave, surge, sway (same as surge), pitch, and roll (same as pitch). For an ideal fluid, the yaw hydrodynamic mass is zero. However, Lamb<sup>45</sup> studied the rotational motion of a sphere in a viscous fluid and identifies a force proportional to angular acceleration that can be considered as a yaw hydrodynamic mass. For a fully immersed oblate spheroid in an ideal fluid with the centers of gravity and pressure coincident, all the off-diagonal terms would be zero. However, for a half-immersed oblate spheroid, the following hydrodynamic forces are coupled:

Surge-Pitch

Sway-Roll

Pitch-Surge

Roll-Sway.

Thus far, hydrodynamic mass and wave damping have been computed for heave, sway, surge, pitch, and roll. Using Lamb's analysis for a rotating sphere, we can approximate the yaw hydrodynamic mass for an oblate spheroid



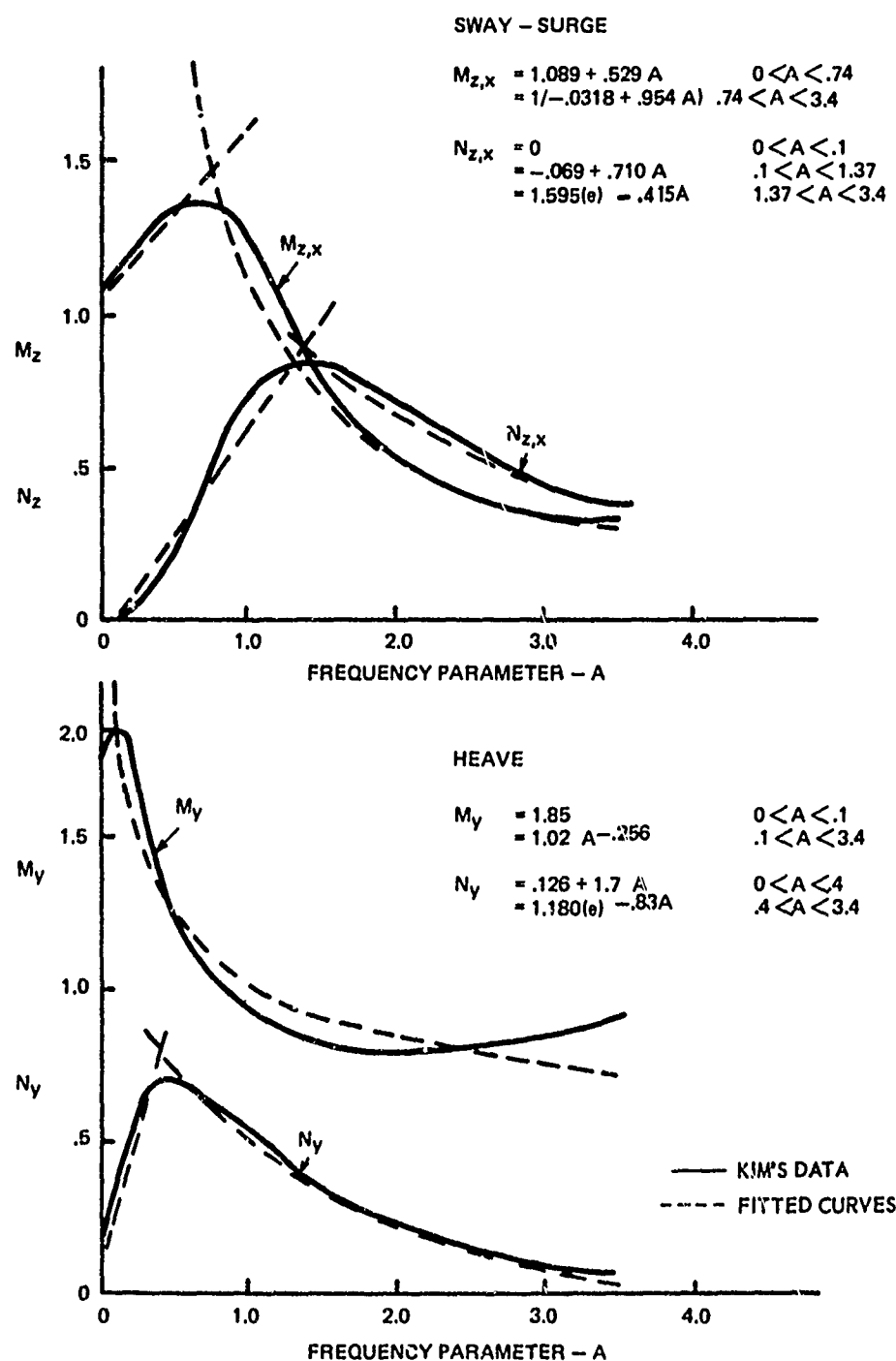


Figure 11. Least-Squares Fits to Kim's Parameters

in a viscous fluid:

$$M_{\alpha\alpha} = \frac{4}{3} \pi \rho A^5 \cdot \frac{1 + \beta A}{1 + 2\beta A + 2\beta^2 A^2} \quad (79)$$

The viscous damping in yaw is

$$N_{\alpha\alpha} = \frac{4}{3} \pi \mu A^3 \cdot \frac{3 + 6\beta A + 6\beta^2 A^2 + 2\beta^3 A^3}{1 + 2\beta A + 2\beta^2 A^2} \quad (80)$$

where

$A$  is the major diameter

$\rho$  is the fluid density

$\mu$  is the viscosity

$\nu$  is the kinematic viscosity

$\beta$  is defined as  $\sqrt{\sigma/2\nu}$

$\sigma$  is the angular frequency of oscillatory motion.

Since the center of pressure and center of gravity of the buoy do not necessarily coincide, force components due to hydrodynamic mass or damping will induce moments about the center of gravity. The projected area of an oblate spheroid in the  $y$ - $x$  or  $z$ - $x$  body planes is a semiellipse. For  $H_D < 0$ , i.e., less than half immersion, the center of pressure is located a distance

$$H_{CP} = \frac{2}{3} \frac{b}{A} \sqrt{(A^2 - H_D^2)^3} \quad (81)$$

below the centroid of the oblate spheroid. For  $H_D > 0$ , i.e., more than half immersion, the center of pressure is located a distance

$$H_{CP} = \frac{\left(\frac{\pi}{2} Ab - \frac{b}{A} H_D \sqrt{A^2 - H_D^2} - Ab \sin^{-1} \frac{H_D}{A}\right) \left(\frac{2}{3} \frac{b}{A} \sqrt{(A^2 - H_D^2)^3}\right)}{\frac{\pi}{2} Ab + \frac{b}{A} H_D \sqrt{A^2 - H_D^2} + Ab \sin^{-1} \left(\frac{H_D}{A}\right)} \quad (82)$$

below the centroid.

In the coordinate system shown, a positive  $y$  acceleration will induce a negative  $\gamma$  moment and, conversely, a positive  $\gamma$  acceleration will induce a negative  $y$  force if the center of gravity is below the center of pressure. Thus, the coupled roll-sway hydrodynamic mass moment of inertia is

$$M_{h_{\gamma y}} = M_{h_{y\gamma}} = -M_{h_{yy}} (H_{CG} - H_{CP}). \quad (83)$$

Also, a positive  $z$  acceleration will induce a positive  $\beta$  moment and vice versa. Thus, the coupled pitch-surge moment is

$$M_{h_{\beta z}} = M_{h_{z\beta}} = M_{h_{zz}} (H_{CG} - H_{CP}). \quad (84)$$

Summarizing the inertial hydrodynamic force coefficients, i.e., the elements of the hydrodynamic mass dyadic for a half-immersed oblate spheroid, we find

$$M_h = \begin{bmatrix} m_{h_{xx}} & 0 & 0 & 0 & 0 & 0 \\ 0 & m_{h_{yy}} & 0 & 0 & 0 & m_{h_{y\gamma}} \\ 0 & 0 & m_{h_{zz}} & 0 & m_{h_{z\beta}} & 0 \\ 0 & 0 & 0 & I_{h_{\alpha\alpha}} & 0 & 0 \\ 0 & 0 & m_{h_{\beta z}} & 0 & I_{h_{\beta\beta}} & 0 \\ 0 & m_{h_{\gamma y}} & 0 & 0 & 0 & I_{h_{\gamma\gamma}} \end{bmatrix}. \quad (85)$$

For the special case of a sphere, the elements of the dyadic are

$$\begin{aligned}
 m_{h_{xx}} &= 1.85 \rho A^3 & 0 < A' < 0.1 \\
 &= (1.02 A'^{-0.256}) \rho A^3 & 0.1 < A' < 3.4 \\
 m_{h_{yy}} = m_{h_{zz}} &= (1.089 + 0.529 A') \rho A^3 & 0 < A' < 0.74 \\
 &= (1.0 / (-0.0318 + 0.954 A')) \rho A^3 & 0.74 < A' < 3.4 \\
 I_{h_{\alpha\alpha}} = I_{h_{\beta\beta}} = I_{h_{\gamma\gamma}} &= \frac{4}{3} \pi \rho A^5 \cdot \frac{1 + \beta A}{1 + 2\beta A + 2\beta^2 A^2} \\
 m_{h_{yyr}} = m_{h_{\gamma r}} &= -m_{h_{yy}} (H_{CG} - H_{CP}) \\
 m_{h_{z\beta}} = m_{h_{\beta z}} &= m_{h_{zz}} (H_{CG} - H_{CP}),
 \end{aligned}$$

where

$$A' \text{ is defined as } \frac{A \sigma^2}{g}$$

$A$  is the sphere radius

$\sigma$  is the angular frequency

$\rho$  is the fluid density

$$\beta \text{ is defined as } \sqrt{\sigma / 2\nu}$$

$\nu$  is the kinematic viscosity

$H_{CG}, H_{CP}$  are locations of centers of gravity and pressure.

In a similar fashion, the dissipative force coefficients due to surface wave generation are

$$N = \begin{bmatrix} n_{xx} & 0 & 0 & 0 & 0 & 0 \\ 0 & n_{yy} & 0 & 0 & 0 & n_{yy} \\ 0 & 0 & n_{zz} & 0 & n_{z\beta} & 0 \\ 0 & 0 & 0 & 0 & 0 & 0 \\ 0 & 0 & n_{\beta z} & 0 & n_{\beta\beta} & 0 \\ 0 & n_{yy} & 0 & 0 & 0 & n_{yy} \end{bmatrix} \quad (86)$$

Again, for the special case of a sphere, the elements of the dyadic are

$$\begin{aligned}
 n_{xx} &= (0.126 + 1.7 \cdot A') \rho \sigma A^3 & 0 < A' < 0.4 \\
 &= (1.18 e^{-0.83 A'}) \rho \sigma A^3 & 0.4 < A' < 3.4 \\
 n_{yy} = n_{zz} &= 0 / & 0 < A' < 0.1 \\
 &= (-0.069 + 0.71 A') \rho \sigma A^3 & 0.1 < A' < 1.37 \\
 &= (1.595 e^{-0.415 A'}) \rho \sigma A^3 & 1.37 < A' < 3.4 \\
 n_{\beta\beta} = n_{\gamma\gamma} &= 0 \\
 n_{\gamma\gamma} = n_{\gamma\gamma} &= -n_{yy} (H_{CG} - H_{CP}) \\
 n_{z\beta} = n_{\beta z} &= n_{zz} (H_{CG} - H_{CP}) .
 \end{aligned}$$

Dissipative forces due to viscosity are assumed to follow a velocity-squared drag law. There is some question as to the validity of representing an unsteady force with a coefficient based upon steady flow experimental measurements. Martin<sup>46</sup> has found that the mean drag coefficient for a plate started impulsively from rest is an order of magnitude greater than for steady flow. However, there is no general, analytical method available to compute the viscous forces for a fully turbulent, oscillatory flow. Schlichting<sup>47</sup> cites use of a method of successive approximations for unsteady laminar flow. Since viscous forces,  $f(a^2)$ , are an order of magnitude less than hydrodynamic inertia and wave damping forces,  $f(a^3)$ , and because steady currents are acting on the buoy, the viscous forces are assumed to follow a velocity-squared drag law for subcritical Reynold's numbers.

Analagous to the hydrodynamic mass dyadic, the viscous force matrix will contain ten elements. The viscous force coefficient matrix is

$$D = \begin{bmatrix} d_{xx} & 0 & 0 & 0 & 0 & 0 \\ 0 & d_{yy} & 0 & 0 & 0 & d_{yx} \\ 0 & 0 & d_{zz} & 0 & d_{z\beta} & 0 \\ 0 & 0 & 0 & d_{\alpha\alpha} & 0 & 0 \\ 0 & 0 & d_{\beta z} & 0 & d_{\beta\beta} & 0 \\ 0 & d_{xy} & 0 & 0 & 0 & d_{yx} \end{bmatrix}, \quad (87)$$

where

$$d_{xx} = \frac{\rho}{2} C_{DH} A_H$$

$$d_{yy} = d_{zz} = \frac{\rho}{2} C_{DS} A_S$$

$$d_{\alpha\alpha} = d_{\beta\beta} = d_{yy} = \frac{4}{3} \pi \mu H^3 \frac{3 + 6\beta H + 6\beta^2 H^2 + 2\beta^3 H^3}{1 + 2\beta H + 2\beta^2 H^2}$$

$$d_{yx} = d_{xy} = -d_{yy} (H_{CG} - H_{CP})$$

$$d_{z\beta} = d_{\beta z} = d_{zz} (H_{CG} - H_{CP})$$

The projected area in heave is

$$A_H \cong \pi b^2 \quad (88)$$

and in surge or sway is

$$A_S = \frac{\pi}{2} H b + \frac{b}{H} H_D \sqrt{H^2 - H_D^2} + H b \sin^{-1} \frac{H_D}{H} \quad (89)$$

For half-immersed spheroids, Hoerner<sup>49</sup> shows plots of drag coefficient

(surge or sway) versus the ratio of vertical to horizontal axis dimensions.

Hoerner's plot for a subcritical drag coefficient is fitted by the function

$$C_{Ds} = 0.354 A/b \quad Re < 10^5; \text{ subcritical}$$

for various spheroids. The drag coefficient in heave is approximated with one-half the value for a sphere,  $C_{DH} = 0.3$ .

### 3.1.5 Ocean Waves

In order to compute the magnitude of the hydrodynamic forces with the coefficients just derived, the relative motion of the fluid surrounding the buoy, relative to the buoy, must be computed. A mathematical model of the sea state must be developed.

The following hypothesis offered by St. Denis and Pierson<sup>24</sup> in 1953 has been verified by Dalzell,<sup>49,50</sup> Gerritsma,<sup>51</sup> and others for the motions of ships in a random seaway:

1. Assume that the sea can be represented as the linear sum of elementary waves, each traveling in the manner described by the classical Airy formulas of linearized water wave theory. Each component wave train will have random phase.
2. Weight the component waves to have the same spectral characteristics as the observed sea state.
3. Assume that the body response to a random sea is the sum of its responses to the various frequency components.

Within the constraints imposed by the assumptions made in the derivation of the hydrodynamic coefficients, i. e., body dimensions are small compared with

a wavelength, the St. Denis-Pierson hypothesis should be better suited to the case of a buoy, with dimensions on the order of 10 ft, than to ships, with dimensions on the order of 100 ft. (For example, as a worst case, a 10-ft buoy in waves with 100-ft wavelengths would only cause a peak error of 3.3 percent in the computed elevation of the mean waterplane. This error will decrease as the wavelengths become longer.)

From the Airy formulas, water particle motions in deep water for waves traveling along the  $z$  axis are described as follows:

Wave Height

$$\chi_w = A_w \sin(kz - \sigma t) \quad (90A)$$

Vertical Velocity Component

$$\dot{\chi}_w = -\frac{A_w g k}{\sigma} \cos(kz - \sigma t) \quad (90B)$$

Horizontal Velocity Component

$$\dot{z}_w = \frac{A_w g k}{\sigma} \sin(kz - \sigma t) \quad (90C)$$

Vertical Acceleration Component

$$\ddot{\chi}_w = -A_w g k \sin(kz - \sigma t) \quad (90D)$$

Horizontal Acceleration Component

$$\ddot{z}_w = -A_w g k \cos(kz - \sigma t) \quad (90E)$$



Wave Slope

$$\begin{aligned}\beta_w &= -\text{TAN}^{-1}(A_w k \cos(kz - \sigma t)) \\ &\cong -A_w k \cos(kz - \sigma t)\end{aligned}\quad (90 F)$$

Angular Velocity of Free Surface

$$\dot{\beta}_w \cong -A_w k \sigma \sin(kz - \sigma t) \quad (90 G)$$

Angular Acceleration of Free Surface

$$\ddot{\beta}_w \cong A_w k \sigma^2 \cos(kz - \sigma t) \quad (90 H)$$

where

$k$  is the wave number  $(k = 2\pi/L_0)$

$L_0$  is the wavelength

$\sigma$  is the angular frequency

$t$  is the time.

The assumption that body dimensions are small compared with wavelengths implies that body displacements are small compared with wavelengths. Thus, we find that

$$X_w \cong -A_w \sin \sigma t, \quad (91 A)$$

$$\dot{X}_w \cong -A_w \sigma \cos \sigma t, \quad (91 B)$$

$$\ddot{X}_w \cong -A_w \sigma^2 \sin \sigma t, \quad (91 C)$$

$$\ddot{X}_w \cong A_w \sigma^2 \sin \sigma t, \quad (91D)$$

$$\ddot{Z}_w \cong -A_w \sigma^2 \cos \sigma t, \quad (91E)$$

$$\beta_w \cong A_w k \cos \sigma t, \quad (91F)$$

$$\dot{\beta}_w \cong -A_w k \sigma \sin \sigma t, \quad (91G)$$

and

$$\ddot{\beta}_w \cong -A_w k \sigma^2 \cos \sigma t. \quad (91H)$$

Transforming the water mass velocities and accelerations to body coordinates, we see that the velocities are

$$\begin{bmatrix} \dot{X}_{w2} \\ \dot{Y}_{w2} \\ \dot{Z}_{w2} \end{bmatrix} = \Omega \cdot \begin{bmatrix} \dot{X}_w \\ 0 \\ \dot{Z}_w \end{bmatrix}, \quad (92A)$$

and that the accelerations are

$$\begin{bmatrix} \ddot{X}_{w2} \\ \ddot{Y}_{w2} \\ \ddot{Z}_{w2} \end{bmatrix} = \Omega \cdot \begin{bmatrix} \ddot{X}_w \\ 0 \\ \ddot{Z}_w \end{bmatrix}. \quad (92B)$$

The location of the intersection of the free surface and the "vertical" axis of the buoy is

$$H_D = X_{06} \cos \beta \cos \gamma + X_2 - X_W \cos \beta \cos \gamma . \quad (93)$$

In order to develop a random wave model, the statistical properties of the sea state must be described. The development of wind waves on a body of water is either limited by the distance to land in the direction from which the wind blows (fetch limited) or by the length of time during which the wind acts on the water surface (duration limited). For the fetch limited case, Bretschneider<sup>52</sup> normalized the original wind wave forecasting relations of Sverdrup and Munk<sup>53</sup> and included much additional data. Bretschneider's dimensionless curves have been approximated by piecewise linear functions by Patton.<sup>54</sup> The approximate functions are as follows:

#### Significant Period

$$\bar{T}_{1/3} = 2.47 \times 10^{-2} \quad \bar{F} < 2.0 \times 10^{-2} \quad (94A)$$

$$\text{LOG } \bar{T}_{1/3} = -1.136 + 0.283 \text{ LOG } \bar{F} \quad 2 \times 10^{-2} < \bar{F} < 1.2 \times 10^5 \quad (94B)$$

$$\bar{T}_{1/3} = 2.0 \quad \bar{F} > 1.2 \times 10^5 \quad (94C)$$

#### Significant Height

$$\bar{H}_{1/3} = 5.74 \times 10^{-4} \quad \bar{F} < 1.6 \times 10^{-2} \quad (95A)$$

$$\text{LOG } \bar{H}_{1/3} = -2.5 + 0.415 \text{ LOG } \bar{F} \quad 1.6 \times 10^{-2} < \bar{F} < 5.0 \times 10^4 \quad (95B)$$

$$\bar{H}_{1/3} = 2.82 \times 10^{-1} \quad \bar{F} > 5.0 \times 10^4 \quad (95C)$$

Weigel<sup>55</sup> extends Bretschneider's dimensionless curves to the case of duration limited wind waves. These curves are approximated by

Significant Period

$$\text{LOG } \bar{T}_{1/3} = -0.2 + 0.224 \text{ LOG } \bar{D} \quad (96)$$

Significant Height

$$\text{LOG } \bar{H}_{1/3} = -2.272 + 0.3282 \text{ LOG } \bar{D} \quad (97)$$

where

$$\bar{T}_{1/3} = \frac{g T_{1/3}}{2\pi WV}, \text{ the dimensionless significant period}$$

$$\bar{H}_{1/3} = \frac{g H_{1/3}}{WV^2}, \text{ the dimensionless significant height}$$

$$\bar{F} = \frac{g F}{WV^2}, \text{ the fetch parameter}$$

$$\bar{D} = \frac{g D}{WV}, \text{ the duration parameter}$$

$T_{1/3}$  is the significant period

$H_{1/3}$  is the significant wave height

$F$  is the fetch

$D$  is the duration

$g$  is the gravitational constant

$WV$  is the wind velocity

In order to determine if the waves are fetch or duration limited, the minimum duration for a given fetch must be determined. From Bretschneider's curves, the minimum duration is given by

$$\text{LOG} \left( \frac{D_{\min} \cdot WV}{F} \right) = 1.477 - 0.255 \text{ LOG } \bar{F} \quad (98)$$

If the duration ( $D$ ) is less than the minimum duration ( $D_{\min}$ ) the waves are duration limited; if greater, the waves are fetch limited.

For a given wind speed, fetch, and duration, the significant wave height and period can be computed by using the above equations. Longuet-Higgins<sup>56</sup> and Bretschneider<sup>52</sup> have shown that the distributions of wave heights and squared periods can be represented by Rayleigh distributions. Thus, the wave height

distribution is

$$p(H) = \frac{\pi H}{2 \bar{H}^2} e^{-\frac{\pi}{4} \frac{H^2}{\bar{H}^2}}, \quad (99)$$

and the wave period distribution is

$$p(T) = 2.7 \frac{T^3}{\bar{T}^4} e^{-0.675 \left(\frac{T}{\bar{T}}\right)^4} \quad (100)$$

The mean wave height and periods are

$$\bar{H} = 0.625 H_{1/3} \quad (101)$$

and

$$\bar{T} = 0.758 T_{1/3} \quad (102)$$

Ocean wind wave amplitude spectra are of the form

$$S_{H^2}(\omega) = A \omega^m e^{-B\omega^n} \quad (103)$$

Pierson and Moskowitz<sup>57</sup> analyzed 54 data sets and evaluated A, B, m, and n.

The exponent m was set equal to -5 and n was found to vary between 2 and 4 depending on the wind speed. Kottler<sup>58</sup> optimized the parameters by using a least-squares fit of each data set used by Pierson-Moskowitz and proposed the form

$$S_{H^2}(\omega) = 10 \cdot \omega^{-5.5} e^{(-b\omega^{-4.5})} + C, \quad (104)$$

where

$$b = (1.75 \times 10^5) WV^{-4.305}$$

$$C = 0.03054 e^{(0.154 \cdot WV)}$$

The Bretschneider spectrum, given by

$$S_{H^2}(\omega) = \alpha g^2 \omega^{-5} e^{-0.675 \left( \frac{g}{WV \omega F_2} \right)^4}, \quad (105)$$

where

$$F_1 = \frac{g \bar{H}}{WV^2}$$

$$F_2 = \frac{g \bar{T}}{2\pi WV}$$

$$\alpha = 3.437 \frac{F_1^2}{F_2^4},$$

was chosen for this study since it closely resembles the optimized spectrum and is integrable.

St. Denis and Pierson<sup>24</sup> proposed a random wave height model in 1953 of the form

$$x_w(t) = \int_0^\infty \cos(\omega t + \epsilon(\omega)) \cdot \sqrt{S_{H^2}(\omega)} d\omega, \quad (106)$$

where  $\epsilon(\omega)$  is a random variable whose values are equally probable for any value between 0 and  $2\pi$ . The integral is not an integral in the Riemann sense since the function is discontinuous because of the random variable. The expression indicates that the random wave heights can be represented as a finite number of cosine waves of different frequency, each having random phase. Let the spectral density  $S_{H^2}(\omega)$  be partitioned into  $N$  frequency bands (figure 12) in such a manner that

$$0 < \omega_0 < \omega_1 < \omega_2 \cdots < \omega_N = W,$$

where the spectral density is essentially zero if  $\omega$  is greater than  $W$ .

The width of the  $n$ th band is

$$\Delta\omega_n = \omega_n - \omega_{n-1}, \quad (107)$$

and the mean angular frequency of the  $n$ th band is

$$\bar{\omega}_n = \frac{1}{2}(\omega_n + \omega_{n-1}). \quad (108)$$

The random wave height model is now defined as

$$X_w(t) = \sum_{n=1}^N \sqrt{S_{H^2}(\bar{\omega}_n) \Delta\omega_n} \cos(\bar{\omega}_n t + \epsilon_n),$$

where  $\epsilon_n$ ,  $n = 1, 2, 3, \dots, N$  are independent random variables distributed uniformly over the interval 0 to  $2\pi$ . Borgman<sup>59</sup> indicates that an equally spaced subdivision  $\Delta\omega_n = W/N$  will result in  $X_w(t)$  repeating itself with period  $2\pi/\bar{\omega}_1$ . Borgman



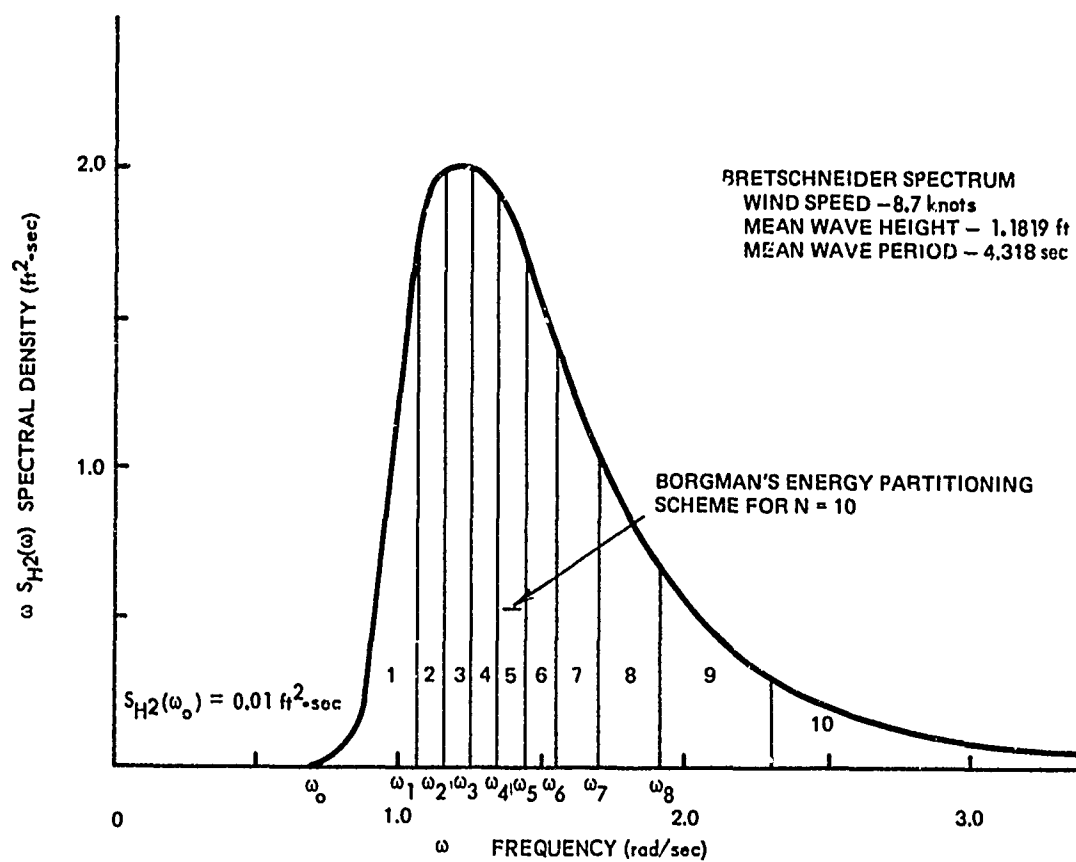


Figure 12. Borgman's Energy Partitioning in a Bretschneider Spectrum

partitions the spectrum on an energy basis using the cumulative spectrum given by

$$S_{H^2}(\omega) = 2 \int_0^\omega S_{H^2}(\omega) d\omega ; \quad (109)$$

thus,

$$S_{H^2}(\bar{\omega}_n) \Delta \omega_n \cong \frac{1}{2} (\bar{S}_{H^2}(\omega_n) - \bar{S}_{H^2}(\omega_{n-1})) ; \quad (110)$$

hence,

$$x_w(t) = \frac{1}{\sqrt{2}} \sum_{n=1}^N \sqrt{\bar{S}_{H^2}(\omega_n) - \bar{S}_{H^2}(\omega_{n-1})} \cos(\bar{\omega}_n t + \epsilon_n). \quad (111)$$

The periodicity is avoided if the set of  $\omega_n$  values are chosen to make

$$\bar{S}_{H^2}(\omega_n) - \bar{S}_{H^2}(\omega_{n-1}) \quad \text{constant for all } n. \quad \text{Let}$$

$$\bar{S}_{H^2}(\omega_n) - \bar{S}_{H^2}(\omega_{n-1}) = h^2 ; \quad (112)$$

then, the instantaneous wave height is

$$x_w(t) = \frac{h}{\sqrt{2}} \sum_{n=1}^N \cos(\bar{\omega}_n t + \epsilon_n), \quad (113)$$

The frequencies,  $\bar{\omega}_n$ , are given by

$$S_{H^2}(\bar{\omega}_n) = \frac{n}{N} \bar{S}_{H^2}(\infty) \quad n=1, 2, \dots, N, \quad (114)$$

which corresponds to an equal subdivision of the energy coordinate axis for

$$S_{H^2}(\omega) .$$

Using the Bretschneider-Pierson spectral density of the form

$$S_{H^2}(\omega) = \frac{AB}{\omega^5} e^{-B/\omega^4} , \quad (115)$$

which is directly integrable, we find that

$$\bar{S}_{H^2}(\omega) = 2 \int_0^\omega \frac{AB}{s^5} e^{-B/s^4} ds = \frac{A}{2} e^{-B/\omega^4} . \quad (116)$$

Integrating out to infinity, we find that

$$\bar{S}_{H^2}(\infty) = \frac{A}{2} ,$$

and

$$\omega_n = \left[ \frac{B}{\text{LOG}_e(N/n)} \right]^{1/4} , \quad (117)$$

where the coefficient is given by

$$B = -0.675 \left( \frac{g}{WV F_2} \right)^4 . \quad (118)$$

Next, we define the various elements of the random sea state model:

#### Wave Height

$$X_w(t) = \frac{1}{2} \sum_{n=1}^N \sqrt{S_{H^2}(\bar{\omega}_n) \Delta \omega_n} \sin(\bar{\omega}_n t + \epsilon_n) \quad (119)$$

Vertical Velocity Component

$$\dot{\chi}_w(t) = \frac{1}{2} \sum_{n=1}^N -\bar{\omega}_n \sqrt{S_{H^2}(\bar{\omega}_n) \Delta \omega_n} \cos(\bar{\omega}_n t + \epsilon_n) \quad (120)$$

Horizontal Velocity Component

$$\dot{\xi}_w(t) = \frac{1}{2} \sum_{n=1}^N -\bar{\omega}_n \sqrt{S_{H^2}(\bar{\omega}_n) \Delta \omega_n} \sin(\bar{\omega}_n t + \epsilon_n) \quad (121)$$

Vertical Acceleration Component

$$\ddot{\chi}_w(t) = \frac{1}{2} \sum_{n=1}^N \bar{\omega}_n^2 \sqrt{S_{H^2}(\bar{\omega}_n) \Delta \omega_n} \sin(\bar{\omega}_n t + \epsilon_n) \quad (122)$$

Horizontal Acceleration Component

$$\ddot{\xi}_w(t) = \frac{1}{2} \sum_{n=1}^N -\bar{\omega}_n^2 \sqrt{S_{H^2}(\bar{\omega}_n) \Delta \omega_n} \cos(\bar{\omega}_n t + \epsilon_n) \quad (123)$$

Wave Slope

$$\beta_w(t) = \frac{1}{2} \sum_{n=1}^N k_n \sqrt{S_{H^2}(\bar{\omega}_n) \Delta \omega_n} \cos(\bar{\omega}_n t + \epsilon_n) \quad (124)$$

Angular Velocity of Free Surface

$$\dot{\beta}_w(t) = \frac{1}{2} \sum_{n=1}^N -k_n \bar{\omega}_n \sqrt{S_{H^2}(\bar{\omega}_n) \Delta \omega_n} \sin(\bar{\omega}_n t + \epsilon_n) \quad (125)$$

Angular Acceleration of Free Surface

$$\ddot{\beta}_w(t) = \frac{1}{2} \sum_{n=1}^N -k_n \bar{\omega}_n^2 \sqrt{S_{H^2}(\bar{\omega}_n) \Delta \omega_n} \cos(\bar{\omega}_n t + \epsilon_n) \quad (126)$$

Again, the wave height, velocity components, and acceleration components must be transformed to body coordinates according to equations (92A), (92B), and (93).

A ten-component, random sea state model was programmed in FORTRAN for use with the UNIVAC 1108 digital computer at the Naval Underwater Systems Center, New London Laboratory. This program is shown in appendix B as subroutine "RWAVE." The ten-component model was found to truncate the low and high ends of the spectrum (the first and ninth frequency components). Since the low-frequency end of the spectrum is important in the computation of the response of mechanical systems, Borgman's frequency partition method was modified to include the low-frequency energy by the following numerical scheme:

1. Use a trial and error method to compute the frequency at which the value of the spectral density rises above some threshold value, for example,  $S_{H^2}(\omega) > 0.01 \text{ ft}^2$ . Let this frequency be denoted  $\omega_0$ .

2. Thus,

$$\bar{\omega}_1 = \frac{1}{2}(\omega_1 - \omega_0)$$

and

$$\Delta\omega_1 = \omega_1 - \omega_0.$$

3. Use the energy computed for the second partition  $\bar{S}_{H^2}(\omega_2) - \bar{S}_{H^2}(\omega_1)$  to compute the component amplitude.

This method accounts for the energy in the low-frequency end of the spectrum.

### 3.1.6 Numerical Solution of the Equations of Motion

Having computed the wind wave displacements, velocities, and accelerations, we can now compute the hydrostatic and hydrodynamic forces acting on the buoy (terms B and H in equation (5)). The hydrostatic forces and moments depend on the position and orientation of the waterplane relative to the buoy. The wave height, given by equation (91A) for a sinusoidal wave model or by equation (119) for a random wave model, must be transformed to buoy coordinates. The transformation is

$$X_{w2} = X_w \cos \beta \cos \gamma - X_{og} \cos \beta \cos \gamma, \quad (127)$$

where  $X_{og}$  is the vertical height of the center of gravity of the buoy below the mean waterplane with no buoy pitch or roll. The transformed wave height must be subtracted from the heave motion of the buoy in order to apply equation (93), the location of the intersection of the waterplane and the "vertical" axis of the buoy. Restricting the study to waves traveling along the  $x$  axis of the coordinate system, the wave slope  $\beta_w$  in the inertial coordinate system is given by equation (91F), for sinusoidal waves and by equation (124) for the random wave model. The attitude of the waterplane, relative to the buoy coordinates, is described by the angles  $\beta_s = \beta - \beta_w$  and  $\gamma_s = \gamma$ . The slope of the sea surface is

$$\beta' = \cos^{-1}(\cos \gamma_s \cos \beta_s). \quad (128)$$

With the location (equation (93)) and slope (equation (128)), the buoyant forces and moments for a sphere are given by equations (49), (55), and (56).

In a similar manner, the hydrodynamic forces are computed by considering water mass movements relative to the buoy. With the assumption that the buoy dimensions are small relative to the wavelength and applying the Froude-Kryloff hypothesis\* for the viscous forces, we find that water mass velocities and accelerations are given by equations (91B), (91C), (91D), (91E), (91G), and (91H) for a sinusoidal wave model and by equations (120), (121), (122), (123), (125), and (126) for a random wave model. Water mass accelerations are simply transformed to buoy coordinates (equation (100B)) and subtracted from buoy accelerations to compute the motion of the buoy relative to the water mass. The relative acceleration is

$$\ddot{\mathbf{Q}}' = \ddot{\mathbf{Q}} - \Omega \cdot \ddot{\mathbf{Q}}_w, \quad (129)$$

where

$\ddot{\mathbf{Q}}'$  is the acceleration vector relative to water mass

$\ddot{\mathbf{Q}}$  is the buoy acceleration

$\ddot{\mathbf{Q}}_w$  is the water mass acceleration.

Water mass velocities are more complex because ocean currents exist and must be included. There is a difference in reference frame that must be resolved since buoy velocities cause a reactive force (i.e., a positive buoy velocity

---

\*The presence of the buoy does not appreciably change water mass movements in the vicinity of the buoy.

causes a negative force) while waves and currents cause active forces (positive velocities cause positive forces). The velocity vector of the buoy, relative to the water mass, is given by

$$\dot{Q}'' = \dot{Q} - \Omega \cdot \dot{Q}_w - \Omega \cdot \dot{Q}_c, \quad (130)$$

where

$\dot{Q}$  is the buoy velocity vector

$\dot{Q}_w$  is the particle velocity vector due to waves

$\dot{Q}_c$  is the current velocity vector.

For current velocity components  $C^u$  and  $C^w$  acting in the positive  $y_0$  and  $z_0$  directions, respectively, the current velocity vector is

$$\dot{Q}_c = \begin{bmatrix} 0 \\ CV \\ CW \end{bmatrix} \quad (131)$$

For viscous dissipative forces, which are functions of the velocity squared, the velocities are

$$\dot{Q}'^2 = \dot{Q}' \cdot \dot{Q}'. \quad (132)$$

The absolute value is used in order to preserve the sign convention.

If the buoy were free floating, not moored, the equations of motion for the buoy could now be integrated for a given set of environmental conditions to solve for the buoy response.



The equations of motion for a spherical buoy are summarized. Equation (5) is

$$M \ddot{Q} = MG - B - H - V - T.$$

In the  $R_2$  coordinate system, the heave acceleration is given by

$$\begin{aligned} \ddot{x} = \frac{1}{m} \bigg[ & mg \cos \gamma \cos \beta - B \cos \gamma \cos \beta \\ & - m_{h_{xx}} \cdot \ddot{x}' - n_{xx} \cdot \dot{x}' - d_{xx} \cdot \dot{x}'' |\dot{x}''| - W_{x_2} \\ & + T_x \cos \gamma \cos \beta + T_y \sin \gamma + T_z \cos \gamma \sin \beta \bigg]. \end{aligned}$$

The sway acceleration is given by

$$\begin{aligned} \ddot{y} = \frac{1}{m} \bigg[ & mg \sin \gamma \cos \beta - B \sin \gamma \cos \beta - m_{h_{yy}} \cdot \ddot{y}' \\ & - m_{h_{yx}} \cdot \ddot{x}' - n_{yy} \cdot \dot{y}' - n_{yx} \cdot \dot{x}' - d_{yy} \cdot \dot{y}'' |\dot{y}''| \\ & - d_{yx} \cdot \dot{x}'' |\dot{x}''| - W_{y_2} - T_x \sin \gamma \cos \beta \\ & + T_y \cos \gamma - T_z \sin \gamma \sin \beta \bigg]. \end{aligned}$$

The surge acceleration is given by

$$\begin{aligned} \ddot{z} = \frac{1}{m} \bigg[ & -mg \sin \beta + B \sin \beta - m_{h_{zz}} \cdot \ddot{z}' - m_{h_{z\beta}} \cdot \ddot{\beta}' \\ & - n_{zz} \cdot \dot{z}' - n_{z\beta} \cdot \dot{\beta}' - d_{zz} \cdot \dot{z}'' |\dot{z}''| - d_{z\beta} \cdot \dot{\beta}'' |\dot{\beta}''| \\ & - W_{z_2} - T_x \sin \beta + T_z \cos \beta \bigg]. \end{aligned}$$

The yaw acceleration is given by

$$\ddot{\alpha} = \frac{1}{I_{\alpha\alpha}} \left[ -I_{h\alpha\alpha} \cdot \ddot{\alpha} - d_{\alpha\alpha} \cdot \dot{\alpha} \cdot |\dot{\alpha}| \right].$$

The pitch acceleration is given by

$$\begin{aligned} \ddot{\beta} = \frac{1}{I_{\beta\beta}} \left[ -M_{\beta} - I_{h\beta\beta} \cdot \ddot{\beta}' - m_{h\beta z} \cdot \ddot{z}' - n_{\beta z} \cdot \dot{z}' \right. \\ \left. - d_{\beta\beta} \cdot \dot{\beta}' |\dot{\beta}'| - d_{\beta z} \cdot \dot{z}' |\dot{z}'| - W_{\beta z} \right. \\ \left. - H_{ML} (-T_x \sin \beta + T_z \cos \beta) \right]. \end{aligned}$$

The roll acceleration is given by

$$\begin{aligned} \ddot{\gamma} = \frac{1}{I_{\gamma\gamma}} \left[ -M_{\gamma} - I_{h\gamma\gamma} \cdot \ddot{\gamma}' - m_{h\gamma y} \cdot \ddot{y}' - n_{\gamma y} \cdot \dot{y}' \right. \\ \left. - d_{\gamma\gamma} \cdot \dot{\gamma}' |\dot{\gamma}'| - d_{\gamma y} \cdot \dot{y}' |\dot{y}'| - W_{\gamma z} \right. \\ \left. - H_{ML} (-T_x \sin \gamma \cos \beta + T_y \cos \gamma - T_z \sin \gamma \sin \beta) \right]. \end{aligned}$$

Hydrodynamic inertias and wave damping are computed for motions of the buoy

relative to the water mass. Thus, for waves traveling along the  $z$  axis, we

see that

$$\begin{array}{lll} \ddot{x}' = \ddot{x} - \ddot{x}_{w2} & \dot{x}' = \dot{x} - \dot{x}_{w2} & x' = x - x_{w2} \\ \ddot{y}' = \ddot{y} & \dot{y}' = \dot{y} & y' = y \\ \ddot{z}' = \ddot{z} - \ddot{z}_{w2} & \dot{z}' = \dot{z} - \dot{z}_{w2} & z' = z - z_{w2} \\ \ddot{\alpha}' = \ddot{\alpha} & \dot{\alpha}' = \dot{\alpha} & \alpha' = \alpha \\ \ddot{\beta}' = \ddot{\beta} - \ddot{\beta}_{w2} & \dot{\beta}' = \dot{\beta} - \dot{\beta}_{w2} & \beta' = \beta - \beta_{w2} \\ \ddot{\gamma}' = \ddot{\gamma} & \dot{\gamma}' = \dot{\gamma} & \gamma' = \gamma \end{array},$$

where the subscript  $w_2$  indicates that the computed wave induced water particle motions are transformed to the buoy coordinates. The viscous drag forces and moments must include a contribution due to the steady-state currents; thus,

$$\begin{aligned}\dot{X}'' &= \dot{X}' \\ \dot{Y}'' &= \dot{Y}' - GV \\ \dot{Z}'' &= \dot{Z}' - GW \\ \dot{\alpha}'' &= \dot{\alpha}' \\ \dot{\beta}'' &= \dot{\beta}' \\ \dot{\gamma}'' &= \dot{\gamma}'\end{aligned}$$

The draft of the buoy is  $H_d = H_{CG} + X'$  where  $H_{CG}$  is the height of the center of gravity of the buoy from the bottom of the buoy hull. The buoyant force is

$$B = \rho g \pi R^3 \left[ \frac{2}{3} + \frac{H_d}{R} \cos \beta' - \frac{H_d^3}{3R^3} \cos^3 \beta' \right].$$

The pitch and roll buoyant moments are given by

$$M_{\beta} = B \cdot (Z_{CB} \cos \beta' + (H_{CG} - X_{CB}) \sin \beta')$$

and

$$M_{\gamma} = B \cdot (Y_{CB} \cos \gamma' + (H_{CG} - X_{CB}) \sin \gamma').$$

The hydrodynamic inertia coefficients are summarized in equation (85). Wave damping coefficients are summarized in equation (86). Viscous drag force coefficients are summarized in equation (87). Finally, wind forces are shown in equation (18).

With all the coefficients in the equations of motion defined and with the sea state model available as a forcing function, the dynamics of a free-floating buoy\* (no mooring line) can be investigated by numerical solution of equation (5). The matrix equations of motion can be rewritten to yield six, coupled, second-order, ordinary differential equations with nonconstant coefficients — three force equations and three moment equations. They can be rewritten as twelve first-order equations.

These equations can be solved numerically in the time domain for the six buoy motions using a standard higher order numerical integration algorithm (usually Milne Predictor-Corrector methods or Runge-Kutta methods). In this study, a fourth-order, Runge-Kutta method was used to integrate the buoy equations of motion on a UNIVAC 1108 digital computer. Although a bit slower than Predictor-Corrector methods, the Gill's Method Runge-Kutta subroutine is available on the UNIVAC 1108 and was found to be easier to implement for large numbers of coupled, second-order differential equations.

Errors in the fourth-order, Runge-Kutta method are on the order of  $h^5$ , where  $h$  is the integration step size. For the smaller oceanographic buoys, it was found that a step size on the order of  $10^{-2}$  sec was required for numerical stability. If a step size of  $5 \times 10^{-3}$  were used, the error would be on the order of  $3.125 \times 10^{-12}$ .

The computer programs used are described in detail in appendix B.

---

\*The mooring line tension force will be developed in the next section on cable dynamics and the equations of motion for the buoy will be coupled with those for the cable.

### 3.2 Cable Dynamics

A study of the dynamics of cables in the ocean environment must include hydrodynamic forces acting on the cable and be capable of including nonlinear stress-strain properties for the cable. Since oceanic currents may flow in various directions at different depths and the excitation at the ends of the cable may be described by a three-dimensional force vector, the analysis must be conducted in three dimensions.

#### 3.2.1 The Cable Equations

Consider a free body of a cable segment of length  $dS_0$  (figure 13) being acted upon by an external force per unit length,  $\vec{Q}$ , and assume perfect flexibility. The geometric center of the cable segment lies at a point  $(x_0, y_0, z_0)$  in a cartesian coordinate system. The external force  $\vec{Q} dS_0$  acting on the cable segment can be resolved into components; they are

$$\vec{Q} dS_0 = X dS_0 \cdot \hat{i} + Y dS_0 \cdot \hat{j} + Z dS_0 \cdot \hat{k} . \quad (133)$$

Writing Newton's Second Law, we see that in the  $x$  direction

$$\mu(S_0) dS_0 \frac{\partial^2 x}{\partial t^2} = X dS_0 + [\vec{T}(S_0 + dS_0) - \vec{T}(S_0)] \cdot \hat{i} ; \quad (134A)$$

in the  $y$  direction

$$\mu(S_0) dS_0 \frac{\partial^2 y}{\partial t^2} = Y dS_0 + [\vec{T}(S_0 + dS_0) - \vec{T}(S_0)] \cdot \hat{j} ; \quad (134B)$$

and in the  $z$  direction,

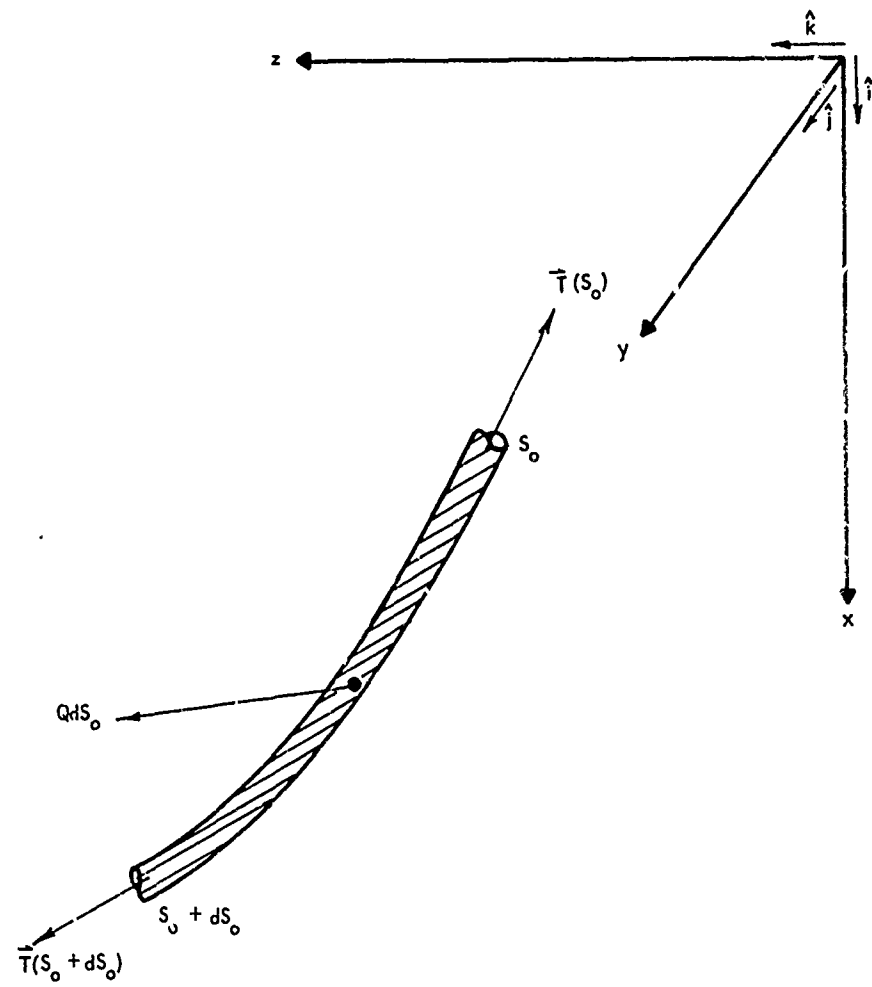


Figure 13. Free Body of a Cable Segment

$$\mu(S_0) dS_0 \frac{\partial^2 z}{\partial t^2} = Z dS_0 + [\vec{T}(S_0 + dS_0) - \vec{T}(S_0)] \cdot \hat{k}, \quad (134C)$$

where  $\mu(S_0)$  is the mass per unit length of the cable. Divide through by  $dS_0$  and let  $dS_0 \rightarrow 0$ . Taking the limit, we can write equation (134A) as

$$\mu(S_0) \frac{\partial^2 x}{\partial t^2} = \lim_{dS_0 \rightarrow 0} \left( X + \frac{1}{dS_0} [\vec{T}(S_0 + dS_0) - \vec{T}(S_0)] \cdot \hat{i} \right),$$

or

$$\mu(S_0) \frac{\partial^2 x}{\partial t^2} = X + \frac{\partial \vec{T}}{\partial S_0} \cdot \hat{i}. \quad (135A)$$

and, in a similar manner, equations (134B) and (134C) become

$$\mu(S_0) \frac{\partial^2 y}{\partial t^2} = Y + \frac{\partial \vec{T}}{\partial S_0} \cdot \hat{j} \quad (135B)$$

and

$$\mu(S_0) \frac{\partial^2 z}{\partial t^2} = Z + \frac{\partial \vec{T}}{\partial S_0} \cdot \hat{k}. \quad (135C)$$

Define the vector  $\vec{r}$  from the origin to a point  $S_0$  on the cable segment.

The vector is defined as

$$\vec{r} = x \cdot \hat{i} + y \cdot \hat{j} + z \cdot \hat{k}.$$

A vector tangent to the cable is

$$\frac{\partial \vec{r}}{\partial S_0} = \frac{\partial x}{\partial S_0} \cdot \hat{i} + \frac{\partial y}{\partial S_0} \cdot \hat{j} + \frac{\partial z}{\partial S_0} \cdot \hat{k}.$$

The unit vector tangent to the cable is

$$\frac{\frac{\partial \vec{r}}{\partial S_0}}{\left| \frac{\partial \vec{r}}{\partial S_0} \right|} = \frac{\frac{\partial \vec{r}}{\partial S_0}}{\sqrt{\left( \frac{\partial x}{\partial S_0} \right)^2 + \left( \frac{\partial y}{\partial S_0} \right)^2 + \left( \frac{\partial z}{\partial S_0} \right)^2}} .$$

At point  $S_0$ , the tension  $\vec{T}$  is tangential to the cable if the cable is assumed to be perfectly flexible (i. e., the cable cannot support bending moments). The tension is

$$\vec{T} = T \frac{\left( \frac{\partial \vec{r}}{\partial S_0} \right)}{\sqrt{\left( \frac{\partial x}{\partial S_0} \right)^2 + \left( \frac{\partial y}{\partial S_0} \right)^2 + \left( \frac{\partial z}{\partial S_0} \right)^2}} ,$$

where  $T$  is the magnitude of the tension. The  $x$  component of the change of tension along the cable is

$$\frac{\partial T}{\partial S_0} \cdot \hat{i} = \frac{\partial}{\partial S_0} (T \cdot \hat{i}) = \frac{\partial}{\partial S_0} \left( \frac{T}{\left| \frac{\partial \vec{r}}{\partial S_0} \right|} \cdot \frac{\partial x}{\partial S_0} \right) . \quad (136)$$

Substituting equation (136) into equation (135A), we find that

$$\mu(S_0) \frac{\partial^2 x}{\partial t^2} = X + \frac{\partial}{\partial S_0} \left( \frac{T}{\left| \frac{\partial \vec{r}}{\partial S_0} \right|} \cdot \frac{\partial x}{\partial S_0} \right) , \quad (137A)$$

and in a similar manner for the  $y$  and  $z$  forces, we find that

$$\mu(S_0) \frac{\partial^2 y}{\partial t^2} = Y + \frac{\partial}{\partial S_0} \left( \frac{T}{\left| \frac{\partial \vec{r}}{\partial S_0} \right|} \cdot \frac{\partial y}{\partial S_0} \right) \quad (137B)$$



and

$$\mu(S_0) \frac{\partial^2 \bar{z}}{\partial t^2} = \bar{Z} + \frac{\partial}{\partial \bar{s}} \left( \frac{T}{|\frac{\partial \bar{r}}{\partial \bar{s}}|} \cdot \frac{\partial \bar{z}}{\partial \bar{s}} \right). \quad (137C)$$

The strain,  $(\epsilon)$ , is defined as

$$\epsilon \equiv \frac{dS - dS_0}{dS_0} = \left| \frac{\partial \bar{r}}{\partial \bar{s}} \right| - 1, \quad (138)$$

where  $S$  is the strained length of the cable. Substituting equation (138) into equations (137A), (137B), and (137C), we can write the equations of motion as follows:

$$\mu(S_0) \frac{\partial^2 \bar{x}}{\partial t^2} - \frac{\partial}{\partial \bar{s}_0} \left( \frac{T}{1+\epsilon} \cdot \frac{\partial \bar{x}}{\partial \bar{s}_0} \right) - \bar{X} = 0, \quad (139A)$$

$$\mu(S_0) \frac{\partial^2 \bar{y}}{\partial t^2} - \frac{\partial}{\partial \bar{s}_0} \left( \frac{T}{1+\epsilon} \cdot \frac{\partial \bar{y}}{\partial \bar{s}_0} \right) - \bar{Y} = 0, \quad (139B)$$

and

$$\mu(S_0) \frac{\partial^2 \bar{z}}{\partial t^2} - \frac{\partial}{\partial \bar{s}_0} \left( \frac{T}{1+\epsilon} \cdot \frac{\partial \bar{z}}{\partial \bar{s}_0} \right) - \bar{Z} = 0. \quad (139C)$$

In addition, the auxiliary equation (138) becomes

$$\epsilon = \frac{dS}{dS_0} - 1.$$

A constitutive relation,

$$T = T(\epsilon), \quad (140)$$

must also be defined.

This set of equations is standard for cable systems and has been developed by Cristecu,<sup>60</sup> Schram,<sup>61</sup> Whicker,<sup>62</sup> Lindsay,<sup>63</sup> and others.

It is desirable to transform the equations of motion to a "natural" coordinate system (i.e., a coordinate system aligned normal and tangential to the cable), because hydrodynamic forces are usually defined as normal and tangential to the cable. The coordinate systems are shown in figure 14. Rotating about the y axis, the transform is

$$A1 = \begin{bmatrix} \cos \theta & 0 & \sin \theta \\ 0 & 1 & 0 \\ -\sin \theta & 0 & \cos \theta \end{bmatrix} .$$

Rotating about the z axis, the transform is

$$A2 = \begin{bmatrix} \cos \phi & \sin \phi & 0 \\ -\sin \phi & \cos \phi & 0 \\ 0 & 0 & 1 \end{bmatrix} .$$

For both rotations, we have that

$$A = A2 \cdot A1 ;$$

thus,

$$A = \begin{bmatrix} \cos \phi \cos \theta & \sin \phi & \cos \phi \sin \theta \\ -\sin \phi \cos \theta & \cos \phi & -\sin \phi \sin \theta \\ -\sin \theta & 0 & \cos \theta \end{bmatrix} . \quad (141)$$

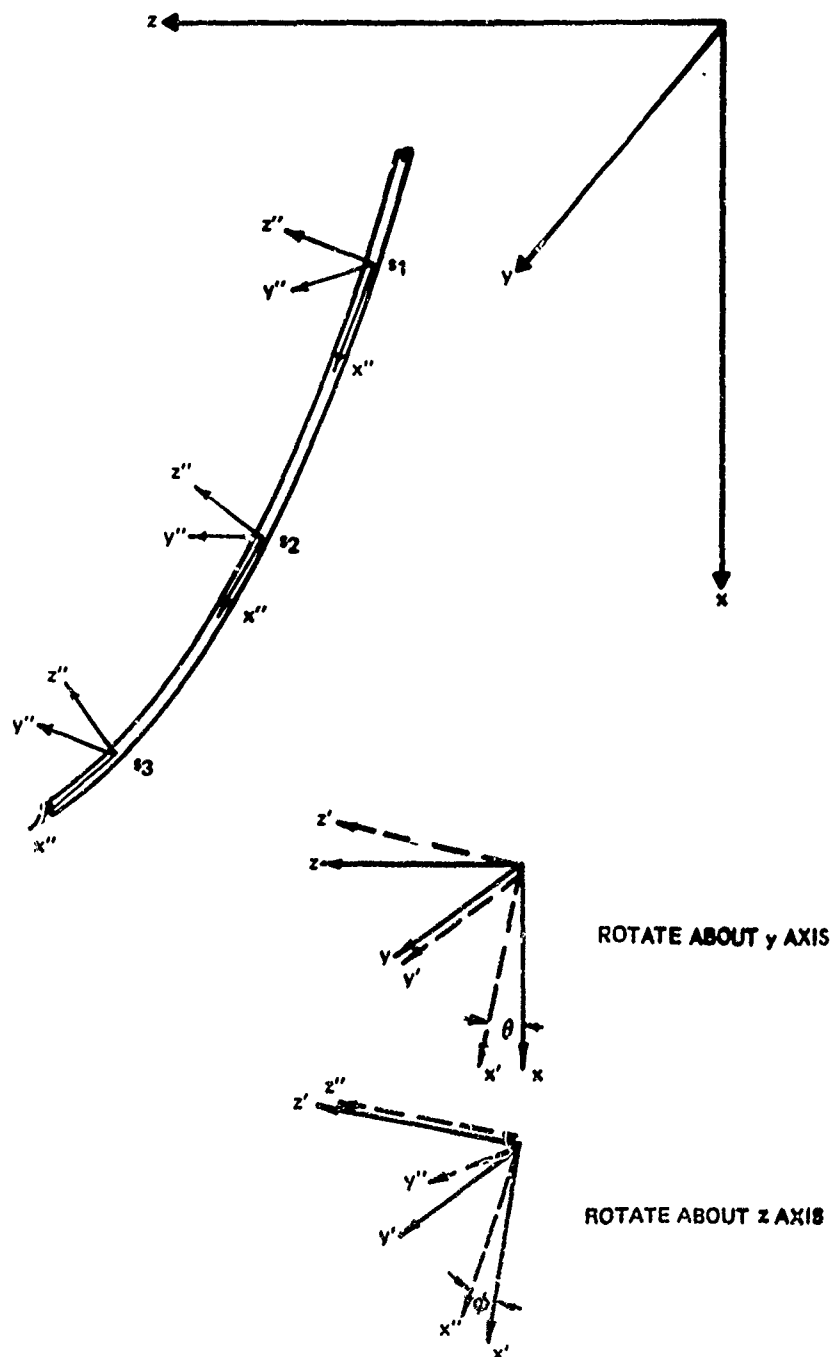


Figure 14. Cable Coordinates

A is the transform matrix from the  $x, y, z$  coordinate system to the  $x'', y'', z''$  system. Since A is orthogonal, we see that  $A^{-1} = A^t$ ; thus,

$$A^{-1} = \begin{bmatrix} \cos \phi \cos \theta & -\sin \phi \cos \theta & -\sin \theta \\ \sin \phi & & \\ \cos \phi \sin \theta & -\sin \phi \sin \theta & \cos \theta \end{bmatrix} . \quad (142)$$

In the double-primed system, let  $x''$  be along the cable and  $z''$  and  $y''$  normal to each other and the cable. Since  $\frac{1}{1+\epsilon} \left( \frac{\partial \vec{r}}{\partial S_0} \right)$  is a unit vector tangent to the cable,  $\frac{1}{1+\epsilon} \left( \frac{\partial \vec{r}}{\partial S_0} \right)$  transforms to  $\begin{bmatrix} 1 \\ 0 \\ 0 \end{bmatrix}$  in the double-primed coordinate system. This transformation is

$$\frac{1}{1+\epsilon} \left( \frac{\partial \vec{r}}{\partial S_0} \right) = A^{-1} \begin{bmatrix} 1 \\ 0 \\ 0 \end{bmatrix} ,$$

or

$$\left( \frac{1}{1+\epsilon} \right) \begin{bmatrix} \frac{\partial x}{\partial S_0} \\ \frac{\partial y}{\partial S_0} \\ \frac{\partial z}{\partial S_0} \end{bmatrix} = \begin{bmatrix} \cos \phi \cos \theta \\ \sin \phi \\ \cos \phi \sin \theta \end{bmatrix} . \quad (143)$$

The components of equation (143) are

$$\frac{\partial x}{\partial S_0} = (1+\epsilon) \cos \phi \cos \theta , \quad (144A)$$

$$\frac{\partial y}{\partial S_0} = (1+\epsilon) \sin \phi , \quad (144B)$$

and

$$\frac{\partial z}{\partial S_0} = (1+\epsilon) \cos \phi \sin \theta . \quad (144C)$$

Let H, G, and I be forces per unit length acting on the cable along the  $x''$ ,  $y''$ , and  $z''$  axes, respectively. In earth coordinates, the cable forces per unit length are

$$\begin{bmatrix} X \\ Y \\ Z \end{bmatrix} = A^{-1} \begin{bmatrix} H \\ G \\ I \end{bmatrix} . \quad (145)$$

Writing equations (139A), (139B), and (139C) in vector form (in the unprimed coordinate system), we see that

$$\begin{bmatrix} \frac{\partial}{\partial S_0} (T \cos \phi \cos \theta) \\ \frac{\partial}{\partial S_0} (T \sin \phi) \\ \frac{\partial}{\partial S_0} (T \cos \phi \sin \theta) \end{bmatrix} + A^{-1} \begin{bmatrix} H \\ G \\ I \end{bmatrix} = \mu(S_0) \begin{bmatrix} \frac{\partial u}{\partial t} \\ \frac{\partial v}{\partial t} \\ \frac{\partial w}{\partial t} \end{bmatrix} , \quad (146)$$

where  $u$ ,  $v$ , and  $w$  are velocities in the  $x$ ,  $y$ , and  $z$  directions, respectively.

Transforming to the double-primed coordinate system, equation (146) becomes

$$A \begin{bmatrix} \frac{\partial}{\partial S_0} (T \cos \phi \cos \theta) \\ \frac{\partial}{\partial S_0} (T \sin \phi) \\ \frac{\partial}{\partial S_0} (T \cos \phi \sin \theta) \end{bmatrix} + \begin{bmatrix} H \\ G \\ I \end{bmatrix} = \mu(S_0) A \begin{bmatrix} \frac{\partial u}{\partial t} \\ \frac{\partial v}{\partial t} \\ \frac{\partial w}{\partial t} \end{bmatrix} . \quad (147)$$

The first term on the left is

$$\begin{aligned}
 & \left[ \begin{aligned}
 & \frac{\partial T}{\partial S_0} (\cos^2 \phi \cos^2 \theta + \sin^2 \phi + \cos^2 \phi \sin^2 \theta) \\
 & + T \frac{\partial \phi}{\partial S_0} (-\cos^2 \theta \cos \phi \sin \phi + \sin \phi \cos \phi - \sin^2 \theta \sin \phi \cos \phi) \\
 & + T \frac{\partial \theta}{\partial S_0} (-\cos^2 \phi \sin \theta \cos \theta + \cos^2 \phi \sin \theta \cos \theta) \\
 & \frac{\partial T}{\partial S_0} (-\cos^2 \theta \sin \phi \cos \phi + \cos \phi \sin \phi - \sin^2 \theta \sin \phi \cos \phi) \\
 & + T \frac{\partial \phi}{\partial S_0} (\cos^2 \theta \sin^2 \phi + \cos^2 \phi + \sin^2 \theta \sin^2 \phi) \\
 & + T \frac{\partial \theta}{\partial S_0} (\sin \phi \cos \theta \sin \theta \cos \phi - \sin \phi \cos \theta \sin \theta \cos \phi) \\
 & \frac{\partial T}{\partial S_0} (-\sin \theta \cos \phi \cos \theta + \sin \theta \cos \theta \cos \phi) \\
 & + T \frac{\partial \phi}{\partial S_0} (\cos \theta \sin \theta \sin \phi - \cos \theta \sin \theta \sin \phi) \\
 & + T \frac{\partial \theta}{\partial S_0} (\cos \phi \sin^2 \theta + \cos \phi \cos^2 \theta)
 \end{aligned} \right]
 \end{aligned}$$

which can be reduced to

$$\begin{bmatrix} \frac{\partial T}{\partial S_0} \\ T \frac{\partial \phi}{\partial S_0} \\ T \cos \phi \frac{\partial \theta}{\partial S_0} \end{bmatrix}$$

(148)

Now consider the term on the right side of equation (147),

$$\mu(S_0) A \begin{bmatrix} \frac{\partial u}{\partial t} \\ \frac{\partial v}{\partial t} \\ \frac{\partial w}{\partial t} \end{bmatrix}$$

If  $U$ ,  $V$ , and  $W$  are the velocity components along the  $x''$ ,  $y''$ , and  $z''$  axes, respectively, the velocity components in inertial coordinates are

$$\begin{bmatrix} u \\ v \\ w \end{bmatrix} = A^{-1} \begin{bmatrix} U \\ V \\ W \end{bmatrix} ;$$

then, the acceleration components are

$$\begin{bmatrix} \frac{\partial u}{\partial t} \\ \frac{\partial v}{\partial t} \\ \frac{\partial w}{\partial t} \end{bmatrix} = \frac{\partial}{\partial t} (A^{-1}) \begin{bmatrix} U \\ V \\ W \end{bmatrix} + A^{-1} \begin{bmatrix} \frac{\partial U}{\partial t} \\ \frac{\partial V}{\partial t} \\ \frac{\partial W}{\partial t} \end{bmatrix} .$$

Multiply through by the mass density and the transformation matrix  $(A)$ ,

$$\mu(S) A \begin{bmatrix} \frac{\partial u}{\partial t} \\ \frac{\partial v}{\partial t} \\ \frac{\partial w}{\partial t} \end{bmatrix} = \mu(S) A \frac{\partial}{\partial t} (A^{-1}) \begin{bmatrix} U \\ V \\ W \end{bmatrix} + \mu(S) A A^{-1} \begin{bmatrix} \frac{\partial U}{\partial t} \\ \frac{\partial V}{\partial t} \\ \frac{\partial W}{\partial t} \end{bmatrix} . \quad (149)$$

Considering the first term on the right of equation (149), we see that

$$\frac{\partial}{\partial t} (A^{-1}) = \frac{\partial}{\partial t} \begin{bmatrix} \cos \phi \cos \theta & -\sin \phi \cos \theta & -\sin \theta \\ \sin \phi & \cos \phi & 0 \\ \cos \phi \sin \theta & -\sin \phi \sin \theta & \cos \theta \end{bmatrix}$$

or

$$= \begin{bmatrix} \begin{pmatrix} -\sin\theta \sin\phi \frac{\partial\phi}{\partial t} \\ -\cos\phi \sin\theta \frac{\partial\theta}{\partial t} \end{pmatrix} & \begin{pmatrix} -\cos\theta \cos\phi \frac{\partial\phi}{\partial t} \\ +\sin\phi \sin\theta \frac{\partial\theta}{\partial t} \end{pmatrix} & \begin{pmatrix} -\cos\theta \frac{\partial\theta}{\partial t} \end{pmatrix} \\ \begin{pmatrix} \cos\phi \frac{\partial\phi}{\partial t} \end{pmatrix} & \begin{pmatrix} -\sin\phi \frac{\partial\phi}{\partial t} \end{pmatrix} & 0 \\ \begin{pmatrix} -\sin\theta \sin\phi \frac{\partial\phi}{\partial t} \\ +\cos\phi \cos\theta \frac{\partial\theta}{\partial t} \end{pmatrix} & \begin{pmatrix} -\sin\theta \cos\phi \frac{\partial\phi}{\partial t} \\ -\sin\phi \cos\theta \frac{\partial\theta}{\partial t} \end{pmatrix} & \begin{pmatrix} -\sin\theta \frac{\partial\theta}{\partial t} \end{pmatrix} \end{bmatrix}$$

A further expansion of  $A \frac{\partial}{\partial t} (A^{-1})$  gives

$$\begin{bmatrix} \begin{pmatrix} -\cos^2\theta \cos\phi \sin\phi \frac{\partial\phi}{\partial t} \\ -\cos^2\phi \cos\theta \sin\theta \frac{\partial\theta}{\partial t} \\ +\sin\phi \cos\phi \frac{\partial\phi}{\partial t} \\ -\sin^2\theta \cos\phi \sin\phi \frac{\partial\phi}{\partial t} \\ +\cos^2\phi \cos\theta \sin\theta \frac{\partial\theta}{\partial t} \end{pmatrix} & \begin{pmatrix} -\cos^2\theta \cos^2\phi \frac{\partial\phi}{\partial t} \\ +\sin\phi \sin\theta \cos\phi \cos\theta \frac{\partial\theta}{\partial t} \\ -\sin^2\phi \frac{\partial\phi}{\partial t} \\ -\sin^2\theta \cos^2\phi \frac{\partial\phi}{\partial t} \\ -\sin\phi \sin\theta \cos\phi \cos\theta \frac{\partial\theta}{\partial t} \end{pmatrix} & \begin{pmatrix} -\cos\phi \cos^2\theta \frac{\partial\theta}{\partial t} \\ -\cos\phi \sin^2\theta \frac{\partial\theta}{\partial t} \end{pmatrix} \\ \begin{pmatrix} \cos^2\theta \sin^2\phi \frac{\partial\phi}{\partial t} \\ +\sin\phi \sin\theta \cos\theta \cos\phi \frac{\partial\theta}{\partial t} \\ +\cos^2\phi \frac{\partial\phi}{\partial t} \\ +\sin^2\phi \sin^2\theta \frac{\partial\phi}{\partial t} \\ -\sin\phi \sin\theta \cos\theta \cos\phi \frac{\partial\theta}{\partial t} \end{pmatrix} & \begin{pmatrix} \cos^2\theta \sin\phi \cos\phi \frac{\partial\phi}{\partial t} \\ -\sin^2\phi \cos\theta \sin\theta \frac{\partial\theta}{\partial t} \\ -\cos\phi \sin\phi \frac{\partial\phi}{\partial t} \\ +\sin^2\theta \sin\phi \cos\phi \frac{\partial\phi}{\partial t} \\ +\sin^2\phi \sin\theta \cos\theta \frac{\partial\theta}{\partial t} \end{pmatrix} & \begin{pmatrix} \cos^2\theta \sin\phi \frac{\partial\theta}{\partial t} \\ +\sin^2\theta \sin\phi \frac{\partial\theta}{\partial t} \end{pmatrix} \\ \begin{pmatrix} \sin\theta \cos\theta \sin\phi \frac{\partial\phi}{\partial t} \\ +\sin^2\theta \cos\phi \frac{\partial\theta}{\partial t} \\ -\sin\phi \cos\theta \sin\theta \frac{\partial\phi}{\partial t} \\ +\cos^2\theta \cos\phi \frac{\partial\theta}{\partial t} \end{pmatrix} & \begin{pmatrix} \sin\theta \cos\theta \cos\phi \frac{\partial\phi}{\partial t} \\ -\sin^2\theta \sin\phi \frac{\partial\theta}{\partial t} \\ -\sin\theta \cos\theta \cos\phi \frac{\partial\phi}{\partial t} \\ -\cos^2\theta \sin\phi \frac{\partial\theta}{\partial t} \end{pmatrix} & \begin{pmatrix} \sin\theta \cos\theta \frac{\partial\theta}{\partial t} \\ -\sin\theta \cos\theta \frac{\partial\theta}{\partial t} \end{pmatrix} \end{bmatrix}$$

The above matrix can be reduced, and we find that



$$A \frac{\partial}{\partial t} (A^{-1}) = \begin{bmatrix} 0 & -\frac{\partial \phi}{\partial t} & -\cos \phi \frac{\partial \theta}{\partial t} \\ \frac{\partial \phi}{\partial t} & 0 & \sin \phi \frac{\partial \theta}{\partial t} \\ \cos \phi \frac{\partial \theta}{\partial t} & -\sin \phi \frac{\partial \theta}{\partial t} & 0 \end{bmatrix}, \quad (150)$$

Substituting into equation (149), the accelerations become

$$\mu(S_0) A \begin{bmatrix} \frac{\partial u}{\partial t} \\ \frac{\partial v}{\partial t} \\ \frac{\partial w}{\partial t} \end{bmatrix} = \mu(S_0) \begin{bmatrix} \frac{\partial U}{\partial t} - V \frac{\partial \phi}{\partial t} - W \cos \phi \frac{\partial \theta}{\partial t} \\ \frac{\partial V}{\partial t} + U \frac{\partial \phi}{\partial t} + W \sin \phi \frac{\partial \theta}{\partial t} \\ \frac{\partial W}{\partial t} + U \cos \phi \frac{\partial \theta}{\partial t} - V \sin \phi \frac{\partial \theta}{\partial t} \end{bmatrix}. \quad (151)$$

Substituting equations (148) and (151) into equation (147) and writing the component equations, we obtain the equations of motion:

$$\frac{\partial T}{\partial S_0} + H = \mu(S_0) \left( \frac{\partial U}{\partial t} - V \frac{\partial \phi}{\partial t} - W \cos \phi \frac{\partial \theta}{\partial t} \right) \quad (152)$$

$$T \frac{\partial \phi}{\partial S_0} + G = \mu(S_0) \left( \frac{\partial V}{\partial t} + U \frac{\partial \phi}{\partial t} + W \sin \phi \frac{\partial \theta}{\partial t} \right) \quad (153)$$

$$T \cos \phi \frac{\partial \theta}{\partial S_0} + I = \mu(S_0) \left( \frac{\partial W}{\partial t} + U \cos \phi \frac{\partial \theta}{\partial t} - V \sin \phi \frac{\partial \theta}{\partial t} \right). \quad (154)$$

In addition, we have the strain definition,

$$\frac{\partial S}{\partial S_0} = 1 + \epsilon, \quad (155)$$

and the constitutive relation,

$$T = T(\epsilon) \quad (156)$$

Equations (152) through (156) give five equations in eight unknowns

$(T, \phi, \theta, U, V, W, S \& \epsilon)$ . Three more geometrical equations can be developed by considering the velocities. The velocities are

$$\begin{bmatrix} u \\ v \\ w \end{bmatrix} = A^{-1} \begin{bmatrix} U \\ V \\ W \end{bmatrix},$$

and the space derivative of the velocity vector is

$$\frac{\partial}{\partial S_0} \begin{bmatrix} u \\ v \\ w \end{bmatrix} = \frac{\partial}{\partial S_0} (A^{-1}) \begin{bmatrix} U \\ V \\ W \end{bmatrix} + A^{-1} \begin{bmatrix} \frac{\partial U}{\partial S_0} \\ \frac{\partial V}{\partial S_0} \\ \frac{\partial W}{\partial S_0} \end{bmatrix}. \quad (157)$$

Consider the left-hand term of equation (157). The space derivative of the

velocity, vector becomes

$$\frac{\partial}{\partial S_0} \begin{bmatrix} u \\ v \\ w \end{bmatrix} = \frac{\partial}{\partial S_0} \begin{bmatrix} \frac{\partial x}{\partial t} \\ \frac{\partial y}{\partial t} \\ \frac{\partial z}{\partial t} \end{bmatrix} = \frac{\partial}{\partial t} \begin{bmatrix} \frac{\partial x}{\partial S_0} \\ \frac{\partial y}{\partial S_0} \\ \frac{\partial z}{\partial S_0} \end{bmatrix}.$$

From equations (144A), (144B), and (144C), we see that

$$\frac{\partial}{\partial S_0} \begin{bmatrix} u \\ v \\ w \end{bmatrix} = \frac{\partial}{\partial t} \begin{bmatrix} (1+\epsilon) \cos \phi \cos \theta \\ (1+\epsilon) \sin \phi \\ (1+\epsilon) \cos \phi \sin \theta \end{bmatrix}.$$

(158)

Rewrite equation (157) and transform with A; thus

$$A A^{-1} \begin{bmatrix} \frac{\partial U}{\partial S_0} \\ \frac{\partial V}{\partial S_0} \\ \frac{\partial W}{\partial S_0} \end{bmatrix} = A \frac{\partial}{\partial S_0} \begin{bmatrix} u \\ v \\ w \end{bmatrix} - A \frac{\partial}{\partial S_0} (A^{-1}) \begin{bmatrix} U \\ V \\ W \end{bmatrix}$$

and

$$\begin{bmatrix} \frac{\partial U}{\partial S_0} \\ \frac{\partial V}{\partial S_0} \\ \frac{\partial W}{\partial S_0} \end{bmatrix} = A \frac{\partial}{\partial t} \begin{bmatrix} (1+\epsilon) \cos \phi \cos \theta \\ (1+\epsilon) \sin \phi \\ (1+\epsilon) \cos \phi \sin \theta \end{bmatrix} - A \frac{\partial}{\partial S_0} (A^{-1}) \begin{bmatrix} U \\ V \\ W \end{bmatrix}.$$

(159)

By analogy with the development of equation (148), the first term on the right-hand side of the above equation is

$$\begin{bmatrix} \frac{\partial \epsilon}{\partial t} \\ (1+\epsilon) \frac{\partial \phi}{\partial t} \\ (1+\epsilon) \cos \phi \frac{\partial \theta}{\partial t} \end{bmatrix} .$$

By analogy with the development of equation (150), the second term on the right-hand of equation (159) is

$$\begin{bmatrix} 0 & -\frac{\partial \phi}{\partial S_0} & -\cos \phi \frac{\partial \theta}{\partial S_0} \\ \frac{\partial \phi}{\partial S_0} & 0 & \sin \phi \frac{\partial \theta}{\partial S_0} \\ \cos \phi \frac{\partial \theta}{\partial S_0} & -\sin \phi \frac{\partial \theta}{\partial S_0} & 0 \end{bmatrix} .$$

Substituting into equation (159), and writing the component equations gives

$$\frac{\partial U}{\partial S_0} = \frac{\partial \epsilon}{\partial t} - \left( -V \frac{\partial \phi}{\partial S_0} - W \cos \phi \frac{\partial \theta}{\partial S_0} \right) , \quad (160A)$$

$$\frac{\partial V}{\partial S_0} = (1+\epsilon) \frac{\partial \phi}{\partial t} - \left( U \frac{\partial \phi}{\partial S_0} + W \sin \phi \frac{\partial \theta}{\partial S_0} \right) , \quad (160B)$$

and

$$\frac{\partial W}{\partial S_0} = (1+\epsilon) \cos \phi \frac{\partial \theta}{\partial t} - \left( U \cos \phi \frac{\partial \theta}{\partial S_0} - V \sin \phi \frac{\partial \theta}{\partial S_0} \right) . \quad (160C)$$

Rewriting the constitutive relation, we obtain the time derivative of tension:

$$\frac{\partial T}{\partial t} = \frac{dT}{d\epsilon} \frac{\partial \epsilon}{\partial t} .$$

Finally, the equations are summarized as follows:

$$\frac{\partial T}{\partial S_0} - \mu(S_0) \left( \frac{\partial U}{\partial t} - V \frac{\partial \phi}{\partial t} - W \cos \phi \frac{\partial \theta}{\partial t} \right) + H = 0, \quad (161)$$

$$T \frac{\partial \phi}{\partial S_0} - \mu(S_0) \left( \frac{\partial V}{\partial t} + U \frac{\partial \phi}{\partial t} + W \sin \phi \frac{\partial \theta}{\partial t} \right) + G = 0, \quad (162)$$

$$T \cos \phi \frac{\partial \theta}{\partial S_0} - \mu(S_0) \left( \frac{\partial W}{\partial t} + U \cos \phi \frac{\partial \theta}{\partial t} - V \sin \phi \frac{\partial \theta}{\partial t} \right) + I = 0, \quad (163)$$

$$\frac{\partial U}{\partial S_0} - \frac{\partial \epsilon}{\partial t} + \left( -V \frac{\partial \phi}{\partial S_0} - W \cos \phi \frac{\partial \theta}{\partial S_0} \right) = 0, \quad (164)$$

$$\frac{\partial V}{\partial S_0} - (1+\epsilon) \frac{\partial \phi}{\partial t} + \left( U \frac{\partial \phi}{\partial S_0} + W \sin \phi \frac{\partial \theta}{\partial S_0} \right) = 0, \quad (165)$$

$$\frac{\partial W}{\partial S_0} - (1+\epsilon) \cos \phi \frac{\partial \theta}{\partial t} + \left( U \cos \phi \frac{\partial \theta}{\partial S_0} - V \sin \phi \frac{\partial \theta}{\partial S_0} \right) = 0 \quad (166)$$

and

$$\frac{\partial T}{\partial t} - \frac{dT}{d\epsilon} \frac{\partial \epsilon}{\partial t} = 0. \quad (167)$$

We have seven, nonlinear, partial differential equations in seven unknowns.

Using the constitutive relation equation (167), these reduce to six equations with six unknowns. Jeffrey and Taniuti<sup>64</sup> show that an analytic solution in the form of a power series for a single, nonlinear, hyperbolic, partial differential equation can only be obtained locally, or "in the small" for a point  $P$  on a noncharacteristic curve  $\mathcal{T}$  in the time-space plane. Physically, it is known that the

flexible cable can propagate both tensile stress waves and transverse flexural waves. It is also known that the characteristic velocity of the transverse waves is a function of the state of stress of the cable. Thus, the usual method of characteristics approach to solve nonlinear wave equations is not tractable because the characteristics diverge in the time-space domain. Solutions must be obtained simultaneously at the same locations in the time-space domain in order to continually update the transverse wave characteristic. A numerical method, which is an extension of Hartree's "hybrid" method,<sup>65-70</sup> will be employed to conduct simultaneous integrations at nodal points of a rectangular grid in the time-space domain. Because this method utilizes integration along characteristics in the immediate vicinity of the time-space grid nodal points, it is necessary to rewrite the cable equations in their "normal" form, i.e., characteristic equations.

First, the characteristics must be found. Assume a linear variation of tension with strain. Equation (167) reduces to

$$T = \frac{dT}{d\epsilon} \epsilon = K \epsilon .$$

Rewriting equations (161) through (166) in the form  $AU_t + BU_s + C = 0$  (168)

gives

$$\begin{bmatrix} 0 & \mu V & \mu W \cos \phi & -\mu & 0 & 0 \\ 0 & -\mu U & -\mu W \sin \phi & 0 & -\mu & 0 \\ 0 & 0 & -\mu(U \cos \phi - V \sin \phi) & 0 & 0 & -\mu \\ -1 & 0 & 0 & 0 & 0 & 0 \\ 0 & -(1+\epsilon) & 0 & 0 & 0 & 0 \\ 0 & 0 & -(1+\epsilon) \cos \phi & 0 & 0 & 0 \end{bmatrix} \begin{bmatrix} \partial \epsilon / \partial t \\ \partial \phi / \partial t \\ \partial \theta / \partial t \\ \partial U / \partial t \\ \partial V / \partial t \\ \partial W / \partial t \end{bmatrix} + C = 0$$

$$+ \begin{bmatrix} \frac{dT}{d\epsilon} & 0 & 0 & 0 & 0 & 0 \\ 0 & \epsilon \frac{dT}{d\epsilon} & 0 & 0 & 0 & 0 \\ 0 & 0 & \epsilon \frac{dT}{d\epsilon} \cos \phi & 0 & 0 & 0 \\ 0 & -V & -W \cos \phi & 1 & 0 & 0 \\ 0 & U & W \sin \phi & 0 & 1 & 0 \\ 0 & 0 & (U \cos \phi - V \sin \phi) & 0 & 0 & 1 \end{bmatrix} \begin{bmatrix} \frac{\partial \epsilon}{\partial S_0} \\ \frac{\partial \phi}{\partial S_0} \\ \frac{\partial \theta}{\partial S_0} \\ \frac{\partial U}{\partial S_0} \\ \frac{\partial V}{\partial S_0} \\ \frac{\partial W}{\partial S_0} \end{bmatrix} + \begin{bmatrix} H \\ G \\ I \\ 0 \\ 0 \\ 0 \end{bmatrix} = 0$$

Rewriting equation (168), we see that

$$A^{-1} A U_t + A^{-1} B U_s + A^{-1} C = 0 ,$$

or

$$U_t + A^{-1} B U_s + A^{-1} C = 0 . \quad (169)$$

The six characteristics are derived from equation (169). This derivation is shown in detail in appendix C. From appendix C the six equations (equations (161) through (166)) yield six characteristics:

$$\lambda_1 = + \sqrt{\frac{1}{\mu(S_0)} \frac{dT}{d\epsilon}} , \quad (170)$$

$$\lambda_2 = - \sqrt{\frac{1}{\mu(S_0)} \frac{dT}{d\epsilon}} , \quad (171)$$

$$\lambda_3 = + \sqrt{\frac{1}{\mu(S_0)} \frac{\epsilon}{(1+\epsilon)} \frac{dT}{d\epsilon}} , \quad (172)$$

$$\lambda_4 = -\sqrt{\frac{1}{\mu(s_0)} \frac{\epsilon}{(1+\epsilon)} \frac{dT}{d\epsilon}} , \quad (173)$$

$$\lambda_5 = +\sqrt{\frac{1}{\mu(s_0)} \frac{\epsilon}{(1+\epsilon)} \frac{dT}{d\epsilon}} , \quad (174)$$

and

$$\lambda_6 = -\sqrt{\frac{1}{\mu(s_0)} \frac{\epsilon}{(1+\epsilon)} \frac{dT}{d\epsilon}} . \quad (175)$$

Rewrite the cable equations in their normal form using the characteristics. To find the characteristic equations, we can write equation (161) in terms of  $\epsilon$  using the constitutive relation (equation (167)) multiplied by  $\frac{1}{\mu}$  and subtract from equation (164) multiplied by  $ds$ . This operation is

$$\begin{aligned} & \left[ \frac{1}{\mu} \frac{dT}{d\epsilon} \frac{\partial \epsilon}{\partial s} dt - \left( \frac{\partial U}{\partial t} dt - V \frac{\partial \phi}{\partial t} dt - W \cos \phi \frac{\partial \theta}{\partial t} dt \right) \right. \\ & \quad \left. + \frac{1}{\mu} H dt \right] \\ & + \left[ \frac{\partial U}{\partial s} ds - \frac{\partial \epsilon}{\partial t} ds + \left( -V \frac{\partial \phi}{\partial s} ds - W \cos \phi \frac{\partial \theta}{\partial s} ds \right) \right] = 0 . \end{aligned} \quad (176)$$

Since there are only two independent variables,  $s$  and  $t$ , the total differential of any dependent variable, for example  $U$ , is

$$dU = \frac{\partial U}{\partial s} ds + \frac{\partial U}{\partial t} dt . \quad (177)$$



The variables in equation (176) are expanded as follows:

$$-\frac{1}{\mu} \frac{dT}{d\epsilon} \frac{\partial \epsilon}{\partial s} dt - \frac{\partial \epsilon}{\partial t} ds + \frac{\partial U}{\partial t} dt + \frac{\partial U}{\partial s} ds - V \frac{\partial \phi}{\partial t} dt - V \frac{\partial \phi}{\partial s} ds - W \cos \phi \frac{\partial \theta}{\partial t} dt - W \cos \phi \frac{\partial \theta}{\partial s} ds - \frac{1}{\mu} H dt = 0, \quad (178)$$

or

$$-\frac{1}{\mu} \frac{dT}{d\epsilon} \frac{\partial \epsilon}{\partial s} dt - \frac{\partial \epsilon}{\partial t} ds + dU - V d\phi - W \cos \phi d\theta - \frac{1}{\mu} H dt = 0. \quad (179)$$

In terms of the characteristic values,  $\lambda$ , we see that

$$\left(-\lambda_{1,2}^2 \frac{\partial \epsilon}{\partial s} - \frac{1}{\mu} H\right) dt - \frac{\partial \epsilon}{\partial t} ds + dU - V d\phi - W \cos \phi d\theta = 0, \quad (180)$$

where  $\lambda_{1,2} = \pm \sqrt{\frac{1}{\mu} \frac{dT}{d\epsilon}}$  are the axial wave characteristics

in the  $t$ - $s$  plane; hence,

$$\frac{ds}{dt} = \pm \sqrt{\frac{1}{\mu} \frac{dT}{d\epsilon}}.$$

The characteristic equation becomes

$$-\sqrt{\frac{1}{\mu} \frac{dT}{d\epsilon}} \cdot d\epsilon + dU - V d\phi - W \cos \phi d\theta - \frac{1}{\mu} H dt = 0. \quad (181)$$

This equation represents the motion of the cable in the axial direction (stretching).

If we let the  $\alpha$  characteristic be associated with  $+\sqrt{\frac{1}{\mu} \frac{dT}{d\epsilon}}$  and represent disturbances traveling down the cable, we see that

$$\frac{dU}{d\alpha} - \sqrt{\frac{1}{\mu} \frac{dT}{d\epsilon}} \frac{d\epsilon}{d\alpha} - V \frac{d\phi}{d\alpha} - W \cos \phi \frac{d\theta}{d\alpha} - \frac{1}{\mu} H \frac{dt}{d\alpha} = 0. \quad (182)$$

Similarly, let  $\beta$  be associated with disturbances traveling up the cable,

$$-\sqrt{\frac{1}{\mu} \frac{dT}{d\epsilon}} ; \text{ then,}$$

$$\frac{dU}{d\beta} + \sqrt{\frac{1}{\mu} \frac{dT}{d\epsilon}} \frac{d\epsilon}{d\beta} - V \frac{d\phi}{d\beta} - W \cos \phi \frac{d\theta}{d\beta} - \frac{1}{\mu} H \frac{dt}{d\beta} = 0. \quad (183)$$

Again. equation (162) multiplied by  $(1/\mu) dt$  is subtracted from equation (165)

multiplied by  $ds$  to give

$$\begin{aligned} \frac{\partial V}{\partial s} ds + \frac{\partial V}{\partial t} dt + U \frac{\partial \phi}{\partial s} ds + U \frac{\partial \phi}{\partial t} dt + W \sin \phi \frac{\partial \theta}{\partial s} ds \\ + W \sin \phi \frac{\partial \theta}{\partial t} dt - (1+\epsilon) \frac{\partial \phi}{\partial t} ds - \frac{\epsilon}{\mu} \frac{dT}{d\epsilon} \frac{\partial \phi}{\partial s} dt - \frac{1}{\mu} G dt = 0. \end{aligned}$$

Dividing through by  $(1+\epsilon)$ , we find that

$$\begin{aligned} -\left(\frac{1}{\mu} \frac{\epsilon}{(1+\epsilon)} \frac{dT}{d\epsilon} \frac{\partial \phi}{\partial s} dt + \frac{\partial \phi}{\partial t} ds\right) + \frac{1}{(1+\epsilon)} U d\phi + \frac{1}{(1+\epsilon)} dV \\ + \frac{1}{(1+\epsilon)} W \sin \phi d\theta - \frac{1}{\mu(1+\epsilon)} G dt = 0. \end{aligned}$$

The transverse wave characteristics in the  $t$ - $s$  plane are

$$\lambda_{3,4} = \pm \sqrt{\frac{1}{\mu} \frac{\epsilon}{(1+\epsilon)} \frac{dT}{d\epsilon}} ;$$

hence,

$$\frac{ds}{dt} = \pm \sqrt{\frac{1}{\mu} \frac{\epsilon}{(1+\epsilon)} \frac{dT}{d\epsilon}},$$

and

$$dV - (1+\epsilon) \sqrt{\frac{1}{\mu} \frac{\epsilon}{(1+\epsilon)} \frac{dT}{d\epsilon}} d\phi + U d\phi + W \sin \phi d\theta - \frac{1}{\mu} G dt = 0.$$

Let the  $\alpha$  characteristic be associated with  $+\sqrt{\frac{1}{\mu} \frac{\epsilon}{(1+\epsilon)} \frac{dT}{d\epsilon}}$  and

represent disturbances traveling down the cable in the  $y''$ - $x''$  plane:

$$\frac{dV}{d\alpha} - \left( (1+\epsilon) \sqrt{\frac{1}{\mu} \frac{\epsilon}{(1+\epsilon)}} \frac{dT}{d\epsilon} + U \right) \frac{d\phi}{d\alpha} + W \sin\phi \frac{d\theta}{d\alpha} - \frac{1}{\mu} G \frac{dt}{d\alpha} = 0. \quad (184)$$

Let the  $\beta$  characteristic be associated with  $-\sqrt{\frac{1}{\mu} \frac{\epsilon}{(1+\epsilon)}} \frac{dT}{d\epsilon}$  and represent disturbances traveling up the cable in the  $y'' - x''$  plane:

$$\frac{dV}{d\beta} + \left( (1+\epsilon) \sqrt{\frac{1}{\mu} \frac{\epsilon}{(1+\epsilon)}} \frac{dT}{d\epsilon} - U \right) \frac{d\phi}{d\beta} + W \sin\phi \frac{d\theta}{d\beta} - \frac{1}{\mu} G \frac{dt}{d\beta} = 0. \quad (185)$$

Finally, equation (163) multiplied by  $(\frac{1}{\mu})dt$  is subtracted from equation (166) multiplied by  $ds$  to give

$$\begin{aligned} & -(1+\epsilon) \cos\phi \left( \frac{\partial\theta}{\partial t} ds + \frac{1}{\mu} \frac{\epsilon}{(1+\epsilon)} \frac{dT}{d\epsilon} \frac{\partial\theta}{\partial s} dt \right) + dW \\ & + (U \cos\phi - V \sin\phi) d\theta - \frac{1}{\mu} I dt = 0. \end{aligned}$$

The transverse wave characteristic in the  $t-s$  plane is

$$\lambda_{s,t} = \pm \sqrt{\frac{1}{\mu} \frac{\epsilon}{(1+\epsilon)}} \frac{dT}{d\epsilon};$$

hence

$$\frac{ds}{dt} = \pm \sqrt{\frac{1}{\mu} \frac{\epsilon}{(1+\epsilon)}} \frac{dT}{d\epsilon}.$$

and

$$dW - (1+\epsilon) \cos\phi \sqrt{\frac{1}{\mu} \frac{\epsilon}{(1+\epsilon)}} \frac{dT}{d\epsilon} \cdot d\theta + (U \cos\phi - V \sin\phi) d\theta - \frac{1}{\mu} I dt = 0.$$

Let the  $\alpha$  characteristic be associated with  $+\sqrt{\frac{1}{\mu} \frac{\epsilon}{(1+\epsilon)}} \frac{dT}{d\epsilon}$  and

represent disturbances traveling down the cable in the  $z'' - x''$  plane:

$$\frac{dW}{d\alpha} - \left( (1+\epsilon) \cos\phi \sqrt{\frac{1}{\mu} \frac{\epsilon}{(1+\epsilon)}} \frac{dT}{d\epsilon} - (U \cos\phi - V \sin\phi) \right) \frac{d\theta}{d\alpha} - \frac{1}{\mu} I \frac{dt}{d\alpha} = 0. \quad (186)$$

Let the  $\beta$  characteristic be associated with  $-\sqrt{\frac{1}{\mu} \frac{\epsilon}{(1+\epsilon)}} \frac{dT}{d\epsilon}$  and

represent disturbances traveling up the cable in the  $z'' - x''$  plane:

$$\frac{dW}{d\beta} + \left( (1+\epsilon) \cos\phi \sqrt{\frac{1}{\mu} \frac{\epsilon}{(1+\epsilon)} \frac{dT}{d\epsilon}} + (U \cos\phi - V \sin\phi) \right) \frac{d\theta}{d\beta} - \frac{1}{\mu} I \frac{dt}{d\beta} = 0 \quad (187)$$

The characteristic equations are now summarized. For tensile waves traveling down the cable with velocity  $+\sqrt{\frac{1}{\mu(s)} \frac{dT}{d\epsilon}}$ , we have

$$\frac{dU}{d\alpha} - \sqrt{\frac{1}{\mu(s)} \frac{dT}{d\epsilon}} \frac{d\epsilon}{d\alpha} - V \frac{d\phi}{d\alpha} - W \cos\phi \frac{d\theta}{d\alpha} - \frac{1}{\mu(s)} H \frac{dt}{d\alpha} = 0 \quad (188)$$

For tensile waves traveling up the cable with velocity  $-\sqrt{\frac{1}{\mu(s)} \frac{dT}{d\epsilon}}$ , we have

$$\frac{dU}{d\beta} + \sqrt{\frac{1}{\mu(s)} \frac{dT}{d\epsilon}} \frac{d\epsilon}{d\beta} - V \frac{d\phi}{d\beta} - W \cos\phi \frac{d\theta}{d\beta} - \frac{1}{\mu(s)} H \frac{dt}{d\beta} = 0 \quad (189)$$

For transverse waves in the  $y'' - x''$  plane traveling down the cable with velocity  $+\sqrt{\frac{1}{\mu(s)} \frac{\epsilon}{(1+\epsilon)} \frac{dT}{d\epsilon}}$ , we have

$$\frac{dV}{d\alpha} - \left( (1+\epsilon) \sqrt{\frac{1}{\mu(s)} \frac{\epsilon}{(1+\epsilon)} \frac{dT}{d\epsilon}} + U \right) \frac{d\phi}{d\alpha} + W \sin\phi \frac{d\theta}{d\alpha} - \frac{1}{\mu(s)} G \frac{dt}{d\alpha} = 0 \quad (190)$$

For transverse waves in the  $y'' - x''$  plane traveling up the cable with velocity  $-\sqrt{\frac{1}{\mu(s)} \frac{\epsilon}{(1+\epsilon)} \frac{dT}{d\epsilon}}$ , we have

$$\frac{dV}{d\beta} + \left( (1+\epsilon) \sqrt{\frac{1}{\mu(s)} \frac{\epsilon}{(1+\epsilon)} \frac{dT}{d\epsilon}} - U \right) \frac{d\phi}{d\beta} + W \sin\phi \frac{d\theta}{d\beta} - \frac{1}{\mu(s)} G \frac{dt}{d\beta} = 0 \quad (191)$$

For transverse waves in the  $z'' - x''$  plane traveling down the cable with velocity  $+\sqrt{\frac{1}{\mu(s)} \frac{\epsilon}{(1+\epsilon)} \frac{dT}{d\epsilon}}$ , we have

$$\frac{dW}{d\alpha} - \left( (1+\epsilon) \cos \phi \sqrt{\frac{1}{\mu(s)} \frac{\epsilon}{(1+\epsilon)} \frac{dT}{d\epsilon}} - (U \cos \phi - V \sin \phi) \right) \frac{d\theta}{d\alpha} - \frac{1}{\mu(s)} I \frac{dt}{d\alpha} = 0 \quad (192)$$

For transverse waves in the  $z'' - x''$  plane traveling up the cable with velocity

$$-\sqrt{\frac{1}{\mu(s)} \frac{\epsilon}{(1+\epsilon)} \frac{dT}{d\epsilon}}, \text{ we have}$$

$$\frac{dW}{d\beta} + \left( (1+\epsilon) \cos \phi \sqrt{\frac{1}{\mu(s)} \frac{\epsilon}{(1+\epsilon)} \frac{dT}{d\epsilon}} + (U \cos \phi - V \sin \phi) \right) \frac{d\theta}{d\beta} - \frac{1}{\mu(s)} I \frac{dt}{d\beta} = 0 \quad (193)$$

Equations (188) through (193) form the basis for a numerical solution of the three-dimensional equations of motion for a buoy mooring cable. The original set of six partial differential equations with six unknowns has been transformed to a set of six ordinary differential equations with six unknowns with the restriction that integration operations must be carried out along characteristic curves.

The solution of sets of coupled, nonlinear, partial differential equations with different characteristic velocities is usually accomplished by assuming that the equations can be decoupled. At best, they can then be linearized and a separation of variables method can be used to obtain an analytical solution. At worst, the normal forms can be integrated numerically along characteristics.

Examination of the functional form of the transverse wave characteristics show that they are dependent on the state of stress in the cable. Thus, the cable equations can not be decoupled if they are subject to time or space varying forces. Also, the particular cable system studied here is a combined initial value — boundary value system:

1. All the dependent parameters are known at time = 0.
2. The displacements at the lower bound (anchor) are constants for all time and their time derivations are zero.
3. The displacements at the upper bound (buoy motions) must be solved for simultaneously as are cable motions.

Buoy system cable motions, as posed here, can best be handled numerically with a modification of Hartree's method, i.e., solving for the values of the dependent variables at rectangular grid nodes in the time-space domain. Hartree's method, as described by Ames,<sup>66</sup> was developed for a single hyperbolic equation whose coefficients may be time or space dependent. In this study, the basic method will be extended for a set of coupled hyperbolic equations with variable coefficients.

### 3.2.2 Finite-Difference Methods

Consider a rectangular grid in the time-space plane (figure 15). Assume that the values of the six independent parameters are known at the nodal points on the  $j$ th time line. It is desired to advance the solution to the nodal points on the  $(j + 1)$ th time line; specifically, for the  $i$ th point  $R$ . If the characteristics are known at point  $R$ , characteristic lines can be drawn back from  $R$  to intersect the  $j$ th time line. The six parameter values at points  $B$ ,  $A$ , and  $D$  can be linearly interpolated to find the values at each intersection point,  $P_1$ ,  $P_2$ ,  $Q_1$ , and  $Q_2$ . Now, the characteristic equations, (188) through (193), can be used to advance the solution to point  $R$ . For tensile waves, the length between point  $A$  and point  $P_1$  in the grid is

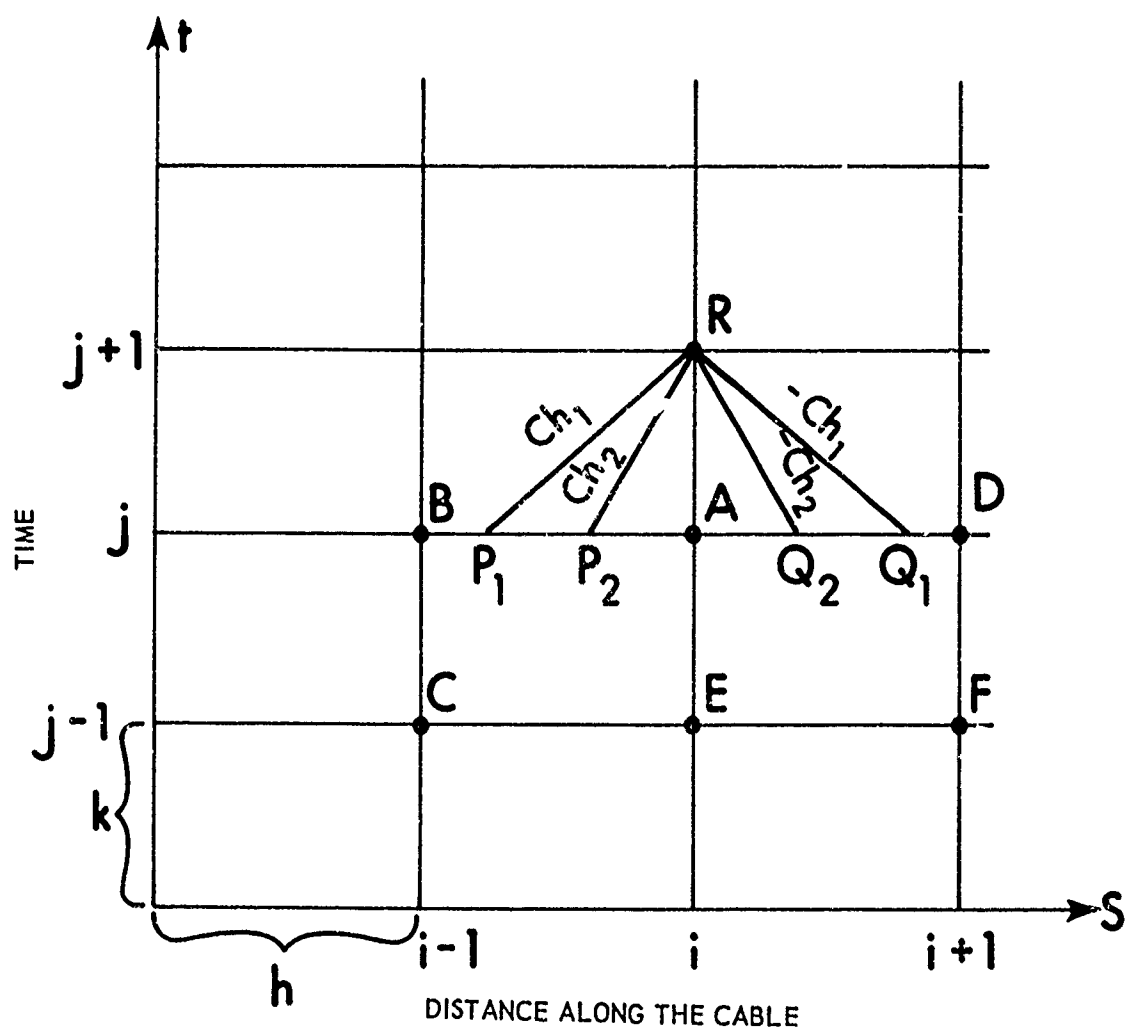


Figure 15. Grid for Adaptation of Hartree's Method

$$S_R - S_{P_1} = \frac{1}{2} (Ch_{1R} + Ch_{1P_1}) \cdot k$$

If constant cable mass and modulus is assumed, the tensile characteristic is independent of the tension; thus,

$$Ch_{1R} = Ch_{1P_1} = Ch_1 = \sqrt{\frac{1}{\mu} \frac{dT}{d\epsilon}}$$

The location of point  $P_1$  is given by  $S_R - S_{P_1} = Ch_1 \cdot k$ ; in a similar manner, point  $Q_1$  (associated with tensile waves propagating up the cable) is given by  $S_R - S_{Q_1} = -Ch_1 \cdot k$ . For tensile waves traveling down the cable, the finite-difference equation is

$$\begin{aligned} U_R - U_{P_1} - \frac{1}{2} (Ch_{1R} + Ch_{1P_1}) (\epsilon_R - \epsilon_{P_1}) - \frac{1}{2} (V_R + V_{P_1}) (\phi_R - \phi_{P_1}) \\ - \frac{1}{2} (W_R + W_{P_1}) \left[ \cos\left(\frac{1}{2} (\phi_R + \phi_{P_1})\right) \right] (\theta_R - \theta_{P_1}) \\ - \frac{1}{\mu} \cdot \frac{1}{2} (H_R + H_{P_1}) \cdot k = 0 \end{aligned} \quad (194)$$

For tensile waves traveling up the cable, the finite-difference equation is

$$\begin{aligned} U_R - U_{Q_1} + \frac{1}{2} (Ch_{1R} + Ch_{1Q_1}) (\epsilon_R - \epsilon_{Q_1}) - \frac{1}{2} (V_R + V_{Q_1}) (\phi_R - \phi_{Q_1}) \\ - \frac{1}{2} (W_R + W_{Q_1}) \left[ \cos\left(\frac{1}{2} (\phi_R + \phi_{Q_1})\right) \right] (\theta_R - \theta_{Q_1}) \\ - \frac{1}{\mu} \cdot \frac{1}{2} (H_R + H_{Q_1}) \cdot k = 0 \end{aligned} \quad (195)$$

For transverse waves in the  $y'' - x''$  plane traveling down the cable, point  $P_2$  is located by

$$S_R - S_{P_2} = \frac{1}{2} (Ch_{2R} + Ch_{2P_2}) \cdot k,$$

where

$$Ch_{2R} = \sqrt{\frac{1}{\mu} \frac{\epsilon}{(1+\epsilon)} \frac{dT}{d\epsilon}}$$



The finite-difference equation is

$$\begin{aligned}
 V_R - V_{P_2} - \frac{1}{2} (Ch_{2R} + Ch_{2P_2}) (\phi_R - \phi_{P_2}) \\
 + \frac{1}{2} (W_R + W_{P_2}) \left[ \sin\left(\frac{1}{2} (\phi_R + \phi_{P_2})\right) \right] (\theta_R - \theta_{P_2}) \\
 - \frac{1}{\mu} \cdot \frac{1}{2} (G_R + G_{P_2}) \cdot k = 0 .
 \end{aligned} \tag{196}$$

For transverse waves in the  $y'' - x''$  plane traveling up the cable, point  $Q_2$  is located by

$$S_R - S_{Q_2} = -\frac{1}{2} (Ch_{2R} + Ch_{2Q_2}) \cdot k .$$

The finite-difference equation is

$$\begin{aligned}
 V_R - V_{Q_2} + \frac{1}{2} (Ch_{2R} + Ch_{2Q_2}) (\phi_R - \phi_{Q_2}) \\
 + \frac{1}{2} (W_R + W_{Q_2}) \left[ \sin\left(\frac{1}{2} (\phi_R + \phi_{Q_2})\right) \right] (\theta_R - \theta_{Q_2}) \\
 - \frac{1}{\mu} \cdot \frac{1}{2} (G_R + G_{Q_2}) \cdot k = 0 .
 \end{aligned} \tag{197}$$

For transverse waves in the  $z'' - x''$  plane traveling down the cable (note that the characteristics for the transverse waves are the same), the finite-difference equation is

$$\begin{aligned}
 W_R - W_{P_2} - \left\{ \frac{1}{2} [(1+\epsilon_R) Ch_{2R} + (1+\epsilon_{P_2}) Ch_{2P_2}] \cos\left(\frac{1}{2} (\phi_R + \phi_{P_2})\right) \right. \\
 \left. - \frac{1}{2} (U_R + U_{P_2}) \cos\left(\frac{1}{2} (\phi_R + \phi_{P_2})\right) + \frac{1}{2} (V_R + V_{P_2}) \sin\left(\frac{1}{2} (\phi_R + \phi_{P_2})\right) \right\} (\theta_R - \theta_{P_2}) \\
 - \frac{1}{\mu} \cdot \frac{1}{2} (I_R + I_{P_2}) \cdot k = 0 .
 \end{aligned} \tag{198}$$

For transverse waves in the  $z'' - x''$  plane traveling up the cable, the finite-

difference equation is

$$\begin{aligned}
 W_R - W_{Q_2} + \left\{ \frac{1}{2} [(1+\epsilon_R) Ch_{2R} + (1+\epsilon_{Q_2}) Ch_{2Q_2}] \cos\left(\frac{1}{2}(\phi_R + \phi_{Q_2})\right) \right. \\
 \left. + \frac{1}{2} (U_R + U_{Q_2}) \cos\left(\frac{1}{2}(\phi_R + \phi_{Q_2})\right) - \frac{1}{2} (V_R + V_{Q_2}) \sin\left(\frac{1}{2}(\phi_R + \phi_{Q_2})\right) \right\} (\theta_R - \theta_{Q_2}) \\
 - \frac{1}{\mu} \cdot \frac{1}{2} (I_R + I_{Q_2}) \cdot k = 0 .
 \end{aligned} \tag{199}$$

Rewriting the six finite-difference equations, we see that

$$\begin{aligned}
 U_R - \frac{1}{2} (Ch_{1R} + Ch_{1P_1}) \epsilon_R - \frac{1}{2} (V_R + V_{P_1}) \phi_R - \frac{1}{2} (W_R + W_{P_1}) \left[ \cos\left(\frac{1}{2}(\phi_R + \phi_{P_1})\right) \right] \theta_R \\
 + \left\{ -U_{P_1} + \frac{1}{2} (Ch_{1R} + Ch_{1P_1}) \epsilon_{P_1} + \frac{1}{2} (V_R + V_{P_1}) \phi_{P_1} + \frac{1}{2} (W_R + W_{P_1}) \left[ \cos\left(\frac{1}{2}(\phi_R + \phi_{P_1})\right) \right] \theta_{P_1} \right. \\
 \left. - \frac{1}{\mu} \cdot \frac{1}{2} (H_R + H_{P_1}) \cdot k \right\} = 0 ,
 \end{aligned} \tag{200}$$

$$\begin{aligned}
 U_R + \frac{1}{2} (Ch_{1R} + Ch_{1Q_1}) \epsilon_R - \frac{1}{2} (V_R + V_{Q_1}) \phi_R - \frac{1}{2} (W_R + W_{Q_1}) \left[ \cos\left(\frac{1}{2}(\phi_R + \phi_{Q_1})\right) \right] \theta_R \\
 + \left\{ -U_{Q_1} - \frac{1}{2} (Ch_{1R} + Ch_{1Q_1}) \epsilon_{Q_1} + \frac{1}{2} (V_R + V_{Q_1}) \phi_{Q_1} + \frac{1}{2} (W_R + W_{Q_1}) \left[ \cos\left(\frac{1}{2}(\phi_R + \phi_{Q_1})\right) \right] \theta_{Q_1} \right. \\
 \left. - \frac{1}{\mu} \cdot \frac{1}{2} (H_R + H_{Q_1}) \cdot k \right\} = 0 ,
 \end{aligned} \tag{201}$$

$$\begin{aligned}
 V_R - \frac{1}{2} ((1+\epsilon_R) Ch_{2R} + (1+\epsilon_{P_2}) Ch_{2P_2}) \phi_R + \frac{1}{2} (W_R + W_{P_2}) \left[ \sin\left(\frac{1}{2}(\phi_R + \phi_{P_2})\right) \right] \theta_R \\
 + \left\{ -V_{P_2} + \frac{1}{2} ((1+\epsilon_R) Ch_{2R} + (1+\epsilon_{P_2}) Ch_{2P_2}) \phi_{P_2} \right. \\
 \left. - \frac{1}{2} (W_R + W_{P_2}) \left[ \sin\left(\frac{1}{2}(\phi_R + \phi_{P_2})\right) \right] \theta_{P_2} - \frac{1}{\mu} \cdot \frac{1}{2} (G_R + G_{P_2}) \cdot k \right\} = 0 ,
 \end{aligned} \tag{202}$$

$$\begin{aligned}
& V_R + \frac{1}{2} \left( (1+\epsilon_R) Ch_{2R} + (1+\epsilon_{Q_2}) Ch_{2Q_2} \right) \phi_R + \frac{1}{2} (W_R + W_{Q_2}) \left[ \sin\left(\frac{1}{2}(\phi_R + \phi_{Q_2})\right) \right] \theta_R \\
& + \left\{ -V_{Q_2} - \frac{1}{2} \left( (1+\epsilon_R) Ch_{2R} + (1+\epsilon_{Q_2}) Ch_{2Q_2} \right) \phi_{Q_2} \right. \\
& \left. - \frac{1}{2} (W_R + W_{Q_2}) \left[ \sin\left(\frac{1}{2}(\phi_R + \phi_{Q_2})\right) \right] \theta_{Q_2} - \frac{1}{\mu} \frac{1}{2} (G_R + G_{Q_2}) \cdot k \right\} = 0, \quad (203)
\end{aligned}$$

$$\begin{aligned}
& W_R - \left\{ \frac{1}{2} \left( (1+\epsilon_R) Ch_{2R} + (1+\epsilon_{P_2}) Ch_{2P_2} \right) \cos\left(\frac{1}{2}(\phi_R + \phi_{P_2})\right) \right. \\
& \left. - \frac{1}{2} (U_R + U_{P_2}) \cos\left(\frac{1}{2}(\phi_R + \phi_{P_2})\right) + \frac{1}{2} (V_R + V_{P_2}) \sin\left(\frac{1}{2}(\phi_R + \phi_{P_2})\right) \right\} \theta_R \\
& + \left[ \left\{ \text{SAME COEFFICIENT} \right\} \theta_{P_2} - \frac{1}{\mu} \cdot \frac{1}{2} (I_R + I_{P_2}) \cdot k \right] = 0, \quad (204)
\end{aligned}$$

and

$$\begin{aligned}
& W_R + \left\{ \frac{1}{2} \left( (1+\epsilon_R) Ch_{2R} + (1+\epsilon_{Q_2}) Ch_{2Q_2} \right) \cos\left(\frac{1}{2}(\phi_R + \phi_{Q_2})\right) \right. \\
& \left. + \frac{1}{2} (U_R + U_{Q_2}) \cos\left(\frac{1}{2}(\phi_R + \phi_{Q_2})\right) - \frac{1}{2} (V_R + V_{Q_2}) \sin\left(\frac{1}{2}(\phi_R + \phi_{Q_2})\right) \right\} \theta_R \\
& + \left[ - \left\{ \text{SAME COEFFICIENT} \right\} \theta_{Q_2} - \frac{1}{\mu} \cdot \frac{1}{2} (I_R + I_{Q_2}) \cdot k \right] = 0. \quad (205)
\end{aligned}$$

In determinant form, they become

$$\begin{aligned}
& U_R + 0 + 0 + A_{14} \epsilon_R + A_{15} \phi_R + A_{16} \theta_R + A_{17} = 0 \\
& U_R + 0 + 0 + A_{24} \epsilon_R + A_{25} \phi_R + A_{26} \theta_R + A_{27} = 0 \\
& 0 + V_R + 0 + 0 + A_{35} \phi_R + A_{36} \theta_R + A_{37} = 0 \\
& 0 + V_R + 0 + 0 + A_{45} \phi_R + A_{46} \theta_R + A_{47} = 0 \\
& 0 + 0 + W_R + 0 + 0 + A_{56} \theta_R + A_{57} = 0 \\
& 0 + 0 + W_R + 0 + 0 + A_{66} \theta_R + A_{67} = 0,
\end{aligned}$$

where the  $A_{ij}$  are the coefficients in the preceding set of equations, (200) through (205). The six simultaneous equations are solved to give

$$\begin{array}{r} W_R + A_{56} \theta_R = -A_{57} \\ -(W_R + A_{66} \theta_R = -A_{67}) \\ \hline (A_{56} - A_{66}) \theta_R = A_{67} - A_{57} \end{array}$$

$$\therefore \theta_R = \frac{(A_{67} - A_{57})}{(A_{56} - A_{66})} ,$$

$$W_R + A_{56} \theta_R = -A_{57} \quad \therefore W_R = -A_{57} - A_{56} \theta_R ,$$

$$\begin{array}{r} V_R + A_{35} \phi_R = -A_{36} \theta_R - A_{37} \\ -(V_R + A_{45} \phi_R = -A_{46} \theta_R - A_{47}) \\ \hline (A_{35} - A_{45}) \phi_R = (A_{46} - A_{36}) \theta_R + A_{47} - A_{37} \end{array}$$

$$\therefore \phi_R = \frac{(A_{46} - A_{36}) \theta_R + A_{47} - A_{37}}{(A_{35} - A_{45})} ,$$

$$V_R + A_{35} \phi_R = -A_{36} \theta_R - A_{37} \quad \therefore V_R = -A_{35} \phi_R - A_{36} \theta_R - A_{37} ,$$

$$\begin{array}{r} U_R + A_{14} \epsilon_R = -A_{15} \phi_R - A_{16} \theta_R - A_{17} \\ -(U_R + A_{24} \epsilon_R = -A_{25} \phi_R - A_{26} \theta_R - A_{27}) \\ \hline (A_{14} - A_{24}) \epsilon_R = (A_{25} - A_{15}) \phi_R + (A_{26} - A_{16}) \theta_R + A_{27} - A_{17} \end{array}$$

$$\therefore \epsilon_R = \frac{(A_{25} - A_{15}) \phi_R + (A_{26} - A_{16}) \theta_R + A_{27} - A_{17}}{(A_{14} - A_{24})} ,$$

and

$$U_R = -A_{14} \epsilon_R - A_{15} \phi_R - A_{16} \theta_R - A_{17} .$$

The numerical procedure within the time-space plane grid is as follows:

Step 1

Compute the coefficients of the six simultaneous equations using the values previously computed along the two preceding iso-time lines.

Parameters between grid points are estimated by linear interpolation along an iso-time line; for example,

$$U_{P_1} = U_A - (h_{P_1}/h)(U_A - U_B),$$

where

$$h_{P_1} = S_A - S_{P_1}.$$

Accelerations are needed to compute the hydrodynamic mass terms in the loading functions. Accelerations are estimated by using an Euler numerical approximation along an iso-space line, for example,

$$\dot{U}_R = (U_R - U_A)/k.$$

In order to begin the iteration, assume that the values of the parameters at point R are equal to the values at point A.

Step 2

Solve the simultaneous equations for the six parameters at point R.

Step 3

Go back to step 1 using the new values at R in the coefficients and recompute values at R.

Step 4

Repeat this procedure three times. \*

---

\*A more efficient method would be to specify an error and iterate until the computed parameter values converge within the error band. However, three iterations were found to give good convergence.

From the above scheme, it is obvious that solutions along two iso-time lines are needed to start the iteration. Use the initial conditions along the cable at  $t = 0$  to fill in the parameter values at points C, E, and F. Assign these same values to points along the cable at  $t = k$  to obtain parameter values at points B, A, and D. Begin iteration at grid point (1, 2);  $S = h$ ,  $t = 2k$ , and iterate down the cable. At the lower end of the cable, set  $S = h$  and  $t = 3k$  and repeat.

Velocities along the upper boundary are described by the motion of the cable end. However, at the beginning of each new iso-time line, strain and angles must be computed at  $S = 0$  for the previous time increment. Hartree's method can not be used here because parameter values at times less than 0 are not available. A linear extrapolation along the previous iso-time line is used to obtain the required values; for example,

$$\textcircled{A} S=0 ; \epsilon_B = \epsilon_A - (\epsilon_D - \epsilon_A) .$$

The same problem exists along the lower boundary; only here the velocities are set to 0. Once again the values of strain and angles are determined by linear extrapolation along the previous iso-time line.

This method fails to converge if points  $P_1$  or  $P_2$  fall outside the space interval A-D. Since the locations of these points are determined by the characteristics, the minimum relative size of the space-to-time increment is equal to the value of the greatest characteristic. The tensile wave characteristic is always greater than the transverse wave characteristic; thus,

$$\left( \frac{h}{k} \right)_{\min} = Ch_1 .$$

The maximum space increment is determined by the size of the smallest wavelength in the cable. The transverse wave characteristic will determine the smallest wavelength. If the transverse wave characteristic is known to be 250 ft/sec and the cable is being excited by a sinusoid with a 2-sec period, the wavelength will be 500 ft in length. At least ten points are needed to describe a sinusoid; thus, the maximum size of the space increment is 50 ft. The time increment for a 3,000-ft/sec tensile wave characteristic is

$$k_{max} = \frac{h}{Ch_1} = \frac{50 \text{ ft.}}{3000 \text{ ft./sec}} = 0.01667 \text{ sec.}$$

Note that the characteristics must always be real, finite values. If the characteristics are zero or imaginary, the equations become ultrahyperbolic with multiple solutions for a given set of initial conditions. In this system, this is possible if the tensions are less than zero. Transverse wave characteristics are then imaginary and the problem is indeterminate. This study is further constrained by the requirement that the tension must be greater than zero at all times over the whole length of cable.

### 3.2.3 Cable Loading Functions

The loading functions H, G, and I (figure 16) in the cable equations are composed of the weight components in the double-primed coordinate system, the steady-state and dynamic drag components (viscous forces), and hydrodynamic inertia components (acceleration proportional forces).

The weight components are found by simply transforming the weight per unit length from the inertial coordinate system to the cable coordinates. The weight components are  $W_c'' = A \cdot W_c$ , or

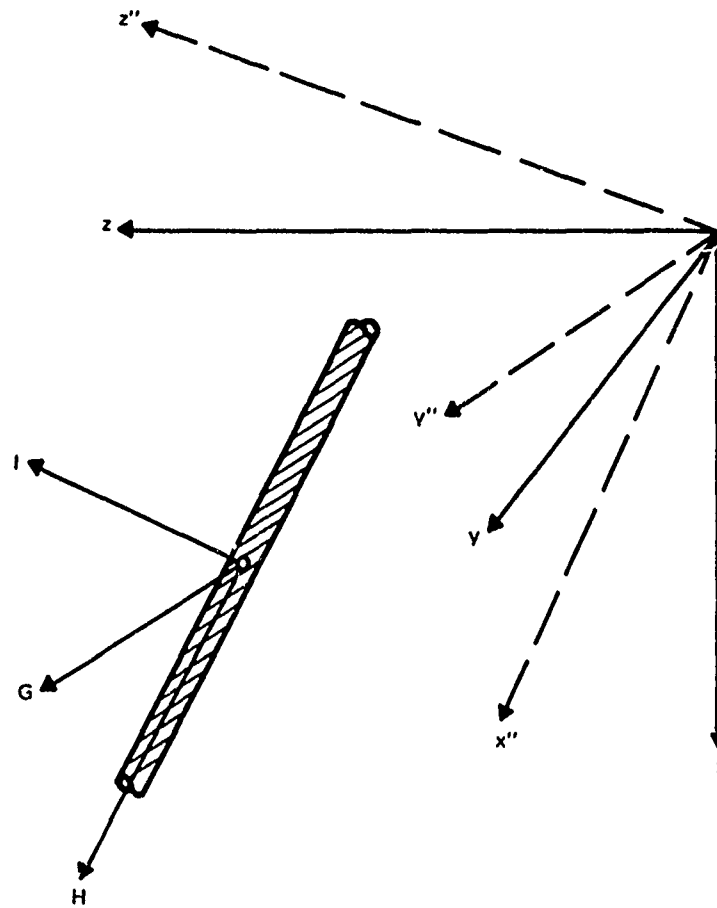


Figure 16. Cable Loading Functions



$$W_c'' = \begin{bmatrix} w_c \cos \phi \cos \theta \\ -w_c \sin \phi \cos \theta \\ -w_c \sin \theta \end{bmatrix} . \quad (206)$$

Drag forces are assumed to follow a velocity-squared drag law of the form:

$$D = \frac{1}{2} \rho C_d A V^2 . \quad (207)$$

On a unit length basis, they become

$$D = \frac{1}{2} \rho C_d d V |V| , \quad (208)$$

where  $d$  is the cable diameter. In order to maintain a sign convention, equation (208) is rewritten as

$$D = \frac{1}{2} \rho C_d d V |V| . \quad (209)$$

Casarella and Parsons<sup>71</sup> have reviewed the state of the art for analysis of hydrodynamic forces on cable systems. Two approaches are described: the use of loading functions\* to compute the normal and tangential drag force components, and the direct computation of normal and tangential drag using normal and tangential drag coefficients. The latter method, used by Wilson<sup>11, 12</sup> for mooring problems, is employed in this study because it lends itself to three-dimensional cable problems and only requires a simple transformation of the relative velocity components to cable coordinates. The first method requires

---

\*Loading functions are defined as the ratio of the hydrodynamic force component of interest to the drag force when the cable is oriented normal to the flow.

multiple transformations to define the normal and tangential forces and to resolve them into three force components.

If the current velocity components are given by

$$G_s = \begin{bmatrix} 0 \\ V_s \\ W_s \end{bmatrix}$$

(no vertical currents) and the velocity components of the cable element are

$$\begin{bmatrix} \dot{X} \\ \dot{Y} \\ \dot{Z} \end{bmatrix},$$

then the velocity components of the water relative to the cable are

$$\begin{bmatrix} U_R \\ V_R \\ W_R \end{bmatrix} = \begin{bmatrix} 0 - \dot{X} \\ V_s - \dot{Y} \\ W_s - \dot{Z} \end{bmatrix}.$$

Transforming to cable coordinates gives

$$\begin{bmatrix} U_R'' \\ V_R'' \\ W_R'' \end{bmatrix} = \begin{bmatrix} -\dot{X} \cos \phi \cos \theta + (V_s - \dot{Y}) \sin \phi + (W_s - \dot{Z}) \cos \phi \sin \theta \\ \dot{X} \sin \phi \cos \theta + (V_s - \dot{Y}) \cos \phi - (W_s - \dot{Z}) \sin \phi \sin \theta \\ \dot{X} \sin \theta + (W_s - \dot{Z}) \cos \theta \end{bmatrix}.$$

The drag force components are now written:

$$D_{X''} = \frac{1}{2} \rho C_{DT} d U_R'' |U_R''|, \quad (210A)$$

$$D_{Y''} = \frac{1}{2} \rho C_{DN} d V_R'' |V_R''|, \quad (210B)$$

and

$$D_{Z''} = \frac{1}{2} \rho C_{DN} d W_R'' |W_R''|. \quad (210C)$$

Hoerner,<sup>48</sup> Wilson,<sup>11</sup> and others show plots of normal and tangential drag coefficients versus Reynolds number for stranded cables. Wilson's data were used in the G. S. A. program "CURFIT," and the following expressions for normal and tangential drag coefficients were developed:

$$\begin{aligned} C_{DN} &= 1.32027 + 10.6962/Re & 0 < Re < 100, \\ &= 1.4 & 100 < Re < 5 \times 10^5, \end{aligned} \quad (211A)$$

$$C_{DT} = 0.60546 \cdot (Re^{-0.475}) \quad 0 < Re < 5 \times 10^5, \quad (211B)$$

where  $Re = \frac{Vd}{\nu}$ ;  $\nu$  is the kinematic viscosity. These expressions are valid only in the subcritical Reynolds number region ( $Re < 5 \times 10^5$ ). However, since this Reynolds number would apply to a 2-in.-diameter cable moving at 35 knots, it is felt that the range of Reynolds numbers covered is adequate.

Hydrodynamic inertia forces are defined normal and tangential to the cable. Transforming the accelerations to cable coordinates and assuming steady ocean currents, we find that the accelerations become

$$\begin{bmatrix} \ddot{X}'' \\ \ddot{Y}'' \\ \ddot{Z}'' \end{bmatrix} = \begin{bmatrix} \ddot{X} \cos \phi \cos \theta + \ddot{Y} \sin \phi + \ddot{Z} \cos \phi \sin \theta \\ -\ddot{X} \sin \phi \cos \theta + \ddot{Y} \cos \phi - \ddot{Z} \sin \phi \sin \theta \\ -\ddot{X} \sin \theta + \ddot{Z} \cos \theta \end{bmatrix} .$$

The hydrodynamic inertia force vector is

$$\begin{bmatrix} F_{hx} \\ F_{hy} \\ F_{hz} \end{bmatrix} = \begin{bmatrix} m_{hxx}'' & 0 & 0 \\ 0 & m_{hyy}'' & 0 \\ 0 & 0 & m_{hzz}'' \end{bmatrix} \cdot \begin{bmatrix} \ddot{X}'' \\ \ddot{Y}'' \\ \ddot{Z}'' \end{bmatrix} .$$

The hydrodynamic mass dyadic is a diagonal matrix due to the axisymmetry of the cable. Also, for a cylindrical object of infinite length, the tangential hydrodynamic mass ( $m_{hxx}''$ ) is zero. For a smooth, constant diameter cable, the normal hydrodynamic masses ( $m_{hyy}''$ ,  $m_{hzz}''$ ) are equal.

Lamb,<sup>45</sup> Basset,<sup>72</sup> and others have used potential flow theory to compute the normal hydrodynamic mass of a circular cylinder:

$$m_{hN} = \pi \rho d^2 / 4 . \quad (212)$$

Miller<sup>73</sup> and Miller and Hagist<sup>74</sup> have investigated the frequency dependence of hydrodynamic mass for various bodies. Their data show a linear decrease in hydrodynamic mass with increasing frequency in the Stokes number region  $0 < St. < 3 \times 10^5$ . By using Miller's data for a 5:1 cylinder,<sup>74</sup> we can see that the slope is  $-1.62 \times 10^{-6}$ . Equation (212) is modified to include the frequency dependence as follows:

$$m_{hN} = (1.0 - (1.62 \times 10^{-6}) \cdot \frac{\omega d^2}{\nu}) \pi \rho d^2 / 4 ; 0 < \frac{\omega d^2}{\nu} < 3 \times 10^5 . \quad (213)$$

The components of the hydrodynamic inertia force are

$$F_{hx} = 0 , \quad (214A)$$

$$F_{h_{my}} = m_{h_N} \cdot \ddot{Y}'' , \quad (214B)$$

and

$$F_{h_{mx}} = m_{h_N} \cdot \ddot{X}'' . \quad (214C)$$

The loading functions are summarized by using equations (206), (210), and (214):

$$H = w_c \cos \phi \cos \theta + (0.60546 \cdot (Re_{v''})^{-0.4758}) \frac{\rho}{2} d U_R'' |U_R''| , \quad (215A)$$

$$G = -w_c \sin \phi \cos \theta + C_{DN_{V''}} \frac{\rho}{2} d V_R'' |V_R''| + (1.0 - (1.62 \times 10^{-6}) \cdot \frac{\omega d^2}{\nu}) \pi \rho \frac{d^2}{4} \cdot \ddot{Y}'' , \quad (215B)$$

and

$$I = -w_c \sin \theta + C_{DN_{W''}} \frac{\rho}{2} d W_R'' |W_R''| + (1.0 - (1.62 \times 10^{-6}) \cdot \frac{\omega d^2}{\nu}) \pi \rho \frac{d^2}{4} \cdot \ddot{X}'' , \quad (215C)$$

where

$$Re_{v''} = \frac{U'' d}{\nu}$$

$$Re_{v''} = \frac{V'' d}{\nu}$$

$$Re_{w''} = \frac{W'' d}{\nu}$$

$$C_{DN_v''} = 1.32027 + 10.6962 / Re_v'' \quad 0 < Re_v'' < 100$$

$$= 1.4 \quad 100 < Re_v'' < 5 \times 10^5$$

$$C_{DN_w''} = 1.32027 + 10.6962 / Re_w'' \quad 0 < Re_w'' < 100$$

$$= 1.4 \quad 100 < Re_w'' < 5 \times 10^5$$

### 3.2.4 Lumped-Mass Model

The finite-difference analysis for cable dynamics can become very expensive in computer time and can require large amounts of computer "storage" because of the large arrays. A lumped-mass analysis can offer significant savings in computational time at the expense of simulation accuracy. In general, the lumped-mass analysis will truncate the high-frequency response of the system. However, for many engineering applications, the high-frequency, low-amplitude response is not of interest, and the cable can be represented as a small number of lumped masses.

Assume that a uniform cable of length  $L$  can be broken up into  $N$  segments of equal length (figure 17). The length of each segment is

$$\Delta L = L / N.$$

Assume that the properties (weight, mass, hydrodynamic forces, etc.) of the cable can be concentrated at points 2, 3, ...,  $N$ , which are located  $\Delta L$ ,

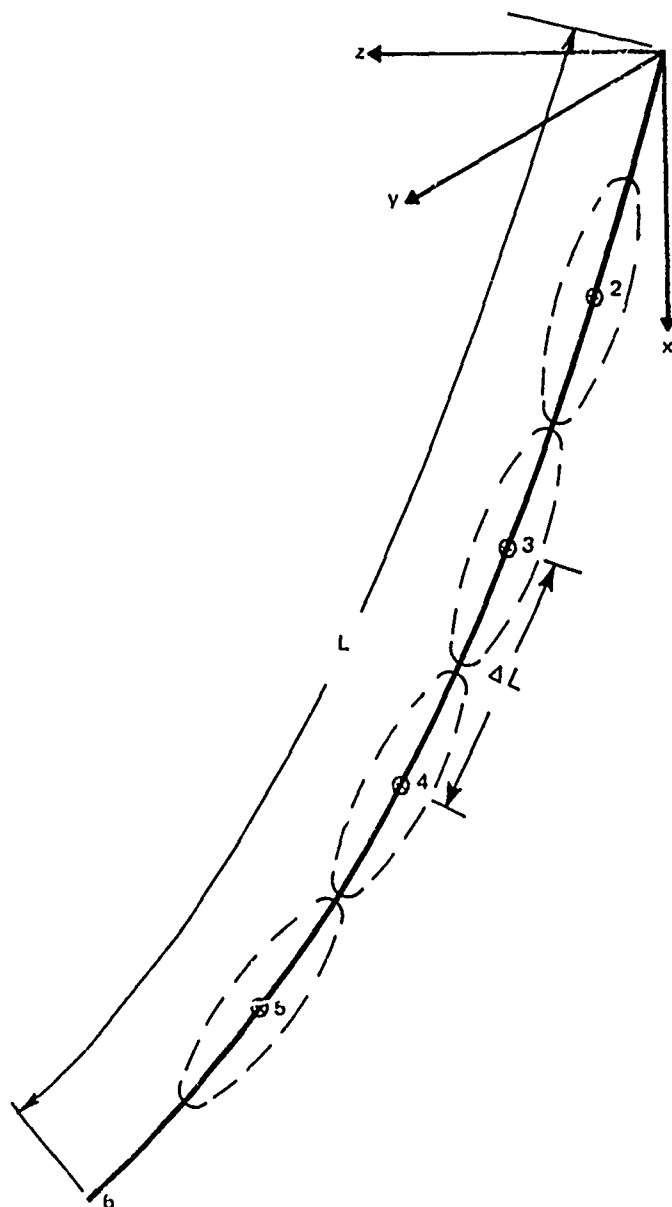


Figure 17. Segments for a Five-Element, Lumped-Mass Model

$2\Delta L, \dots, (N-1)\Delta L$  from the upper end of the cable. All the forces acting on the cable span from  $(N-1)\Delta L \pm \frac{\Delta L}{2}$  are concentrated at the  $n$ th mass point. Cristecu's cable equations, (135A), (135B), and (135C), are written for each mass point:

$$\mu(S_0)\Delta L \frac{d^2 X_n}{dt^2} = X_n \Delta L + (\vec{T}_n \cdot \hat{i} - \vec{T}_{n-1} \cdot \hat{i}), \quad (216A)$$

$$\mu(S_0)\Delta L \frac{d^2 Y_n}{dt^2} = Y_n \Delta L + (\vec{T}_n \cdot \hat{j} - \vec{T}_{n-1} \cdot \hat{j}), \quad (216B)$$

and

$$\mu(S_0)\Delta L \frac{d^2 Z_n}{dt^2} = Z_n \Delta L + (\vec{T}_n \cdot \hat{k} - \vec{T}_{n-1} \cdot \hat{k}). \quad (216C)$$

This is equivalent to modeling the cable with a system of spring-mass elements as shown in figure 18. In order to compute the forces acting on each mass element, the cable angles ( $\phi$  and  $\theta$ ) for each cable element must be defined. From the geometry between the  $n$ th and  $(N+1)$ th mass element, we see that

$$\theta_n = \sin^{-1} \left( \frac{(Z_{n+1} - Z_n)}{\sqrt{(X_{n+1} - X_n)^2 + (Z_{n+1} - Z_n)^2}} \right) \quad (217)$$

and

$$\phi_n = \sin^{-1} \left( \frac{(Y_{n+1} - Y_n)}{\sqrt{(X_{n+1} - X_n)^2 + (Y_{n+1} - Y_n)^2 + (Z_{n+1} - Z_n)^2}} \right). \quad (218)$$

Tensions between the lumped masses are computed by using the elastic properties of the cable and the deformation of the cable. If the effective cable



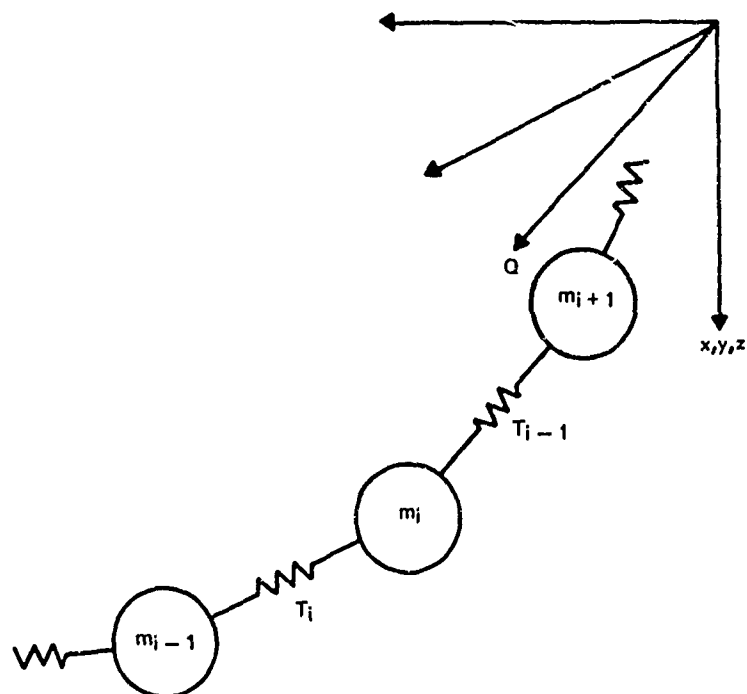


Figure 18. Lumped-Mass Model

modulus is  $E_c$  and the deformation of the cable of length  $\Delta L$  is  $\delta$ , the spring constant along the cable is

$$K_{x''} = \frac{F}{\delta} = \frac{\pi \frac{d^2}{4} \sigma}{\delta} = \pi \frac{d^2}{4} \frac{E_c}{\Delta L} \quad (219)$$

The stretched length between the  $n$ th and  $(N + 1)$ th mass element is

$$\sqrt{(x_{n+1} - x_n)^2 + (y_{n+1} - y_n)^2 + (z_{n+1} - z_n)^2}.$$

If the difference between the stretched length of the cable and the unstretched length ( $\Delta L$ ) is less than zero, the tension is zero since the cable can not support compression. (This is analogous to the ultrahyperbolic equations that occur in the finite-difference analysis if tensions go to zero.) Otherwise, the tension in the  $n$ th cable segment is defined as

$$T_{n_{x''}} = K_{x''} \left( \sqrt{(x_{n+1} - x_n)^2 + (y_{n+1} - y_n)^2 + (z_{n+1} - z_n)^2} - \Delta L \right). \quad (220)$$

Transforming to inertial coordinates, the tension becomes

$$T_n = A^{-1} \cdot \begin{bmatrix} T_{n_{x''}} \\ 0 \\ 0 \end{bmatrix} = \begin{bmatrix} T_{n_{x''}} \cos \phi_n \cos \theta_n \\ T_{n_{x''}} \sin \phi_n \\ T_{n_{x''}} \cos \phi_n \sin \theta_n \end{bmatrix}. \quad (221)$$

These tension components are used in equations (216) to compute the tension difference across the mass element.

As before, the forces  $X_n \Delta L$ ,  $Y_n \Delta L$  and  $Z_n \Delta L$  acting on each mass element consist of weight, viscous drag, and hydrodynamic inertia

forces. The weight force vector per unit length is

$$W_c = \begin{bmatrix} w_c \\ 0 \\ 0 \end{bmatrix},$$

where  $w_c$  is the weight per unit length in water of the cable. Again, if the current velocity components at the  $n$ th element are

$$C_s = \begin{bmatrix} 0 \\ V_{sn} \\ W_{sn} \end{bmatrix}$$

and the velocity components of the  $n$ th element are

$$\begin{bmatrix} \dot{x}_n \\ \dot{y}_n \\ \dot{z}_n \end{bmatrix},$$

then the relative velocity components are

$$\begin{bmatrix} U_{Rn} \\ V_{Rn} \\ W_{Rn} \end{bmatrix} = \begin{bmatrix} 0 - \dot{x}_n \\ V_{sn} - \dot{y}_n \\ W_{sn} - \dot{z}_n \end{bmatrix}, \quad (222)$$

If the mean cable angles at the  $n$ th mass element are computed, we find

$$\bar{\phi}_n = \frac{1}{2} (\phi_n + \phi_{n-1}) \quad (223A)$$

and

$$\bar{\theta}_n = \frac{1}{2} (\theta_n + \theta_{n-1}) . \quad (223B)$$

The relative velocity components are transformed to cable coordinates as follows:

$$U_{R_n}'' = -\dot{\chi}_n \cos \bar{\phi}_n \cos \bar{\theta}_n + (V_{S_n} - \dot{y}_n) \sin \bar{\phi}_n + (W_{S_n} - \dot{z}_n) \cos \bar{\phi}_n \sin \bar{\theta}_n ,$$

$$V_{R_n}'' = \dot{\chi}_n \sin \bar{\phi}_n \cos \bar{\theta}_n + (V_{S_n} - \dot{y}_n) \cos \bar{\phi}_n - (W_{S_n} - \dot{z}_n) \sin \bar{\phi}_n \sin \bar{\theta}_n ,$$

and

$$W_{R_n}'' = \dot{\chi}_n \sin \bar{\theta}_n + (W_{S_n} - \dot{z}_n) \cos \bar{\theta}_n .$$

The drag forces per unit length are

$$D_{\chi_n}'' = \frac{1}{2} \rho C_{DT} d U_{R_n}'' |U_{R_n}''| ,$$

$$D_{y_n}'' = \frac{1}{2} \rho C_{DN} d V_{R_n}'' |V_{R_n}''| ,$$

and

$$D_{z_n}'' = \frac{1}{2} \rho C_{DN} d W_{R_n}'' |W_{R_n}''| ,$$

where the drag coefficients are computed from equations (211A) and (211B).

The accelerations of the nth mass element in cable coordinates are

$$\ddot{\chi}_n'' = \ddot{\chi}_n \cos \bar{\phi}_n \cos \bar{\theta}_n + \ddot{y}_n \sin \bar{\phi}_n + \ddot{z}_n \cos \bar{\phi}_n \sin \bar{\theta}_n ,$$

$$\ddot{y}_n'' = -\ddot{\chi}_n \sin \bar{\phi}_n \cos \bar{\theta}_n + \ddot{y}_n \cos \bar{\phi}_n - \ddot{z}_n \sin \bar{\phi}_n \sin \bar{\theta}_n ,$$

and

$$\ddot{z}_n'' = -\ddot{\chi}_n \sin \bar{\theta}_n + \ddot{z}_n \cos \bar{\theta}_n .$$

The hydrodynamic inertia force components per unit length are

$$F''_{hm_{x_n}} = 0 \quad , \quad (224A)$$

$$F''_{hm_{y_n}} = -m_{h_n} \cdot \ddot{Y}_n \quad , \quad (224B)$$

and

$$F''_{hm_{z_n}} = -m_{h_n} \cdot \ddot{Z}_n \quad , \quad (224C)$$

where  $m_{h_n}$  is computed from equation (213). The drag and hydrodynamic inertia forces per unit length are summed and transformed back to inertial coordinates and added to the weight force; thus,

$$\begin{bmatrix} X_n \\ Y_n \\ Z_n \end{bmatrix} = \begin{bmatrix} w_c \\ 0 \\ 0 \end{bmatrix} + A^{-1} \cdot \begin{bmatrix} D''_{x_n} + 0 \\ D''_{y_n} + F''_{hm_{y_n}} \\ D''_{z_n} + F''_{hm_{z_n}} \end{bmatrix} . \quad (225)$$

All terms have been defined in the equations of motion for the cable elements. The three equations, (216A), (216B), and (216C), must be integrated simultaneously for each mass element. Thus, if the cable is broken up into ten segments, there will be nine mass elements, each having three degrees of freedom. Therefore, there will be  $9 \times 3 \times 2 = 54$  simultaneous first-order equations. Note that the upper half of the first cable length and the lower half of the last cable length are not included in these equations of motion. These cable segments are assumed to be moving with the upper and lower boundaries

and their properties should be lumped in with the properties of the buoy and anchor. The computer program developed for the lumped-mass simulation of cable dynamics will be discussed in a later section.

### 3.3 Steady-State Buoy System Configurations

As an introduction to the coupling of the buoy and cable equations of motion and the resulting computer programs, the steady-state buoy system configuration (zeroth-order case of buoy system dynamics) will be investigated. The specification of the proper mooring line length for a moored buoy system is critical in the design of the system in order to avoid tow-under of the buoy, minimize the "watch circle" of the buoy, reduce steady-state tensions in the moor, etc. This analysis offers a method to select the proper mooring line length for a given buoy, water depth, and current.

If the time dependent terms in the cable equations (equations (161) through (167)) are allowed to go to zero, we find that

$$\frac{\partial T}{\partial S_0} + H = 0 \quad , \quad (226)$$

$$T \frac{\partial \phi}{\partial S_0} + G = 0 \quad , \quad (227)$$

$$T \cos \phi \frac{\partial \theta}{\partial S_0} + I = 0 \quad , \quad (228)$$

and

$$\epsilon = \frac{1}{K} T \quad . \quad (229)$$

Letting cable velocities go to zero in the loading functions, we find that

$$H = w_c \cos \phi \cos \theta + (0.60546 \cdot (Re_{U_R''})^{-0.4756}) \frac{\rho}{2} d U_R'' |U_R''| ,$$

$$G = -w_c \sin \phi \cos \theta + C_{DN_{V''}} \frac{\rho}{2} d V_R'' |V_R''| ,$$

and

$$I = -w_c \sin \theta + C_{DN_{W''}} \frac{\rho}{2} d W_R'' |W_R''| ,$$

where

$$U_R'' = V_S \sin \phi + W_S \cos \phi \sin \theta$$

$$V_R'' = V_S \cos \phi - W_S \sin \phi \sin \theta$$

$$W_R'' = W_S \cos \theta$$

$$\begin{aligned} C_{DN_{V''}} &= 1.32027 + 10.6962 / Re_{V''} \\ &= 1.4 \end{aligned}$$

$$0 < Re_{V''} < 100$$

$$100 < Re_{V''} < 5 \times 10^5$$

$$\begin{aligned} C_{DN_{W''}} &= 1.32027 + 10.6962 / Re_{W''} \\ &= 1.4 \end{aligned}$$

$$0 < Re_{W''} < 100$$

$$100 < Re_{W''} < 5 \times 10^5$$

$$Re_{U''} = \frac{U'' d}{\nu}$$

$$Re_{V''} = \frac{V'' d}{\nu}$$

$$Re_{W''} = \frac{W'' d}{\nu} .$$

Expanding equations (226), (227), and (228) to include the loading functions and taking total derivatives, we find that the steady-state cable equations become

$$\frac{dT}{dS_0} = -w_c \cos \phi \cos \theta - (0.60546 (Re_{U_R''}^{-0.4758})) \frac{\rho}{2} dU_R'' |U_R''|, \quad (230)$$

$$\frac{d\phi}{dS_0} = \frac{1}{T} \left( w_c \sin \phi \cos \theta - C_{DN_{V''}} \frac{\rho}{2} dV_R'' |V_R''| \right), \quad (231)$$

$$\frac{d\theta}{dS_0} = \frac{1}{T \cos \phi} \left( w_c \sin \theta - C_{DN_{W''}} \frac{\rho}{2} dW_R'' |W_R''| \right), \quad (232)$$

and

$$\frac{dS}{dS_0} = 1 + \epsilon = 1 + \frac{1}{K} T. \quad (233)$$

Before integrating these equations, the upper boundary conditions (at the buoy) must be determined. The tension at the buoy is

$$T_B = \sqrt{(Disp - W_B)^2 + Drag^2}, \quad (234)$$

where

Disp is the buoy displacement

Drag is the buoy drag force due to surface currents

$W_B$  is the buoy weight.

For convenience, let the  $z$  axis of the inertial coordinate system be aligned with the surface current. Then, the initial buoy moor angle is

$$\theta_0 = \tan^{-1} \left( \frac{Drag}{(Disp - W_B)} \right), \quad (235)$$

and the initial moor transverse angle is

$$\phi_0 = 0. \quad (236)$$



Unfortunately, the displacement and drag of the buoy are functions of the cable tension at the buoy. Thus, a trial and error solution must be used. For a given current profile,  $V_s = f_1(x)$ ;  $W_s = f_2(x)$ , the depth of water is the controlling parameter. When the vertical projection of the cable is equal to the depth of water, the correct solution has been obtained. The differential equations defining the cable shape (equations (230) to (233)) are controlled by the unstressed cable length  $S_0$ . Each iteration must take into account the stretch in the segment before the  $x$  component of segment is computed. Thus, if the integration step size is  $dS_0$  and the tension and angles for that segment are  $T$ ,  $\theta$ , and  $\phi$ , the stretched length is

$$dS = (1 + \epsilon) dS_0. \quad (237)$$

From the cable properties, we see that

$$\epsilon = \frac{\sigma}{E_c} = \frac{4T}{\pi d^2 E_c}.$$

Rewriting equation (237), we see that the stretched length increment is

$$dS = \left( 1 + \frac{4T}{\pi d^2 E_c} \right) dS_0. \quad (238)$$

The components of the cable incremental length  $dS$  are

$$dx = dS \cos \phi \cos \theta,$$

$$dy = dS \sin \phi,$$

and

$$dz = dS \cos \phi \sin \theta.$$

Since both the displacement and drag of the buoy are functions of the draft of the buoy (equations (52) and (95) developed for an oblate spheroid — similar equations can be developed for buoys of different shape), the draft  $H$  is incremented upward from its "free-floating" value, i. e., as if the buoy were floating on a calm surface with no mooring. The configuration of the cable is then computed using a fourth-order, Runge-Kutta numerical integration algorithm for the given current structure, which may vary in magnitude and direction as a function of depth. The components of the incremental length  $dS$  are computed and summed. The  $x$  component of the end of the cable is tested logically to see if it falls within a specified error band about the water depth. If the computed vertical projection is less than the water depth, the buoy draft is incremented upward and the process is repeated. If the computed vertical projection falls within the error band, the solution can be accepted or the width of the error band can be reduced and the process repeated until the solution achieves the desired accuracy. This process is shown schematically in figure 19.

This method has been programmed in FORTRAN IV and is shown in appendix B. Subroutines are included for the displacement and drag of oblate spheroids, spherical buoys, cylindrical buoys (cans or spars), torroidal buoys ("donut" buoys), and discus buoys ("monster" buoys). The user must input the buoy characteristics (weight, dimensions, etc.) the cable characteristics (diameter, length, cable modulus, and weight per foot in water — negative if buoyant), and the environmental characteristics (water depth, current structure, etc.). The output includes unstretched length, stretched length, tensions,

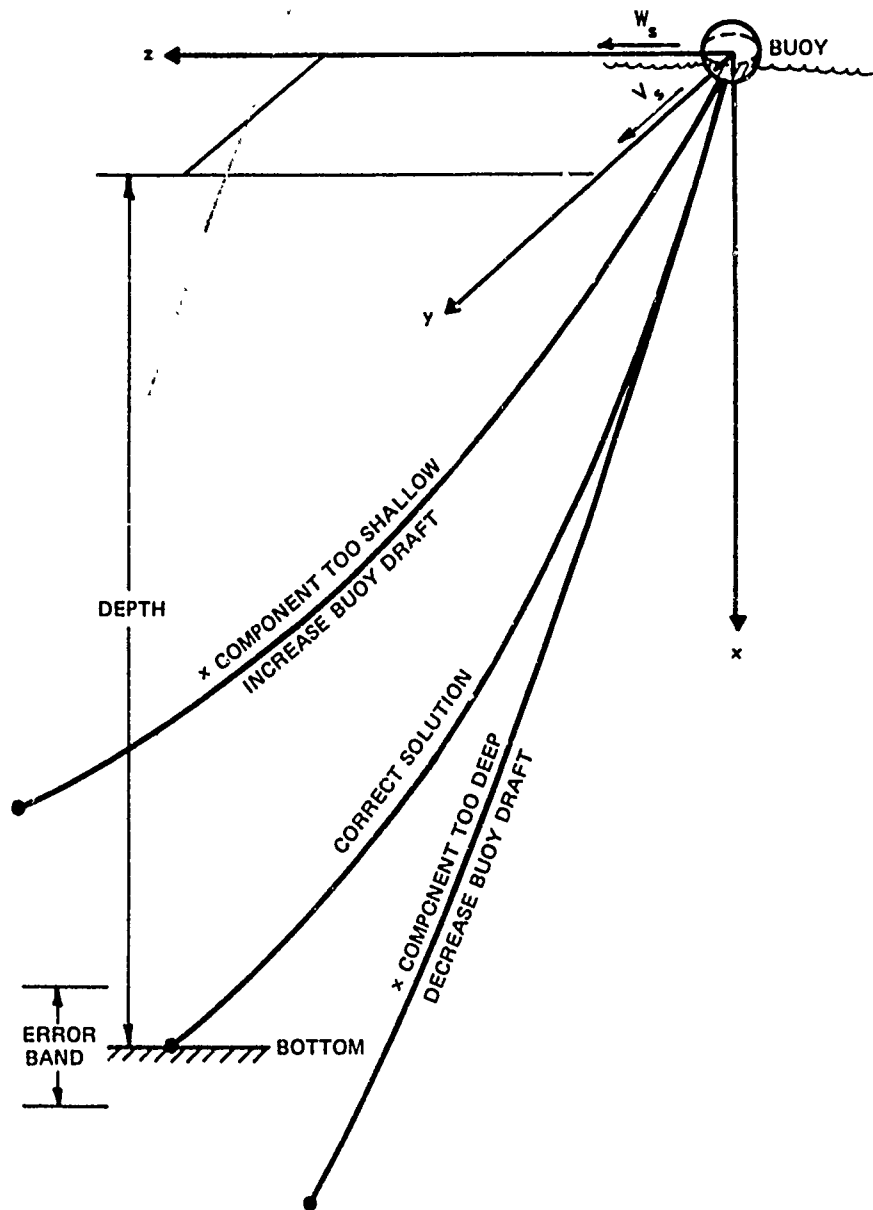


Figure 19. Buoy System Configuration Computation Procedures

the cable angles, and the  $x$ ,  $y$ ,  $z$  coordinates of each integration step. The step size of the buoy draft is incremented upward as some percentage of the total buoy draft (as if it were fully submerged). Downward buoy draft increments are taken as half the prior upward increments to avoid a lock-step situation where the solution swings between two values and never converges. Subsequent draft increments are halved to avoid the same situation. If the initial error band specified is too narrow and the solution overshoots the error band, the solution may converge too slowly. A limiter is built in to stop the program after 15 configurations are computed. The user should then open up the initial error band. If the buoy draft is increased to its maximum value, the program prints out a statement that the buoy sinks and the computation stops. This indicates that the buoy tows under either because it has insufficient excess buoyancy or the system drag is too high.

If the mooring line is made up of more than one type of cable, rope, or chain, logical "IF" statements are used to change the cable properties at the proper cable lengths. The writer has found that at the transition of cable to chain, the integration step size must be reduced to ensure numerical stability.

Also, if the mooring line has objects (instruments, buoys, weights, etc.) attached to it, the change in tension and angles across the discontinuity must be computed from the free body of the object (figure 20). If the cable parameters just above the discontinuity are  $T_H$ ,  $\phi_H$  and  $\theta_H$ , the tension components at that point are

$$T_{Hx} = T_H \cos \phi_H \cos \theta_H, \quad (239A)$$

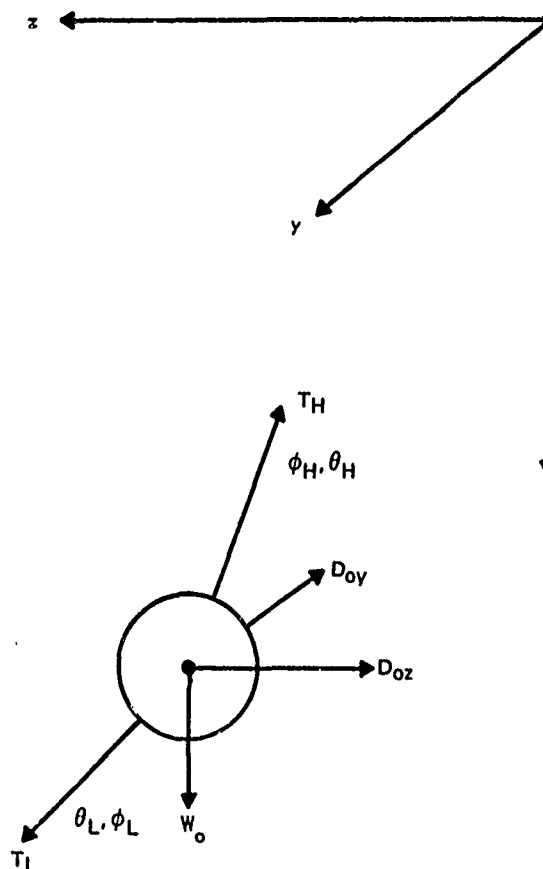


Figure 20. Free Body of an Object on the Mooring Line

$$T_{Hy} = T_H \sin \phi_H , \quad (239B)$$

and

$$T_{Hz} = T_H \cos \phi_H \sin \theta_H . \quad (239C)$$

By summing the forces on the free body, we can determine the tension components below the discontinuity. The tension components are

$$T_{Lx} = T_{Hx} - W_0 ,$$

$$T_{Ly} = T_{Hy} + D_{0y} ,$$

and

$$T_{Lz} = T_{Hz} + D_{0z} ,$$

where

$W_0$  is the in-water weight of the object

$D_{0y}$  is the drag of the object in the minus  $y$  direction

$D_{0z}$  is the drag of the object in the minus  $z$  direction .

The cable tension just below the discontinuity is

$$T_L = \sqrt{T_{Lx}^2 + T_{Ly}^2 + T_{Lz}^2} , \quad (240)$$

and the cable angles become

$$\theta_L = \tan^{-1}(T_{Lz} / T_{Lx}) , \quad (241)$$

and

$$\phi_L = \text{TAN}^{-1} \left( T_{Ly} / \sqrt{T_{Lx}^2 + T_{Lz}^2} \right). \quad (242)$$

The integration down the cable can resume using the new tension and angles.

The process can be repeated for other objects along the mooring line.

Computer programs developed for buoy system statics and dynamics are shown and discussed in appendix B. The experimental data taken and the validation of the analytical models will now be discussed.

#### IV. EXPERIMENTAL MEASUREMENTS AND COMPARISON WITH MODELS

##### 4.1 Steady-State Buoy System Configurations

The steady-state analysis of the buoy system configuration is important since it serves as the set of initial conditions for the dynamic analysis. Also, the steady-state analysis is the first step for the buoy system designer to ensure that his system will not tow-under or have other undesirable static characteristics. The analysis for both shallow and deep water oceanographic buoy systems are compared with data taken at sea to validate the steady-state analysis.

##### 4.1.1 Torroid and Current Meter Array at Station BRAVO

On 22 August 1967, the writer installed a buoy-supported, current meter array at station BRAVO ( $41^{\circ} 51.15'N$ ,  $71^{\circ} 46.50'W$ ) at the Block Island — Fishers Island (BIFI) Oceanographic and Acoustic Range in Block Island Sound. This array was recovered on 19 September 1967, and the current meter data were analyzed. The components of the array are shown in figure 21. The three Braincon type 316 current meters were suspended below the buoy at cable lengths of 15, 60, and 105 ft. The buoy and array were moored with a 70-lb Danforth anchor and a 100-lb lead weight to keep the line pull horizontal. The buoy used in this experiment is shown in figure 22.



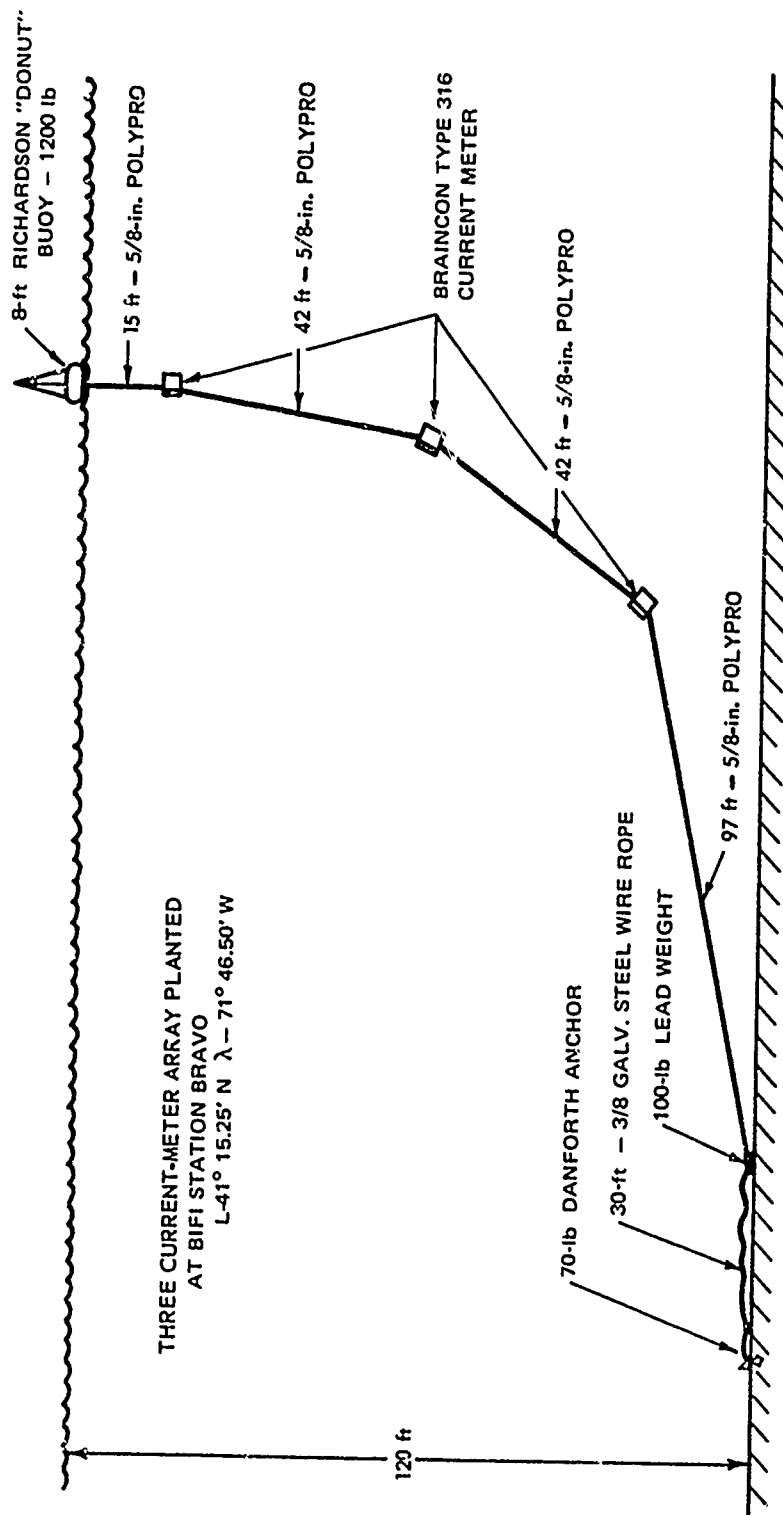


Figure 21. Current Meter Array at Station BRAVO

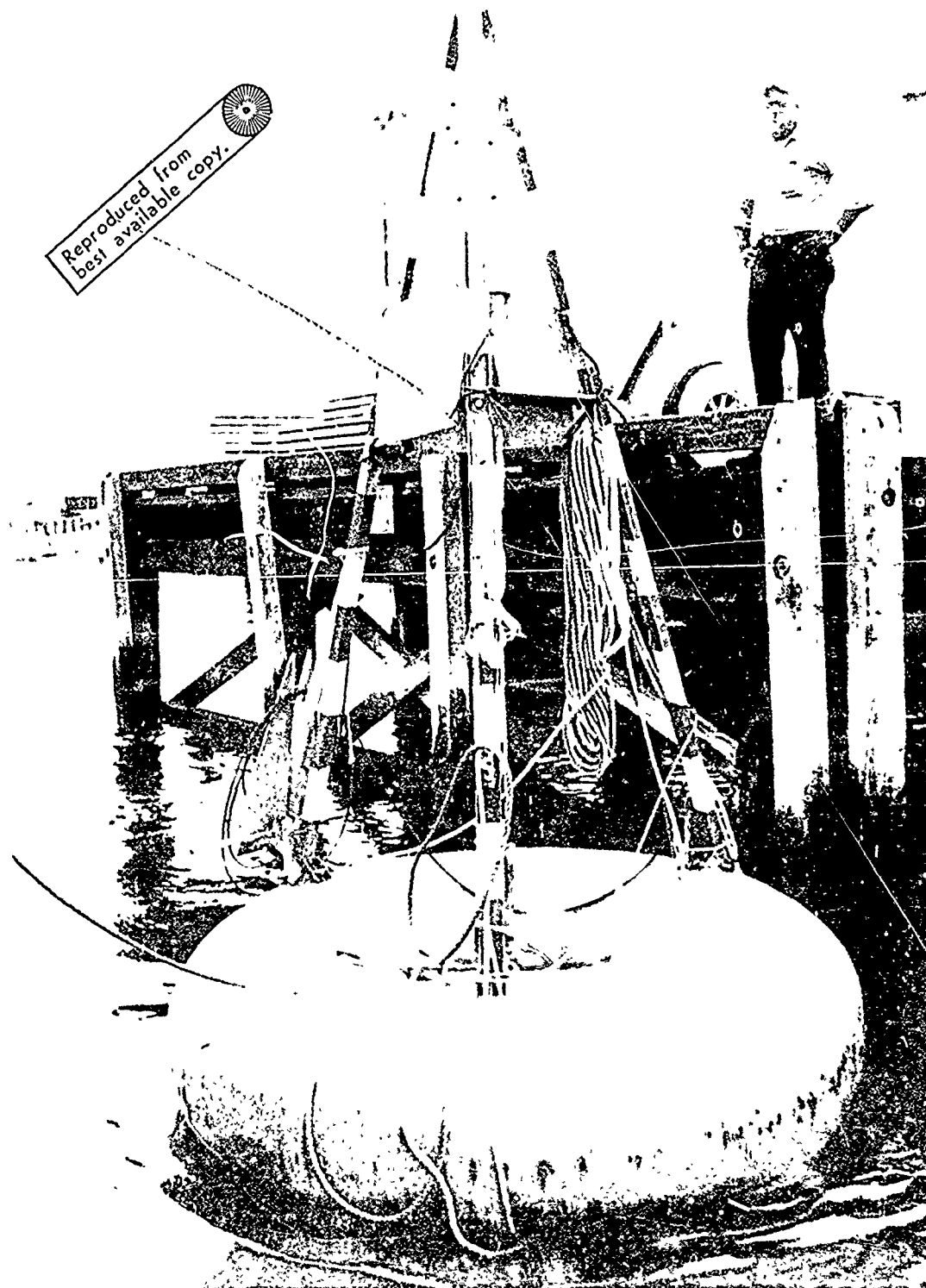


Figure 22. Torroidal Buoy Used for the Three-Current-Meter Array

Twenty-eight samples of the current meter data were selected and are shown in table 1. Data from the bottom current meter were highly variable and erratic and were not regarded as reliable. The data shown are 10-min time averages due to the photographic method used to record data. The instruction manual for the type 316 current meter<sup>75</sup> gives the following ranges and accuracies:

	<u>Range</u>	<u>Accuracy</u>
Current speed	0.5 - 5 knots	$\pm 0.15$ knot
Current direction	0 - 360 deg	$\pm 5$ deg
Current meter tilt	0 40 deg	$\pm 1$ deg
Timing mechanism	5 months	$\pm 10$ sec/day.

The weight in sea water of the current meter is given in the instruction manual as 67 lb. The cylindrical body of the current meter is  $8\frac{1}{2}$  in. in diameter by  $38\frac{3}{4}$  in. long with a 36-in. vertical vane attached to align it with the flow. Sunblad<sup>76</sup> gives a normal drag coefficient of 0.59 based on frontal area derived from tow tank data for the type 316 current meter.

The torroidal buoy has an 8-ft outer diameter and a 3-ft hole through the center. The buoy weighed 1200 lb in air. The mooring line was 5/8-in.-diameter polypropylene rope having 0.02 lb/ft buoyancy. The 3/8-in.-diameter wire rope at the anchor weighed 0.2 lb/ft. The cable modulus of elasticity for the polypropylene rope was taken as  $1.67 \times 10^5$  lb/in.<sup>2</sup> (50° F) and for the steel cable as  $12.0 \times 10^6$  lb/in.<sup>2</sup>.

Williams<sup>77</sup> and Nalwalk *et al.*<sup>78</sup> have made current measurements at station BRAVO and have found a two-layer current structure. On an ebb tide

TABLE 1. CURRENT METER DATA — STATION BRAVO

Time (hr)	Speed (knots)			Direction (deg) Reference to Magnetic North			Observed Tilt Angle (deg $\pm$ 1 deg)		
	15	60	105	15	60	105	15	60	105
.333	1.177	1.27	.701	278	270	301	10	22	40
.666	1.205	1.16	1.04	276	276	310	10	20	40
1.000	1.079	1.08	1.11	281	277	300	7	18	40
1.333	1.099	1.07	1.84	284	283	257	6	14	40
1.666	.945	.928	.498	292	282	217	6	11	18
2.000	.836	.713	.777	290	276	206	5	7	41
2.333	.717	.578	1.031	286	273	119	4	7	40
2.666	.538	.497	4.688	298	284	115	4	5	40
3.000	.509	.341	3.92	316	302	171	3	3	10
3.333	.378	.214	.110	335	316	160	2	4	17
3.666	.420	.159	.069	27	188	151	3	1	7
49.0	1.253	1.086	.764	290	280	215	15	25	18
50.0	1.169	1.088	1.386	298	275	202	15	25	40
51.0	.940	.943	.697	291	272	246	10	20	40
52.0	.748	.516	.523	308	289	110	6	11	40
53.0	.617	.265	1.472	21	91	109	5	5	9
54.0	.790	.578	.687	83	89	17	5	5	0
55.0	.908	.666	.901	93	86	56	4	10	40
56.0	.824	.814	1.964	90	169	1	5	5	19
20.0	.632	.699	.756	71	96	1	5	5	40
21.0	.578	.345	.859	41	104	5	5	5	5
22.0	.630	.363	1.394	283	242	312	6	15	40
23.0	.910	.845	4.539	283	267	305	10	23	40
24.0	1.178	1.108	2.141	278	268	309	16	30	41
25.0	1.219	.985	.545	283	260	306	14	30	40
26.0	1.158	1.050	1.283	288	257	306	15	26	18
27.0	.893	.700	1.894	298	257	201	9	20	18
28.0	.691	.42	.832	347	254	111	6	6	40

(current setting to the east) the bottom layer appears to set to the northeast. On a flood tide (current setting to the west) the bottom layer sets to the northwest. Williams and Nalwalk never observed bottom currents greater than 1.5 knots, which make the data from the bottom current meter questionable. Also, the high tilt angles of the bottom current meter preclude proper response of the Savonius rotor to the ambient currents. In the following study, which was made to compare predicted current meter tilt angles with observed tilt angles, the current is modeled as an upper layer having a thickness of 70 ft and a bottom layer with a thickness of 50 ft. The current speed and direction of the upper layer is approximated by the mean of the speeds and directions from the two upper current meters. The speed and direction of the lower layer is assumed to be equal to the speed and direction from the bottom current meter. Bottom currents greater than 1.5 knots were set equal to the value of the upper layer current.

The computer program for steady-state buoy configurations shown in appendix B was modified to include the effects of the current meters and lead weight by solving the free body at each object (equations (239A) through (242)). The torroidal buoy subroutine was used and cable configurations were integrated with a fourth-order Runge-Kutta algorithm using a 1-ft step size. Current meter tilt angles were computed by balancing moments on each current meter. The program was run on the GSA-360 time sharing computer and results for the first ten cases are shown in table 2 and in figure 23. Average tilt angle errors for the ten cases are as follows:

TABLE 2. COMPARISON OF OBSERVED CURRENT METER TILT ANGLES  
WITH DATA COMPUTED BY INTEGRATION OF CABLE EQUATIONS

Time (hr)	Observed Tilt Angle (deg $\pm$ 1 deg)				Computed Tilt Angle (deg)			Tilt Angle Error (deg)		
	15	60	105		15	60	105	15	60	105
.333	10	22	40		10.59	20.62	49.86	.59	-1.38	—
.666	10	20	40		9.91	19.39	48.82	-.09	-.61	—
1.000	7	18	40		8.38	16.69	44.87	1.38	-1.31	—
1.333	6	14	40		8.31	16.33	49.00	2.31	2.33	—
1.866	6	11	18		6.46	13.27	34.32	.46	2.27	16.32
2.000	5	7	41		4.45	9.25	25.82	-.55	2.25	—
2.333	4	7	40		3.11	6.50	13.50	-.89	-.50	—
2.666	4	5	40		1.99	4.17	10.92	-2.01	-.83	—
3.000	3	3	10		1.34	2.81	8.49	-1.66	-.19	-1.51
3.333	2	4	17		.65	1.37	5.38	-1.35	-2.63	-11.62
Average error 0.22 0.20 1.06										
Overall average error -0.49										

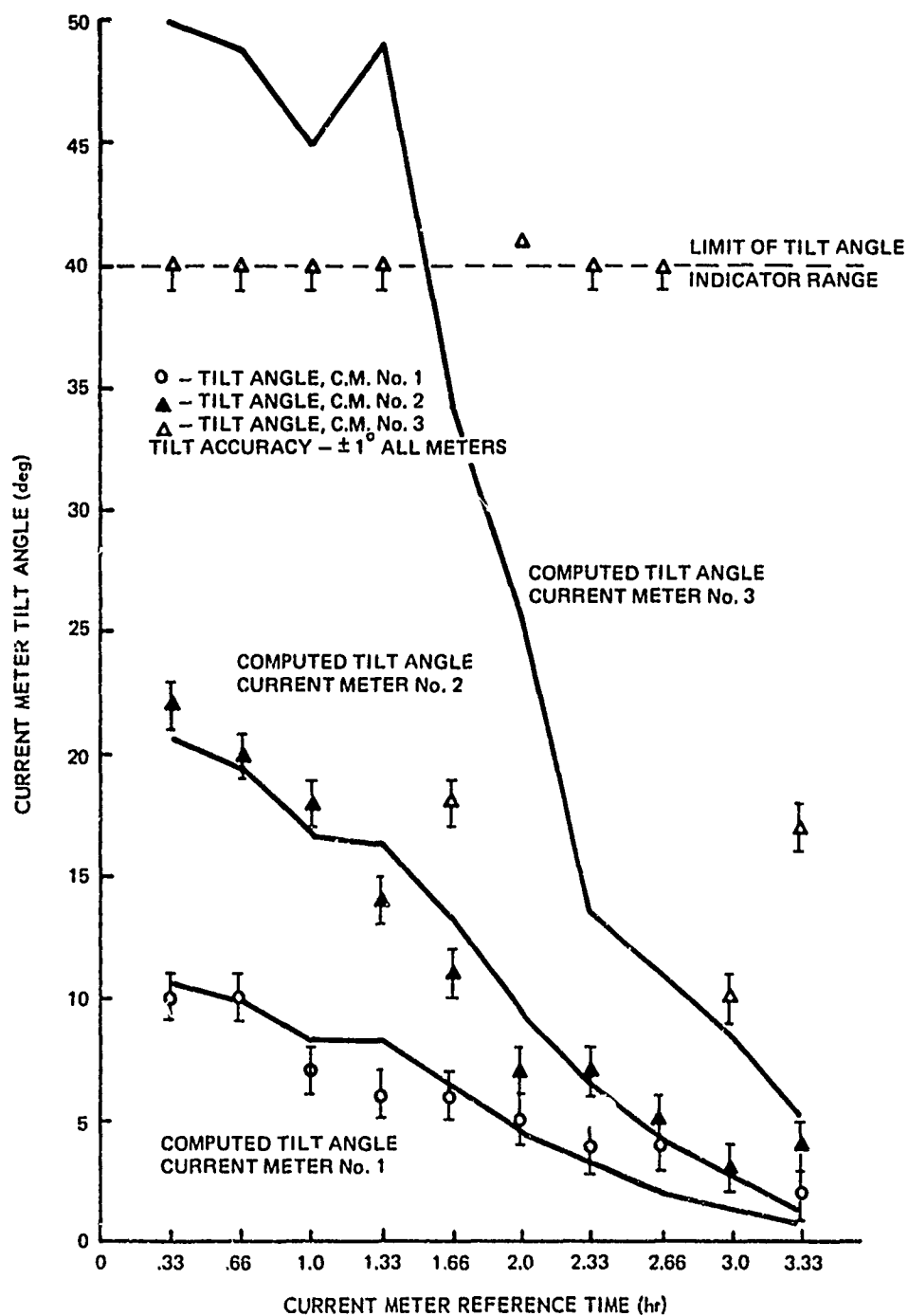


Figure 23. Current Meter Tilt Angles Computed by Integrating Down the Cable Compared With Observed Data

Upper current meter	+ 0.22 deg
Middle current meter	+ 0.2 deg
Lower current meter*	+ 1.06 deg
Overall average error	+ 0.49 deg.

With the exception of the lower current meter, these errors fall within the  $\pm 1$  deg accuracy of the tilt indicator indicating good agreement of the computer model with observed data. The computer study indicated that the 100-lb weight was never picked up off the bottom by the strongest currents and that the weight and drag of the current meters control the buoy system configuration to a greater degree than the weight and drag of the polypropylene rope. With this in mind, a simple statics model of the buoy system was developed; it was assumed that the rope was not deflected between current meters and that half of the drag force acting on each rope span could be assumed to be concentrated at the end of the current meter to which it was attached. Since the tensions in the integrated cable configurations were observed to be very small, the buoy draft was computed for the buoy weight and the weight of the current meters only. Thus, the vertical force component is equal to the weight of the current meters. The simplified model is shown on figure 24. Lateral deflections computed by the integrated configurations were very small; thus, the simplified model was restricted to two dimensions. Drag forces on the rope spans and on the current meters were computed as if the currents were acting normal to the rope or current meter. The small buoyancy and the stretch of the rope were neglected.

---

\*The errors of the lowest current meter were not computed for data where the observed tilt angle was 40 deg.



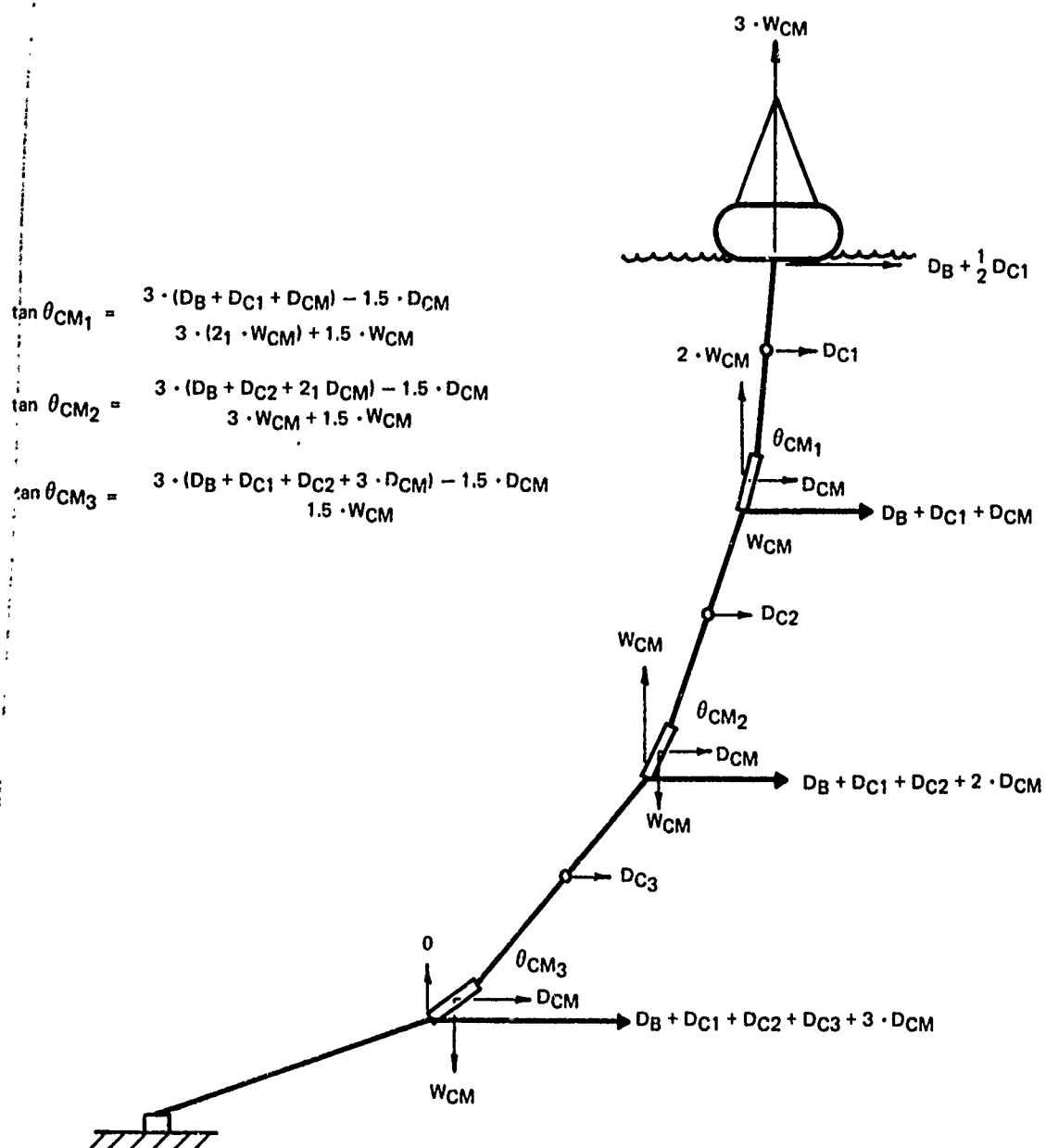


Figure 24. A Simple Statics Model of the Current Meter Array

Buoy system configurations for the case at current meter reference time of 0.333 hr are shown in figure 25 and are quite similar. Computed current meter tilt angles were compared with the observed tilt angles. The angles were computed by using a uniform current equal to the mean value of the current speeds from the upper two current meters. The angles are shown in table 3 and on figure 26. The average errors for the first ten data sets are as follows:

Upper current meter	- 2.15 deg
Middle current meter	- 0.26 deg
Lower current meter	+ 7.64 deg
Overall average error	+ 1.74 deg.

These errors indicate that the simple statics model is about three times less accurate than integration down the cable but may be adequate for engineering applications. The average errors for 28 data sets are as follows:

Upper current meter	- 3.77 deg
Middle current meter	- 2.69 deg
Lower current meter	16.66 deg
Overall average error	3.4 deg.

The preceding study indicates that the steady-state buoy system configuration model can predict current meter inclination angles to within  $\frac{1}{2}$  deg on the average. No tension data were recorded; thus, the steady-state tension errors were not computed. The shallow water buoy system described above is most heavily influenced by the weight and drag of the current meters. In most deep water buoy systems, the weight and drag of the mooring cables are the predominant forces.

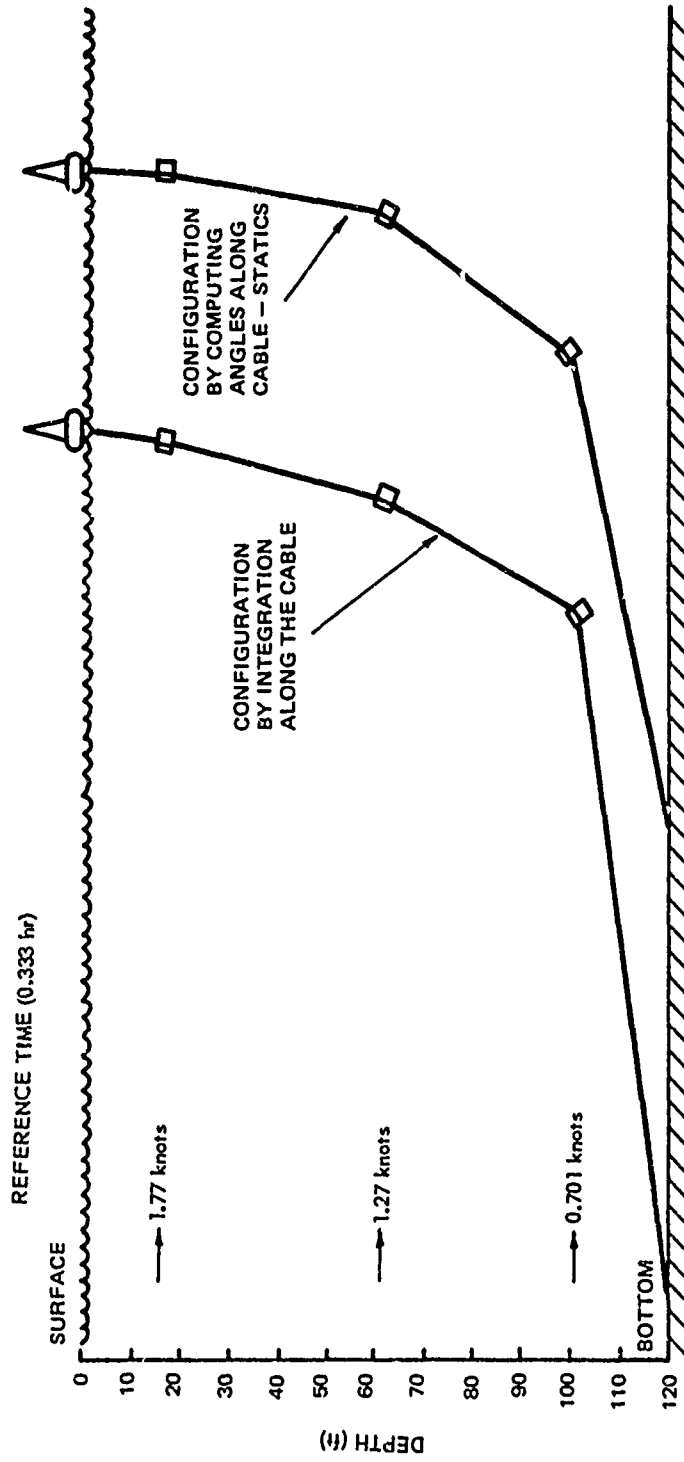


Figure 25. Comparison of Computed Buoy System Configurations

TABLE 3. COMPARISON OF OBSERVED CURRENT METER TILT ANGLES  
WITH DATA COMPUTED BY ASSUMING NO CABLE CURVATURE

Time (hr)	Speed (knots)		Observed Tilt Angle (deg + 1 deg)			Computed Tilt Angle (deg)			Tilt Angle Error (deg)		
	15	60	15	60	105	15	60	105	15	60	105
.33	1.177	1.27	10	22	40	6.90	20.77	62.53	-3.10	-1.12	-
.66	1.205	1.16	10	20	40	6.45	19.50	60.90	-3.55	-.50	-
1.00	1.079	1.08	7	18	40	5.38	16.45	56.27	-1.62	-1.55	-
1.33	1.099	1.07	6	14	40	5.43	16.59	56.51	-.57	2.59	-
1.66	.945	.928	6	11	18	4.06	12.53	48.42	-1.94	1.53	30.42
2.00	.836	.713	5	7	40	2.78	8.64	37.62	-2.22	1.64	-
2.33	.717	.578	4	7	40	1.94	6.06	28.31	-2.06	-.94	-
2.66	.538	.497	4	5	40	1.24	3.88	18.99	-2.76	-1.12	-
3.00	.509	.341	3	3	10	.84	2.62	13.07	-2.16	-.38	3.07
3.33	.378	.214	2	4	17	.41	1.27	6.42	-1.59	-2.73	10.58
3.66	.420	.159	3	1	7	.39	1.22	6.15	-2.61	.22	-.85
49.0	1.253	1.086	15	25	18	6.31	19.11	60.36	-8.69	-5.89	42.36
50.0	1.169	1.088	15	25	40	5.88	17.88	58.57	-9.12	-7.12	-
51.0	.940	.943	10	20	40	4.10	12.66	48.72	-5.90	-7.34	-
52.0	.748	.516	6	11	40	1.85	5.78	27.17	-4.15	-5.22	-
53.0	.617	.265	5	5	9	.90	2.82	14.03	-4.10	-2.18	5.03
54.0	.790	.576	5	5	10	2.17	6.76	31.01	-2.83	1.76	21.01
55.0	.908	.666	4	10	40	2.87	8.92	38.51	-1.13	-1.08	-
56.0	.824	.814	5	5	19	3.10	9.64	40.76	-1.90	4.64	21.76
20.0	.632	.699	5	5	40	2.05	6.40	29.64	-2.95	1.40	-
21.0	.578	.345	5	5	5	.99	3.09	15.31	-4.01	-1.91	10.31
22.0	.630	.363	6	15	40	1.14	3.57	17.58	-4.86	-11.43	-
23.0	.910	.845	10	23	40	3.56	11.04	44.70	-6.44	-11.96	-
24.0	1.178	1.108	16	30	41	6.03	18.31	59.22	-9.97	-11.69	-
25.0	1.219	.985	14	30	40	5.61	17.10	57.35	-8.39	-12.90	-
26.0	1.158	1.056	15	26	18	5.66	17.25	57.58	-9.34	-8.75	39.58
27.0	.893	.699	9	20	18	2.93	9.12	39.15	-6.07	-10.88	21.15
28.0	.691	.342	6	6	40	1.24	3.87	18.92	-4.76	-2.13	-

28 Set average error -3.77 -2.69 16.66

Overall average error 3.4

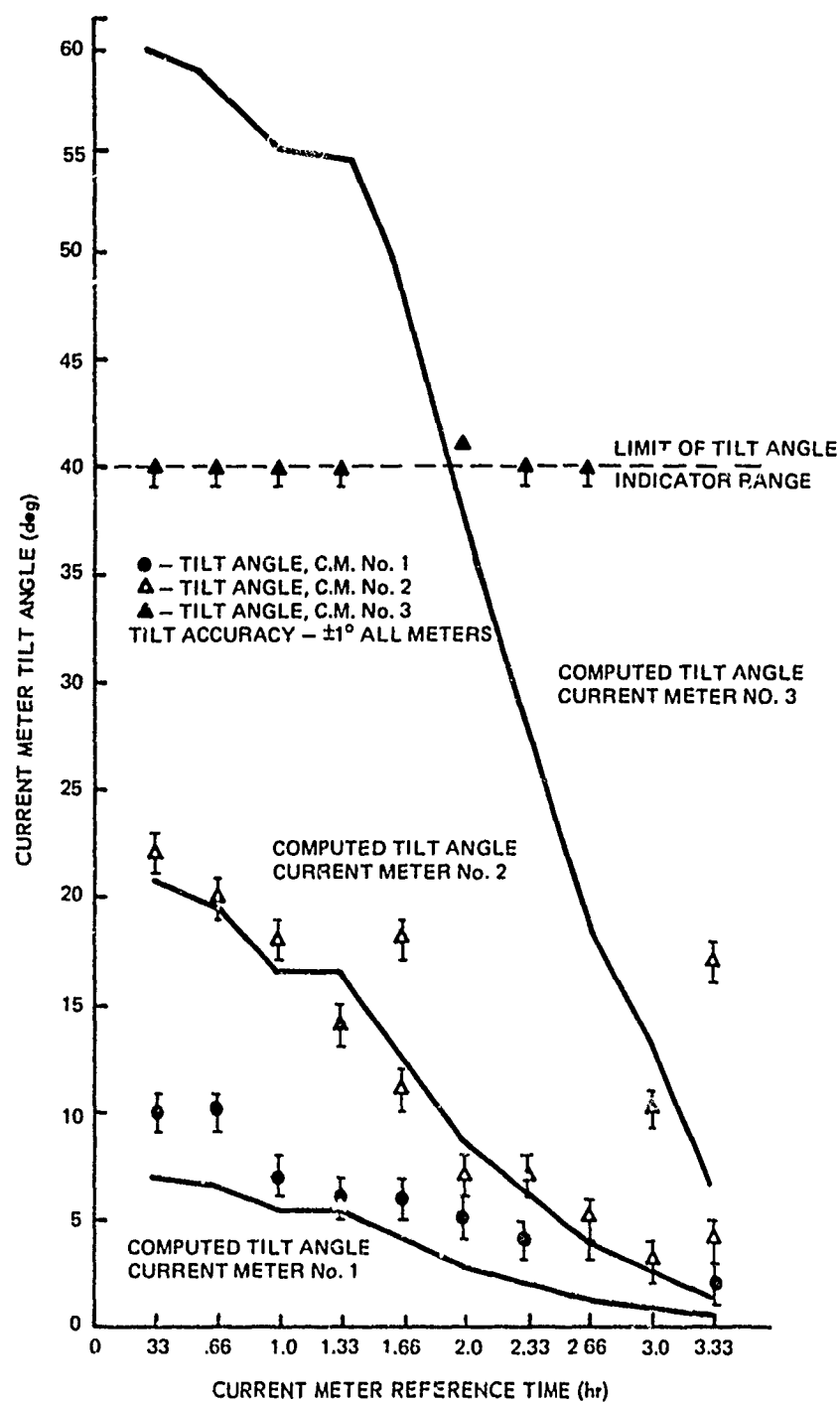


Figure 26. Current Meter Tilt Angles Computed by Simple Statistics Model Compared With Observed Data

#### 4.1.2 WHOI Mooring No. 279

Millard<sup>37</sup> describes tension measurements made on a taut-moored buoy system. The buoy system (figure 27) was installed in water 2685 m deep at Woods Hole Oceanographic Institution Site D. Tensions were recorded at four locations along the mooring line, and currents were recorded at a depth of 12 m for the  $2\frac{1}{2}$  months that the buoy system was on station. Berteaux and Walden<sup>79</sup> describe the properties of the wire rope and plaited nylon rope used in this buoy system as follows:

	<u>Diameter (in.)</u>	<u>Weight/ft in Sea Water (lb/ft)</u>
1/4-in. 1 × 50 wire rope	0.25	0.090
5/8-in. plaited nylon	0.625	0.01047.

The cable modulus for the wire rope was taken as  $1.682 \times 10^7$  lb/in.<sup>2</sup>.

Nylon rope is subject to both elastic and inelastic deformation when loaded.

New rope, when first loaded, will acquire a permanent deformation, the amount of which depends on the initial load. Furthermore, if the load is left on the rope, the rope is subject to creep and the permanent deformation increases with time. Martin<sup>14</sup> discusses the various mechanisms for the deformation of nylon rope. Using Martin's curve for the percent stretch versus load for the 5/8-in.-diameter plaited nylon rope, the rope modulus is computed as follows:

$$E = 3.52 \times 10^5 \text{ lb/in.}^2 ; 0 < T < 1000 \text{ lb}$$

$$E = 6.79 \times 10^5 \text{ lb/in.}^2 ; 1000 < T < 2000 \text{ lb}$$

$$E = 1.041 \times 10^6 \text{ lb/in.}^2 ; 2000 < T .$$

- PURPOSE OF TEST - EVALUATION OF MOORING CONFIGURATION AS SHOWN OVER A TWO MONTH PERIOD - MEASUREMENT OF MOORING TENSION STRETCH 13%
- PROCEDURE - LAUNCH BUOY, PAY OUT MOORING LINE, ATTACH BALLS, LAUNCH ANCHOR, CHECK ANCHORING, RETRIEVE NEXT CRUISE
- EQUIPMENT - AS SHOWN

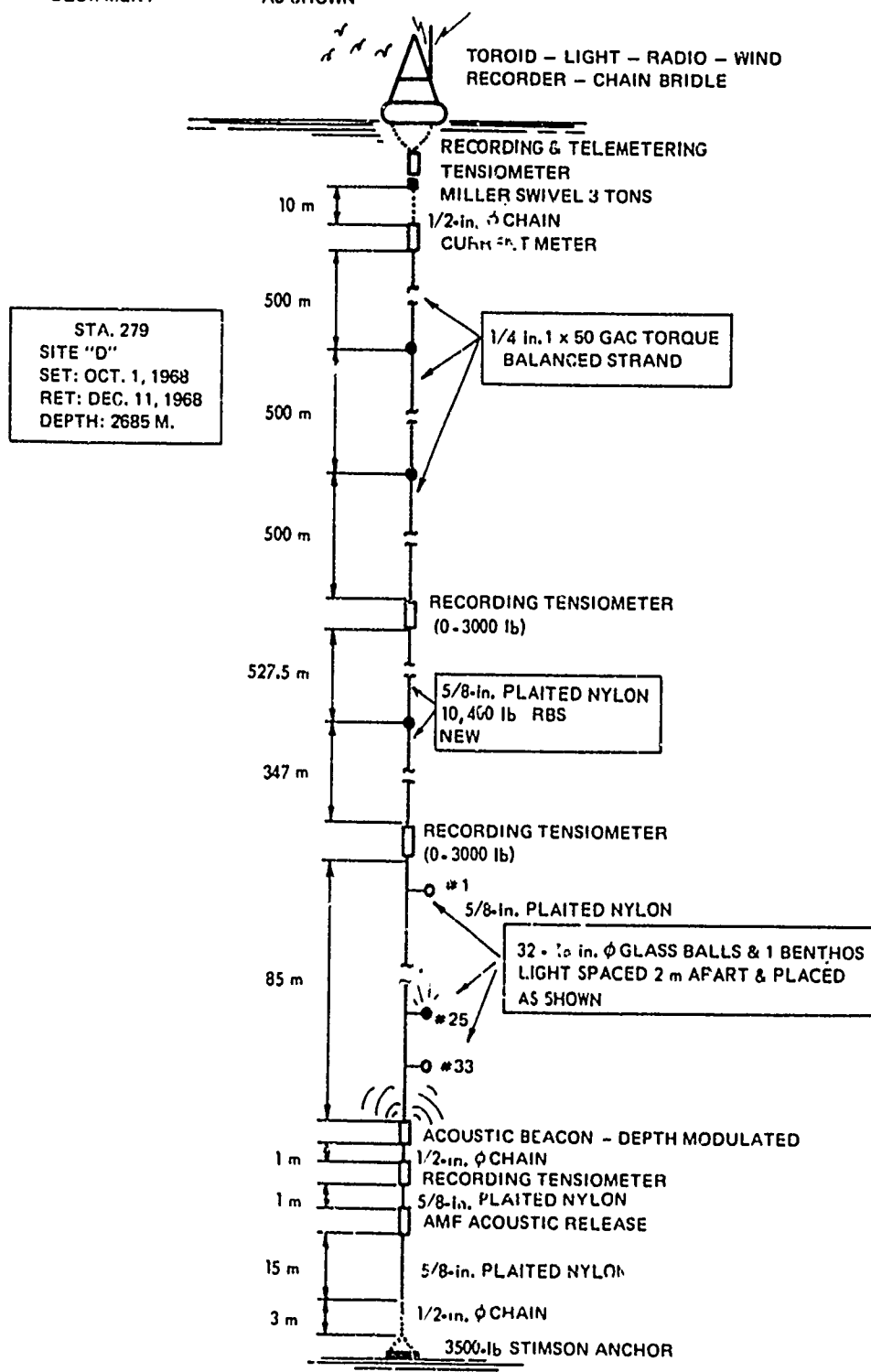


Figure 27. Woods Hole Oceanographic Institution Mooring No. 279

Webster<sup>80</sup> measured currents for a 2-month period at site D. Webster's data were curve-fitted using the program CURFIT on the GSA time-sharing computer, and the following function for the current strength as a function of depth was developed:

$$C = 2.6 \cdot C_s \cdot D^{-0.418},$$

where

$C$  is the current (ft/sec)

$C_s$  is the surface current (ft/sec)

$D$  is the depth (meters).

The steady-state buoy system configuration computer program was modified to include Webster's current profile, Martin's elastic properties for the nylon rope, and the cable properties given by Berteaux and Walden. Since information on the variations of current direction with depth was not available, the currents were assumed to be acting in the same direction at all depths. Furthermore, the initial inelastic stretch due to the emplantment and the dynamic wave loads is not known. The no-current elastic stretch of the nylon rope was assumed, and the tensions in the system were computed while currents acted on the system. Tensions at the junction of the wire rope and nylon rope are shown in figure 28 as functions of the surface current and of the no-current elastic stretch. Data taken by Millard at the same location on the mooring line are also shown on figure 28. Because of the creep properties of the nylon rope, the inelastic stretch will increase and the no-current elastic stretch will decrease as time increases. The shape of the tension curve will remain roughly the same, but the tension bias will decrease with time. Since the



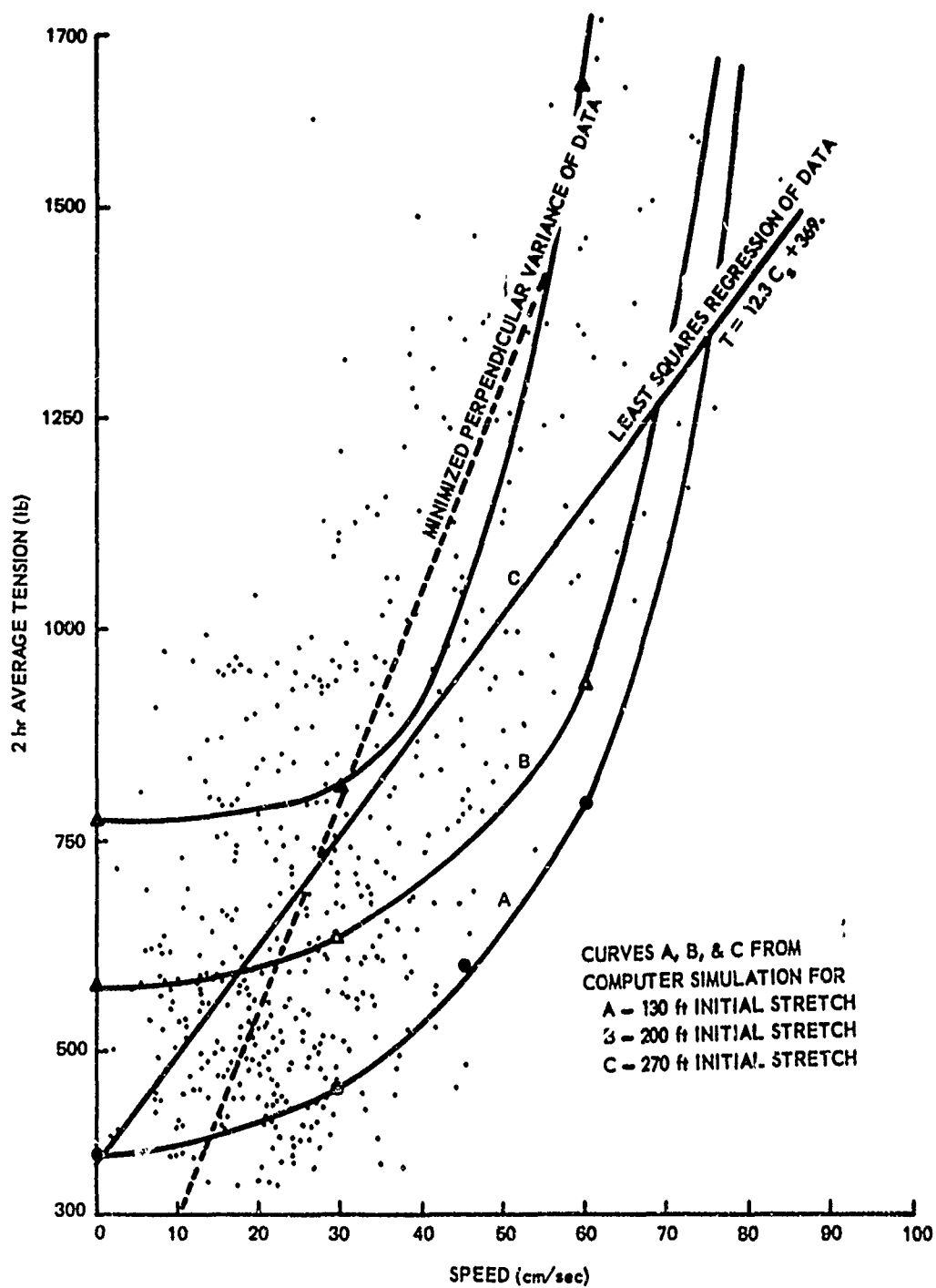


Figure 28. Comparisons of WHOI Data With Computed Mean Mooring Line Tensions

creep properties of the nylon rope are not known, computation of errors between observed and computed tensions in this case is of little value.

Millard analyzed the tension versus surface current data shown on figure 28 and least-squares fitted the linear function:

$$T = 12.3 \cdot C_s + 369 \text{ .}$$

Least-squares linear fits to the computed curves A, B, and C are

$$T = 12.59 \cdot C_x + 608 \text{ ,}$$

$$T = 12.25 \cdot C_s + 381 \text{ ,}$$

and

$$T = 12.10 \cdot C_s + 203 \text{ .}$$

Slopes of the computed linearized functions are in very close agreement, which indicates that the functional form of the computed tensions is accurate.

From this comparison, it is obvious that more experimentation on the elastoplastic properties of nylon rope is needed in order to predict the steady-state configurations of deep ocean, taut-moored buoy systems. Also, a deep ocean buoy system should be installed with both recording tensiometers and inclinometers to better validate the steady-state computer model.

#### 4.2 Experimental Measurements of Buoy System Dynamics

In order to validate the computer simulation of buoy system dynamics, buoy motions as measured at sea will be correlated with computer simulated buoy system response to the same environmental conditions.

Two oceanographic buoys were equipped with motion sensing instrumentation and installed in Block Island Sound. The smaller of the two buoys, a

3½-ft-diameter sphere, was installed in March 1970 off Great Salt Pond entrance, Block Island, Rhode Island. The larger buoy, an 8-ft-diameter torroid was installed at station BRAVO during May 1970. A description of the instrumentation and a discussion of the measurements taken are presented in reference 81.

#### 4.2.1 Spherical Buoy at Station D

The 3½-ft-diameter spherical buoy is shown in figure 29. This buoy was loaned to the writer by Dr. A. Nalwalk, of the Marine Sciences Institute of the University of Connecticut. The buoy was equipped with the following instrumentation:

Heave motion statistical accelerometers

Current meter

Heave accelerometer

Surge Accelerometer

Sway accelerometer

Pitch pendulous potentiometer

Roll pendulous potentiometer

Cable pitch pendulous potentiometer

Cable roll pendulous potentiometer

Cable tension gage

Thermis.or.

The buoy system was installed in 62 ft of water, west of Great Salt Pond entrance at Block Island by the Research Vessel, UCONN, on 2 March 1970.

The 1½-in.-diameter, 14-conductor armored cable was laid along the bottom to

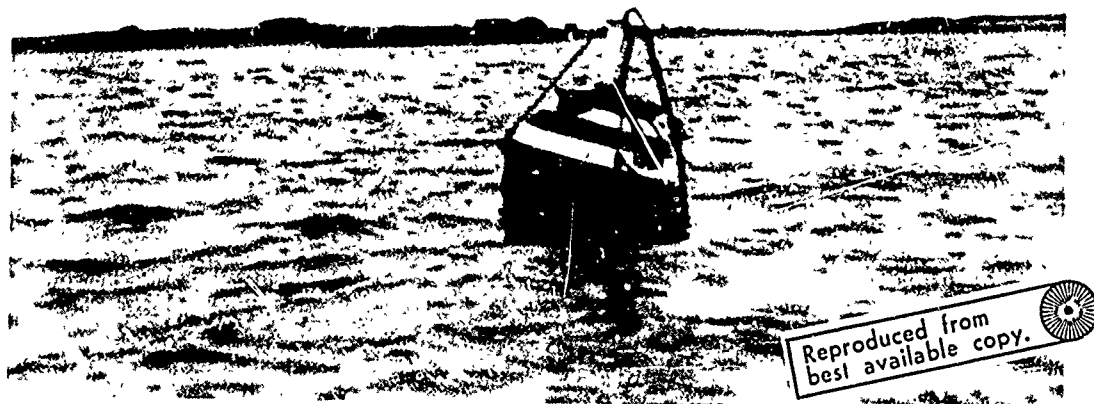


Figure 29. Spherical Buoy at Block Island Station D

the beach and was carried over the beach to the BIFI field station: A Snodgrass wave sensor was also installed off the beach in 25 ft of water. The arrangement of cables and instruments is shown schematically in figure 30.

Two weeks of statistical heave accelerometer data were collected. Some buoy motion data were also recorded. The electrical conductors in the cable began to fail after a month of use and a number of attempts were made to repair the cable in order to continue collecting data. The buoy broke loose during a storm in early November 1970 and is missing.

The statistical accelerometers were designed to count at 0.35-, 0.50-, 0.65-, 0.80-, 1.20-, 1.35-, 1.50-, and 1.65-g heave acceleration levels. The pulses from the accelerometers actuated counters in the van at the BIFI Field Station, and the total count was recorded daily. Sea state data were based on estimates by the resident engineer (Carl T. Milner) and by Coast Guard observations reported by the ESSA Marine Weather Service. Data were recorded during the period 4 March to 12 March 1970.

Data from the 22 observations of positive acceleration counts were used to generate figure 31, a plot of the counts per hour versus acceleration level for various sea states. The negative acceleration counters did not work, because of the failure of leads in the cable. Figure 31 indicates that for any sea state greater than sea state 0, the buoy will always undergo 1.2-g accelerations at a rate of 1,000/hr. The number of cycles per hour for higher acceleration levels will increase with increasing sea state. Figure 32 is the conditional probability of the buoy exceeding various positive acceleration levels given that the buoy exceeds 1.2-g level accelerations. Figure 33 shows the buoy heave acceleration

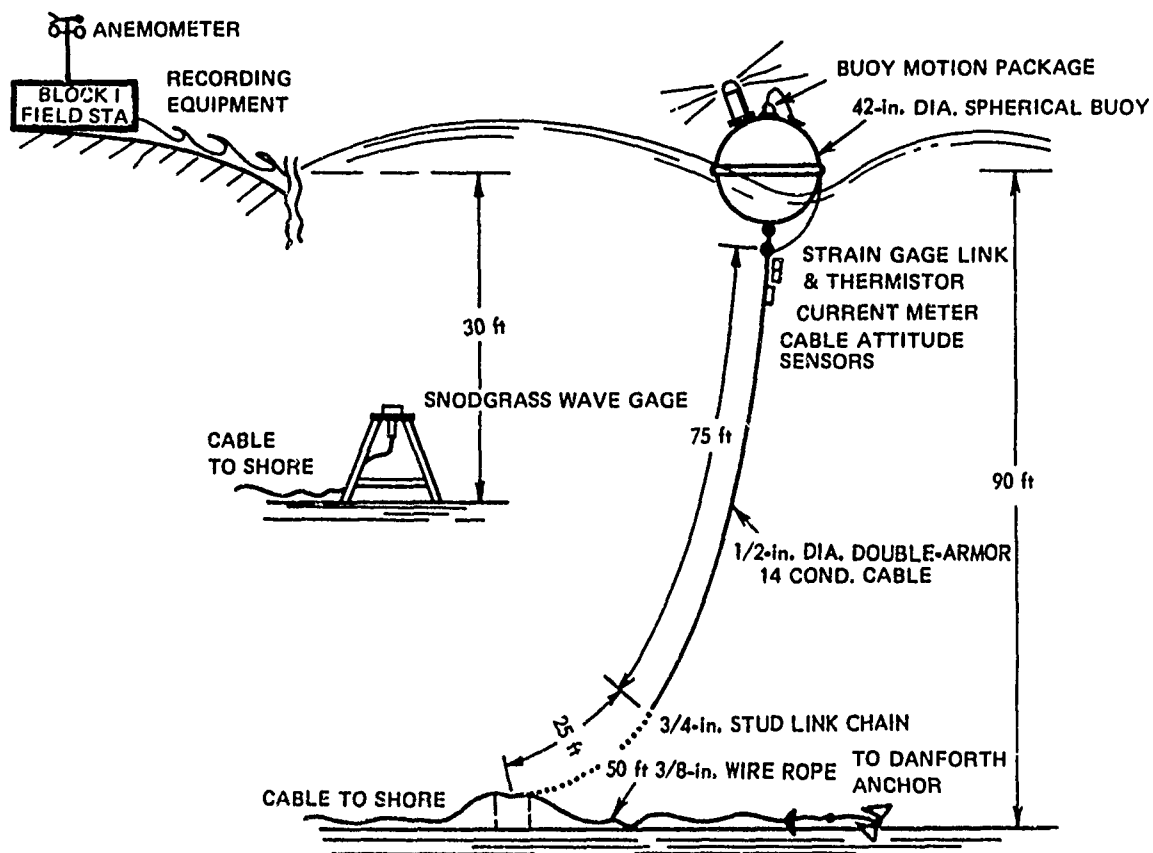


Figure 30. Spherical Buoy System at Block Island

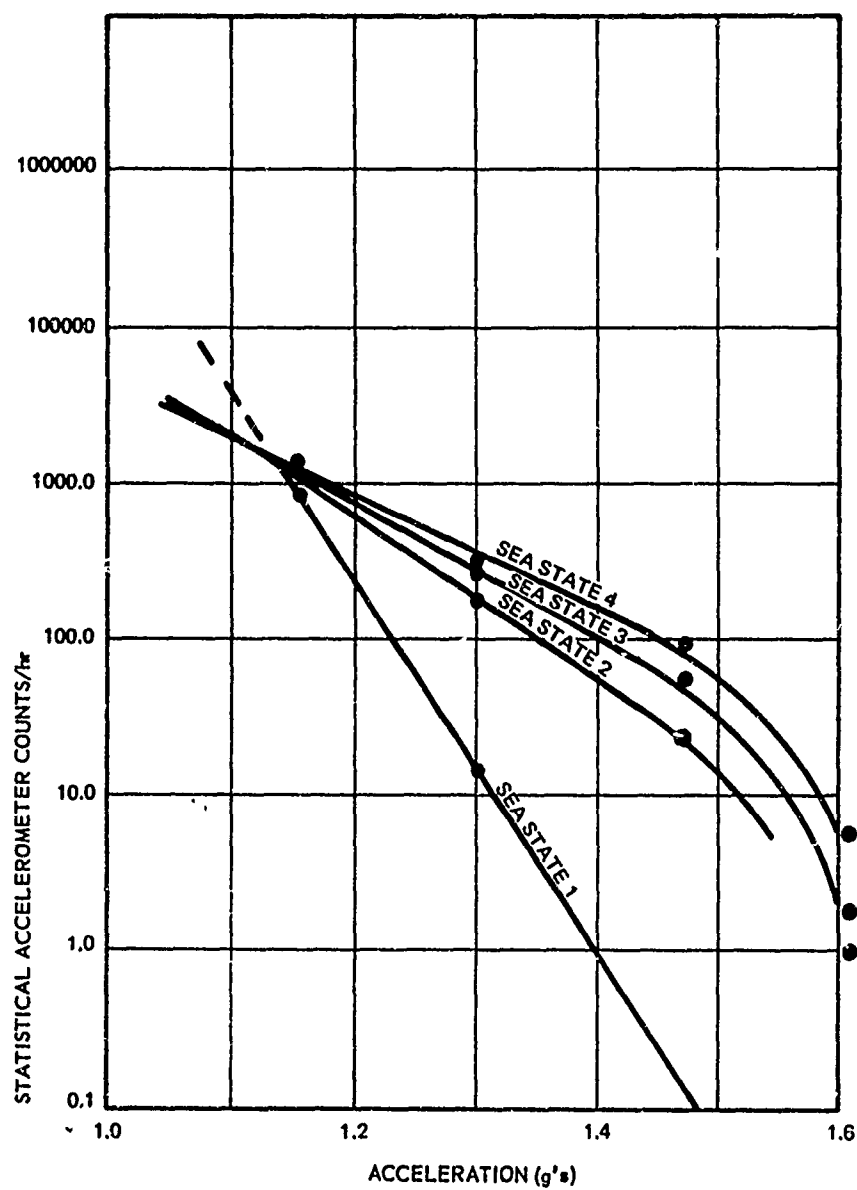


Figure 31. Statistical Accelerometer Data for Heave Motions

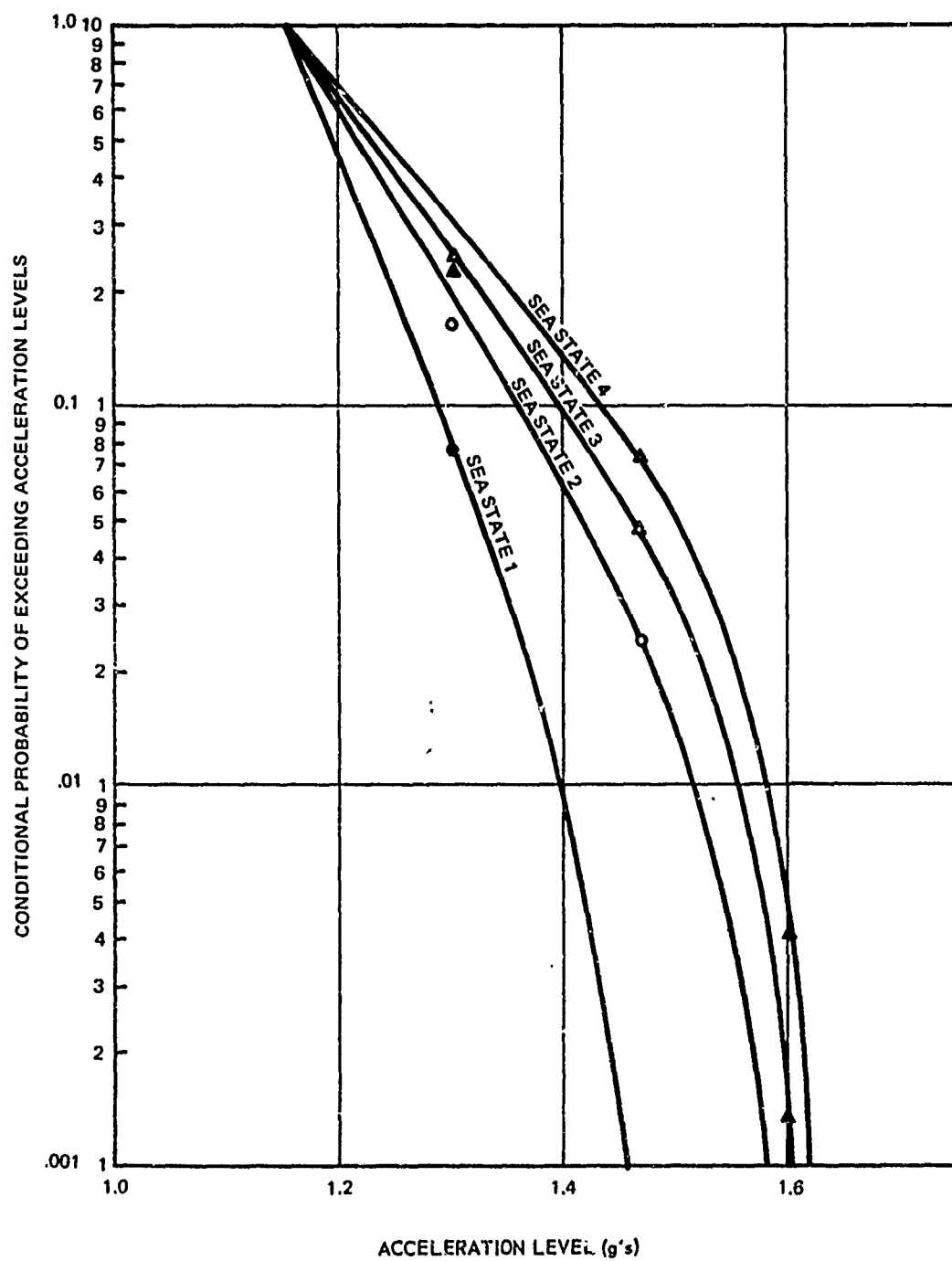


Figure 32. Conditional Probabilities for Heave Motions



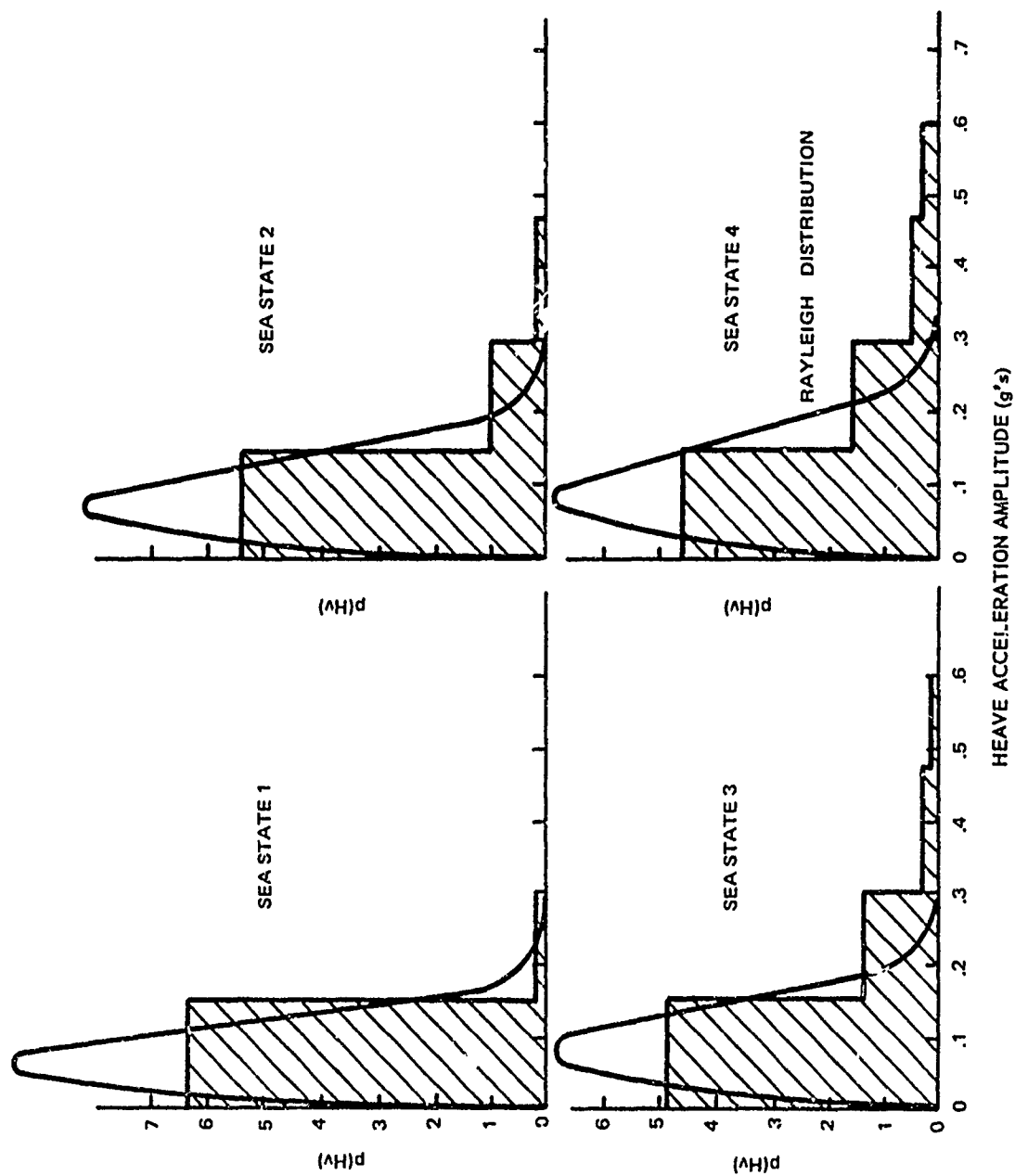


Figure 33. Spherical Buoy Heave Acceleration Amplitude Distributions

amplitude histogram for various sea state conditions. Rayleigh distributions are plotted over the histograms and were computed by using the mean of the histograms. Longuet-Higgins<sup>55</sup> and Bretschneider<sup>51</sup> have shown that the distribution of wave heights is given by the Rayleigh distribution.

Analog data of the spherical buoy motions were also recorded. On 16 March 1970, the following records were obtained on a two-channel strip chart recorder:

- Wave height (20 min)
- Buoy heave and buoy surge (15 min)
- Buoy heave and buoy pitch (10 min)
- Buoy heave and buoy roll (10 min)
- Buoy heave and cable pitch (10 min)
- Buoy heave and cable roll (10 min).

Winds were 15 to 20 knots, northeast, with an estimated sea state 3 at the buoy. Results of a simple "quick look" analysis are shown in figures 34 through 37.

One-hundred samples of each record were digitized and analyzed on the GSA-440 time sharing computer. Figure 34 shows means, variances, and standard deviations for each parameter. In addition, the correlation matrix for simple product-moment correlations is shown. Parameters that should be coupled appear to be coupled, and parameters that should be decoupled appear to be decoupled. For example, heave-surge, heave-pitch, and surge-pitch are coupled, and heave-roll, surge-roll, and pitch-roll are decoupled. Also, cable angles are mildly coupled to buoy displacements but decoupled from buoy angles.

<u>VARIABLE</u>	<u>MEAN</u>	<u>VARIANCE</u>	<u>STANDARD DEVIATION</u>			
HEAVE ACCELERATION	0 g	0.0242 g <sup>2</sup>	0.1555 g			
SURGE ACCELERATION	0 g	0.00978 g <sup>2</sup>	0.0991 g			
PITCH ANGLE	1.1 deg BOW DOWN	104.2 deg <sup>2</sup>	10.20 deg			
ROLL ANGLE	14.3 deg PORT	55.3 deg <sup>2</sup>	7.58 deg			
CABLE PITCH	-27.1 deg	24.0 deg <sup>2</sup>	4.90 deg			
CABLE ROLL	-7.3 deg	16.2 deg <sup>2</sup>	4.01 deg			
<u>THE CORRELATION MATRIX</u>						
	<u>HEAVE</u>	<u>SURGE</u>	<u>PITCH</u>	<u>ROLL</u>	<u>CABLE PITCH</u>	<u>CABLE ROLL</u>
HEAVE	1.0	0.4806	0.6050	-0.0706	0.2435	0.0454
SURGE		1.0	-0.4199	0.0054	-0.1605	0.1975
PITCH			1.0	-0.1021	0.0063	-0.0946
ROLL				1.0	0.2121	-0.3813
CABLE PITCH					1.0	-0.2282
CABLE ROLL						1.0

Figure 34. Spherical Buoy Motion Parameter Statistics

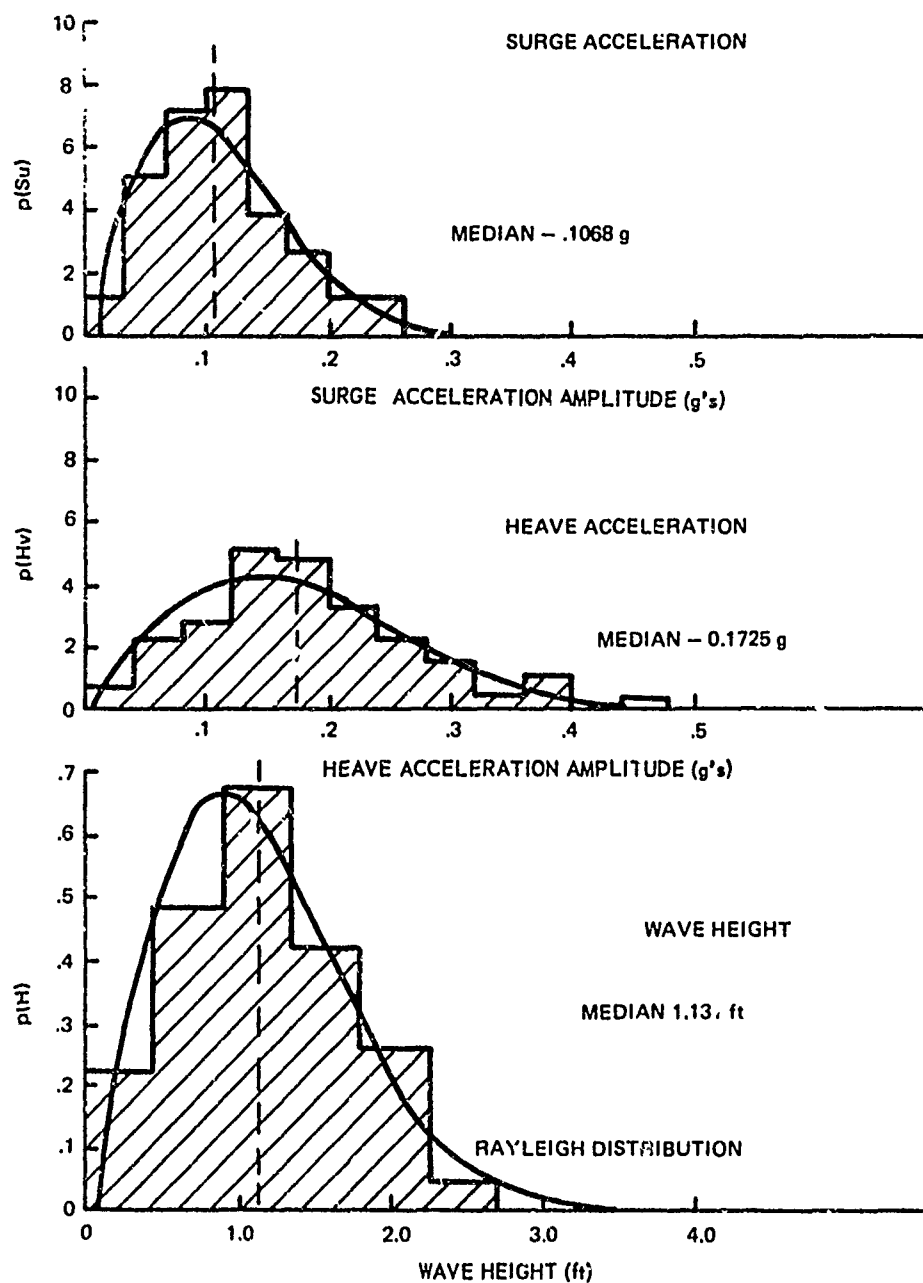


Figure 35. Spherical Buoy Motion Amplitude Histograms — Wave Height, Heave, and Surge

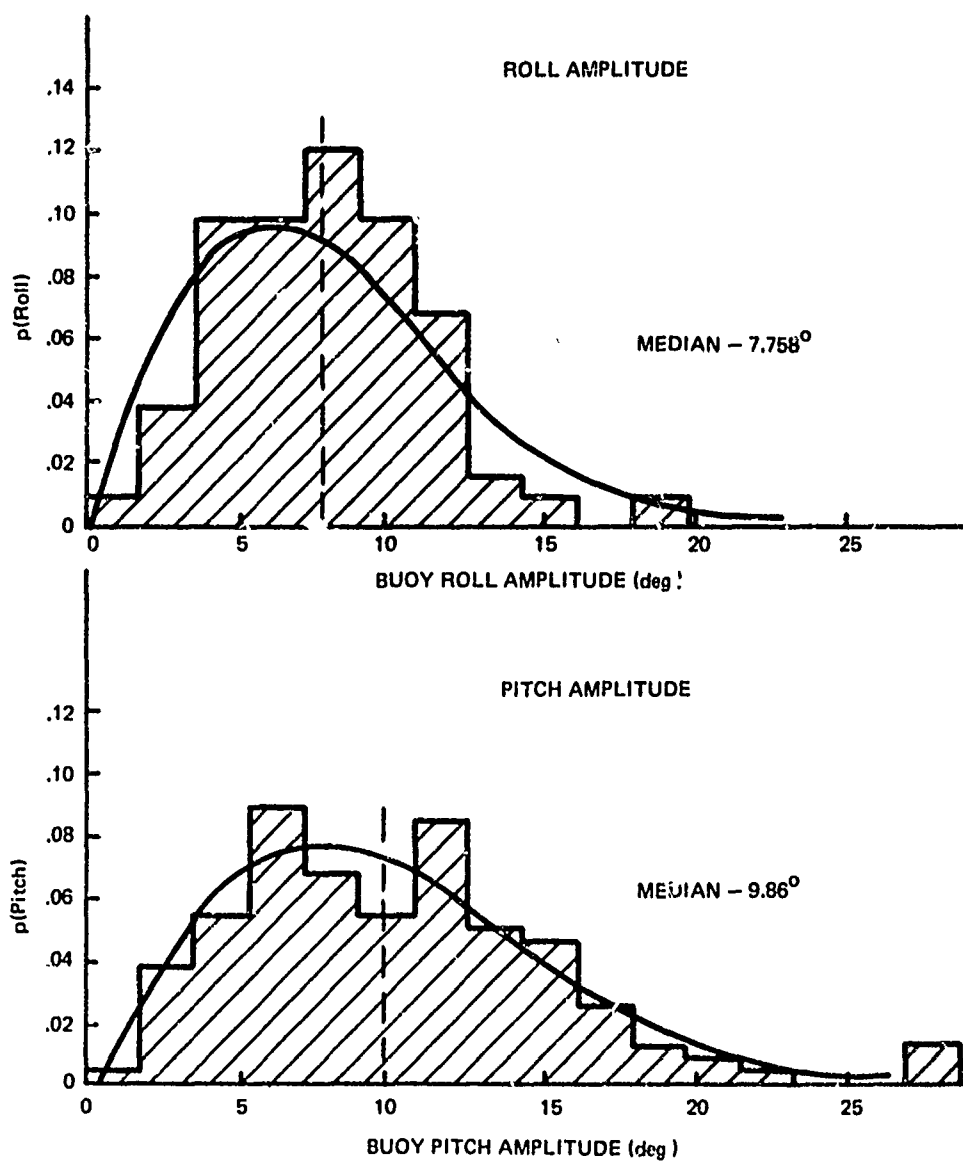


Figure 36. Spherical Buoy Motion Amplitude Histograms — Pitch and Roll

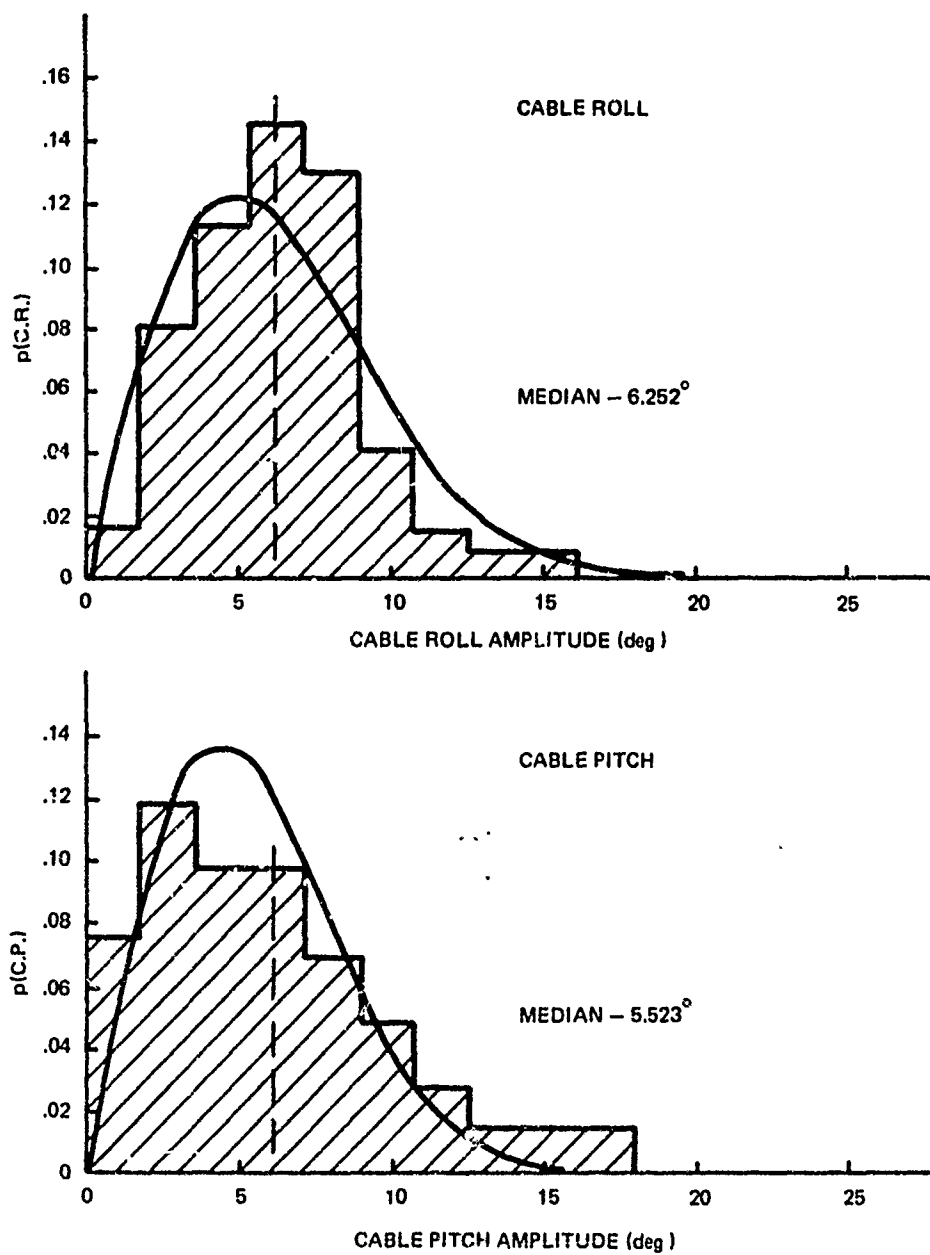


Figure 37. Spherical Buoy Motion Amplitude Histograms — Cable Pitch and Roll

One hundred amplitudes from each parameter record were digitized and were used to generate parameter amplitude histograms. These probability distributions are shown in figures 35 and 37. The median amplitudes were computed and were used to compute Rayleigh distributions, which are plotted over the histograms. The Rayleigh distributions of the form

$$p(H) = \frac{\pi}{2} \frac{H}{\bar{H}^2} e^{-\frac{\pi}{2} \frac{H^2}{\bar{H}^2}},$$

where

$p(H)$  is the probability of parameter  $H$

$H$  is the parameter

$\bar{H}$  is the mean value of the parameter,

were found to match the histograms quite well. The fact that the amplitude probability distributions all appear to fit a Rayleigh distribution indicates a linear transform from wave height to buoy response.

If the functions relating the mean buoy motion amplitude parameters to sea state were known, the probability distribution for any parameter in any sea state can be computed from the Rayleigh distribution.

From the statistical accelerometer data, the mean heave acceleration amplitude can be plotted versus mean wave height (using Vine and Volkman's<sup>80</sup> relations for sea state and mean wave height). This curve, shown in figure 38, can be approximated in the region  $H = 1$  to 10 ft with the linear function:

$$\bar{H}_v = 0.11 + 0.0086 \bar{H}.$$

Assuming a linear transform for the other motion parameters and averaging pitch and roll amplitude means, we can write a set of linear equations for the

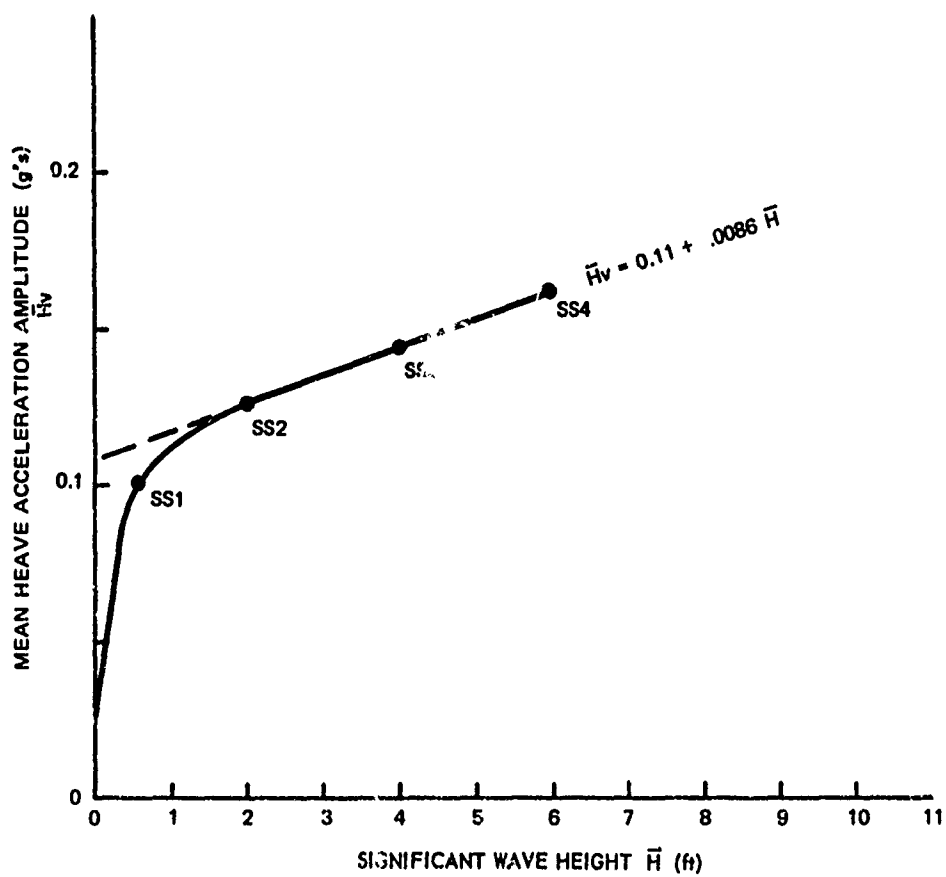


Figure 38. Heave Response of the Spherical Buoy



mean motion amplitudes. In addition, these equations can be substituted into the Rayleigh equation to find the amplitude probability distribution for any parameter. The linear equations and their amplitude distributions are as follows:

For  $1 < H < 10$  ft, the mean heave acceleration amplitude is

$$\overline{H_v} = 0.11 + 0.0086 \overline{H},$$

The amplitude probability distribution is

$$p(H_v) = \frac{\pi}{2} \frac{H_v}{\overline{H_v}^2} e^{-\frac{\pi}{4} \frac{H_v^2}{\overline{H_v}^2}}.$$

The mean surge acceleration amplitude is

$$\overline{S_v} = 0.0688 + 0.00537 \overline{H},$$

and the probability distribution is

$$p(S_v) = \frac{\pi}{2} \frac{S_v}{\overline{S_v}^2} e^{-\frac{\pi}{4} \frac{S_v^2}{\overline{S_v}^2}}.$$

The mean sway acceleration amplitude is

$$\overline{S_w} = 0.0688 + 0.00537 \overline{H},$$

and the probability distribution is

$$p(S_w) = \frac{\pi}{2} \frac{S_w}{\overline{S_w}^2} e^{-\frac{\pi}{4} \frac{S_w^2}{\overline{S_w}^2}}.$$

The mean pitch angle amplitude is

$$\overline{P_t} = 5.59 + 0.436 \overline{H},$$

and the probability distribution is

$$p(P_t) = \frac{\pi}{2} \frac{P_t}{\overline{P_t}^2} e^{-\frac{\pi}{4} \frac{P_t^2}{\overline{P_t}^2}}.$$

The mean roll angle amplitude is

$$\overline{R_l} = 5.59 + 0.436 \overline{H},$$

and the probability distribution is

$$p(RL) = \frac{\pi}{2} \frac{RL}{RL^2} e^{-\frac{\pi}{4} \frac{RL}{RL^2}}.$$

The mean cable pitch angle amplitude is

$$\overline{CPt} = 3.41 + 0.294 \bar{H},$$

and the probability distribution is

$$p(CPt) = \frac{\pi}{2} \frac{CPt}{CPt^2} e^{-\frac{\pi}{4} \frac{CPt^2}{CPt^2}}.$$

The mean cable roll angle amplitude is

$$\overline{CRL} = 3.41 + 0.294 \bar{H},$$

and the probability distribution is

$$p(CRL) = \frac{\pi}{2} \frac{CRL}{CRL^2} e^{-\frac{\pi}{4} \frac{CRL^2}{CRL^2}}.$$

The preceding empirical equations will serve as a first-order approximation to the buoy motion parameters for the spherical buoy and can be used for design purposes.

#### 4.2.2 Torroidal Buoy at Station BRAVO

An 8-ft-diameter, torroidal oceanographic buoy was outfitted with buoy motion sensing instrumentation and telemetry and was installed in Block Island Sound during May-June 1970. The buoy (figure 39) was installed by the USCGC MARIPOSA on 30 April 1970 at station BRAVO in 120 ft of water. A telemetry receiving station was established in the generator building at the Watch Hill Lighthouse, Watch Hill, Rhode Island (figures 40 and 41). A schematic of the instrumentation arrangement is shown in figures 42 and 43. A detailed description of the instrumentation, circuitry, and calibrations is described in reference 81.

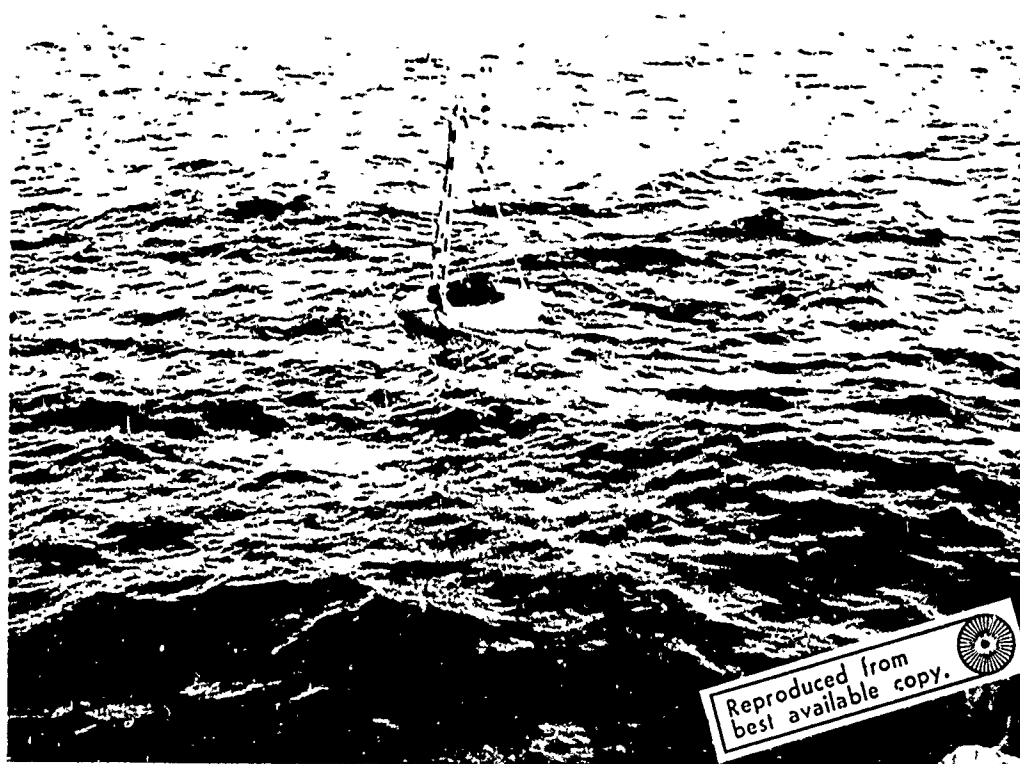


Figure 39. Torroidal Buoy at Station BRAVO

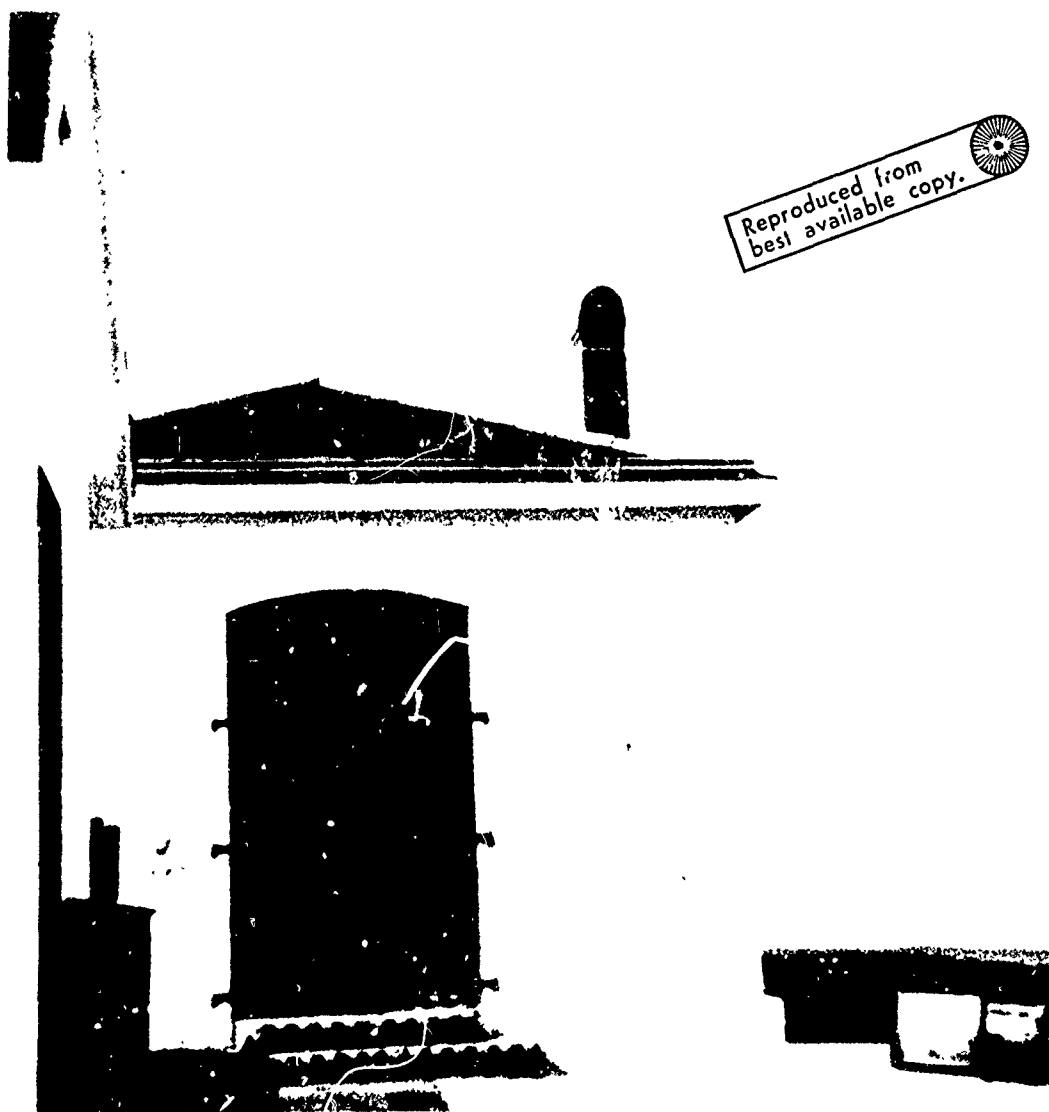


Figure 40. The Shore Station at Watch Hill Lighthouse

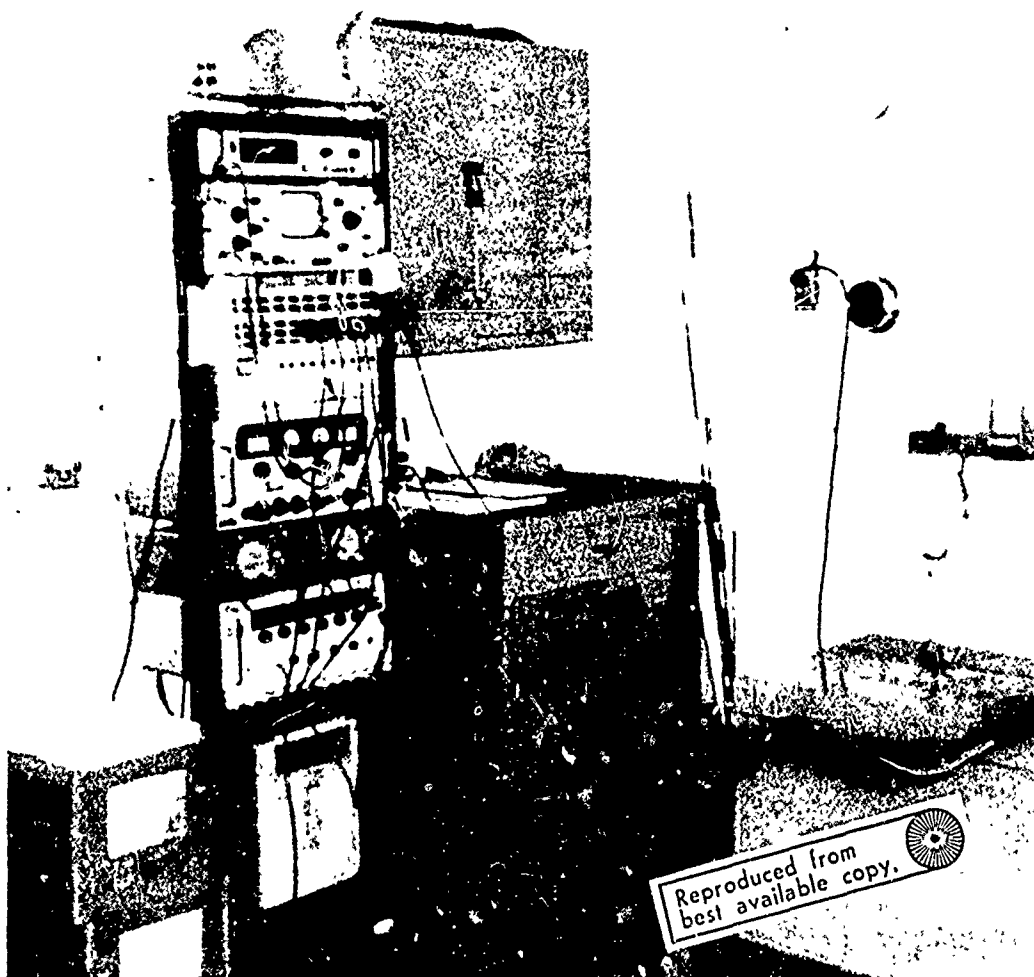


Figure 41. Telemetry Receiver and Recording Equipment

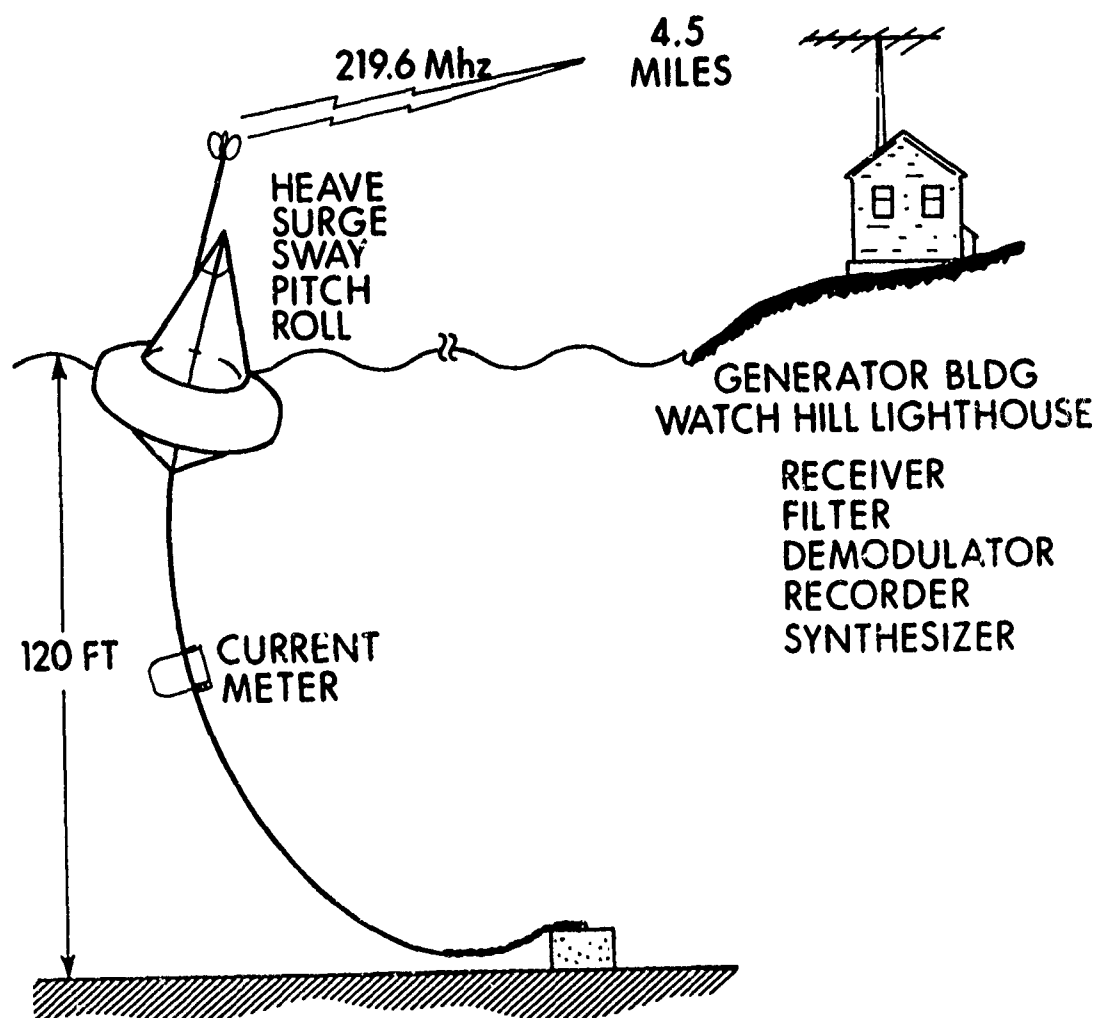


Figure 42. Torroidal Buoy Motion Experiment Setup

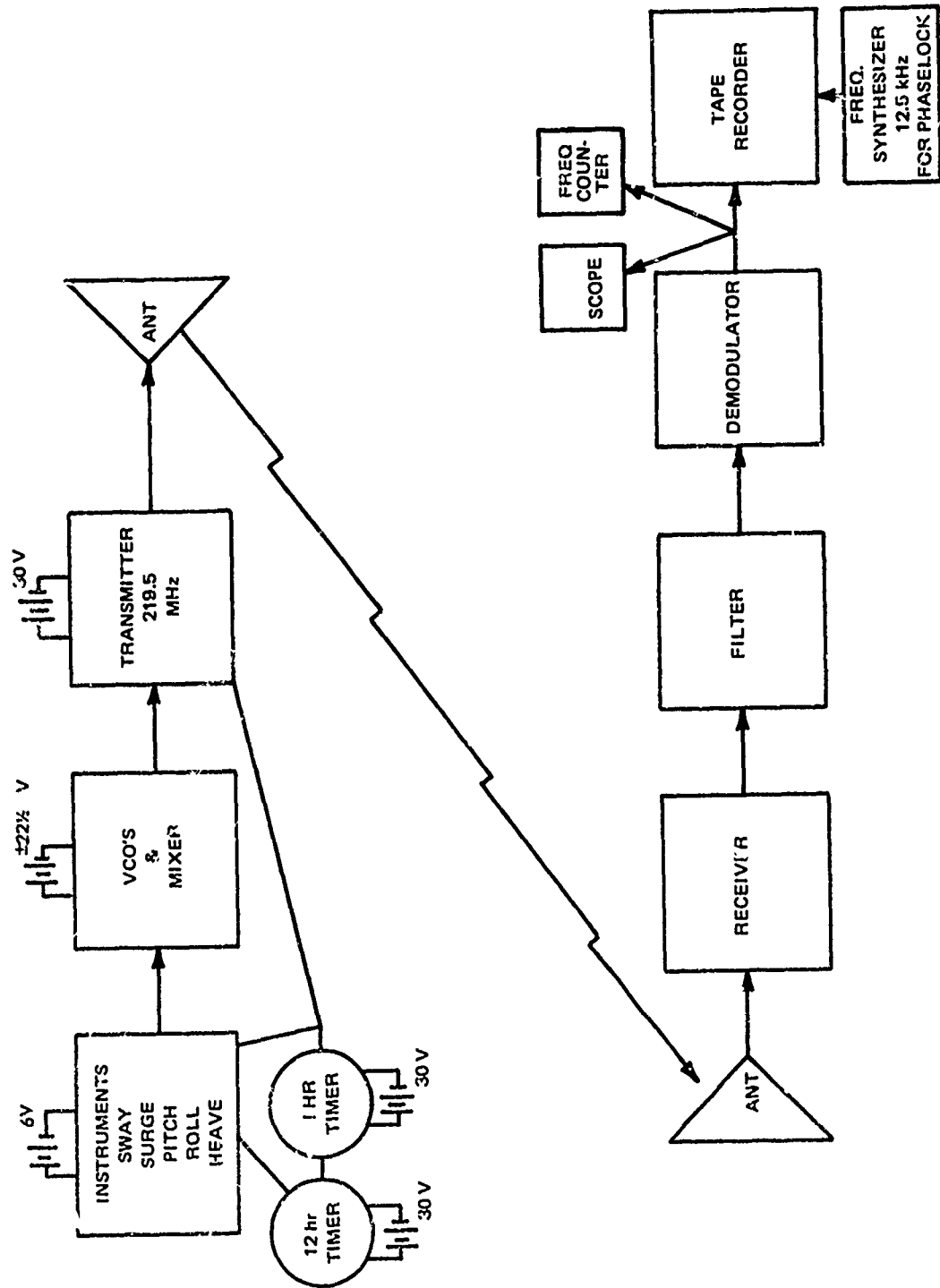


Figure 43. Buoy Motion Telemetry System

The buoy contained the following motion sensing instrumentation:

Heave accelerometer

Surge accelerometer

Sway accelerometer

Pitch angle potentiometer

Roll angle potentiometer.

In addition, a self-recording current meter was attached to the mooring cable at a depth of 60 ft. Wind speeds were recorded on a paper tape recorder at the Watch Hill Lighthouse. Wind directions were logged every 4 hr by the duty personnel at the Lighthouse. Also, the ESSA weather reports on 163.5 kHz were monitored during each data run, and reported conditions at Coast Guard Stations bordering Block Island Sound were logged on the data sheets.

The buoy transmitted data every 12 hr for a  $\frac{1}{2}$ -hr time period. Each data transmission was preceded by a calibration sequence consisting of two voltage levels from the potentiometer sensors. The FM signals from the buoy containing the five mixed frequencies were demodulated and recorded on an FM tape recorder. The composite signal and a 12.5-kHz phase-lock signal were also recorded on two AM channels.

During the 51 days the buoy was on station, 55 data transmissions were recorded. The only major problem encountered was the failure of the operational amplifier that mixed the five frequencies from the voltage controlled oscillators in the buoy. This component was replaced and tests continued. Structurally, the only failure was the loss of a cotter pin on a shackle holding one of the three chain bridle legs under the buoy. The loss of this pin allowed



the shackle to come undone in such a manner that the buoy bridle had only two active legs. The buoy was recovered on 19 June 1970 by the USCGC REDWOOD.

Because of the large amount of recorded data, a simple "quick look" analysis of the data was performed by playing back the recorded data for each of the five motion parameters on a "memoscope." A 2-min sample of each parameter for each run was traced out. The mean width of the band trace-out was measured, and the value of the parameter double amplitude (in volts) was logged. This value was assumed to be the "significant" amplitude, i.e., the mean of the highest one-third of the amplitudes. It was found that the data on the pitch channel were too noisy to be used in this fashion; thus, pitch was not included in this analysis. The logged values of buoy heave, surge, and sway acceleration amplitudes along with buoy roll angle amplitude are shown in table 4. The environmental conditions are also shown for each run.

The statistics of the measured parameters are shown in figure 44. The matrix of simple product-moment correlation coefficients is also shown. These statistics were computed on the GSA-440 time sharing computer. Inspection of the correlation matrix indicates that all the significant buoy motions are well correlated. In addition, they correlate well with wind speed and, to a lesser extent, with computed wind wave height. A similar analysis was conducted with current speed. The elements of that correlation matrix are as follows:

	<u>Heave</u>	<u>Sway</u>	<u>Surge</u>	<u>Roll</u>
Current	0.1537	-0.00572	0.1040	-0.0237.

Thus, it appears that buoy motion amplitudes are not correlated with current speed. Buoy motions are not significantly affected by current speed.

TABLE 4. SUMMARY OF OBSERVED ENVIRONMENTAL AND BUOY RESPONSE DATA  
FOR THE TORROIDAL BUOY BRAVO

Date (1967)	Time (hr)	Wind		Computed Depth & Current			Computed Wind Waves			Observed Waves				Parameter Double Amplitude from Memoscope (V)				Mean Roll (V)	Mean Pitch (V)
		Speed (knots)	Direction (deg)	Duration (hr)	Water Depth (ft)	Surface Current (knots)	Set (deg)	H <sub>1/3</sub> (ft)	T <sub>1/3</sub> (sec)	Swell (ft)	Wind (ft)	Heave	Sway	Surge	Pitch	Roll			
4/30	2230	-	-	-	120.0	1.00	065	-	-	-	-	-	-	0.3	-	-	-		
5/1	1030	8.0	135.0	2.0	120.1	0.66	065	1.597	5.270	1.0	-	0.5	0.45	0.5	-	-	-0.55		
5/1	2230	-	-	-	120.3	0.615	065	-	-	-	-	-	-	-	-	-	-		
5/2	1030	6.3	130.0	2.0	120.4	0.234	065	1.719	5.467	1.5	1	0.5	0.55	0.65	-	0.25	-0.5		
5/3	2230	0	-	-	123.2	0.456	265	-	-	2.0	0	0.25	0.15	0.2	-	0.18	-0.5		
5/4	2230	3.5	22.5	2.0	121.7	1.04	265	0.306	2.31	1.5	0	0.25	0.2	0.15	0.15	0.25	-0.35		
5/5	1030	4.3	202.5	1.0	122.1	1.26	265	0.472	2.87	1.0	0	0.18	0.15	0.14	-	0.2	-0.55		
5/5	2100	8.0	180.0	3.0	123.6	1.30	265	1.600	5.27	3.0	1.0	0.5	0.55	0.55	-	0.2	-0.5		
5/6	0900	14.8	292.5	5.0	122.6	0.95	265	1.717	3.459	2.5	1.5	0.5	0.5	0.45	-	0.2	-0.5		
5/6	2100	34.5	292.5	10.0	123.5	0.93	265	4.670	5.01	2.0	1.5	0.85	0.6	0.65	-	0.2	-0.5		
5/7	0900	16.9	292.5	12.0	122.1	0.50	265	2.006	3.66	1.0	1.75	0.55	0.45	0.52	-	0.28	-0.52		
5/7	2100	17.0	292.5	12.0	122.8	0.36	265	2.019	3.67	0.5	0	0.56	0.58	0.52	-	0.32	-0.52		
5/8	0900	10.4	281.0	4.0	121.8	0	-	1.136	2.97	0.75	0.5	0.52	0.75	0.65	-	0.28	-0.5		
5/8	2100	10.0	225.0	3.5	122.1	0	-	2.169	4.68	1.5	0	0.5	0.55	0.4	-	0.25	-0.55		
5/9	0900	0	225.0	-	121.3	0.41	065	-	-	1.0	0	0.2	0.25	0.1	-	0.15	-0.5		
5/10	0900	0.87	225.0	-	121.0	0.68	065	-	-	1.5	0	0.45	0.35	0.32	-	0.32	-0.52		
5/10	2100	10.0	225.0	1.0	120.6	0.58	065	2.495	6.59	1.0	1.0	0.65	0.5	0.55	-	0.40	-0.60		
5/11	0900	3.9	292.5	1.0	121.1	0.73	065	0.380	2.57	2.0	0	0.40	0.37	0.45	-	0.40	-0.55		
5/11	2100	0	-	-	120.7	0.66	065	-	-	1.25	0	-	-	-	-	-	-		
5/12	0900	0	270.0	-	120.7	0.75	065	-	-	1.0	0	0.6	0.5	0.5	-	0.45	-0.52		
5/12	2100	12.2	90.0	1.5	120.9	0.66	065	3.714	8.04	1.0	1.0	0.3	0.35	0.36	-	0.40	-0.62		
5/14	2100	8.7	45.0	4.0	120.9	0.39	065	0.698	2.27	-	1.5	0.65	0.7	0.65	-	0.45	-0.6		
5/15	0900	7.8	45.0	1.0	120.7	0.23	065	1.519	4.96	1.5	0.5	0.65	0.5	0.4	-	0.20	-0.5		
5/16	0900	11.3	90.0	3.0	120.8	0	-	3.186	7.44	2.5	1.0	0.25	0.25	0.21	-	0.11	-0.26		
5/17	0900	20.9	135.0	10.0	121.2	0.46	265	9.097	9.66	-	4.5	0.8	0.65	0.75	-	6.50	-0.6		
5/18	0900	20.9	67.5	10.0	120.7	0.78	265	4.562	5.94	2.5	4.0	-	-	-	-	-	-		
5/25	0830	18.2	90.0	3.0	120.9	0.88	065	8.265	11.989	-	2.5	0.8	0.65	0.65	-	0.5	-0.75		
5/25	2030	17.3	135.0	12.0	121.1	0.87	065	6.41	8.022	-	1.75	0.4	0.55	0.4	-	0.25	-0.65		
5/26	0830	0	-	-	120.5	1.08	065	-	-	1.0	0	0.45	0.4	0.3	-	0.2	-0.65		
5/26	2020	21.7	202.5	3.0	120.6	0.99	065	3.73	5.106	2.25	0.5	0.8	0.5	0.7	0.25	0.25	-0.5		

TABLE 4. (Cont'd) SUMMARY OF OBSERVED ENVIRONMENTAL AND BUOY RESPONSE DATA  
FOR THE TORROIDAL BUOY BRAVO

Date (1967)	Time (hr)	Wind			Computed Depth & Current			Computed Wind Waves			Observed Waves			Parameter Double Amplitude from Memoscope (V)				Mean Pitch (V)	Mean Roll (V)
		Speed (knots)	Direction (deg)	Duration (hr)	Water Depth (ft)	Surface Current (knots)	Set (deg)	H <sub>1/3</sub> (ft)	T <sub>1/3</sub> (sec)	Waves	Swell (ft)	Wind (ft)	Heave	Sway	Surge	Pitch	Roll		
5/27	0830	4.8	315.0	6.0	120.2	1.05	065	0.348	1.754	2.5	0.3	-	-	-	-	-	-	-	-
5/27	2030	13.0	315.0	11.0	120.3	0.92	065	1.116	2.703	2.0	0.5	0.8	0.6	0.5	-	-	0.2	-	-0.55
5/28	0830	4.4	315.0	0.5	120.1	0.74	065	0.483	2.899	2.0	0	0	0.25	0.3	0.35	-	0.2	-	-0.55
5/28	2030	4.4	225.0	6.0	120.3	0.65	065	0.483	2.814	1.5	0.3	0.3	0.45	0.5	0.24	-	0.2	-	-0.6
5/29	2030	3.5	135.0	5.0	120.7	0.23	065	0.306	2.306	1.0	0.5	0.5	0.25	0.2	0.25	-	0.15	-	-0.6
5/30	2030	8.7	135.0	6.0	121.9	0.90	265	1.888	5.731	-	1.5	1.5	0.45	0.4	0.35	-	0.2	-	-0.6
5/31	2030	10.4	270.0	4.0	122.1	0.82	265	1.136	2.968	-	2.0	2.0	0.6	0.7	0.75	-	0.4	-	-0.7
6/1	0830	7.4	270.0	0.5	122.7	1.15	265	1.366	4.874	-	1.5	1.5	0.55	0.55	0.55	-	0.25	-	-0.52
6/1	2030	4.3	225.0	2.5	123.2	1.29	265	0.461	2.83	-	2.0	2.0	0.48	0.5	0.55	-	0.2	-	-0.65
6/2	0830	2.2	225.0	2.0	122.2	1.28	265	0.121	1.449	1.0	1.0	1.0	0.45	0.5	0.45	-	0.25	-	-0.65
6/2	2030	7.8	225.0	2.0	123.4	1.32	265	1.518	5.138	2.0	0	0	0.75	0.6	0.55	-	0.25	-	-0.64
6/3	0830	4.3	225.0	3.0	122.4	1.12	265	0.461	2.832	1.0	1.5	1.5	0.55	0.44	0.45	-	0.24	-	-0.6
6/3	2030	4.8	225.0	8.0	123.5	1.02	265	0.430	2.026	-	1.5	1.5	0.54	0.58	0.6	-	0.25	-	-0.55
6/4	0830	4.3	315.0	7.0	123.3	0.72	265	0.306	1.672	-	0.5	0.5	0.3	0.35	0.3	-	0.25	-	-0.65
6/4	2030	0	180.0	-	123.3	0.70	265	-	-	1.0	0	0	0.35	0.35	0.3	-	0.32	-	-0.65
6/5	0830	8.7	30.0	2.5	122.2	0.22	265	.888	5.731	1.5	0	0	0.28	0.2	0.25	-	0.18	-	-0.6
6/5	2030	0	135.0	-	122.9	0.22	265	-	-	1.0	0	0	0.25	0.2	0.25	-	0.15	-	-0.6
6/7	2030	2.6	225.0	0.5	122.2	0.47	265	0.168	1.713	3.0	0	0	-	-	-	-	-	-	-
6/8	0830	0	270.0	-	1.2	0.45	065	-	-	2.5	0	0	-	-	-	-	-	-	-
6/8	2030	4.3	225.0	9.0	121.3	0.375	065	0.341	1.800	1.5	0	0.4	0.4	0.55	0.4	-	0.25	-	-0.6
6/9	0830	0	225.0	-	120.8	0.756	065	-	-	1.0	0	0	0.3	0.45	0.3	-	0.25	-	-0.6
6/9	2030	8.7	225.0	8.0	121.0	0.72	065	1.159	3.210	0	-	-	-	-	-	-	-	-	-
6/10	0830	0	-	-	120.6	0.78	065	-	-	1.0	0	0	-	-	-	-	-	-	-
6/10	2030	5.0	180.0	-	120.9	0.72	065	0.624	3.294	1.0	0.33	1.47	-	-	-	-	-	-	-
6/11	0830	0	-	-	120.6	0.72	065	-	-	1.0	0	0	-	-	-	-	-	-	-
6/11	2030	8.7	225.0	1.0	120.9	0.636	065	1.888	5.732	1.0	1.0	1.0	-	-	-	-	-	-	-
6/12	0830	0	225.0	-	120.5	0.483	065	-	-	1.0	0	0	-	-	-	-	-	-	-
Means -		7.44			120.0	0.70138							0.4773	0.45386	0.43431		0.26465		0.5625

<u>VARIABLE</u>	<u>MEAN</u>	<u>VARIANCE</u>	<u>STANDARD DEVIATION</u>			
WIND	8.198 (knots)	52.72 (knots <sup>2</sup> )	7.261 (knots)			
SIGNIFICANT WAVE HEIGHT	1.62 ft	4.44 ft <sup>2</sup>	2.10 ft			
SIGNIFICANT HEAVE ACCELERATION AMPLITUDE	0.197 g	0.00574 g <sup>2</sup>	0.0758 g			
SIGNIFICANT SWAY ACCELERATION AMPLITUDE	0.1397 g	0.0024 g <sup>2</sup>	0.049 g			
SIGNIFICANT SURGE ACCELERATION AMPLITUDE	0.135 g	0.00284 g <sup>2</sup>	0.0532 g			
SIGNIFICANT ROLL AMPLITUDE	14 deg	25.9 deg <sup>2</sup>	5.09 deg			
CURRENT	0.7022 (knots)	0.1435 (knots <sup>2</sup> )	0.3787 (knots)			
<u>THE CORRELATION MATRIX</u>						
	<u>WIND</u>	<u>WAVE</u>	<u>HEAVE</u>	<u>SWAY</u>	<u>SURGE</u>	<u>ROLL</u>
WIND	1.0	0.7699	0.6418	0.4839	0.5852	0.1997
WAVE		1.0	0.4989	0.3765	0.4553	0.4134
HEAVE			1.0	0.8058	0.8448	0.4671
SWAY				1.0	0.8642	0.4885
SURGE					1.0	0.5571
ROLL						1.0

Figure 44. Torroidal Buoy Motion Statistics for 6-week Period

The GSA-440 computer was also used to fit curves to the observed parameter significant amplitudes. Six curves were fitted using least-squares methods.

In general, the linear plot had the best index of determination when fitted to the data. Figures 45 through 50 show the observed buoy motion significant amplitudes plotted versus wind speed, computed significant wave height, and buoy heave acceleration. The least-mean-squares linear curve is shown on each plot. The least-mean-squares linear functions were transformed to engineering units and are summarized in figure 51. If the buoy motion amplitudes are assumed to be distributed by the Rayleigh distribution, the mean amplitude is  $62\frac{1}{2}$  percent of the significant amplitude. The empirical equations shown in figure 51 were again transformed in such a manner that they are in terms of mean amplitudes. They are shown in figure 52.

The cumulative probability distributions for wind, current, observed and computed wave height, and buoy motion amplitudes are shown in figures 53 through 55 for the time period that the buoy was on station.

A complete spectral analysis was performed on two runs of buoy motion data taken on 10 and 11 June 1970. A Fast Fourier Transform method that is programmed and is available on the NUSC UNIVAC 1108 computer was used to compute power spectra and cross correlations. The data were digitized at a rate of 64 samples per second on automatic data processing equipment by the Data Analysis Branch at NUSC. A set of buoy motion spectra for the second data run, which was taken at 2030 EDST, on 11 June 1970, is shown in figures 56 through 61. The wind was at 10 knots from the southwest and had been blowing

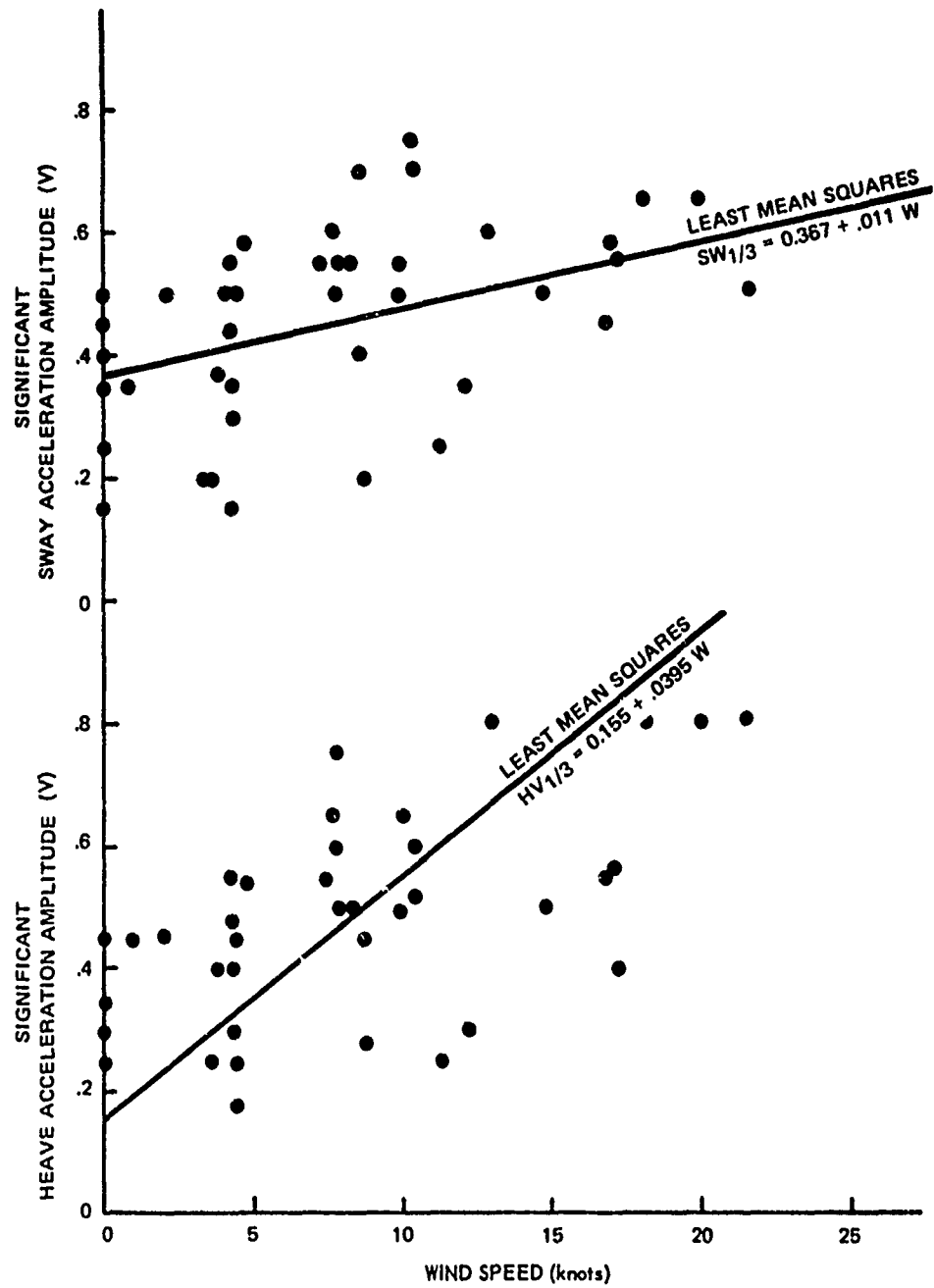


Figure 45. Buoy Motions versus Wind Speed — Heave and Sway

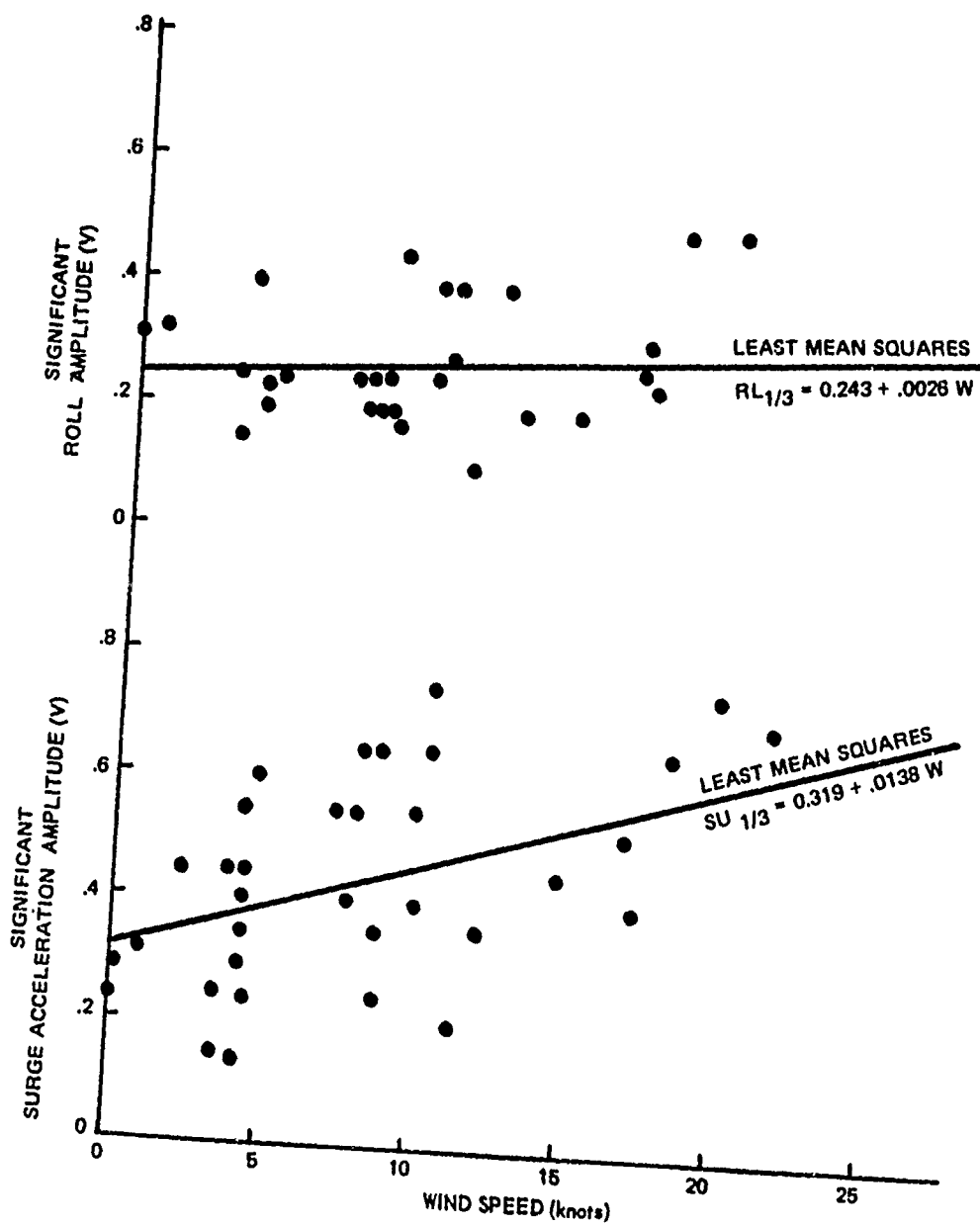


Figure 46. Buoy Motions versus Wind Speed — Surge and Roll

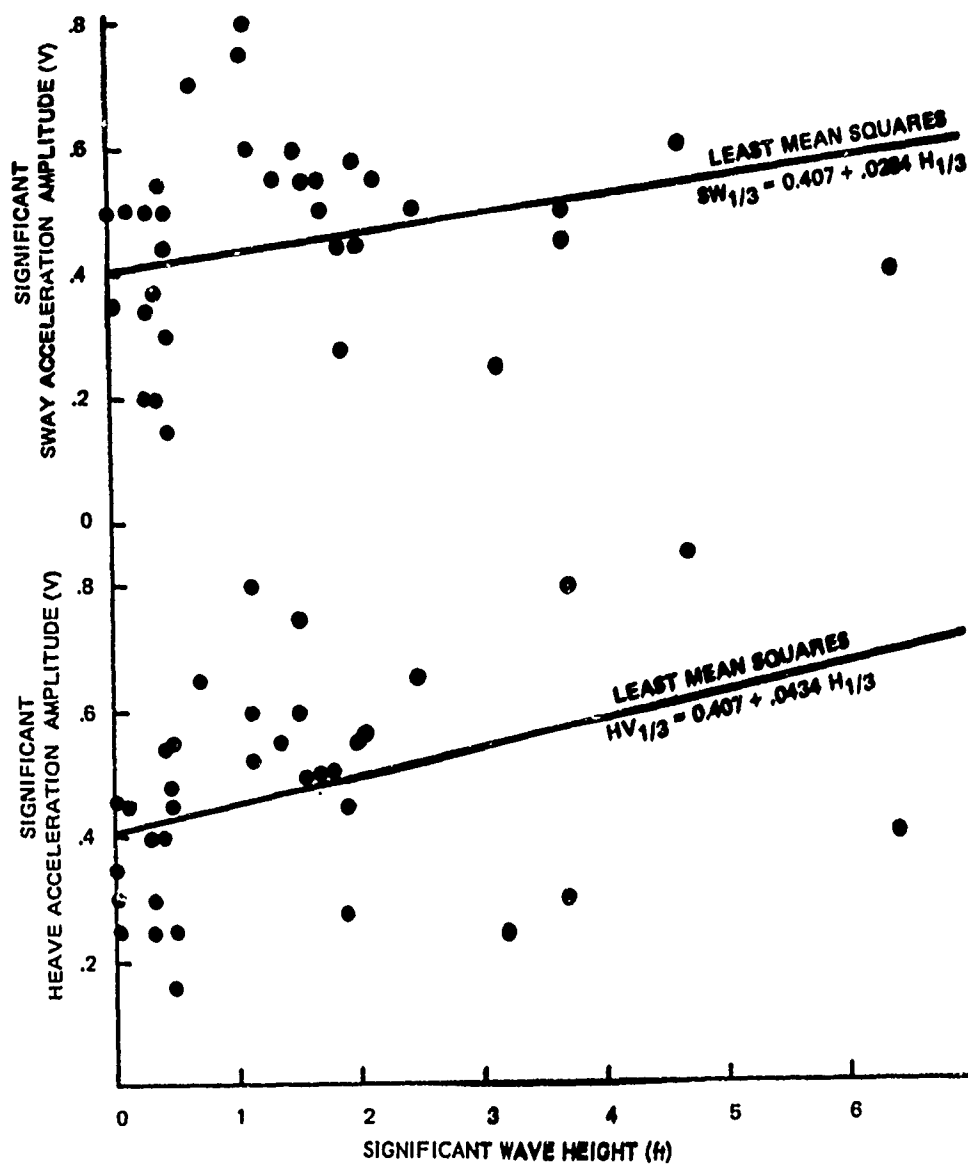


Figure 47. Buoy Motions versus Wave Height — Heave and Sway



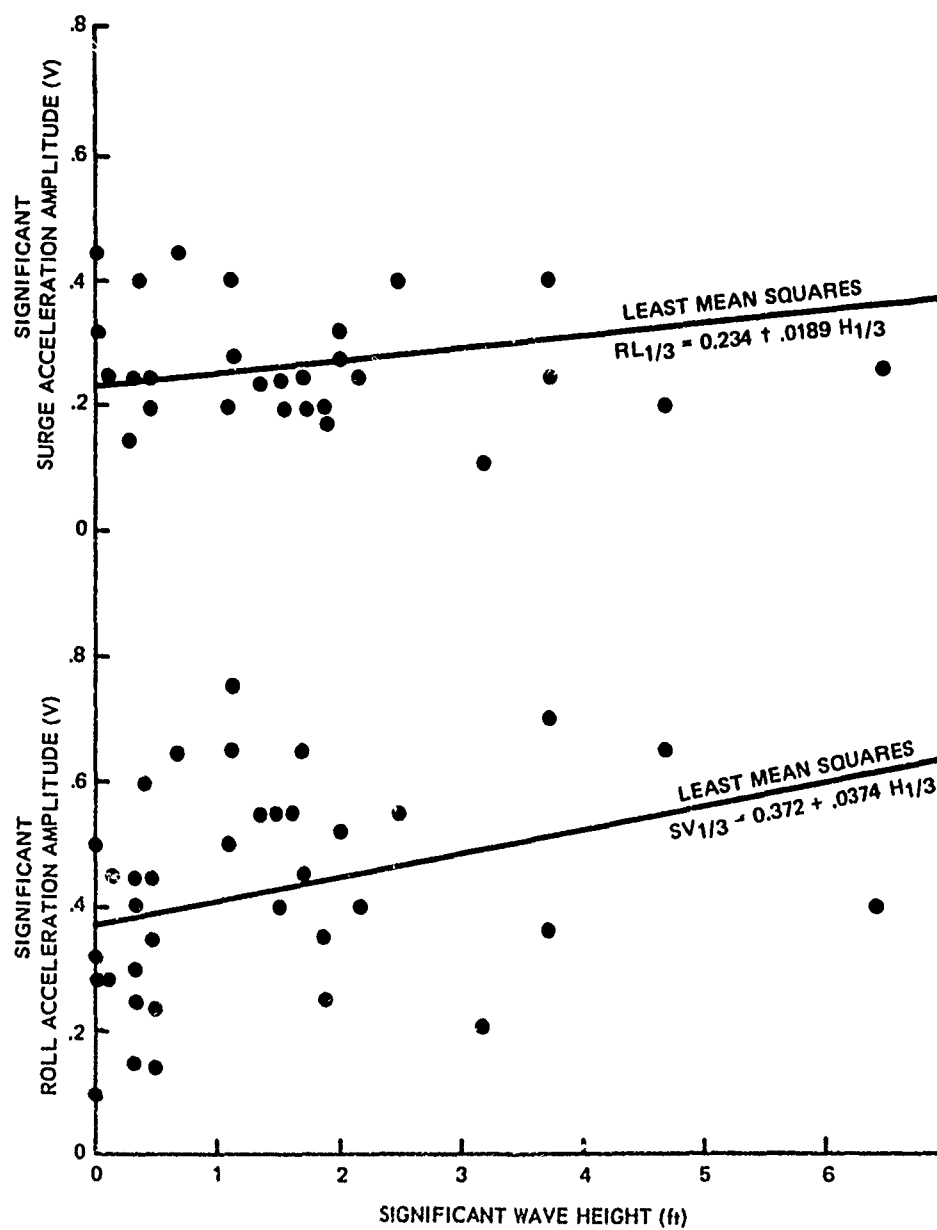


Figure 48. Buoy Motions versus Wave Height — Surge and Roll

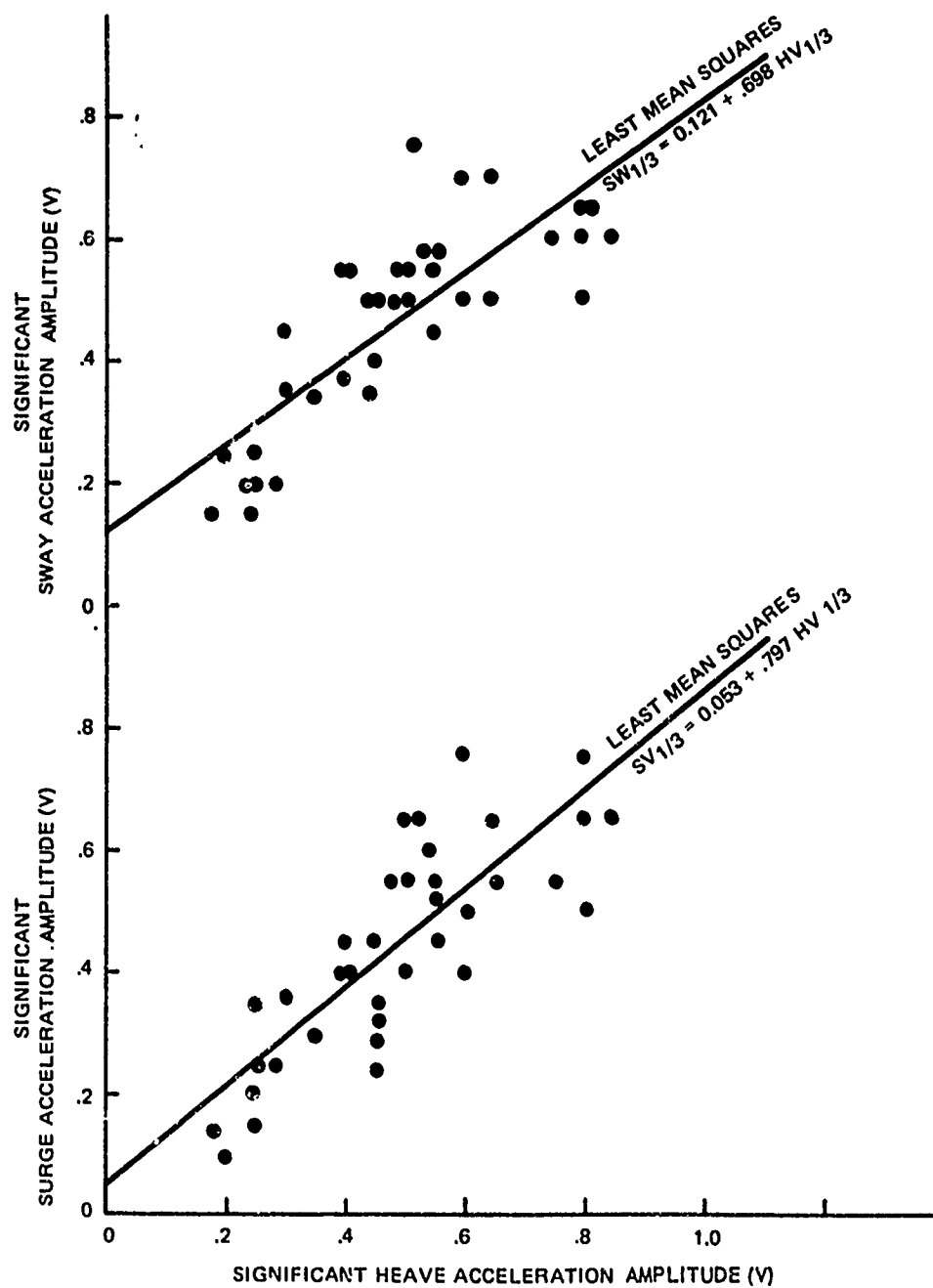


Figure 49. Surge and Sway Motions versus Heave Motion

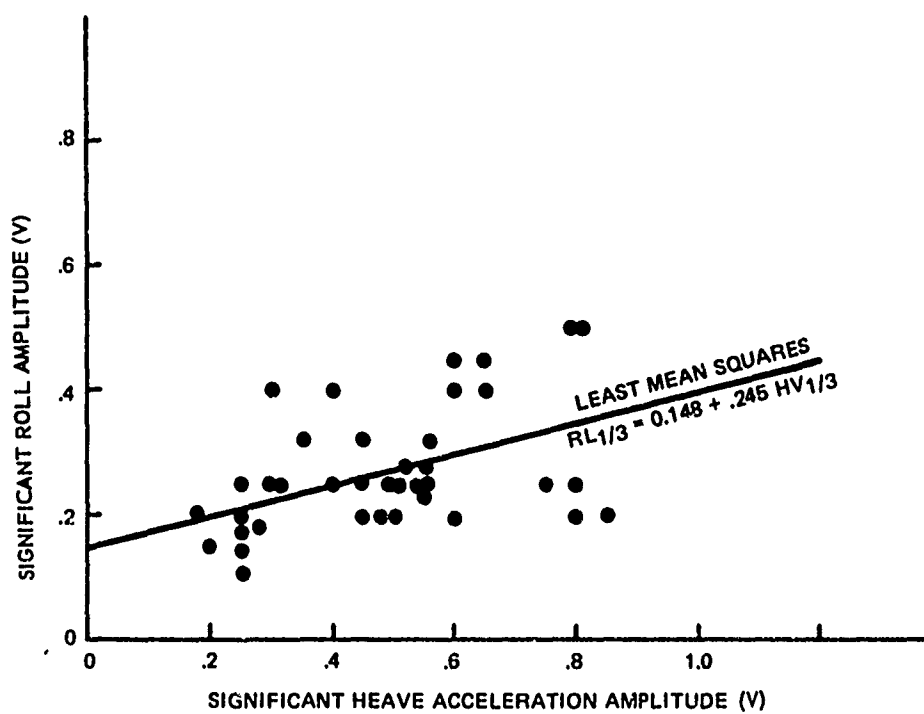


Figure 50. Roll Motion versus Heave Motion

1. ON WIND (W in knots)

HEAVE ACCELERATION  $Hv_{1/3} = 0.0064 + 0.0163 \cdot W \text{ (g's)}$

SWAY-SURGE ACCELERATION  $Su_{1/3} = Sw_{1/3} = 0.1056 + 0.003825 \cdot W \text{ (g's)}$

PITCH-ROLL ANGLE  $Pi_{1/3} = Ri_{1/3} = 12.83^\circ + 0.1373 \cdot W \text{ (deg)}$

2. ON SIGNIFICANT WAVE HEIGHT ( $H_{1/3}$  in ft)

HEAVE ACCELERATION  $Hv_{1/3} = 0.168 + 0.01792 \cdot H_{1/3} \text{ (g's)}$

SWAY-SURGE ACCELERATION  $Su_{1/3} = Sw_{1/3} = 0.120 + 0.01015 \cdot H_{1/3} \text{ (g's)}$

PITCH-ROLL ANGLE  $Pi_{1/3} = Ri_{1/3} = 12.36 + 1.0 \cdot H_{1/3} \text{ (deg)}$

3. ON HEAVE ACCELERATION AMPLITUDE ( $Hv_{1/3}$  in g's)

SWAY-SURGE ACCELERATION  $Su_{1/3} = Sw_{1/3} = 0.0268 + 0.557 \cdot Hv_{1/3} \text{ (g's)}$

PITCH-ROLL ANGLE  $Pi_{1/3} = Ri_{1/3} = 7.82 + 31.35 \cdot Hv_{1/3} \text{ (deg)}$

Figure 51. Empirical Equations for Significant Buoy Motion Amplitudes  
(Based on Linear, Least-Mean-Squares Equations)

1. ON WIND (W in knots)

HEAVE ACCELERATION

$$\overline{H_v} = 0.004 + 0.0102 \cdot W \text{ (g's)}$$

SWAY-SURGE ACCELERATION

$$\overline{S_u} = \overline{S_w} = 0.066 + 0.002394 \cdot W \text{ (g's)}$$

PITCH-ROLL ANGLE

$$\overline{P_i} = \overline{R_l} = 8.03 + 0.086 \cdot W \text{ (deg)}$$

$$p(H_v) = \frac{\pi}{2} \cdot \frac{H_v}{\overline{H_v}^2} \cdot e^{-\left(\frac{\pi}{4} \cdot \frac{H_v^2}{\overline{H_v}^2}\right)} \quad p(S_w) = p(S_u) = \frac{\pi}{2} \cdot \frac{S_u}{\overline{S_u}^2} \cdot e^{-\left(\frac{\pi}{4} \cdot \frac{S_u^2}{\overline{S_u}^2}\right)}$$

$$p(P_i) = p(R_l) = \frac{\pi}{2} \cdot \frac{R_l}{\overline{R_l}^2} \cdot e^{-\left(\frac{\pi}{4} \cdot \frac{R_l^2}{\overline{R_l}^2}\right)}$$

2. ON MEAN WAVE HEIGHT ( $\overline{H}$  in ft)

HEAVE ACCELERATION

$$\overline{H_v} = 0.105 + 0.01792 \cdot \overline{H} \text{ (g's)}$$

SWAY-SURGE ACCELERATION

$$\overline{S_w} = \overline{S_u} = 0.075 + 0.01015 \cdot \overline{H} \text{ (g's)}$$

PITCH-ROLL ANGLE

$$\overline{P_i} = \overline{R_l} = 7.72^\circ + 1.0 \cdot \overline{H} \text{ (deg)}$$

(NOTE THAT THE PROBABILITY DISTRIBUTIONS ARE THE SAME AS ABOVE.)

3. ON MEAN HEAVE ACCELERATION AMPLITUDE ( $\overline{H_v}$  in g's)

SWAY-SURGE ACCELERATION

$$\overline{S_w} = \overline{S_u} = 0.01674 + 0.557 \cdot \overline{H_v} \text{ (g's)}$$

PITCH-ROLL ANGLE

$$\overline{P_i} = \overline{R_l} = 4.89 + 31.35 \cdot \overline{H_v} \text{ (deg)}$$

Figure 52. Empirical Equations for Mean Buoy Motion Amplitudes

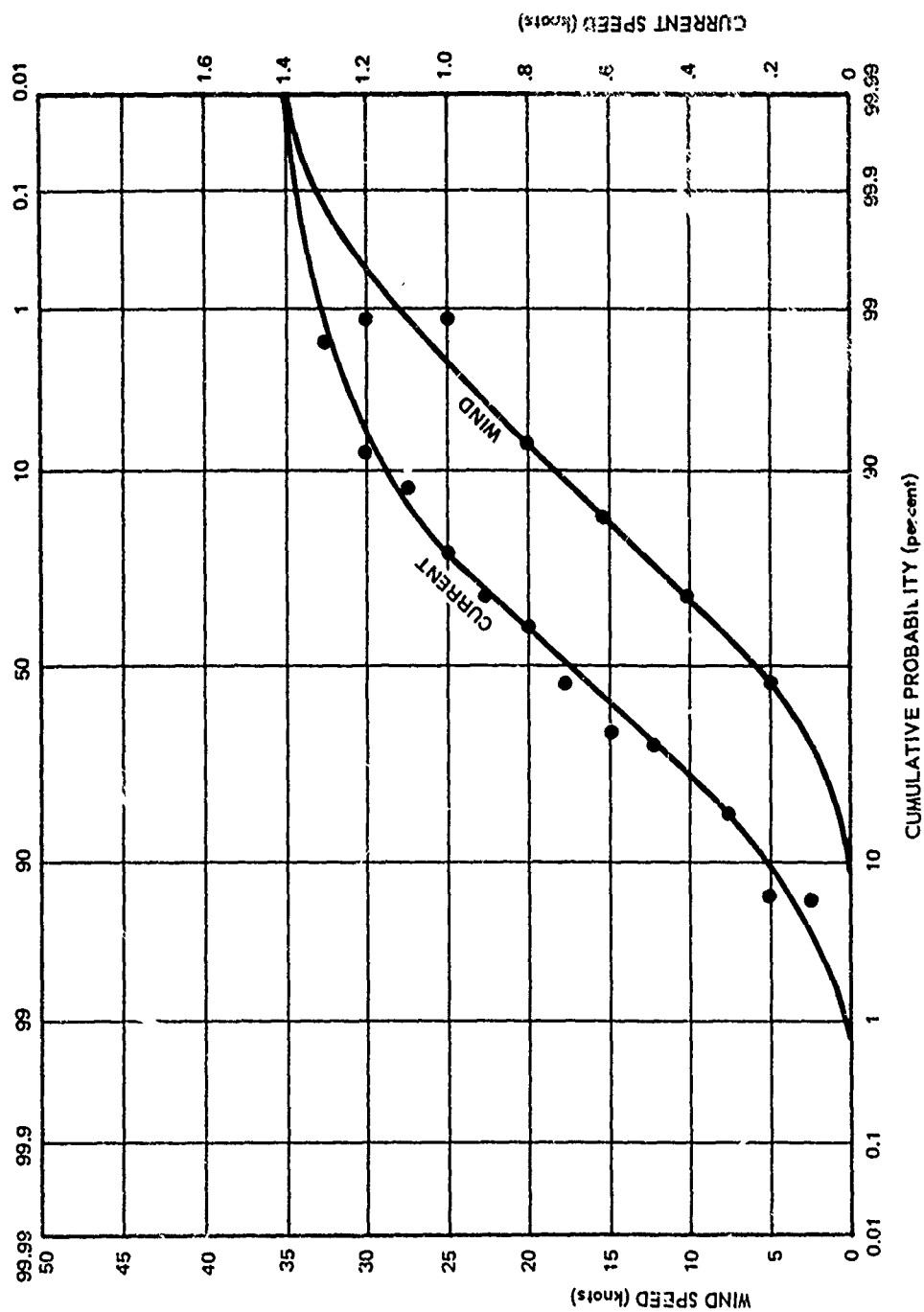


Figure 53. Wind and Current Cumulative Distributions

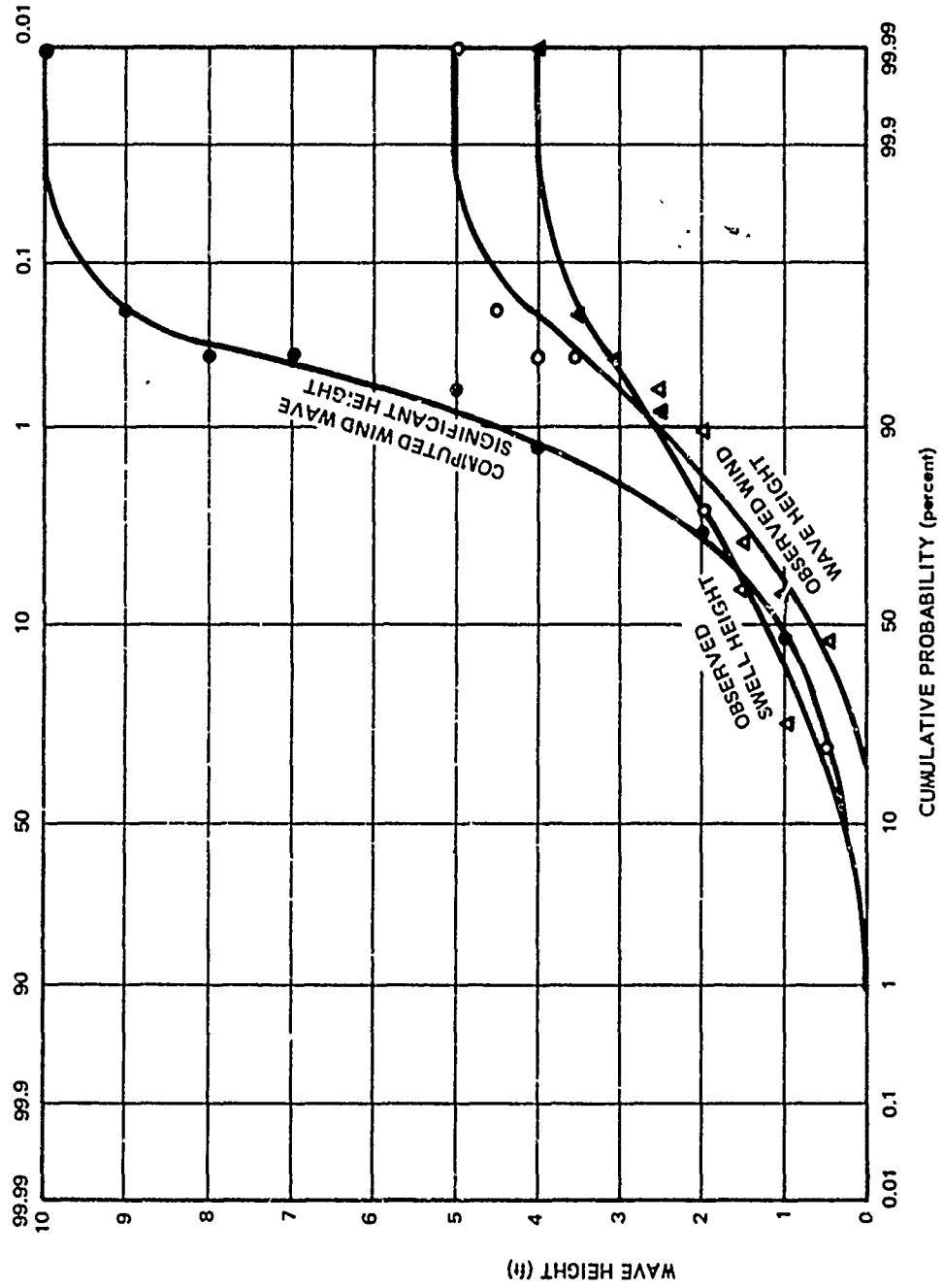


Figure 54. Significant Wave Height Cumulative Distributions

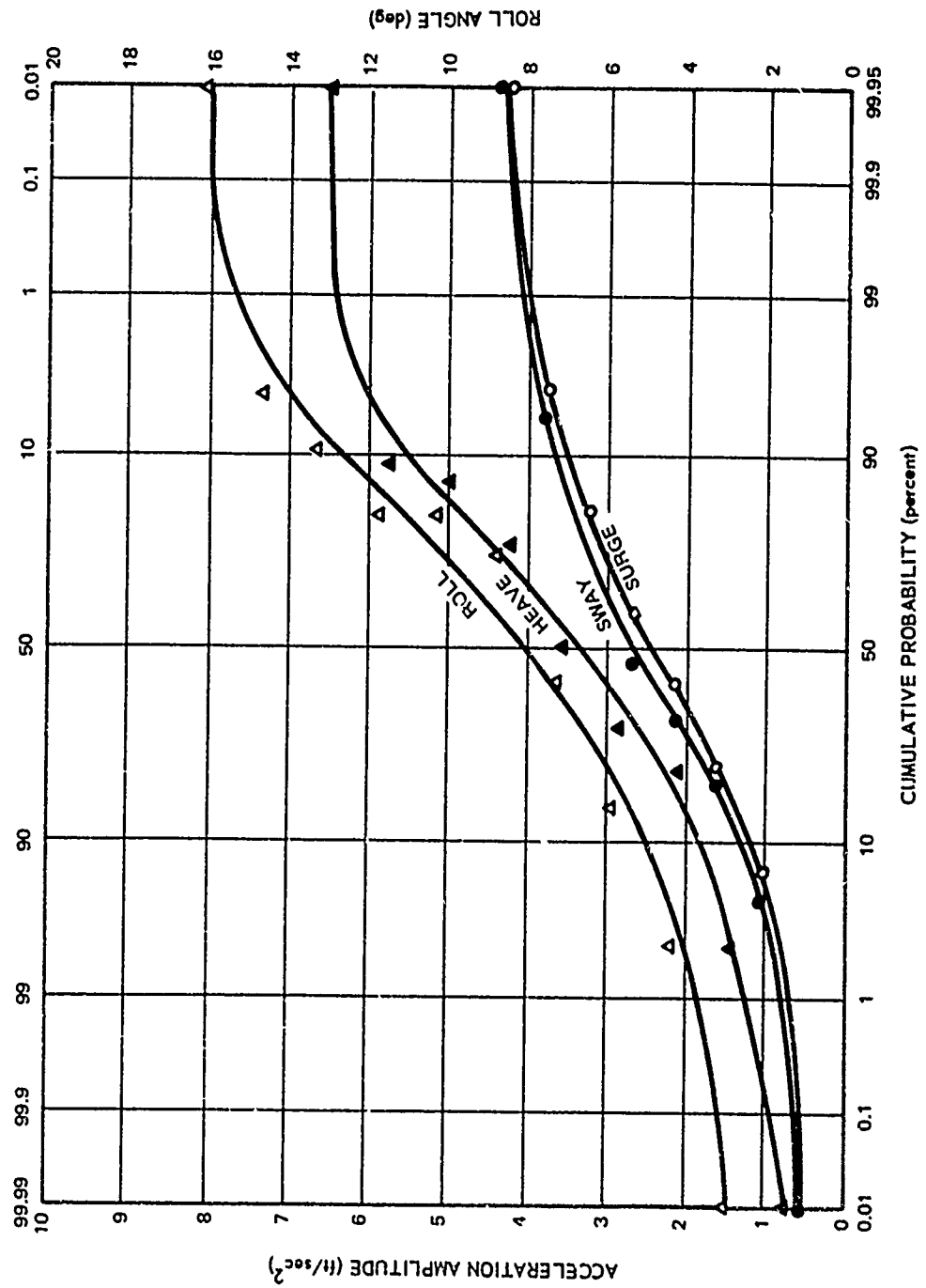


Figure 55. Significant Buoy Motion Cumulative Distributions



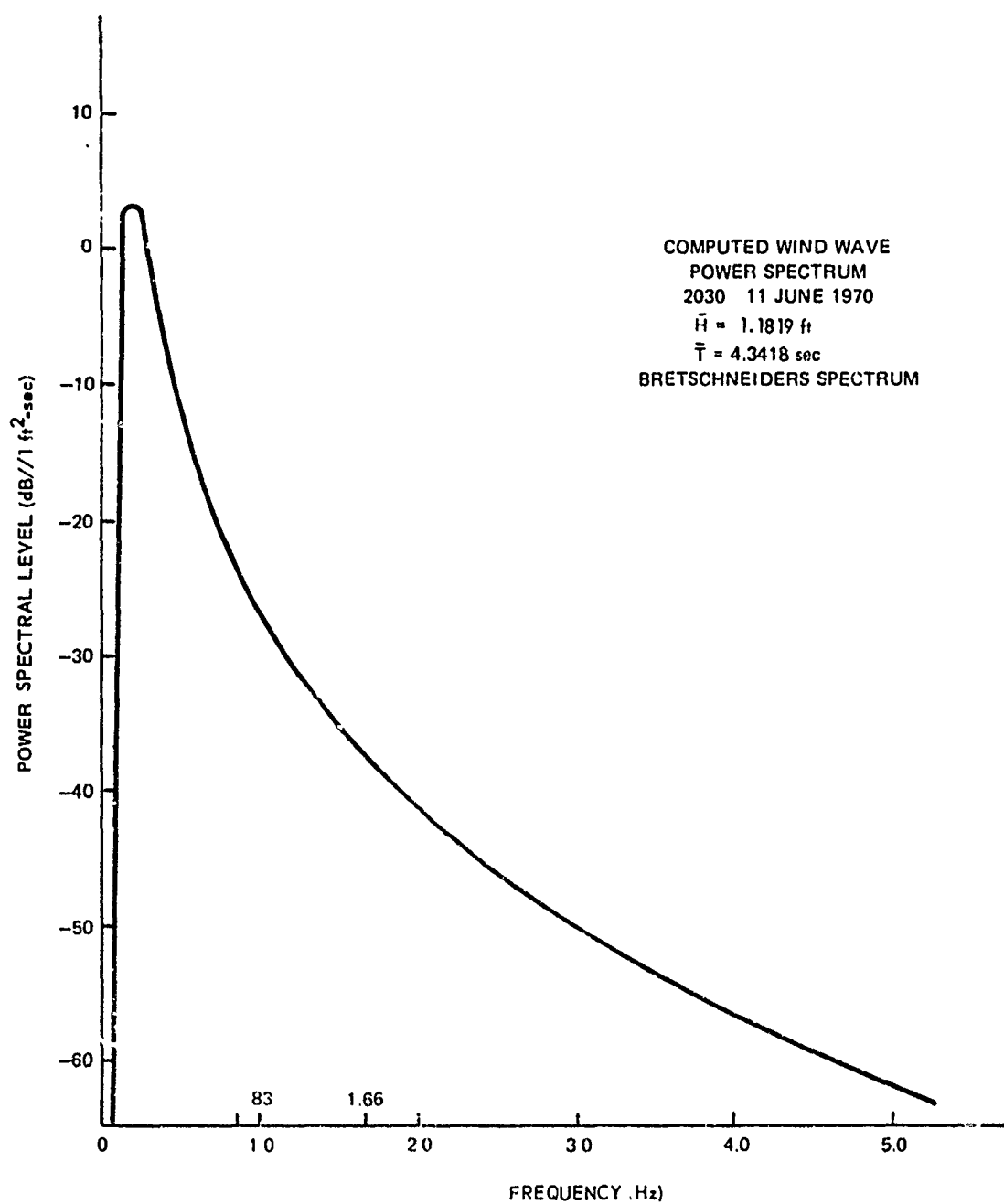


Figure 56. Computed Wind Wave Spectral Levels — 2030 hr, 11 June 1970

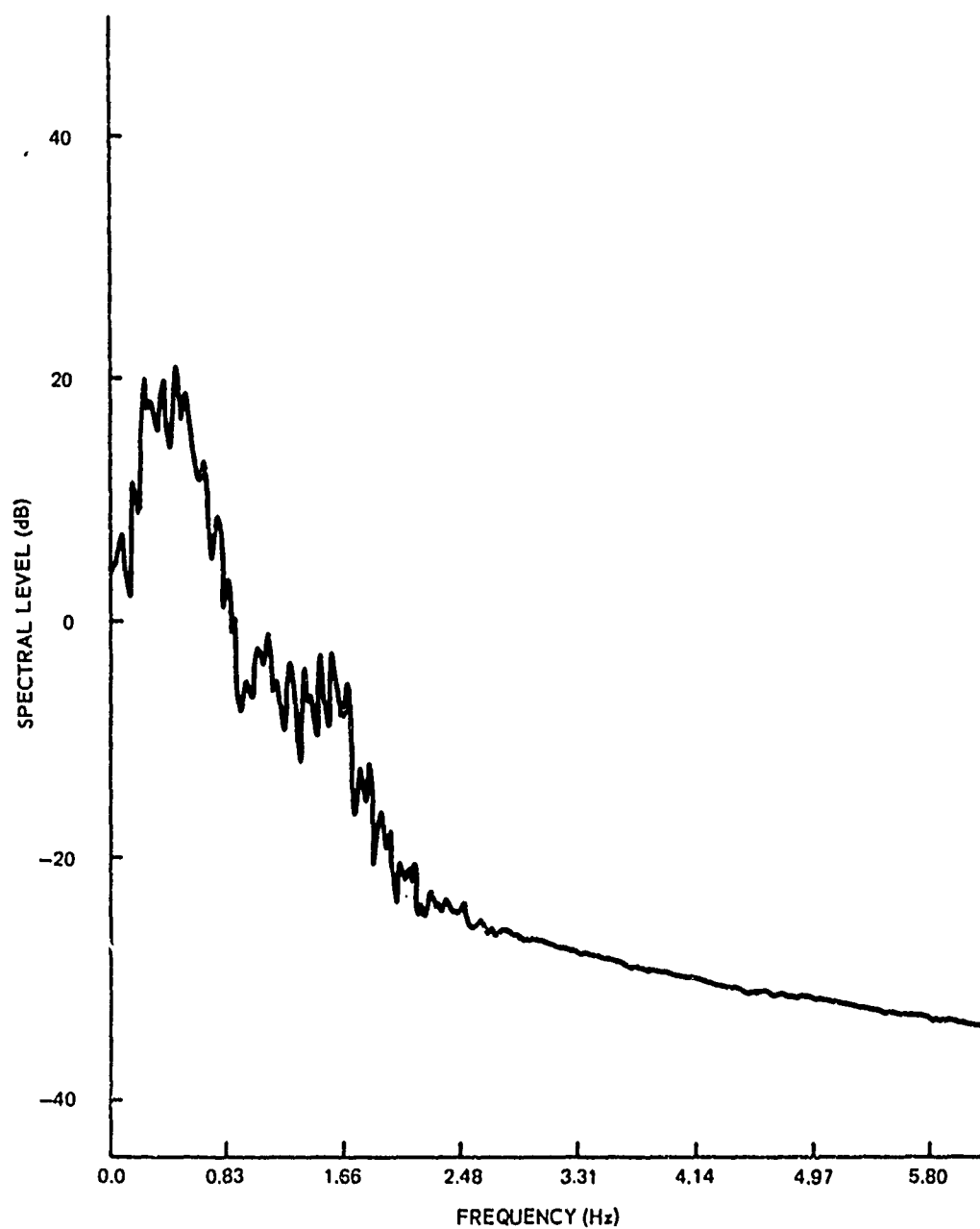


Figure 57. Observed Heave Spectral Levels

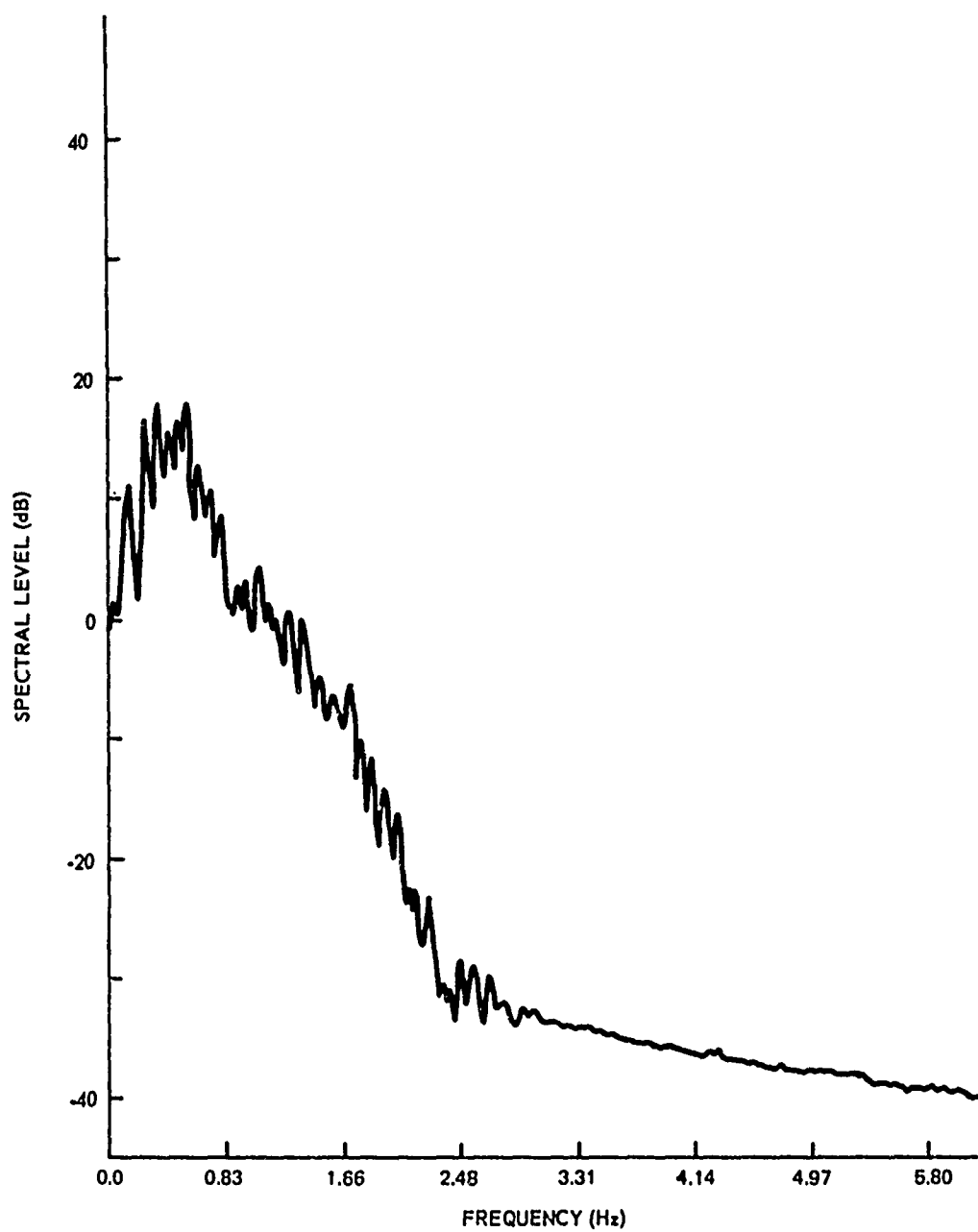


Figure 58. Observed Surge Spectral Levels

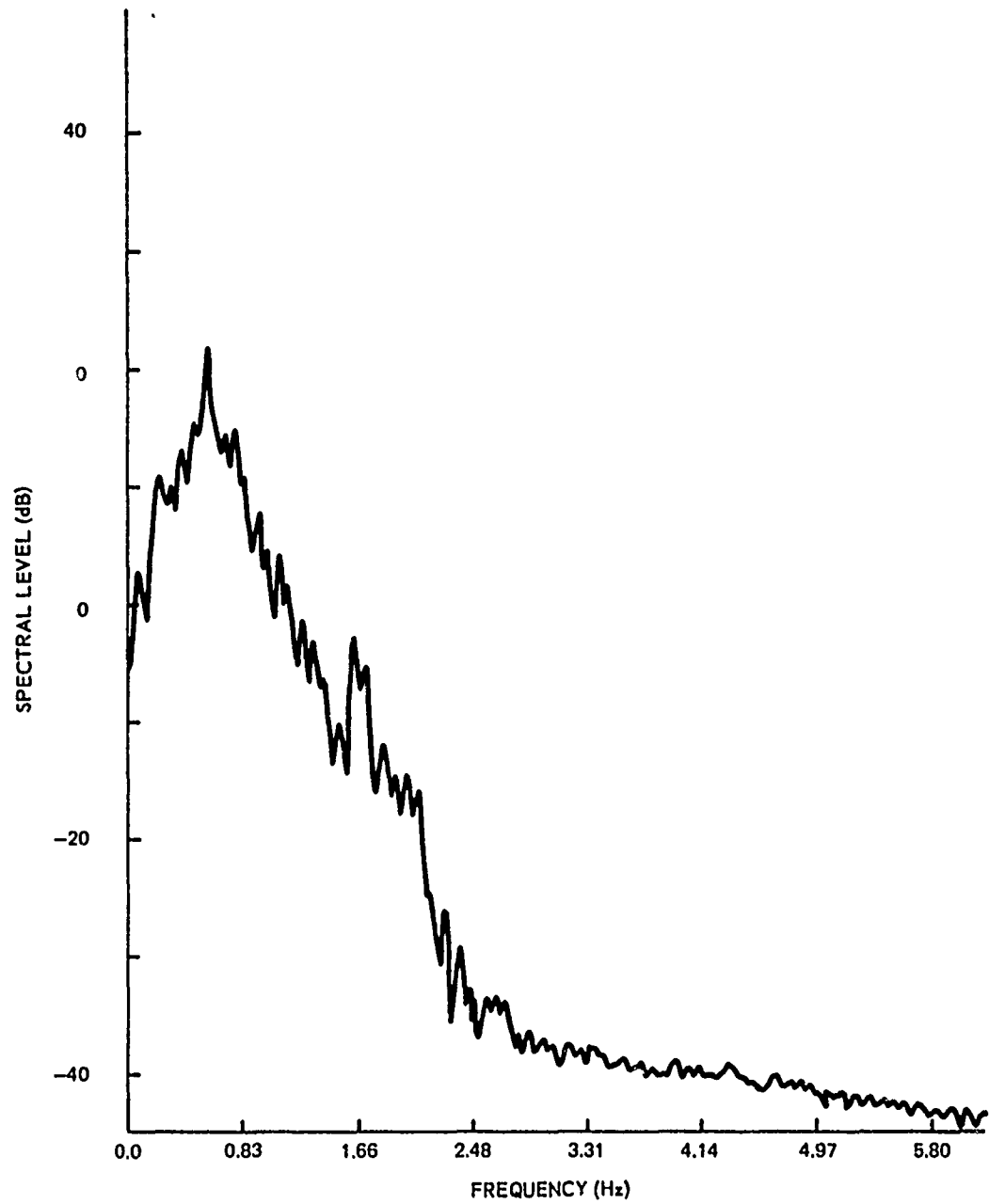


Figure 59. Observed Sway Spectral Levels

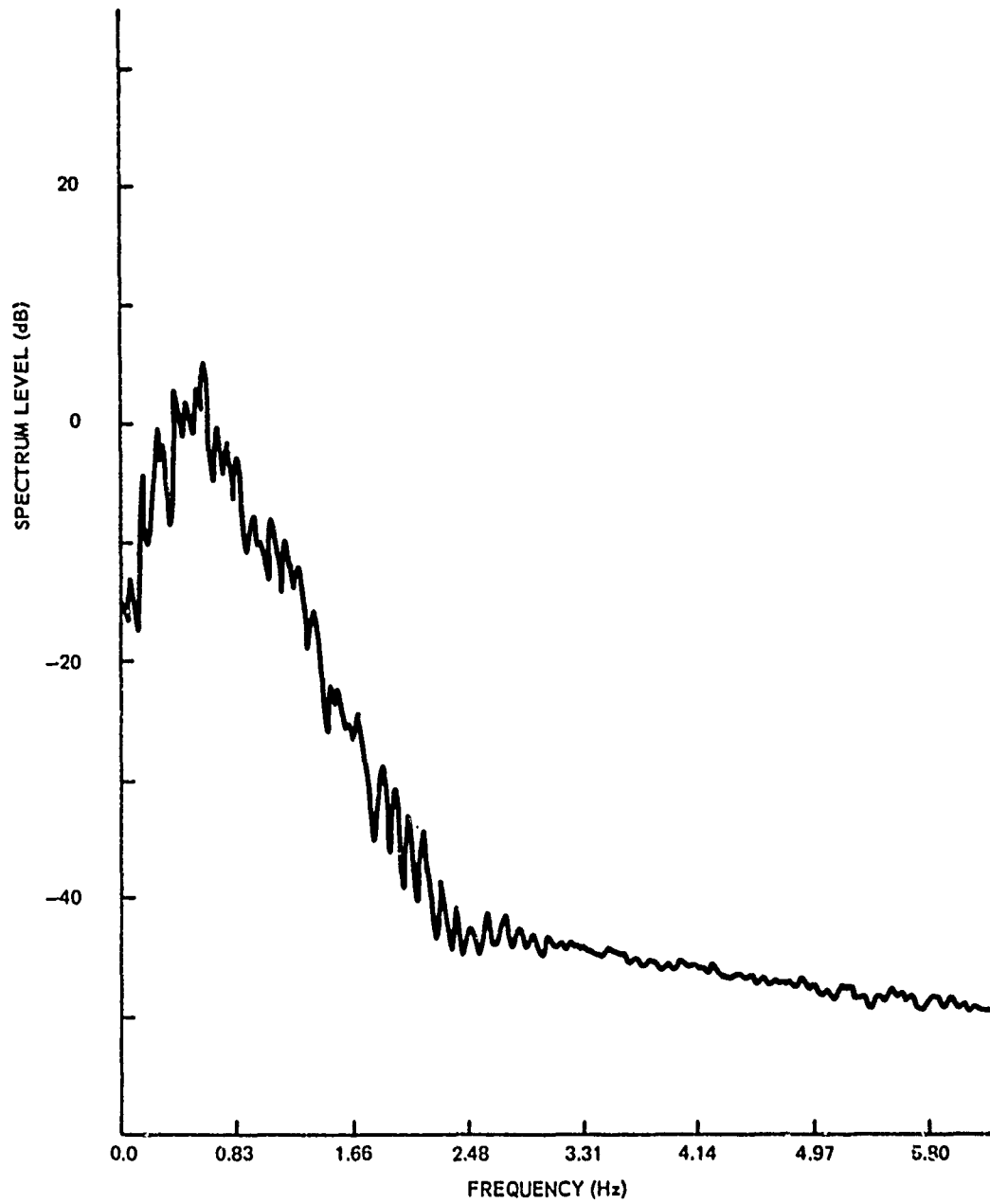


Figure 60. Observed Pitch Spectral Levels

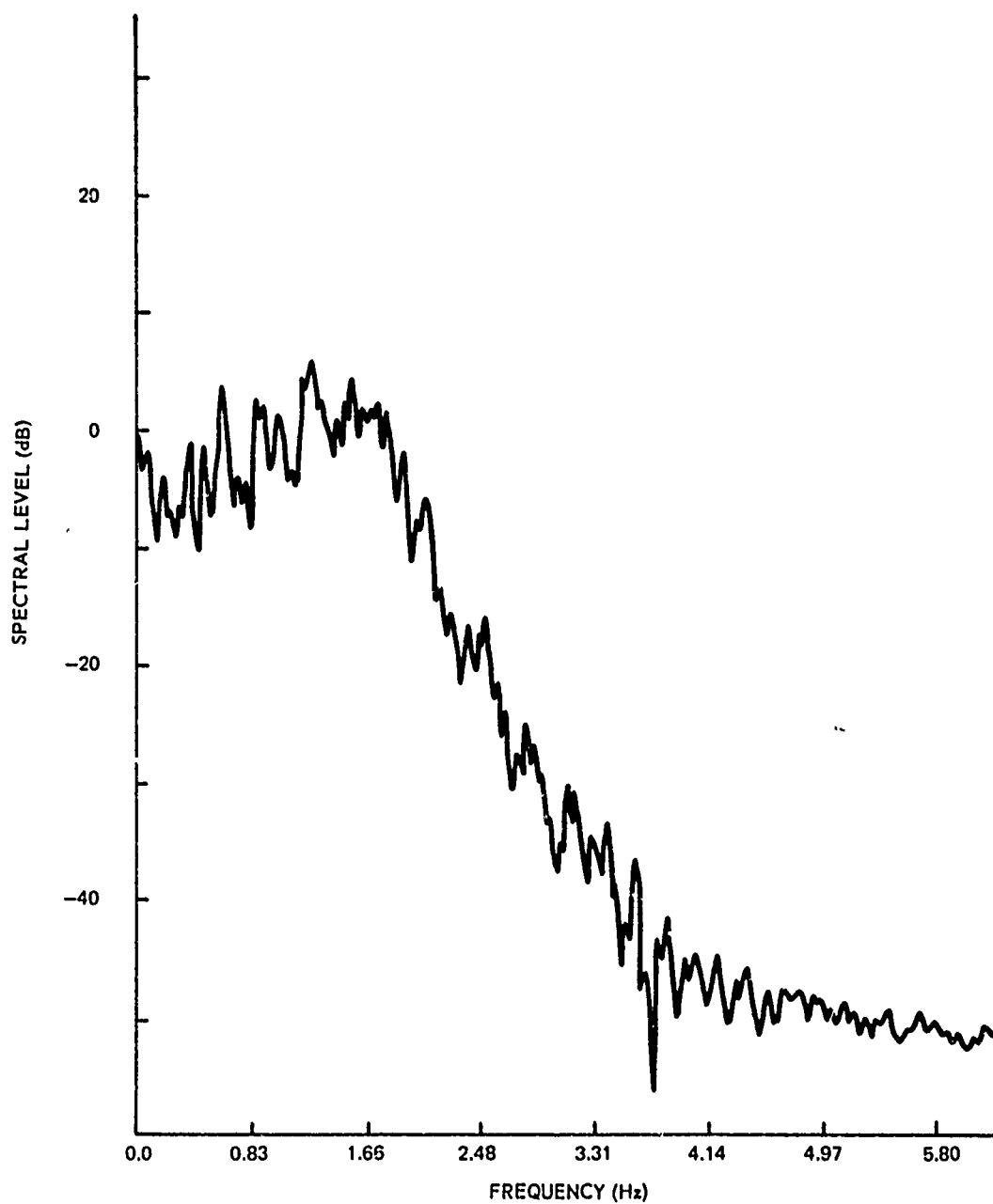


Figure 61. Observed Roll Spectral Levels

steady at that strength for 1 hr. The wind wave spectrum was computed by using a two-parameter Bretschneider spectrum. Figure 56 shows the computed wind wave power spectrum. Figures 57 through 61 show the buoy motion power spectra. Figure 57, the buoy heave acceleration power spectra, shows a peak in the energy around 0.5 rad/sec ( $T = 12.5$  sec). There is also a peak around 1.5 rad/sec, which corresponds to the peak of the computed wind wave power spectrum.

The peak at the lower frequency may be caused by swell; a 1-ft swell from the south was observed visually during the data run. The same type of energy distribution is seen in the other spectra. Buoy roll angle and sway acceleration spectra indicate relatively more energy at wind wave frequencies; thus, it is concluded that the buoy was oriented in such a manner that the sway-heave plane was close to a southwest-northeast orientation.

Buoy motion parameters were cross-correlated with buoy heave acceleration and are shown in figures 62 through 65. These plots indicate the existence of two modes with rather strong coupling between motion parameters. If a linear system is assumed, the input and output spectra can be related by the transfer function:

$$S_{A^2}(\omega) = H(\omega)^2 \cdot S_{H^2}(\omega),$$

where

$S_{A^2}(\omega)$  is the buoy motion power spectrum

$S_{H^2}(\omega)$  is the wave height power spectrum

$H(\omega)$  is the transfer function.

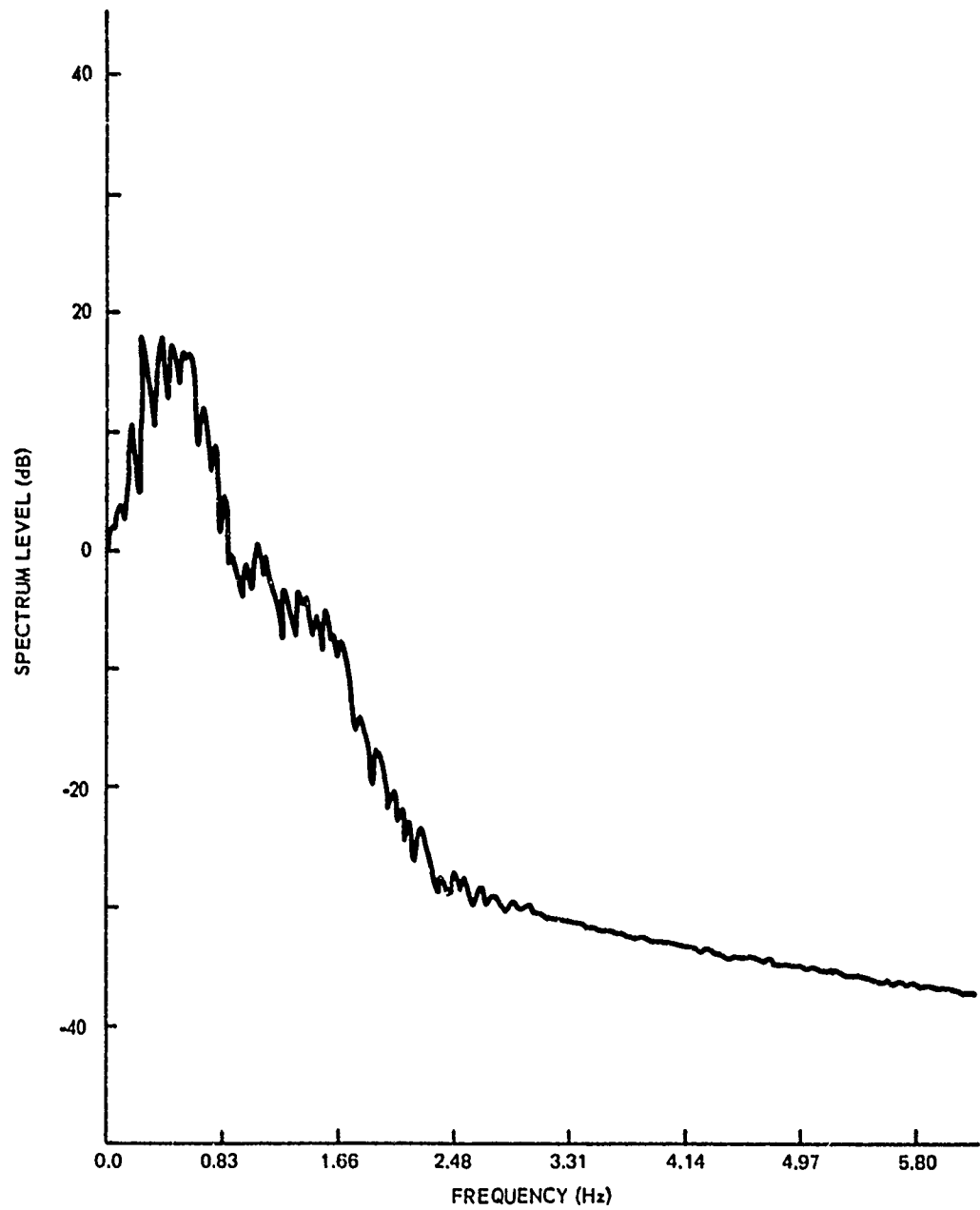


Figure 62. Cross-Spectral Levels of Surge and Heave



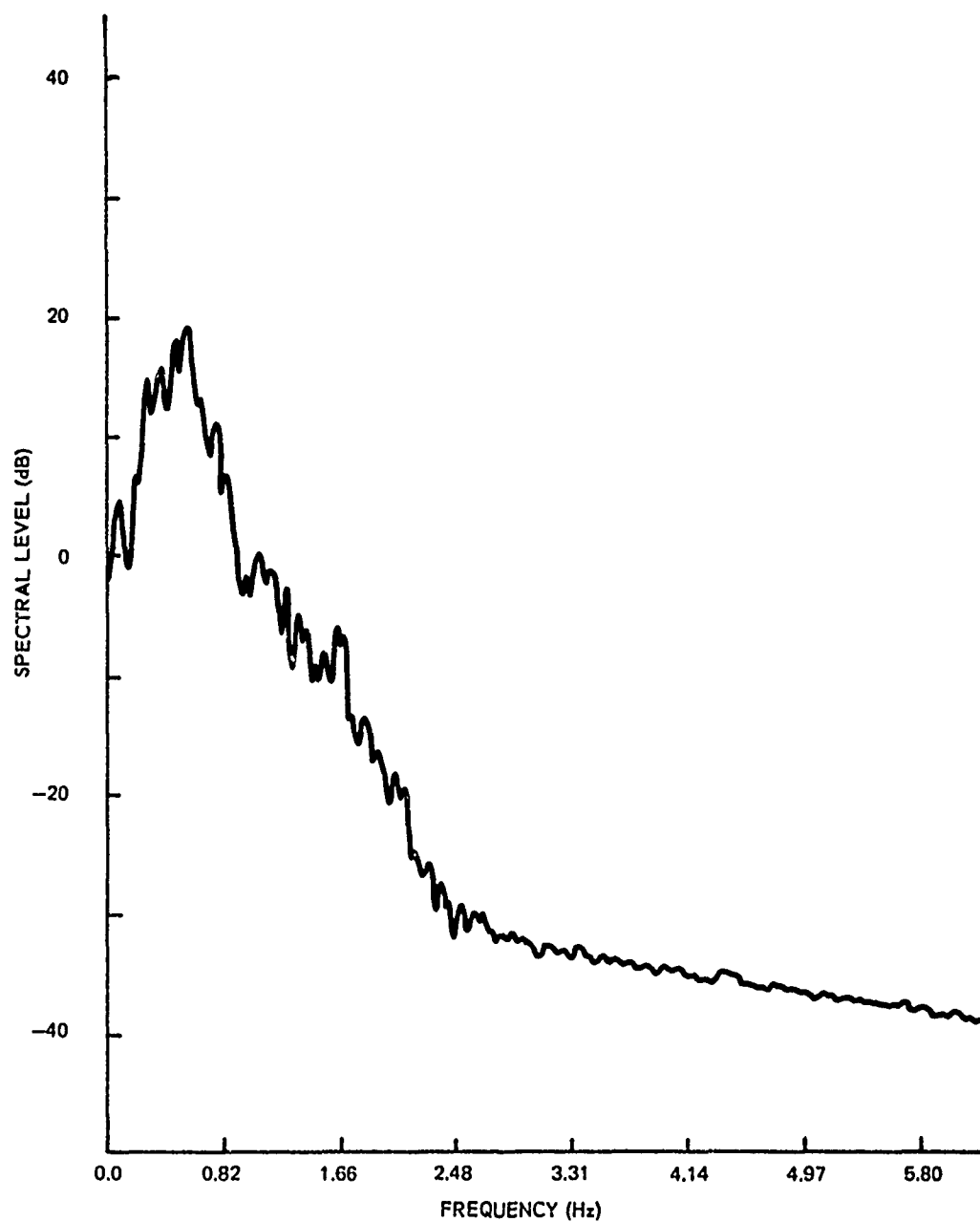


Figure 63. Cross-Spectral Levels of Sway and Heave

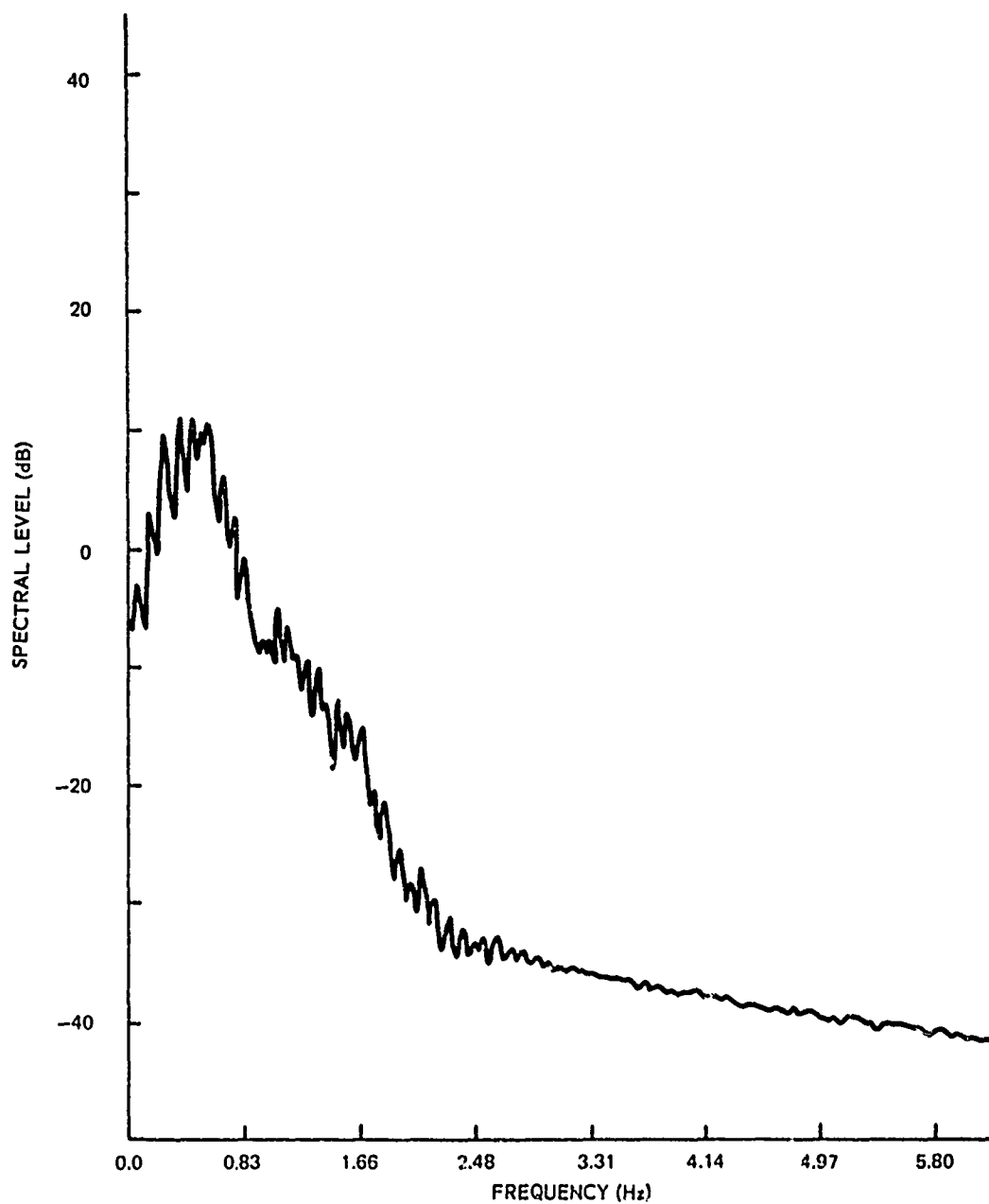


Figure 64. Cross-Spectral Levels of Pitch and Heave

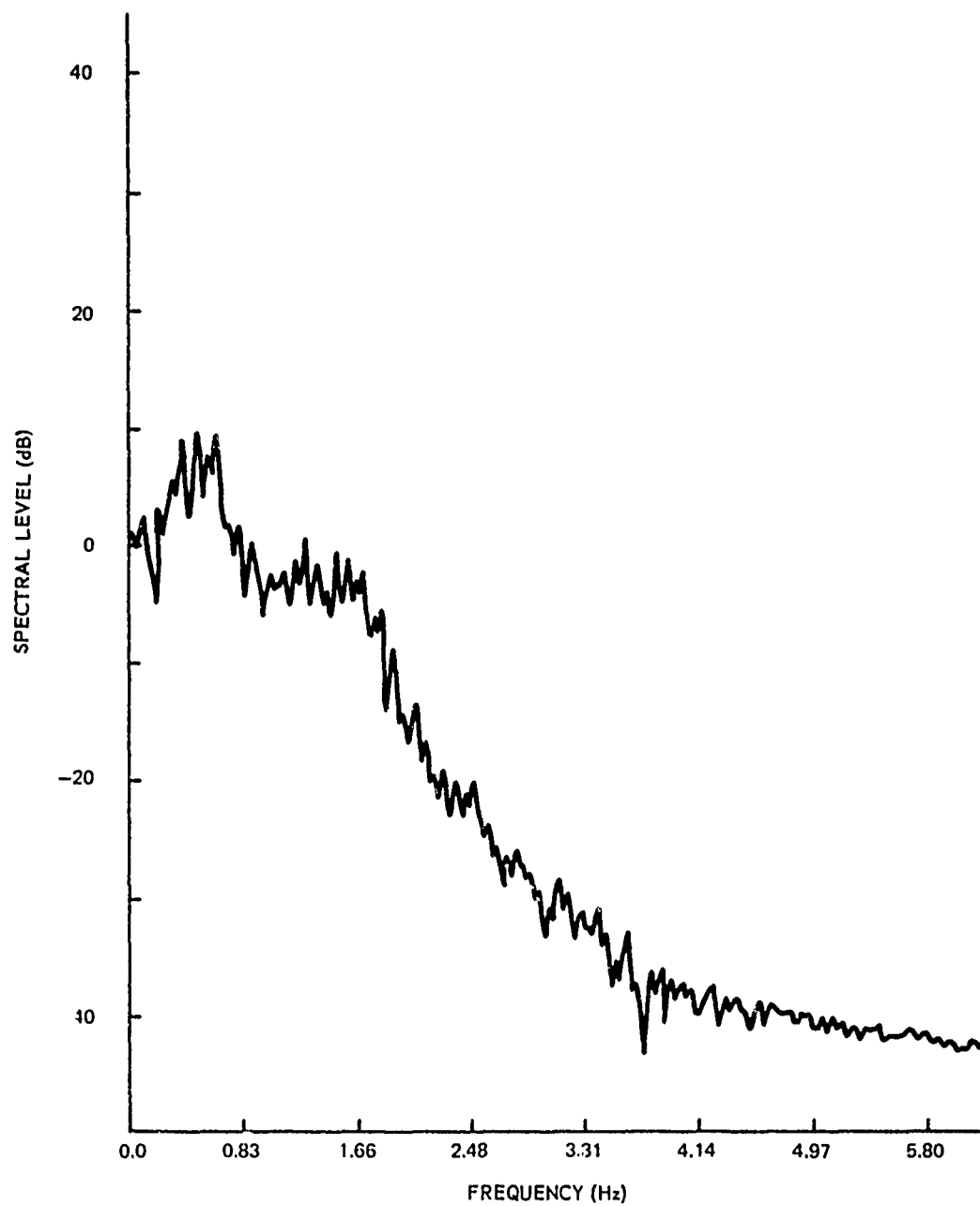


Figure 65. Cross-Spectral Levels of Roll and Heave

Wave spectra determined by Williams<sup>77</sup> for similar conditions in Block Island Sound indicate that swell appears in the wave spectrum as a horizontal line to the left of the wind wave peak and is about 5 dB down from the peak. Figure 56 was modified to include swell. The buoy motion power spectra were smoothed and the difference in decibels between them and the wave spectrum (including swell) were plotted as the square of the absolute value of the transfer function in decibels. Figures 66 through 70 show the transfer functions and indicate the existence of two modes. The relative magnitudes of the peaks indicate that the modes are a heave mode (low frequency) and a roll mode (high frequency). Observations made by the writer while servicing the buoy at sea indicate that the sway-surge mode has the lowest frequency, the heave mode has the next highest frequency, and the pitch-roll mode has the highest frequency.

These spectra indicate that the heave, surge, and sway motions of the buoy are primarily excited by the sea swell, whereas buoy pitch and roll are excited by the higher frequency wind waves.

Analysis of measured buoy motion data for the  $3\frac{1}{2}$ -ft spherical buoy and for the 8-ft torroidal buoy have yielded sets of empirical equations that can be used to predict mean buoy motions and amplitude distributions for various sea states. Buoy motion amplitude distributions appear to follow a Rayleigh distribution, which indicates that the dynamic system is linear or near-linear.

Spectra for the torroidal buoy indicate the existence of a heave mode and a pitch-roll mode within the range of wave frequencies. In general, both buoys are hard-coupled to the sea surface in heave. The torroidal buoy appears to respond in pitch-roll motions to a greater extent than does the spherical buoy.

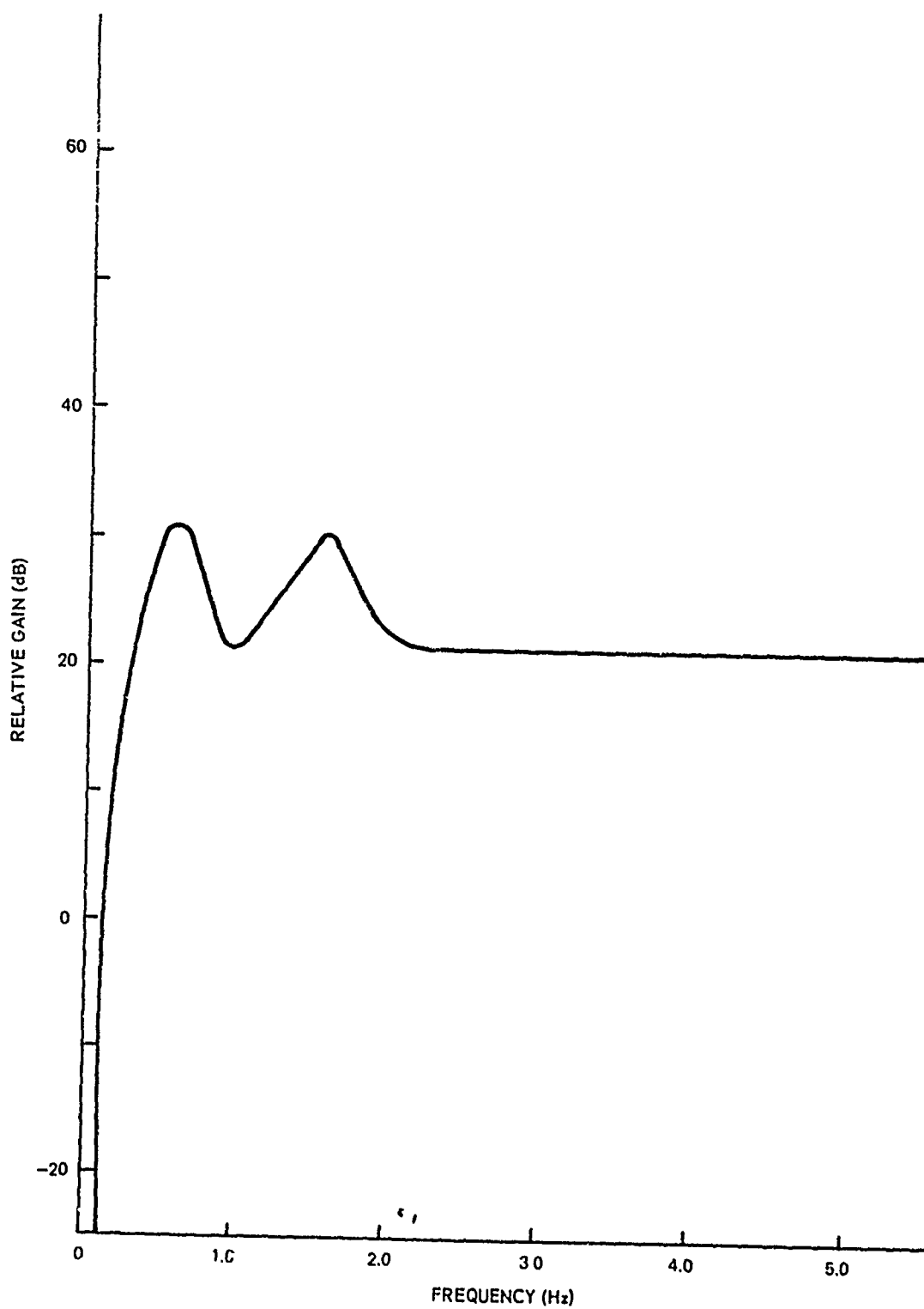


Figure 66. Gain Function for Heave and Wave Height

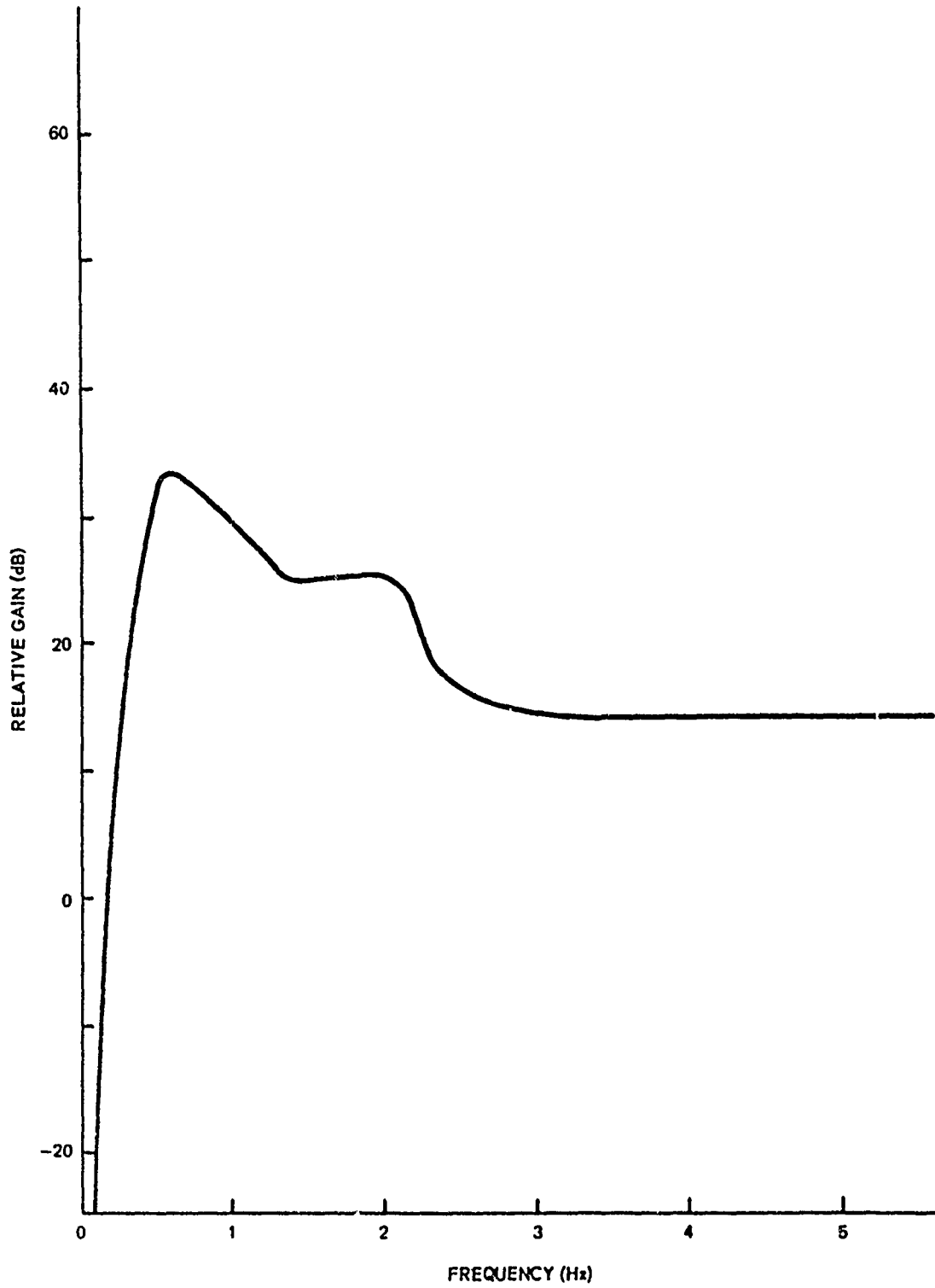


Figure 67. Gain Function for Sway and Wave Height

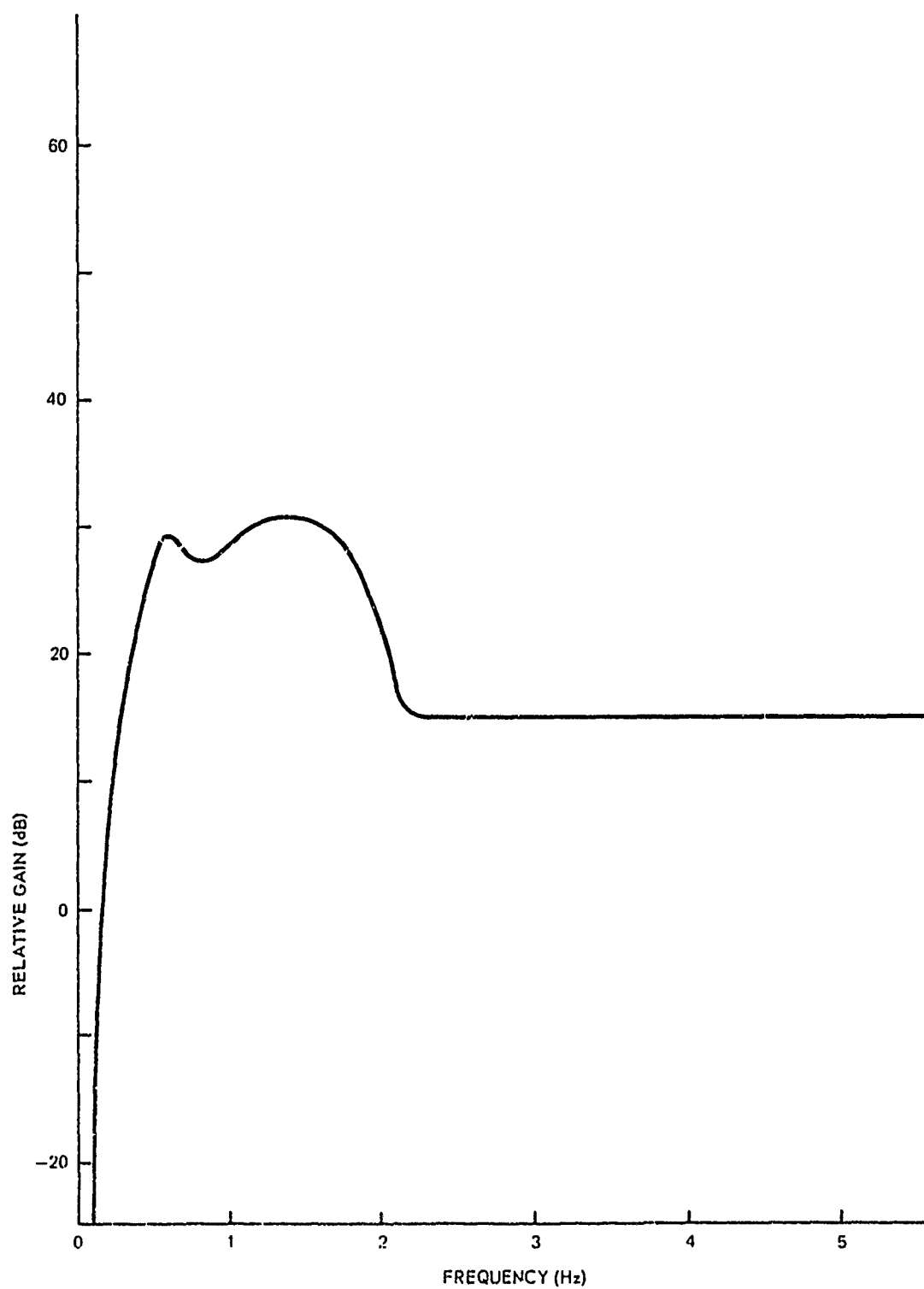


Figure 68. Gain Function for Surge and Wave Height

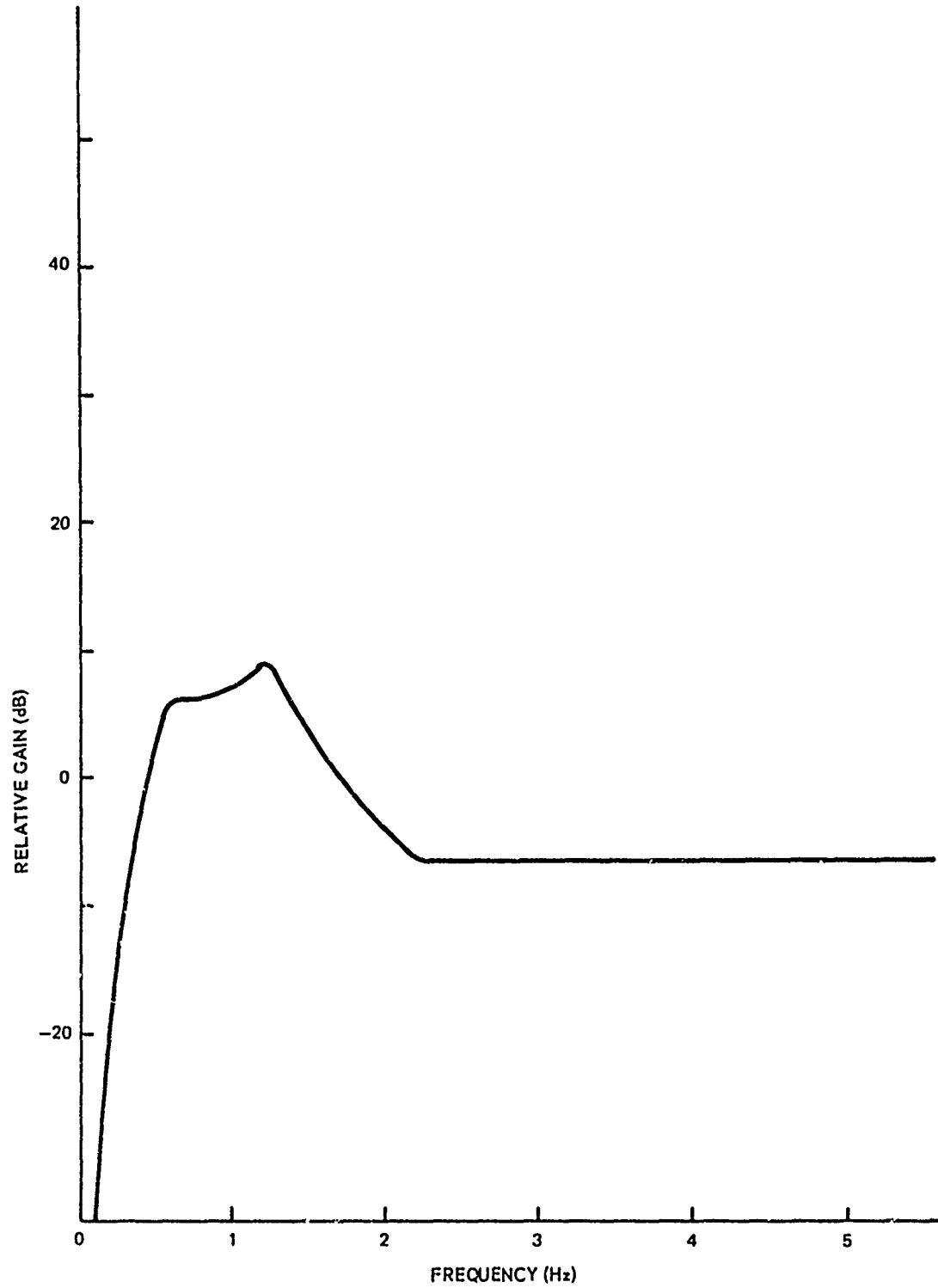


Figure 69. Gain Function for Pitch and Wave Height



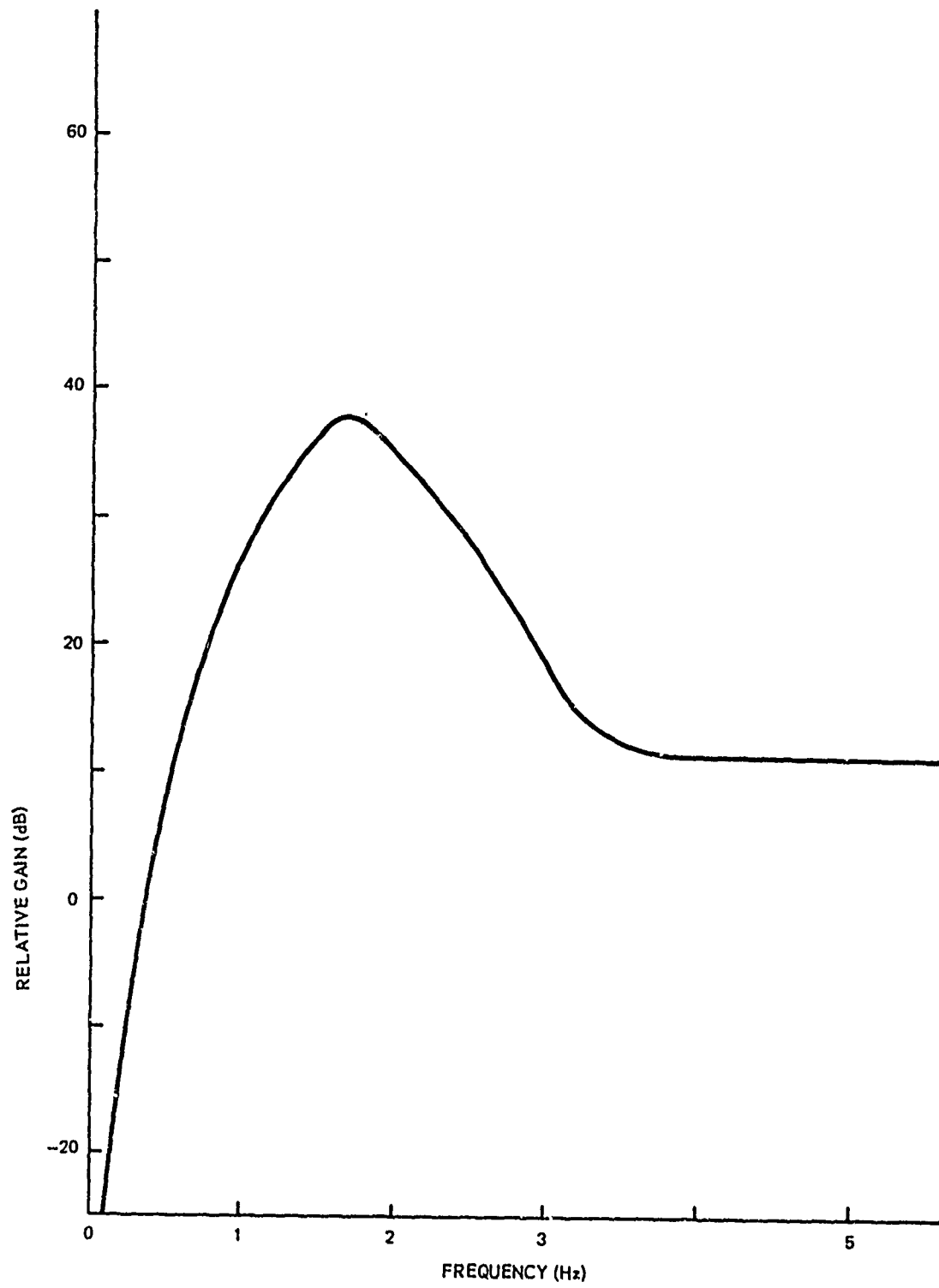


Figure 70. Gain Function for Roll and Wave Height

### 4.3 Simulation and Comparison of Buoy System Dynamics

#### 4.3.1 Spherical Buoy at Station D

Steady-state configurations of the spherical buoy system, installed at Station D, are shown in figure 71 for various uniform currents. Very little of the 3/4-in. DiLock chain is picked up off the bottom even under the worst current conditions — 1 knot. Steady-state tensions never go over 100 lb, and the watch circle radius can vary from 38 ft at 0 knot to 62 ft at 1 knot. These configurations were computed on the GSA time-sharing computer using the steady-state buoy system configuration program shown in appendix B. The Savonius rotor current meter used in the spherical buoy system failed 3 days after emplantment, thus; cable angles can not be correlated with current strength for this buoy system. However, the computed configurations are used as initial conditions for the buoy system dynamics simulation when current strength and direction are computed from the Coast and Geodetic Survey current tables.<sup>83</sup>

The lumped-mass dynamic equations of motion for the cable and the equations of motion for the spherical buoy were programmed and solved numerically in the time domain using a fourth-order, Runge-Kutta numerical integration scheme. Five mooring line mass elements were used — three for the cable and two for the chain. The buoy was allowed six degrees of freedom (heave, surge, sway, yaw, pitch, and roll), and each mooring line mass element was allowed three degrees of freedom ( $x_1$ ,  $y$ , and  $z$ ). The program shown in appendix B can accept wind and current vectors coming from any

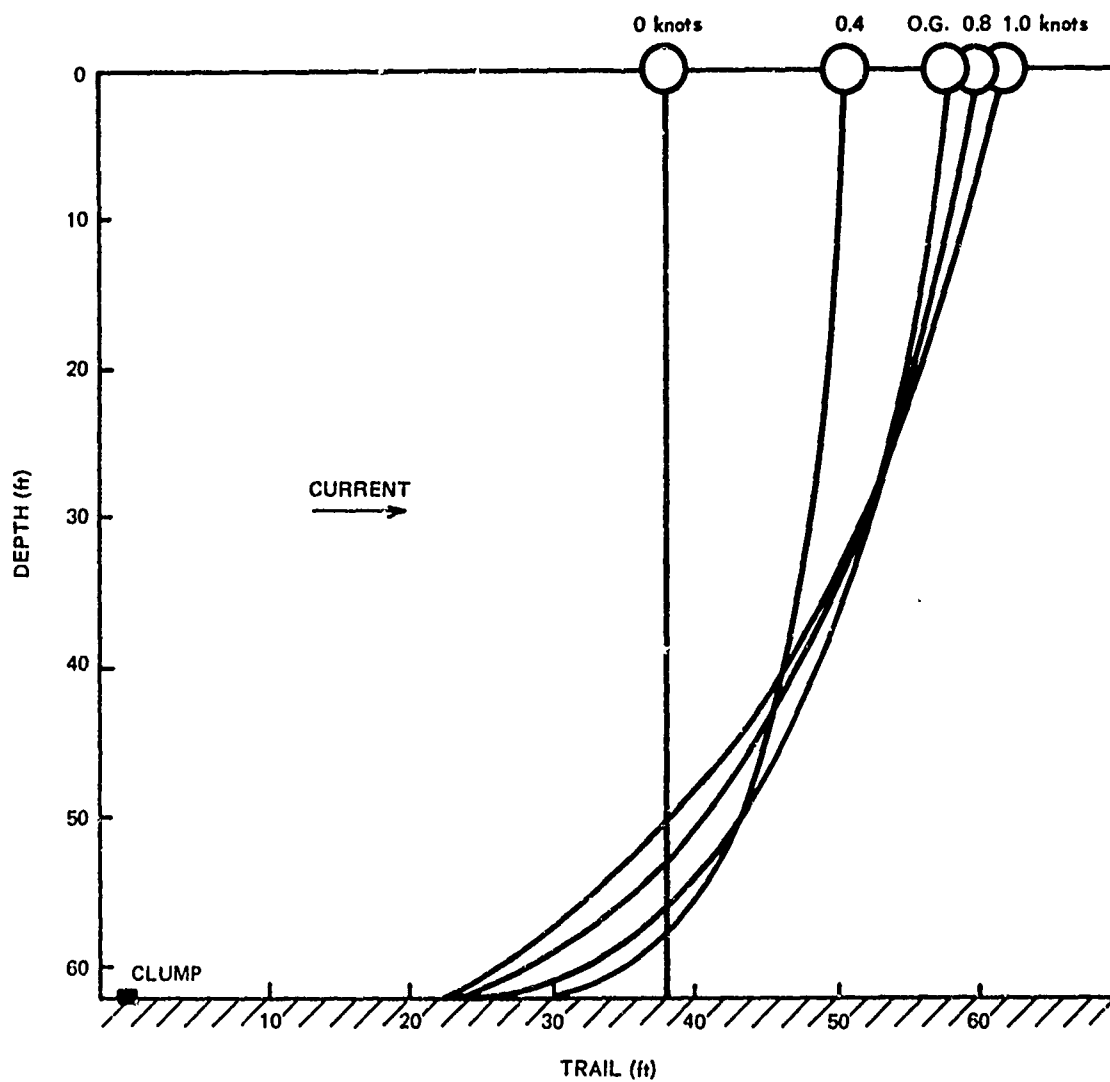


Figure 71. Computed Steady-State Configurations of the Spherical Buoy System

direction; however, the waves are assumed to be two-dimensional and are constrained to come in on the  $z$  axis of the inertial coordinate system. A complete listing of the input data needed to describe the spherical buoy system is shown in appendix D. Mean wave heights and periods were computed from reference 82 for various sea state conditions. The spherical buoy system dynamics model was excited with the ten-component random wave model based upon a two-parameter Bretschneider spectrum having the mean wave height and period for each sea state. The average wind strength and direction and the average current strength over the time period in which the statistical accelerometers were in operation were also used to force the model. The wave amplitudes for each component were allowed to build linearly over two component wave periods. This procedure minimized transient motions. The solution was allowed to proceed in time as transients decayed. Finally, buoy heave accelerations were sampled over a time period, and the mean heave acceleration amplitude was computed.

These computed amplitudes are shown in figure 72 and are compared with the amplitudes derived from the statistical accelerometer data. The computer model overestimates the heave acceleration amplitudes at the lower sea states and agrees quite well at the higher sea states. Since the observed sea states are based upon the Block Island resident engineer's visual observations, a plus or minus one sea state error band is shown in figure 72 for the observed data. It is concluded that the computer model provides a conservative estimate of buoy accelerations for design purposes.

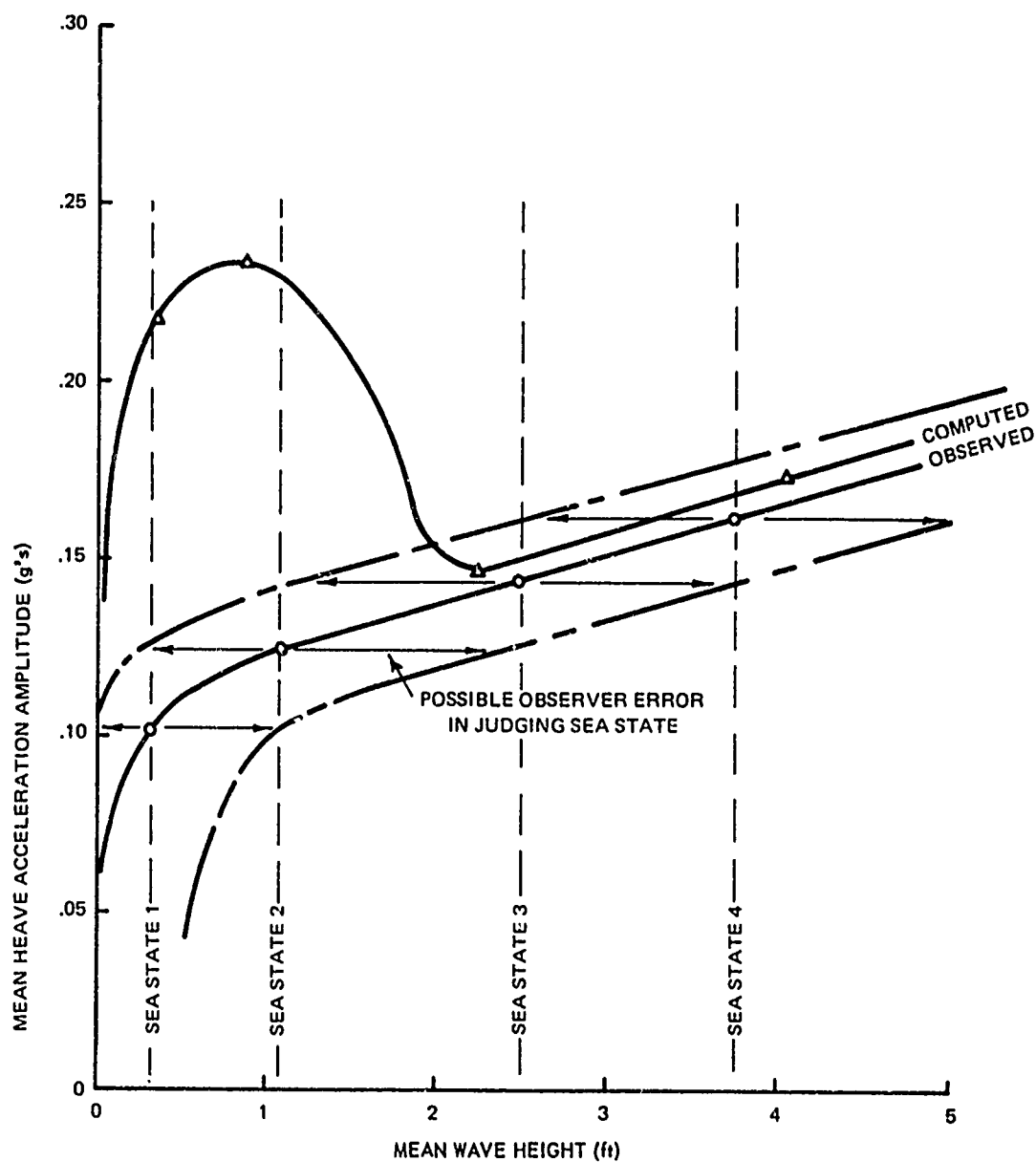


Figure 72. Observed and Simulated Heave Motions of the Spherical Buoy

On 16 March 1970, strip chart recordings of the buoy motion instrumentation were made. The computed Bretschneider wind wave spectrum for that location, date, and time based upon the observed wind speed, direction, and duration is shown in figure 73. This spectrum was used to determine component amplitudes for the random sea forcing function. The observed wind and the current as computed from the tidal current tables were also used to force the model on the UNIVAC 1108. Computed buoy heave, sway, and surge accelerations, pitch, roll, cable pitch, and cable roll were sampled in the same manner as the observed data and were analyzed on the GSA time-sharing computer.

The reduced spherical buoy motion parameters based upon computed motions and observed motions are shown on figures 74 and 75, respectively. Since the spherical buoy was not equipped with a yaw sensing device, the motions designated surge and sway and pitch and roll are not known relative to the  $z$  axis, along which the waves are traveling. Visual observations made from the beach while the data were being recorded indicated that the buoy was aligned in one direction with little or no yaw motion. A comparison of figures 34 and 75 indicates that the observed sway may really have been surge and that pitch and roll should be interchanged. Figure 75 reflects these changes.

A comparison of figures 74 and 75 indicates that the computer model predicts buoy heave accelerations with good engineering accuracy (-9.5 percent error for heave acceleration standard deviation), underestimates buoy sway accelerations (-71 percent error for sway acceleration standard deviation), and overestimates buoy pitch and roll motion (+54 percent error for pitch angle and

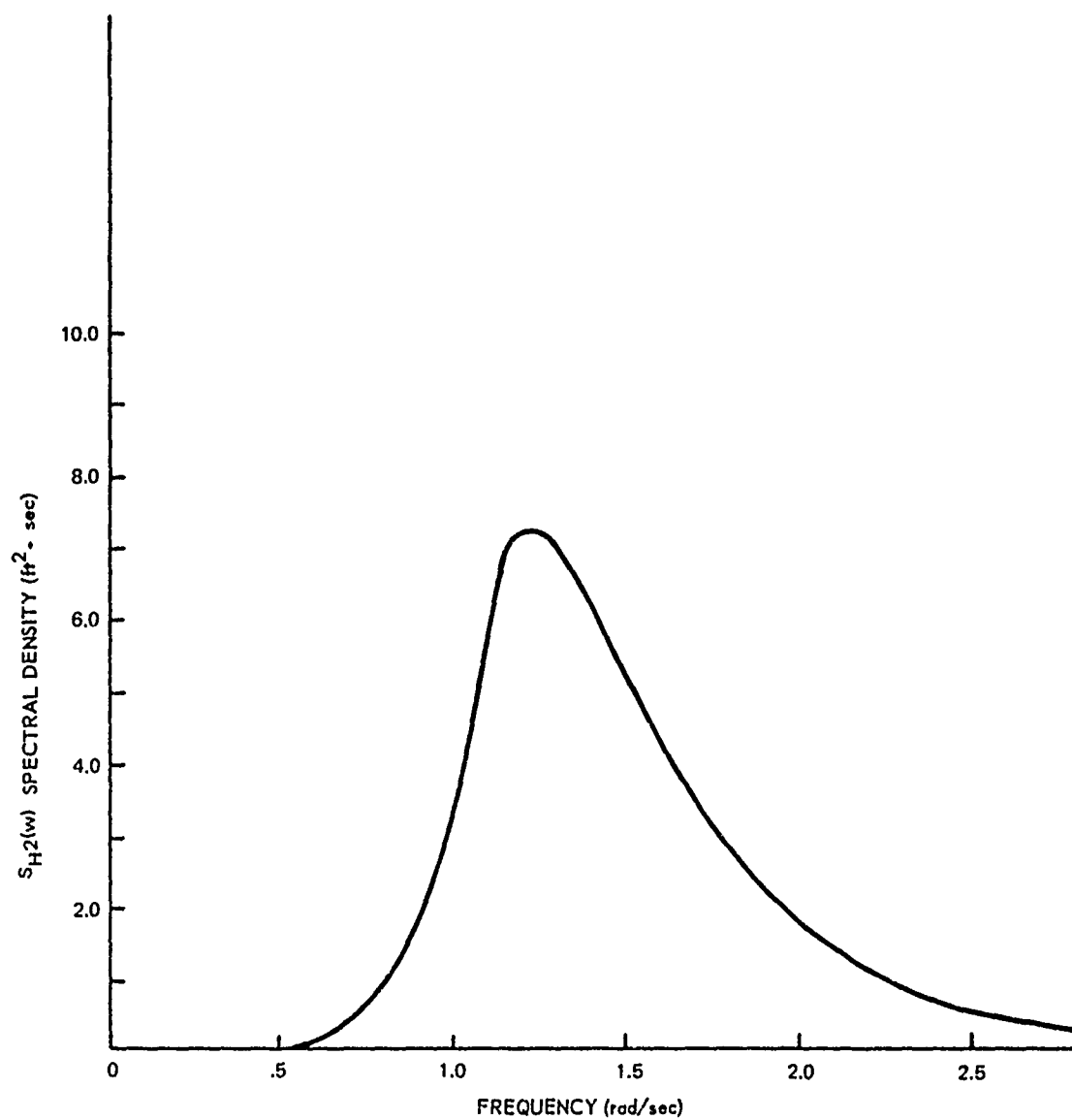


Figure 73. Bretschneider Spectrum — 1200 hr; 16 March 1970 Station D

<u>VARIABLE</u>	<u>MEAN</u>	<u>VARIANCE</u>	<u>STANDARD DEVIATION</u>				
HEAVE ACCELERATION	0 g	0.0198 g <sup>2</sup>	0.1408 g				
SWAY ACCELERATION	0 g	0.0009 g <sup>2</sup>	0.0288 g				
SURGE ACCELERATION	0 g	0.0015 g <sup>2</sup>	0.0390 g				
PITCH	-1.37 deg	137.00 deg <sup>2</sup>	11.70 deg				
ROLL	-1.01 deg	315.07 deg <sup>2</sup>	17.75 deg				
CABLE PITCH	-19.37 deg	13.38 deg <sup>2</sup>	3.66 deg				
CABLE ROLL	38.29 deg	15.72 deg <sup>2</sup>	3.97 deg				
<u>THE CORRELATION MATRIX</u>							
	<u>HEAVE</u>	<u>SWAY</u>	<u>SURGE</u>	<u>PITCH</u>	<u>ROLL</u>	<u>CABLE PITCH</u>	<u>CABLE ROLL</u>
HEAVE	1.0	0.4774	-0.2632	-0.1251	-0.0410	0.2660	-0.3602
SWAY		1.0	-0.6762	-0.6023	-0.5559	0.1582	-0.2172
SURGE			1.0	0.1980	0.3751	0.1502	0.1979
PITCH				1.0	0.7363	-0.3377	0.2582
ROLL					1.0	-0.1546	0.3268
CABLE PITCH						1.0	0.0388
CABLE ROLL							1.0

Figure 74. Simulated Spherical Buoy Motion Parameter Statistics



<u>VARIABLE</u>	<u>MEAN</u>	<u>VARIANCE</u>	<u>STANDARD DEVIATION</u>				
HEAVE ACCELERATION	0 g	0.0242 g <sup>2</sup>	0.1555 g				
SWAY ACCELERATION	0 g	0.0098 g <sup>2</sup>	0.0991 g				
SURGE ACCELERATION	—	—	—				
PITCH	14.3 deg	55.3 deg <sup>2</sup>	7.58 deg				
ROLL	1.1 deg	104.2 deg <sup>2</sup>	10.20 deg				
CABLE PITCH	-7.3 deg	16.2 deg <sup>2</sup>	4.01 deg				
CABLE ROLL	-27.1 deg	24.0 deg <sup>2</sup>	4.90 deg				
<u>THE CORRELATION MATRIX</u>							
	<u>HEAVE</u>	<u>SWAY</u>	<u>SURGE</u>	<u>PITCH</u>	<u>ROLL</u>	<u>CABLE PITCH</u>	<u>CABLE ROLL</u>
HEAVE	1.0	0.4806	—	-0.0706	0.6050	0.0454	0.2435
SWAY		1.0	—	0.0054	-0.4199	0.1975	-0.1605
SURGE			1.0	—	—	—	—
PITCH				1.0	-0.1021	-0.3813	-0.2121
ROLL					1.0	-0.0946	0.0063
CABLE PITCH						1.0	-0.2282
CABLE ROLL							1.0

Figure 75. Observed Spherical Buoy Motion Parameter Statistics

+74 percent error for roll angle standard deviations). Mooring line pitch and roll angle standard deviations are underestimated by -33.6 percent and -19.0 percent, respectively.

The simple product-moment correlation matrix for the observed data indicates moderate coupling for heave-sway, heave-roll, sway-roll, and pitch-cable pitch. Because of the axial symmetry of the buoy, it is expected that heave-pitch and surge-pitch would also be coupled. The simulated buoy motion correlation matrix indicates coupling between heave-sway, sway-surge, sway-pitch, sway-roll, and pitch-roll. The modal coupling indicated by the two correlation matrices do not agree. This poor agreement is probably due to the rather short sample time used to compute the product moment correlations. An error estimate based upon an assumed bandpass white noise sea spectrum with a bandwidth of 1 Hz indicates normalized errors of about 22 percent in the standard deviations and about 48 percent in the product-moment correlations. The comparison of simulated buoy motions with observed buoy motions for this case indicates reasonable agreement for parameter standard deviations but poorer agreement for product moment correlations. In view of the limited amount of data and its relatively poor quality, this particular comparison will not be extended.

### 1.3.2 Torroidal Buoy at Station BRAVO

The buoy motion computer model with lumped-mass cable elements was modified and input values were changed in order to simulate motions of the torroidal buoy BRAVO. A subroutine to compute the buoyant forces and moments

by polar integration around the torroid as a function of its draft and tilt angle was incorporated in the program (appendix E). A subroutine to compute simple statistical properties (mean, variance, and standard deviation) of the input wave height and output buoy motions (heave, surge, and sway accelerations and pitch and roll angles) was also incorporated in the program.

Winds were assumed to act from the southwest (the predominant wind direction during May and June), and an average ebb current of 0.7 knot was assumed (uniform in depth, setting to the east). Thus, the buoy system coordinate system has the  $z$  axis pointing southwest and the  $y$  axis pointing southeast (figure 76). The S-M-B method was used to compute the mean wave height and period for winds of 5, 10, 15, 20, and 25 knots for the southwest winds with an assumed duration of 4 hr. The computed mean wind wave heights and periods for station BRAVO are shown in figure 77. Resulting Bretschneider spectra for these conditions are shown in figure 78. These spectra were used to compute random wave component amplitudes and frequencies which, in turn, forced the buoy motion computer model.

Initial runs with a five-element cable model were found to be very time-consuming in machine time since the relatively low mass and high elastic modulus of the cable elements required that numerical integration step sizes on the order of 0.001 sec be used for numerical stability. A step size of 0.0005 sec was used for accuracy. The program was rewritten, and inputs were recomputed for a three-element mooring line model. Cable masses were concentrated at the current meter in the middle of the cable, and the lengths of heavy anchor chain were broken up to form the other two mooring line lumped masses. This

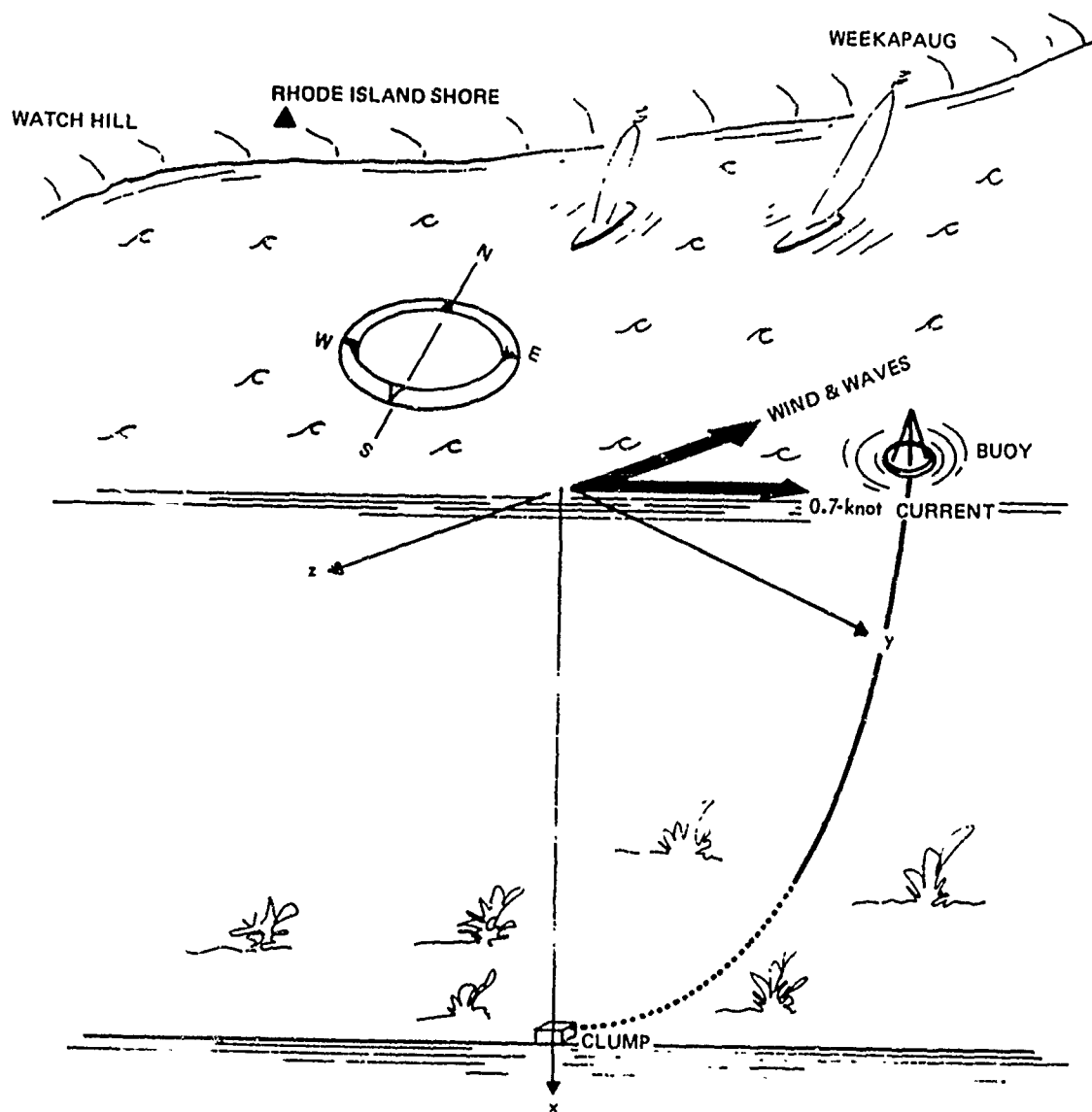


Figure 76. Torroidal Buoy BRAVO with Ebb Current and Southwest Winds

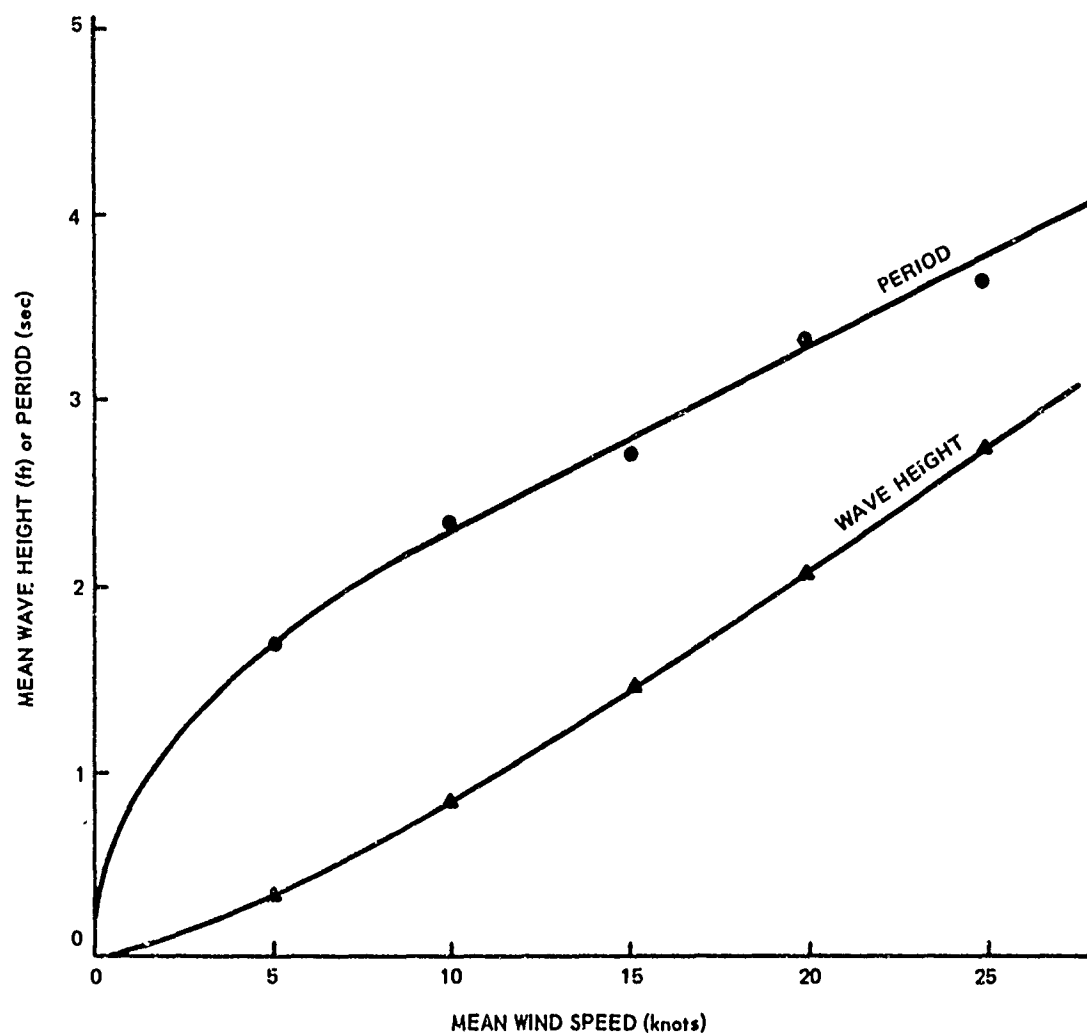


Figure 77. Computed Mean Wave Heights and Periods at Station BRAVO

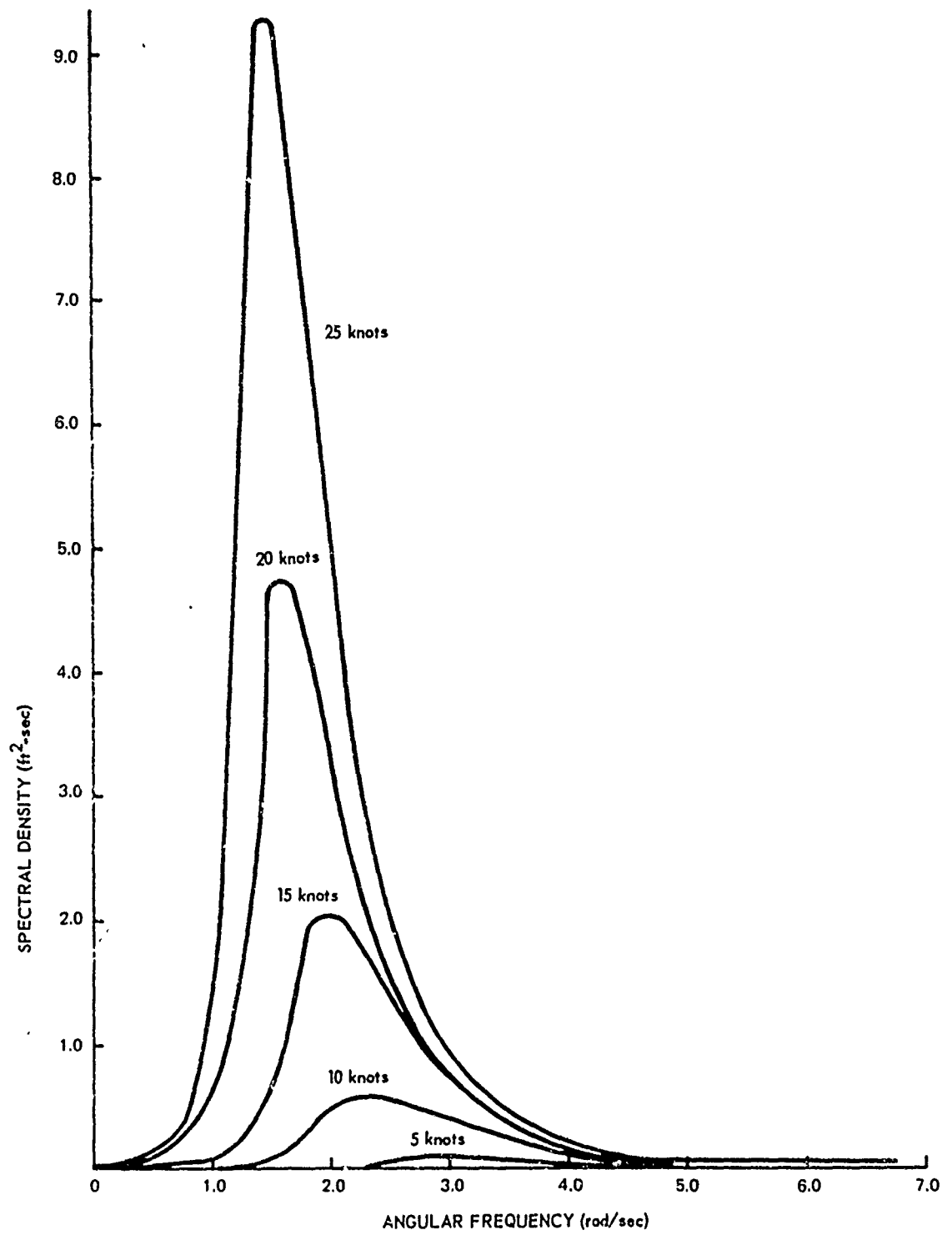


Figure 78. Computed Wind Wave Spectra

procedure greatly reduced the highest natural frequency of the system and the step size could be increased to 0.01 sec before numerical instability occurred. A step size of 0.005 sec, which allowed an order of magnitude increase in computational speed, was used. No significant difference was seen in computed buoy motions when using the three-lump or five-lump cable model.

The run procedure is as follows. First, the model is acted upon by the mean wind and current components (no waves) and allowed to converge to its steady-state configuration. Then, the random wave components are introduced and buoy motions sampled at every integration for 60 sec. Each run required about 20 min of computer time on the UNIVAC 1108. The ratio of computer time to solution time was 9.15:1.

The results of four runs with mean wind speeds of 5, 10, 15, and 20 knots are shown in figures 79, 80, and 81. The least-mean-squares plots of the observed data, as shown in figures 45 through 50 and as summarized in figure 51, are also shown in figures 79, 80, and 81. Since the yaw orientation of the buoy was not known during the at-sea measurements, the coefficients of the surge and sway empirical functions and of the pitch and roll empirical functions were averaged. Also, since the winds and waves in the computer model are acting along the  $z$  axis, only heave, surge, and pitch motions are compared with observed data. The average error indicated in the simulation over the range of wind speeds considered are as follows:

#### 1. On Mean Wind Speed

Mean heave acceleration amplitude	+14.45 percent
Mean surge acceleration amplitude	-63.6 percent

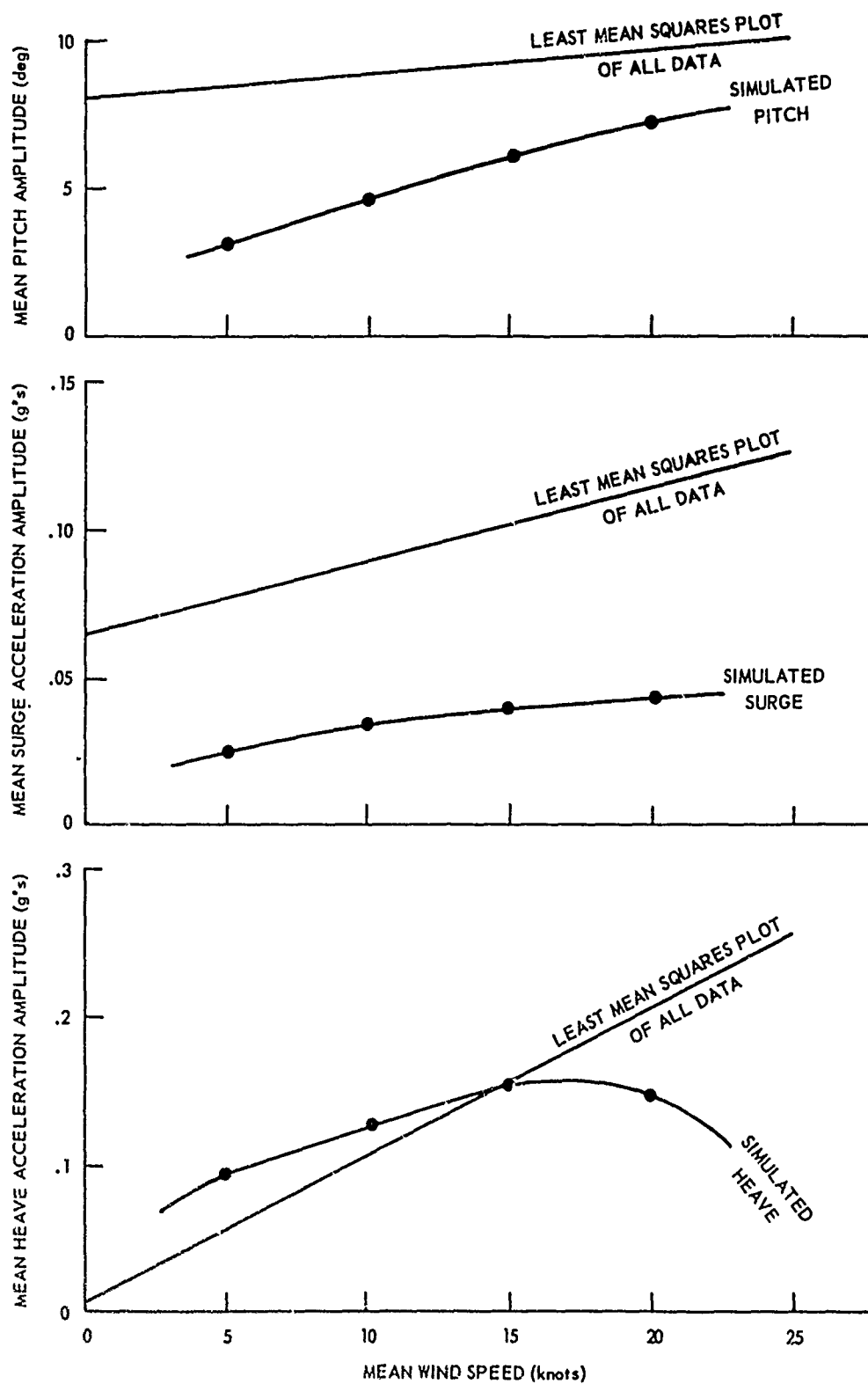


Figure 79. Simulated and Observed Buoy Motions versus Wind Speed



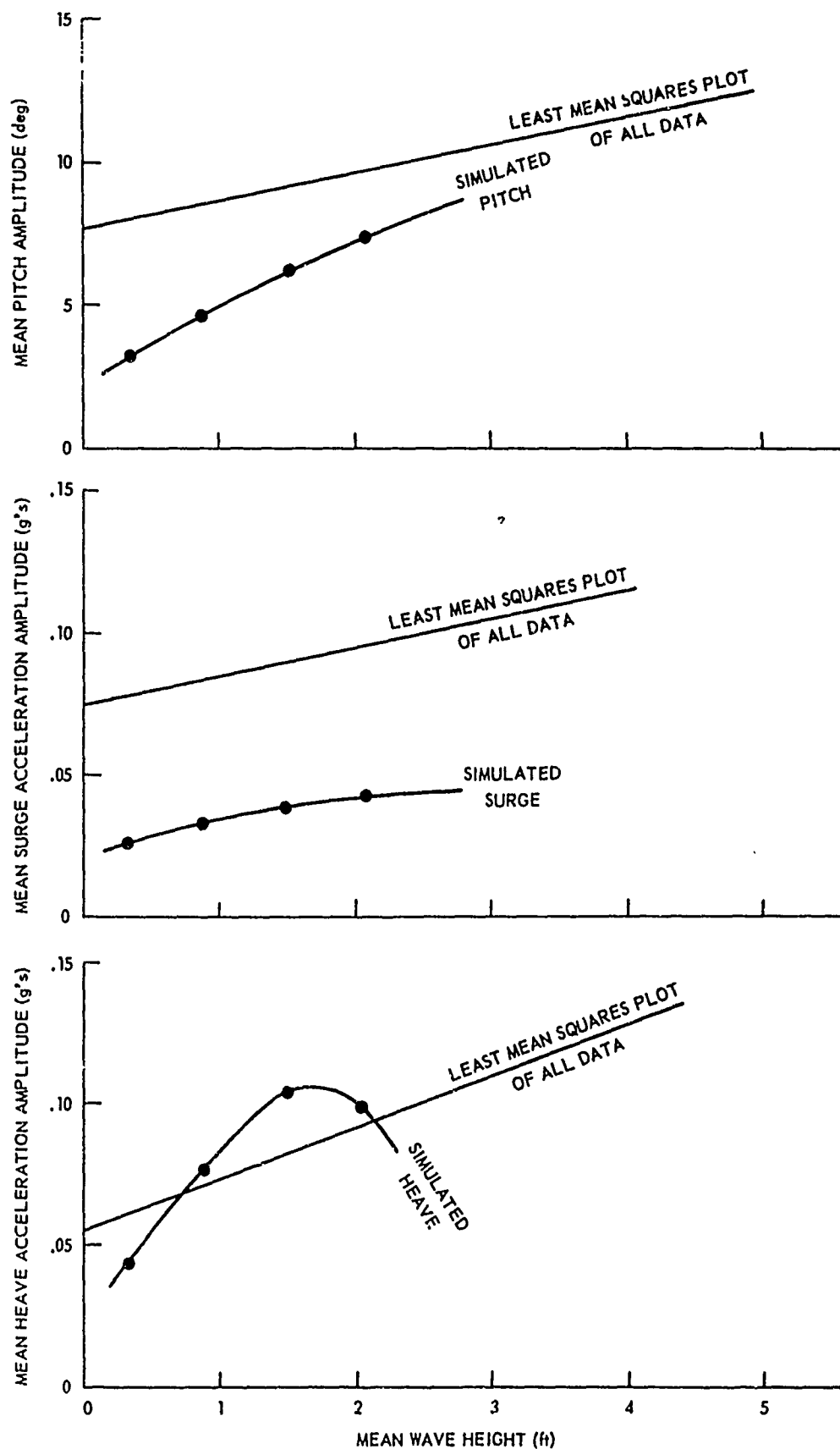


Figure 80. Simulated and Observed Buoy Motions versus Wave Height

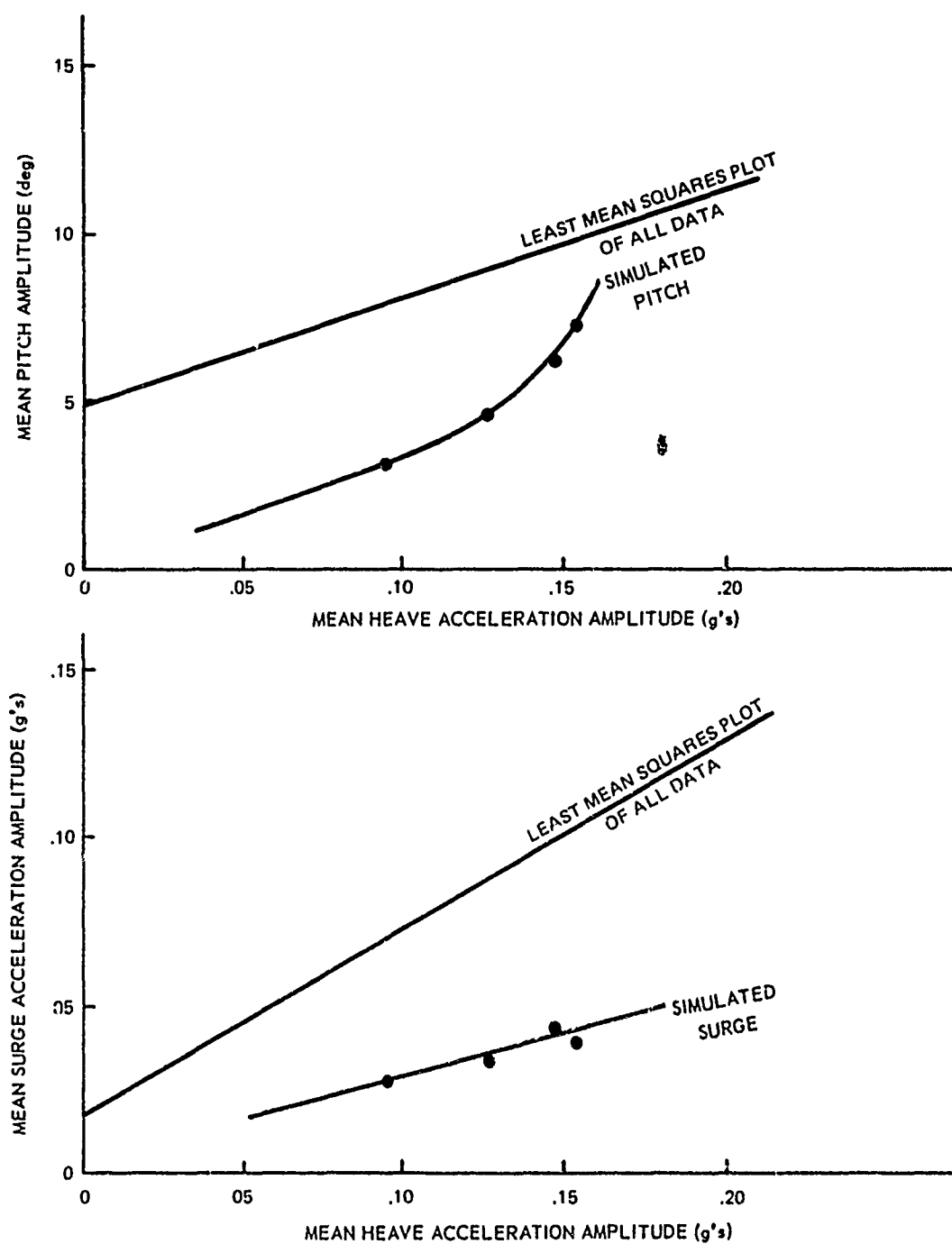


Figure 81. Simulated and Observed Surge and Pitch versus Heave

Mean pitch angle amplitude	-42.4 percent
----------------------------	---------------

## 2. On Mean Wave Height\*

Mean heave acceleration amplitude	+2.22 percent
-----------------------------------	---------------

Mean surge acceleration amplitude	-60.15 percent
-----------------------------------	----------------

Mean pitch angle amplitude	-41.43 percent
----------------------------	----------------

## 3. On Mean Heave Acceleration Amplitude

Mean surge acceleration amplitude	-60.4 percent
-----------------------------------	---------------

Mean pitch angle amplitude	-42.3 percent.
----------------------------	----------------

Again, assuming bandpass-limited white noise spectra of about 1-Hz bandwidth, note that the error in the standard deviations of the simulated buoy motion is about +13 percent. Also, known and estimated errors in the sensors and instrumentation (including possible observer error in reading the memoscope) indicate an overall error of +20.13 percent in the observed data.

The differences in observed and computed mean heave acceleration amplitudes fall within these error bands and thus indicate that the computer model offers reasonable accuracy for this motion. However, even if these error bands are taken into account, the model is systematically underestimating surge and pitch motions. Since surge and sway motions are underestimated with both the spherical buoy and with the torroidal buoy, it is suspected that the transverse hydrodynamic mass and damping used in the model may be in error. Recent

---

\*Note that wave heights for the observed data were based upon visual observations while wave heights for the simulated buoy motions were computed by the S-M-B method.

communications with E. Geller and R. Canada, who are affiliated with the National Data Buoy Project, have indicated that the results of their model buoy tests in towing basins do not agree with present theory because surge and sway hydrodynamic forces are less than predicted analytically. This communication confirms the above suspicion, but judgment is reserved until more test tank data are published.

The environmental conditions as measured during the data run of 11 June 1970 at 2030 EDT were used as input to the computer model, and buoy motions were computed. Power spectra for wave height, buoy heave accelerations, buoy sway acceleration, buoy surge acceleration, buoy pitch motions, and buoy roll motions were computed by a Fast Fourier Transform method.<sup>84-86</sup> A total of 1,024 samples, sampled at 0.06-sec intervals for each parameter, were transformed. The samples were smoothed by averaging over a 0.3-sec interval to prevent aliasing in the spectra. Eight ensemble averages were used, and they resulted in 64 statistical degrees of freedom and a standard error of 17.66 percent. The frequency resolution is 0.0163 Hz. Williams<sup>87</sup> states that a resolution on the order of 0.02 Hz is adequate to define ocean swell spectral peaks in his study of ocean wave spectra in Block Island Sound.

The input wave spectrum is shown in figure 82 along with the frequencies of the components that form the "random" wave forcing function. Figure 83 shows the computed spectrum level of the "random" wave model compared with the theoretical spectrum level. As expected, the "random" wave model exhibits characteristics of narrow-band white noise, which is reasonable since it is made up of a finite number of sine wave components close to one another in

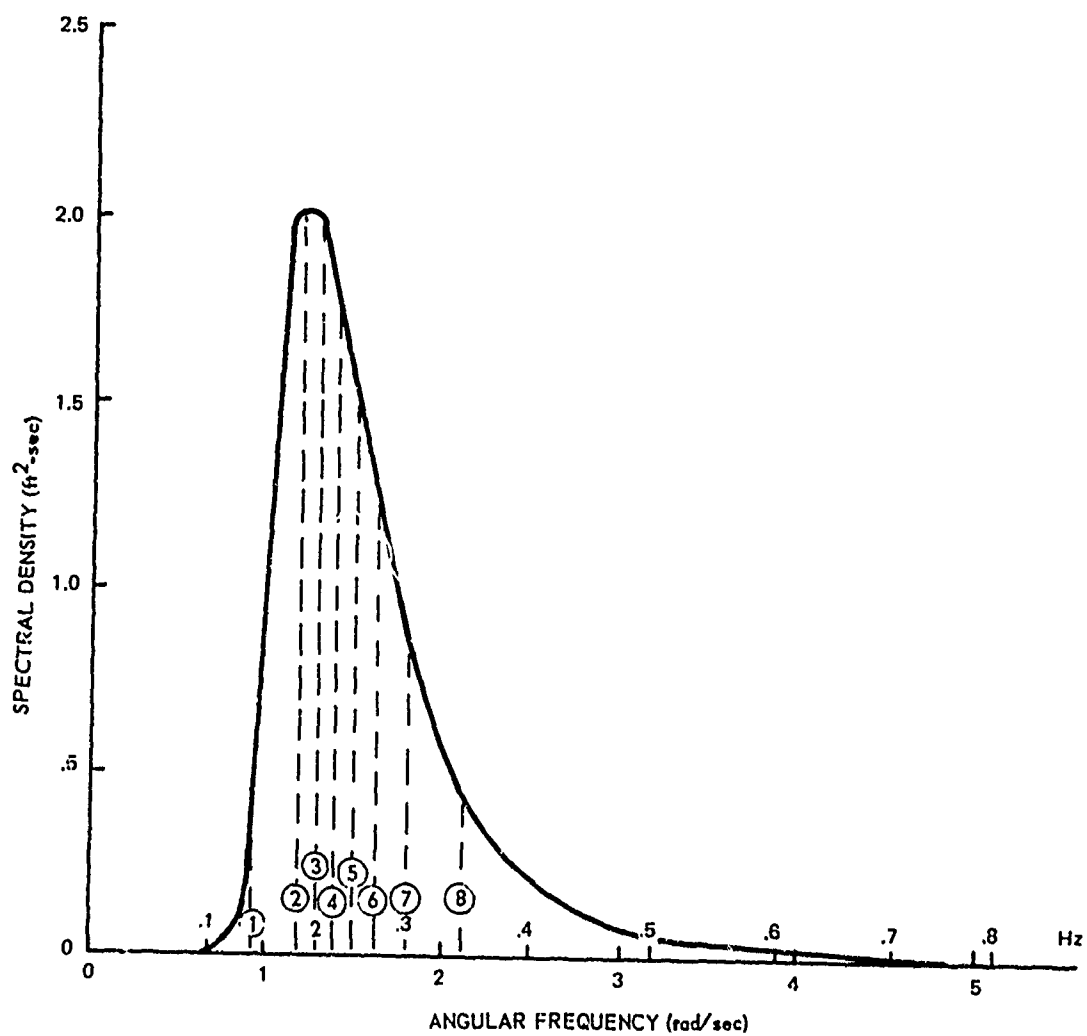


Figure 82. Wave Height Spectrum — 2030 hr, 11 June 1970

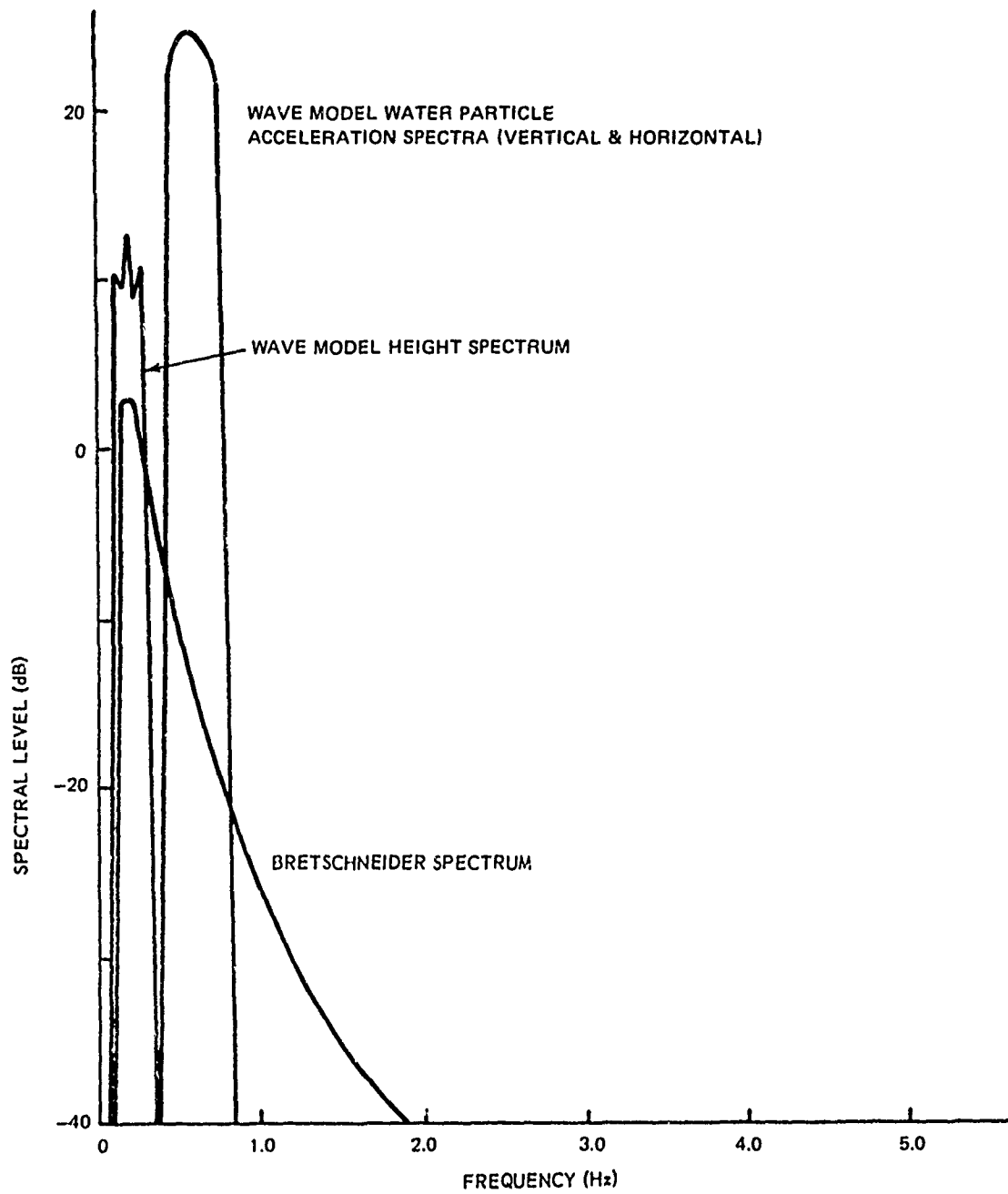


Figure 83. Simulated Wave Height Spectral Levels

the frequency domain.

The standard deviations for the input wave height and the output buoy motions are as follows:

Wave height	0.4807 ft
Heave acceleration	1.9321 ft/sec <sup>2</sup>
Sway acceleration	0.4217 ft/sec <sup>2</sup>
Surge acceleration	0.4974 ft/sec <sup>2</sup>
Pitch angle	2.98 deg
Roll angle	4.437 deg.

Output spectral levels are shown in figures 84 through 88. In general, the spectra exhibit more deterministic properties than the buoy motion spectra from the at-sea data. More smoothing was done on the at-sea spectra than on the simulated spectra, but the at-sea spectra do not appear to have the narrow-band characteristics of the simulated spectra, especially in heave, surge, and pitch. This indicates that the model may be inadequately damped. The natural frequency of the buoy in heave when at middraft is computed to be 0.36 Hz. The heave, surge, and pitch spectra exhibit peaks at about this frequency. Since surge and pitch are decoupled from heave hydrodynamically, the coupling must be effected through the cable tensions acting on the buoy.

The second peak in the heave spectrum is located at about the same frequency as the peak of the water particle acceleration spectra. The forcing function component due to the heave hydrodynamic inertia force caused by water particle acceleration is driving the buoy in this frequency range. The surge spectrum also indicates that this forcing mechanism is active in that mode.

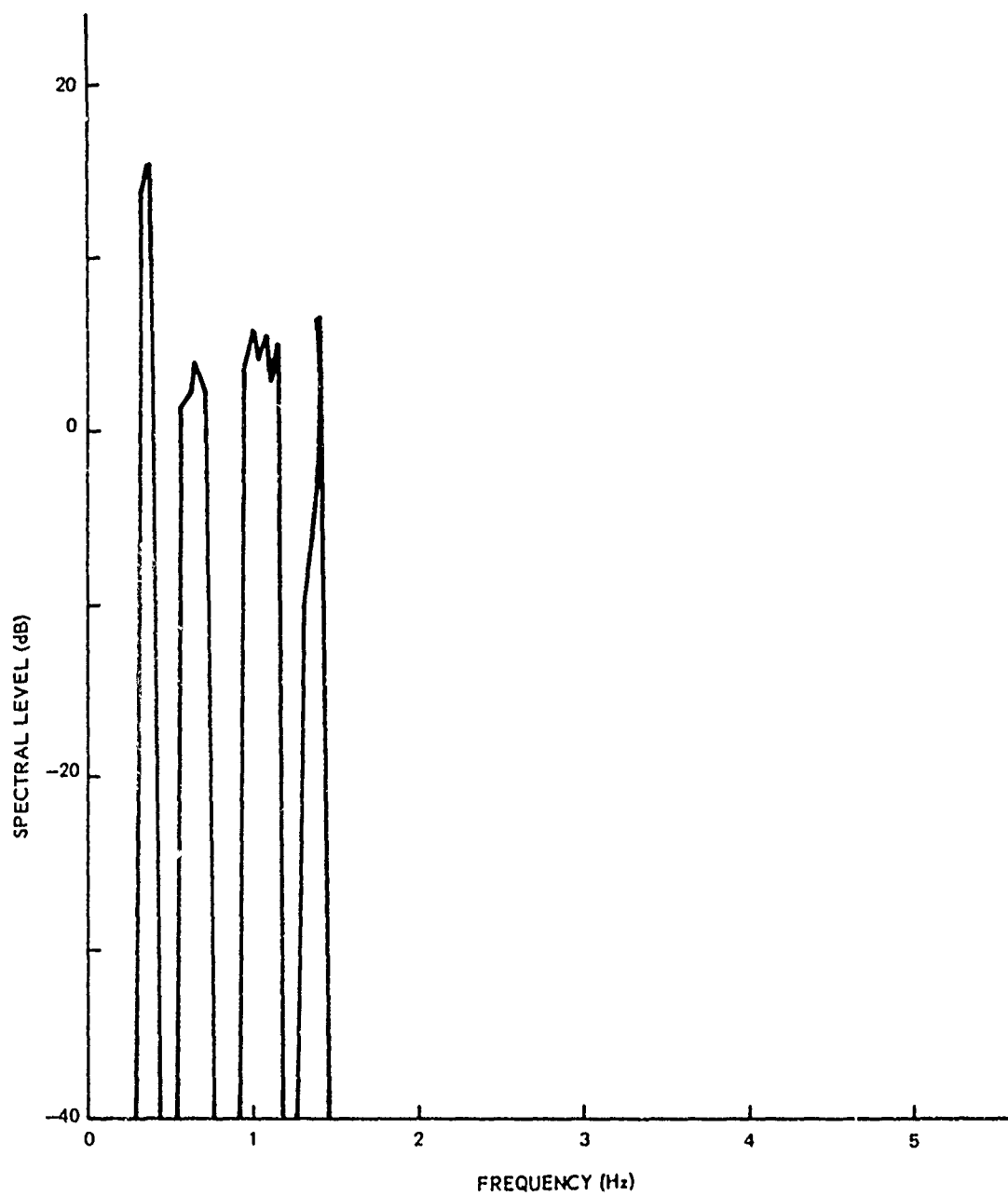


Figure 84. Simulated Heave Spectral Levels



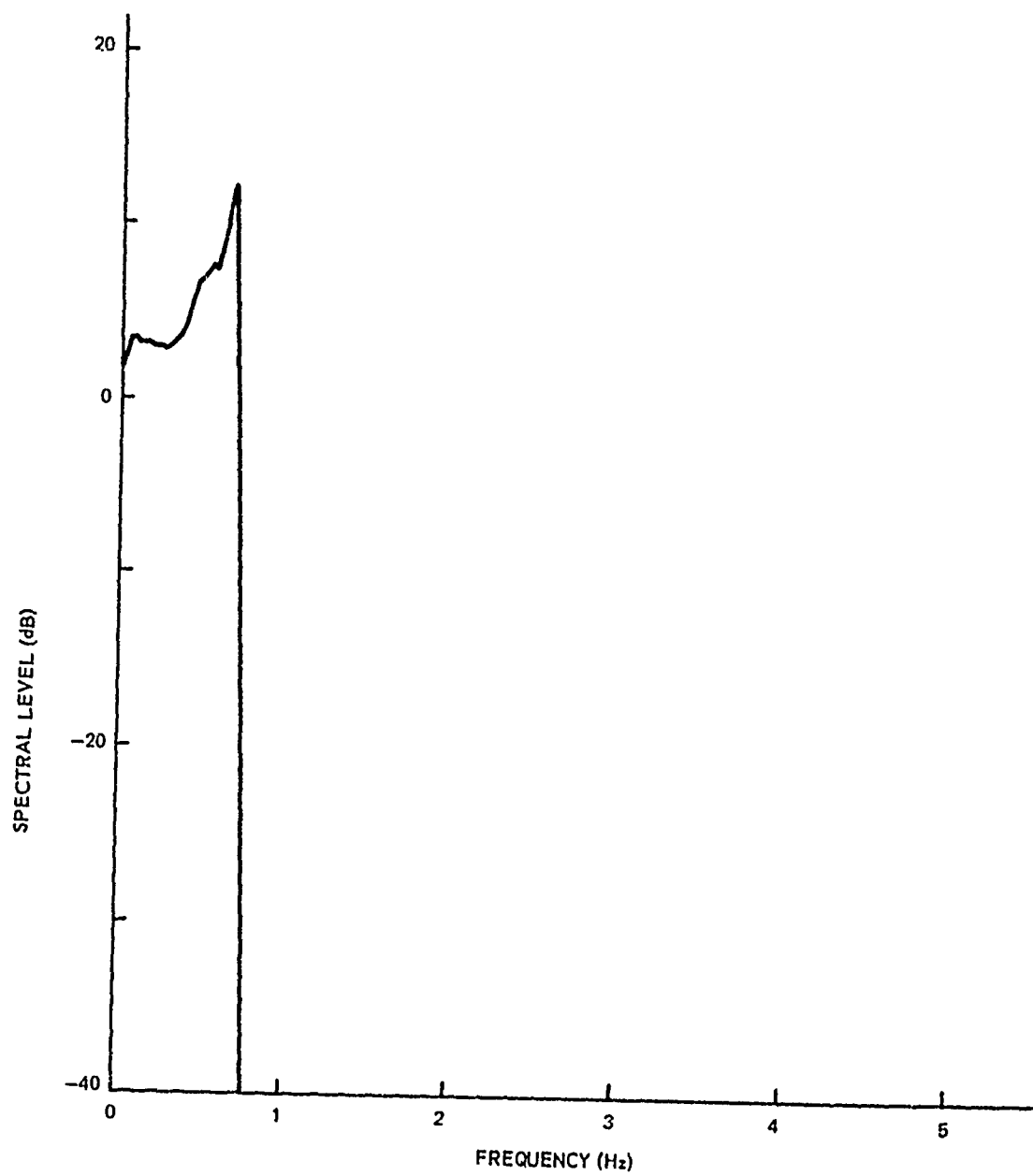


Figure 85. Simulated Sway Spectral Levels

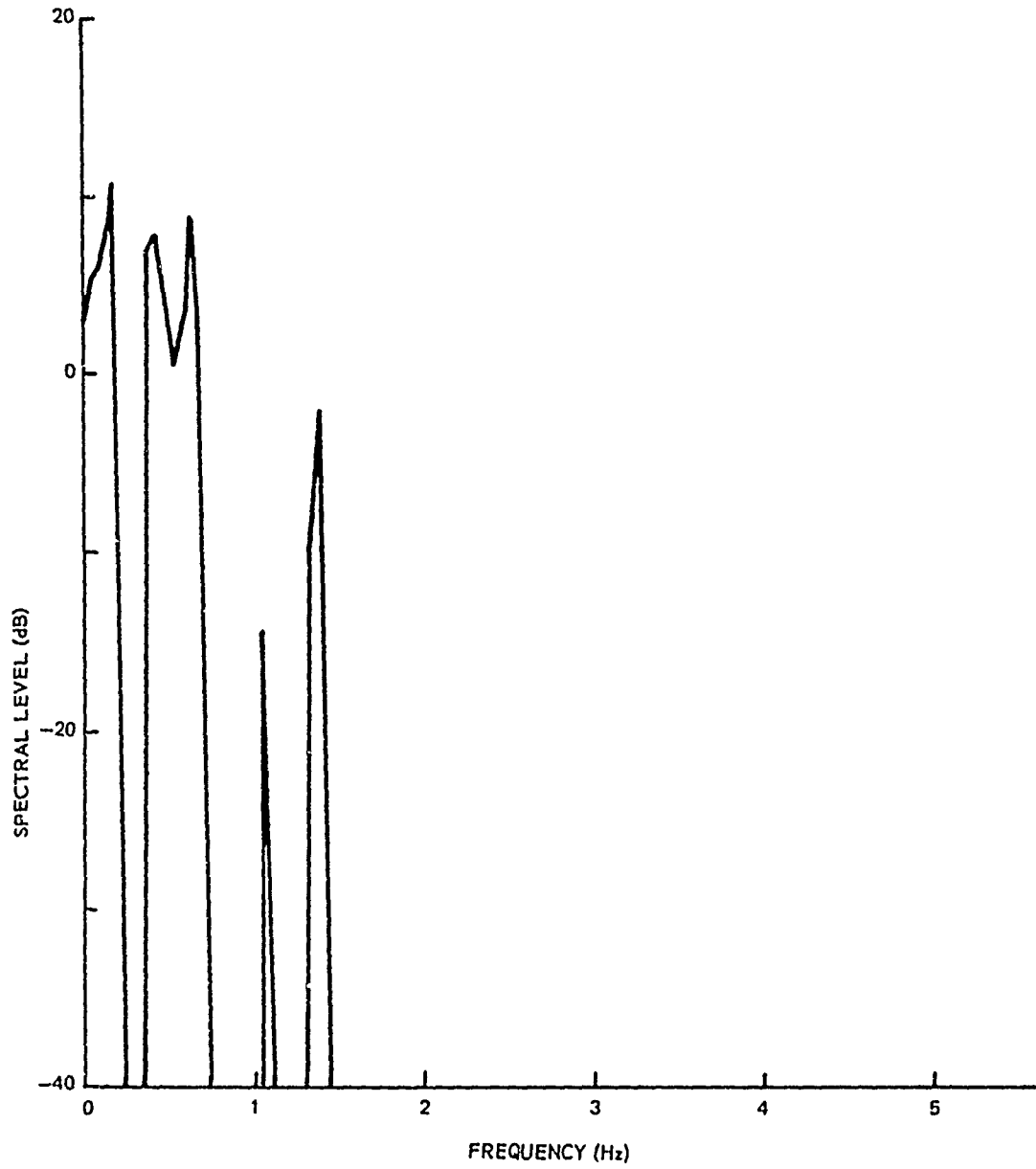


Figure 86. Simulated Surge Spectral Levels

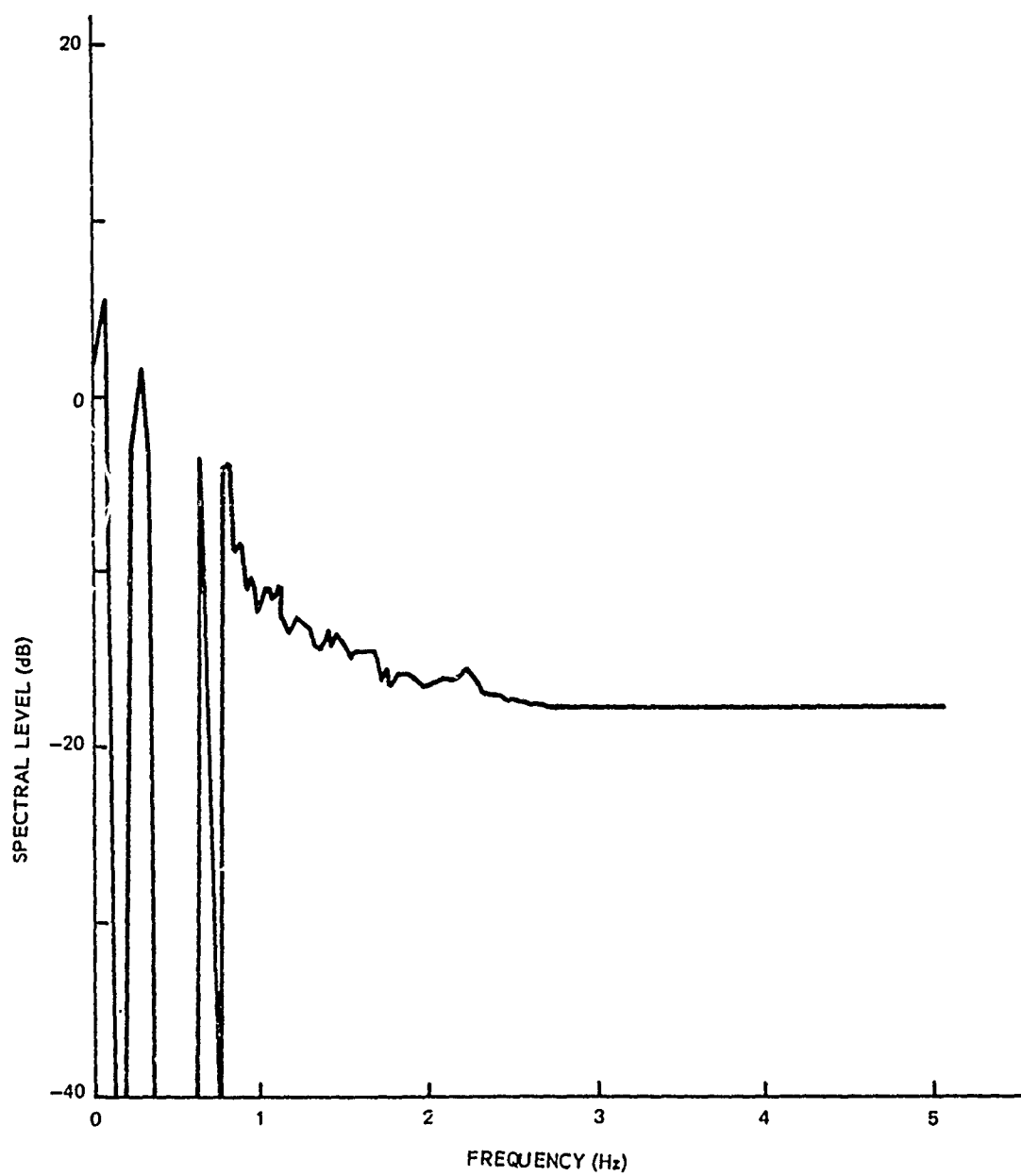


Figure 87. Simulated Pitch Spectral Levels

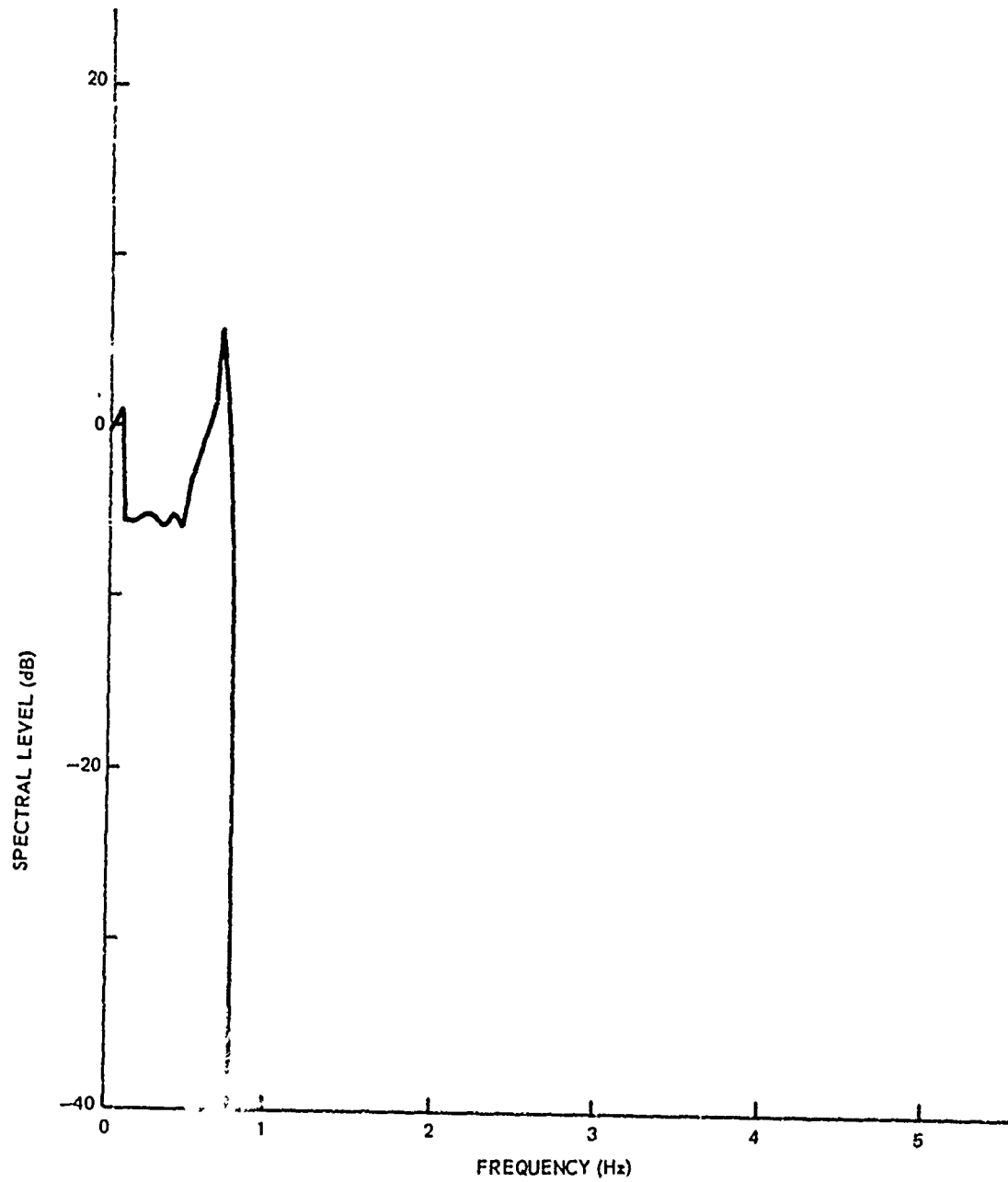


Figure 88. Simulated Roll Spectral Levels

Both pitch and roll spectra show peaks at this frequency. Pitch and roll motions have computed natural frequencies at about 0.7 Hz and would tend to respond to this forcing mechanism through coupling from surge and sway motions. Since the water particle motions are constrained to the  $x - z$  plane, one would not expect a response out of plane. However, the current vector has an out-of-plane component; thus, the mooring line tension force will have an out-of-plane component. Heave and surge motions will couple into sway and roll motions because of the mooring line tension. This coupling also illustrates another unusual feature of this dynamic system in that the response of the system is strongly dependent on the mean values of the system element spatial locations — a strong argument against linearized, decoupled models of buoy systems.

Both heave and surge show peaks at higher frequencies (1.05 and 1.4 Hz). These peaks are probably due to natural frequencies for the lumped-mass cable model. Sway and roll spectra have nearly the same shape and thus indicate a strong coupling in these modes. Surge and sway (also, pitch and roll through coupling) indicate some response at very low frequencies. This is due to the lowest natural frequency of the buoy system in a horizontal mode. If the analogy is made with a pendulum having a length order of magnitude with the water depth, the natural frequency of this motion would be quite low.

The heave spectrum computed from the experimental data (figure 57) indicates a peak at 0.4 Hz, which agrees well with the peak in the simulated heave spectrum due to the buoys natural frequency in heave. Surge, sway, pitch, and roll spectra all have spikes at 0.6 Hz. This is in agreement with

the peaks in the simulated sway, surge, pitch, and roll spectra. All the spectra, especially in roll, indicate energy at frequencies out to 2 Hz. This energy may be due to vibration in the mooring line coupling into the buoy.

This comparison of simulated buoy motions with observed buoy motions for the torroid buoy at station BRAVO on 11 June 1970 indicates that the computer model is distributing energy in its response in about the same way as the actual buoy system. However, the model is apparently underdamped and is filtering out some energy between natural frequencies. Again, more test tank data are needed for buoy hulls to determine their hydrodynamic characteristics.

The simulations of buoy system dynamics for the spherical and torroidal buoys moored in Block Island Sound have used the lumped-mass model of cable dynamics. In the course of this research, it was found that if mean tensions in the cable are very low or if a number of force discontinuities are present along the cable (both conditions common to shallow water moorings), the finite-difference method is usually not suitable. With very low tensions, the cable equations can go ultrahyperbolic, which could cause the numerical method to break down. When many force discontinuities are in the line, a large number of nodes are needed in the cable segments between the discontinuities in addition to equation of motion for each discontinuity. The resulting computational time becomes prohibitive.

#### 4.3.3 WHOI Mooring No. 238

In order to validate the buoy dynamics simulation using the finite-difference cable model, mooring line tension data taken with WHOI mooring No. 238 (reference 37) is compared with simulated tension data for the same

buoy system. WHOI mooring No. 238 is essentially the same as WHOI mooring No. 279 (figure 27) and was moored at the same location. Tensions were measured just below the toroidal surface buoy and were telemetered ashore. Computed inputs for the simulation of WHOI mooring No. 279 are shown in appendix D, and the buoy system dynamics program incorporating the finite-difference cable model is shown in appendix B. Since the WHOI data are shown against wind speed, the primary input is wind speed. The fetch was assumed to be 100 miles for this location in the North Atlantic, and wind durations were taken to be 24 hr. The Webster current profile, with a surface current of 1.5 ft/sec, was assumed to act in the direction of the wind for all cases.

Strains and cable angles at each node must be read in as initial conditions. The steady-state buoy system configuration program was used to compute these parameters for each wind speed and the given current profile. The initial cable angles are shown in figures 89 and 90. The standard deviation for the cable tension just below the buoy was computed for each run. Millard<sup>37</sup> presents a "scattergram" of "dynamic tension amplitude" versus 2-hr mean wind speed. Tensions were recorded on a Rustrak recorder, which has a very slow chart speed — on the order of centimeters per day. Thus, this "amplitude" was read by measuring the breadth of a very thick line. This actually represents the tension difference between the highest and lowest tension that occurred in a 2-hr period. It is assumed that these "amplitudes" correspond to the highest 1/10th wave heights found in wind-wave height distributions. The WHOI data of "dynamic tension amplitude" versus wind speed is shown in figure 91.

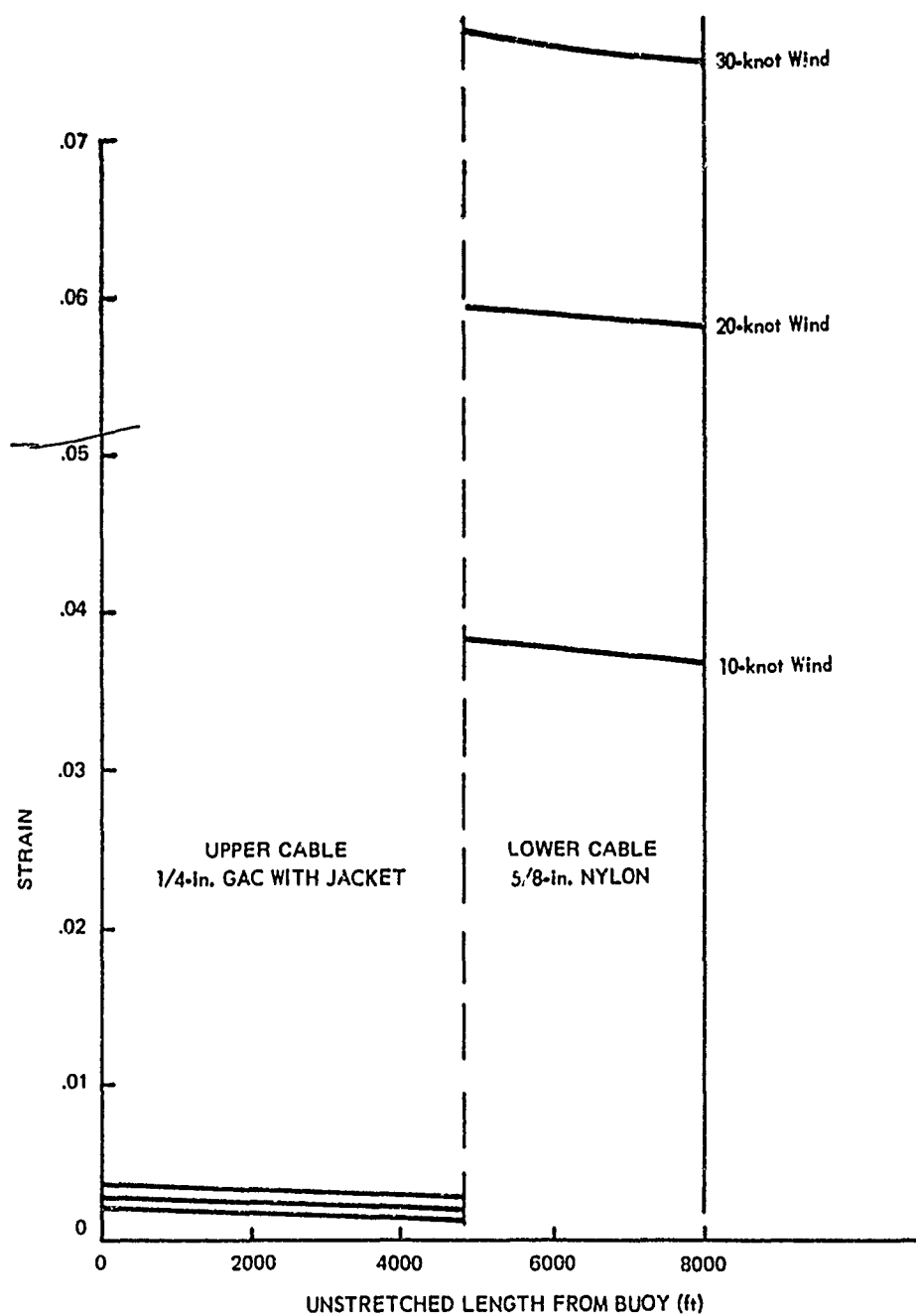


Figure 89. Initial Strains for WHOI Mooring No. 238



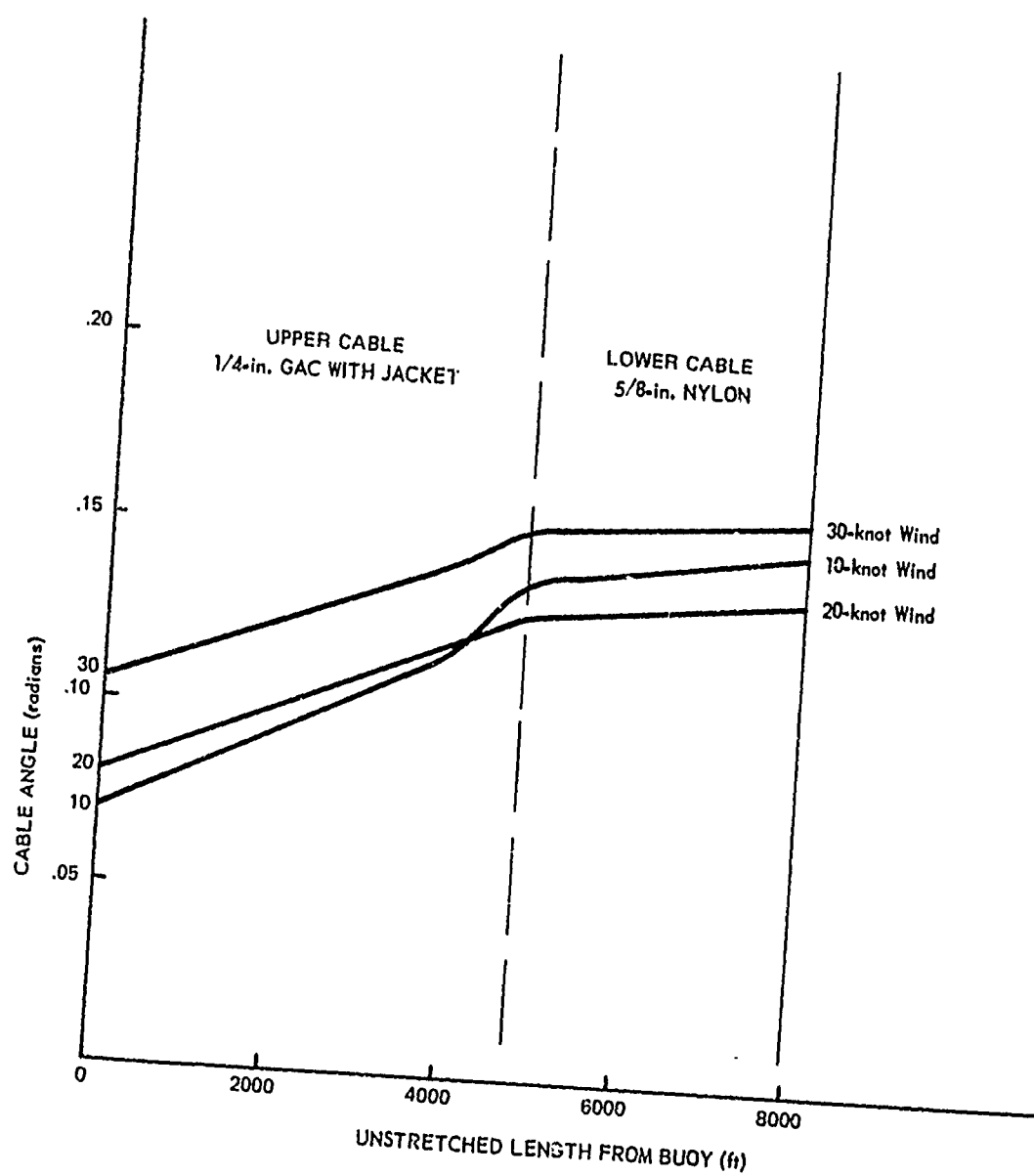


Figure 90. Initial Angles for WHOI Mooring No. 238

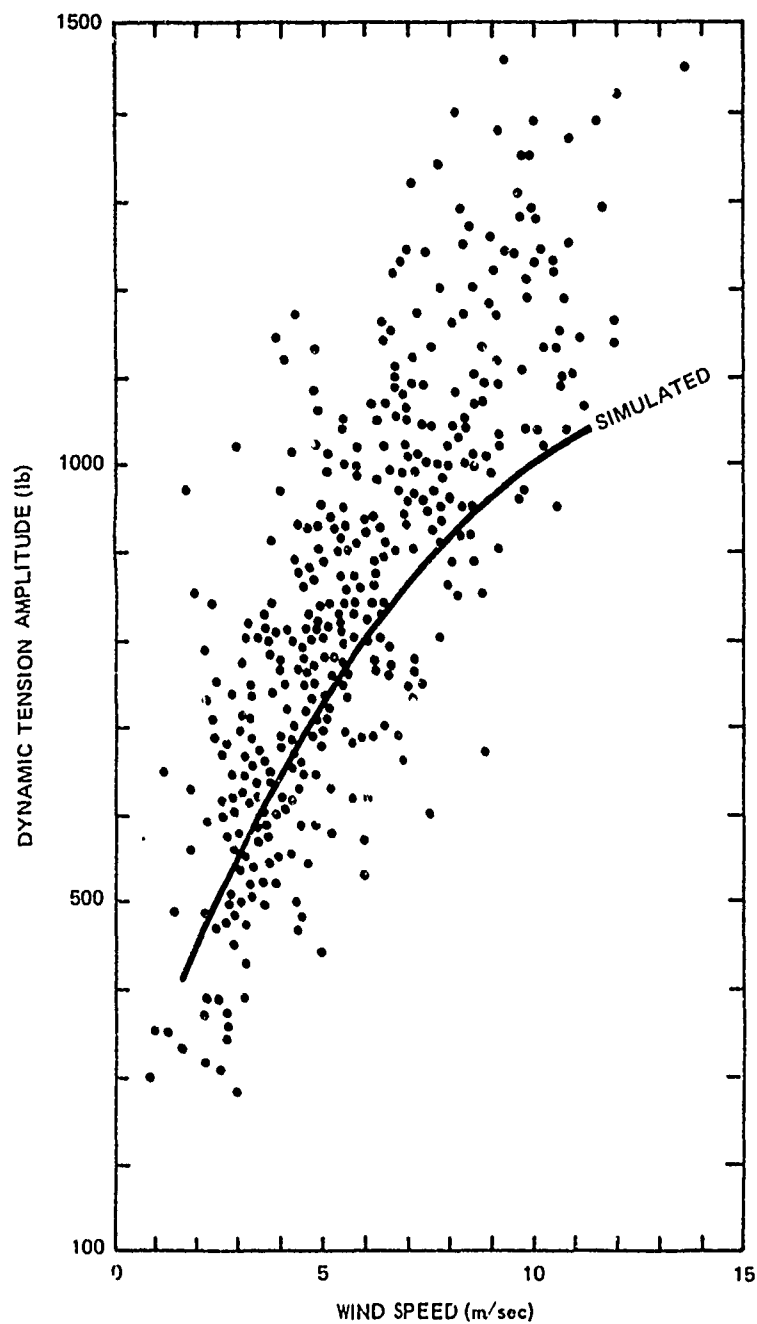


Figure 91. Computed and Observed Tension Amplitudes at 12 m for WHOI Mooring No. 238

Tension standard deviations for each run were first converted to mean amplitudes by assuming sinusoidal variations, converted to highest 1/10th amplitudes by assuming a Rayleigh distribution, and finally converted to double amplitudes. The resulting expression is

$$T_{\text{WHOI}} = (1.57)(2.03)(2.0) \cdot T_{\text{SD}} .$$

The simulated "dynamic tension amplitudes" are plotted in figure 91. Errors for the simulation were not computed in this case since the meaning of the WHOI "dynamic tension amplitude" is not clear. However, the simulation computes dynamic tensions that are order of magnitude and that increase with increasing wind speed. A better set of buoy motion and tension measurements are needed for deep sea buoy systems in order to fully validate the buoy motion dynamic simulation with the finite-difference cable model.

## V. SUMMARY

### 5.1 Restatement of the Problem

The object of this investigation was to evaluate the forces acting on the components of a simple buoy system exposed to the oceanic environment and to develop a numerical model of buoy system dynamics to simulate buoy system response. Axisymmetric buoy hull shapes were considered in general, and hydrostatic and hydrodynamic forces and moments on oblate spheroids were studied. The set of integro-differential equations of motion for the buoy were reduced to a set of ordinary differential equations with nonconstant coefficients by using frequency dependent hydrodynamic force coefficients published in the literature.

A "quasi-random" wind wave model was developed to simulate the motions of the water masses in the immediate vicinity of the buoy. Wind wave properties were computed with the S-M-B method from the mean wind speed, fetch, and duration. Borgman's energy partitioning method was applied to a two-component Bretschneider spectrum, and sinusoidal wave component amplitudes and frequencies were computed. The random phase components were summed to compute instantaneous water particle motions.

Major assumptions made in the investigation of buoy dynamics include the following:

1. Dissipative forces can be separated into those due to surface wave generation and those due to viscous drag.

2. Infinitesimal buoy motions exist; this assumption was made by John<sup>22, 23</sup> in the derivation of the hydrodynamic force and moment integrals and subsequently by Kim,<sup>42</sup> who evaluated the integrals for oblate spheroids.

3. The Haskind hypothesis is valid; i.e., it is assumed that the general problem of an object moving on a free surface in response to gravity waves on that free surface can be linearized to the extent that the velocity potential for that motion is the sum of

- a. the linearized velocity potential of the gravity waves alone,
- b. the velocity potential of the object moving on the free surface with no waves, and
- c. the velocity potential due to the waves generated by the motion of the body.

The Haskind hypothesis was used in order to apply Kim's coefficients for oblate spheroids, which were derived for objects oscillating on a free surface, to the case of objects oscillating on a free surface with gravity waves.

4. The St. Denis-Pierson hypothesis is valid, i.e., it was assumed that the sea can be represented as the linear sum of elementary waves of random phase.

5. Body dimensions are small compared with a wavelength. This assumption was made in order to use the computed water particle motions as the motions of the mass of water in the immediate vicinity of the buoy hull.

Equations of motion for an elastic cable capable of supporting both axial and transverse waves simultaneously were written. A unique finite-difference numerical technique, an extension of Hartree's method for hyperbolic partial differential equations, was developed for the solution of sets of coupled hyperbolic equations. A lumped-mass cable model was also developed. Major assumptions made in the development of the cable dynamics model are that the cable is homogeneous and perfectly flexible and that hysteresis damping is negligible compared with viscous damping. The equations of motion for the buoy and cable were programmed and solved numerically on a UNIVAC 1108 digital computer in the time domain. Two types of buoy hulls were considered — a spherical buoy and a torroidal buoy. Both shallow water and deep water moorings were simulated using the lumped-mass and finite-difference cable models. Simulated data were compared with observed data in two steady-state cases and in three dynamics cases.

## 5.2 Conclusions

Steady-state buoy system configurations were simulated using the method described in chapter III for a shallow water buoy system and for a deep water buoy system. Comparison of simulated to observed configuration parameters (current meter tilt angles for the shallow water mooring and mean tensions for the deep water mooring) indicate good agreement between the computer model configurations and the configurations of the actual buoy systems. Although this comparison of a few bits of data from two buoy systems does not constitute a full validation of the steady-state buoy system configuration model (angles and tensions all along the mooring line for many current profiles and winds and for

many different buoy systems should be simulated and correlated for a full validation), it does indicate that the simulation errors are on the order of 5 percent, which is adequate for engineering analysis.

Buoy system dynamics were simulated for three cases (two shallow water moorings where the lumped-mass cable model was used and one deep water mooring where the finite-difference cable model was used), and simulated buoy motion parameters were compared with observed parameters. In general, the lumped-mass cable model is more adaptable to shallow water buoy systems, which, if slack-moored, tend to have very low tensions at the bottom and cable angles that approach  $\pi/2$  and, if taut-moored, tend to have very high dynamic strain levels, which can cause slack cable. The lumped-mass cable model can handle these cases easily (if tensions on an element go to zero, the element simply free falls through the water), whereas the finite-difference cable model breaks down with slack cable conditions since the equations of motion are ultrahyperbolic and possess an infinite number of equally valid solutions. Also, the lumped-mass model is more adaptable when the mooring line contains a number of mass or force discontinuities, i.e., instruments, subsurface buoys, sentinels, etc.

The comparison for both shallow water cases, one a spherical buoy and the other a Richardson torroid, indicate that the surge and sway hydrodynamic forces were underestimated in the simulation. Also, the comparison of observed to simulated shallow water torroidal buoy motion spectral levels indicates that the simulation is underdamped in all modes. There is good agreement in simulated and observed heave motions, the most important motion parameter

for the buoy system designer. In general, the simulation appears to predict heave motions within  $\pm 15$  percent and the other motions within  $\pm 50$  percent. Since the environmental conditions were not monitored at either buoy during the motion measurements but were inferred from wind speeds measured ashore, from computed tidal currents based upon previous current measurements, and from visual observations of sea conditions, it is impossible to draw conclusions on the validity of the model, except that it computes buoy system motions that are order of magnitude with observed motions.

The comparison of simulated deep sea buoy system dynamics using the finite-difference model is inconclusive because of uncertainties in monitoring the environment and in the statistical meaning of the tension data collected.

## 5.2 Suggestions for Further Study

Future research in the area of buoy system dynamics should involve the emplacement and the fitting of motion sensing instrumentation to a wide spectrum of oceanic buoy system types — both shallow and deep water. The environment at each site should be adequately monitored (winds, waves, and currents), and a complete set of buoy system motions should be recorded. The measurements should include angles and tensions along the mooring line as well.

Another key area that should be investigated involves the hydrodynamic forces acting on a body on the free surface of a fluid when the free surface is subjected to random gravity waves. John's analysis assumed infinitesimal body motions in order to linearize the free surface boundary conditions. Kim's analysis assumed sinusoidal body motions in order to evaluate the hydrodynamic force and moment integrals. An investigation of the validity of these assumptions



should be made in order to better understand the nature of the body-fluid interaction. Also, test tank data are needed to validate theoretical force and moment coefficients.

Extension of the analysis presented in this dissertation to nonaxisymmetric buoy hulls to include cross-coupled hydrodynamic forces and moments in the other modes would be of significance as a more general study of buoy system dynamics.

Finally, more research on the behavior of wire ropes and synthetic lines that are used in the ocean environment is needed for the prediction of buoy system performance.

## REFERENCES

1. J. D. Isaacs et al., Development and Testing of Taut-Nylon Moored Instrument Stations, Scripps Institution of Oceanography, Report 65-5, San Diego, Calif., 15 April 1965. 86 pp.
2. W. S. Richardson et al., "Current Measurements from Moored Buoys," Deep Sea Research, Vol. 10, No. 4, October 1963, pp. 369-388.
3. G. H. Volkman, Mooring Summary 1967, Woods Hole Oceanographic Institution, Report 68-80, Woods Hole, Mass., 1968, 69 pp.
4. G. I. Volkman, Mooring Summary 1968, Woods Hole Oceanographic Institution, Report 69-35, Woods Hole, Mass. 1968, 70 pp.
5. J. E. Smith, Structures in Deep Ocean Engineering — Manual for Underwater Construction, U. S. Naval Civil Engineering Laboratory Report 284-7, Port Hueneme, Cal., October 1965, Ch. 7.
6. F. Webster, "Some Perils of Measurement from Moored Ocean Buoys," Transcript of the 1964 Buoy Technology Symposium, Marine Technology Society, Washington, D. C., 25 March 1964, pp. 33-48.
7. F. Webster, "A scheme for Sampling Deep-Sea Currents from Moored Buoys," Transcript of the Second International Buoy Technology Symposium, Marine Technology Society, Washington, D. C., 20 September 1967, pp. 419-431.
8. S. O. Marcus, "Evaluation of NOMAD-II Data in Their Meteorological and Oceanographic Applications," Transcript of the Second International Buoy Technology Symposium, Marine Technology Society, Washington, D. C., 20 September 1967, pp. 395-408.
9. L. C. Huff, "Evaluation of the NOMAD Wind Measurement Subsystem," Transcript of the Second International Buoy Technology Symposium, Marine Technology Society, Washington, D. C., 20 September 1967, pp. 395-408.
10. G. C. Day, "Wind Measurements from Moored Buoys," Woods Hole Oceanographic Institution Reference No. 70-19, Woods Hole, Mass., May 1970.

11. B. W. Wilson, Characteristics of Anchor Cables in Uniform Ocean Currents, Texas A & M Report TR No. 204-1, Texas A & M University, College Station, Texas, April 1960.
12. B. W. Wilson, Characteristics of Deep-Sea Anchor Cables in Strong Ocean Currents, Texas A & M Report 204-3, Texas A & M University, College Station, Texas, 3 February 1961.
13. K. T. Patton, "On the Equilibrium Configuration of Moored Surface Buoys in Currents," U. S. Navy Underwater Sound Laboratory Technical Memorandum No. 2212-212-68, U. S. Navy Underwater Sound Laboratory, New London, Conn., 25 October 1968.
14. W. D. Martin, "Tension and Geometry of Single Point Moored Surface Buoy System." M. S. Thesis, Dept. of Naval Architecture and Marine Engineering, Massachusetts Institute of Technology, Cambridge, Mass., 8 November 1968.
15. L. Euler, Scientia Navalis, 1749.
16. The Papers of William Froude, ed. by A. D. Duckworth, The Institution of Naval Architects, London, 1955, 359 pp.
17. A. Kriloff, "A General Theory of the Oscillations of a Ship on Waves," Transactions of the Institution of Naval Architects, Vol. 40, 1898, pp. 135-212.
18. F. M. Lewis, "The Inertia of Water Surrounding a Vibrating Ship," Transactions of the Society of Naval Architects and Marine Engineers, Vol. 37, 1929, pp. 1-20.
19. M. D. Haskind, "Oscillation of a Ship on a Calm Sea," Izvestia Akademii Nauk, S.S.S.R., Otdelenie Technicheskikh Nauk, No. 1, 1946. 23-24, English Translation: Technical and Research Bulletin No. 1-12, The Society of Naval Architects and Marine Engineering 1953.
20. M. D. Haskind and I. S. Riman, "A Method of Determining the Pitching and Heaving Characteristics of Ships," Izvestia Akademii Nauk, S.S.S.R., Otdelenie Technicheskikh Nauk, No. 10 (1946) 1373-1383, English Translation: David Taylor Model Basin, Translation No. 253, 1955.
21. M. D. Haskind, "The Exciting Forces and Wetting of Ships." Izvestia Akademii Nauk, S.S.S.R., Otdelenie Technicheskikh Nauk, No. 7, 1957. pp. 65-79, English Translation: David Taylor Model Basin Translation No. 307, March 1962.

22. F. John, "On the Motion of Floating Bodies, I," Communications on Pure and Applied Mathematics, Vol. 2, 1949.
23. F. John, "On the Motion of Floating Bodies. II, Simple Harmonic Motions," Communications on Pure and Applied Mathematics, Vol. 3, 1950, pp. 45-101.
24. M. St. Denis and W. J. Pierson, "On the Motions of Ships in Confused Seas," Transactions of the Society of Naval Architects and Marine Engineers, Vol. 61, (1953) pp. 280-332.
25. B. V. Korvin-Kroukovsky, "Investigation of Ships Motions in Regular Waves," Transactions of the Society of Naval Architects and Marine Engineers, Vol. 65, 1957.
26. B. V. Korvin-Kroukovsky, "Pitching and Heaving Motions of a Ship in Regular Waves," Transactions of the Society of Naval Architects and Marine Engineers, Vol. 65, 1957.
27. B. V. Korvin-Kroukovsky, "Theory of Seakeeping," The Society of Naval Architects and Marine Engineers, 1961, New York.
28. J. K. Lunde and S. W. Doroff, Proceedings of the Fifth Symposium on Naval Hydrodynamics - Ship Motion, Drag Reduction, Office of Naval Research Publication ACR-112, Dept. of the Navy, Washington, D. C., September, 1964, 1154 pp.
29. R. F. Devereux, Development of an Ocean Data Telemetering Buoy, General Dynamics/Convair Division Report GD/C-65-018, San Diego, Calif., May 1965, 255 pp.
30. R. F. Devereux, et al., Some Observations from a Prototype Ocean Data Station Buoy in Hurricane Betsy 6-8 Sept., 1965, General Dynamics/Convair Division Report GDIC-65-203, San Diego, Calif., 1 October 1965, 57 pp.
31. S. T. Uyeda, et al., "Two Experimental Moorings of a Large Oceanographic Buoy in 13,000 feet of Water Near Bermuda," Transactions of the Second International Buoy Technology Symposium, Marine Technology Society, Washington, D.C., 20 September 1967, pp. 85-104.
32. R. D. Gaul and N. L. Brown, "A Comparison of Wave Measurements from a Free-Floating Wave Meter and the Monster Buoy," Transactions of the Second International Buoy Technology Symposium, Marine Technology Society, Washington, D.C., 20 September 1967, pp. 473-494.

33. R. G. Paquette, et al., The Dynamics of Simple Deep-Sea Buoy Moorings, General Motors Defense Research Corp., Report No. TR-65-79, Santa Barbara, Calif., November 1965, 167 pp.
34. L. E. Bivens and B. R. Swann, "Moored Buoy Performance Measurement," Transactions of the Second International Buoy Technology Symposium, Marine Technology, Washington, D.C., 20 September 1967, pp. 245-267.
35. P. Rudnick, "Motion of a Large Spar Buoy in Sea Waves," Journal of Ship Research, Vol. 11, No. 4, December 1967, pp. 257-260.
36. R. Blumberg and C. D. Osborn, "Computer Aided Design of Submerged Ocean Buoy Systems," Proceedings of the 1969 Offshore Technology Conference, Houston, Texas, 18 May 1969, Paper No. OTC-1133, pp. 497-504.
37. R. C. Millard, Jr., "Observations of Static and Dynamic Tension Variations from Surface Moorings," Woods Hole Oceanographic Institution Reference No. 69-29, Woods Hole, Mass., May 1969, 23 pp.
38. J. H. Nath, Dynamics of Single Point Ocean Moorings of a Buoy — A Numerical Model for Solution by Computer, Oregon State University, Department of Oceanography Report No. 69-10, Corvallis, Oregon, July 1969, 109 pp.
39. F. H. Hsu and K. A. Blenkarn, "Analysis of Peak Mooring Force Caused by Slow Vessel Drift Oscillation in Random Seas," Proceedings of the 1970 Offshore Technology Conference, Houston, Texas, Paper No. OTC 1159, 22 April 1970, pp. 135-147.
40. B. G. Burke, "The Analysis of Drilling Vessel Motions in a Random Sea," Proceedings of the 1970 Offshore Technology Conference, Houston, Texas, Paper No. OTC 1219, 22 April 1970, pp. 701-716.
41. The Collected Papers of Sir Thomas Havelock on Hydrodynamics, ed. by C. Wigley, Office of Naval Research, Dept. of the Navy Report ONR/ACR-103, Washington, D.C. 11 March 1963, pp. 627.
42. W. D. Kim, "Oscillations of a Rigid Body on a Free Surface," Journal of Fluid Mechanics, Vol. 21, 1965, pp. 427-451.
43. R. Barakat, "Vertical Motion of a Floating Sphere in a Sine-Wave Sea," Journal of Fluid Mechanics, Vol. 13, 1962, pp. 540-569.
44. G. Birkhoff, Hydrodynamics, Princeton University Press, Princeton, N. J. 1960.

45. H. Lamb, Hydrodynamics, 6th ed., Dover Publications, New York, 1932, 738 pp.
46. M. Martin, "Roll Damping Due to Bilge Keels," PhD dissertation, State University of Iowa, Iowa City, Iowa, 1959.
47. H. Schlichting, Boundary Layer Theory, 4th ed., McGraw-Hill Book Co., Inc., New York, 1960, 644 pp.
48. S. F. Hoerner, Fluid Dynamic Drag, published by author, Midland Park, N. J., 1958.
49. J. F. Dalzell, Cross-Spectral Analysis of Ship Model Motions: A Destroyer Model in Irregular Long-Crested Head Seas, Stevens Institute of Technology — Davidson Laboratory Report No. 810, 1962.
50. J. F. Dalzell, Some Further Experiments on the Application of Linear Superposition Techniques to the Responses of a Destroyer Model in Extreme Long-Crested Head Seas, Stevens Institute of Technology — Davidson Laboratory Report No. 918, 1962.
51. J. Gerritsma, Ship Motions in Longitudinal Waves, International Ship Building Progress, No. 7, 1960, pp. 49-76.
52. C. L. Bretschneider, "Wave Variability and Wave Spectra for Wind-Generated Gravity Waves," Technical Memorandum No. 118, Beach Erosion Board, U. S. Army Corps of Engineers, 1959.
53. H. U. Sverdrup and W. H. Munk, Wind Sea and Swell: Theory of Relations for Forecasting, Hydrographic Office, Pub. No. 601, U. S. Department of the Navy, 1947.
54. K. T. Patton, "Prediction of Wind Waves in Block Island Sound," U. S. Navy Underwater Sound Laboratory Technical Memorandum No. 2212-78-69, 8 April 1969.
55. R. L. Weigel, Some Engineering Aspects of Wave Spectra: Ocean Wave Spectra-Proceedings of a Conference, Prentice-Hall, Inc., Englewood Cliffs, N. J., 1963.
56. M. S. Longuet-Higgins, "On the Statistical Distribution of the Heights of Sea Waves," Journal of Marine Research, Vol. 11, No. 3, 1952, pp. 345-366.
57. W. J. Pierson and L. Moskowitz, "A Proposed Spectral Form for Fully Developed Wind Seas Based on the Similarity Theory of S. A. Kitaigorodskii," Journal of Geophysical Research, Vol. 69, No. 24, 1964, pp. 5181-5190.

58. C. F. Kottler, Jr., "A Wind Wave Co-Cumulative Spectral Model," Journal of Ship Research, Vol. 14, No. 4, December 1970, pp. 277-296.
59. L. E. Borgman, Ocean Wave Simulation for Engineering Design, Hydraulic Engineering Laboratory — University of California Technical Report HEL-9-13, October 1967, 44 pp.
60. N. Cristecu, "Rapid Motions of Extensible Strings," Journal of Mechanics of Physics and Solids, 1964, Vol. 12, pp. 269-273.
61. J. W. Schram, "A Three-Dimensional Analysis of a Towed System," PhD. dissertation, Rutgers — The State University, New Brunswick, N. J., 1968.
62. L. F. Whicker, "The Oscillatory Motion of Cable Towed Bodies," PhD. dissertation, University of California, 1957.
63. R. B. Lindsay, Mechanical Radiation, McGraw-Hill Book Company, Inc., New York, 1960, 415 pp.
64. A. Jeffrey and T. Taniuti, Non-Linear Wave Propagation, Academic Press, New York, 1964, 369 pp.
65. D. R. Hartree, Numerical Analysis, 2nd ed., Oxford University Press, London, 1958.
66. W. F. Ames, Nonlinear Partial Differential Equations in Engineering, Academic Press, New York, 1965, 512 pp.
67. Nonlinear Partial Differential Equations — A Symposium on Methods of Solution, ed. by W. F. Ames, Academic Press, New York, 1967, 316 pp.
68. D. Greenspan, Introduction to Partial Differential Equations, McGraw-Hill Book Company, Inc., New York, 1961, 195 pp.
69. L. Fox, Numerical Solution of Ordinary and Partial Differential Equations, Pergamon Press, Oxford, G. B., 1962, 509 pp.
70. G. F. D. Duff and D. Naylor, Differential Equations of Applied Mathematics, John Wiley & Sons, Inc., New York, 1966, 423 pp.
71. M. Casarella and M. Parsons, "Cable Systems Under Hydrodynamic Loading," Marine Technology Society Journal, Vol. 4, No. 4, July-August 1970.

72. A. B. Basset, A Treatise on Hydrodynamics, 2 vols., Dover Publications, Inc., New York, 1961 (first published 1888).
73. R. R. Miller, The Effects of Frequency and Amplitude of Oscillation on the Hydrodynamic Mass of Irregular Shaped Bodies, " M. S. Thesis, University of Rhode Island, Kingston, R. I., 1965.
74. R. R. Miller and W. M. Hagist, Experimental Determination of the Hydrodynamic Mass, University of Rhode Island, Division of Engineering Research and Development Report to U. S. Navy Underwater Sound Laboratory, Kingston, R. I., 1965.
75. "Instruction Bulletin — Type 316 Histogram Current Meter," Braincon Corp., Marion, Mass. April 1965.
76. R. L. Sunblad. "The Histogram Current Meter," Instrument Society of America, Conference Preprint, date unknown.
77. R. G. Williams, Physical Oceanography of Block Island Sound, U. S. Navy Underwater Sound Laboratory Report No. 966, New London, Conn., 1 July 1969.
78. A. J. Nalwalk et al., Final Report of Oceanographic Measurements Along the Block Island-Fishers Island (BIFI) Range in Block Island Sound from January 1969 through June 1970., University of Connecticut—Marine Research Laboratory Report to Navy Underwater Sound Laboratory, Noank, Conn., December 1970.
79. H. O. Berteaux and R. G. Walden, Analysis and Experimental Evaluation of Single Point Moored Buoy Systems, Woods Hole Oceanographic Institution Report No. 69-36, Woods Hole, Mass., May 1969.
80. F. Webster, "Vertical Profiles of Horizontal Ocean Currents," Deep Sea Research, Vol. 16, No. 1, 1969, pp 85-98.
81. Patton, K. T., "Buoy Motions in Block Island Sound — Preliminary Data," NUSC Technical Memorandum No. 2212-29-71, Naval Underwater Systems Center, New London Laboratory, New London, Conn., March 1971, 87 pp.
82. A. Vine and C. H. Volkman, "Nomogram for Wind Waves at Sea," Undersea Technology, Vol. 5, No. 5, May 1964, p. 37.
83. "1970 Tidal Current Tables — Atlantic Coast of North America," U. S. Dept. of Commerce, Environmental Science Services Administration, Coast and Geodetic Survey, Rockville, Md., 1959.



84. J. S. Bendat and A. G. Piersol, Measurement and Analysis of Random Data, John Wiley & Sons, Inc., New York, 1966.
85. J. F. Ferrie and A. H. Nuttall, "Availability of Fisher's FFT Algorithm," NUSC Technical Memorandum No. 2070-21-71, Naval Underwater Systems Center, New London Laboratory, New London, Conn., January 1971, 11 pp.
86. A. H. Nuttall, Spectral Estimation by Means of Overlapped Fast Fourier Transform Processing of Windowed Data, NUSC Report No. 4169, Naval Underwater Systems Center, New London Laboratory, New London, Conn., October 1971, 40 pp.
87. R. G. Williams, "Estimating Ocean Wind Wave Spectra by Means of Underwater Sound," PhD. dissertation, New York University — Dept. of Meteorology and Oceanography, New York, 1971, 186 pp.

## Appendix A

### ANGULAR STABILITY OF AXISYMMETRIC BUOYS

It is known from visual observation and from collected motion data that buoys do not become unstable in the sense of Liapunov; i.e., buoy motions will not build to infinity. However, buoys will undergo large excursions and can be upset. For example, a buoy that undergoes gross heaving motions in the sea so that it is alternately awash and then rises out of water to fall over on its side would be deemed unstable by the casual observer; however, the buoy would actually be stable since its motions are bounded and do not tend to infinity with time. Of course, if this buoy housed meteorologic or oceanographic instrumentation, it would be of little value because of its wild motions.

The "stability" of this type of motion is best described in the pitch (or roll) phase plane, i.e., a plot of pitch angular velocity versus pitch. However, pitching (and rolling) motions are heavily influenced by the draft of the buoy, i.e., the location of the center of buoyancy relative to the center of gravity. Thus, the heave motions and resulting buoy draft must be considered. Because the righting moment depends on the location of the center of buoyancy relative to the center of gravity, the pitch (or roll) equations of motion are similar to the nonlinear equations of motion for a pendulum.

A wide spectrum of axisymmetric buoy shapes will be considered, ranging from a spar buoy with a high draft-to-beam ratio to a discus buoy with a low

draft-to-beam ratio (figure A-1). First, consider the spar buoy. In the absence of external forces (mooring line tensions, etc.), static stability is maintained only if the center of gravity is below the center of buoyancy:

$$L_{CG} < H/2 .$$

This is obvious from the undamped pitch equation of motion for the spar buoy:

$$I_B \ddot{\beta} + \rho g \frac{\pi}{4} B^2 H \left( \frac{H}{2} - L_{CG} \right) \sin \beta = 0 .$$

Also, if the buoy is tilted at extreme angles, we see that

$$\beta > \pi \quad \text{or} \quad \beta < -\pi .$$

The spar buoy will not return to its initial equilibrium position but will undergo a complete revolution and seek equilibrium at either  $2\pi$  or  $-2\pi$ . A typical pitch phase plane for the spar buoy is shown on figure A-2 for two possible conditions:

$$1. L_{CG} < H/2$$

$$2. L_{CG} > H/2 .$$

Note that if the buoy is initially unstable,  $L_{CG} > H/2$ , it is stable at  $\pm \pi$ ; i.e., it is stable upside down.

A cable attached to the bottom of the spar buoy will tend to stabilize the buoy. Adding a restoring moment due to the cable tension in the equation of motion yields

$$I_B \ddot{\beta} + \rho g \frac{\pi}{4} B^2 H \left( H/2 - L_{CG} \right) \sin \beta + K L_{CG} (1 - \cos \beta) L_{CG} \sin \beta = 0 ,$$

where  $K$  is a cable spring constant. For a stable system, the sum of the two restoring moment terms must be positive. Solving for  $L_{CG}$ , we see that

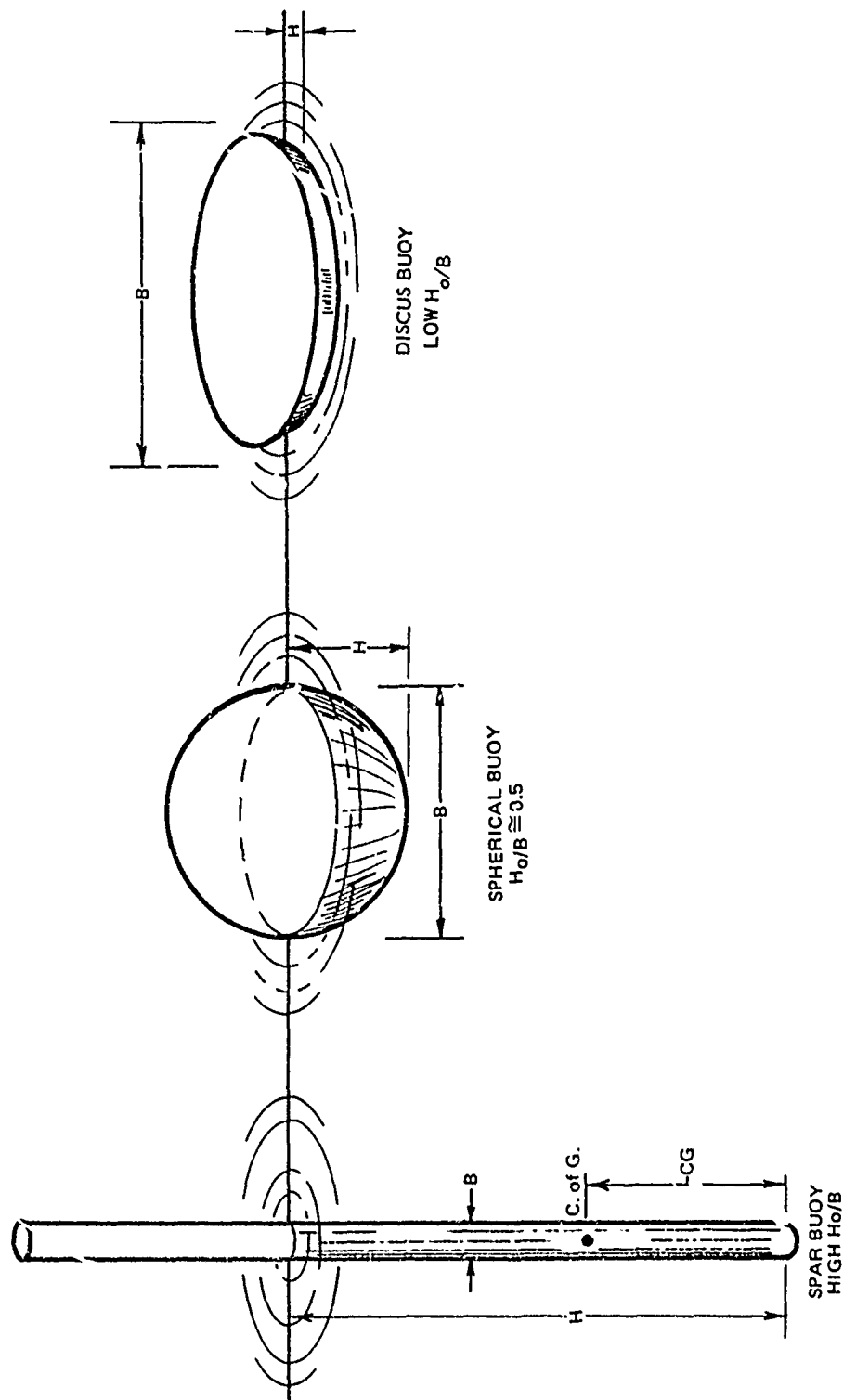


Figure A-1. Axisymmetric Buoy Shapes

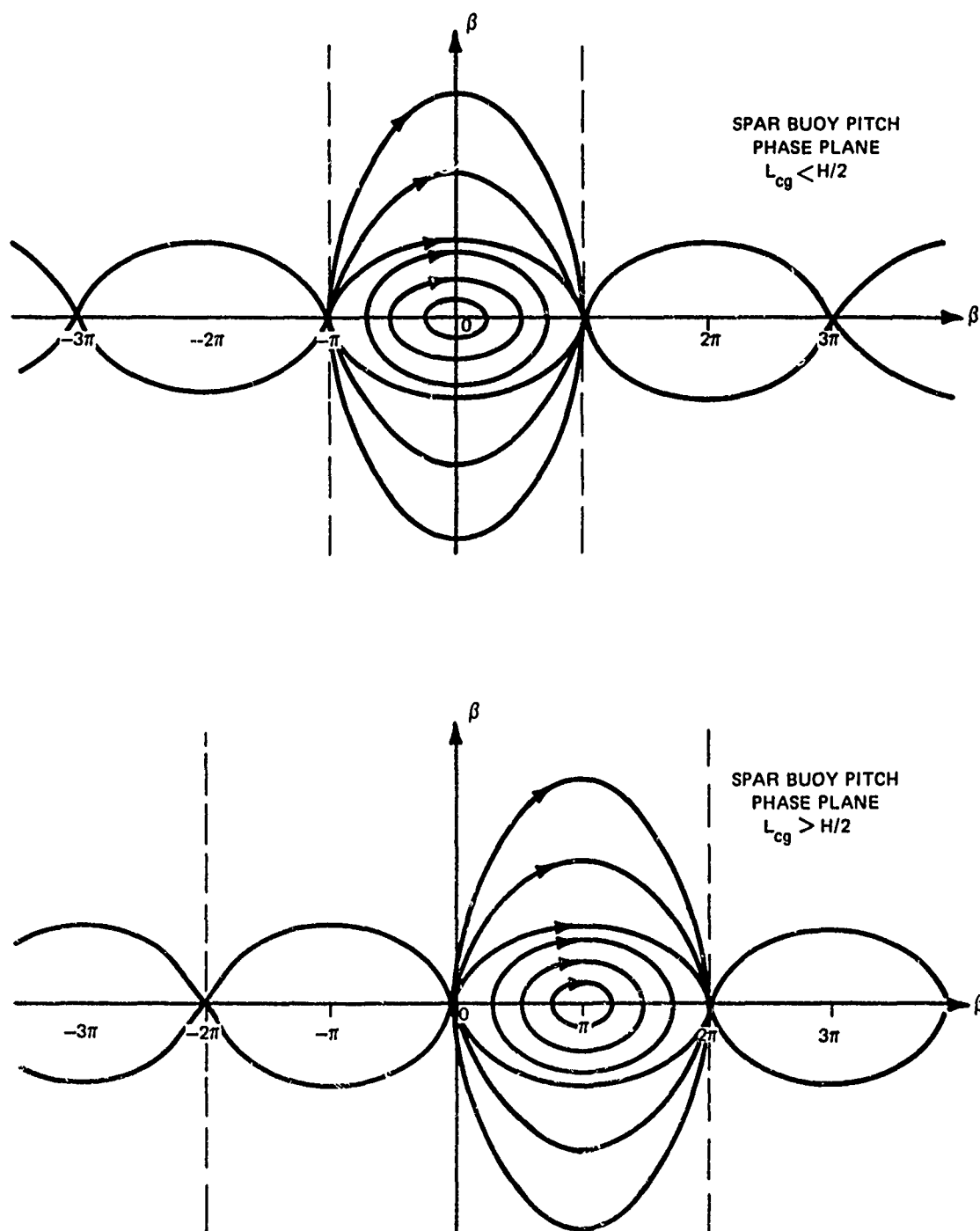


Figure A-2. Spar Buoy Phase Planes

$$L_{CG} = \frac{C}{2} + \frac{1}{2} \sqrt{C} \cdot \sqrt{C-2H} ,$$

where

$$C = \frac{\rho g \pi B^2 H}{4K(1-\cos\beta)} .$$

In general, a spar buoy is designed to minimize heave response. Thus, the shallowest buoy draft would be the static draft of the buoy minus one-half the largest wave height:

$$H_{MIN} = H_0 - \frac{1}{2} \eta_{MAX} .$$

For a stable buoy, we see that

$$L_{CG} < \frac{H_{MIN}}{2} = \frac{H_0 - \frac{1}{2} \eta_{MAX}}{2} .$$

The spherical buoy shape is subject to the same types of moments, but the study is complicated by the fact that the center of buoyancy will deviate from the vertical axis of the buoy as the buoy pitches. If the center of gravity lies below the center of buoyancy ( $5/8 H$  from the bottom), the buoy is positively stable and will have a phase plane representation similar to that shown in figure A-2 for the spar buoy. The upper phase plane applies if  $L_{CG} < 5/8 H$ , and the lower phase plane applies if  $L_{CG} > H$ . However, the buoy is neutrally stable if  $5/8 H < L_{CG} < H$ , since the center of buoyancy is always directly below the center of gravity. In this situation there is no definite stable position, because there is no restoring moment. Again, the tension of a mooring line attached below the center of buoyancy will stabilize the buoy.

Any buoy with a draft-to-beam ratio less than 0.5 and a hull height-to-beam ratio less than 1 can be bistable; i.e., it can be stable right side up or

upside down. Torroid and discus buoys are of this class. If the center of gravity is located far below the buoy hull (achieved by means of ballast weights on a boom or tripod), the phase plane is similar to the upper curve for the spar buoy. If the center of gravity is far above the buoy hull (due to heavy instruments or equipment), the lower curve for the spar buoy phase plane would apply — the buoy is stable when upside down. If the center of gravity is near the geometric center of the buoy hull, the buoy is equally stable right side up or upside down. The phase plane for this situation is shown on figure A-3. Inspection of figure A-3 indicates that the width of the stable (in the sense that the buoy is right-side-up) region in the phase plane can vary from  $2\pi$  to 0 depending on the vertical location of the center of gravity.

This simple discussion of buoy stability did not consider other modes of possible unstable motion since they have never been observed to offer serious problems. Cross-coupled moments due to the hydrodynamic forces acting on the buoy and the horizontal tension components were neglected in this discussion. Even with these restrictions, a few design guides are apparent. The buoy should be designed with the center of gravity below the center of buoyancy if at all possible. Also, the mooring line attachment point should be as low as possible to offer the greatest righting moment if the buoy does capsize.

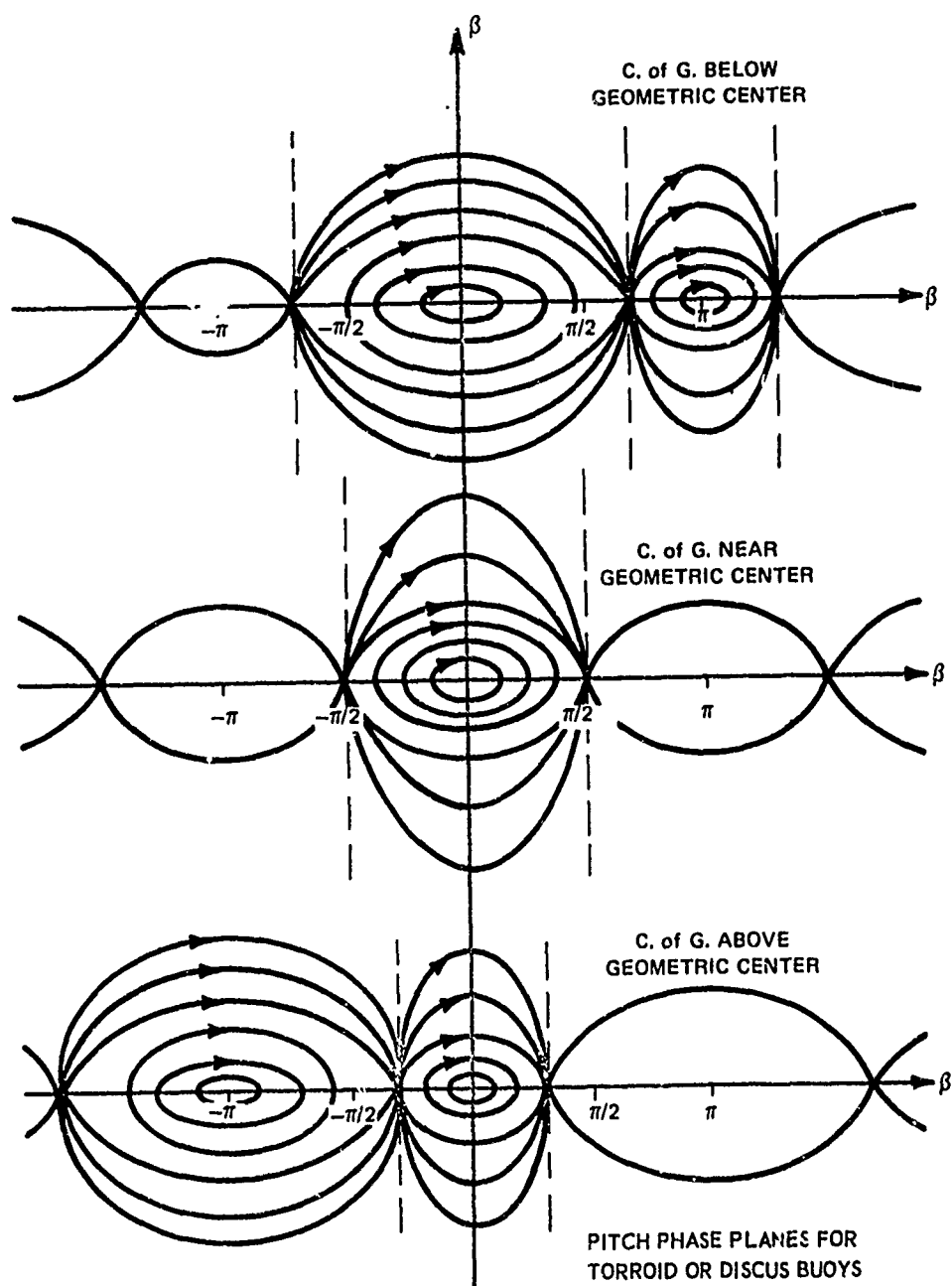


Figure A-3. Torroid or Discus Buoy Phase Planes





## Appendix B

### COMPUTER PROGRAMS FOR THE MODELS

#### Steady-State Buoy System Configurations

This program computes the three-dimensional spatial configuration, tensions, and strains of either an elastic or inelastic buoy system mooring line. Winds from any compass direction can act on the buoy, and currents that vary in strength and direction as a function of depth can act on the buoy and mooring line. The mooring line can be composed of segments having different properties (weight in water, mass, drag, elasticity, etc.). Point mass discontinuities (to simulate current meters, hydrophones, etc.) can also be accounted for.

The basic cable equations (equations (230) to (233)) and a discussion of the development of this program are included in chapter III of the main text. The logic employed in this program is shown in figure B-1, which generally illustrates the computational operations.

The input data are as follows:

1. Buoy major diameter (ft)
2. Buoy minor diameter (ft)
  - a. Vertical diameter for an oblate spheroid
  - b. Hole diameter for a torroid

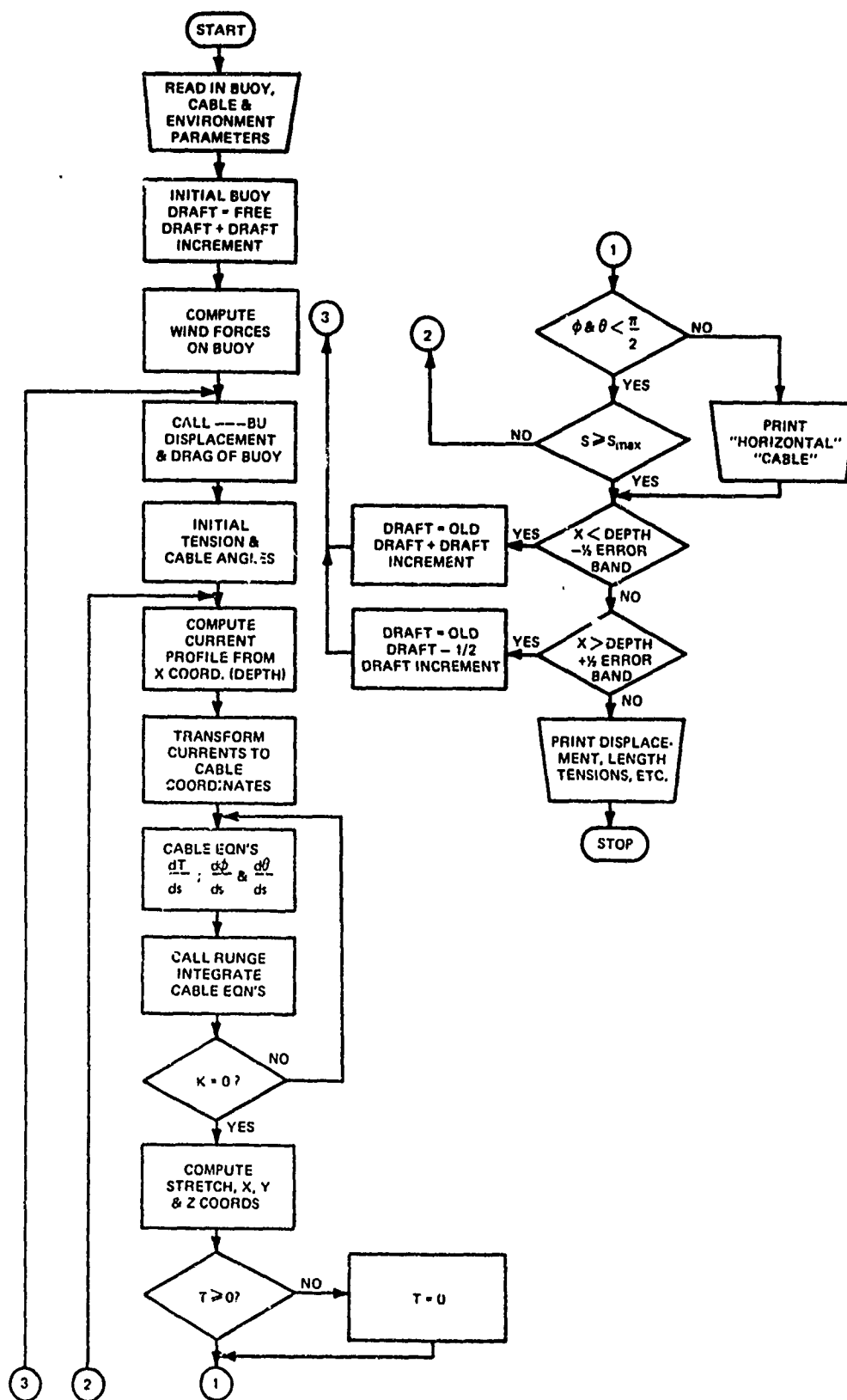


Figure B-1. Steady-State Buoy System Configuration Flow Chart

- c. 0 for a cylinder
- d. 0 for a sphere
- 3. Buoy weight (lb)
- 4. Maximum draft of hull (ft)
- 5. Free draft with no mooring line (ft)
- 6. Buoy windage ( $\text{ft}^2$ )
- 7. Wind drag coefficient
- 8. Cable diameter (in.)
- 9. Cable weight in water per unit length (lb/ft)
- 10. Effective cable modulus of elasticity ( $\text{lb/in.}^2$ )
- 11. Unstretched cable length (ft)
- 12. Surface current (knots)
- 13. Water depth (ft)
- 14. Wind speed component in y direction (ft/sec)
- 15. Wind speed components in z direction (ft/sec).

The integration step size "B" is normally set at 1/100th of the total cable length. However, if the cable properties are changed from a lightweight line to a very heavy line (for example, anchor chain), the step size should be changed in inverse proportion to the in-water weights. Also, the normal and tangential drag coefficients ("DRGON" and "DRGCT") should be changed accordingly if the mooring line section is not circular, for example, hair-faired cable and chain. Occasionally, the solution will not converge into the depth error band. This occurs if the first draft increment is too large and the computed x dimension of the mooring line "overshoots" the depth. With each overshoot, the buoy draft

3

increment is halved; thus, convergence may be very slow. The initial buoy draft increment should be halved if this occurs.

PATTON

DATE 060372 PAGE 3

BI FOR S1279J5:279  
 UNIVAC 1106 FORTRAN V LEVEL 2206 0023  
 THIS COMPILATION WAS DONE ON 06 MAR 72 AT 10112156

## MAIN PROGRAM

STORAGE USED (BLOCK, NAME, LENGTH)

0001 \*CODE 000645  
 0000 \*DATA 000617  
 0002 \*BLANK 000000

## EXTERNAL REFERENCES (BLOCK, NAME)

0003 ORLBU  
 0004 RUNGE  
 0005 NROCS  
 0006 NIOCS  
 0007 SORT  
 0010 ATAN  
 0011 SIN  
 0012 COS  
 0013 NERFSS  
 0014 NERRAG  
 0015 NADUS  
 0016 NSTOPS

## STORAGE ASSIGNMENT FOR VARIABLES (BLOCK, TYPE, RELATIVE LOCATION, NAME)

0001 000453 10L 0000 00047 100F 0000 000551 101F 0000 000553 102F 0000 000455 104F  
 0000 00057 106F 0000 000475 12L 0001 000476 12L 0001 000522 2710  
 0001 000275 3L 0001 000355 4L 0001 000116 7L 0001 000440 9L  
 0000 R 000503 B 0000 R 000462 B01 0000 R 000443 B02 0000 R 000512 C 0000 R 000540 CRENT  
 0000 R 000575 CUR 0000 R 000535 CWXC 0000 R 000536 CHYC 0000 R 000537 CHZC 0000 R 000540 D  
 0000 R 000511 DC 0000 R 000515 ODP 0000 R 000516 DM 0000 R 000571 DIA 0000 R 000543 DS  
 0000 R 000521 DISP 0000 R 000522 DRB 0000 R 000542 DRCN 0000 R 000541 DRECT 0000 R 000543 DS  
 0000 R 000544 DX 0000 R 000545 DY 0000 R 000546 DZ 0000 R 000510 E 0000 R 000473 EC 0000 I 000504 K  
 0000 R 000517 H 0000 R 000545 HFREE 0000 I 000505 M 0000 R 000152 PRL 0000 R 000503 K  
 0000 I 000520 L 0000 R 000505 S 0000 R 000474 SM 0000 R 000527 STR 0000 R 000506 TEN  
 0000 R 000502 RHO 0000 R 000532 UC 0000 R 000530 V 0000 R 000533 VC 0000 R 000501 VIS  
 0000 R 000531 W 0000 R 000447 WAREA 0000 R 000444 WB 0000 R 000474 WC 0000 R 000470 WCD  
 0000 R 000513 WFY 0000 R 000516 WFX 0000 R 000477 WINDY 0000 R 000470 WINDZ 0000 R 000472 WTC  
 0000 R 000523 X 0000 R 000524 Y 0000 R 000525 Z

00100 1\* C  
 00100 2\* C  
 00100 3\* C  
 00100 4\* C  
 00100 5\* C

DATE 060372 PAGE 8

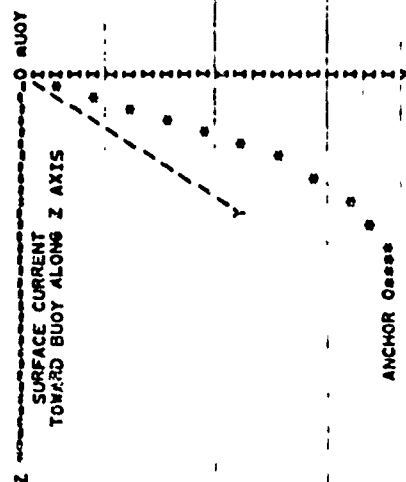
PATTON

00100	6*	C
00100	7*	C
00100	8*	C
00100	9*	C
00100	10*	C
00100	11*	C
00100	12*	C
00100	13*	C
00100	14*	C
00100	15*	C
00100	16*	C
00100	17*	C
00100	18*	C
00100	19*	C
00100	20*	C
00100	21*	C
00100	22*	C
00100	23*	C
00100	24*	C
00100	25*	C
00100	26*	C
00100	27*	C
00100	28*	C
00100	29*	C
00100	30*	C
00100	31*	C
00100	32*	C
00100	33*	C
00100	34*	C
00100	35*	C
00100	36*	C
00100	37*	C
00100	38*	C
00100	39*	C
00100	40*	C
00100	41*	C
00100	42*	C
00100	43*	C
00100	44*	C
00100	45*	C
00100	46*	C
00100	47*	C
00100	48*	C
00100	49*	C
00100	50*	C
00101	51*	C
00103	52*	C
00103	53*	C
00103	54*	C
00103	55*	C
00104	56*	C
00104	57*	C
00104	58*	C
00104	59*	C
00104	60*	C
00104	61*	C
00104	62*	C
00104	63*	C

THIS PROGRAM COMPUTES STEADY STATE BUOY SYSTEM CONFIGURATIONS.  
THE DRAFT OF THE BUOY CONTROLS THE BUOY'S DISPLACEMENT AND  
DRAG WHICH DETERMINE THE UPPER BOUNDARY CONDITIONS ON THE CABLE.  
THE CABLE CONFIGURATION IS COMPUTED AND ITS VERTICAL PROJECTION  
IS TESTED AGAINST THE WATER DEPTH - IF SHALLOW, THE BUOY DRAFT  
IS INCREASED - IF TOO DEEP, THE BUOY DRAFT IS DECREASED.

UNITS ARE IN FEET, POUNDS, SECONDS

COORDINATE SYSTEM



BEGIN ITERATION AT THE FREE FLOATING DRAFT OF THE BUOY. I.E. - AS  
IF THERE WERE NO MOORING CABLE.  
DIMENSION D(3), R(3)  
DIMENSION TEN(100), PHI(100), THE(100)  
READ IN THE BUOY PARAMETERS - MAJOR DIAMETER, MINOR DIAMETER,  
WEIGHT, MAXIMUM HULL DRAFT, ANCHOR DRAFT  
READ 100, B01, B02, B03, B04, B05, B06, B07, B08, B09, B10, B11, B12, B13, B14, B15, B16, B17, B18, B19, B20, B21, B22, B23, B24, B25, B26, B27, B28, B29, B30, B31, B32, B33, B34, B35, B36, B37, B38, B39, B40, B41, B42, B43, B44, B45, B46, B47, B48, B49, B50, B51, B52, B53, B54, B55, B56, B57, B58, B59, B60, B61, B62, B63, B64, B65, B66, B67, B68, B69, B70, B71, B72, B73, B74, B75, B76, B77, B78, B79, B80, B81, B82, B83, B84, B85, B86, B87, B88, B89, B90, B91, B92, B93, B94, B95, B96, B97, B98, B99, B100  
READ IN THE BUOY WINDAGE AND WIND DRAG COEFFICIENT  
READ 102, WAREA, WCD  
READ IN THE CABLE PARAMETERS - DIAMETER(INCHES), WEIGHT PER FOOT  
IN WATER, CABLE MODULUS(LB/50. IN.), LENGTH  
READ 103, DIA, WTC, EC, SM

PATTON DATE 06/13/82 PAGE 5

```

C READ IN THE ENVIRONMENTAL PARAMETERS - SURFACE CURRENT (KTS.)
C WATER DEPTH AND WIND COMPONENTS
C READ 102, CUR, DEEP
C READ 102, WINDY, WINDZ
C THE KINEMATIC VISCOSITY AND DENSITY FOR SALT WATER AT 10 DEG. F
C VISAL, KSE=5
C RHO=1.992
C 100 FORMAT(5F10.3)
C 101 FORMAT(4F15.4)
C 102 FORMAT(2F10.3)
C 104 FORMAT(8F2.3)
C THE INTEGRATION STEP SIZE IS .01 OF THE CABLE LENGTH
C BE, E1=SH
C N=3
C M=0
C K=0
C J=1
C E1=K4, SEC
C DC=0.1A/12.0
C C=1.69*CUR
C WIND FORCES ON THE BUOY
C WY20.00344*WCD*WAREA*WINDY*ABS(WINDY)
C WZ20.00344*WCD*WAREA*WINDZ*ABS(WINDZ)
C INITIAL ERROR BAND WIDTH = 2*E1//20
C DOPDEEP/20.0
C THE INITIAL BUOY DRAFT INCREMENT
C DHEM/20.0
C HEMREE*DH
C 7 CONTINUE
C L=1
C CALL ORLBU(8D1,8D2,H,HM,RHO,C,DISP,DBB)
C X=0.0
C Y=0.0
C Z=0.0
C S=0.0
C STR=0.0
C R(1)=SQRT(((DISP-WB)*2)+((DRB*WFZ)*2)+MF*2)
C R(2)=ATAN(WFZ/SQRT(((DRB*WFZ)*2)+((DISP-WB)*2)))
C R(3)=ATAN((DRB*WFZ)/(DISP-WB))
C 5 CONTINUE
C COMPUTE THE CURRENT PROFILE - DIRECTION AND MAGNITUDE - AS A
C FUNCTION OF DEPTH, RELATIVE TO THE SURFACE CURRENT. EXPRESS AS Y
C AND Z COMPONENTS GOING IN THE NEGATIVE DIRECTIONS.
C FOR A UNIFORM CURRENT
C V=0.0
C W=0.0
C UCS=STN(R(2))*VCOS(R(2))*SIN(R(3))
C VCS=VCOS(R(2))*W*SIN(R(2))*SIN(R(3))
C WCS=VCOS(R(3))
C IF MORE THAN ONE TYPE OF CABLE IS USED IN THE MOD, CHANGE CABLE
C CHARACTERISTICS HERE. USE A LOGICAL IF AT THE PROPER LENGTH.
C REFERRED TO CHANGE THEM BACK BEFORE THE NEXT CONFIGURATION IS
C COMPUTED
C 00117 64*
C 00117 65*
C 00125 66*
C 00131 67*
C 00131 68*
C 00131 69*
C 00135 70*
C 00136 71*
C 00137 72*
C 00140 73*
C 00141 74*
C 00142 75*
C 00142 76*
C 00143 77*
C 00144 78*
C 00145 79*
C 00146 80*
C 00147 81*
C 00150 82*
C 00151 83*
C 00152 84*
C 00152 85*
C 00153 86*
C 00154 87*
C 00154 88*
C 00154 89*
C 00155 90*
C 00155 91*
C 00156 92*
C 00157 93*
C 00160 94*
C 00161 95*
C 00162 96*
C 00163 97*
C 00164 98*
C 00165 99*
C 00166 100*
C 00167 101*
C 00170 102*
C 00171 103*
C 00172 104*
C 00173 105*
C 00173 106*
C 00173 107*
C 00173 108*
C 00173 109*
C 00173 110*
C 00174 111*
C 00174 112*
C 00176 113*
C 00177 114*
C 00200 115*
C 00200 116*
C 00200 117*
C 00200 118*
C 00200 119*
C 00200 120*
C 00200 121*

```

PATTON

C IF INSTRUMENTS, SINKERS, OR OTHER CONCENTRATED FORCES ARE ACTING ON  
C THE MOORING LINE, CHANGE THE TENSIONS AND ANGLES BY USING A  
C LOGICAL IF AT THE PROPER LENGTH(S) AND THEN SOLVING FOR THE  
C STATIC FORCES ON THE FREEBODY OF THE ITEM.

CWXC=WC\*Cos(R(2))\*Cos(R(3))  
CWYC=WC\*Sin(R(2))\*Cos(R(3))  
CWZC=WC\*Sin(R(3))  
CRENTEUC=DC/VIS  
DRGCTE=6055\*(CRENTE\*-4759)  
DRGCTE1=4

3 CONTINUE

DTEN/DS  
D(1)=-CWXC+0.5\*RH0\*DRGCT\*DC\*UC\*ABS(UC)

DPHI/DS  
D(2)=-CWYC+0.5\*RH0\*DRGCT\*DC\*VC\*ABS(VC)/R(1)

D(3)=-CWZC+0.5\*RH0\*DRGCT\*DC\*WC\*ABS(WC)/R(1)\*Cos(R(2))  
CALL RUNGE(N,R,D,S,B,M,K)

DS=DS\*(1.0+1.272\*R(1)/E\*(DC\*\*2))  
DX=DS\*Cos(R(2))\*Cos(R(3))

X=X+DX

TEN(L)=R(1)

PHI(L)=R(2)

THE(L)=R(3)

L=L+1

IF(L-SN13.6,6

TEST THE X COORDINATE AGAINST THE WATER DEPTH

6 IFIX-(DEEP-DDP)/8.9,9

8 H=H+DH

J=J+1

IF(J-15)17,18,15

17 GO TO 7

9 IFIX-(DEEP+DDP)/10,11,11

11 DH=DH/2

GO TO 7

DDP=DDP/2.0

DH=DH/2

ERROR BAND HALF WIDTH MUST BE GREATER THAN THE STEP SIZE

IF(DDP-B/2.)/12.7,7

18 WRITE(6,105)

106 FORMAT(15H NO CONVERGENCE)

12 WRITE(6,107)

107 FORMAT(21H DRAFT DISPLACEMENT)

WRITE(6,102)H/DISP

X=X,0

Y=Y,0

Z=Z,0

DO 82 L=1,100

S=8\*L

DS=DS\*(1.0+1.272\*TEN(L)/E\*(DC\*\*2))

DX=DS\*Cos(PHI(L))\*Cos(THE(L))

DY=DS\*Sin(PHI(L))

DZ=DS\*Cos(PHI(L))\*Sin(THE(L))

STR=STR+DS

X=X+DX

00200 122\*  
00201 123\*  
00202 124\*  
00203 125\*  
00204 126\*  
00205 127\*  
00206 128\*  
00207 129\*  
00208 130\*  
00209 131\*  
00210 132\*  
00211 133\*  
00212 134\*  
00213 135\*  
00214 136\*  
00215 137\*  
00216 138\*  
00217 139\*  
00218 140\*  
00219 141\*  
00220 142\*  
00221 143\*  
00222 144\*  
00223 145\*  
00224 146\*  
00225 147\*  
00226 148\*  
00227 149\*  
00228 150\*  
00229 151\*  
00230 152\*  
00231 153\*  
00232 154\*  
00233 155\*  
00234 156\*  
00235 157\*  
00236 158\*  
00237 159\*  
00238 160\*  
00239 161\*  
00240 162\*  
00241 163\*  
00242 164\*  
00243 165\*  
00244 166\*  
00245 167\*  
00246 168\*  
00247 169\*  
00248 170\*  
00249 171\*  
00250 172\*  
00251 173\*  
00252 174\*  
00253 175\*  
00254 176\*  
00255 177\*  
00256 178\*  
00257 179\*



DATE 060372 PAGE 7

PATTON

00302 180\*  
 00303 181\*  
 00304 182\*  
 00305 183\*  
 00306 184\*  
 00321 185\*  
 00322 186\*

Y=Y\*0Y

Z=Z\*0Z

PHI(L)=57.4\*PHI(L)

THE(L)=57.4\*THE(L)

=2 \*RIYE(5,104)S/STR\*TEN(L)\*PHI(L)\*THE(L)\*X.Y.Z

STOP

END

END OF UNIVAC 1108 FORTRAN V COMPILATION. 0 \*DIAGNOSTIC MESSAGE(S)

**PAYTON**

DATE 060372 PAGE 8

UNIVAC 1108 FORTRAN V LEVEL 2206 0023  
THIS COMPILATION WAS DONE ON 06 MAR 72 AT 10:12:58

10:12:58.591

SUBROUTINE OGLEU  
ENTRY POINT 000126

STORAGE USED (BLOCK, NAME, LENGTH)

0001	*CODE	000142
0000	*DATA	000034
0002	*DLANK	000000

EXTERNAL REFERENCES (BLOCK, NAME)

0003	SGRT
0004	ASIN
0005	NERRYJ

 STORAGE ASSIGNMENT FOR VARIABLES (BLOCK, TYPE, RELATIVE LOCATION, NAME) |

0000 R 000000 A  
0000 000016 INJPS  
-----  
0000 R 000004 AD  
0000 R 000003 VOL  
-----  
0000 R 000001 B  
0000 R 000005 CD  
-----  
0000 R 000002 HD

00101	1*	SUBROUTINE OBLAURED1, BD2, H, RH0, C, DISP, ORB,
00101	2*	DISPLACEMENT AND ORAG FOR AN OBLATE SPHEROIDAL BODY
00103	3*	A=BD2/2,
00104	4*	B=BD1/2,
00105	5*	IF HM=0,
00106	6*	IF HM=0, A1HO=A
00110	7*	VOL=3.416*A*(B**2)*(.666*(H/A)+.333*(H/A**3)).
00111	8*	AD=1.571*(A*B*(B/A)+H*D*SQRT((A**2-H**2))+A*B*ASIN(HD/ABS(A)))
00112	9*	DISP=32.2*RH0*VOL
00113	10*	CD=.354*A/B
00114	11*	ORB=0.5*RH0*CD*AD*C*ABS(C)
00115	12*	RETURN
00116	13*	END

END OF UNIVAC 1108 FORTRAN V COMPILATION. 0 \*DIAGNOSTIC MESSAGE(S)\*

PATTON

DATE 060372 PAGE 9

10112:59.698

G1 FOR TORBU, TORBU  
UNIVAC 1108 FORTRAN V LEVEL 2206 0023  
THIS COMPILATION WAS DONE ON 06 MAR 72 AT 10112:59

SUBROUTINE TORBU ENTRY POINT 000166

STORAGE USED (BLOCK, NAME, LENGTH)

0001 \*CODE 000207  
0000 \*DATA 000033  
0002 \*BLANK 000000

EXTERNAL REFERENCES (BLOCK, NAME)

0003 SURT  
0004 ATAN  
0005 NERR35

STORAGE ASSIGNMENT FOR VARIABLES (BLOCK, TYPE, RELATIVE LOCATION, NAME)

0001 000124 3L 0001 000086 6L 0001 000130 6L 0000 000000 4R6 0000 000000 4R6 0000 000000 4R6

```

00101 1* SUBROUTINE TORBU(R,E,F,H,C,DRB,DISP)
00101 2* DISPLACEMENT AND DRAG FOR A TORROIDAL BUOY WITH CANS
00101 3* E IS TORROID DIA. (00) - F IS CAN XSECT AREA
00103 4* IF (H-R)/4,4,5
00106 5* 4 CONTINUE
00107 6* ARG5(R-H)/R
00110 7* A12(R*2)*((1.572-ATAN(ARG/SCRT(1.0-ARG)))
00110 8* 1 - (H-H)*SCRT((R*2)-((R-H)*2))
00111 9* GO TO 6
00112 10* 5 CONTINUE
00113 11* IF (H-2.0*R)/2,3,3
00116 12* 2 ARG5(R-(2.0*R-H))/R
00117 13* A123.1416*(R*2)-((R*2)*((1.572-ATAN(ARG/SCRT(1.0-ARG)))
00117 14* 1 - (H-R)*SCRT((R*2)-((R-H)*2))
00120 15* GO TO 6
00121 16* 3 A123.1416*(R*2)
00122 17* 6 CONTINUE
00123 18* B=(E-2.0*R)/2.0
00124 19* DRB=(A1+2.0*B*H)*0.5*(C*2)
00125 20* DRB=2.0*DRB
00126 21* DISP=(6.2832*B*(1+F*H)*E*0
00127 22* RETURN
00130 23* END

```

END OF UNIVAC 1108 FORTRAN V COMPILATION. 0 \*DIAGNOSTIC MESSAGE(S)

PATTON

DATE 080372 PAGE 10

J1 FOR CYLBU,CYLB  
 UNIVAC 1108 FORTRAN V LEVEL 2206 0023  
 THIS COMPILATION WAS DONE ON 06 MAR 72 AT 10:13:01

10:13: 0.910

SUBROUTINE CYLBU ENTRY POINT 000041

STORAGE USED (BLOCK, NAME, LENGTH)

0001 \*CODE 000054  
 0000 \*DATA 000014  
 0002 \*BLANK 000000

EXTERNAL REFERENCES (BLOCK, NAME)

0003 MERRS

STORAGE ASSIGNMENT FOR VARIABLES (BLOCK, TYPE, RELATIVE LOCATION, NAME)

0000 000004 INJPS

00101 1\* SUBROUTINE CYLBU(BD1,BD2,H,L,RHO,C,DISP,DRB)  
 00101 2\* C DISPLACEMENT AND DRAG OF A CYLINDRICAL BUOY (CAN OR SPAR)  
 00103 3\* IF(MAGE.L)HEL  
 00105 4\* DISP=25.3\*(BD1\*2)\*RHOSH  
 00106 5\* DRB=0.5\*RHO\*1.\*BD1\*H\*C\*ABS(C)  
 00107 6\* RETURN  
 00110 7\* END

END OF UNIVAC 1108 FORTRAN V COMPILATION. 0 \*DIAGNOSTIC MESSAGE(S)

PATTON

SI FOR DISBU,DISBU  
 UNIVAC 1108 FORTRAN V LEVEL 2205 0023  
 THIS COMPILATION WAS DONE ON 06 MAR 72 AT 10:13:02

DATE 060372 PAGE 11

10:13: 1.936

SUBROUTINE DISBU ENTRY POINT 000134

STORAGE USED (BLOCK, NAME, LENGTH)

0001 \*CODE 000171  
 0000 \*DATA 000026  
 0002 \*BLANK 000000

EXTERNAL REFERENCES (BLOCK, NAME)

0003 NERRIS

STORAGE ASSIGNMENT FOR VARIABLES (BLOCK, TYPE, RELATIVE LOCATION, NAME)

0001 000006 3L 0001 000037 4L 0001 000126 9L 0000 000000 01 0000 000007 INCHPS  
 0000 R 000001 RAD

00101 16 SUBROUTINE DISBU(R,F,L,H,C,DNB,DISP)  
 00101 20 C DISPLACEMENT AND DRAG FOR A DISC BUOY  
 00101 30 C  
 00101 40 F IS HEIGHT OF BEVEL - F IS WIDTH OF BEVEL  
 00101 50 IF(H-E).2,3,3  
 00106 50 2 A122.00R0H-(H02)\*F/Z  
 00107 60 DR001.20A10(C002)  
 00110 70 RAD00-F\*H0F/Z  
 00111 80 DISP=64.001.00720H0((RAD002)+RAD0(R-F)+((R-F)\*002))  
 00112 90 YD 0  
 00113 100 3 IF(H-1,10,5,5  
 00115 110 5 HCL  
 00117 120 4 A122.00R0E-E0F+2.00\*(H-E)\*R  
 00120 130 DR001.20A10(C002)  
 00121 140 DISP=64.001.00720E0((R002)+R0(R-F)+((R-F)\*002))3.10100(R002)\*0(H-E)  
 00122 150 9 RETURN  
 00123 160 END

END OF UNIVAC 1108 FORTRAN V COMPILATION. 0 \*DIAGNOSTIC MESSAGE(S)

## PATTON

01 FOR SPHBU,SPHBU  
UNIVAC 1108 FORTRAN V LEVEL 2206 0023  
THIS COMPILATION WAS DONE ON 06 MAR 72 AT 10113103

DATE 060372 PAGE 12

101131 3.106

SUBROUTINE SPHBU ENTRY POINT 000075

STORAGE USED (BLOCK, NAME, LENGTH)

0001 \*CODE 000116  
0000 \*DATA 000024  
0002 \*BLANK 000000

EXTERNAL REFERENCES (BLOCK, NAME)

0003 SORT  
0004 ATAN  
0005 NEPR35

STORAGE ASSIGNMENT FOR VARIABLES (BLOCK, TYPE, RELATIVE LOCATION, NAME)

0001 000010 2L 0000 R 000000 ARG 0000 R 000001 AT 0000 000011 INJBS

```

00101 1* SUBROUTINE SPHBU(R,H,C,DRB,DISP)
00101 2* C DISPLACEMENT AND DRAG FOR A SPHERICAL BUOY
00103 3* IF(H=2.0)R(2,3)=3
00106 4* 3 H=2.0R
00107 5* 2 ARG=(R-H)/R
00110 6* A1=(R+2)*I(1.572-ATAN(ARG/SORT(1.0-ARG)))
00110 7* 1=(R-H)*SORT((R+2)-((R-H)*2))
00112 8* DRB=4*PI*H*(C+2)
00112 9* DISP=4*0.2*16*(R-H/3.0)*(H+2)
00113 10* RETURN
00114 11* END

```

END OF UNIVAC 1108 FORTRAN V COMPILATION. 0 \*DIAGNOSTIC MESSAGES)

PATTON

DATE 060372 PAGE 13

10113: 4.230

DI FOR RUNGE RUNGE  
UNIVAC 1108 FORTRAN V LEVEL 2206 10023  
THIS COMPILATION WAS DONE ON 06 MAR 72 AT 10113104

SUBROUTINE RUNGE (BLOCK, NAME, LENGTH)

ENTRY POINT 000134

0001 \*CODE 000163  
0000 \*DATA 000053  
0002 \*BLANK 000000

EXTERNAL REFERENCES (BLOCK, NAME)

0003 MERR28  
0004 MERR35

STORAGE ASSIGNMENT FOR VARIABLES (BLOCK, TYPE, RELATIVE LOCATION, NAME)

0001 000021 IL 0001 000121 10L 0001 000023 1070 0001 000054 1206 0001 000102 1306  
0001 000030 SL 0001 000032 4L 0001 000036 SL 0001 000074 7L 0001 000117 9L  
0000 R 000021 A 0000 1 000020 I 0000 000033 INPS 0000 000000 0

00101 1\* SUBROUTINE RUNGE(N,Y,F,X,H,M,K)  
00101 2\* C THIS ROUTINE PERFORMS RUNGE KUTTA CALCULATIONS BY GILLIS METHOD  
00103 3\* DIMENSION Y(16),F(16),G(16)  
00104 4\* M=41  
00105 5\* 60 TO (1.4/513.7)\*M  
00106 6\* 1.00 8 121.0  
00111 7\* 2 011120.0  
00113 8\* A20.5  
00114 9\* 80 TO 9  
00115 10\* 3 A21.707107  
00116 11\* C IF YOU NEED MORE ACCURACY USE A21.707107811805578244  
00117 12\* 4 23140.84H  
00117 13\* 5 00.5 121.0  
00122 14\* Y(11:Y(1)+A\*(F(1)-H\*(Y(1))))  
00123 15\* 6 01112.00A\*H\*(Y(1)+1.0-3.0A)\*G(11)  
00125 16\* A20.2928932  
00125 17\* C IF YOU NEED MORE ACCURACY USE A20.2928932118130426756  
00126 18\* 60 TO 9  
00127 19\* 7 00.5 121.0  
00132 20\* 8 Y(11:Y(1)+H\*(F(1)/6.0-0.0(1)/3.0  
00136 21\* H\*U.0  
00135 22\* K2.0  
00136 23\* 80 TO 10  
00137 24\* 9 K21.0  
00137 25\* 10 RETURN  
00141 26\* END

### Buoy System Dynamics for the Spherical Buoy

This program simulates the motions of a spherical buoy exposed to winds, currents, and a random sea. The mooring line is simulated as five, elastically connected, lumped masses. Cable weights, drag forces, and inertia forces are concentrated at each mass. The buoy is allowed six degrees of freedom, and each mooring line mass element is allowed three translational degrees of freedom. With a total of 21 degrees of freedom, 42 first-order differential equations are integrated simultaneously in the time domain.

The equations of motion for the buoy and the development of the forces acting on the buoy are presented in chapter III of the main text. The lumped-mass cable equations are also shown in that chapter.

Major computational procedures in this program are shown in figure B-2.

The input data are as follows:

1. Buoy hull radius (ft)
2. Height of the center of gravity of the buoy above the mooring line connection point on the buoy (ft)
3. Height of the mooring line connection point below the buoy hull (ft)
4. Buoy weight (lb)
5. Buoy structural and floodwater mass ( $\text{lb-sec}^2/\text{ft}$ )
6. Yaw mass moment of inertia ( $\text{lb-sec}^2/\text{ft}$ )
7. Pitch mass moment of inertia ( $\text{lb-sec}^2/\text{ft}$ )
8. Roll mass moment of inertia ( $\text{lb-sec}^2/\text{ft}$ )
9. Effective buoy wind drag coefficient (dimensionless)



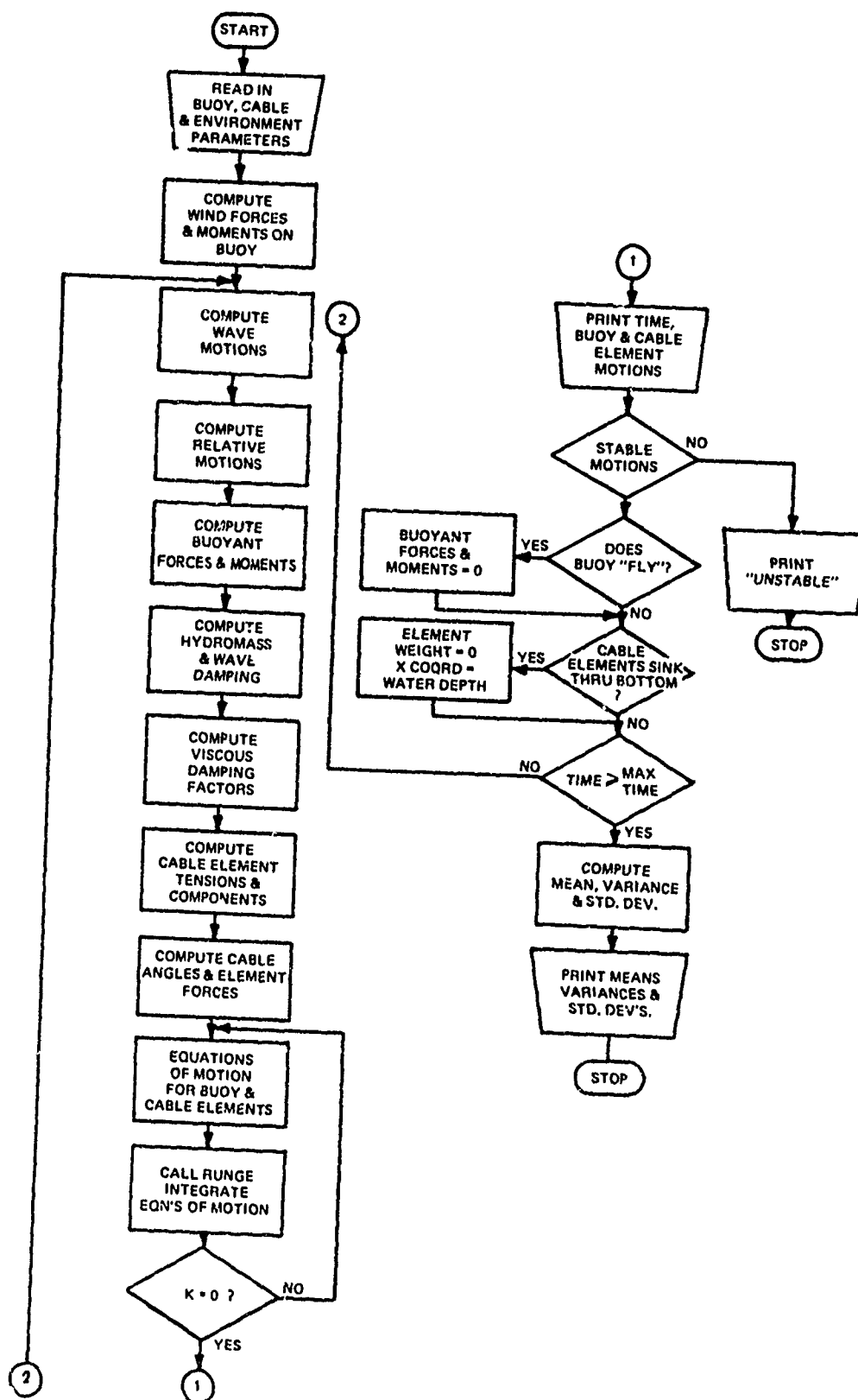


Figure B-2. Spherical Buoy Dynamics Simulation Flow Chart

10. Effective buoy wind lift coefficient (dimensionless)
11. Buoy windage (profile area) ( $\text{ft}^2$ )
12. Buoy plan area ( $\text{ft}^2$ )
13. Height of the wind center of pressure above the center of gravity of the buoy (ft)
14. Mean wave height (ft)
15. Mean wave period (sec)
16. The unstretched cable lengths between mass elements (ft) (6 required)
17. Upper mooring line segment diameter (ft)
18. Upper mooring line segment weight in water per unit length (lb/ft)
19. Upper mooring line segment mass per unit length ( $\text{lb-sec}^2/\text{ft}$ )
20. Lower mooring line segment diameter (ft)
21. Lower mooring line segment weight in water per unit length (lb/ft)
22. Lower mooring line segment mass per unit length ( $\text{lb-sec}^2/\text{ft}$ )
23. Surface current y component (ft/sec)
24. Surface current z component (ft/sec)
25. Wind speed y component (ft/sec)
26. Wind speed z component (ft/sec)
27. Initial buoy displacements x, y, and z (ft)
28. Initial cable element displacements (including the anchor clump) x, y, and z for each of 6 sets (ft).

The user of this program should first estimate the highest natural frequency in the system. In general, the upper mooring line segment will be lightest and the highest natural frequencies are in the axial mode along the

cable. Using the same variable names as those in the program we can estimate the highest natural frequency:

$$f_{HI} = \frac{1}{2\pi} \sqrt{\frac{2 EA}{DCSM1 \cdot CLO(2)}} ,$$

where

EA is the cable modulus\* (lb)

DCSM1 is the mass per unit length of the upper mooring line segment  
(lb-sec<sup>2</sup>/ft<sup>2</sup>)

CLO(2) is the unstretched cable length between the first and second  
cable mass elements (ft).

If the cable lengths were very short or the cable modulus were very high in the lower mooring line segment, an estimate should be made of its highest natural frequency also.

For numerical stability, the integration step size should be about 1/20th the shortest period present. Thus, the step size is computed:

$$R = 0.05 (1/f_{HI}) .$$

In this program, the wave component amplitudes, frequencies, and phase angles are computed externally and are listed in the body of the program (MOMEG, AMP, and PHS). The water depth (DEEP) is also listed, and the x coordinate of the mooring anchor clump should be set equal to the water depth. The total time of the simulation is controlled by a logical "IF" statement (statement

---

\*The cable modulus is the product of the cable material elastic modulus and the actual cable cross-sectional area.

no. 491), which shifts to the "STOP" control if the maximum simulated time is exceeded.

In this program, buoy motion output data are not printed for the first 6 sec of simulation as initial transients decay. After this time, the following buoy system outputs are printed every 800 time steps:

Simulation time (sec)

Water particle vertical acceleration (ft/sec<sup>2</sup>)

Buoy heave acceleration (ft/sec<sup>2</sup>)

Buoy sway acceleration (ft/sec<sup>2</sup>)

Buoy surge acceleration (ft/sec<sup>2</sup>)

Buoy pitch angle (deg)

Buoy roll angle (deg).



# BUOY DYNAMICS

```

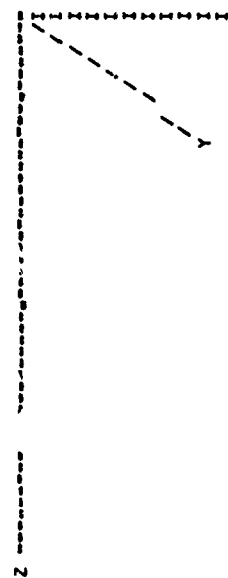
0000 K 000566 DGG6      0000 R 000572 DGGY      0000 R 000475 DGMW      0000 R 000515 DGM1      0000 R 000524 DGM2
0000 K 000600 DGN      0000 R 000421 UGN1      0000 R 000422 DGM2      0000 R 000372 DGT      0000 R 000417 DGT1
0000 K 000620 DGT2      0000 R 000561 UGN2      0000 R 000567 DGY6      0000 R 000562 DGY7      0000 R 000570 DGT2
0000 K 000653 DGT2      0000 R 000405 UJA1      0000 R 000410 DIA2      0000 R 000406 DMC1      0000 R 000411 DMC2
0000 K 000670 DGM      0000 R 000511 UX1      0000 R 000517 DX2      0000 R 000471 DYW      0000 R 000512 DY1
0000 K 000620 QY2      0000 R 000472 QZ4      0000 R 000513 DZ1      0000 R 000521 DZ2      0000 R 000601 EA
0000 K 000613 EAL      0000 R 000414 EA2      0000 R 000556 ETA      0000 R 000612 FAL      0000 R 000613 FBT
0000 K 000614 FGM      0000 R 000549 FR      0000 R 000607 FX      0000 R 000610 FY      0000 R 000611 FZ
0000 K 000637 GMM2      0000 R 000375 GMIN      0000 R 000467 GNM      0000 R 000510 GMI      0000 R 000525 H
0000 K 000526 HBT      0000 R 000533 HBT2      0000 R 000527 HGM      0000 R 000536 HGM2      0000 K 000531 HP
0000 K 000453 I      0000 I 000445 J      0000 I 000451 K      0000 I 000452 M      0000 I 000452 M
0000 K 000347 V3      0000 K 000336 MAA      0000 R 000334 MBB      0000 R 000343 MBB2      0000 R 000343 MBB2
0000 K 000335 MGG      0000 K 000346 MGG2      0000 K 000344 MGY      0000 R 000337 MXXB      0000 R 000340 MXXG
0000 K 000331 MXX      0000 R 000341 MMYG      0000 R 000332 MYY      0000 R 000342 MZZB      0000 R 000333 MZZ2
0000 K 000273 MMEG      0000 R 000350 MU      0000 I 000446 N      0000 R 000354 NAF      0000 R 000355 NBB
0000 K 000360 NXX      0000 K 000366 NSZ      0000 R 000356 NGG      0000 R 000362 NGX      0000 R 000364 NGY
0000 K 000620 NY      0000 K 000357 NXB      0000 R 000361 NXX      0000 R 000351 NXX      0000 R 000363 NYG
0000 K 000352 NY      0000 K 000362 NXX      0000 R 000353 NZZ      0000 R 000404 PEN      0000 R 000317 PHS
0000 K 000447 P      0000 R 000623 SPI      0000 R 000621 STE      0000 R 000144 T      0000 R 000265 TEN
0000 K 000332 VBB      0000 R 000460 VELBB      0000 R 000461 VELB      0000 R 000455 VELX      0000 R 000456 VELYB
0000 K 000457 VELZB      0000 R 000335 VCG      0000 R 000400 WAREA      0000 R 000401 WAREL      0000 R 000372 WB
0000 K 000573 WC      0000 R 000376 WCD      0000 R 000377 WCL      0000 R 000402 WCPHT      0000 R 000415 WC1
0000 K 000416 W2      0000 R 000443 WFSY      0000 R 000444 WFGM      0000 R 000440 WFX      0000 R 000441 WFY
0000 K 000442 WF2      0000 R 000454 WHT      0000 R 000443 WHTM      0000 R 000436 WINDY      0000 R 000437 WINDZ
0000 K 000504 WK      0000 R 000370 XCG      0000 R 000547 XHM      0000 R 000371 XML      0000 R 000603 XMPT
0000 K 000462 X*      0000 R 000509 X1      0000 R 000062 Y      0000 R 000604 YMPT      0000 R 000463 YW
0000 K 000605 ZMPT      0000 R 000564 Z*      0000 R 000564 Z*

```

THIS PROGRAM COMPUTES THE RESPONSE OF AN AXI-SYMMETRIC BUOY  
EXPOSED TO THE OCEAN ENVIRONMENT  
UNITS ARE IN FT., LB., SEC

DIMENSION D(50),Y(150),T(25),CW(25),CLF(25),CLO(6),TEN(6)  
DIMENSION MONEG(10),AMP(10),PHS(10)

REAL MONEG  
REAL MXX,MYY,MZZ,MHBB,MHGG,MHAA,MHXB,MHXY,MHYZ,MHZZ,MHBB  
REAL MHT,MHBT,MHGX,MHGX,MHGX,MHGX,MHGX,MHGX,MHGX,MHGX,MHGX,MHGX  
REAL MXX,MYY,MZZ,MHBB,MHGG,MHAA,MHXB,MHXY,MHYZ,MHZZ,MHBB  
THE COORDINATE SYSTEM



```

00100 1* C
00100 2* C
00100 3* C
00100 4* C
00101 5*
00101 6*
00101 7*
00101 8*
00101 9*
00101 10* C
00101 11* C
00101 12* C
00101 13* C
00101 14* C
00101 15* C
00101 16* C
00101 17* C
00101 18* C
00101 19* C
00101 20* C
00101 21* C
00101 22* C
00101 23* C
00101 24* C
00101 25* C
00101 26* C
00101 27* C

```

DATE 100172 PAGE 5

I I I I I I I I I I X

## BUOY DYNAMICS

```

00107 28* C
00107 29* C
00107 30* C
00107 31* C
00107 32* C
00107 33* C
00107 34* C
00107 35* C
00107 36* C
00107 37* C
00107 38* C
00110 39* 102 FORMAT(8F10.2)
00111 40* 103 FORMAT(11H BUOY SINKS)
00112 41* 105 FORMAT(6F10.2)
00113 42* 106 FORMAT(9H UNSTABLE)
00114 43* 107 FORMAT(5F10.4)
00115 44* 108 FORMAT(2F10.4)
00116 45* 109 FORMAT(3F10.4)
00116 46* C READ IN THE BUOY PARAMETERS
00116 47* C BUOY RADIUS, MT. OF C.OF G. FROM MOOR POINT AND THE LENGTH OF THE
00116 48* C MOOR POINT BELOW THE BOTTOM OF THE BUOY
00117 49* C HEAD 109.8R,XCG,XML
00117 50* C INERTIAS
00124 51* C HEAD 107.WB,MB,ALIN,BYIN,GNIN
00124 52* C WIND LIFT AND DRAG COEFFICIENTS AND AREAS
00133 53* C HEAD 107.WCD,WCL,WAREA,WAREL,WCPHT
00133 54* C
00133 55* C THE VISCOSITY OF THE WATER AT 40 DEG F
00142 56* MU=2.735E-5
00142 57* C
00142 58* C THE WAVE PARAMETERS
00143 59* READ 108.WHTM,PER
00147 60* WMEG(1)=1.7357
00151 61* WMEG(2)=2.2326
00152 62* WMEG(3)=2.3953
00153 63* WMEG(4)=2.5665
00153 64* WMEG(5)=2.7613
00154 65* WMEG(6)=3.0013
00155 66* WMEG(7)=3.3310
00156 67* WMEG(8)=3.8899
00157 68* WMEG(9)=682.07
00160 69* AMP(1)=0.3046
00161 70* AMP(2)=0.1565
00162 71* AMP(3)=0.1563
00163 72* AMP(4)=0.1562
00164 73* AMP(5)=0.1561
00165 74* AMP(6)=0.1559
00166 75* AMP(7)=0.1555
00167 76* AMP(8)=0.1537
00170 77* AMP(9)=0
00171 78* PHS(1)=0.657
00172 79* PHS(2)=0.435
00173 80* PHS(3)=5.545
00174 81* PHS(4)=3.220
00175 82* PHS(5)=0.575
00176 83* PHS(6)=5.20
00177 84* PHS(7)=4.655
00400 85* PHS(8)=6.255

```

DATE 100172 PAGE 6

## BUOY DYNAMICS

```

00201 PH5(9)=0.306
00202 C
00203 C THE CABLE PARAMETERS
00204 C THE CABLE LENGTHS BETWEEN ELEMENTS
00205 C READ 105,CLO(1),CLO(2),CLO(3),CLO(4),CLO(5),CLO(6)
00206 C
00207 C THE UPPER CABLE PROPERTIES
00208 C READ 109,DIA1,DWC1,DSCM1
00209 C
00210 C THE LOWER CABLE PROPERTIES
00211 C READ 109,DIA2,DWC2,DSCM2
00212 C
00213 C EA1=2.16E5
00214 C
00215 C EAZ=EA1
00216 C
00217 C WCI=UWC1*CLO(1)
00218 C
00219 C WC2=UWC2*CLO(5)
00220 C
00221 C DGT1=0.05*DIA1*CLO(1)
00222 C
00223 C UGT2=0.2*DIA2*CLO(5)
00224 C
00225 C DGN1=1.2*DIA1*CLO(1)
00226 C
00227 C DGN2=1.2*DIA2*CLO(5)
00228 C
00229 C CSM1=DSCM1*CLO(1)
00230 C
00231 C CSM2=DSCM2*CLO(5)
00232 C
00233 C CHMT1=0.0
00234 C
00235 C CHMT2=0.753*(DIA2**2)*CLO(5)
00236 C
00237 C CHN1=1.56*(DIA1**2)*CLO(1)
00238 C
00239 C CHN2=1.56*(DIA2**2)*CLO(5)
00240 C
00241 C THE WATER DEPTH
00242 C DEEP=62.0
00243 C
00244 C THE CURRENTS IN THE WATER COLUMN
00245 C READ THE Y AND Z COMPONENTS OF THE SURFACE CURRENT
00246 C READ 108,CYS,CZS
00247 C
00248 C IF THE CURRENT VARIATIONS WITH DEPTH, INSERT THE FUNCTIONS FOR
00249 C STRENGTH AND DIRECTION
00250 C
00251 C FOR A UNIFORM CURRENT
00252 C CYS=CYS
00253 C CZS=CZS
00254 C
00255 C THE WIND ACTING ON THE BUOY
00256 C READ THE Y AND Z COMPONENTS OF THE MEAN WIND
00257 C READ 108,WINDY,WINDZ
00258 C
00259 C WFX=0.0034*WCL*WAREA*WINDY**2*WINDZ**2)
00260 C
00261 C WFT=0.0034*WCD*WAREA*WINDY*ABS(WINDY)
00262 C
00263 C WFBT=0.0034*WCD*WAREA*WINDZ*ABS(WINDZ)
00264 C
00265 C WFGM2=WFX+WFBT
00266 C
00267 C JE1
00268 C
00269 C N=42
00270 C
00271 C REO=0.0005
00272 C
00273 C A=0.0
00274 C
00275 C K=0
00276 C
00277 C M=0
00278 C
00279 C THE INITIAL CONDITIONS
00280 C ALL ACCELERATIONS AND VELOCITIES ARE ZERO
00281 C DO 58 I=1,412
00282 C
00283 C D(I)=0.0
00284 C
00285 C 58 Y(I)=0.0
00286 C
00287 C READ THE INITIAL BUOY DISPLACEMENTS - X,Y,Z
00288 C READ 109,Y(2),Y(4),Y(6)
00289 C
00290 C THE INITIAL BUOY ANGLES ARE ZERO

```



DATE 100172 PAGE 7

## BUOY DYNAMICS

```

00303 144 Y(8)=0.0
00304 145 Y(10)=0.0
00305 146 Y(12)=0.0
00306 147 READ THE INITIAL CABLE DISPLACEMENTS
00307 148 DO 53 I=14,44,6
00308 149 53 READ 109,Y(I),Y(I+2),Y(I+4)
00309 150 5 CONTINUE
00310 151 WHT=A*WHTM/(2.0*PER)
00311 152 IF (A.GE.(2.0*PER))WHT=B*WHTM
00312 153 VELXB=Y(1)
00313 154 VELYB=Y(3)
00314 155 VELZB=Y(5)
00315 156 VELXB=Y(9)
00316 157 VELGB=Y(11)
00317 158 THE WAVES
00318 159 FOR A SINGLE TRAIN OF WAVES, ASSUME THEY ARE COMING IN ON THE
00319 160 Z AXIS
00320 161 XW=0.0
00321 162 YW=0.0
00322 163 ZW=0.0
00323 164 ALW=0.0
00324 165 BTW=0.0
00325 166 GWW=0.0
00326 167 DXW=0.0
00327 168 DYW=0.0
00328 169 DZW=0.0
00329 170 UALW=0.0
00330 171 DBTW=0.0
00331 172 UGNW=0.0
00332 173 DDYW=0.0
00333 174 DDZW=0.0
00334 175 DDALW=0.0
00335 176 DDBTW=0.0
00336 177 DDGNW=0.0
00337 178 DO 14 I=1,9
00338 179 WK=(MOMEG(I)**2)/32.2
00339 180 ANGA=MOMEG(I)/MS(I)
00340 181 XW=XW+AMP(I)*SIN(ANG)
00341 182 ZW=ZW+AMP(I)*COS(ANG)
00342 183 BTW=BTW+WK*AMP(I)*COS(ANG)
00343 184 DXW=DXW+MOMEG(I)*AMP(I)*COS(ANG)
00344 185 DZW=DZW-MOMEG(I)*AMP(I)*SIN(ANG)
00345 186 DBTW=DBTW-WK*MOMEG(I)*AMP(I)*SIN(ANG)
00346 187 DXW=DXW+MOMEG(I)*2*AMP(I)*SIN(ANG)
00347 188 DZW=DZW-MOMEG(I)*2*AMP(I)*COS(ANG)
00348 189 DDZW=DDZW-WK*(MOMEG(I)*2)*AMP(I)*COS(ANG)
00349 190 14 DDBTW=DDBTW-WK*(MOMEG(I)*2)*AMP(I)*COS(ANG)
00350 191
00351 192 THE BUOY MOTIONS RELATIVE TO THE WATER MASS
00352 193 DISPLACEMENTS
00353 194 X1=Y(2)-XW
00354 195 BT1=Y(10)-BTW
00355 196 GM1=Y(12)-GMW
00356 197 VELOCITIES
00357 198 OX1=Y(1)-DXW
00358 199 OY1=Y(3)-DYW
00359 200 DZ1=Y(5)-DZW
00360 201 DAL1=Y(7)-DALW

```



DAYE 100172 PAGE 9

## BUOY DYNAMICS

```

00460 260* FR=((6.2832/PER)*2)*BR/32.2
00461 261* BLAMB=SORT((6.25/(PER*HU)))
00462 262* BA=BLAMB*RR
00463 263* HYDRODYNAMIC FORCE MOMENT ARM
00464 264* XHM=XLG-XML-0.625*H
00465 265* HEAVE
00466 266* IF(FR,GE,0.1)GO TO 31
00467 267* CMX=1.85
00468 268* GO TO 33
00469 269* 31 IF(FR,GE,3.4)GO TO 32
00470 270* CMX=1.02*(FR*(-.256))
00471 271* GO TO 33
00472 272* 32 CMX=1.0
00473 273* CMY=1.0
00474 274* S=AY-SURGE
00475 275* 33 IF(FR,GE,0.74)GO TO 34
00476 276* CMY=1.069+0.529*FR
00477 277* GO TO 35
00478 278* 34 CMY=1.0/(-0.0318+0.95*FR)
00479 279* CMZ=CMY
00480 280* MXX=1.988*(BR*3)*CMX
00481 281* MYY=1.988*(BR*3)*CMY
00482 282* MZZ=1.988*(BR*3)*CMZ
00483 283* YAB
00484 284* MAA=16.65*(BR*5)*(1.0+8A)/(1.0+2.0*8A+2.0*(BA*2))
00485 285* PITCH AND ROLL
00486 286* MAB=MYZZ*(XHM*2)
00487 287* MGG=MHBB
00488 288* CROSS-COUPLED HYDROMASSES
00489 289* MABX=0.0
00490 290* MABY=0.0
00491 291* MABZ=0.0
00492 292* MXYG=MYYY*XHM
00493 293* MXYZ=MYYG
00494 294* MABZ=MYZB
00495 295* MABY=MYG
00496 296*
00497 297* THE DAMPING DUE TO WAVE GENERATION
00498 298*
00499 299* HEAVE
00500 300* IF(FR,GE,0.4)GO TO 41
00501 301* CMX=0.126+0.17*FR
00502 302* GO TO 42
00503 303* 41 CMX=1.18*EXP(-0.83*FR)
00504 304* 42 IF(FR,LE,0.1)CMY=0.0
00505 305* IF(FR,GE,1.37)GO TO 44
00506 306* CMY=-0.069+0.71*FR
00507 307* GO TO 43
00508 308* 44 CMY=1.595*EXP(-0.415*FR)
00509 309* 43 NXX=1.988*FR*(BR*3)*CMXX
00510 310* NY=1.988*FR*(BR*3)*CMY
00511 311* NZZ=NY
00512 312* PITCH AND ROLL
00513 313* NAA=4.195*HU*(BR*3)*3.0+6.0*BA*6.0*(BA*2)+2.0*(BA*3))
00514 314* 1/(1.0+2.0*BA+2.0*(BA*2))
00515 315* NBB=NAA*NZZ*(XHM*2)
00516 316* NGG=MBB
00517 317* CROSS COUPLED WAVE DAMPING

```

DATE 100172 PAGE 10

## BUOY DYNAMICS

```

00543 318* NXB=0.0
00544 319* NBX=0.0
00545 320* TXG=0.0
00546 321* NGX=0.0
00547 322* NYG=-NY*XXH
00550 323* NZB=-NYG
00551 324* NBZ=NB
00552 325* NGY=NYG
00552 326*
00552 327* C THE VISCOUS DAMPING AND DRAG
00552 328* C
00553 329* AREAS
00553 330* ARXX=3.1416*(BR**2)
00554 331* IFH.GT.(0.95*BR))GO TO 47
00556 332* ETA=2.0*ATAN((SQRT(2.0*HBR-(H**2)))/(BR-H))
00557 333* ARYY=0.5*(BR**2)*ETA*SIN(ETA))
00560 334* GO TO 49
00561 335* 47 IFH.GT.(1.05*BR))GO TO 46
00563 336* ARYY=1.5708*(BR**2)
00564 337* GO TO 49
00565 338* 46 HP=2.0*BR-H
00566 339* ETA=2.0*ATAN((SQRT(2.0*HP*BR-(HP**2)))/(BR-HP))
00567 340* ARYY=BR**2*13.1416*0.5*(ETA*SIN(ETA))
00570 341* 49 ARZZ=ARYY
00571 342* IFH.GE.(2.0*BR) ARYY=3.1416*(BR**2)
00573 343* OGXX=0.497*ARXX
00574 344* OGYY=0.497*ARZZ
00575 345* OGZZ=0.497*ARZZ
00576 346* OGAA=0.0
00577 347* OGBB=0.0
00580 348* UGGG=0.0
00580 349* C CROSS-COUPLED VISCOUS DRAG
00601 350* OGYY=-DGY*(XHM**2)
00602 351* OGZB=-DGYG
00603 352* OGBZ=DGBZ
00604 353* OGGT=DGTG
00604 354* C
00604 355* C TENSIONS AND FORCES FOR THE 5 ELEMENT LUMP MASSCABLE MODEL
00604 356* C THE FIRST THREE ELEMENTS ARE CABLE, THE LAST TWO ARE CHAIN
00605 357* WC=WC1
00606 358* CSN=CSN1
00607 359* CHNTECHNT1
00610 360* CHNTECHN1
00611 361* DGT=DGT1
00612 362* DGN=DGN1
00613 363* EA=EA1
00614 364* CABK=EA/CLO(1)
00615 365* XMPY=Y(2)+XCG*COS(Y(10))*COS(Y(12))
00616 366* YMPY=Y(4)-XCG*COS(Y(10))*SIN(Y(12))
00617 367* ZMPT=Y(6)+XCG*SIN(Y(10))*COS(Y(12))
00620 368* CL=SQRT(((XMPY-Y(14))**2)+((YMPY-Y(16))**2)+((ZMPT-Y(18))**2))
00621 369* TEN(1)=CABK*(CL-CLO(1))
00622 370* IF(TEN(1)).LE.0.0)TEN(1)=0.0
00624 371* T(4)=TEN(1)*(Y(14)-XMPY)/CL
00625 372* T(6)=TEN(1)*(Y(16)-YMPY)/CL
00626 373* T(6)=TEN(1)*(Y(18)-ZMPT)/CL
00627 374* ADD 30 LBS. TO ACCOUNT FOR THE INSTRUMENT PACKAGE UNDER THE BUOY
00631 375* FYT(4)+30.0
00631 375* FYT(5)

```

BUOY DYNAMICS DATE 100172 PAGE 11

```

376* FZ=I(6)
377* FAL=0.0
378* FBT=-XCG*(F2-COS(Y(10))*COS(Y(12))+FX*SIN(Y(10))*COS(Y(12)))
379* FBP=-ACG*(FY-COS(Y(10))*COS(Y(12))+FX*SIN(Y(12))*COS(Y(10)))
380* CPIT=57.4*ATAN((Y(18)-ZMPT)/(Y(14)-XMPY))
381* CROLL=57.4*ATAN((Y(16)-YMPT)/SQRT((Y(14)-XMPY)**2+(Y(18)-ZMPT)**2))
382* 1.0021
383* 00 71 I=13.37*6
384* K1=((11-1)/2)-2
385* NT=((11-1)/6)
386* CL=SQRT((Y(11)-Y(17))**2+((Y(13)-Y(19))**2)+
387* 1.((Y(15)-Y(11))**2))
388* IF(NT.GE.4)GO TO 72
389* 60 TO 73
390* CHARACTERISTICS OF THE LOWER PART OF THE MOORING LINE
391* 72 #C=62
392* CSM=CSM2
393* CHMT=CHMT2
394* CMN=CMN2
395* DGT=DGT2
396* DNE=DNE2
397* EA=EA2
398* CABK=EA/CLO(NT)
399* TEN(NT)=CABK*(CL-CLO(NT))
400* IF(TEN(NT).LE.0.0)TEN(NT)=0.0
401* THE TENSION COMPONENTS
402* T(K1+3)=TEN(NT)*((Y(17)-Y(11))/CL
403* T(K1+4)=TEN(NT)*((Y(19)-Y(13))/CL
404* T(K1+5)=TEN(NT)*((Y(11)-Y(15))/CL
405* THE SINES AND COSINES OF THE CABLE ANGLES
406* STHE=Y(11)-Y(15)/SQRT((Y(11)-Y(15))**2+
407* 1.((Y(17)-Y(11))**2))
408* CTHE=Y(17)-Y(11)/SQRT((Y(17)-Y(11))**2+
409* 1.((Y(19)-Y(13))**2))
410* SPHE=Y(19)-Y(13)/CL
411* CPHE=SQRT((Y(11)-Y(17))**2+((Y(15)-Y(13))**2))/CL
412* CM(K1)=CSM+CHMT*CPHE*CTHE
413* CM(K1+1)=CSM+CMN*CPHE
414* CM(K1+2)=CSM+CMN*CTHE
415* CUR=Y(11)*CPHE*CTHE+Y(17)*CY+Y(19)*CY-CTHE*CPHE*STHE
416* CVR=Y(11)*SPHE*CTHE+Y(17)*CY+Y(19)*CY-CTHE*SPHE*STHE
417* CAR=Y(11)*STHE+Y(17)*CTHE
418* CLF(K1)=DGT*CPHE*CTHE*CUR+DGN*SPHE*CTHE*CVR+ABS(CVR)
419* 1-DGN*STHE*CMN*ABS(CVR)
420* CLF(K1+1)=DGT*SPHE*CUR+DGN*CPHE*CVR+ABS(CVR)
421* CLF(K1+2)=DGT*CPHE*STHE*CUR+DGN*SPHE*STHE*CVR+ABS(CVR)
422* 1-DGN*CTHE*CMR*ABS(CVR)
423* 50 CONTINUE
424* DDY1=Y(11)-VELXB)/R
425* DDY2=Y(13)-VELYB)/R
426* DDZ1=Y(15)-VELZB)/R
427* DDZ2=Y(19)-VELZB)/R
428* DDGM1=Y(11)-V/LGB)/R
429* THE EQUATIONS OF MOTION FOR THE BUOY
430* HEAVE -X MOTION
431* D(1)=(WB-BXB-BXB-BXB+MHXX*DDY1-MHXB*DDZ1-MHXB*DDGM1-NXX*DX1
432*
433*

```

BUOY DYNAMICS DATE 100172 PAGE 12

```

00712 434 1 -AXB*DBT1-NX*OCM1-DGX*DX2*ABS(DX2)+FX+FX)/(MB+MHXX)
00713 435 D(2)=Y(1)
00714 436 C
00715 437 C
00716 438 SWAY - Y MOTION
00717 439 D(3)=(PHY*DDYH-WYNG*DDGM1-NY*DY1-NYG*DDGM1-DGY*DY2*ABS(DY2)
00718 440 D(4)=Y(13)
00719 441 C
00720 442 SURGE - Z MOTION
00721 443 D(5)=(MZZ*DDW-W*ZB*DBT1-NZZ*DZ1-MZB*DBT1-OGZZ*DZ2*ABS(DZ2)
00722 444 D(6)=Y(5)
00723 445 C
00724 446 YAW - ALPHA MOTION
00725 447 D(7)=(MHA*DDAL-W*AA*DAL1-DGAA*DAL2*ABS(DAL2)+FAL)/(ALIN+MHA)
00726 448 D(8)=Y(7)
00727 449 C
00728 450 PITCH - BETA MOTION
00729 451 D(9)=(-BAX-BBX-WHBX*DDX1-MHBX*DDZ1+WHB*DBT1-NBX*DX1-NBB*DBT1
00730 452 1 -NBZ*DZ1-DGZ*DZ2*ABS(DZ2)-DGB*DBT2*ABS(DBT2)+FBT+FBT)/
00731 453 2 (BTIN+MHB)
00732 454 D(10)=Y(9)
00733 455 C
00734 456 C
00735 457 ROLL - GAMMA MOTION
00736 458 U(1)=(-BGX-BGG-MHGX*DDX1-WHG*DDZ1+MHGG*DDGM1-NGX*DX1-NGY*DY1
00737 459 1 -NGG*DDGM1-DGG*DY2*ABS(DY2)-DGG*DDGM2*ABS(DGM2)+FGM+FGM)/
00738 460 2 (GMH+MHGG)
00739 461 D(12)=Y(11)
00740 462 C
00741 463 EQUATIONS OF MOTION FOR A 5 LUMP MODEL
00742 464 DO 81 I=1,5,37.6
00743 465 KIE(I-1)/2)-2
00744 466 ELEMENT X MOTION
00745 467 U(1)=(-T(KI)+T(KI-3)-CLF(KI))/CM(KI)
00746 468 D(1)=Y(1)
00747 469 C
00748 470 ELEMENT Y MOTION
00749 471 D(1+2)=(-T(KI+1)+T(KI-4)-CLF(KI+1))/CM(KI+1)
00750 472 D(1+3)=Y(1+2)
00751 473 C
00752 474 ELEMENT Z MOTION
00753 475 D(1+4)=(-T(KI+2)+T(KI-5)-CLF(KI+2))/CM(KI+2)
00754 476 D(1+5)=Y(1+4)
00755 477 C
00756 478 CALL RUNGE(N,Y,D,A,R,M,K)
00757 479 GO TO (50,40),K
00758 480 40 ALFA=57.4*Y(8)
00759 481 BETA=57.4*Y(10)
00760 482 GAMMA=57.4*Y(12)
00761 483 IF(J.EG.200)GO TO 51
00762 484 JEU+1
00763 485 GO TO 52
00764 486 51 CONTINUE
00765 487 WHITE(4,108)*D(1)
00766 488 JZ1
00767 489 C
00768 490 52 CONTINUE
00769 491 INSTABILITY LIMITER
00770 492 DO 60 I=1,N
00771 493 60 IF(Y(I).GE.1000.0)GO TO 92
00772 494 THE CABLE ELEMENTS CAN'T SINK THRU THE BOTTC
00773 495 DO 218 I=14,38.6

```

DATE 100172 PAGE 13

## BUOY DYNAMICS

```

00772 492* 218 IF(Y(1).GE.DEEP(1)).DEEP
00775 493* IF(A.GE.26.0)60 TO 88
00777 494* 60 TO 5
01000 495* 92 WRITE(4,106)
01002 496* 88 STOP
01003 497* END

```

END OF UNIVAC 1106 FORTRAN V COMPILATION. 0 \*DIAGNOSTIC\* MESSAGE(S)

## BUOY DYNAMICS

G1 FOR RUNGE, RUNGE  
UNAVAC 1108 FORTRAN V LEVEL 2206 0023  
THIS COMPILE WAS DONE ON 10 JAN 72 AT 15:08:22

DATE 100172 PAGE 14

15: 8:22.132

SUBROUTINE RUNGE ENTRY POINT 000134

STORAGE USED (BLOCK, NAME, LENGTH)

0001 \*CODE 000163  
0002 \*DATA 000115  
0003 \*BLANK 000000

EXTERNAL REFERENCES (BLOCK, NAME)

0003 NEMR25  
0004 NEMR33

STORAGE ASSIGNMENT FOR VARIABLES (BLOCK, TYPE, RELATIVE LOCATION, NAME)

0001	000021 1L	0001	000121 10L	0001	000023 1076	0001	000054 1206	0001	000102 1306
0001	000030 3L	0001	000032 4L	0001	000036 5L	0001	000074 7L	0001	000117 9L
0000	N 000063 A	0000	1 000062 I	0000	000075 INJPS	0000	R 000000 Q		

```

00101 1* C SUBROUTINE RUNGE(H,Y,F,X,H,M,K)
00101 2* THIS ROUTINE PERFORMS RUNGE KUTTA CALCULATIONS BY GILL'S METHOD
00103 3* DIMENSION Y(50),F(50),U(50)
00104 4* MEM=1
00105 5* GO TO (1,4,5,3,7),M
00106 6* 1 DO 2 I=1,N
00107 7* 2 Q(I)=0.0
00108 8* A=0.5
00109 9* GO TO 9
00110 10* 3 A=1.707107
00111 11* C IF YOU NEED MORE ACCURACY USE A=1.7071067811865475244
00112 12* 4 X=X+0.5*H
00113 13* 5 DO 6 I=1,N
00114 14* Y(I)=Y(I)+A*(F(I)+H*Q(I))
00115 15* 6 Q(I)=(2.0*A*H*(F(I)+(1.0-3.0*A)*Q(I))
00116 16* A=0.2428932
00117 17* C IF YOU NEED MORE ACCURACY USE A=0.2928932188134524756
00118 18* 7 DO 8 I=1,N
00119 19* 8 Y(I)=Y(I)+H*(F(I)+6.0*Q(I))/3.0
00120 20* M=0.0
00121 21* K=2
00122 22* GO TO 10
00123 23* 9 K=1
00124 24* 10 RETURN
00125 25* END
00126 26*

```



### Buoy System Dynamics for the Torroidal Buoy at Station BRAVO

The previous program, developed for the spherical buoy, was modified to simulate the torroidal buoy dynamics. As indicated in figure B-3, the basic computational procedures remain the same as for the spherical buoy. However, the wave component amplitudes, frequencies, and phase angles are computed in a subroutine (RWAVE) in the program and do not have to be listed in the program. The buoyant forces and moments for the torroidal buoy are also computed in a subroutine (TORBU) using an integration method developed in appendix E. Finally, since the output motions were to be displayed as spectrum, subroutines using Fast Fourier Transform (FFT) methods were employed to compute the spectra.

Buoy hull hydrodynamic force functions in the program were modified according to Kim's data for a half-beam to draft ratio of 3.2:1. Terms are included to account for the hydrodynamic mass and drag of the three-leg chain bridle under the buoy, and the effective hydrodynamic centers are modified to account for the bridle. The computed inputs for the torroidal buoy are shown in appendix D.

A three-element, lumped-mass cable model was used in this simulation since the actual masses in the system were concentrated at three places along the mooring line (the current meter, the sentinel, and halfway down the 3/4-in. chain). Initial runs using a five-lump cable model were compared with runs using a three-lump cable model, and no significant difference in buoy motions was noted. However, there was an order of magnitude increase in computational speed since the two, high-natural-frequency cable lumps were summed into the

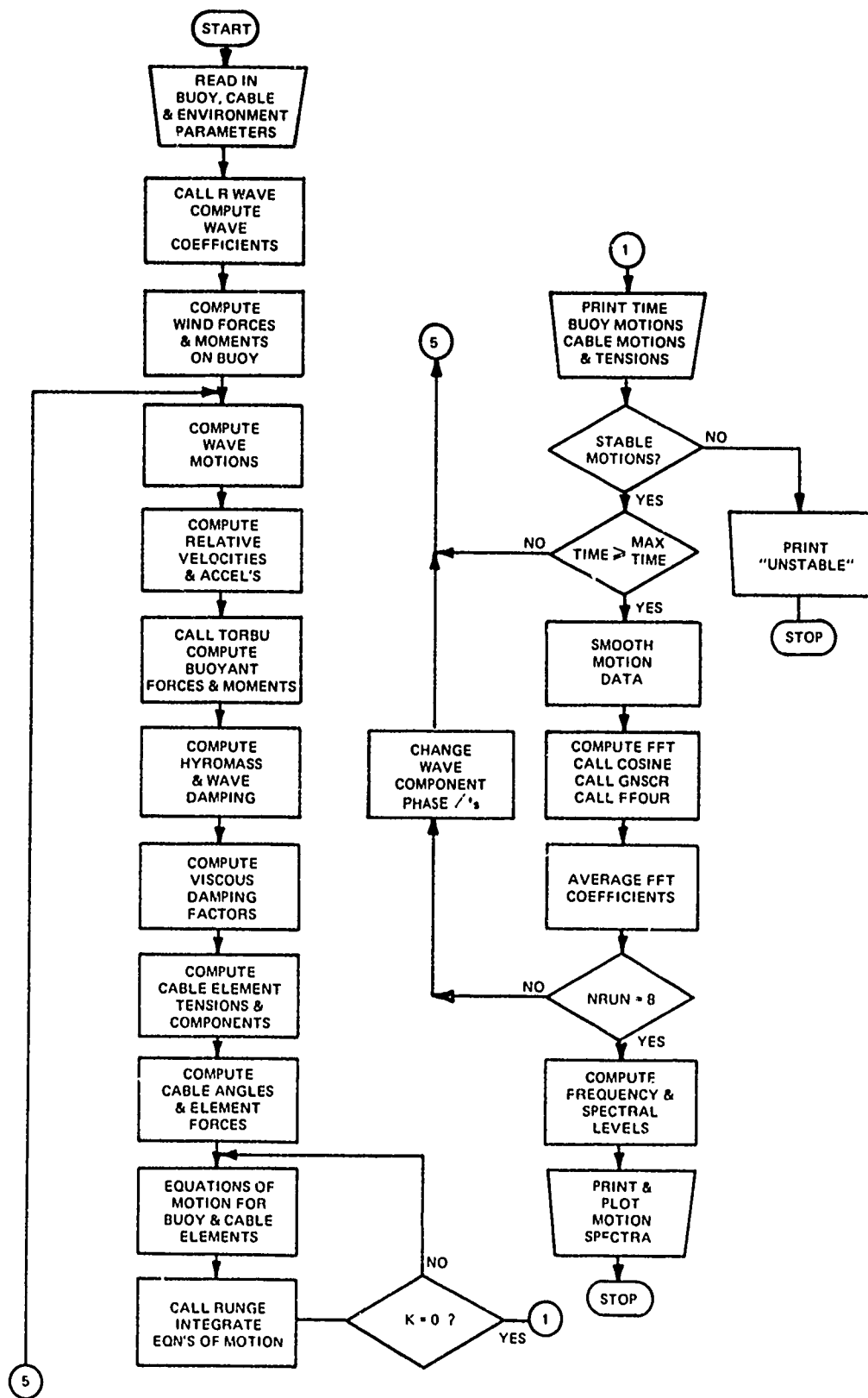


Figure B-3. Torroidal Buoy BRAVO Dynamics Simulation Flow Chart

current meter lump.

Input data for this program are as follows:

1. Buoy hull radius (ft)
2. Height of the center of gravity of the buoy above the mooring line connection point on the buoy (ft)
3. Height of the mooring line connection point below the buoy hull (ft)
4. Buoy weight (lb)
5. Buoy structural and floodwater mass ( $\text{lb-sec}^2/\text{ft}$ )
6. Yaw mass moment of inertia ( $\text{lb-sec}^2/\text{ft}$ )
7. Pitch mass moment of inertia ( $\text{lb-sec}^2/\text{ft}$ )
8. Roll mass moment of inertia ( $\text{lb-sec}^2/\text{ft}$ )
9. Effective buoy wind drag coefficient (dimensionless)
10. Effective buoy wind lift coefficient (dimensionless)
11. Buoy windage (profile area) ( $\text{ft}^2$ )
12. Buoy plan area ( $\text{ft}^2$ )
13. Height of the wind center of pressure above the center of gravity of the buoy (ft)
14. Mean wind speed causing the wind waves (ft/sec)
15. Wind duration (hr)
16. Surface current y component (ft/sec)
17. Surface current z component (ft/sec)
18. Wind y component (ft/sec)
19. Wind z component (ft/sec)
20. Initial displacements of the buoy x, y, and z (ft)

21. Initial cable displacements (including the anchor clump) x, y, and z for each of four sets (ft)

Again, the user should estimate the highest natural frequency in the system and adjust the integration step size as required. Computed buoy motions are sampled every 12th time step, and 1024, or  $2^{10}$ , samples are stored. Simple statistical estimates (mean, variance, and standard deviation) of the output motions are computed. Each data point is smoothed to reduce aliasing by averaging with the four data points closest to it in time. Spectra are computed using FFT subroutines and are smoothed for plotting. Statements 557 through 595 plot the spectral levels in dB. A Stromberg Datagraphics, Inc. integrated graphics system peripheral to the Naval Underwater Systems Center UNIVAC 1108 computer was used for this procedure.

DATE 230272 PAGE 3 12:43:57.53

# BUOY DYNAMICS

Q FOR 51670-51676  
UNIVAC 1108 FORTRAN V LEVEL 2206 0023  
THIS COMPILATION WAS DONE ON 23 FEB 72 AT 12:43:57

## MAIN PROGRAM

### STORAGE USED (BLOCK, NAME, LENGTH)

0001 CODE 003731  
0000 DATA 045324  
0002 BLANK 000000

### EXTERNAL REFERENCES (BLOCK, NAME)

0003 RAVE  
0004 TORBU  
0005 RUNGE  
0006 DSTAT  
0007 COSINE  
0010 GNSCR  
0011 FF0UR  
0012 MUESG  
0013 OBJCTG  
0014 SUBJCG  
0015 GRIDG  
0016 LABELG  
0017 TITLGG  
0020 LINESG  
0021 PAGEG  
0022 EATIG  
0023 NUOCs  
0024 NI02s  
0025 SIN  
0026 COS  
0027 SHT  
0030 NEXP0s  
0031 EXP  
0032 NERR2s  
0033 NWDUS  
0034 ALOG10  
0035 NSTOPs

### STORAGE ASSIGNMENT FOR VARIABLES (BLOCK, TYPE, RELATIVE LOCATION, NAME)

0001	002501	1003G	0001	002567	1021G	0000	015022	103F	0001	002604	1030G	0001	002640	1042G
0000	015025	105F	0000	015027	106F	0000	015032	107F	0000	015034	108F	0000	015036	109F
0000	015040	112F	0000	015042	116F	0000	015045	117F	0000	015054	120F	0000	015052	121F
0000	015054	122F	0000	015056	123F	0000	015060	124F	0000	015062	127F	0000	003405	130L
0001	003503	131L	0001	003531	132L	0001	003557	133L	0001	003605	134L	0001	003633	135L
0001	003661	136L	0001	000217	262G	0001	000230	274G	0001	000576	31L	0001	000247	312G
0001	000612	32L	0001	000264	326G	0001	000614	33L	0001	000555	374G	0001	002117	40L
0001	000707	41L	0001	000717	42L	0001	002601	450L	0001	000275	5L	0001	001513	50L
0001	000257	500L	0001	002145	51L	0001	002167	52L	0001	001173	556G	0001	002040	641G

BUOY DYNAMICS	DATE	230272	PAGE
0001 004171 701G	0001 002203 707G	0001 002330 757G	0001 003725 89L
0000 003712 92L	0000 004612 A	0000 002110 ACX	0000 002510 ACY
0000 003010 ACTC	0000 003160 ACZ	0000 001501 ACZC	0000 0014552 ALIN
0000 004626 AL*	0000 000305 AMP	0000 0014646 ANG	0000 0014754 AXMN
0000 004760 AXSD	0000 0014765 AXVK	0000 0014767 ATMN	0000 0014770 AYVR
0000 004772 AZMN	0000 0014774 AZSD	0000 0014773 AZVR	0000 0014670 B8B
0000 004672 B8X	0000 0014757 BETA	0000 0014673 BGG	0000 0014507 BIN
0000 004677 BLAMB	0000 003510 BPIT	0000 0015012 BPITC	0000 0014777 BPSD
0000 004770 BVR	0000 004546 BR	0000 0015000 BRMN	0000 0015013 BROLC
0000 0045002 BVS	0000 0015001 BRVH	0000 0014553 BTIN	0000 0014650 BTI
0000 004771 BXB	0000 0014674 BXR	0000 0014667 BXX	0000 0000383 CHMN
0000 0000330 CMT	0000 0014730 CL	0000 0000226 CLF	0000 0000175 CM
0000 0014702 CMX	0000 0014703 CMT	0000 0014704 CMZ	0000 0014706 CNY
0000 0000367 CDS1	0000 0014745 CPH1	0000 0000331 CSM	0000 0014746 CUR
0000 0014747 CUR	0000 0014750 CWR	0000 0014573 CY	0000 0014574 CZ
0000 004572 C25	0000 0000000 O	0000 0014634 DALW	0000 0014663 DAL2
0000 0015160 DATA	0000 0005356 DATAS	0000 0021100 DATB	0000 0025160 DATC
0000 0007666 DATCS	0000 0031160 DATD	0000 0011032 DATDS	0000 0012176 DATES
0000 0001160 DATE	0000 0013342 DATFS	0000 0014635 DBTW	0000 0014664 DBT2
0000 004642 DBALW	0000 0014643 DC9TW	0000 0014754 DDBT1	0000 0014755 DDGM1
0000 0014637 DDXW	0000 0014751 DDY1	0000 0014650 DDYM	0000 0014651 DDZM
0000 0014753 DDZ1	0000 0014570 DEEP	0000 0014713 DGA	0000 0014721 DGBZ
0000 0014715 DGG5	0000 0014722 DGGY	0000 0014636 DGM	0000 0014663 DGM2
0000 0000362 DGM	0000 0000355 DGT	0000 0014710 DGTG	0000 0014711 DGY
0000 0014720 DGTB	0000 0014712 DGTZ	0000 0015014 DPAX	0000 0015016 DPAY
0000 0015017 DPT	0000 0015020 DPHL	0000 0014653 DPL	0000 0014632 DX1
0000 0014660 DX2	0000 0014632 DPL	0000 0014653 DY1	0000 0014633 DZM
0000 0014654 D21	0000 0014662 D22	0000 0014723 EA	0000 0014567 EA2
0000 0014734 FAL	0000 0014735 FBT	0000 0014736 FGM	0000 0004615 FRQ
0000 0014731 FX	0000 0014732 FY	0000 0014733 FZ	0000 0014554 GMIN
0000 0014630 GMA	0000 0014631 G1	0000 0014666 H	0000 0015005 IP
0000 0000767 ISC4	0000 0014613 J	0000 0014600 K	0000 0014614 L
0000 0014607 M	0000 0014526 MB	0000 0014515 MHAA	0000 0014524 MHBX
0000 0014522 MHBZ	0000 0014514 MHGG	0000 0014525 MHGX	0000 0014516 MHBX
0000 0014517 MHKG	0000 0014510 MHXX	0000 0014520 MHYG	0000 0014521 MHBZ
0000 0014512 MHZZ	0000 0000273 HMEG	0000 0014527 HJ	0000 0014533 NAA
0000 0014534 HBB	0000 0014537 HBB	0000 0014535 HNZ	0000 0014541 NGX
0000 0014543 NGT	0000 0015004 HL	0000 0015003 NN	0000 0015021 NPLT
0000 0014610 NHUN	0000 0014740 NT	0000 0014536 NXB	0000 0014530 NXX
0000 0014542 NYG	0000 0014531 NYT	0000 0014544 NZB	0000 0003220 PAX
0000 0003451 PAY	0000 0003702 PAZ	0000 0014565 PER	0000 0004133 PPT
0000 0004364 PRL	0000 0002767 PNY	0000 0014500 O	0000 0014744 SPHT
0000 0014742 STE	0000 0000144 T	0000 0000285 TEN	0000 0014622 VELBB
0000 0014616 VLLXB	0000 0014617 VELYB	0000 0014620 VELZB	0000 0014560 WAREL
0000 0014551 WB	0000 0000350 WC	0000 0014555 WCD	0000 0014561 WCPHT
0000 0014602 WFBT	0000 0014603 WFGM	0000 0014577 WFX	0000 0014601 WZ
0000 0014615 WHT	0000 0014562 WINDS	0000 0014575 WINDZ	0000 0014576 WINDZ
0000 0014645 WA	0000 0014761 WVMN	0000 0014763 WUSD	0000 0014547 XCG
0000 0014710 XCPRS	0000 0014701 XMM	0000 0014550 XNL	0000 0014623 XM
0000 0015160 XAV	0000 0015006 XWVC	0000 0014647 XI	0000 0014726 YMPT
0000 0014624 YW	0000 0005046 Z	0000 0014727 ZMPT	0000 0014625 ZW

00100 1\* C THIS PROGRAM COMPUTES THE RESPONSE OF AN AXI-SYMMETRIC BUOY  
 00100 2\* C EXPOSED TO THE OCEAN ENVIRONMENT  
 00100 3\* C UNITS ARE IN FT\*,LB\*,SEC



DATE 230272 PAGE 6

## BUOY DYNAMICS

```

00137 62* 107 FORMAT(5F10.4)
00140 63* 108 FORMAT(2F10.4)
00141 64* 109 FORMAT(3F10.4)
00142 65* 112 FORMAT(4F8.2)
00143 66* 116 FORMAT(1F10.4,4F8.2)
00144 67* 117 FORMAT(1F8.4,11F8.2)
00145 68* 120 FORMAT(1F10.4)
00146 69* 121 FORMAT(1F20.4)
00147 70* 122 FORMAT(1F30.4)
00150 71* 123 FORMAT(1F40.4)
00151 72* 124 FORMAT(1F50.4)
00152 73* 127 FORMAT(6F10.4)
00152 74* C READ IN THE BUOY PARAMETERS
00152 75* C BUOY RADIUS, HT. OF C.OF G. FROM MOOR POINT AND THE LENGTH OF THE
00152 76* C MOOR POINT BELOW THE BOTTOM OF THE BUOY
00152 77* C READ 109,HR,XCG,XML
00153 78* C INERTIAS
00160 79* C READ 107,WB,MB,ALIN,BTIN,GMIN
00160 80* C WIND LIFT AND DRAG COEFFICIENTS AND AREAS
00167 81* C READ 107,WCD,WCL,WALEA,WAREL,WCPHT
00167 82* C
00167 83* C THE VISCOSITY OF THE WATER AT 40 DEG F
00176 84* MU=2.735E-5
00176 85* C
00176 86* C READ THE MEAN WIND SPEED AND DURATION CAUSING THE WIND WAVES
00177 87* C READ 108,WINDS,DUR
00203 88* C CALL KWAVE(WINDS,DUR,WHTM,PER,MONEG,AMP,PHS)
00203 89* C
00203 90* C THE CABLE PARAMETERS
00203 91* C THE CABLE LENGTHS BETWEEN ELEMENTS
00204 91* CLO(1)=53.0
00205 93* CLO(2)=47.0
00206 94* CLO(3)=50.0
00207 95* CLO(4)=145.0
00210 96* CSM(1)=2.08
00211 97* CSM(2)=8.54
00212 98* CSM(3)=20.96
00213 99* CHMT(1)=0.1975
00214 100* CHMT(2)=0.0
00215 101* CHMT(3)=0.666
00216 102* CHMN(1)=1.5362
00217 103* CHMN(2)=1.228
00220 104* CHMN(3)=2.908
00221 105* WC(1)=34.51
00222 106* WC(2)=254.2
00223 107* WC(3)=624.5
00224 108* DGT(1)=0.5942
00225 109* DGT(2)=0.940
00226 110* DGT(3)=1.10
00227 111* DGN(1)=3.142
00230 112* DGN(2)=8.75
00231 113* DGN(3)=6.49
00232 114* EAI=2.16E5
00233 115* EAI=EA1
00233 116* C THE WATER DEPTH
00234 117* DEEP=120.9
00234 118* C
00234 119* C THE CURRENTS IN THE WATER COLUMN

```



DATE 230272 PAGE 7

## BUOY DYNAMICS

```

00234 C      READ THE Y AND Z COMPONENTS OF THE SURFACE CURRENT
00235 READ 108,CYS,CZS
00236 C      IF THE CURRENT VARIES WITH DEPTH, INSERT THE FUNCTIONS FOR
00237 STRENGTH AND DIRECTION
00238 C
00239 C      FOR A UNIFORM CURRENT
00240 CYS=CYS
00241 CZS=CZS
00242 C
00243 C      THE WIND ACTING ON THE BUOY
00244 READ THE Y AND Z COMPONENTS OF THE MEAN WIND
00245 READ 108,WINDY,WINDZ
00246 WFX=-0.0034*WCL*WAREA*(WINDY**2+WINDZ**2)
00247 WFY=-0.0034*WCU*WAREA*WINDY*ABS(WINDY)
00248 WFZ=-0.0034*WCU*WAREA*WINDZ*ABS(WINDZ)
00249 WFBT=-WFZ*WCPHT
00250 WFGM=-WFX*WCPHT
00251 N=30
00252 K=0.005
00253 R=0.005
00254 K=0
00255 M=0
00256 NRUNE=1
00257 UO 440 I=1,612
00258 DATAS(I)=0.0
00259 DATBS(I)=0.0
00260 DATCS(I)=0.0
00261 DATDS(I)=0.0
00262 DATFS(I)=0.0
00263 C      THE INITIAL CONDITIONS
00264 C      ALL ACCELERATIONS AND VELOCITIES ARE ZERO
00265 DO 58 I=1,41,2
00266 D(I)=0.0
00267 Y(I)=0.0
00268 C      READ THE INITIAL BUOY DISPLACEMENTS - X,Y,Z
00269 READ 109,Y(2),Y(4),Y(6)
00270 C      THE INITIAL BUOY ANGLES ARE ZERO
00271 Y(8)=0.0
00272 Y(10)=0.0
00273 Y(12)=0.0
00274 C      READ THE INITIAL CABLE DISPLACEMENTS
00275 DO 53 I=14,32,6
00276 53 READ 109,Y(1),Y(1+2),Y(1+4)
00277 C      INPUTS AND OPERATIONS FOR THE POWER SPECTRA COMPUTATIONS
00278 500 CONTINUE
00279 A=0.0
00280 J=1
00281 DO 59 L=1,20*8
00282 ACX(L)=0.0
00283 ACY(L)=0.0
00284 ACZ(L)=0.0
00285 BP1(L)=0.0
00286 BP2(L)=0.0
00287 59 XW(L)=0.0
00288 L=1
00289 5 CONTINUE
00290 WHT=A*WHTM/(2.0*PER)
00291 177

```

DATE 230272 PAGE 8

## BUOY DYNAMICS

```

00342 178* IF(A*GE,(2.0*PER))WHT=HMTM
00344 179* VELXB=Y(1)
00345 180* VELYB=Y(3)
00346 181* VELZB=Y(5)
00347 182* VELDB=Y(9)
00350 183* VELGB=Y(11)
00350 184* THE WAVES
00350 185* FOR A SINGLE TRAIN OF WAVES, ASSUME THEY ARE COMING IN ON THE
00350 186* Z AXIS
00351 187* XW=0.0
00352 188* YW=0.0
00353 189* ZW=0.0
00354 190* ALW=0.0
00355 191* BTW=0.0
00356 192* GHW=0.0
00357 193* DXW=0.0
00360 194* DYW=0.0
00361 195* DZW=0.0
00362 196* DALW=0.0
00363 197* DBTW=0.0
00364 198* DGMW=0.0
00365 199* DOXW=0.0
00366 200* DOYW=0.0
00367 201* DOZW=0.0
00370 202* DOALW=0.0
00371 203* DOBTW=0.0
00372 204* DOGMW=0.0
00373 205* DO 14 1=1.9
00376 206* WK=(MOMEG(1)*2)/32.2
00377 207* ANG=A*MOMEG(1)*PHS(1)
00400 208* XW=XW+AMP(1)*SIN(ANG)
00401 209* ZW=ZW+AMP(1)*COS(ANG)
00402 210* DTW=BTW+K*AMP(1)*COS(ANG)
00403 211* DXW=DXW+MOMEG(1)*AMP(1)*COS(ANG)
00404 212* DZW=DZW+MOMEG(1)*AMP(1)*SIN(ANG)
00405 213* DBTW=DBTW+WK*MOMEG(1)*AMP(1)*SIN(ANG)
00406 214* DOXW=DOXW+(MOMEG(1)*2)*AMP(1)*SIN(ANG)
00407 215* DOZW=DOZW+(MOMEG(1)*2)*AMP(1)*COS(ANG)
00410 216* DOBTW=DOBTW-WK*(MOMEG(1)*2)*AMP(1)*COS(ANG)
00410 217* THE BUOY MOTIONS RELATIVE TO THE WATER MASS
00410 218* DISPLACEMENTS
00410 219* X1=Y(2)-XW
00412 220* BT1=Y(10)-BTW
00413 221* GM1=Y(12)-GMW
00414 222* VELOCITIES
00414 223* DX1=Y(1)-DXW
00415 224* DY1=Y(3)-DYW
00416 225* DZ1=Y(5)-DZW
00417 226* DAL1=Y(7)-DALW
00420 227* DGM1=Y(11)-DGMW
00421 228* DBT1=Y(9)-DBTW
00422 229* DGM1=Y(11)
00423 230* WATER MASS VELOCITIES RELATIVE TO THE BUOY INCLUDING CURRENTS
00423 231* DX2=DX1
00424 232* DY2=DY1-CY
00425 233* DZ2=DZ1-CZ
00426 235*

```

DATE 230272 PAGE 9

## BUOY DYNAMICS

```

00*27 230* DAL2=DAL1
00*30 237* DBT2=UBT1
00*31 238* DGM2=DGM1
00*31 239* C
00*31 240* C
00*31 241* C
00*32 242* THE BUOYANCY FORCES AND MOMENTS
00*33 243* HXCG=X1-XHL
00*34 244* CALL TORBU(M,BT1,BXX,BB8,BXB,BBX)
00*35 245* CALL TORBU(M,GML,BXX,BGG,BXG,BGX)
00*35 246* 30 CONTINUE
00*35 247* C
00*35 248* C
00*35 249* C
00*36 250* THE HYDRODYNAMIC MASSES AND MOMENTS OF INERTIA
00*37 251* THE DIMENSIONLESS FREQUENCY
00*38 252* FR=(16.2832/PER)**2*(BR/32.2
00*39 253* BLAMB=SQRT(6.25/(PER*MU))
00*40 254* BA=BLAMB*BR
00*41 255* HYDRODYNAMIC FORCE MOMENT ARM
00*42 256* XHM=4.16
00*43 257* HEAVE
00*44 258* IF(FR.GE.0.2)GO TO 31
00*45 259* CHX=2.31
00*46 260* GO TO 33
00*47 261* 31 IF(FR.GE.2.4)GO TO 32
00*48 262* CHX=1.35725*(FR*(-.330597))
00*49 263* GO TO 33
00*50 264* 32 CHX=1.0
00*51 265* SWAY-SURGE
00*52 266* 33 CMZ=CMY
00*53 267* MXX=1.988*(BR**3)*CHX
00*54 268* MYY=1.988*(BR**3)*CMY*U.8045)
00*55 269* MZZ=MYY
00*56 270* YAW
00*57 271* MAAA=16.65*(BR**5)*(1.0*BA)/(1.0+2.0*BA+2.0*(BA**2))
00*58 272* PITCH AND ROLL
00*59 273* MBBB=MZZ*(XHM**2)
00*60 274* MGGG=MBBB
00*61 275* CROSS-COUPLED HYDROMASSES
00*62 276* MBBX=0.0
00*63 277* MGBX=0.0
00*64 278* MXXB=0.0
00*65 279* MXXG=0.0
00*66 280* MYYG=-MYY*XHM
00*67 281* MZZB=-MYYG
00*68 282* MGBZ=MZZB
00*69 283* MGY=MYYG
00*70 284* C
00*71 285* C
00*72 286* THE DAMPING DUE TO WAVE GENERATION
00*73 287* HEAVE
00*74 288* IF(FR.GE.0.8)GO TO 41
00*75 289* CHXX=FR/10.132617*0.873644*FR)
00*76 290* GO TO 42
00*77 291* 41 CNXX=1.2476*EXP(-0.37376*FR)
00*78 292* 42 CNY=0.14
00*79 293* 43 NXX=1.988*FR*(BR**3)*CNXX
00*80 294* NYY=1.988*FR*(BR**3)*CNY
00*81 295*

```

DATE 230272 PAGE 10

BUOY DYNAMICS

```

00503 294*  NZZENY
00504 295*  PITCH AND ROLL
00505 296*  NAA=4.195*PI*(BR**3)*(3.0+6.0*BA+6.0*(BA**2)+2.0*(BA**3))
00506 297*  1/(1.0+2.0*BA+2.0*(BA**2))
00507 298*  NBB=NAA+NZZ*((1.282-0.5*H)**2)
00508 299*  NGG=NBB
00509 300*  CROSS COUPLED WAVE DAMPING
00510 301*  NXB=0.0
00511 302*  NBY=0.0
00512 303*  NXG=0.0
00513 304*  NYG=0.0
00514 305*  NYG=-NYA*(1.282-0.5*H)
00515 306*  NZB=-NYG
00516 307*  NBZ=NZB
00517 308*  NGY=NYG
00518 309*  C
00519 310*  C
00520 311*  THE VISCOUS DAMPING AND DRAG
00521 312*  AREAS
00522 313*  ARXX=3.1416*(BR**2)
00523 314*  DGY=15.5
00524 315*  DGZ=15.6
00525 316*  DGA=0.0
00526 317*  DGB=0.0
00527 318*  DGG=0.0
00528 319*  XCPRS=3.25
00529 320*  CROSS-COUPLED VISCOUS DRAG
00530 321*  DGYG=DGY*(XCPRS**2)
00531 322*  DGZG=DGYG
00532 323*  DGGG=DGG
00533 324*  DGGY=DGYG
00534 325*  C
00535 326*  TENSIONS AND FORCES FOR THE 3 LUMP MASS CABLE MODEL
00536 327*  THE FIRST ELEMENT IS CABLE , THE LAST TWO ARE CHAIN
00537 328*  EAE=1
00538 329*  CABR=EA/CLO(1)
00539 330*  XMP1=Y(2)+XCG*COY(Y(10))*COY(Y(12))
00540 331*  YMP1=Y(4)-XCG*COY(Y(10))*SIN(Y(12))
00541 332*  ZMP1=Y(6)+XCG*SIN(Y(10))*COY(Y(12))
00542 333*  CL=SQRT((XMP1-Y(14))**2+((YMP1-Y(16))**2+((ZMP1-Y(18))**2))
00543 334*  TEN(1)=CABR*(CL-CLO(1))
00544 335*  IF(TEN(1).LE.0)TEN(1)=0.0
00545 336*  T(4)=TEN(1)*Y(14)-XMP1/CL
00546 337*  T(5)=TEN(1)*Y(16)-YMP1/CL
00547 338*  T(6)=TEN(1)*Y(18)-ZMP1/CL
00548 339*  ADD 165 LBS. TO ACCOUNT FOR THE CHAINS UNDER THE BUOY
00549 340*  FX=T(4)+165.0
00550 341*  FY=T(5)
00551 342*  FZ=T(6)
00552 343*  FAL=0.0
00553 344*  FBT=-XCG*(-FZ*COY(Y(10))*COY(Y(12))+FX*SIN(Y(10))*COY(Y(12)))
00554 345*  FGM=-XCG*(FY*COY(Y(10))*COY(Y(12))+FX*SIN(Y(12))*COY(Y(10)))
00555 346*  DO 71 I=13,25,6
00556 347*  KI=((I-1)/2)-2
00557 348*  NT=((I-1)/6)
00558 349*  NP=NT-1
00559 350*  CL=SQRT(((Y(I+1)-Y(I+7))**2+((Y(I+3)-Y(I+9))**2)+
00560 351*  1*((Y(I+5)-Y(I+11))**2))

```

DATE 230272 PAGE 11

## BUOY DYNAMICS

```

00564 352* 73 CABK=EA/CLO(NT)
00565 353* TEN(NT)=CABK*(CL-CLO(NT))
00566 354* IF(TEN(NT).LE.0)TEN(NT)=0.0
00567 355* C THE TENSION COMPONENTS
00568 356* T(K1+3)=TEN(NT)*(Y(I+7)-Y(I+1))/CL
00569 357* T(K1+4)=TEN(NT)*(Y(I+9)-Y(I+3))/CL
00570 358* T(K1+5)=TEN(NT)*(Y(I+11)-Y(I+5))/CL
00571 359* C THE SINES AND COSINES OF THE CABLE ANGLES
00572 360* STHE=(Y(I+11)-Y(I+5))/SQRT((Y(I+1)-Y(I+7))**2)
00573 361* 1+(Y(I+5)-Y(I+1))/SQRT((Y(I+1)-Y(I+7))**2)
00574 362* CTHE=(Y(I+7)-Y(I+1))/SQRT((Y(I+1)-Y(I+7))**2)
00575 363* 1+(Y(I+5)-Y(I+1))/SQRT((Y(I+1)-Y(I+7))**2)
00576 364* SPHI=(Y(I+9)-Y(I+3))/CL
00577 365* CPHI=SQRT((Y(I+1)-Y(I+7))**2)+(Y(I+5)-Y(I+1))**2)/CL
00578 366* CUR=Y(I)*CPHI*CTHE+(Y(I+2)-CY)*SPHI*(Y(I+4)-CZ)*CPHI*STHE
00579 367* CVR=Y(I)*SPHI*CTHE+(Y(I+2)-CY)*CPHI*(Y(I+4)-CZ)*SPHI*STHE
00580 368* CWR=Y(I)*STHE*(Y(I+4)-CZ)*CTHE
00581 369* C CABLE MASSES
00582 370* CM(K1)=CSM(NP)*CHMT(NP)*CPHI*CTHE
00583 371* CM(K1+1)=CSM(NP)*CHMT(NP)*CPHI
00584 372* CM(K1+2)=CSM(NP)*CHMT(NP)*CTHE
00585 373* C CABLE LOADING FUNCTIONS
00586 374* CLF(K1)=DGT(NP)*CPHI*CTHE*CUR*ABS(CUR)-DGN(NP)*SPHI*CTHE*CVR*
00587 375* 1*ABS(CVR)-DGN(NP)*STHE*CUR*ABS(CUR)-YC(NP)
00588 376* CLF(K1+1)=DGT(NP)*SPHI*CTHE*CUR*ABS(CUR)-DGN(NP)*CPHI*CTHE*ABS(CVR)
00589 377* 71 CLF(K1+2)=DGT(NP)*CPHI*STHE*CUR*ABS(CUR)-DGN(NP)*SPHI*STHE
00590 378* 1*CVR*ABS(CVR)+DGN(NP)*CTHE*CUR*ABS(CVR)
00591 379* 50 CONTINUE
00592 380* DDY1=(Y(I)-VELXB)/R
00593 381* DDY2=(Y(I)-VELYB)/R
00594 382* DDZ1=(Y(I)-VELZB)/R
00595 383* DDY1=(Y(I)-VELXB)/R
00596 384* DDGM1=(Y(I)-VELGB)/R
00597 385* DDY1=0.0
00598 386* DDZ1=0.0
00599 387* DDY1=0.0
00600 388* DDZ1=0.0
00601 389* DDGM1=0.0
00602 390* C THE EQUATIONS OF MOTION FOR THE BUOY
00603 391* HEAVE - X MOTION
00604 392* D(1)=(WB-BXX-BXB-BXG+MHXX+DDY1-MHXB+DDBT1-MHXB+DDGM1-MHXX+DDX1
00605 393* 1-MHXB+DDBT1-MHXB+DDGM1-DDGX+DDX2)*ABS(DDX2)+MFX+FY)/(MB+MHXX)
00606 394* D(2)=Y(I)
00607 395* C SWAY - Y MOTION
00608 396* D(3)=(MHYY+DDY1-MHYY+DDGM1-MHYY+DDY1-MHYY+DDGM1-DDGY+DY2)*ABS(DY2)
00609 397* 1-DDGY+DDGM1-DDGY+DY2)/(MB+MHYY)
00610 398* D(4)=Y(I)
00611 399* C SURGE - Z MOTION
00612 400* D(5)=(MHZZ+DDZ1-MHZZ+DDZ1-MHZZ+DDZ1-MHZZ+DDZ1-MHZZ+DDZ1-MHZZ+DDZ1
00613 401* 1-DDZB+DDZ1-MHZZ+DDZ1-MHZZ+DDZ1-MHZZ+DDZ1-MHZZ+DDZ1-MHZZ+DDZ1
00614 402* D(6)=Y(I)
00615 403* C YAW - ALPHA MOTION
00616 404* D(7)=(MHAA+DDAL1-MHAA+DDAL1-MHAA+DDAL1-MHAA+DDAL1-MHAA+DDAL1-MHAA+DDAL1
00617 405* 1-MHAA+DDAL1-MHAA+DDAL1-MHAA+DDAL1-MHAA+DDAL1-MHAA+DDAL1-MHAA+DDAL1
00618 406* D(8)=Y(I)
00619 407* C
00620 408* C
00621 409*

```

DATE 230272 PAGE 12

## BUOY DYNAMICS

```

00633 410* D(8)=Y(7)
00633 411* C
00633 412* C
00633 413* PITCH - BETA MOTION
00634 414* D(9)=(-BXX-BB8-MHBX*DDX1-MHBZ*DDZ1+MHB8*DDBT-MBX*DX1-NBB*DBT1
00634 415* 1 -M2Z*O21-DGB2*O22*ABS(O22)-DGB8*DBT2*ABS(DBT2)+WBT*FBT)/
00634 416* 2 (BTIN+MHB8)
00635 417* D(10)=Y(9)
00635 418* C
00635 419* C
00636 420* ROLL- GAMMA MOTION
00636 421* D(11)=(-BGX-BUG-MHGX*DDX1-NHGY*DDY1+MHGG*DDGM-MGX*DX1-NGY*DY1
00637 422* 1 -MGG*DDM1-DGY*DY2*ABS(O22)-DGGG*DDGM2*ABS(DGM2)+WFGM*FGM)/
00637 423* 2 (GMIN+MHGG)
00637 424* D(12)=Y(11)
00637 425* C
00637 426* C
00637 427* EQUATIONS OF MOTION FOR A 3 LUMP MODEL OF THE CABLE
00637 428* DO 81 I=1,25,6
00637 429* KI=((I-1)/2)-2
00637 430* ELEMENT X MOTION
00637 431* D(1)=(-T(KI)+T(KI+3)-CLF(KI))/CM(KI)
00637 432* D(1+1)=Y(1)
00637 433* C
00637 434* C
00637 435* ELEMENT Y MOTION
00637 436* D(1+2)=(-T(KI+1)+T(KI+4)-CLF(KI+1))/CM(KI+1)
00637 437* D(1+3)=Y(1+2)
00637 438* C
00637 439* C
00637 440* ELEMENT 2 MOTION
00637 441* D(1+4)=(-T(KI+2)+T(KI+5)-CLF(KI+2))/CM(KI+2)
00637 442* D(1+5)=Y(1+4)
00637 443* C
00637 444* C
00637 445* CALL RUNGE(N,Y,D,A,R,M,K)
00637 446* GO TO (50,40),K
00637 447* 40 ALPHA=57.4*Y(8)
00637 448* BETA=57.4*Y(10)
00637 449* GAMMA=57.4*Y(12)
00637 450* C
00637 451* IF(A,LE,5.0)GO TO 52
00637 452* IF(J,EQ,12)GO TO 51
00637 453* J=J+1
00637 454* GO TO 52
00637 455* 51 CONTINUE
00637 456* J=1
00637 457* XWV(L)=XW
00637 458* ACX(L)=D(1)
00637 459* ACY(L)=D(3)
00637 460* ACZ(L)=D(5)
00637 461* BPIT(L)=Y(10)
00637 462* BROL(L)=Y(12)
00637 463* L=L+2
00637 464* 52 CONTINUE
00637 465* C
00637 466* C
00637 467* INSTABILITY LIMITER
00637 468* DO 60 I=1,30
00637 469* 60 IF(Y(I),GT,10000.0)GO TO 92
00637 470* THE CABLE ELEMENTS CANT SINK THRU THE BOTTOM
00637 471* DO 218 I=1,26,6
00637 472* 218 IF(Y(I),GE,DEEPIY(I)=DEEP
00637 473* IF(L,EQ,2049)GO TO 88
00637 474* GO TO 5
00637 475* 88 CONTINUE
00637 476* C
00637 477* C
00637 478* COMPUTE SIMPLE STATISTICAL PROPERTIES
00637 479* C
00637 480* C
00637 481* C
00637 482* C
00637 483* C
00637 484* C
00637 485* C
00637 486* C
00637 487* C
00637 488* C
00637 489* C
00637 490* C
00637 491* C
00637 492* C
00637 493* C
00637 494* C
00637 495* C
00637 496* C
00637 497* C
00637 498* C
00637 499* C
00637 500* C
00637 501* C
00637 502* C
00637 503* C
00637 504* C
00637 505* C
00637 506* C
00637 507* C
00637 508* C
00637 509* C
00637 510* C
00637 511* C
00637 512* C
00637 513* C
00637 514* C
00637 515* C
00637 516* C
00637 517* C
00637 518* C
00637 519* C
00637 520* C
00637 521* C
00637 522* C
00637 523* C
00637 524* C
00637 525* C
00637 526* C
00637 527* C
00637 528* C
00637 529* C
00637 530* C
00637 531* C
00637 532* C
00637 533* C
00637 534* C
00637 535* C
00637 536* C
00637 537* C
00637 538* C
00637 539* C
00637 540* C
00637 541* C
00637 542* C
00637 543* C
00637 544* C
00637 545* C
00637 546* C
00637 547* C
00637 548* C
00637 549* C
00637 550* C
00637 551* C
00637 552* C
00637 553* C
00637 554* C
00637 555* C
00637 556* C
00637 557* C
00637 558* C
00637 559* C
00637 560* C
00637 561* C
00637 562* C
00637 563* C
00637 564* C
00637 565* C
00637 566* C
00637 567* C
00637 568* C
00637 569* C
00637 570* C
00637 571* C
00637 572* C
00637 573* C
00637 574* C
00637 575* C
00637 576* C
00637 577* C
00637 578* C
00637 579* C
00637 580* C
00637 581* C
00637 582* C
00637 583* C
00637 584* C
00637 585* C
00637 586* C
00637 587* C
00637 588* C
00637 589* C
00637 590* C
00637 591* C
00637 592* C
00637 593* C
00637 594* C
00637 595* C
00637 596* C
00637 597* C
00637 598* C
00637 599* C
00637 600* C
00637 601* C
00637 602* C
00637 603* C
00637 604* C
00637 605* C
00637 606* C
00637 607* C
00637 608* C
00637 609* C
00637 610* C
00637 611* C
00637 612* C
00637 613* C
00637 614* C
00637 615* C
00637 616* C
00637 617* C
00637 618* C
00637 619* C
00637 620* C
00637 621* C
00637 622* C
00637 623* C
00637 624* C
00637 625* C
00637 626* C
00637 627* C
00637 628* C
00637 629* C
00637 630* C
00637 631* C
00637 632* C
00637 633* C
00637 634* C
00637 635* C
00637 636* C
00637 637* C
00637 638* C
00637 639* C
00637 640* C
00637 641* C
00637 642* C
00637 643* C
00637 644* C
00637 645* C
00637 646* C
00637 647* C
00637 648* C
00637 649* C
00637 650* C
00637 651* C
00637 652* C
00637 653* C
00637 654* C
00637 655* C
00637 656* C
00637 657* C
00637 658* C
00637 659* C
00637 660* C
00637 661* C
00637 662* C
00637 663* C
00637 664* C
00637 665* C
00637 666* C
00637 667* C
00637 668* C
00637 669* C
00637 670* C
00637 671* C
00637 672* C
00637 673* C
00637 674* C
00637 675* C
00637 676* C
00637 677* C
00637 678* C
00637 679* C
00637 680* C
00637 681* C
00637 682* C
00637 683* C
00637 684* C
00637 685* C
00637 686* C
00637 687* C
00637 688* C
00637 689* C
00637 690* C
00637 691* C
00637 692* C
00637 693* C
00637 694* C
00637 695* C
00637 696* C
00637 697* C
00637 698* C
00637 699* C
00637 700* C
00637 701* C
00637 702* C
00637 703* C
00637 704* C
00637 705* C
00637 706* C
00637 707* C
00637 708* C
00637 709* C
00637 710* C
00637 711* C
00637 712* C
00637 713* C
00637 714* C
00637 715* C
00637 716* C
00637 717* C
00637 718* C
00637 719* C
00637 720* C
00637 721* C
00637 722* C
00637 723* C
00637 724* C
00637 725* C
00637 726* C
00637 727* C
00637 728* C
00637 729* C
00637 730* C
00637 731* C
00637 732* C
00637 733* C
00637 734* C
00637 735* C
00637 736* C
00637 737* C
00637 738* C
00637 739* C
00637 740* C
00637 741* C
00637 742* C
00637 743* C
00637 744* C
00637 745* C
00637 746* C
00637 747* C
00637 748* C
00637 749* C
00637 750* C
00637 751* C
00637 752* C
00637 753* C
00637 754* C
00637 755* C
00637 756* C
00637 757* C
00637 758* C
00637 759* C
00637 760* C
00637 761* C
00637 762* C
00637 763* C
00637 764* C
00637 765* C
00637 766* C
00637 767* C
00637 768* C
00637 769* C
00637 770* C
00637 771* C
00637 772* C
00637 773* C
00637 774* C
00637 775* C
00637 776* C
00637 777* C
00637 778* C
00637 779* C
00637 780* C
00637 781* C
00637 782* C
00637 783* C
00637 784* C
00637 785* C
00637 786* C
00637 787* C
00637 788* C
00637 789* C
00637 790* C
00637 791* C
00637 792* C
00637 793* C
00637 794* C
00637 795* C
00637 796* C
00637 797* C
00637 798* C
00637 799* C
00637 800* C
00637 801* C
00637 802* C
00637 803* C
00637 804* C
00637 805* C
00637 806* C
00637 807* C
00637 808* C
00637 809* C
00637 810* C
00637 811* C
00637 812* C
00637 813* C
00637 814* C
00637 815* C
00637 816* C
00637 817* C
00637 818* C
00637 819* C
00637 820* C
00637 821* C
00637 822* C
00637 823* C
00637 824* C
00637 825* C
00637 826* C
00637 827* C
00637 828* C
00637 829* C
00637 830* C
00637 831* C
00637 832* C
00637 833* C
00637 834* C
00637 835* C
00637 836* C
00637 837* C
00637 838* C
00637 839* C
00637 840* C
00637 841* C
00637 842* C
00637 843* C
00637 844* C
00637 845* C
00637 846* C
00637 847* C
00637 848* C
00637 849* C
00637 850* C
00637 851* C
00637 852* C
00637 853* C
00637 854* C
00637 855* C
00637 856* C
00637 857* C
00637 858* C
00637 859* C
00637 860* C
00637 861* C
00637 862* C
00637 863* C
00637 864* C
00637 865* C
00637 866* C
00637 867* C
00637 868* C
00637 869* C
00637 870* C
00637 871* C
00637 872* C
00637 873* C
00637 874* C
00637 875* C
00637 876* C
00637 877* C
00637 878* C
00637 879* C
00637 880* C
00637 881* C
00637 882* C
00637 883* C
00637 884* C
00637 885* C
00637 886* C
00637 887* C
00637 888* C
00637 889* C
00637 890* C
00637 891* C
00637 892* C
00637 893* C
00637 894* C
00637 895* C
00637 896* C
00637 897* C
00637 898* C
00637 899* C
00637 900* C
00637 901* C
00637 902* C
00637 903* C
00637 904* C
00637 905* C
00637 906* C
00637 907* C
00637 908* C
00637 909* C
00637 910* C
00637 911* C
00637 912* C
00637 913* C
00637 914* C
00637 915* C
00637 916* C
00637 917* C
00637 918* C
00637 919* C
00637 920* C
00637 921* C
00637 922* C
00637 923* C
00637 924* C
00637 925* C
00637 926* C
00637 927* C
00637 928* C
00637 929* C
00637 930* C
00637 931* C
00637 932* C
00637 933* C
00637 934* C
00637 935* C
00637 936* C
00637 937* C
00637 938* C
00637 939* C
00637 940* C
00637 941* C
00637 942* C
00637 943* C
00637 944* C
00637 945* C
00637 946* C
00637 947* C
00637 948* C
00637 949* C
00637 950* C
00637 951* C
00637 952* C
00637 953* C
00637 954* C
00637 955* C
00637 956* C
00637 957* C
00637 958* C
00637 959* C
00637 960* C
00637 961* C
00637 962* C
00637 963* C
00637 964* C
00637 965* C
00637 966* C
00637 967* C
00637 968* C
00637 969* C
00637 970* C
00637 971* C
00637 972* C
00637 973* C
00637 974* C
00637 975* C
00637 976* C
00637 977* C
00637 978* C
00637 979* C
00637 980* C
00637 981* C
00637 982* C
00637 983* C
00637 984* C
00637 985* C
00637 986* C
00637 987* C
00637 988* C
00637 989* C
00637 990* C
00637 991* C
00637 992* C
00637 993* C
00637 994* C
00637 995* C
00637 996* C
00637 997* C
00637 998* C
00637 999* C
00637 1000* C

```

DATE 230272 PAGE 13

## BUOY DYNAMICS

```

00720 4000 CALL DSTAT(XAV,WVMN,WVVR,WVSD)
00721 4001 CALL DSTAT(ACX,AXMN,AXVR,AXSD)
00722 4002 CALL DSTAT(ACY,AYMN,AYVR,AYSD)
00723 4003 CALL DSTAT(ACZ,AZMN,AZVR,AZSD)
00724 4004 CALL DSTAT(BPIT,BPMN,BPVR,BPSD)
00725 4005 CALL DSTAT(BROL,BRMN,BRVR,BRSD)
00726 4006 #RITE(4,127)WVMN,AXMN,AYMN,AZMN,BPMN,BPMN
00727 4007 #RITE(4,127)WVSD,AXSD,AYSD,AZSD,BPSD,BPSD
00728 4008 #RITE(4,127)WVVR,AXVR,AYVR,AZVR,BPVR,BPVR
00729 4009 SMOOTH THE MOTION DATA TO MINIMIZE ALIASING
00730 4010 DO 433 L=5,2043,2
00731 4011 XWV(L)=(XWV(L-4)+XWV(L-2)+XWV(L)+XWV(L+2)+XWV(L+4))/5.0
00732 4012 ACX(L)=(ACX(L-4)+ACX(L-2)+ACX(L)+ACX(L+2)+ACX(L+4))/5.0
00733 4013 ACY(L)=(ACY(L-4)+ACY(L-2)+ACY(L)+ACY(L+2)+ACY(L+4))/5.0
00734 4014 ACZ(L)=(ACZ(L-4)+ACZ(L-2)+ACZ(L)+ACZ(L+2)+ACZ(L+4))/5.0
00735 4015 BPIT(L)=(BPIT(L-4)+BPIT(L-2)+BPIT(L)+BPIT(L+2)+BPIT(L+4))/5.0
00736 4016 BROL(L)=(BROL(L-4)+BROL(L-2)+BROL(L)+BROL(L+2)+BROL(L+4))/5.0
00737 4017 COMPUTE POWER SPECTRA
00738 4018 B1N=1024
00739 4019 Q=B1N
00740 4020 CALL COSINE(COSI,B1N)
00741 4021 CALL GNSCR(ISCR,Q)
00742 4022
00743 4023
00744 4024 WAVE HEIGHT
00745 4025 CALL FFOUR(DATB,COSI,ISCR,Q,B1N,-1)
00746 4026 CALL FFOUR(DATC,COSI,ISCR,Q,B1N,-1)
00747 4027 CALL FFOUR(DATD,COSI,ISCR,Q,B1N,-1)
00748 4028 CALL FFOUR(DATE,COSI,ISCR,Q,B1N,-1)
00749 4029 CALL FFOUR(DATF,COSI,ISCR,Q,B1N,-1)
00750 4030 USE 8 ENSEMBLE AVERAGES
00751 4031 AVERAGE THE COEFFICIENTS OVER 8 RUNS
00752 4032 DO 410 I=1,306
00753 4033 DATAS(I)=DATAS(I)+DATA(I)
00754 4034 DATBS(I)=DATBS(I)+DATB(I)
00755 4035 DATCS(I)=DATCS(I)+DATC(I)
00756 4036 DATDS(I)=DATDS(I)+DATD(I)
00757 4037 DATES(I)=DATES(I)+DATE(I)
00758 4038 DATFS(I)=DATFS(I)+DATF(I)
00759 4039 IF(NRUN.EQ.8)GO TO 450
00760 4040 NRUN=NRUN+1
00761 4041 PHS(10)=PHS(1)
00762 4042 DO 404 NN=1,9
00763 4043 NL=NN+1
00764 4044 PHS(NN1)=PHS(NL)
00765 4045 GO TO 500
00766 4046 DO 411 I=1,306
00767 4047 DATA(I)=DATAS(I)/8.0
00768 4048 DATB(I)=DATBS(I)/8.0
00769 4049 DATC(I)=DATCS(I)/8.0
00770 4050 DATD(I)=DATDS(I)/8.0
00771 4051 DATE(I)=DATES(I)/8.0
00772 4052 DATF(I)=DATFS(I)/8.0
00773 4053 IP=I/2
00774 4054 FRQ(IP)=I/61.44
00775 4055 XWVC=(DATA(I-3)+DATA(I-2)+DATA(I-1)+DATA(I)
00776 4056 +DATA(I+1)+DATA(I+2)+DATA(I+3))/7.0
00777 4057
00778 4058
00779 4059
00780 4060
00781 4061
00782 4062
00783 4063
00784 4064
00785 4065
00786 4066
00787 4067
00788 4068
00789 4069
00790 4070
00791 4071
00792 4072
00793 4073
00794 4074
00795 4075
00796 4076
00797 4077
00798 4078
00799 4079
00800 4080
00801 4081
00802 4082
00803 4083
00804 4084
00805 4085
00806 4086
00807 4087
00808 4088
00809 4089
00810 4090
00811 4091
00812 4092
00813 4093
00814 4094
00815 4095
00816 4096
00817 4097
00818 4098
00819 4099
00820 4100
00821 4101
00822 4102
00823 4103
00824 4104
00825 4105
00826 4106
00827 4107
00828 4108
00829 4109
00830 4110
00831 4111
00832 4112
00833 4113
00834 4114
00835 4115
00836 4116
00837 4117
00838 4118
00839 4119
00840 4120
00841 4121
00842 4122
00843 4123
00844 4124
00845 4125
00846 4126
00847 4127
00848 4128
00849 4129
00850 4130
00851 4131
00852 4132
00853 4133
00854 4134
00855 4135
00856 4136
00857 4137
00858 4138
00859 4139
00860 4140
00861 4141
00862 4142
00863 4143
00864 4144
00865 4145
00866 4146
00867 4147
00868 4148
00869 4149
00870 4150
00871 4151
00872 4152
00873 4153
00874 4154
00875 4155
00876 4156
00877 4157
00878 4158
00879 4159
00880 4160
00881 4161
00882 4162
00883 4163
00884 4164
00885 4165
00886 4166
00887 4167
00888 4168
00889 4169
00890 4170
00891 4171
00892 4172
00893 4173
00894 4174
00895 4175
00896 4176
00897 4177
00898 4178
00899 4179
00900 4180
00901 4181
00902 4182
00903 4183
00904 4184
00905 4185
00906 4186
00907 4187
00908 4188
00909 4189
00910 4190
00911 4191
00912 4192
00913 4193
00914 4194
00915 4195
00916 4196
00917 4197
00918 4198
00919 4199
00920 4200
00921 4201
00922 4202
00923 4203
00924 4204
00925 4205
00926 4206
00927 4207
00928 4208
00929 4209
00930 4210
00931 4211
00932 4212
00933 4213
00934 4214
00935 4215
00936 4216
00937 4217
00938 4218
00939 4219
00940 4220
00941 4221
00942 4222
00943 4223
00944 4224
00945 4225
00946 4226
00947 4227
00948 4228
00949 4229
00950 4230
00951 4231
00952 4232
00953 4233
00954 4234
00955 4235
00956 4236
00957 4237
00958 4238
00959 4239
00960 4240
00961 4241
00962 4242
00963 4243
00964 4244
00965 4245
00966 4246
00967 4247
00968 4248
00969 4249
00970 4250
00971 4251
00972 4252
00973 4253
00974 4254
00975 4255
00976 4256
00977 4257
00978 4258
00979 4259
00980 4260
00981 4261
00982 4262
00983 4263
00984 4264
00985 4265
00986 4266
00987 4267
00988 4268
00989 4269
00990 4270
00991 4271
00992 4272
00993 4273
00994 4274
00995 4275
00996 4276
00997 4277
00998 4278
00999 4279
01000 4280
01001 4281
01002 4282
01003 4283
01004 4284
01005 4285
01006 4286
01007 4287
01008 4288
01009 4289
01010 4290
01011 4291
01012 4292
01013 4293
01014 4294
01015 4295
01016 4296
01017 4297
01018 4298
01019 4299
01020 4300
01021 4301
01022 4302
01023 4303
01024 4304
01025 4305
01026 4306
01027 4307
01028 4308
01029 4309
01030 4310
01031 4311
01032 4312
01033 4313
01034 4314
01035 4315
01036 4316
01037 4317
01038 4318
01039 4319
01040 4320
01041 4321
01042 4322
01043 4323
01044 4324
01045 4325
01046 4326
01047 4327
01048 4328
01049 4329
01050 4330
01051 4331
01052 4332
01053 4333
01054 4334
01055 4335
01056 4336
01057 4337
01058 4338
01059 4339
01060 4340
01061 4341
01062 4342
01063 4343
01064 4344
01065 4345
01066 4346
01067 4347
01068 4348
01069 4349
01070 4350
01071 4351
01072 4352
01073 4353
01074 4354
01075 4355
01076 4356
01077 4357
01078 4358
01079 4359
01080 4360
01081 4361
01082 4362
01083 4363
01084 4364
01085 4365
01086 4366
01087 4367
01088 4368
01089 4369
01090 4370
01091 4371
01092 4372
01093 4373
01094 4374
01095 4375
01096 4376
01097 4377
01098 4378
01099 4379
01100 4380
01101 4381
01102 4382
01103 4383
01104 4384
01105 4385
01106 4386
01107 4387
01108 4388
01109 4389
01110 4390
01111 4391
01112 4392
01113 4393
01114 4394
01115 4395
01116 4396
01117 4397
01118 4398
01119 4399
01120 4400
01121 4401
01122 4402
01123 4403
01124 4404
01125 4405
01126 4406
01127 4407
01128 4408
01129 4409
01130 4410
01131 4411
01132 4412
01133 4413
01134 4414
01135 4415
01136 4416
01137 4417
01138 4418
01139 4419
01140 4420
01141 4421
01142 4422
01143 4423
01144 4424
01145 4425
01146 4426
01147 4427
01148 4428
01149 4429
01150 4430
01151 4431
01152 4432
01153 4433
01154 4434
01155 4435
01156 4436
01157 4437
01158 4438
01159 4439
01160 4440
01161 4441
01162 4442
01163 4443
01164 4444
01165 4445
01166 4446
01167 4447
01168 4448
01169 4449
01170 4450
01171 4451
01172 4452
01173 4453
01174 4454
01175 4455
01176 4456
01177 4457
01178 4458
01179 4459
01180 4460
01181 4461
01182 4462
01183 4463
01184 4464
01185 4465
01186 4466
01187 4467
01188 4468
01189 4469
01190 4470
01191 4471
01192 4472
01193 4473
01194 4474
01195 4475
01196 4476
01197 4477
01198 4478
01199 4479
01200 4480
01201 4481
01202 4482
01203 4483
01204 4484
01205 4485
01206 4486
01207 4487
01208 4488
01209 4489
01210 4490
01211 4491
01212 4492
01213 4493
01214 4494
01215 4495
01216 4496
01217 4497
01218 4498
01219 4499
01220 4500
01221 4501
01222 4502
01223 4503
01224 4504
01225 4505
01226 4506
01227 4507
01228 4508
01229 4509
01230 4510
01231 4511
01232 4512
01233 4513
01234 4514
01235 4515
01236 4516
01237 4517
01238 4518
01239 4519
01240 4520
01241 4521
01242 4522
01243 4523
01244 4524
01245 4525
01246 4526
01247 4527
01248 4528
01249 4529
01250 4530
01251 4531
01252 4532
01253 4533
01254 4534
01255 4535
01256 4536
01257 4537
01258 4538
01259 4539
01260 4540
01261 4541
01262 4542
01263 4543
01264 4544
01265 4545
01266 4546
01267 4547
01268 4548
01269 4549
01270 4550
01271 4551
01272 4552
01273 4553
01274 4554
01275 4555
01276 4556
01277 4557
01278 4558
01279 4559
01280 4560
01281 4561
01282 4562
01283 4563
01284 4564
01285 4565
01286 4566
01287 4567
01288 4568
01289 4569
01290 4570
01291 4571
01292 4572
01293 4573
01294 4574
01295 4575
01296 4576
01297 4577
01298 4578
01299 4579
01300 4580
01301 4581
01302 4582
01303 4583
01304 4584
01305 4585
01306 4586
01307 4587
01308 4588
01309 4589
01310 4590
01311 4591
01312 4592
01313 4593
01314 4594
01315 4595
01316 4596
01317 4597
01318 4598
01319 4599
01320 4600
01321 4601
01322 4602
01323 4603
01324 4604
01325 4605
01326 4606
01327 4607
01328 4608
01329 4609
01330 4610
01331 4611
01332 4612
01333 4613
01334 4614
01335 4615
01336 4616
01337 4617
01338 4618
01339 4619
01340 4620
01341 4621
01342 4622
01343 4623
01344 4624
01345 4625
01346 4626
01347 4627
01348 4628
01349 4629
01350 4630
01351 4631
01352 4632
01353 4633
01354 4634
01355 4635
01356 4636
01357 4637
01358 4638
01359 4639
01360 4640
01361 4641
01362 4642
01363 4643
01364 4644
01365 4645
01366 4646
01367 4647
01368 4648
01369 4649
01370 4650
01371 4651
01372 4652
01373 4653
01374 4654
01375 4655
01376 4656
01377 4657
01378 4658
01379 4659
01380 4660
01381 4661
01382 4662
01383 4663
01384 4664
01385 4665
01386 4666
01387 4667
01388 4668
01389 4669
01390 4670
01391 4671
01392 4672
01393 4673
01394 4674
01395 4675
01396 4676
01397 4677
01398 4678
01399 4679
01400 4680
01401 4681
01402 4682
01403 4683
01404 4684
01405 4685
01406 4686
01407 4687
01408 4688
01409 4689
01410 4690
01411 4691
01412 4692
01413 4693
01414 4694
01415 4695
01416 4696
01417 4697
01418 4698
01419 4699
01420 4700
01421 4701
01422 4702
01423 4703
01424 4704
01425 4705
01426 4706
01427 4707
01428 4708
01429 4709
01430 4710
01431 4711
01432 4712
01433 4713
01434 4714
01435 4715
01436 4716
01437 4717
01438 4718
01439 4719
01440 4720
01441 4721
01442 4722
01443 4723
01444 4724
01445 4725
01446 4726
01447 4727
01448 4728
01449 4729
01450 4730
01451 4731
01452 4732
01453 4733
01454 4734
01455 4735
01456 4736
01457 4737
01458 4738
01459 4739
01460 4740
01461 4741
01462 4742
01463 4743
01464 4744
01465 4745
01466 4746
01467 4747
01468 4748
01469 4749
01470 4750
01471 4751
01472 4752
01473 4753
01474 4754
01475 4755
01476 4756
01477 4757
01478 4758
01479 4759
01480 4760
01481 4761
01482 4762
01483 4763
01484 4764
01485 4765
01486 4766
01487 4767
01488 4768
01489 4769
01490 4770
01491 4771
01492 4772
01493 4773
01494 4774
01495 4775
01496 4776
01497 4777
01498 4778
01499 4779
01500 4780
01501 4781
01502 4782
01503 4783
01504 4784
01505 4785
01506 4786
01507 4787
01508 4788
01509 4789
01510 4790
01511 4791
01512 4792
01513 4793
01514 4794
01515 4795
01516 4796
01517 4797
01518 4798
01519 4799
01520 4800
01521 4801
01522 4802
01523 4803
01524 4804
01525 4805
01526 4806
01527 4807
01528 4808
01529 4809
01530 4810
01531 4811
01532 4812
01533 4813
01534 4814
01535 4815
01536 4816
01537 4817
01538 4818
01539 4819
01540 4820
01541 4821
01542 4822
01543 4823
01544 4824
01545 4825
01546 4826
01547 4827
01548 4828
01549 4829
01550 4830
01551 4831
01552 4832
01553 4833
01554 4834
01555 4835
01556 4836
01557 4837
01558 4838
01559 4839
01560 4840
01561 4841
01562 4842
01563 4843
01564 4844
01565 4845
01566 4846
01567 4847
01568 4848
01569 4849
01570 4850
01571 4851
01572 4852
01573 4853
01574 4854
01575 4855
01576 4856
01577 4857
01578 4858
01579 4859
01580 4860
01581 4861
01582 4862
01583 4863
01584 4864
01585 4865
01586 4866
01587 4867
01588 4868
01589 4869
01590 4870
01591 4871
01592 4872
01593 4873
01594 4874
01595 4875
01596 4876
01597 4877
01598 4878
01599 4879
01600 4880
01601 4881
01602 4882
01603 4883
01604 4884
01605 4885
01606 4886
01607 4887
01608 4888
01609 4889
01610 4890
01611 4891
01612 4892
01613 4893
01614 4894
01615 4895
01616 4896
01617 4897
01618 4898
01619 4899
01620 4900
01621 4901
01622 4902
01623 4903
01624 4904
01625 4905
01626 4906
01627 4907
01628 4908
01629 4909
01630 4910
01631 4911
01632 4912
01633 4913
01634 4914
01635 4915
01636 4916
01637 4917
01638 4918
01639 4919
01640 4920
01641 4921
01642 4922
01643 4923
01644 4924
01645 4925
01646 4926
01647 4927
01648 4928
01649 4929
01650 4930
01651 4931
01652 4932
01653 4933
01654 4934
01655 4935
01656 4936
01657 4937
01658 4938
01659 4939
01660 4940
01661 4941
01662 4942
01663 4943
01664 4944
01665 4945
01666 4946
01667 4947
01668 4948
01669 4949
01670 4950
01671 4951
01672 4952
01673 4953
01674 4954
01675 4955
01676 4956
01677 4957
01678 4958
01679 4959
01680 4960
01681 4961
01682 4962
01683 4963
01684 4964
01685 4965
01686 4966
01687 4967
01688 4968
01689 4969
01690 4970
01691 4971
01692 4972
01693 4973
01694 4974
01695 4975
01696 4976
01697 4977
01698 4978
01699 4979
01700 4980
01701 4981
01702 4982
01703 4983
01704 4984
01705 4985
01706 4986
01707 4987
01708 4988
01709 4989
01710 4990
01711 4991
01712 4992
01713 4993
01714 4994
01715 4995
01716 4996
01717 4997
01718 4998
01719 4999
01720 5000
01721 5001
01722 5002
01723 5003
01724 5004
01725 5005
01726 5006
01727 5007
01728 5008
01729 5009
01730 5010
01731 5011
01732 5012
01733 5013
01734 5014
01735 5015
01736 5016
01737 5017
01738 5018
01739 5019
01740 5020
01741 5021
01742 5022
01743 5023
01744 5024
01745 5025
01746 5026
01747 5027
01748 5028
01749 5029
01750 5030
01751 5031
01752 5032
01753 5033
01754 5034
01755 5
```

DATE 230272 PAGE 14

## BUOY DYNAMICS

```

01047 520* ACXC=IDATB(I-3)+DATB(I-2)+DATB(I-1)+DATB(I)
01047 521* 1 +DATB(I+1)+DATB(I+2)+DATB(I+3))/7.0
01050 528* ACYC=IDATC(I-3)+DATC(I-2)+DATC(I-1)+DATC(I)
01050 529* 1 +DATC(I+1)+DATC(I+2)+DATC(I+3))/7.0
01051 530* ACZC=IDATD(I-3)+DATD(I-2)+DATD(I-1)+DATD(I)
01051 531* 1 +DATD(I+1)+DATD(I+2)+DATD(I+3))/7.0
01052 532* BPITC=(DATE(I-3)+DATE(I-2)+DATE(I-1)+DATE(I)
01052 533* 1 +DATE(I+1)+DATE(I+2)+DATE(I+3))/7.0
01053 534* BROLC=(DATF(I-3)+DATF(I-2)+DATF(I-1)+DATF(I)
01053 535* 1 +DATF(I+1)+DATF(I+2)+DATF(I+3))/7.0
01054 536* IF(XAVC.LE.0.0001)XAVC=0.0001
01056 537* IF(ACXC.LE.0.0001)ACXC=0.0001
01060 538* IF(ACYC.LE.0.0001)ACYC=0.0001
01062 539* IF(ACZC.LE.0.0001)ACZC=0.0001
01064 540* IF(BPITC.LE.0.0001)BPITC=0.0001
01066 541* IF(BROLC.LE.0.0001)BROLC=0.0001
01070 542* PAV(IP)=10.0*ALOG10(XAVC)
01071 543* PAX(IP)=10.0*ALOG10(ACXC)
01072 544* PAY(IP)=10.0*ALOG10(ACYC)
01073 545* PAZ(IP)=10.0*ALOG10(ACZC)
01074 546* PPT(IP)=10.0*ALOG10(BPITC)
01075 547* PRL(IP)=10.0*ALOG10(BROLC)
01076 548* DPAX=PAV(IP)-PAV(IP)
01077 549* DPAY=PAY(IP)-PAY(IP)
01100 550* DPAZ=PAZ(IP)-PAZ(IP)
01101 551* DPPT=PPPT(IP)-PPPT(IP)
01102 552* DPRL=PRL(IP)-PRL(IP)
01103 553* 164 WRITE(4,117)FRQ(IP),PMV(IP),PAX(IP),PAY(IP),PAZ(IP),PPT(IP),
01103 554* 1 PRL(IP),DPAX,DPAY,DPAZ,DPPT,DPRL
01103 555* C
01103 556* C
01103 557* PLOT THE SPECTRA
01122 557* NPLT=0
01123 558* CALL MODESG(Z,0)
01124 559* 130 NPLT=NPLT+1
01125 560* CALL OBJCTG(Z,500.,500.,3600.,3000.)
01126 561* CALL SUBJEG(Z,0.,40.5.,40.)
01127 562* CALL GRIDG(Z,1.,10.,0.,0.)
01130 563* CALL LABELG(Z,0.1.,0.12)
01131 564* CALL LABELG(Z,1.,10.,0.,4)
01132 565* IF(NPLT.EQ.1)GO TO 131
01134 566* IF(NPLT.EQ.2)GO TO 132
01136 567* IF(NPLT.EQ.3)GO TO 133
01140 568* IF(NPLT.EQ.4)GO TO 134
01142 569* IF(NPLT.EQ.5)GO TO 135
01144 570* IF(NPLT.EQ.6)GO TO 136
01146 571* 131 CALL TITLEG(Z,9,9HFREQUENCY,8.8HUB LEVEL,13.13HWAVE SPECTRUM)
01147 572* .CALL LINESG(Z,153,FRQ,PMV)
01150 573* CALL PAGEG(Z,0.1,1)
01151 574* GO TO 130
01152 575* 132 CALL TITLEG(Z,9,9HFREQUENCY,8.8HUB LEVEL,14.14HHEAVE SPECTRUM)
01153 576* CALL LINESG(Z,153,FRQ,PAX)
01154 577* CALL PAGEG(Z,0.1,1)
01155 578* GO TO 130
01156 579* 133 CALL TITLEG(Z,9,9HFREQUENCY,8.8HUB LEVEL,13.13HSWAY SPECTRUM)
01157 580* CALL LINESG(Z,153,FRQ,PAY)
01160 581* CALL PAGEG(Z,0.1,1)
01161 582* GO TO 130
01162 583* 134 CALL TITLEG(Z,9,9HFREQUENCY,8.8HUB LEVEL,14.14HSURGE SPECTRUM)

```



```

01163      584*      BUOY DYNAMICS
01164      585*      CALL LINESG(2,153,FRQ,PAZ)
01165      586*      CALL PAGEG(2,0,1,1)
01166      587*      GO TO 130
01167      588*      135 CALL TITLEG(2,9,9HFREQUENCY,8,8HUB LEVEL,14,14HPITCH SPECTRUM)
01168      589*      CALL LINESG(2,153,FRQ,PPT)
01169      590*      CALL PAGEG(2,0,1,1)
01170      591*      GO TO 130
01171      592*      136 CALL TITLEG(2,9,9HFREQUENCY,8,8HUB LEVEL,13,13HROLL SPECTRUM)
01172      593*      CALL LINESG(2,153,FRQ,PRL)
01173      594*      CALL PAGEG(2,0,1,1)
01174      595*      CALL EXITG(2)
01175      596*      GO TO 89
01176      597*      92 WRITE(4,105)
01177      598*      89 STOP
01178      599*      END
01201
01204
01205
END OF UNIVAC 1108 FORTRAN V COMPILATION.      0 *DIAGNOSTIC* MESSAGE(S)
DATE 230272 PAGE 15

```

# BUOY DYNAMICS

W1 FOR WAVE, H WAVE  
UNIVAC 1106 FORTKATH V LEVEL 2206 0023  
THIS COMPILATION WAS DONE ON 23 FEB 72 AT 12:44:04

UATE 230272 PAGE 16

12:44: 4.826

SUBROUTINE KWAVE ENTRY POINT 000417  
STORAGE USED (BLOCK, NAME, LENGTH)

0001 \*CODE 000452  
0000 \*DATA 000173  
0002 \*BLANK 000000

## EXTERNAL REFERENCES (BLOCK, NAME)

0003 ALOG10  
0004 NEXP63  
0005 ALUG  
0006 EXP  
0007 SINT  
0008 \*ENR33

## STORAGE ASSIGNMENT FOR VARIABLES (BLOCK, TYPE, RELATIVE LOCATION, NAME)

0001 000207 1436 0001 000303 1616 0001 000321 1676 0001 000235 402L  
0000 K 000052 APAR 0000 R 000053 BPAR 0000 R 000012 DMWG 0000 R 000336 402L  
0000 K 000037 FPAR 0000 K 000043 FPARL 0000 R 000050 FP1 0000 R 000042 DURMIN 0000 R 000055 G  
0000 K 000047 HSPAR 0000 K 000046 HSPARL 0000 R 000134 INJP\$ 0000 I 000054 IS 0000 R 000056 OM  
0000 K 000000 DMG 0000 K 000045 P3PAR 0000 R 000044 P3PARL 0000 R 000057 SPEC  
0000 K 000041 TPAN 0000 K 000040 TPARL

00101 1\* SUBROUTINE KWAVE(WINDS,DUR,WHT4,PER,MOMEG,AMP,PHS)  
00101 4\* USE THE BREITSCHEIDER WAVE METHOD TO COMPUTE THE MEAN WAVE  
00101 3\* HEIGHT AND PERIOD  
00101 4\* USE A 15 MILE FETCH AT STATION BRAVO  
00103 5\* DIMENSION OMEG(10),MOMEG(10),DMWG(10),SPEC(10),PHS(10),AMP(10)  
00104 6\* REAL MOMEG  
00105 7\* FETCH=9.12E4  
00105 8\* FETCH LIMITED CASE  
00106 9\* FPAR=32.2\*FETCH/(WINDS\*\*2)  
00107 10\* TPAN=1.477-0.225\*ALOG10(FPAR)  
00110 11\* FPAR=10.0\*\*TPANL  
00112 12\* DURMIN=TPAN\*FETCH/(WINDS\*3600.0)  
00112 13\* IF (DUR-DURMIN)303,304,304  
00115 14\* UURATION LIMITED CASE  
00115 15\* FPAR=DUR\*WINDS\*3600.0/FETCH  
00116 16\* FPAR=5.78-3.915\*ALOG10(TPAN)  
00117 17\* FPAR=10.0\*\*FPARL  
00120 18\* P3PARL=-1.13+0.283\*ALOG10(FPAR)  
00121 19\* P3PAR=10.0\*\*P3PARL  
00122 20\* IF (FPAR,LT,0.02)P3PAR=0.0247

DATE 230272 PAGE 17

## BUOY DYNAMICS

```

00124 21* IF (FPAR.GT.1.2E5) P3PAR=2.0
00126 22* PER=0.14*P3PAR*WINDS
00128 23* H3PAR=-2.5*0.415*ALOG10(FPAR)
00130 24* H3PAR=10.0**H3PARL
00131 25* IF (FPAR.LT.0.016) H3PAR=0.00057
00133 26* IF (FPAR.GT.5.0E4) H3PAR=0.082
00135 27* WIND=0.01942*H3PAR*(WINDS**2)
00137 28* C COMPUTE FREQUENCIES AND AMPLITUDES FOR A 9 COMPONENT WAVE MODEL
00138 29* F1=32.2*WINDM/(WINDS**2)
00140 31* F2=32.2*PER/(6.2832*WINDS)
00141 32* APAR=3.437*(F1**2)/(F2**4)
00142 33* BPAR=-0.675*(1.32.2/(WINDS*F2))**4)
00144 34* DO 401 IS=1,9
00146 35* G=10.0/IS
00148 36* 401 OMEG(1S)=(-BPAR/(ALOG(G)))*0.25
00150 37* OMEG(10)=500.0
00151 38* OMEG=0
00152 39* 402 OMEG=OM+0.05
00153 40* SPECT=(1037.0*APAR/(OM**5))*EXP(BPAR/(OM**4))
00154 41* IF (SPECT.LE.0.001) GO TO 402
00156 42* HMEG(1)=OM+0.5*(OMEG(1)-OM)
00157 43* DO 403 IS=2,9
00158 44* HMEG(1S)=OMEG(1S)+OMEG(1S)-OMEG(1S)
00160 45* DO 404 IS=1,8
00161 46* SPEC(1S)=(1037.0*APAR/(HMEG(1S)**5))
00162 47* 1*EXP(BPAR/(HMEG(1S)**4))
00163 48* 404 AMP(1S)=0.5*SGRT(SPEC(1S)*HMEG(1S))
00164 49* AMP(9)=0.0
00165 50* C USE A RANDOM NUMBER TABLE TO SELECT RANDOM PHASE ANGLES FR
00166 51* EACH COMPONENT
00167 52* PHS(1)=0.306
00168 53* PHS(2)=6.235
00169 54* PHS(3)=4.635
00170 55* PHS(4)=5.20
00171 56* PHS(5)=0.575
00172 57* PHS(6)=3.220
00173 58* PHS(7)=5.546
00174 59* PHS(8)=0.435
00175 60* PHS(9)=0.657
00176 61* RETURN
00177 62* END
00178 63*

```

END OF UNIVAC 1108 FORTRAN V COMPILATION. 0 \*DIAGNOSTIC\* MESSAGE(S)

## BUOY DYNAMICS

1 FOR TORQU, TORBU  
 11VAC 1106 FORTHAI, V LEVEL 2206 0023  
 THIS COMPILATION WAS DONE ON 23 FEB 72 AT 12:44:06

DATE 230272 PAGE 18

12:44: 6.542

SUBROUTINE TORBU ENTRY POINT 000340

STORAGE USED (BLOCK, NAME, LENGTH)

0001 ALJLE 000363  
 0000 ALJTA 000061  
 0002 ALJAK 000000

EXTERNAL REFERENCES (BLOCK, NAME)

0003 SIN  
 0004 COS  
 0005 SORT  
 0006 ATAN  
 0007 NERH35

STORAGE ASSIGNMENT FOR VARIABLES (BLOCK, TYPE, RELATIVE LOCATION, NAME)

0001 000145 10L 0001 000225 11L 0001 000220 16L  
 0001 000275 20L 0001 000230 3L 0001 000132 8L  
 0000 K 000013 AK 0000 K 000011 2a' 0000 R 000014 ARTY  
 0000 K 000001 GAM 0000 K 000017 HB 0000 000041 INJP\$  
 0000 K 000003 AT 0000 000070 VOLX 0000 R 000007 VOLX  
 0000 K 000005 ZGBH 0001 000231 18L  
 0001 000245 19L 0001 000016 9L  
 0000 R 000012 ALF 0000 R 000002 OGAM  
 0000 R 000004 RS 0000 R 000017 XM

00101 1\* C  
 00101 2\* C  
 00101 3\* C  
 00101 4\* C  
 00101 5\* C  
 00101 6\* C  
 00101 7\* C  
 00101 8\* C  
 00101 9\* C  
 00101 10\* C  
 00101 11\* C  
 00101 12\* C  
 00101 13\* C  
 00101 14\* C  
 00101 15\* C  
 00101 16\* C  
 00101 17\* C  
 00101 18\* C  
 00101 19\* C  
 00101 20\* C  
 00101 21\* C

SUBROUTINE TORBU(M,TIL,BXX,BTT,BAT,BTX)  
 THIS SUBROUTINE COMPUTES THE DISPLACEMENT AND RIGHTING MOMENT  
 FOR THE 8 FOOT DIA. RICHARDSON BUOY USED IN THE BUOY MOTION  
 EXPERIMENT  
 J=1  
 GAM=-1.5708  
 OGAM=0.1  
 RT=2.75  
 RS=1.25  
 ZGBH=1.202  
 VOL=0.0  
 VOLX=0.0  
 9 CONTINUE  
 HB=(ZGBH-M)\*(1.0-COS(TIL))\*RT\*SIN(TIL)\*SIN(GAM)  
 IF(J.EQ.1)HB=H  
 IF(HB.LE.0.0)HB=0.0  
 IF(HB.GT.(0.99\*RS))GO TO 8  
 IF(HB.GE.(1.99\*RS))GO TO 11  
 ART=2.0\*HB\*(RS\*\*2)/(RS-HB)\*\*2-1.0  
 IF(ART.GE.25.0)GO TO 16  
 ALF=2.0\*ATAN(ART)

DATE 230272 PAGE 19

## BUOY DYNAMICS

```

00131 22* AN=0.5*(RS**2)*(ALF-SIN(ALF))
00132 23* GO TO 18
00133 24* 8 CONTINUE
00134 25* IF(HB.GT.(1.01*RS))GO TO 10
00135 26* AN=1.5708*HS*HS
00136 27* GO TO 18
00137 28* 10 ARTY=((RS**2)/((RS-(2.0*HS-HB)**2))-1.0
00138 29* IF(ARTY.LE.0.0)ARTY=0.0
00139 30* ART=SQRT(ARTY)
00140 31* IF(ART.GE.25.0)GO TO 16
00141 32* ALF=2.0*ATAN(ART)
00142 33* AN=3.1416*(RS**2)-0.5*(RS**2)*(ALF-SIN(ALF))
00143 34* GO TO 18
00144 35* 16 AN=1.5708*(RS**2)
00145 36* GO TO 18
00146 37* 11 AR=3.1416*(RS**2)
00147 38* IF(J.EQ.1)GO TO 3
00148 39* GO TO 19
00149 40* 3 BXX=402.124*RT*AR
00150 41* J=2
00151 42* GO TO 9
00152 43* 19 VOL=VOL+UGAM*HT*AR
00153 44* X=RT*SIN(GAM)
00154 45* VOLX=VOLX+X*UGAM*HT*AR
00155 46* GAM=GAM+UGAM
00156 47* IF(GAM.GE.1.57)GO TO 20
00157 48* GO TO 9
00158 49* 20 BXTIL=128.0*VOL
00159 50* BXT=BXTIL-BXX
00160 51* C THE RIGHTING ARM
00161 52* XME=(VOLX/VOL)*COS(TIL)-(ZGBH-H)*SIN(TIL)
00162 53* BTT=dBXTIL/dXM
00163 54* BTK=BXT*AM
00164 55* RETURN
00165 56* END
00166 57*
00167 58*
00168 59*
00169 60*
00170 61*
00171 62*
00172 63*
00173 64*
00174 65*
00175 66*
00176 67*
00177 68*
END OF UNIVAC 1108 FORTRAN V COMPILATION. 0 *DIAGNOSTIC* MESSAGE(S)

```

DATE 230272 PAGE 20 12:44: 0.120

# BUOY DYNAMICS

W1 FOR RUNGE, RUNGE  
UNIVAC 1104 FORTHMAN V LEVEL 2206 0023  
THIS COMPILATION WAS DONE ON 23 FEB 72 AT 12:44:08

SUBROUTINE RUNGE ENTRY POINT 000134  
STORAGE USED (BLOCK, NAME, LENGTH)

0001 \*COLE 000163  
0000 \*DATA 000115  
0002 \*BLANK 000000

## EXTERNAL REFERENCES (BLOCK, NAME)

0003 NEHR23  
0004 NEHR35

## STORAGE ASSIGNMENT FOR VARIABLES (BLOCK, TYPE, RELATIVE LOCATION, NAME)

Block	Type	Relative Location	Name
0001	000021 1L	0001 000121 10L	
0001	000030 3L	0001 000032 4L	
0000	R 000063 A	0000 1 000062 I	
0001	000054 120G	0001 000023 107G	
0001	000074 7L	0001 000036 5L	
0000	R 000000 Q	0000 000075 INJPS	
0001	000102 130G	0001 000102 130G	
0001	000117 9L	0001 000117 9L	

00101 1\* C SUBROUTINE RUNGE(I,Y,F,X,H,M,K)  
00101 2\* THIS ROUTINE PERFORMS RUNGE KUTTA CALCULATIONS BY GILL'S METHOD  
00103 3\* DIMENSION Y(50),F(50),Q(50)  
00104 4\* M=M+1  
00105 5\* GO TO (1,4,5,3,7),M  
00106 6\* 1 DO 2 I=1,N  
00111 7\* 2 Q(I)=0.0  
00113 8\* A=0.5  
00114 9\* GO TO 9  
00115 10\* 3 A=1.707107  
00116 12\* 4 X=X+0.5\*M  
00117 13\* 5 DO 6 I=1,N  
00122 14\* Y(I)=Y(I)+A\*(F(I)\*H-Q(I))  
00123 15\* 6 Q(I)=2.0\*A\*(H\*(F(I)+(1.0-3.0\*A)\*Q(I))  
00125 16\* A=0.2928932  
00125 17\* C IF YOU NEED MORE ACCURACY USE A=0.2928932188134524756  
00126 18\* GO TO 9  
00127 19\* 7 DO 8 I=1,N  
00132 20\* 8 Y(I)=Y(I)+H\*(F(I)+6.0\*(I)/3.0  
00134 21\* M=0.0  
00135 22\* K=2  
00136 23\* GO TO 10  
00137 24\* 9 K=1  
00140 25\* 10 RETURN  
00141 26\* END

# BUOY DYNAMICS

M1 FOR USTAT, DSTAT  
 UNIVAC 1106 FORTRAN V LEVEL 2206 0023  
 THIS COMPILATION WAS DONE ON 23 FEB 72 AT 12:44:09

DATE 230272 PAGE 22

12:44: 9.365

SUBROUTINE USTAT ENTRY POINT 000045

STORAGE USED (BLOCK, NAME, LENGTH)

0001 \*CODE 000062  
 0000 \*DATA 000017  
 0002 \*BLANK 000000

EXTERNAL REFERENCES (BLOCK, NAME)

0003 SORT  
 0004 NERR35

STORAGE ASSIGNMENT FOR VARIABLES (BLOCK, TYPE, RELATIVE LOCATION, NAME)

0001 000012 110G 0000 000005 INJPS 0000 I 000003 J 0000 I 000000 N 0000 R 000001 S  
 0000 R 000002 S1

00101 1\* SUBROUTINE DSTAT(PAR,PRMN,PRVR,PRSD)  
 00103 2\* DIMENSION PAR(2048)  
 00104 3\* N=1024  
 00105 4\* S=0.0  
 00106 5\* S1=0.0  
 00107 6\* DO 3 J=1,2047,2  
 00112 7\* S=S+PAR(J)  
 00113 8\* 3 S1=S1+PAR(J)\*PAR(J)  
 00115 9\* PRMN=S/N  
 00116 10\* PRVR=(S1-PRMN\*S)/N  
 00117 11\* PRSD=SQRT(PRVR)  
 00120 12\* RETURN  
 00121 13\* END

END OF UNIVAC 1106 FORTRAN V COMPILATION. 0 \*DIAGNOSTIC\* MESSAGE(S)

DATE 230272 PAGE 23 12:44:10.490

BUOY DYNAMICS

WA FJM FFOUR,FFOUR  
UNLAC 1100 FORTRAN V LEVEL 2406 0023  
THIS COMPILEATION WAS DONE ON 25 FEB 72 AT 12:44:10

SUBROUTINE FFOUR ENTRY POINT 000324

STORAGE USED (BLOCK, NAME, LENGTH)

0001 \*CODE 000357  
0000 \*DATA 000051  
0002 \*BLANK 000000

EXTERNAL REFERENCES (BLOCK, NAME)

0003 UNSCR  
0004 NERR33

STORAGE ASSIGNMENT FOR VARIABLES (BLOCK, TYPE, RELATIVE LOCATION, NAME)

0001	000021	10L	0001	000175	153G	0001	000257	170G	0001	000304	4L
0001	000023	40L	0001	000041	60L	0001	000024	80L	0001	000153	91L
0001	000223	94L	0000	C	000001	A	0000	R	0000	C	000013
0000	I	000006	INDEX	0000	000021	INJPS	0000	I	000005	LINC	0000
0000	I	000007	LOC1	0000	I	000004	THTA	0000	I	000010	Y
				0000	I	000003	TINC	0000	R	000010	Y

SUBROUTINE FFOUR(X,C,ISCR,T,BIN,J)

00101 1\*  
00103 2\*  
00104 3\*  
00105 4\*  
00106 5\*  
00107 6\*  
00110 7\*  
00111 8\*  
00112 9\*  
00113 10\*  
00114 11\*  
00115 12\*  
00116 13\*  
00117 14\*  
00120 15\*  
00121 16\*  
00122 17\*  
00123 18\*  
00124 19\*  
00127 20\*  
00132 21\*  
00133 22\*  
00134 23\*  
00135 24\*  
00136 25\*

COMPLEX EX(1),A  
INTEGER I,TINC,THTA,BIN  
DIMENSION CSE(2),C(1),ISCR(1)  
EQUIVALENCE (E,CSE)  
2 TINC=BIN/T  
LINC=T/2  
10 LOC=LINC  
40 THTA=0  
80 CSE(1)=C(THTA+1)  
INDEX=BIN/4+1-THTA  
CSE(2)=-C(INDEX)  
60 LOC=LOC+1  
LOC1=LOC-LINC  
E=E\*(X(LOC1)-X(LOC))  
X(LOC1)=X(LOC1)+X(LOC)  
X(LOC)=E  
THTA=THTA+TINC  
IF(THTA-BIN/2) 20,30,30  
20 IF(THTA-BIN/4) 80,50,50  
50 INDEX=BIN/2+1-THTA  
CSE(1)=-C(INDEX)  
INDEX=THTA-(BIN/4-1)  
CSE(2)=-C(INDEX)  
GO TO 60

FF8  
FF9  
FF10  
FF11

FF13  
FF14  
FF15  
FF16  
FF17  
FF18  
FF19  
FF20

FF23



```

00137      26*
00142      27*
00143      28*
00144      29*
00147      30*
00150      31*
00151      32*
00152      33*
00155      34*
00156      35*
00157      36*
00160      37*
00162      38*
00163      39*
00165      40*
00166      41*
00167      42*
00172      43*
00173      44*
00174      45*
00176      46*
00177      47*
00200      48*

      BUOY DYNAMICS
      30 IF (LOC-T) 90,91,91
      90 LOC=LOC+LINC
         GO TO 40
      91 IF (2-LINC) 92,93,94
      92 LINC=LINC/2
         TINC=TINC+TINC
         GO TO 10
      93 DO 100 LUC=2,T,2
         LOC=LOC-1
         EX(LOC)=X(LOC)
         X(LOC)=X(LOC)+X(LOC)
      100 X(LOC)=E
      94 CALL UNSCR(X,ISCR,T)
         Y=1.0/T
         I2=T/2+1
         DO 3 I=2,I2
            AX(I)
            X(I)=CMPLX(REAL(X(T+2-I)),Y,AIMAG(X(T+2-I)))*Y
            X(T+2-I)=CMPLX(REAL(A),Y,AIMAG(A))*Y
            X(I)=CMPLX(REAL(X(I)),Y,AIMAG(X(I)))*Y
         4 RETURN
      END

      ENO OF UNIVAC 1108 FORTRAN V COMPILATION.      0 *DIAGNOSTIC* MESSAGE(S)

```

DATE 230272 PAGE 24

FF24  
FF25  
FF26  
FF27  
FF28  
FF29  
FF30  
FF31  
FF32  
FF33  
FF34  
FF35

FF38

## BUOY DYNAMICS

QA FOR GNSCR,GNSCR  
UNIVAC 1108 FORTRAN V LEVEL 2206 0023  
THIS COMPILATION WAS DONE ON 23 FEB 72 AT 12:44:12

DATE 230272 PAGE 25

12:44:12. 93

SUBROUTINE GNSCR ENTRY POINT 000062

STORAGE USED (BLOCK, NAME, LENGTH)

0001 \*CODE 000075  
0000 \*DATA 000024  
0002 \*BLANK 000000

EXTERNAL REFERENCES (BLOCK, NAME)

0003 MERR35

STORAGE ASSIGNMENT FOR VARIABLES (BLOCK, TYPE, RELATIVE LOCATION, NAME)

0001 000013 11L 0001 000020 1116 0001 000046 8L  
0000 1 000001 M 0000 1 000002 N 0000 1 000000 TM 0000 1 000003 J

00101 1\*  
00103 2\*  
00104 3\*  
00105 4\*  
00106 5\*  
00107 6\*  
00110 7\*  
00113 8\*  
00114 9\*  
00116 10\*  
00121 11\*  
00122 12\*  
00123 13\*  
00124 14\*  
00125 15\*

SUBROUTINE GNSCR(SCR,T)  
INTEGER T,TM,SCR(1)  
SCR(1)=1  
M=1  
N=1  
TM=T/2  
11 DO 9 J=1,M  
N=N+1  
9 SCR(N)=TM+SCR(J)  
IF(T-SCR(N)) 8,8,10  
10 M=M+M  
TM=TM/2  
GO TO 11  
8 RETURN  
END

FF44  
FF45  
FF46  
FF47  
FF48  
FF49  
FF50  
FF51  
FF52  
FF53  
FF54  
FF55  
FF56

CND OF UNIVAC 1108 FORTRAN V COMPILATION. 0 \*DIAGNOSTIC\* MESSAGE(S)

BUOY DYNAMICS

QA FOR UNSCR,UNSCR  
UNIVAC 1108 FORTRAN V LEVEL 2206 0023  
THIS COMPILATION WAS DONE ON 23 FEB 72 AT 12:44:13

DATE 230272 PAGE 26

12:44:13.208

SUBROUTINE UNSCR ENTRY POINT 000047

STORAGE USED (BLOCK, NAME, LENGTH)

0001 \*CODE 000061  
0000 \*DATA 000023  
0002 \*BLANK 000000

EXTERNAL REFERENCES (BLOCK, NAME)

0003 NEHR35

STORAGE ASSIGNMENT FOR VARIABLES (BLOCK, TYPE, RELATIVE LOCATION, NAME)

0001 000012 1066 0001 000030 9L 0000 C 000000 E 0000 I 000003 I 0000 000004 INUMPS

00101 1\* SUBROUTINE UNSCR(X,SCR,T)  
00103 2\* COMPLEX E,X(I)  
00104 3\* INTEGER T,SCR(I)  
00105 4\* DO 9 J=1,T  
00110 5\* I=SCR(J)  
00111 6\* IF(J-I) 9,9,10  
00114 7\* 10 E=X(J)  
00115 8\* X(J)=X(I)  
00116 9\* X(I)=E  
00117 10\* 9 CONTINUE  
00121 11\* RETURN  
00122 12\* END

PF62  
PF63  
PF64  
PF65  
PF67  
PF68  
PF69  
PF70

END OF UNIVAC 1108 FORTRAN V COMPILATION. 0 \*DIAGNOSTIC\* MESSAGE(S)

DATE 230272 PAGE 27  
1234514.245

BUOY DYNAMICS  
QA FOR COSINE, COSINE  
UNIVAC 1100 FORTRAN V LEVEL 2206 0023  
THIS COMPILATION WAS DONE ON 25 FEB 72 AT 12:44:14

SUBROUTINE COSINE ENTRY POINT 000126  
STORAGE USED (BLOCK, NAME, LENGTH)

0001 \*CODE 000141  
0000 \*DATA 000053  
0002 \*BLANK 000000

EXTERNAL REFERENCES (BLOCK, NAME)

0003 RND  
0004 UCOS  
0005 OSIN  
0006 NERR3s

STORAGE ASSIGNMENT FOR VARIABLES (BLOCK, TYPE, RELATIVE LOCATION, NAME)

0001 000060 1206 0000 D 000000 ANG 0000 D 000002 CS 0000 I 000013 INDEX  
0000 000030 INJPS 0000 I 000012 INTB 0000 I 000014 J 0000 R 000000 RND 0000 D 000004 SN  
0000 D 000010 SNJ

00100 1\* C \*\*\* SUBROUTINE COSINE \*\*\* 10/14/70 \*\*\* A.M. NUTTALL  
00101 2\* SUBROUTINE COSINE (C, BIN)  
00102 3\* DOUBLE PRECISION ANG, CS, SN, CSJ, SNJ  
00103 4\* INTEGER BIN  
00104 5\* DIMENSION C(1)  
00105 6\* ANG=6.2831853071795864800/BIN  
00106 7\* INTB=BIN/8  
00107 8\* INDEX=2\*INTB+1  
00108 9\* CS=DCOS(ANG)  
00109 10\* SN=OSIN(ANG)  
00110 11\* CSJ=1.000  
00111 12\* SNJ=0.000  
00112 13\* C(1)=1.0  
00113 14\* C(INDEX)=0.0  
00114 15\* DO 9 J=1, INTB  
00115 16\* ANG=CSJ\*CS-SNJ\*SN  
00116 17\* SNJ=CSJ\*SN+SNJ\*CS  
00117 18\* CSJ=ANG  
00118 19\* C(J+1)=RND(CSJ)  
00119 20\* C(INDEX-J)=RND(SNJ)  
00120 21\* RETURN  
00121 22\* END  
00131

END OF UNIVAC 1100 FORTRAN V COMPILATION. 0 \*DIAGNOSTIC MESSAGE(S)

## BUOY DYNAMICS

01 ASM RND,RND  
 ASSEMBLER 8LSD 2454 0007  
 THIS ASSEMBLY WAS DONE ON 23 FEB 72 AT 12:44:15

DATE 230272 PAGE 28

12:44:15.517

000001	01	000000	71 13 00 13 1	000000	DL	REGNAM	AD=0,X11	• ASSOCIATE REG'S WITH MEM'S
000002		000001	76 17 04 00 0	000014	FCL		A4,A0	• GENERATE CODE UNDER L.C.1
000003		000002	01 00 04 00 0	000000	SA		A4,SPOX	• ENTRY POINT FOR X=END(DX)
000004		000003	73 13 03 00 0	000011	LDSL		A4,SPOX	• A4 <-- SINGL(IX)
000005		000004	73 02 04 00 0	000011	SSL		A4,9	• SPDX <-- A4
000006		000005	73 03 00 00 0	000017	JN		A4,9	• A3 <-- C,A4 <-- H XXX
000007		000006	45 00 01 00 0	000001	TOP		A0,NEG	• A4 <-- H
000008		000007	74 04 00 00 0	000030	J		FIN	• JUMP IF DX < 0
000009		000008	10 00 02 00 0	000002	LA		A1,(000000,0)	• SKIP NI IF ROUNO UP
000010		000009	52 00 02 00 0	000020	TE		A2,(000077777777)	• NO JUMP UP, EXIT
000011		000010	74 04 00 00 0	000033	J		A2,A4	• AD <-- 000777777777
000012		000011	14 16 03 00 0	000001	AA,U		FIN1	• SKIP NI IF M = 7'S
000013		000012	10 00 04 00 0	000003	LA		A3,1	• NO, JUST INCREMENT
000014		000013	73 03 03 00 0	000011	DSL		A4,(04000000,0)	• C <-- C+1
000015		000014	74 04 00 00 0	000031	J		A3,9	• H <-- 400000000000
000016		000015	05 00 00 00 0	000016	TEP		FIN2	• A4 <-- C,M
000017		000016	74 04 00 00 0	000030	J		FIN	• EXIT
000018		000017	44 00 01 00 0	000001	LA		A1,(000000,0)	• SKIP NI IF ROUNO UP
000019		000018	05 00 00 00 0	000016	SZ		A2	• NO ROUNO UP, EXIT
000020		000019	52 00 02 00 0	000020	TE		A2,A4	• A2 <-- 0
000021		000020	74 04 00 00 0	000037	J		FIN3	• SKIP NI IF M = 0'S
000022		000021	15 16 03 00 0	000001	ANA,U		A3,1	• NO, JUST DECREMENT
000023		000022	10 00 04 00 0	000011	LA		A4,(037777777777)	• C <-- C-1
000024		000023	73 03 03 00 0	000014	DSL		A3,9	• H <-- 377777777777
000025		000024	74 04 00 00 0	000031	J		FIN2	• A4 <-- C,M
000026		000025	10 00 04 00 0	000000	LA		A4,SPOX	• EXIT
000027		000026	01 00 04 00 0	000014	SA		A4,A0	• A4 <-- SPOX
000028		000027	74 04 00 00 0	000002	J		2,X11	• A4 <-- A4
000029		000028	10 00 04 00 0	000001	LA		A4,SPOX	• RETURN
000030		000029	01 00 04 00 0	000014	SA		A4,1	• A4 <-- X431
000031		000030	74 04 00 13 0	000002	J		2,X11	• A4 <-- A4
000032		000031	10 00 04 00 0	000000	LA		A4,SPOX	• RETURN
000033		000032	14 16 04 00 0	000001	SA		A4,A0	• A4 <-- X431
000034		000033	01 00 04 00 0	000014	J		2,X11	• A4 <-- A4
000035		000034	74 04 00 13 0	000002	LA		A4,SPOX	• RETURN
000036		000035	10 00 04 00 0	000000	ANA,U		A4,1	• A4 <-- X431
000037		000036	15 16 04 00 0	000001	SA		A4,A0	• A4 <-- A4
000038		000037	01 00 04 00 0	000014	J		2,X11	• RETURN
000039		000038	74 04 00 13 0	000002	+		0	• GENERATE DATA UNDER L.C.0
000040		000039	00000000000000		END			• SINGLE PRECISION DX
000041		000040	00000000000000					
000042		000041	00000000000000					
000043		000042	00000000000000					
000044		000043	00000000000000					
000045		000044	00000000000000					
000046		000045	00000000000000					
000047		000046	00000000000000					
000048		000047	00000000000000					
000049		000048	00000000000000					
000050		000049	00000000000000					
000051		000050	00000000000000					
000052		000051	00000000000000					
000053		000052	00000000000000					
000054		000053	00000000000000					
000055		000054	00000000000000					
000056		000055	00000000000000					
000057		000056	00000000000000					
000058		000057	00000000000000					
000059		000058	00000000000000					
000060		000059	00000000000000					
000061		000060	00000000000000					
000062		000061	00000000000000					
000063		000062	00000000000000					
000064		000063	00000000000000					
000065		000064	00000000000000					
000066		000065	00000000000000					
000067		000066	00000000000000					
000068		000067	00000000000000					
000069		000068	00000000000000					
000070		000069	00000000000000					
000071		000070	00000000000000					
000072		000071	00000000000000					
000073		000072	00000000000000					
000074		000073	00000000000000					
000075		000074	00000000000000					
000076		000075	00000000000000					
000077		000076	00000000000000					
000078		000077	00000000000000					
000079		000078	00000000000000					
000080		000079	00000000000000					
000081		000080	00000000000000					
000082		000081	00000000000000					
000083		000082	00000000000000					
000084		000083	00000000000000					
000085		000084	00000000000000					
000086		000085	00000000000000					
000087		000086	00000000000000					
000088		000087	00000000000000					
000089		000088	00000000000000					
000090		000089	00000000000000					
000091		000090	00000000000000					
000092		000091	00000000000000					
000093		000092	00000000000000					
000094		000093	00000000000000					
000095		000094	00000000000000					
000096		000095	00000000000000					
000097		000096	00000000000000					
000098		000097	00000000000000					
000099		000098	00000000000000					
000100		000099	00000000000000					

Buoy System Dynamics for the Torroidal  
Buoy Used in WHOI Mooring No. 238

This program (figure B-4) is basically the same as the previous program except that the mooring line forces and dynamics are simulated with the finite-difference method described in chapter III of the main text. Subroutine "MOOR" (figure B-5) takes the spatial values of the six variables (strain, two angles, and the velocity components) describing the cable motions and updates them for the next time step. The tension and angles at the top of the cable are then used to compute the mooring line forces acting on the buoy.

For numerical stability, the value of the tensile wave characteristic should never exceed the quotient of the nodal spacing,  $H$ , and the time step,  $K$ , in the subroutine:

$$Ch_1 < H/K.$$

The list of input values is the same as that for the previous program. In this particular program, the mooring line is composed of two segments, and the cable weights, masses, etc. are changed at a cable length of 4800 ft. There are 20 nodes spaced 400 ft apart to simulate dynamics of an 8,000-ft mooring line.

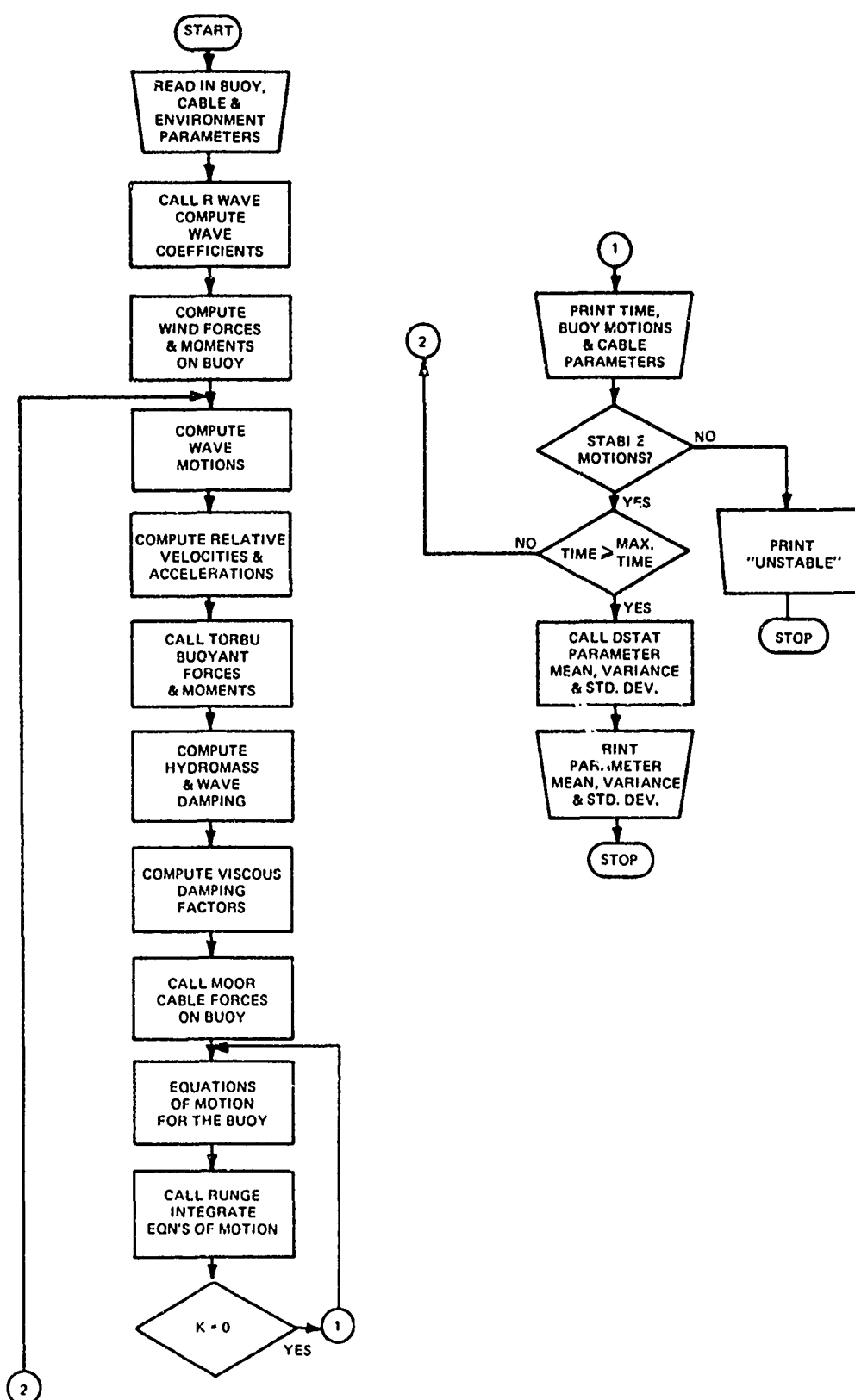


Figure B-4. Torroidal Buoy WHOI Mooring No. 238  
Dynamics Simulation Flow Chart

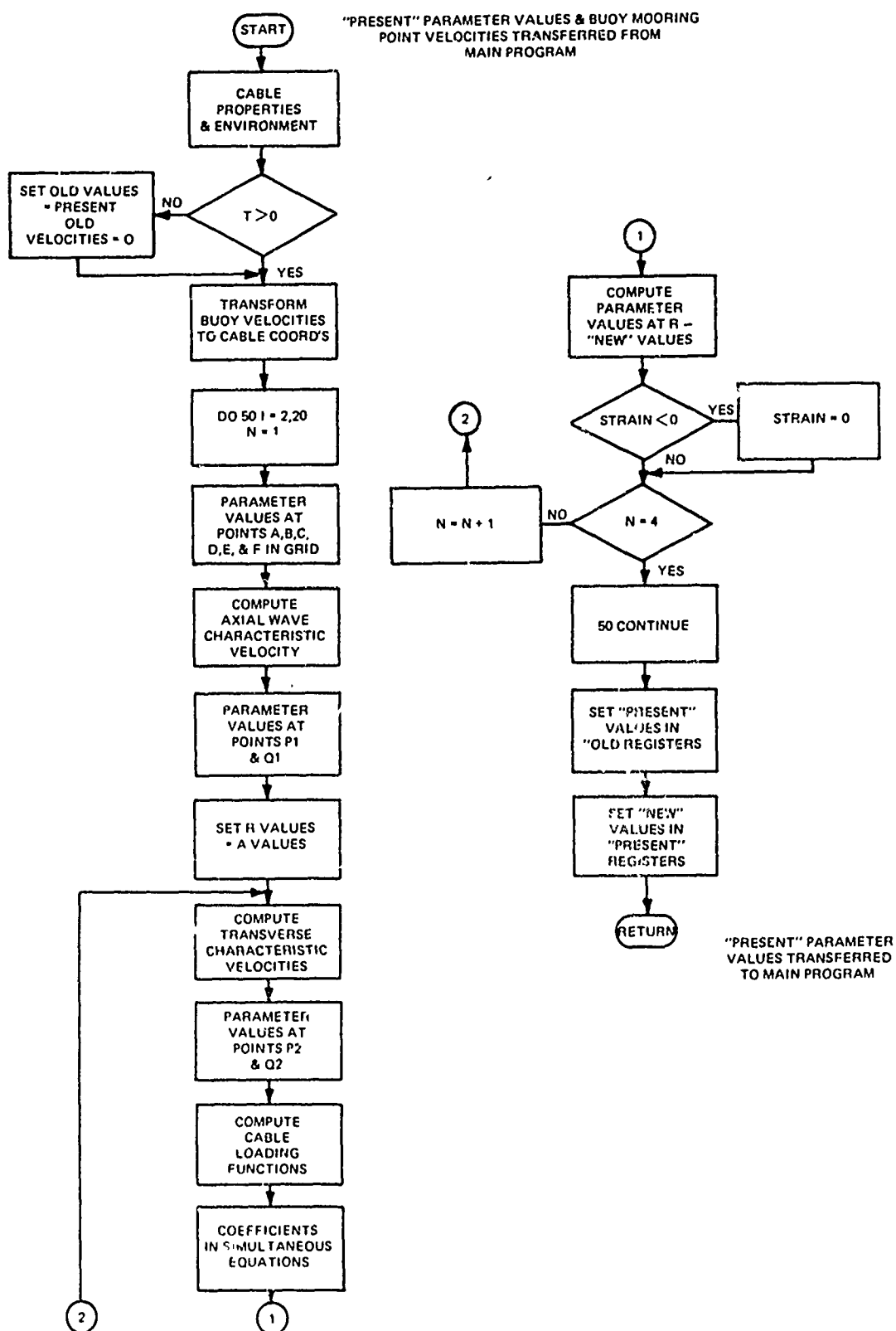


Figure B-5. Finite-Difference Cable Dynamics Simulation Flow Chart



## BOOT DYNAMICS

G FOR 51279.51279  
UNIVAC 1108 FORTRAN V LEVEL 2206 0023  
THIS COMPILATION WAS DONE ON 01 MAY 72 AT 10:50:52

DATE 010572 PAGE 3

10:50:52.667

## MAIN PROGRAM

## STORAGE USED (BLOCK, NAME, LENGTH)

0001 \*CODE 001735  
0000 \*DATA 010637  
0002 \*BLANK 000000

## EXTERNAL REFERENCES (BLOCK, NAME)

0003 RAVE  
0004 TORBU  
0005 MOOR  
0006 RUNGE  
0007 DSTAT  
0010 MRUCS  
0011 NI025  
0012 SURT  
0013 MEXPOS  
0014 LAP  
0015 COS  
0016 SIN  
0017 NEHR25  
0020 MUDUS  
0021 NSTOPS

## STORAGE ASSIGNMENT FOR VARIABLES (BLOCK, TYPE, RELATIVE LOCATION, NAME)

0000	010515	103F	0000	010520	105F	0000	010522	106F	0000	010525	107F	0000	010527	108F
0000	010531	109F	0000	010533	112F	0000	010535	120F	0000	010537	121F	0000	010541	122F
0000	010543	123F	0000	010545	124F	0000	010547	129F	0000	010551	131F	0000	000145	211G
0001	000164	227G	0001	000225	31L	0001	000241	32L	0001	000243	33L	0001	000551	371G
0001	001431	40L	0001	000336	41L	0001	000346	42L	0001	000774	441G	0001	000452	SL
0001	001065	50L	0001	001520	542G	0001	001452	72L	0001	001514	73L	0001	50:53E	87L
0001	001731	88L	0001	001716	92L	0000	010327	A	0000	003232	ACX	0000	004232	ACY
0000	005232	ACZ	0000	010462	ALFA	0000	010274	ALIN	0000	010373	ALW	0000	000206	AMP
0000	010413	ANG	0000	010345	ARXX	0000	010470	AWMN	0000	010472	AWSD	0000	002232	AWV
0000	010471	AVR	0000	010476	AXMN	0000	010500	AXSO	0000	010477	AXVR	0000	010501	AYMN
0000	010503	AYSD	0000	010502	AYVR	0000	010504	AZMN	0000	010477	AXVR	0000	010505	AZVR
0000	010336	BA	0000	010434	BBB	0000	010436	BBX	0000	010463	BETA	0000	010337	BGG
0000	010441	BXX	0000	010335	BLAMB	0000	010270	BR	0000	010506	AZSD	0000	010311	BPSD
0000	010510	BPRV	0000	010270	BR	0000	010512	BRMN	0000	010507	BPMN	0000	010514	BRSD
0000	010513	BTVR	0000	010275	BTIN	0000	010374	BTW	0000	007232	BROL	0000	010435	BXB
0000	010440	BXX	0000	010433	BXX	0000	010340	CMX	0000	010415	BTI	0000	010435	BXB
0000	010343	CXX	0000	010344	CNY	0000	010312	CY	0000	010341	CMY	0000	010342	CMZ
0000	010311	CZ5	0000	000000	D	0000	010401	DALV	0000	010310	CYS	0000	010430	CZ
0000	010402	DBTW	0000	010424	DBT1	0000	010431	DBT2	0000	010422	DAL1	0000	010410	DDBTW
0000	010460	DDBT1	0000	010411	DDGMW	0000	010461	DDGM1	0000	010404	DOXW	0000	010455	DDX1
0000	010405	DOYW	0000	010456	DDY1	0000	010406	DDZW	0000	010457	DOZ1	0000	010351	DGAA

## BUOY DYNAMICS

```

0000 K 010352 DG88      0000 K 010357 DG8Z      0000 R 010353 DG6G      0000 R 010360 DGGY      0000 R 010403 DGMW
0000 K 010423 DG*1      0000 K 010352 DG*2      0000 R 010346 DGAX      0000 R 010347 DGYT      0000 R 010347 DX1
0000 K 010356 DGZB      0000 K 010350 DGZ2      0000 R 010446 DTDE      0000 R 010376 DOWX      0000 R 010400 DZM
0000 K 010425 DX2       0000 K 010377 DY*W      0000 R 010420 DY1      0000 R 010426 DY2      0000 R 010454 FGM
0000 K 010421 DZ1       0000 K 010427 DZ2      0000 R 010452 FAL      0000 R 010453 FBT      0000 I 010464 GAMMA
0000 K 010334 FK        0000 K 010447 FX        0000 R 010450 FY        0000 R 010451 FZ        0000 I 010332 I
0000 K 010276 GMIN      0000 K 010375 GMM        0000 R 010416 GM1      0000 R 010361 H        0000 R 010250 MB
0000 I 010323 J         0000 I 010330 K         0000 I 010333 L         0000 R 010351 M         0000 R 010236 MGG
0000 K 010237 MHAA      0000 K 010235 MHBB      0000 R 010446 MHXB      0000 R 010241 MHXG      0000 R 010232 MHXX
0000 K 010247 MHGX      0000 K 010245 MHGY      0000 R 010240 MHXB      0000 R 010243 MHZZ      0000 R 000174 MONEG
0000 K 010242 MHTG      0000 K 010233 MHTY      0000 R 010243 MHXB      0000 R 010256 NBB      0000 R 010261 NBX
0000 K 010251 MU        0000 I 010324 N         0000 R 010255 NAA      0000 R 010263 NGX      0000 I 010325 NNY
0000 K 010267 NBZ       0000 K 010257 NGG      0000 R 010263 NGX      0000 R 010264 NYG      0000 R 000220 PHS
0000 K 010260 NXB       0000 K 010262 NXG      0000 R 010252 NXX      0000 R 000122 PHI      0000 R 010467 TBSO
0000 K 010266 NZB       0000 K 010254 NZZ      0000 K 010262 KCB      0000 R 000075 STRN      0000 R 010465 TBMN
0000 K 010326 K         0000 K 010442 KCB      0000 K 010050 TEN      0000 R 000232 TENB      0000 R 010443 UBY
0000 K 010466 TBVP      0000 K 010366 VELBB      0000 K 010301 WAEHA      0000 R 010363 VELXB      0000 R 010445 WBY
0000 K 010365 VELZB     0000 K 010300 WCL        0000 K 010302 WCPHT      0000 R 010321 WFBT      0000 R 010362 WMT
0000 K 010277 *CU       0000 K 010316 WFX        0000 R 010317 WFY        0000 R 010320 WFZ        0000 R 010412 WK
0000 K 010322 *FGH      0000 K 010304 WINDS      0000 R 010314 WINDY      0000 R 010315 WINDZ      0000 R 010354 XCPHS
0000 K 010473 WVMN      0000 K 010475 WVSD      0000 R 010474 WVR      0000 R 010271 XCG      0000 R 010414 X1
0000 K 010337 XHP      0000 K 010272 XML      0000 R 010370 XW      0000 R 001232 XWV
0000 K 000024 Y         0000 K 010371 YW        0000 R 010372 ZW

```

DATE 010572 PAGE 4

THIS PROGRAM COMPUTES THE RESPONSE OF AN AXI-SYMMETRIC BUOY

EXPOSED TO THE OCEAN ENVIRONMENT

UNITS ARE IN FT., LB., SEC

```

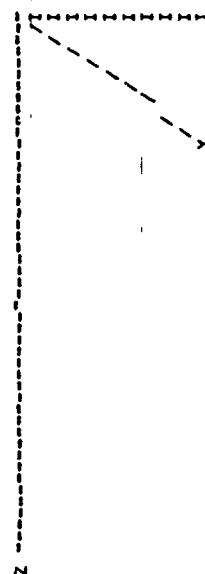
00100 C
00100 1* C
00100 2* C
00100 3* C
00100 4* C
00100 5* C
00100 6* C
00100 7* C
00100 8* C
00100 9* C
00100 10* C
00100 11* C
00100 12* C
00100 13* C
00100 14* C
00100 15* C
00100 16* C
00100 17* C
00100 18* C
00100 19* C
00100 20* C
00100 21* C
00100 22* C
00100 23* C
00100 24* C
00100 25* C
00100 26* C
00100 27* C
00100 28* C
00100 29* C

```

```

DIMENSION D(20),Y(20)
DIMENSION TEN(21),STRN(21),PHI(21),THE(21)
DIMENSION MONEG(10),AMP(10),PHS(10)
DIMENSION TENB(12),XWV(12),AWV(12),ACX(12),ACY(12)
DIMENSION ACZ(12),BPIT(12),BROL(12)
REAL MHXX,MHTY,MHZZ,MHBB,MHGG,MHAA,MHXB,MHXY,MHYZ,MHNB,MHNBZ
REAL MHGX,MHBX,MHGX,MH,MU,MXX,MYY,MZZ,MAA,MNB,MNGG,MNBX,MNBZ
REAL NXG,NGX,NYG,NGY,NZB,NBZ
THE COORDINATE SYSTEM

```



DATE 010572 PAGE 5

BUOY DYNAMICS

00112	30*	C				
00112	31*	C		I		
00112	32*	C		I		
00112	33*	C		I		
00112	34*	C		I		
00112	35*	C		I		
00112	36*	C		I		
00112	37*	C		I		
00112	38*	C		I		
00112	39*	C		I		
00112	40*	C		I		
00112	41*	C		I		
00112	42*	C		I		
00113	43*					
00114	44*					
00115	45*					
00116	46*					
00117	47*					
00120	48*					
00121	49*					
00122	50*					
00123	51*					
00124	52*					
00125	53*					
00126	54*					
00127	55*					
00130	56*	C				
00130	57*	C				
00130	58*	C				
00131	59*	C				
00131	60*	C				
00136	61*	C				
00136	62*	C				
00145	63*	C				
00145	64*	C				
00145	65*	C				
00154	66*	C				
00154	67*	C				
00154	68*	C				
00154	69*	C				
00155	70*	C				
00161	71*	C				
00161	72*	C				
00161	73*	C				
00161	74*	C				
00161	75*	C				
00162	76*	C				
00162	77*	C				
00162	78*	C				
00162	79*	C				
00162	80*	C				
00166	81*	C				
00167	82*	C				
00167	83*	C				
00167	84*	C				
00167	85*	C				
00167	86*	C				
00170	87*	C				

103 FORMAT(11H BUOY SINKS)  
 105 FORMAT(6F10.2)  
 106 FORMAT(9H UNSTABLE)  
 107 FORMAT(5F10.4)  
 108 FORMAT(2F10.4)  
 109 FORMAT(3F10.4)  
 112 FORMAT(8F8.2)  
 120 FORMAT(1F10.4)  
 121 FORMAT(1F20.4)  
 122 FORMAT(1F30.4)  
 123 FORMAT(1F40.4)  
 124 FORMAT(1F50.4)  
 129 FORMAT(3F10.5)  
 131 FORMAT(8F8.5)  
 READ IN THE BUOY PARAMETERS  
 BUOY RADIUS MT. OF C.G. FROM MOOR POINT AND THE LENGTH OF THE  
 MOOR POINT BELOW THE BOTTOM OF THE BUOY  
 READ 109,MR,XCG,XML  
 INERTIAS  
 READ 107,MB,ALIN,BTIN,GWIN  
 WING LIFT AND DRAG COEFFICIENTS AND AREAS  
 READ 107,MCDC,CL,AREA,WARL,NCPT  
 THE VISCOSITY THE WATER AT 40 DEG F  
 MU=2.735E-5  
 READ THE MEAN WIND CAUSING THE SEA STATE (WHICH MAY BE DIFFERENT  
 THAN THE WIND ACTING DURING THE SIMULATION) AND ITS DURATION  
 READ 108,WINDS,SDUR  
 CALL WAVE(WINDS,SDUR,WHT,PER,MONEG,AMP,PHS)  
 THE CURRENTS IN THE WATER COLUMN  
 READ THE Y AND Z COMPONENTS OF THE SURFACE CURRENT  
 READ 108,CYS,CZS  
 IF THE CURRENT VARIES WITH DEPTH, INSERT THE FUNCTIONS FOR  
 STRENGTH AND DIRECTION  
 FOR A UNIFORM CURRENT  
 CY=CYS  
 CZ=CZS  
 THE WIND ACTING ON THE BUOY  
 READ THE WIND COMPONENTS ACTING ON THE BUOY AT THE TIME OF THE  
 SIMULATION  
 READ 108,WINDY,WINDZ

DATE 010572 PAGE 6

## BUOY DYNAMICS

```

00174 88* WFX=-0.0034*WCL*WALE*(WINDY**2+WINDZ**2)
00175 89* WFY=0.0034*WCU*WAREA*(WINDY*ABS(WINDY))
00176 90* WFZ=0.0034*WCD*WAREA*(WINDZ*ABS(WINDZ))
00177 91* WFBT=-WFZ*WCPHT
00200 92* WFGM=-WFX*WCPHT
00201 93* J=1
00202 94* N=12
00203 95* NN=1
00204 96* R=0.0025
00205 97* A=0.0
00206 98* K=0
00207 99* M=0
00207 100* C THE INITIAL CONDITIONS
00207 101* C ALL ACCELERATIONS AND VELOCITIES ARE ZERO
00210 102* O0 58 I=1.41,2
00213 103* O(1)=0.0
00214 104* 56 Y(1)=0.0
00214 105* C READ THE INITIAL BUOY DISPLACEMENTS - X,Y,Z
00216 106* READ 109,Y(2),Y(4),Y(6)
00216 107* C THE INITIAL BUOY ANGLES ARE ZERO
00223 108* Y(8)=0.0
00224 109* Y(10)=0.0
00225 110* Y(12)=0.0
00225 111* C THE INITIAL CONDITIONS FOR THE CABLE
00226 112* DO 2 L=1,21
00231 113* 2 READ 129,STRN(L),PHI(L),THE(L)
00237 114* 30 CONTINUE
00237 115* C THE HYDRODYNAMIC MASSES AND MOMENTS OF INERTIA
00237 116* C
00237 117* C
00237 118* C THE DIMENSIONLESS FREQUENCY
00240 119* FK=((6.2832/PER)**2)*BR/32.2
00241 120* BLAMB=SQRT(6.25/(PER*HU))
00242 121* BA=BLAMB*BR
00242 122* C HYDRODYNAMIC FORCE MOMENT ARM
00243 123* XHM=4.16
00243 124* C HEAVE
00244 125* IF(FR.GE.0.2)GO TO 31
00246 126* CMX=2.31
00247 127* GO TO 33
00250 128* 31 IF(FR.GE.2.4)GO TO 32
00252 129* CMX=1.35725*(FR**(-.330597))
00253 130* GO TO 33
00254 131* 32 CMX=1.0
00254 132* C SWAY-SURGE
00255 133* CMY=0.215
00256 134* C ROLL
00257 135* CMX=1.988*(BR**3)*CMX
00257 136* CMY=1.988*((BR**3)*CMY+0.8045)
00261 137* CMZ=MHY
00261 138* C
00262 139* MH=16.65*(BR**5)/(1.0+BA)/(1.0+2.0*BA+2.0*(BA**2))
00262 140* C PITCH - ROLL
00263 141* MHBL=MH*(XHM**2)
00264 142* MHGB=MH*(YHM**2)
00264 143* C CROSS-COUPLED HYDROMASSES
00265 144* MHBX=0.0
00266 145* MHGX=0.0

```







DATE 010572 PAGE 10

BUOY DYNAMICS

```

00501 320* C ROLL- GAMMA MOTION
00502 321* O(11)=(-BGX-BGG-MHGX-DDX1-MHGY-DDY1+MHGG-DDGM-MNGX-DX1-MNGY-DY1
00503 322* 1 -HGG-DGM1-DGGY-DY2+ABS(UY2)-DGG6-DGM2+ABS(DGM2)+WFGM+FGM)/
00504 323* 2 (GM1+MHGG)
00505 324* O(12)=Y(11)
00506 325* C CALL RUNGE(N,Y,C,A,R,M,K)
00507 326* GO TO (50,40)*K
00508 327* 40 ALFA=57.4*Y(8)
00509 328* BETA=57.4*Y(10)
00510 329* GAMMA=57.4*Y(12)
00511 330* J=J+1
00512 331* IF(J.EQ.20160 TO 72
00513 332* GO TO 73
00514 333* 72 TENB(NN)=TEN(1)/1000.0
00515 334* XWV(NN)=XV
00516 335* AMV(NN)=DOXM
00517 336* ACX(NN)=D(11)
00518 337* ACY(NN)=D(13)
00519 338* ACZ(NN)=D(15)
00520 339* BPIT(NN)=Y(10)
00521 340* BROL(NN)=Y(12)
00522 341* WRITE(4,131)A,X,DDX,D(1),TENB(NN),STRN(1),PHI(1),THE(1)
00523 342* NNN=1
00524 343* 73 CONTINUE
00525 344* C
00526 345* C INSTABILITY LIMITER
00527 346* DO 60 I=1,N
00528 347* 60 IF(Y(1).GE.10000.0)GO TO 92
00529 348* IF(NN.EQ.512)GO TO 87
00530 349* GO TO 5
00531 350* 87 CALL DSTAT(TENB,TBMN,TBVR,IBSO1
00532 351* CALL DSTAT(AMV,AMMN,AMVR,AMSD)
00533 352* CALL DSTAT(XMV,XMMN,XMVR,XMSD)
00534 353* CALL DSTAT(ACX,AXMN,AXVR,AXSD)
00535 354* CALL DSTAT(ACY,AYMN,AYVR,AYSDD)
00536 355* CALL DSTAT(ACZ,AZMN,AZVR,AZSD)
00537 356* CALL DSTAT(BPIT,BPMN,BPVR,BPSD)
00538 357* CALL DSTAT(BROL,BRMN,BRVR,BRSD)
00539 358* WRITE(4,109)TBMN,TBVR,IBSO
00540 359* WRITE(4,109)AMMN,AMVR,AMSD
00541 360* WRITE(4,109)XMMN,XMVR,XMSD
00542 361* WRITE(4,109)AXMN,AXVR,AXSD
00543 362* WRITE(4,109)AYMN,AYVR,AYSDD
00544 363* WRITE(4,109)AZMN,AZVR,AZSD
00545 364* WRITE(4,109)BPMN,BPVR,BPSD
00546 365* WRITE(4,109)BRMN,BRVR,BRSD
00547 366* GO TO 86
00548 367* 92 WRITE(4,166)
00549 368* 88 STOP
00550 369* END
00551 370*
00552 371*

```

END OF UNIVAC 1108 FORTRAN V COMPILATION. 0 \*DIAGNOSTIC\* MESSAGE(S)



## BUOY DYNAMICS

DATE 010572 PAGE 11

Q1 FOR RMAVE,RWAVE  
 UNIVAC 1108 FORTRAN V LEVEL 2206 0023  
 THIS COMPILATION WAS DONE ON 01 MAY 72 AT 10:50:57

10:50:57, 61

SUBROUTINE RMAVE ENTRY POINT 000417

STORAGE USED (BLOCK, NAME, LENGTH)

0001 \*CODE 000452  
 0000 \*DATA 000173  
 0002 \*BLANK 000000

EXTERNAL REFERENCES (BLOCK, NAME)

0003 ALOG10  
 0004 NEXP65  
 0005 ALOG  
 0006 EXP  
 0007 SQRT  
 0010 NERR35

STORAGE ASSIGNMENT FOR VARIABLES (BLOCK, TYPE, RELATIVE LOCATION, NAME)

0001 000207 1436 0001 000303 161G 0001 000321 167G 0001 000235 402L  
 0000 K 000052 FPAR 0000 K 000053 FPAR 0000 R 000012 DOMEK 0000 R 000036 FETCH  
 0000 K 000057 FPAR 0000 K 000043 FPARL 0000 R 000050 FPI 0000 R 000042 DURMIN 0000 R 000055 G  
 0000 K 000047 HSPAR 0000 K 000046 HSPARL 0000 R 000051 FP2 0000 R 000056 OM  
 0000 K 000000 OMEK 0000 K 000045 P3PAR 0000 I 000054 IS 0000 R 000057 SPECT  
 0000 R 000041 TPAR 0000 K 000040 TPARL 0000 R 000024 SPEC

00101 1\* SUBROUTINE RMAVE(WINDS,DUR,WHIM,PER,MOMEK,AMP,PHS)  
 00101 2\* C USE THE BRETTSCHEIDER WAVE METHOD TO COMPUTE THE MEAN WAVE  
 00101 3\* C HEIGHT AND PERIOD  
 00101 4\* C ASSUME A 100 MILE FETCH FOR DEEP SEA BUOYS  
 00103 5\* DIMENSION ONEG(10),MOMEK(10),DOMEK(10),SPEC(10),PHS(10),AMP(10)  
 00104 6\* REAL MOMEK  
 00105 7\* FETCHES,OMES  
 00106 8\* FETCH LIMITED CASE  
 00107 9\* FPAR=32.2\*FETCH/(WINDS\*\*2)  
 00108 10\* TPAR=1.477-0.225\*ALOG10(FPAR)  
 00110 11\* TPAR=10.0\*\*TPARL  
 00111 12\* DURMIN=TPAR\*FETCH/(WINDS\*\*0.0)  
 00112 13\* IF (DUR-DURMIN)303,304,304  
 00112 14\* C DURATION LIMITED CASE  
 00115 15\* 303 TPAR=DUR\*WINDS\*3600.0/FETCH  
 00116 16\* FPAR=5.78-3.915\*ALOG10(TPAR)  
 00117 17\* FPAR=10.0\*\*FPARL  
 00120 18\* 304 P3PAR=-1.156+0.283\*ALOG10(FPAR)  
 00121 19\* P3PAR=10.0\*\*P3PARL  
 00122 20\* IF (FPAR.LT.0.02)P3PAR=0.02\*\*7

DATE 010572 PAGE 12

## BUOY DYNAMICS

```

00124 21 IF (FPAR.GT.1.E5) P3PAR=2.0
00126 22 PER=0.149*P3PAR*WINDS
00127 23 H3PARL=-2.5+0.415*ALOG10(FPAR)
00130 24 H3PAR=10.0+H3PARL
00131 25 IF (FPAR.LT.0.016) H3PAR=0.0057
00133 26 IF (FPAR.GT.5.0E4) H3PAR=0.282
00135 27 WTM=0.01942*H3PAR*(WINDS**2)
00136 28 COMPUTE FREQUENCIES AND AMPLITUDES FOR A 9 COMPONENT WAVE MODEL
00137 29
00137 29 F1=32.2*WTM/(WINDS**2)
00137 30 F2=32.2*WTM/(6.2832*WINDS)
00137 31 APAR=3.437*(F1**2)/(F2**4)
00141 32 BPAR=-0.675*((32.2/(WINDS**F2))**4)
00142 33 DO 401 IS=1,9
00145 34 G=10.0/IS
00145 35 OMEG(1S)=(-BPAR/(ALOG(G)))*0.25
00150 36 OMEG(10)=500.0
00151 37 OM=0.0
00152 38 OM=OM+0.05
00153 39 SPECT=(1037.0*APAR/(OM**5))*EXP(BPAR/(OM**4))
00154 40 IF (SPECT.LE.0.001) GO TO 402
00156 41 OMEG(1)=OM+0.5*(OMEG(1)-OM)
00157 42 OMEG(1)=OMEG(1)-OM
00160 43 DO 403 IS=2,9
00163 44 OMEG(1S)=(OMEG(1S)+OMEG(1S+1))/2.0
00164 45 OMEG(1S)=OMEG(1S+1)-OMEG(1S)
00166 46 DO 404 IS=1,8
00171 47 SPECT(1S)=(1037.0*APAR/((OMEG(1S))**5))
00171 48 1 *EXP(BPAR/((OMEG(1S))**4))
00172 49 404 AMP(1S)=0.5*SORT(SPECT(1S)*OMEG(1S))
00174 50 AMP(9)=0.0
00174 51 USE A RANDOM NUMBER TABLE TO SELECT RANDOM PHASE ANGLES FR
00174 52 EACH COMPONENT
00175 53 PHS(1)=0.306
00176 54 PHS(2)=6.255
00177 55 PHS(3)=4.655
00200 56 PHS(4)=5.20
00201 57 PHS(5)=0.575
00202 58 PHS(6)=3.220
00203 59 PHS(7)=5.545
00204 60 PHS(8)=0.435
00205 61 PHS(9)=0.657
00206 62 RETURN
00207 63 END

```

END OF UNIVAC 1106 FORTRAN V COMPILATION 0 \*DIAGNOSTIC\* MESSAGE(S)

## BUOY DYNAMICS

DATE 010572 PAGE 13

DI FOR TORBU,TORBU

UNIVAC 1108 FORTRAN V LEVEL 2206 0023

THIS COMPILATION WAS DONE ON 01 MAY 72 AT 10:50:58

10:50:58.774

SUBROUTINE TORBU ENTRY POINT 000340

STORAGE USED (BLOCK, NAME, LENGTH)

0001 \*CODE 000363  
 0000 \*DATA 000061  
 0002 \*BLANK 000000

EXTERNAL REFERENCES (BLOCK, NAME)

0003 SIN  
 0004 COS  
 0005 SQR  
 0006 ATAN  
 0007 NEHR35

STORAGE ASSIGNMENT FOR VARIABLES (BLOCK, TYPE, RELATIVE LOCATION, NAME)

0001 000145 10L 0001 000225 11L 0001 000220 16L 0001 000245 19L  
 0001 000275 20L 0001 000236 3L 0001 000132 8L 0001 000012 ALF  
 0000 R 000013 AK 0000 R 000011 ART 0000 R 000014 ARTY 0000 R 000016 BXTIL  
 0000 R 000001 GAM 0000 R 000010 HB 0000 000011 INOPS 0000 R 000002 DGAM  
 0000 R 000003 RI 0000 R 000006 VOL 0000 R 000007 VOLX 0000 R 000004 RS  
 0000 R 000005 ZGBH 0000 R 000015 X 0000 R 000017 XM

00101 1\* SUBROUTINE TORBU(H,TIL,BXX,BTT,BXT,BTX)  
 00101 2\* C THIS SUBROUTINE COMPUTES THE DISPLACEMENT AND RIGHTING MOMENT  
 00101 3\* C FOR THE 8 FOOT CIA. RICHARDSON BUOY USED IN THE BUOY MOTION  
 00101 4\* C EXPERIMENT

00103 5\* J=1  
 00104 6\* GAM=1.5708  
 00105 7\* DGAM=0.1  
 00106 8\* RI=2.75  
 00107 9\* RS=1.25  
 00110 10\* ZGBH=1.282  
 00111 11\* VOL=0.0  
 00112 12\* VOLX=0.0

00113 13\* 9 CONTINUE  
 00114 14\* HB=H-(ZGBH-H)\*(1.0-COS(TIL))+RT\*SIN(TIL)\*SIN(GAM)  
 00115 15\* IF(J.EQ.1)HB=H  
 00117 16\* IF(HB.LE.0.0)HB=0.0  
 00121 17\* IF(HB.GT.(0.99\*RS))GO TO 8  
 00123 18\* IF(HB.GT.(1.1\*99\*RS))GO TO 11  
 00125 19\* ART=SQRT((RS\*\*2)/((RS-HB)\*\*2))-1.0  
 00126 20\* IF(ART.EE.25.0)GO TO 16  
 00130 21\* ALF=2.0\*ATAN(ART)

DATE 010572 PAGE 14

BUOY DYNAMICS

```

00131 22* AH=0.5*(RS**2)*(ALF-SIN(ALF))
00132 23* GO TO 18
00133 24* 8 CONTINUE
00134 25* IF (HM.GT.(1.01*HS))GO TO 10
00135 26* AR=1.5708*RS*HS
00136 27* GO TO 18
00137 28* 10 ARTY=((RS**2)/((RS-(2.0*RS*HB)**2))-1.0
00138 29* IF (ARTY.LT.0.0)ARTY=0.0
00139 30* ART=SQRT(ARTY)
00140 31* IF (ART.GE.25.0)GO TO 16
00141 32* ALF=2.0*ATAN(ART)
00142 33* AH=3.1416*(RS**2)-0.5*(RS**2)*(ALF-SIN(ALF))
00143 34* GO TO 15
00144 35* 16 AR=1.5708*(RS**2)
00145 36* GO TO 18
00146 37* 11 AR=3.1416*(RS**2)
00147 38* 18 IF (J.EQ.1)GO TO 3
00148 39* GO TO 19
00149 40* 3 BXX=02.124*ART*AR
00150 41* J=2
00151 42* GO TO 9
00152 43* 19 VOL=VOL+UGAM*RT*AR
00153 44* X=RT*SIN(GAM)
00154 45* VOLX=VOLX+X*OGAM*RT*AR
00155 46* GAM=GAM+DGAM
00156 47* IF (GAM.GE.1.57)GO TO 20
00157 48* GO TO 9
00158 49* 20 BXTIL=128.0*VOL
00159 50* BXT=BXTIL*81.4
00160 51* C THE RIGHTING ARM
00161 52* XM=(VOLX/VOL)*COS(TIL)-(2GBH*H)*SIN(TIL)
00162 53* BTT=BXTIL*XG
00163 54* BTX=BXT*XM
00164 55* RETURN
00165 56* END

```

END OF UNIVAC 1108 FORTRAN V COMPILATION. 0 \*DIAGNOSTIC\* MESSAGE(S)

## BUOY DYNAMICS

DATE 010572 PAGE 15

10:51:00.349

GI FOR MOOR, MOOR  
 UNIVAC 1108 FORTRAN V LEVEL 2206 0023  
 THIS COMPILATION WAS DONE ON 01 MAY 72 AT 10:51:00

SUBROUTINE MOOR ENTRY POINT 002352

STORAGE USED (BLOCK, NAME, LENGTH)

0001 \*CODE 002412  
 0000 \*DATA 000760  
 0002 \*BLANK 000000

EXTERNAL REFERENCES (BLOCK, NAME)

0003 COS  
 0004 SIN  
 0005 NEXP6S  
 0006 SORT  
 0007 MERR3S

STORAGE ASSIGNMENT FOR VARIABLES (BLOCK, TYPE, RELATIVE LOCATION, NAME)

0001	00065	130G	0001	000215	146G	0001	000577	2L	0001	000074	3L	0001	000363	41L
0001	000351	42L	0001	002267	482G	0001	002306	471G	0001	000374	A	0001	000540	ACUA
0000	000341	ACUB	0000	000542	ACUD	0000	000612	ACUP1	0000	000613	ACUQ1	0000	000551	ACUR
0000	000543	ACVA	0000	000544	ACVB	0000	000545	ACVD	0000	000614	ACVP2	0000	000615	ACVG2
0000	000552	ACVR	0000	000546	ACWA	0000	000547	ACWB	0000	000650	ACWO	0000	000616	ACWP2
0000	000617	ACWQ2	0000	000553	ACWR	0000	000455	CDN	0000	000456	CDT	0000	000626	CGP2
0000	000627	CGQ2	0000	000625	CGR	0000	000457	CHMCN	0000	000458	CHMCT	0000	000628	CHP1
0000	000624	CHQ1	0000	000622	CHR	0000	000550	CHI	0000	000550	CH2P2	0000	000629	CHQ2
0000	000557	CH2K	0000	000551	CIP2	0000	000632	CIG2	0000	000630	CIR	0000	000561	CH2Q2
0000	000451	DIA	0000	000521	DRAGH	0000	000650	DRAGT	0000	000450	DTDE	0000	000453	CMU
0000	000507	EB	0000	000510	ED	0000	000151	EN	0000	000452	EP1	0000	000531	EP2
0000	000530	EQ1	0000	000532	EQ2	0000	000526	ER	0000	000462	H	0000	000524	HP1
0000	000564	HP2	0000	000525	HQ1	0000	000525	HQ2	0000	000463	I	0000	000667	INJPS
0000	000517	N	0000	000511	PHIA	0000	000512	PHIB	0000	000465	PHID	0000	000677	PHIN
0000	000602	PHIP1	0000	000604	PHIP2	0000	000603	PHIQ1	0000	000605	PHIQ2	0000	000536	PHIR
0000	000461	RHO	0000	000450	SMAX	0000	000522	SP1	0000	000522	SP2	0000	000523	SP1
0000	000563	SQ2	0000	000521	SR	0000	000514	THEA	0000	000515	THEB	0000	000516	THEO
0000	000124	THEN	0000	000606	THEP1	0000	000610	THEP2	0000	000607	THEQ1	0000	000611	THEQ2
0000	000537	THER	0000	000464	UA	0000	000465	UB	0000	000466	UC	0000	000467	UD
0000	000470	UE	0000	000471	UF	0000	000400	UN	0000	000472	UG	0000	000473	UH
0000	000566	UF1	0000	000570	JP2	0000	000567	UB1	0000	000571	UG2	0000	000572	UH2
0000	000554	US5	0000	000472	VA	0000	000473	VB	0000	000474	VC	0000	000475	VD
0000	000476	VE	0000	000477	VF	0000	000478	VG	0000	000479	VE	0000	000480	VF
0000	000572	VP1	0000	000573	VP2	0000	000574	VQ1	0000	000575	VQ2	0000	000576	VR
0000	000446	VSM	0000	000555	VSS	0000	000500	WA	0000	000501	WB	0000	000502	WC
0000	000503	WD	0000	000504	WE	0000	000505	WF	0000	000506	WG	0000	000507	WH
0000	000250	WP	0000	000526	WP1	0000	000600	WP2	0000	000527	WQ1	0000	000601	WQ2
0000	000535	WR	0000	000447	WSM	0000	000556	WS5	0000	000448	WTC	0000	000557	WT5

DATE 010572 PAGE 16

## BUOY DYNAMICS

```

00101 SUBROUTINE MOOR(T,K,UBY,VBY,WBY,EP,PHIP,THEP)
00101 THIS SUBROUTINE COMPUTES THE RESPONSE OF A MOORING LINE IN THE
00101 OCEAN ENVIRONMENT TO THE MOTIONS OF A BUOY. THREE DIMENSIONAL
00101 MOTIONS ARE CONSIDERED. COUPLED TENSILE WAVES AND TRANSVERSE WAVES
00101 ARE PROPAGATING UP AND DOWN THE MOORING LINE. THE MOORING CLUMP
00101 IS ASSUMED TO BE OF INFINITE MASS AND RIGIDITY CAUSING 100 PCT
00101 REFLECTION OF WAVES. THE SOLUTION OF THE SET OF PARTIAL
00101 DIFFERENTIAL EQUATIONS IS EFFECTED WITH A METHOD OF CHARACTERISTIC
00101 TECHNIQUE CALLED HARTREE'S METHOD.
00101 THE MOORING LINE HAS 4800 FT. OF 1/4 INCH WIRE ROPE AND 3200 FT.
00101 OF 5/8 NYLON ROPE
00101
00103 DIMENSION UN(21),VN(21),WN(21),PHIN(21),THEN(21),EN(21)
00104 DIMENSION UP(21),VP(21),WP(21),PHIP(21),THEP(21),EP(21)
00105 DIMENSION UO(21),VO(21),WO(21)
00106 DIMENSION A(6,7)
00107 REAL K
00108 THE CABLE PROPERTIES, INITIAL CONDITION* AND COEFFICIENTS
00109 VSM=0.0
00110 WSM=-1.5
00111 SHAX=8000.0
00112 THE WIRE ROPE PROPERTIES
00113 DIA=0.0312
00114 WTC=0.125
00115 CABLE MASS PER UNIT LENGTH X 100
00116 DISTRIBUTE THE MASS OF THE INSTRUMENTS OVER THE CABLE
00117 CMU=0.672
00118 COT=0.05
00119 CON=1.4
00120 CHMCT=0.6
00121 CHMCN=0.00153
00122 OTDE=6.875
00123 RHOS=1.987
00124 H=0.05*SPAX
00125
00126 AMES CRITERIA - H/K GREATER THAN ANY CHARACTERISTIC
00127
00128 IF (T.GT.0.0) GO TO 3
00129 DO 4, I=1,21
00130 VP(I)=0.0
00131 WPI(I)=0.0
00132 WPT(I)=0.0
00133 VOT(I)=0.0
00134 WOT(I)=0.0
00135 WOT(I)=0.0
00136 WOT(I)=0.0
00137 WOT(I)=0.0
00138
00139 4 CONTINUE
00140
00141 TRANSFORM THE BUOY VELOCITIES TO CABLE COORDINATES
00142 UN(1)=UBY.COS(PHIP(1)).COS(THEP(1)).VBY.SIN(PHIP(1))
00143 1 +WBY.COS(PHIP(1)).SIN(THEP(1))
00144 VN(1)=UBY.SIN(PHIP(1)).COS(THEP(1)).VBY.COS(PHIP(1))
00145 1 -WBY.SIN(PHIP(1)).SIN(THEP(1))
00146 WN(1)=UBY.SIN(THEP(1)).WBY.COS(THEP(1))
00147 1 -UN(1)
00148 DO 50 I=2,20
00149 UA=UP(I)
00150 UB=UP(I-1)
00151 UC=UO(I-1)
00152

```

## BUOY DYNAMICS

DATE 010572 PAGE 17

```

00153 UD=UP(I+1)
00154 UE=UO(I)
00155 UF=UO(I+1)
00156 VA=VP(I)
00157 VB=VP(I+1)
00158 VC=VO(I+1)
00159 VD=VP(I+1)
00160 VE=VO(I)
00161 VF=VO(I+1)
00162 WA=WP(I)
00163 WB=WP(I+1)
00164 WC=WO(I+1)
00165 WD=WP(I+1)
00166 WE=WO(I)
00167 WF=WO(I+1)
00168 EA=EP(I)
00169 EB=EP(I+1)
00170 EC=EP(I+1)
00171 ED=EP(I+1)
00172 TH=TH(I+1)
00173 TE=TH(I+1)
00174 TH=TH(I+1)
00175 TH=TH(I+1)
00176 TH=TH(I+1)
00177 TH=TH(I+1)
00178 TH=TH(I+1)
00179 TH=TH(I+1)
00180 TH=TH(I+1)
00181 TH=TH(I+1)
00182 TH=TH(I+1)
00183 TH=TH(I+1)
00184 TH=TH(I+1)
00185 TH=TH(I+1)
00186 TH=TH(I+1)
00187 TH=TH(I+1)
00188 TH=TH(I+1)
00189 TH=TH(I+1)
00190 TH=TH(I+1)
00191 TH=TH(I+1)
00192 TH=TH(I+1)
00193 TH=TH(I+1)
00194 TH=TH(I+1)
00195 TH=TH(I+1)
00196 TH=TH(I+1)
00197 TH=TH(I+1)
00198 TH=TH(I+1)
00199 TH=TH(I+1)
00200 TH=TH(I+1)
00201 TH=TH(I+1)
00202 TH=TH(I+1)
00203 TH=TH(I+1)
00204 TH=TH(I+1)
00205 TH=TH(I+1)
00206 TH=TH(I+1)
00207 TH=TH(I+1)
00208 TH=TH(I+1)
00209 TH=TH(I+1)
00210 TH=TH(I+1)
00211 TH=TH(I+1)
00212 TH=TH(I+1)
00213 TH=TH(I+1)
00214 TH=TH(I+1)
00215 TH=TH(I+1)
00216 TH=TH(I+1)
00217 TH=TH(I+1)
00218 TH=TH(I+1)
00219 TH=TH(I+1)
00220 TH=TH(I+1)
00221 TH=TH(I+1)
00222 TH=TH(I+1)
00223 TH=TH(I+1)
00224 TH=TH(I+1)

```

STRAINS ARE DISCONTINUOUS BETWEEN TWO ADJACENT CABLES  
 USE AN EULER APPROXIMATION TO ESTIMATE THE STRAINS ACROSS THE  
 DISCONTINUITY  
 IF(1.5G.13)EU=2.0\*EP(13)-EP(12)  
 IF(1.5G.14)EB=2.0\*EP(14)-EP(15)  
 PHIA=PHIP(I)  
 PHIB=PHIP(I+1)  
 PHID=PHIP(I+1)  
 THEA=THEP(I)  
 THEB=THEP(I+1)  
 THED=THEP(I+1)  
 CHANGE THE CABLE PROPERTIES AT 4800 FT.  
 IF(1.5G.14)GO TO 42  
 GO TO 41

42 THE NYLON ROPE PROPERTIES  
 DIA=0.052  
 WTC=0.0105  
 CHUC=0.455  
 CHMC=0.00425  
 DTDC=3.06E4  
 41 CONTINUE

THIS SECTION PERFORMS QUADRATURE IN THE T-S PLANE USING HARTREE'S  
 METHOD (A HYBRID METHOD)  
 ARRANGEMENT OF POINTS IN GRID FOR HARTREE'S METHOD

```

J+1      R
      ---
      B--A--O
      ---
J-1      C--E--F
      ---
      I-1 I I+1

```

NEO  
 CH1=11300.0  
 IF(1.5G.14)CH1=2600.0  
 SR=H\*(I-1)

DATE 010572 PAGE 18

## BUOY DYNAMICS

00225 116\* SPI=SK-CH1\*K  
 00226 117\* S01=SR-CH1\*K  
 00227 118\* HP1=SR-SF1  
 00230 119\* H01=HP1  
 00231 120\* ER=EA  
 00232 121\* EP1=EA-(HP1/H)\*(EA-EB)  
 00233 122\* E01=EA\*(H01/H)\*(ED-EA)  
 00234 123\* EP2=EP1  
 00235 124\* EQ2=EQ1  
 00236 125\* UR=UA  
 00237 126\* VR=VA  
 00240 127\* WR=WA  
 00241 128\* PHIR=PHIA  
 00242 129\* THER=THEA  
 00243 130\* ACUA=(UA-UE)/K  
 00244 131\* ACUB=(UB-UC)/K  
 00245 132\* ACUD=(UD-UF)/K  
 00246 133\* ACVA=(VA-VE)/K  
 00247 134\* AVB=(VB-VC)/K  
 00250 135\* ACVD=(VD-VF)/K  
 00251 136\* ACVA=(VA-VE)/K  
 00252 137\* ACWB=(WB-WC)/K  
 00253 138\* ACWD=(WD-WF)/K  
 00254 139\* ACUR=ACUA  
 00255 140\* ACVR=ACVA  
 00256 141\* ACWR=ACWA  
 00257 142\* WEBSTER CURRENT PROFILE  
 00258 143\* WSN=3.9/((SR/3.2802)\*\*0.418)  
 00260 144\* WSH=WSN  
 00261 145\* USS=VSN\*SIN(PHIA)-WSN\*COS(PHIA)\*SIN(THEA)  
 00262 146\* VSS=VSN\*COS(PHIA)-WSN\*SIN(PHIA)\*SIN(THEA)  
 00263 147\* WSS=WSN\*COS(THEA)  
 00264 148\* 2 CONTINUE  
 00265 149\* CH2K=CH1\*SQRTER(1.0+ER))  
 00266 150\* CH2P2=CH1\*SQRTER(EP2/(1.0+EP2))  
 00267 151\* CH2Q2=CH1\*SQRTER(EQ2/(1.0+EQ2))  
 00270 152\* SP2=SR-0.5\*(CH2R+CH2P2)\*K  
 00271 153\* SG2=SR+0.5\*(CH2R+CH2Q2)\*K  
 00272 154\* HP2=SR-SP2  
 00273 155\* H02=S02-SR  
 00274 156\* EP2=EA-(HP2/H)\*(EA-EB)  
 00275 157\* E02=EA\*(H02/H)\*(ED-EA)  
 00276 158\* UP1=UA-(HP1/H)\*(UA-UB)  
 00277 159\* UQ1=UA\*(H01/H)\*(UD-UA)  
 00300 160\* VP2=UA-(HP2/H)\*(UA-UB)  
 00301 161\* UQ2=UA\*(H02/H)\*(UD-UA)  
 00302 162\* VP1=VA-(HP1/H)\*(VA-VB)  
 00303 163\* VQ1=VA\*(H01/H)\*(VD-VA)  
 00304 164\* VP2=VA-(HP2/H)\*(VA-VB)  
 00305 165\* VQ2=VA\*(H02/H)\*(VD-VA)  
 00306 166\* WP1=WA-(HP1/H)\*(WA-WB)  
 00307 167\* WQ1=WA\*(H01/H)\*(WD-WA)  
 00310 168\* WP2=WA-(HP2/H)\*(WA-WB)  
 00311 169\* WQ2=WA\*(H02/H)\*(WD-WA)  
 00312 170\* PHIP1=PHIA-(HP1/H)\*(PHIA-PHIB)  
 00313 171\* PHIQ1=PHIA\*(H01/H)\*(PHIA-PHIB)  
 00314 172\* PHIP2=PHIA-(HP2/H)\*(PHIA-PHIB)  
 00315 173\* PHIQ2=PHIA\*(H02/H)\*(PHIA-PHIB)

C





DATE 010572 PAGE 20

BUOY DYNAMICS

```

00371 232* A(3,3)=0.0
00372 233* A(3,4)=0.0
00373 234* A(3,5)=0.5*((1.0+ER)*CH2R)+((1.0+EP2)*C*H2P2)
00374 235* A(3,6)=0.5*((1.0+ER)*CH2R)+((1.0+EP2)*C*H2P2)*PHIP2
00375 236* A(3,7)=0.5*((1.0+ER)*CH2R)+((1.0+EP2)*C*H2P2)*PHIP2
00376 237* 1-A(3,6)*THEP2-109.0*0.5*(CGR+CGP2)*K/CMU
00377 238* C
00378 239* A(4,1)=0.0
00379 240* A(4,2)=1.0
00380 241* A(4,3)=0.0
00381 242* A(4,4)=0.0
00382 243* A(4,5)=0.5*((1.0+ER)*CH2R)+((1.0+EP2)*CH2O2)
00383 244* A(4,6)=0.5*((1.0+ER)*CH2R)+((1.0+EP2)*CH2O2)*PHIQ2
00384 245* A(4,7)=0.5*((1.0+ER)*CH2R)+((1.0+EP2)*CH2O2)*PHIQ2
00385 246* 1-A(4,6)*THEQ2-100.0*0.5*(CGR+CGQ2)*K/CMU
00386 247* C
00387 248* A(5,1)=0.0
00388 249* A(5,2)=0.0
00389 250* A(5,3)=1.0
00390 251* A(5,4)=0.0
00391 252* A(5,5)=0.0
00392 253* A(5,6)=0.5*((1.0+ER)*CH2R)+((1.0+EP2)*CH2P2)*COS(0.5*(PHIR
00393 254* 1+PHIP2))-0.5*((1.0+ER)*CH2R)+((1.0+EP2)*CH2P2)*COS(0.5*(PHIR
00394 255* 2-0.5*((1.0+ER)*CH2R)+((1.0+EP2)*CH2P2)*COS(0.5*(PHIR+PHIP2)))
00395 256* A(5,7)=0.5*((1.0+ER)*CH2R)+((1.0+EP2)*CH2P2)*K/CMU
00396 257* C
00397 258* A(6,1)=0.0
00398 259* A(6,2)=0.0
00399 260* A(6,3)=1.0
00400 261* A(6,4)=0.0
00401 262* A(6,5)=0.0
00402 263* A(6,6)=0.5*((1.0+ER)*CH2R)+((1.0+EP2)*CH2O2)*COS(0.5*(PHIR
00403 264* 1+PHIQ2))-0.5*((1.0+ER)*CH2R)+((1.0+EP2)*CH2O2)*COS(0.5*(PHIR+PHIQ2))
00404 265* 2-0.5*((1.0+ER)*CH2R)+((1.0+EP2)*CH2O2)*COS(0.5*(PHIR+PHIQ2)))
00405 266* A(6,7)=0.5*((1.0+ER)*CH2R)+((1.0+EP2)*CH2O2)*K/CMU
00406 267* C
00407 268* C
00408 269* C
00409 270* C
00410 271* C
00411 272* C
00412 273* C
00413 274* C
00414 275* C
00415 276* C
00416 277* C
00417 278* C
00418 279* C
00419 280* C
00420 281* C
00421 282* C
00422 283* C
00423 284* C
00424 285* C
00425 286* C
00426 287* C
00427 288* C
00428 289* C
00429 290* C
00430 291* C
00431 292* C
00432 293* C
00433 294* C
00434 295* C
00435 296* C
00436 297* C
00437 298* C
00438 299* C
00439 300* C
00440 301* C
00441 302* C
00442 303* C
00443 304* C
00444 305* C
00445 306* C
00446 307* C
00447 308* C
00448 309* C
00449 310* C
00450 311* C
00451 312* C
00452 313* C
00453 314* C
00454 315* C
00455 316* C
00456 317* C
00457 318* C
00458 319* C
00459 320* C
00460 321* C
00461 322* C
00462 323* C
00463 324* C
00464 325* C
00465 326* C
00466 327* C
00467 328* C
00468 329* C
00469 330* C
00470 331* C
00471 332* C
00472 333* C
00473 334* C
00474 335* C
00475 336* C
00476 337* C
00477 338* C
00478 339* C
00479 340* C
00480 341* C
00481 342* C
00482 343* C
00483 344* C
00484 345* C
00485 346* C
00486 347* C
00487 348* C
00488 349* C
00489 350* C
00490 351* C
00491 352* C
00492 353* C
00493 354* C
00494 355* C
00495 356* C
00496 357* C
00497 358* C
00498 359* C
00499 360* C
00500 361* C
00501 362* C
00502 363* C
00503 364* C
00504 365* C
00505 366* C
00506 367* C
00507 368* C
00508 369* C
00509 370* C
00510 371* C
00511 372* C
00512 373* C
00513 374* C
00514 375* C
00515 376* C
00516 377* C
00517 378* C
00518 379* C
00519 380* C
00520 381* C
00521 382* C
00522 383* C
00523 384* C
00524 385* C
00525 386* C
00526 387* C
00527 388* C
00528 389* C
00529 390* C
00530 391* C
00531 392* C
00532 393* C
00533 394* C
00534 395* C
00535 396* C
00536 397* C
00537 398* C
00538 399* C
00539 400* C
00540 401* C
00541 402* C
00542 403* C
00543 404* C
00544 405* C
00545 406* C
00546 407* C
00547 408* C
00548 409* C
00549 410* C
00550 411* C
00551 412* C
00552 413* C
00553 414* C
00554 415* C
00555 416* C
00556 417* C
00557 418* C
00558 419* C
00559 420* C
00560 421* C
00561 422* C
00562 423* C
00563 424* C
00564 425* C
00565 426* C
00566 427* C
00567 428* C
00568 429* C
00569 430* C
00570 431* C
00571 432* C
00572 433* C
00573 434* C
00574 435* C
00575 436* C
00576 437* C
00577 438* C
00578 439* C
00579 440* C
00580 441* C
00581 442* C
00582 443* C
00583 444* C
00584 445* C
00585 446* C
00586 447* C
00587 448* C
00588 449* C
00589 450* C
00590 451* C
00591 452* C
00592 453* C
00593 454* C
00594 455* C
00595 456* C
00596 457* C
00597 458* C
00598 459* C
00599 460* C
00600 461* C
00601 462* C
00602 463* C
00603 464* C
00604 465* C
00605 466* C
00606 467* C
00607 468* C
00608 469* C
00609 470* C
00610 471* C
00611 472* C
00612 473* C
00613 474* C
00614 475* C
00615 476* C
00616 477* C
00617 478* C
00618 479* C
00619 480* C
00620 481* C
00621 482* C
00622 483* C
00623 484* C
00624 485* C
00625 486* C
00626 487* C
00627 488* C
00628 489* C
00629 490* C
00630 491* C
00631 492* C
00632 493* C
00633 494* C
00634 495* C
00635 496* C
00636 497* C
00637 498* C
00638 499* C
00639 500* C
00640 501* C
00641 502* C
00642 503* C
00643 504* C
00644 505* C
00645 506* C
00646 507* C
00647 508* C
00648 509* C
00649 510* C
00650 511* C
00651 512* C
00652 513* C
00653 514* C
00654 515* C
00655 516* C
00656 517* C
00657 518* C
00658 519* C
00659 520* C
00660 521* C
00661 522* C
00662 523* C
00663 524* C
00664 525* C
00665 526* C
00666 527* C
00667 528* C
00668 529* C
00669 530* C
00670 531* C
00671 532* C
00672 533* C
00673 534* C
00674 535* C
00675 536* C
00676 537* C
00677 538* C
00678 539* C
00679 540* C
00680 541* C
00681 542* C
00682 543* C
00683 544* C
00684 545* C
00685 546* C
00686 547* C
00687 548* C
00688 549* C
00689 550* C
00690 551* C
00691 552* C
00692 553* C
00693 554* C
00694 555* C
00695 556* C
00696 557* C
00697 558* C
00698 559* C
00699 560* C
00700 561* C
00701 562* C
00702 563* C
00703 564* C
00704 565* C
00705 566* C
00706 567* C
00707 568* C
00708 569* C
00709 570* C
00710 571* C
00711 572* C
00712 573* C
00713 574* C
00714 575* C
00715 576* C
00716 577* C
00717 578* C
00718 579* C
00719 580* C
00720 581* C
00721 582* C
00722 583* C
00723 584* C
00724 585* C
00725 586* C
00726 587* C
00727 588* C
00728 589* C
00729 590* C
00730 591* C
00731 592* C
00732 593* C
00733 594* C
00734 595* C
00735 596* C
00736 597* C
00737 598* C
00738 599* C
00739 600* C
00740 601* C
00741 602* C
00742 603* C
00743 604* C
00744 605* C
00745 606* C
00746 607* C
00747 608* C
00748 609* C
00749 610* C
00750 611* C
00751 612* C
00752 613* C
00753 614* C
00754 615* C
00755 616* C
00756 617* C
00757 618* C
00758 619* C
00759 620* C
00760 621* C
00761 622* C
00762 623* C
00763 624* C
00764 625* C
00765 626* C
00766 627* C
00767 628* C
00768 629* C
00769 630* C
00770 631* C
00771 632* C
00772 633* C
00773 634* C
00774 635* C
00775 636* C
00776 637* C
00777 638* C
00778 639* C
00779 640* C
00780 641* C
00781 642* C
00782 643* C
00783 644* C
00784 645* C
00785 646* C
00786 647* C
00787 648* C
00788 649* C
00789 650* C
00790 651* C
00791 652* C
00792 653* C
00793 654* C
00794 655* C
00795 656* C
00796 657* C
00797 658* C
00798 659* C
00799 660* C
00800 661* C
00801 662* C
00802 663* C
00803 664* C
00804 665* C
00805 666* C
00806 667* C
00807 668* C
00808 669* C
00809 670* C
00810 671* C
00811 672* C
00812 673* C
00813 674* C
00814 675* C
00815 676* C
00816 677* C
00817 678* C
00818 679* C
00819 680* C
00820 681* C
00821 682* C
00822 683* C
00823 684* C
00824 685* C
00825 686* C
00826 687* C
00827 688* C
00828 689* C
00829 690* C
00830 691* C
00831 692* C
00832 693* C
00833 694* C
00834 695* C
00835 696* C
00836 697* C
00837 698* C
00838 699* C
00839 700* C
00840 701* C
00841 702* C
00842 703* C
00843 704* C
00844 705* C
00845 706* C
00846 707* C
00847 708* C
00848 709* C
00849 710* C
00850 711* C
00851 712* C
00852 713* C
00853 714* C
00854 715* C
00855 716* C
00856 717* C
00857 718* C
00858 719* C
00859 720* C
00860 721* C
00861 722* C
00862 723* C
00863 724* C
00864 725* C
00865 726* C
00866 727* C
00867 728* C
00868 729* C
00869 730* C
00870 731* C
00871 732* C
00872 733* C
00873 734* C
00874 735* C
00875 736* C
00876 737* C
00877 738* C
00878 739* C
00879 740* C
00880 741* C
00881 742* C
00882 743* C
00883 744* C
00884 745* C
00885 746* C
00886 747* C
00887 748* C
00888 749* C
00889 750* C
00890 751* C
00891 752* C
00892 753* C
00893 754* C
00894 755* C
00895 756* C
00896 757* C
00897 758* C
00898 759* C
00899 760* C
00900 761* C
00901 762* C
00902 763* C
00903 764* C
00904 765* C
00905 766* C
00906 767* C
00907 768* C
00908 769* C
00909 770* C
00910 771* C
00911 772* C
00912 773* C
00913 774* C
00914 775* C
00915 776* C
00916 777* C
00917 778* C
00918 779* C
00919 780* C
00920 781* C
00921 782* C
00922 783* C
00923 784* C
00924 785* C
00925 786* C
00926 787* C
00927 788* C
00928 789* C
00929 790* C
00930 791* C
00931 792* C
00932 793* C
00933 794* C
00934 795* C
00935 796* C
00936 797* C
00937 798* C
00938 799* C
00939 800* C
00940 801* C
00941 802* C
00942 803* C
00943 804* C
00944 805* C
00945 806* C
00946 807* C
00947 808* C
00948 809* C
00949 810* C
00950 811* C
00951 812* C
00952 813* C
00953 814* C
00954 815* C
00955 816* C
00956 817* C
00957 818* C
00958 819* C
00959 820* C
00960 821* C
00961 822* C
00962 823* C
00963 824* C
00964 825* C
00965 826* C
00966 827* C
00967 828* C
00968 829* C
00969 830* C
00970 831* C
00971 832* C
00972 833* C
00973 834* C
00974 835* C
00975 836* C
00976 837* C
00977 838* C
00978 839* C
00979 840* C
00980 841* C
00981 842* C
00982 843* C
00983 844* C
00984 845* C
00985 846* C
00986 847* C
00987 848* C
00988 849* C
00989 850* C
00990 851* C
00991 852* C
00992 853* C
00993 854* C
00994 855* C
00995 856* C
00996 857* C
00997 858* C
00998 859* C
00999 860* C
01000 861* C

```

DATE 010572 PAGE 21

BUGY DYNAMICS

```

00446 290* C THE LOWER BOUNDARY - VELOCITIES ARE ZERO
00450 291* UN(21)=0.0
00451 292* VN(21)=0.0
00452 293* WN(21)=0.0
00453 294* *CF AN EULER APPROXIMATION FOR ANGLES AND STRAIN
00454 295* EN(21)=2.0*EN(20)-EN(19)
00455 296* PHIN(21)=2.0*PHIN(20)-PHIN(19)
00456 297* THEN(21)=2.0*THEN(20)-THEN(19)
00457 298* EN(1)=2.0*EN(2)-EN(3)
00460 300* PHIN(1)=2.0*PHIN(2)-PHIN(3)
00461 301* THEN(1)=2.0*THEN(2)-THEN(3)
00462 302* SET JTH VALUES INTO THE (J-1)TH REGISTERS
00463 303* DO 51 I=1,21
00464 304*   UO(I)=UP(I)
00465 305*   VO(I)=VP(I)
00466 306*   SI WO(I)=WP(I)
00470 307* C SET THE (J+1)TH VALUES INTO THE JTH REGISTERS
00471 308* DO 52 I=1,21
00472 309*   UP(I)=UN(I)
00473 310*   VP(I)=VN(I)
00474 311*   WP(I)=WN(I)
00475 312*   EP(I)=EN(I)
00476 313*   PHIP(I)=PHIN(I)
00477 314*   THEP(I)=THEN(I)
00500 315* RETURN
00501 316* END

```

END OF UNIVAC 1108 FORTRAN V COMPILATION. 0 \*DIAGNOSTIC\* MESSAGE(S)

BUOY DYNAMICS

DATE 010572 PAGE 22

WI FOR RUNGE,RUNGE  
UNIVAC 1108 FORTRAN V LEVEL 2206 0023  
THIS COMPILATION WAS DONE ON 01 MAY 72 AT 10:51:05

10:51: 5.197

SUBROUTINE RUNGE ENTRY POINT 000134

STORAGE USED (BLOCK, NAME, LENGTH)

0001 \*CODE 000163  
0000 \*DATA 000115  
0002 \*BLANK 000000

EXTERNAL REFERENCES (BLOCK, NAME)

0003 NERR23  
0004 NERR135

STORAGE ASSIGNMENT FOR VARIABLES (BLOCK, TYPE, RELATIVE LOCATION, NAME)

Block	Type	Relative Location	Name
0001	00021 1L	0001	000121 10L
0001	00030 3L	0001	000032 4L
0000	000063 A	0000	1 000062 I
0001	000054 1206	0001	000103 1306
0001	000074 7L	0001	000117 9L
0000	R 000000 Q		

00101 14 C SUBROUTINE RUNGE(N,Y,F,X,H,M,K)  
00101 20 THIS ROUTINE PERFORMS RUNGE KUTTA CALCULATIONS BY GILL'S METHOD  
00103 30 MEM\*1  
00104 40 GO TO (1,4,5,3,7),M  
00105 50 1 DO 2 I=1,N  
00106 60 2 Q(I)=0.0  
00107 70 A=0.5  
00108 80 GO TO 9  
00109 90 3 A=1.707107  
00110 100 C IF YOU NEED MORE ACCURACY USE A=1.7071067811865475244  
00111 110 4 X=X+0.5\*H  
00112 120 5 DO 6 I=1,N  
00113 130 Y(I)=Y(I)+A\*(F(I)+H\*Q(I))  
00114 140 6 Q(I)=2.0\*A\*H\*(F(I)+(1.0-3.0\*A)\*Q(I))  
00115 150 A=0.2928932  
00116 160 C IF YOU NEED MORE ACCURACY USE A=0.2928932188134524756  
00117 170 7 DO 8 I=1,N  
00118 180 8 Y(I)=Y(I)+H\*(F(I)+6.0\*Q(I))/3.0  
00119 190 M=0.0  
00120 200 K=2  
00121 210 GO TO 10  
00122 220 9 K=1  
00123 230 10 RETURN  
00124 240  
00125 250  
00126 260 END

## BUOY DYNAMICS

Q1 FOR DSTAT,DSTAT  
 UNIVAC 1106 FORTRAN V LEVEL 2206 0023  
 THIS COMPILATION WAS DONE ON 01 MAY 72 AT 10:51:06

DATE 010572 PAGE 24

10:51: 6.415

SUBROUTINE DSTAT ENTRY POINT 000045

STORAGE USED (BLOCK, NAME, LENGTH)

0001 \*CODE 000062  
 0000 \*DATA 000017  
 0002 \*BLANK 000000

EXTERNAL REFERENCES (BLOCK, NAME)

0003 SORT  
 0004 NERR35

STORAGE ASSIGNMENT FOR VARIABLES (BLOCK, TYPE, RELATIVE LOCATION, NAME)

0001 000012 1106 0000 000005 INJPS 0000 1 000003 J  
 0000 K 000002 S1 0000 1 000001 S

00101  
 00103  
 00107  
 00105  
 00106  
 00107  
 00112  
 00113  
 00115  
 00116  
 00117  
 00120  
 00121

1\* SUBROUTINE DSTAT(PAR,PRMN,PRVR,PRSD)  
 2\* DIMENSION PAR(2048)  
 3\* N=512  
 4\* S=0.0  
 5\* S1=0.0  
 6\* DO 3 J=1,512  
 7\* S=S+PAR(J)  
 8\* PRMN=S/N  
 9\* PRVR=(S1-PRMN\*S)/N  
 10\* PRSD=SORT(PRVK)  
 11\* RETURN  
 12\*  
 13\* END

END OF UNIVAC 1106 FORTRAN V COMPILATION.

0 \*DIAGNOSTIC\* MESSAGE(S)

# Appendix C

## DERIVATION OF THE CABLE CHARACTERISTICS

In order to rewrite the cable equations in their "normal" form, the characteristic roots of the cable equations must be determined. From equation (168) of the main text, we see that  $AU_t + BU_s + C = 0$ ,

$$\begin{bmatrix} 0 & \mu V & \mu W \cos \phi & -\mu & 0 & 0 \\ 0 & -\mu V & -\mu W \sin \phi & 0 & -\mu & 0 \\ 0 & 0 & -\mu(U \cos \phi - V \sin \phi) & 0 & 0 & -\mu \\ -1 & 0 & 0 & 0 & 0 & 0 \\ 0 & -(1+\epsilon) & 0 & 0 & 0 & 0 \\ 0 & 0 & 0 & 0 & 0 & 0 \end{bmatrix} \begin{bmatrix} \partial \epsilon / \partial t \\ \partial \phi / \partial t \\ \partial \theta / \partial t \\ \partial U / \partial t \\ \partial V / \partial t \\ \partial W / \partial t \end{bmatrix}$$

$$+ \begin{bmatrix} \frac{dT}{d\epsilon} & 0 & 0 & 0 & 0 & 0 \\ 0 & \epsilon \frac{dT}{d\epsilon} & 0 & 0 & 0 & 0 \\ 0 & 0 & \epsilon \frac{dT}{d\epsilon} \cos \phi & 0 & 0 & 0 \\ 0 & -V & -W \cos \phi & 1 & 0 & 0 \\ 0 & U & W \sin \phi & 0 & 1 & 0 \\ 0 & 0 & (U \cos \phi - V \sin \phi) & 0 & 0 & 1 \end{bmatrix} \begin{bmatrix} \partial \epsilon / \partial s_0 \\ \partial \phi / \partial s_0 \\ \partial \theta / \partial s_0 \\ \partial U / \partial s_0 \\ \partial V / \partial s_0 \\ \partial W / \partial s_0 \end{bmatrix} + \begin{bmatrix} H \\ G \\ I \\ 0 \\ 0 \\ 0 \end{bmatrix} = 0$$

Multiplying through by the inverse of the  $A$  matrix yields

$$A^{-1}A U_t + A^{-1}B U_s + A^{-1}C = 0,$$

or

$$U_t + A^{-1}B U_s + A^{-1}C = 0.$$

To find the inverse of the  $A$  matrix, partition the  $A$  matrix into four 3-by-3 matrices:

$$A = \begin{bmatrix} D & -\mu I \\ E & 0 \end{bmatrix}$$

$$D = \begin{bmatrix} 0 & \mu V & \mu W \cos \phi \\ 0 & -\mu V & -\mu W \sin \phi \\ 0 & 0 & -\mu(U \cos \phi - V \sin \phi) \end{bmatrix}$$

$$E = \begin{bmatrix} -1 & 0 & 0 \\ 0 & -(1+\epsilon) & 0 \\ 0 & 0 & -(1+\epsilon) \cos \phi \end{bmatrix}.$$

Let  $A^{-1}$  be partitioned in the same way,

$$A^{-1} = \begin{bmatrix} K_1 & K_2 \\ K_3 & K_4 \end{bmatrix};$$

then

$$\begin{bmatrix} D & -\mu I \\ E & 0 \end{bmatrix} \begin{bmatrix} K_1 & K_2 \\ K_3 & K_4 \end{bmatrix} = \begin{bmatrix} I & 0 \\ 0 & I \end{bmatrix},$$

$$DK_1 - \mu K_3 = I$$

$$DK_2 - \mu K_4 = 0$$

$$EK_1 + 0 = 0 \quad E \text{ nonsingular} \therefore K_1 = 0$$

$$EK_2 + 0 = I \therefore K_2 = E^{-1}$$

Substituting into the first equation, we see that

$$K_3 = \frac{1}{\mu} I.$$

From the second equation, we see that

$$K_4 = \frac{1}{\mu} DK_2 = \frac{1}{\mu} DE^{-1}.$$

$$\therefore K_1 = 0$$

$$K_2 = \begin{bmatrix} -1 & 0 & 0 \\ 0 & -\frac{1}{(1+\epsilon)} & 0 \\ 0 & 0 & -\frac{1}{(1+\epsilon)\cos\phi} \end{bmatrix}$$

$$K_3 = \begin{bmatrix} -\frac{1}{\mu} & 0 & 0 \\ 0 & -\frac{1}{\mu} & 0 \\ 0 & 0 & -\frac{1}{\mu} \end{bmatrix}$$

$$K_4 = \begin{bmatrix} 0 & -\frac{V}{(1+\epsilon)} & -\frac{W}{(1+\epsilon)} \\ 0 & \frac{V}{(1+\epsilon)} & \frac{W \sin\phi}{(1+\epsilon)\cos\phi} \\ 0 & 0 & \frac{(U\cos\phi - V\sin\phi)}{(1+\epsilon)\cos\phi} \end{bmatrix}$$



The  $A^{-1}$  matrix is written

$$A^{-1} = \begin{bmatrix} 0 & 0 & 0 & -1 & 0 & 0 \\ 0 & 0 & 0 & 0 & -\frac{1}{(1+\epsilon)} & 0 \\ 0 & 0 & 0 & 0 & 0 & -\frac{1}{(1+\epsilon)\cos\phi} \\ -\frac{1}{\mu} & 0 & 0 & 0 & -\frac{V}{(1+\epsilon)} & -\frac{W}{(1+\epsilon)} \\ 0 & -\frac{1}{\mu} & 0 & 0 & \frac{U}{(1+\epsilon)} & \frac{W\sin\phi}{(1+\epsilon)\cos\phi} \\ 0 & 0 & -\frac{1}{\mu} & 0 & 0 & \frac{(U\cos\phi - V\sin\phi)}{(1+\epsilon)\cos\phi} \end{bmatrix}.$$

$A^{-1}B$

$$A^{-1} \cdot \begin{bmatrix} \frac{dT}{d\epsilon} & 0 & 0 & 0 & 0 & 0 \\ 0 & \epsilon \frac{dT}{d\epsilon} & 0 & 0 & 0 & 0 \\ 0 & 0 & \epsilon \frac{dT}{d\epsilon} \cos\phi & 0 & 0 & 0 \\ 0 & -V & -W\cos\phi & 1 & 0 & 0 \\ 0 & U & W\sin\phi & 0 & 1 & 0 \\ 0 & 0 & (U\cos\phi - V\sin\phi) & 0 & 0 & 1 \end{bmatrix} =$$

$$\begin{bmatrix} 0 & V & W\cos\phi & -1 & 0 & 0 \\ 0 & -\frac{V}{(1+\epsilon)} & -\frac{W\sin\phi}{(1+\epsilon)} & 0 & -\frac{1}{(1+\epsilon)} & 0 \\ 0 & 0 & -\frac{(U\cos\phi - V\sin\phi)}{(1+\epsilon)\cos\phi} & 0 & 0 & -\frac{1}{(1+\epsilon)\cos\phi} \\ -\frac{1}{\mu} \frac{dT}{d\epsilon} & -\frac{UV}{(1+\epsilon)} & -\frac{UW\cos\phi}{(1+\epsilon)} & 0 & -\frac{V}{(1+\epsilon)} & -\frac{W}{(1+\epsilon)} \\ 0 & \left(-\frac{\epsilon}{\mu} \frac{dT}{d\epsilon} + \frac{U^2}{(1+\epsilon)}\right) \left(\frac{2UW\sin\phi}{(1+\epsilon)} - \frac{VW\sin^2\phi}{(1+\epsilon)\cos\phi}\right) & 0 & \frac{U}{(1+\epsilon)} & \frac{W\sin\phi}{(1+\epsilon)\cos\phi} \\ 0 & 0 & \left(-\frac{\epsilon}{\mu} \frac{dT}{d\epsilon} \cos\phi + \frac{(U\cos\phi - V\sin\phi)^2}{(1+\epsilon)\cos\phi}\right) & 0 & 0 & \frac{(U\cos\phi - V\sin\phi)}{(1+\epsilon)\cos\phi} \end{bmatrix}.$$

$$\underline{A^{-1}G}$$

$$\begin{bmatrix} 0 & 0 & 0 & -1 & 0 & 0 \\ 0 & 0 & 0 & 0 & -\frac{1}{(1+\epsilon)} & 0 \\ 0 & 0 & 0 & 0 & 0 & -\frac{1}{(1+\epsilon)\cos\phi} \\ -\frac{1}{\mu} & 0 & 0 & 0 & -\frac{V}{(1+\epsilon)} & -\frac{W}{(1+\epsilon)} \\ 0 & -\frac{1}{\mu} & 0 & 0 & \frac{U}{(1+\epsilon)} & \frac{W\sin\phi}{(1+\epsilon)\cos\phi} \\ 0 & 0 & -\frac{1}{\mu} & 0 & 0 & \frac{(U\cos\phi - V\sin\phi)}{(1+\epsilon)\cos\phi} \end{bmatrix} \begin{bmatrix} H \\ G \\ I \\ 0 \\ 0 \\ 0 \end{bmatrix} = \begin{bmatrix} 0 \\ 0 \\ 0 \\ -\frac{H}{\mu} \\ -\frac{G}{\mu} \\ -\frac{I}{\mu} \end{bmatrix}.$$

To find the characteristics,  $\lambda$ , use  $|A^{-1}B - \lambda I| = 0$ :

$$\begin{bmatrix} 0-\lambda & V & W\cos\phi & -1 & 0 & 0 \\ 0 & -\frac{U}{(1+\epsilon)}-\lambda & -\frac{W\sin\phi}{(1+\epsilon)} & 0 & -\frac{1}{(1+\epsilon)} & 0 \\ 0 & 0 & -M-\lambda & 0 & 0 & -\frac{1}{(1+\epsilon)\cos\phi} \\ -\frac{1}{\mu}\frac{dT}{d\epsilon} & -\frac{UV}{(1+\epsilon)} & -\frac{VW\cos\phi}{(1+\epsilon)} & -\lambda & -\frac{V}{(1+\epsilon)} & -\frac{W}{(1+\epsilon)} \\ 0 & \left(-\frac{\epsilon}{\mu}\frac{dT}{d\epsilon} + \frac{U^2}{(1+\epsilon)}\right) & N & 0 & \left(\frac{U}{(1+\epsilon)} - \lambda\right) & \frac{W\sin\phi}{(1+\epsilon)\cos\phi} \\ 0 & 0 & \left(-\frac{\epsilon}{\mu}\frac{dT}{d\epsilon}\cos\phi + M(U\cos\phi - V\sin\phi)\right) & 0 & 0 & M-\lambda \end{bmatrix} = 0,$$

where

$$M = \frac{U\cos\phi - V\sin\phi}{(1+\epsilon)\cos\phi}$$

$$N = \frac{2UW\sin\phi}{(1+\epsilon)} - \frac{VW\sin^2\phi}{(1+\epsilon)\cos\phi}.$$

The first reduction is

$$-\lambda \begin{bmatrix} -\frac{U}{(1+\epsilon)} - \lambda & -\frac{W \sin \phi}{(1+\epsilon)} & 0 & -\frac{1}{(1+\epsilon)} & 0 \\ 0 & -M - \lambda & 0 & 0 & -\frac{1}{(1+\epsilon) \cos \phi} \\ -\frac{UV}{(1+\epsilon)} & -\frac{UW \cos \phi}{(1+\epsilon)} & -\lambda & -\frac{V}{(1+\epsilon)} & -\frac{W}{(1+\epsilon)} \\ \left(-\frac{\epsilon}{\mu} \frac{dT}{d\epsilon} + \frac{U^2}{(1+\epsilon)}\right) & N & 0 & \left(\frac{U}{(1+\epsilon)} - \lambda\right) & \frac{W \sin \phi}{(1+\epsilon) \cos \phi} \\ 0 & \left(-\frac{\epsilon}{\mu} \frac{dT}{d\epsilon} \cos \phi + M(U \cos \phi - V \sin \phi)\right) & 0 & 0 & M - \lambda \end{bmatrix}$$

$$+ \frac{1}{\mu} \frac{dT}{d\epsilon} \begin{bmatrix} V & W \cos \phi & -1 & 0 & 0 \\ -\frac{U}{(1+\epsilon)} - \lambda & -\frac{W \sin \phi}{(1+\epsilon)} & 0 & -\frac{1}{(1+\epsilon)} & 0 \\ 0 & -M - \lambda & 0 & 0 & -\frac{1}{(1+\epsilon) \cos \phi} \\ -\frac{\epsilon}{\mu} \frac{dT}{d\epsilon} + \frac{U^2}{(1+\epsilon)} & N & 0 & \left(\frac{U}{(1+\epsilon)} - \lambda\right) & \frac{W \sin \phi}{(1+\epsilon) \cos \phi} \\ 0 & \left(-\frac{\epsilon}{\mu} \frac{dT}{d\epsilon} \cos \phi + M(U \cos \phi - V \sin \phi)\right) & 0 & 0 & M - \lambda \end{bmatrix} = 0$$

The second reduction is

$$\lambda^2 \begin{bmatrix} -\frac{U}{(1+\epsilon)} - \lambda & -\frac{W \sin \phi}{(1+\epsilon)} & -\frac{1}{(1+\epsilon)} & 0 \\ 0 & -M - \lambda & 0 & -\frac{1}{(1+\epsilon) \cos \phi} \\ -\frac{\epsilon}{\mu} \frac{dT}{d\epsilon} + \frac{U^2}{(1+\epsilon)} & N & \frac{U}{(1+\epsilon)} - \lambda & \frac{W \sin \phi}{(1+\epsilon) \cos \phi} \\ 0 & -\frac{\epsilon}{\mu} \frac{dT}{d\epsilon} \cos \phi + M(U \cos \phi - V \sin \phi) & 0 & M - \lambda \end{bmatrix}$$

$$-\frac{1}{\mu} \frac{dT}{d\epsilon} \begin{bmatrix} -\frac{U}{(1+\epsilon)} - \lambda & -\frac{W \sin \phi}{(1+\epsilon)} & -\frac{1}{(1+\epsilon)} & 0 \\ 0 & -M - \lambda & 0 & -\frac{1}{(1+\epsilon) \cos \phi} \\ -\frac{\epsilon}{\mu} \frac{dT}{d\epsilon} + \frac{U^2}{(1+\epsilon)} & N & \frac{U}{(1+\epsilon)} - \lambda & \frac{W \sin \phi}{(1+\epsilon) \cos \phi} \\ 0 & -\frac{\epsilon}{\mu} \frac{dT}{d\epsilon} \cos \phi + M(U \cos \phi - V \sin \phi) & 0 & M - \lambda \end{bmatrix} = 0$$

Note that these two matrices are the same. Since they must be nonsingular, we see that

$$\lambda^2 - \frac{1}{\mu} \frac{dT}{d\epsilon} = 0 ;$$

thus,

$$\lambda = \pm \sqrt{\frac{1}{\mu} \frac{dT}{d\epsilon}} .$$

The third reduction is

$$-\frac{1}{(1+\epsilon)} \begin{bmatrix} 0 & -M - \lambda & -\frac{1}{(1+\epsilon) \cos \phi} \\ -\frac{\epsilon}{\mu} \frac{dT}{d\epsilon} + \frac{U^2}{(1+\epsilon)} & N & \frac{W \sin \phi}{(1+\epsilon) \cos \phi} \\ 0 & -\frac{\epsilon}{\mu} \frac{dT}{d\epsilon} \cos \phi + M(U \cos \phi - V \sin \phi) & M - \lambda \end{bmatrix}$$

$$+\left(\frac{U}{(1+\epsilon)}-\lambda\right)\begin{bmatrix}-\frac{U}{(1+\epsilon)}-\lambda & -\frac{W\sin\phi}{(1+\epsilon)} & 0 \\ 0 & -M-\lambda & -\frac{1}{(1+\epsilon)\cos\phi} \\ 0 & -\frac{\epsilon}{\mu}\frac{dT}{d\epsilon}\cos\phi+M(U\cos\phi-V\sin\phi) & M-\lambda\end{bmatrix}=0$$

The fourth reduction is

$$-\frac{1}{(1+\epsilon)}\left(\frac{\epsilon}{\mu}\frac{dT}{d\epsilon}-\frac{U^2}{(1+\epsilon)}\right)\begin{bmatrix}-M-\lambda & -\frac{1}{(1+\epsilon)\cos\phi} \\ -\frac{\epsilon}{\mu}\frac{dT}{d\epsilon}\cos\phi+M(U\cos\phi-V\sin\phi) & M-\lambda\end{bmatrix}$$

$$+\left(\frac{U}{(1+\epsilon)}-\lambda\right)\left(-\frac{U}{(1+\epsilon)}-\lambda\right)\begin{bmatrix}-M-\lambda & -\frac{1}{(1+\epsilon)\cos\phi} \\ -\frac{\epsilon}{\mu}\frac{dT}{d\epsilon}\cos\phi+M(U\cos\phi-V\sin\phi) & M-\lambda\end{bmatrix}=0$$

Again, the matrices are the same; since they must be nonsingular, we see i. at

$$-\frac{1}{(1+\epsilon)}\left(\frac{\epsilon}{\mu}\frac{dT}{d\epsilon}-\frac{U^2}{(1+\epsilon)}\right)+\left(\frac{U}{(1+\epsilon)}-\lambda\right)\left(-\frac{U}{(1+\epsilon)}-\lambda\right)=0,$$

or

$$\lambda = \pm \sqrt{\frac{1}{\mu} \frac{\epsilon}{(1+\epsilon)} \frac{dT}{d\epsilon}}.$$

The fifth reduction is

$$(-M-\lambda)(M-\lambda) - \left( \frac{\epsilon}{\mu} \frac{dT}{d\epsilon} \cos\phi + M(U \cos\phi - V \sin\phi) \right) \left( \frac{-1}{(1+\epsilon)\cos\phi} \right) = 0,$$

or

$$\lambda = \pm \sqrt{\frac{1}{\mu} \frac{\epsilon}{(1+\epsilon)} \frac{dT}{d\epsilon}}.$$

Summarizing, the six characteristics are

$$\lambda_1 = + \sqrt{\frac{1}{\mu(s_0)} \frac{dT}{d\epsilon}}$$

$$\lambda_2 = - \sqrt{\frac{1}{\mu(s_0)} \frac{dT}{d\epsilon}}$$

$$\lambda_3 = + \sqrt{\frac{1}{\mu(s_0)} \frac{\epsilon}{(1+\epsilon)} \frac{dT}{d\epsilon}}$$

$$\lambda_4 = - \sqrt{\frac{1}{\mu(s_0)} \frac{\epsilon}{(1+\epsilon)} \frac{dT}{d\epsilon}}$$

$$\lambda_5 = + \sqrt{\frac{1}{\mu(s_0)} \frac{\epsilon}{(1+\epsilon)} \frac{dT}{d\epsilon}}$$

$$\lambda_6 = - \sqrt{\frac{1}{\mu(s_0)} \frac{\epsilon}{(1+\epsilon)} \frac{dT}{d\epsilon}}.$$

## Appendix D

### COMPUTED INPUT DATA FOR THE SIMULATIONS

This appendix provides computed input data for the following:

1. Steady-state configurations of the 8-ft torroidal buoy and current meter array at Block Island Sound station BRAVO.
2. Steady-state configurations of the 8-ft torroidal buoy and cable used for WHOI Mooring No. 279.
3. Dynamics of the  $3\frac{1}{2}$ -ft spherical buoy and cable at station DELTA off New Harbor, Block Island.
4. Dynamics of the 8-ft torroidal buoy and cable at station BRAVO in Block Island Sound.
5. Dynamics of the 8-ft torroidal buoy and cable used for WHOI Mooring No. 238.

#### Inputs for the Simulation of Steady-State Configurations of the 8-ft Torroid and Current Meter Array at BRAVO

The components used in the buoy system are shown in figure 21 and are described in chapter IV of the main text. The input data are as follows:

- |                                 |           |
|---------------------------------|-----------|
| 1. Buoy diameter BD1            | 8.0 ft    |
| 2. Torroid section diameter BD2 | 2.5 ft    |
| 3. Buoy weight WB               | 1200.0 lb |
| 4. Maximum hull draft HM        | 2.5 ft    |

5. Free draft (when displacement equals buoy weight) HFREE 0.7 ft
6. Buoy windage WAREA  $12.84 \text{ ft}^2$
7. Wind drag coefficient WCD 0.971
8. Cable diameter DIA:
  - Upper line - 5/8-in. polypropylene 0.625 in.
  - Lower line - 3/8-in. wire rope 0.375 in.
9. Cable weight in water per unit length WTC:
  - Upper line - -0.02 lb/ft
  - Lower line - 0.2 lb/ft
10. Cable modulus of elasticity EC:
  - Upper line -  $1.67 \times 10^5 \text{ lb/in.}^2$
  - Lower line -  $1.20 \times 10^7 \text{ lb/in.}^2$
11. Mooring line length SM 235.0 ft
12. Current speeds at three depths:
  - CUR1, CUR2, and CUR3 1.0 to 1.77 knots
13. Current directions at three depths:
  - DIR 1, DIR 2, and DIR 3 0-360 deg
14. Water depth DEEP 120.0 ft
15. Wind speed y component 0.0 ft/sec
16. Wind speed x component 0.0 ft/sec.

The cable properties DIA, WTC, and EC are changed at a cable length of 230.0 ft from the values for the 5/8-in. polypropylene to the values for 3/8-in.



wire rope. Changes in tension and angles across the current meters were found by inserting the following procedures in the program:

1. Use and IF statement to locate the current meters along the mooring line.
2. Use the computed tension and angles to compute the force components acting on the top of the current meter.
3. Solve the statics equations for the current meter by using the current meter in-water weight and computed drag force components to find the force components acting on the bottom of the current meter.
4. Compute the current meter tilt angle.
5. Transform back to cable coordinates to find the new cable tension and angles.
6. Increase the cable length by 3 ft, i.e., the length of the current meter.
7. Continue integration down the cable.

The following data were required to accomplish the above:

Current meter weight in water WCM	67 lb
Current meter drag coefficient CDCM	0.59
Current meter frontal area ARCM	2.285 ft <sup>2</sup>

Current strengths and directions as functions of depth were computed as follows:

1. Average strengths and directions from current meters 1 and 2.
2. For depths of 0 to 70 ft, set the upper layer strength and direction equal to these values.

3. Test current meter 3 strength against mean strength of meters 1 and 2. If greater, set the lower layer current equal to the mean strength in the upper layer.
4. Current strength and direction in the lower layer (70 to 120 ft) set equal to current meter 3 strength and direction.

Integration step size (B) was set equal to 1.0 ft, and the limiting depth error bandwidth DDP was set equal to 1 ft.

Inputs for the Simulation of Steady-State  
Configurations of the 8-ft Torroid and  
Cable Used for WHOI Mooring No. 279

The components used in this mooring are shown in figure 27 and are described in chapter IV of the main text. Buoy dimensions are the same but the buoy weight is increased to account for the instruments in the buoy, the chain bridle, and instruments directly beneath the buoy. The input data are listed as follows:

1. Buoy diameter BD1	8.0 ft
2. Torroid section diameter BD2	2.5 ft
3. Buoy weight WB	2100.0 lb
4. Maximum hull draft HM	2.5 ft
5. Free draft HFREE	1.04 ft
6. Buoy windage WAREA	19.84 ft <sup>2</sup>
7. Buoy wind drag coefficient	0.971
8. Cable diameter DIA:	
Upper cable - 1/4-in. GAC	0.25 in.

Lower cable - 5/8-in. plaited nylon      0.625 in.

9. Cable weight in sea water per unit length WTC:

Upper cable -      0.090 lb/ft

Lower cable -      0.0105 lb/ft

10. Cable modulus of elasticity EC:

Upper cable -       $1.682 \times 10^7$  lb/in.<sup>2</sup>

Lower cable -       $3.52 \times 10^5$  lb/in.<sup>2</sup>     $0 < T < 1000$  lb

$6.79 \times 10^5$  lb/in.<sup>2</sup>     $1000 \text{ lb} < T < 2000 \text{ lb}$

$1.041 \times 10^6$  lb/in.<sup>2</sup>     $2000 \text{ lb} < T$

11. Mooring line length SM      8000.0 ft

12. Surface current CUR      0-1.46 knots

13. Water depth DEEP      8800.0 ft

14. Wind speed y component      0.0 ft/sec

15. Wind speed z component      0.0 ft/sec.

Cable properties were changed at a length of 4800 ft from the buoy and the changes in tension and angles were computed across the instruments in the line as before. The input data for the current meter and tensiometers are listed as follows:

Current meter:

Weight in water      120.0 lb

Drag coefficient      1.4

Frontal area       $2.92 \text{ ft}^2$

## Tensiometer:

Weight in water	50.0 lb
Drag coefficient	1.4
Frontal area	$0.875 \text{ ft}^2$

The drag force acting on the buoy was increased to account for the chain bridle and the instruments directly below the buoy. An effective area-drag coefficient product of  $22.18 \text{ ft}^2$  was added to the area-drag coefficient product of the buoy to account for the instruments and chains.

Inputs for the Simulation of Buoy System  
For the Spherical Buoy

The spherical buoy dimensions were measured and the buoy and its instrumentation were weighed. The center of gravity and mass moments of inertia were calculated from the known weights and dimensions. The cable and chain were weighed in air and the mass and weight in sea water of each were computed. Mean wind wave heights and periods and the frequencies, amplitudes, and phases were computed on the GSA computer by using program RWAVE (see subroutine RWAVE in appendix A) for a given wind speed, a 10-hr duration, and a 15-mile fetch. Input data are listed as follows:

1. Buoy hull radius BR	1.75 ft
2. Center of gravity height XML	0.208 ft
3. Mooring line connection height XML	0.208 ft
4. Buoy weight WB	440.0 lb
5. Buoy mass MB	$13.66 \text{ lb-sec}^2/\text{ft}$
6. Yaw mass moment of inertia ALIN	$11.967 \text{ lb-sec}^2/\text{ft}$

7. Pitch mass moment of inertia BTIN	17.46 lb-sec <sup>2</sup> /ft
8. Roll mass moment of inertia GMJN	19.875 lb-sec <sup>2</sup> /ft
9. Wind drag coefficient WCD	0.5
10. Windage (profile area) WAREA	5.435 ft <sup>2</sup>
11. Wind lift coefficient WCL	0.25
12. Plan area WAREL	4.81 ft <sup>2</sup>
13. Wind center of pressure height	1.068 ft
14. Mean wave height WHTM	0.5 to 4.05 ft
15. Mean wave period PER	2.2 to 6.0 sec
16. Unstretched cable lengths CLO(I)	18.75 ft
	18.75 ft
	18.75 ft
	18.75 ft
	12.5 ft
	12.5 ft
17. Upper cable diameter DIA1	0.0416 ft
18. Upper cable weight in sea water DWC1	0.35 lb/ft
19. Upper cable mass per unit length DCSM1	0.0124 lb-sec <sup>2</sup> /ft <sup>2</sup>
20. Lower cable diameter DIA2	0.125 ft
21. Lower cable weight in sea water DWC2	7.3 lb/ft
22. Lower cable mass per unit length DCSM2	0.233 lb-sec <sup>2</sup> /ft <sup>2</sup>
23. Surface current y component CYS	0.0 ft/sec
24. Surface current z component CZS	0.845 ft/sec
25. Wind y component	-30.0 ft/sec

26. Wind z component	-8.0 ft/sec
27. Initial buoy displacements y(2)	-0.21 ft
y(4)	-41.1 ft
y(6)	62.35 ft
28. Initial cable element displacements y(1)	15.04 ft
	27.54 ft
	38.76 ft
	49.46 ft
	55.95 ft
	62.00 ft
y(1 + 2)	-29.79 ft
	-20.54 ft
	-13.06 ft
	-6.86 ft
	-3.31 ft
	0.00 ft
y(1 + 4)	55.86 ft
	46.06 ft
	34.47 ft
	20.48 ft
	10.43 ft
	0.00 ft.

The highest natural frequency of the system was estimated by using the method described in appendix A, and a time step size ( $\Delta t$ ) of  $5 \times 10^{-4}$  sec was

used. The currents were uniform over the 62-ft water depth. A 30-lb force was added to the vertical cable force component acting on the buoy to account for the instrument package just below the buoy.

Inputs for the Simulation of Buoy System  
Dynamics for Torroidal Buoy BRAVO

Again, buoy dimensions and weights were measured or taken from the manufacturers' drawings, and the properties of the buoy were calculated. The chain bridle below the buoy was assumed to be rigid, and its mass and drag were included in the computations. In this case, each cable element weight, mass, and drag were listed directly in the program since the mooring line was composed of many elements (cable chains, current meter, sentinel, etc.). Input data are listed as follows:

1. Buoy hull radius $R_B$	4.0 ft
2. Center of gravity height $X_{CG}$	13.064 ft
3. Mooring line connection height $X_{ML}$	11.782 ft
4. Buoy weight $W_B$	2100.0 lb
5. Buoy mass $M_B$	65.25 lb
6. Yaw mass moment of inertia $A_{LIN}$	283.44 lb-sec <sup>2</sup> /ft
7. Pitch mass moment of inertia $B_{TIN}$	445.12 lb-sec <sup>2</sup> /ft
8. Roll mass moment of inertia $G_{MIN}$	445.12 lb-sec <sup>2</sup> /ft
9. Wind drag coefficient	0.971
10. Wind lift coefficient	0.25
11. Windage (profile area)	19.84 ft <sup>2</sup>
12. Plan area	50.3 ft <sup>2</sup>

13. Wind center of pressure height	6.19 ft
14. Wind speed causing the waves	
(11 June 1970)	16.9 ft/sec
15. Wind duration	
16. Surface current y component	
(11 June 1970)	-0.21 ft/sec
17. Surface current z component	
(11 June 1970)	-0.597 ft/sec
18. Wind y component	0.0 ft/sec
19. Wind z component	
(11 June 1970)	-16.9 ft/sec
20. Initial buoy displacements y(2)	-0.25 ft
y(4)	-0.7 ft
y(6)	208.6 ft
21. Initial cable element displacements y(I)	64.18 ft
	110.45 ft
	120.91 ft
	120.9 ft
y(I + 2)	-0.8358 ft
	-0.7416 ft
	-0.6817 ft
	0.0 ft
y(I + 4)	200.84 ft
	193.35 ft



144.95 ft

0.0 ft.

In this case, the time step size was taken to be  $5 \times 10^{-3}$  sec. Because of the chain bridle, the hydrodynamic force moment arm was computed to be 4.16 ft below the center of gravity. The surge and sway area-drag coefficient products include the effects of the steel bracing and chain bridle under the buoy.

Inputs for the Simulation of Buoy System  
Dynamics for the Torroidal Buoy and  
Cables Used in WHOI Mooring No. 238

Buoy dimensions, weights, masses, etc. are the same as those for the torroidal buoy at station BRAVO. The wind fetch length in subroutine RWAVE was changed to 100 miles to better simulate deep-sea wind wave conditions. Cable dynamics were simulated with subroutine MOOR, and the six dependent cable properties (tension, two angles, and three velocity components) were calculated at 20 points along the cable. Total unstretched mooring line length was 8000 ft: 4800 ft of 1/4-in. galvanized steel aircraft cable (polyolefin jacketed to 3/8-in. diameter) and 3200 ft of 5/8-in. plaited nylon.

The upper cable properties are listed as follows:

1. Diameter	0.0312 ft
2. Weight per unit length in sea water	0.125 lb/ft
3. Mass per unit length	$0.0054 \text{ lb-sec}^2/\text{ft}^2$
4. Characteristic velocity	11,300.0 ft/sec
5. Elastic modulus-cross section product	$6.87 \times 10^5 \text{ lb}$

The lower cable properties are listed as follows:

- |  |                                      |
|--|--------------------------------------|
| 1. Diameter                              | 0.052 ft                             |
| 2. Weight per unit length in sea water   | 0.0105 lb/ft                         |
| 3. Mass per unit length                  | $0.00455 \text{ lb-sec}^2/\text{ft}$ |
| 4. Characteristic velocity               | $2609.0 \text{ ft/sec}$              |
| 5. Elnetic modulus-cross section product | $3.06 \times 10^4 \text{ lb.}$       |

Cable properties were changed from wire rope to nylon rope at 4800 ft ( $l = 14$ ). The Webster current profile was used to compute steady drag forces on the cable. Numerical stability was maintained by using a time step ( $\Delta t$ ) of 0.02 sec. The  $H/K$  quotient is equal to 20,000 ft/sec, which is larger than the tensile wave speed in the upper cable (11,300 ft/sec). Initial strains and cable angles were computed with the steady-state, buoy system configuration program with the same current profile and a surface current of 1.5 knots. Winds of 10, 20, and 30 knots were used, and the computed steady-state strains and cable angles served as input (initial conditions) to the dynamics model.

Appendix E

BUOYANT FORCES AND MOMENTS FOR  
A TORROIDAL BUOY

In order to simulate the dynamics of the torroidal buoy, a method to compute the buoyant force and righting moment for a given buoy draft and tilt angle was developed. This computation was included in the program as subroutine TORBU, and it updated the buoyant force and moment for each integration time step.

Consider a torroid with major radius  $R$  and minor radius  $r$ , partially immersed in a fluid with a mean draft  $H$  and a tilt angle  $\theta$  (figure E-1). The area of an immersed circular segment with draft  $H_s$  is given by

$$A_s = \frac{1}{2} r^2 (\alpha - \sin \alpha), \quad (E-1)$$

where

$$\alpha = 2 \tan^{-1} \sqrt{\frac{r^2}{(r-H_s)^2} - 1}.$$

If  $H_s > r$ , we can redefine the draft

$$H'_s = 2r - H_s, \quad (E-2)$$

and

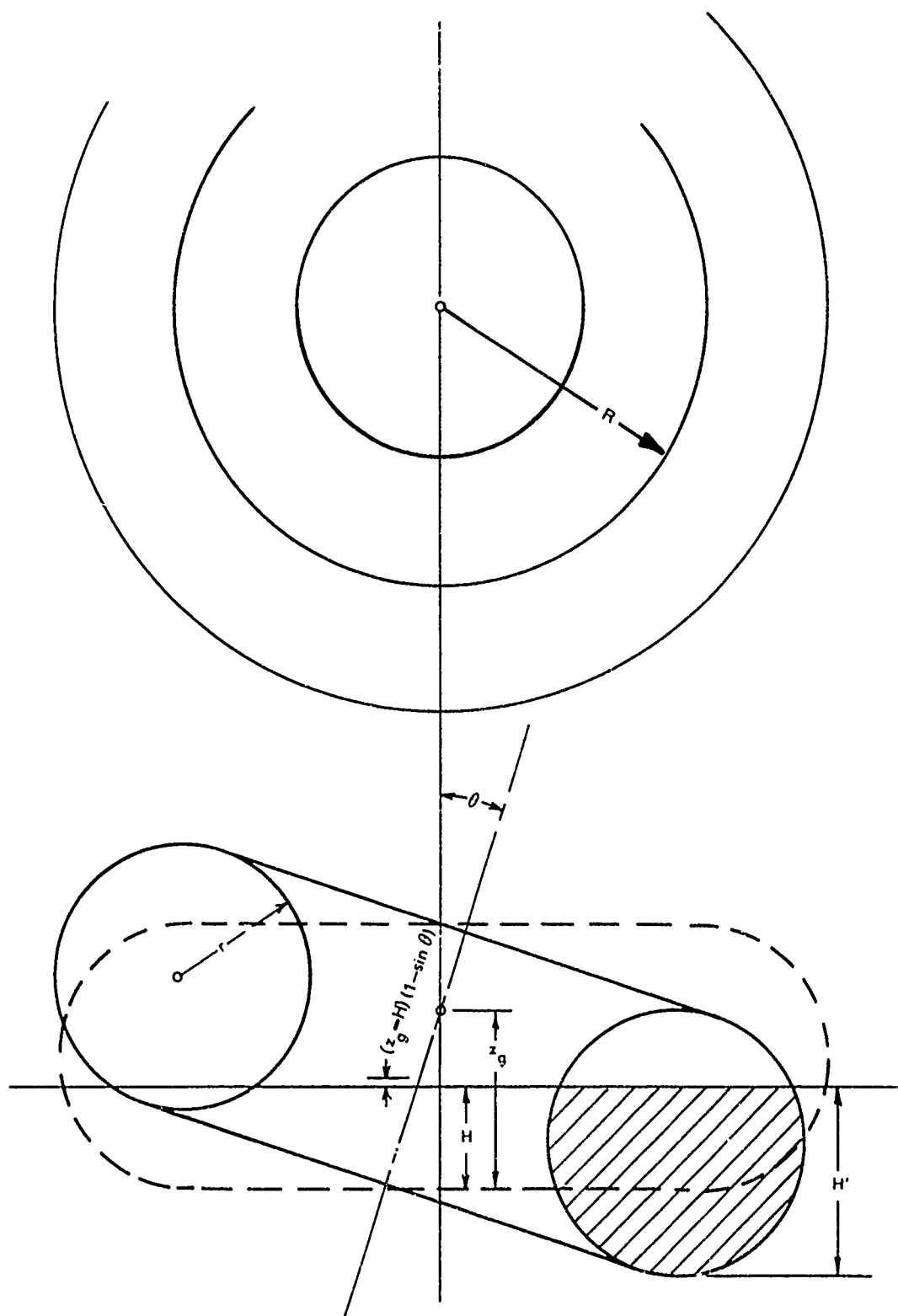


Figure E-1. Torroid Section

$$\alpha' = 2 \tan^{-1} \sqrt{\frac{r^2}{(r-H'_s)^2} - 1}.$$

Thus, the area becomes

$$A_s = \pi r^2 - \frac{1}{2} r^2 (\alpha' - \sin \alpha') \quad (\text{E-3})$$

Define the section draft,  $H_s$ , as a function of  $\phi$ , the radial angle about the torroid axis. The maximum draft in the direction of the tilt angle  $\theta$  ( $\phi = \pi/2$ ) is

$$H_{s_{\max}} = H + R \sin \theta,$$

and the minimum draft is

$$H_{s_{\min}} = H - R \sin \theta.$$

For any angle  $\phi$  around the torroid,

$$H_s = H + R \sin \phi \sin \theta + (\bar{z}_g - H)(1 - \sin \theta). \quad (\text{E-4})$$

The last term represents the small change in the mean draft  $H$  due to the fact that the tilt is about the center of gravity and not about the waterplane center.

By using the draft for any section as defined above, we can compute the immersed area of any section from equation (E-1) or (E-3). The immersed volume is found by integrating around the torroid,

$$V = 2 \cdot \int_{-\pi/2}^{\pi/2} A_s R d\phi, \quad (\text{E-5})$$

and the buoyant force

$$B = 2 \cdot \gamma \cdot R \int_{-\pi/2}^{\pi/2} A_s d\phi, \quad (E-6)$$

where  $\gamma$  is the weight density of the fluid. The centroid of the submerged volume  $V$  is computed in order to find the righting moment:

$$\bar{X} = \frac{2 \cdot \int_{-\pi/2}^{\pi/2} R \sin \phi A_s R d\phi}{2 \int_{-\pi/2}^{\pi/2} A_s R d\phi} \quad (E-7)$$

The righting arm is

$$X_{RA} = \bar{X} \cos \theta - (z_G - H) \sin \theta, \quad (E-8)$$

and the righting moment is

$$M = X_{RA} \cdot B \quad (E-9)$$

The above equations were programmed for subroutine TORBU, and the differential volumes were summed in 2-deg steps around the torroid. Buoy draft and tilt angle are the inputs, and the heave buoyant force, tilt righting moment, cross-coupled tilt-heave buoyant force, and cross-coupled heave-tilt righting moment are the outputs. Plots of the displacement, righting moment, and the cross-coupled force and moment for the Richardson torroid used at station BRAVO are shown in figures (E-2) through (E-5).

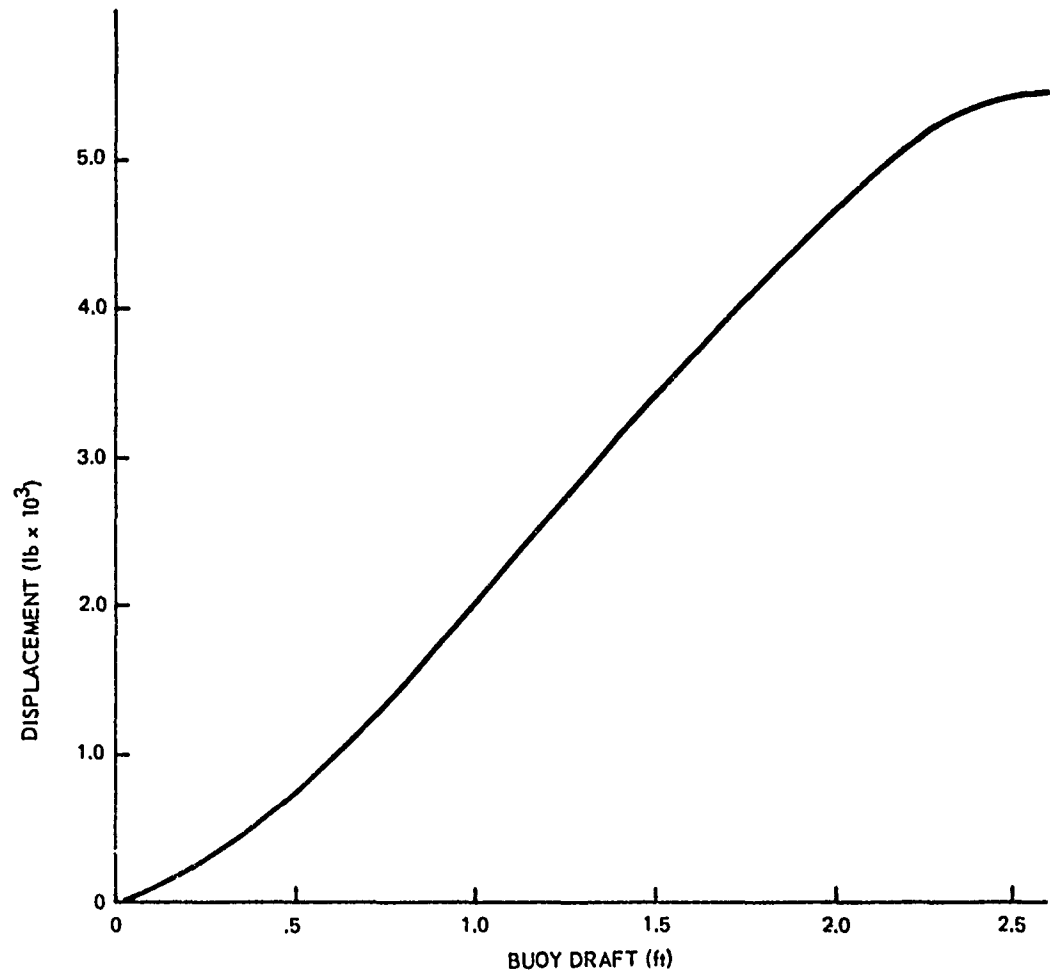


Figure E-2. Torroid (8-ft) Displacement versus Draft

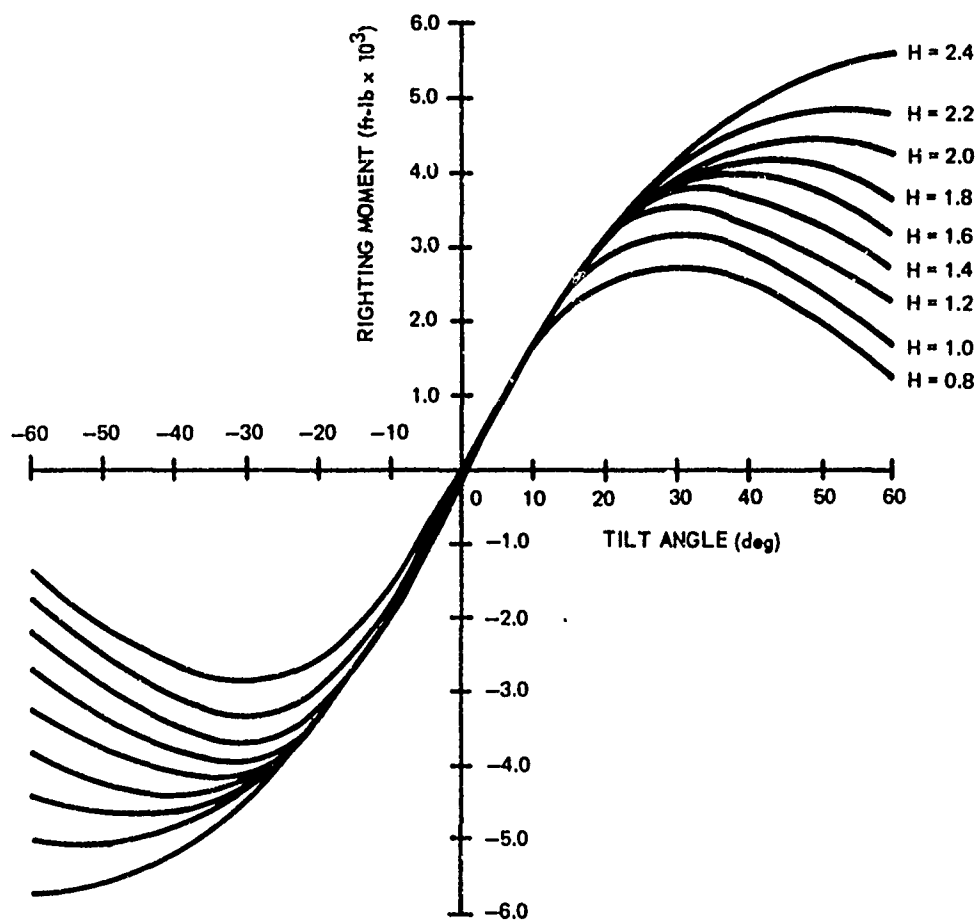


Figure E-3. Torroid (8-ft) Righting Moment versus Tilt Angle



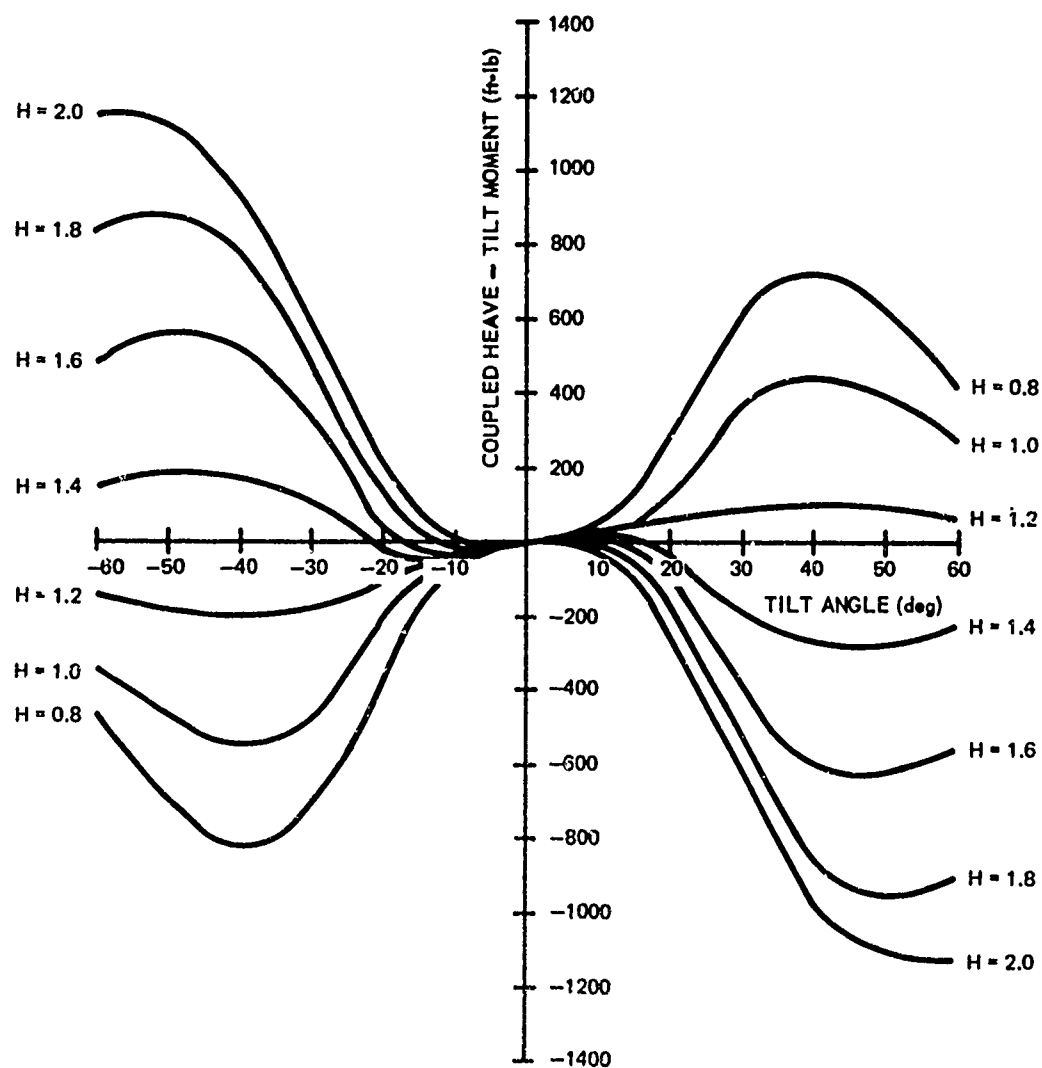


Figure E-4. Torroid (8-ft) Coupled Moment versus Tilt Angle

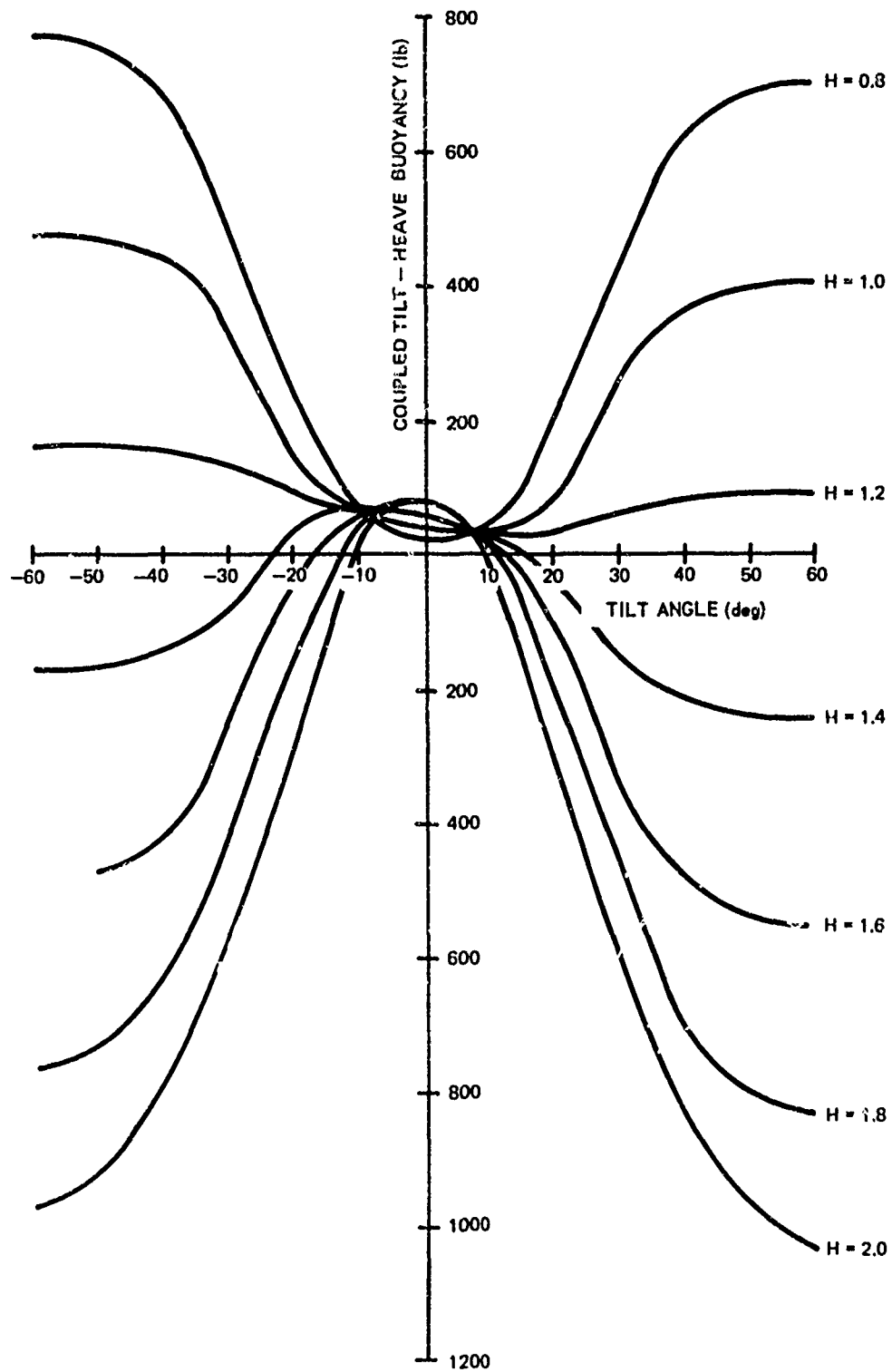


Figure E-5. Torroid (3-ft) Coupled Buoyancy versus Tilt Angle